



European Fuel Cell

Conference & Exhibition



PROCEEDINGS

OF THE 6TH EUROPEAN FUEL CELL | PIERO LUNGI CONFERENCE

Naples

16-18 December, 2015

15 December *Side Events*

organized by



ATENA
FUTURE TECHNOLOGY



UNIVERSITÀ
DEGLI STUDI
DI PERUGIA



UNIVERSITÀ
DEGLI STUDI
DI NAPOLI
"PARTHENOPE"



PROCEEDINGS

OF THE 6TH EUROPEAN FUEL CELL
PIERO LUNGI CONFERENCE



To Piero Lunghi. We miss you a lot.
To you our gratitude for ever.

This book is dedicated to the memory of Piero Lunghi, creator of the European Fuel Cell Technology & Applications Conference, dear friend and colleague, who prematurely passed away in a car accident on damned November 9, 2007.

Piero made significant contributions in the field of fuel cells in the course of his too short career.

He was the eading figure in the formation of the fuel cell research group at the University of Perugia and several activities and research projects initiated by him are still ongoing.

This means that, thanks to Piero, many young people are working in this exciting research field and are coming to Naples to present their results.

Therefore, Piero's memory is in the conference name but Piero's contribution is still in the contents of this book.

The memory of our friend Piero, his great personal generosity and energy, survives in our hearts, his contribution and his tenacity survive in the work of young people who carry on his vision throughout the world.





European Fuel Cell

Conference & Exhibition

EDITED BY
Viviana Cigolotti

CO-EDITED BY
Chiara Barchiesi and Michela Chianella

2015

ENEA
ITALIAN NATIONAL AGENCY FOR NEW TECHNOLOGIES, ENERGY
AND SUSTAINABLE ECONOMIC DEVELOPMENT

Lungotevere Thaon di Revel, 76
00196 ROME

ISBN 978-88-8286-324-1

Naples
16-18 December, 2015

15 December Side Events

organized by



ATENA
FUTURE TECHNOLOGY



UNIVERSITÀ
DEGLI STUDI
DI PERUGIA



UNIVERSITÀ
DEGLI STUDI
DI NAPOLI
"PARTHENOPE"



Senato della Repubblica



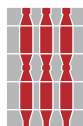
Ministero dello Sviluppo Economico



MINISTERO DELL'AMBIENTE
E DELLA TUTELA DEL TERRITORIO E DEL MARE



REGIONE CAMPANIA



Regione Umbria



COMUNE DI NAPOLI



LOCAL COMMITTEE

Chairman Angelo MORENO

ENEA (Italian National Agency for New Technologies, Energy and Sustainable Economic Development) - Italy

Viviana CIGIOTTI

ENEA (Italian National Agency for New Technologies, Energy and Sustainable Economic Development) - Italy

Chiara BARCHIESI

Dept. of Engineering - University of Perugia - Italy

Michela CHIANELLA

Dept. of Engineering - University of Perugia - Italy

Elio JANNELLI

Dept. of Engineering - University of Naples "Parthenope" - ATENA Scarl Italy

Stephen McPHAIL

ENEA (Italian National Agency for New Technologies, Energy and Sustainable Economic Development) - Italy

Vanessa ROSSI

Dept. of Engineering - University of Perugia - Italy

ORGANIZING COMMITTEE

Australia

Karl Föger, Ceramic Fuel Cells Limited (CFCL)

China

Min-Fang Han, China University of Mining and Technology (CUMT)

Hongmei Yu, Dalian Institute of Chemical Physics

Finland

Jari Kiviaho, VTT Technical Research Center of Finland

Germany

Detlef Stolten, Forschungszentrum Jülich (FZJ)

Christian Sattler, DLR - German Aerospace Center,
Vice-President of N.ERGHY

Olaf Jedicke, Karlsruhe Institut of Technology (KIT)

Italy

Alberto Ravagni, SOFCPower Spa

Gianni Bidini, Università degli Studi di Perugia

Stefano Ubertini, Università degli Studi della Toscana

Marcello Baricco, Università degli Studi di Torino

Luigi Crema, Fondazione Bruno Kessler

Marco Carcassi, Università degli Studi di Pisa

Marcello Capra, Ministero dello Sviluppo Economico

Japan

Takao Watanabe, Central Research Institute
of Electric Power Industry (CRIEPI)

Kenchiro Ota, Yokohama National University

Korea

Tae-Hoon Lim, Korea Institute of Science & Technology (KIST)

Spain

Luis Correas, Hydrogen Aragon - Foundation for the development
of new hydrogen technologies in Aragon

Fernando Palacin, Director at the Foundation
for Hydrogen in Aragon

Iñaki Azkarate, Tecnalia Corporación Tecnológica

USA

Subhash Singhal, Pacific Northwest National Laboratory (PNNL)



SCIENTIFIC COMMITTEE

Bulgaria

Tzvety Bogdanov Tzvetkoff, Hydrogen Technology Centre; NATO - Defence Technologies Laboratory, University of Chemical Technology and Metallurgy

Croatia

Franco Barbir, FESB - University of Split

Denmark

John Bögild Hansen, Haldor Topsøe

Finland

Tiina Koljonen, Technical Research Center of Finland (VTT)

France

Michel Cassir, Chimie Paris Tech (ENSCP)

Deborah Jones, Université Montpellier

Germany

Alexander Michaelis, Fraunhofer-Institut für Keramische Technologien und Systeme - IKTS Dresden

Thomas Pfeifer, Fraunhofer-Institut für Keramische Technologien und Systeme - IKTS Dresden

Ludwig Jörissen, Centrum für Sonnenenergie- und Wasserstoff-Forschung Baden-Württemberg - ZSW

Greece

Tsiakaras Panagiotis, University of Thessaly

Thanos Stubos, National Center for Scientific Research «Demokritos»

Italy

Mauro Scagliotti, R.S.E. Spa – Ricerca sul Sistema Energetico

Aristide Massardo, Università degli Studi di Genova

Maria Giovanna Minutillo, Univ. degli Studi di Napoli Parthenope

Alessandra Perna, Università degli Studi di Cassino

Umberto Desideri, Università degli Studi di Pisa

Angelo Basile, ITM-CNR – Istituto per la Tecnologia delle Membrane del Consiglio Nazionale delle Ricerche

Sergio Ulgiati, Università degli Studi di Napoli Parthenope

Vincenzo Palma, Università degli Studi di Salerno

Cesare Pianese, Università degli Studi di Salerno

Barbara Bosio, Università degli Studi di Genova

Rodolfo Taccani, Università degli Studi di Trieste

Pierluigi Leone, Politecnico di Torino

Nicola Massarotti, Università degli Studi di Napoli "Parthenope"

Luca Andreassi, Università degli Studi di Roma "Tor Vergata"

Andrea Casalegno, Politecnico di Milano

Massimo Santarelli, Politecnico di Torino

Vito Di Noto, Università degli Studi di Padova

Domenico Borrello, Università di Roma "La Sapienza"

Pierangela Cristiani, RSE - Ricerca sul Sistema Energetico S.P.A.

Raffaele Cioffi, Università degli Studi di Napoli "Parthenope"

Japan

Koichi Eguchi, Kyoto University

Netherlands

Kas Hemmes, Delft University of Technology - TU Delft

P.V. Aravind, Delft University of Technology - TU Delft

Portugal

Carmen Rangel, LNEG - National Laboratory of Energy and Geology

Romania

Vasile Stanciu, The National R-D Institute for Cryogenics and Isotopes Technologies - ICIT

Iordache Ioan, Institutul Național de Cercetare-Dezvoltare pentru Tehnologii Criogenice și Izotopice – ICSI Rm. Vâlcea

Slovenia

Stanko Hocevar, National Institute of Chemistry of Slovenia

South Korea

Suk Woo Nam, Korea Institute of Science & Technology (KIST)

Jaeyoung Lee, GIST

Spain

Javier Brey, Hynergreen technologies S.A.

Garcia Luis Alberto, Tecnalia Corporación Tecnológica

David Sanchez, University of Sevilla

Antonio García-Conde, Spanish Hydrogen Association - IEA HIA

Justo Lobato Bajo, University of Castilla-La Mancha

Sweden

Bin Zhu, Royal Institute of Technology

Carina Lagergren, KTH

Switzerland

Olivier Bucheli, EFCF

Turkey

Cigdem Karadag, TUBITAK Marmara Research Center

Atila Ersoz, TUBITAK Marmara Research Center

Isil Isik Gulsac, TUBITAK Marmara Research Center

Fehmi Akgun, TUBITAK Marmara Research Center

UK

Mike Blundell, Coventry University Enterprises - CUE Lt

Vladimir Molkow, University of Ulster

John Irvine, University of St. Andrews

USA

Abdelkader Hilmi, Fuel Cell Energy

Whitney Colella, Pacific Northwest National Laboratory (PNNL)

J. Robert Selman, Illinois Institute of Technology

EFC15 TRACK MANAGERS

Rodolfo Taccani

Pierluigi Leone

Nicola Massarotti

Luca Andreassi

Massimo Santarelli

Carina Lagergren

Alessandra Perna

Isabel Cabrita

Domenico Borrello

Michael Lang

Kas Hemmes

Stephen McPhail

Qingxi Fu

Mariagiovanna Minutillo

Whitney Colella

Giovanni Cinti

Pierangela Cristiani

Ioannis Ieropoulos

Chiara Barchiesi

Giacomo Falcucci

Kas Hemmes

David Sánchez



EXHIBITORS

Precision FLUID CONTROLS



Precision Fluid Controls S.r.l., founded in 1997, is currently selling on the whole Italian market and abroad instrumentation for level, pressure, flow and temperature monitoring.

We distribute a wide range of products, according to leading Representatives companies, on a sole distribution basis. Our instrumentation is suitable both for the process control (chemical industry, shipbuilding and heavy industry) and laboratories. Precision is able to supply you with the right solution to your exigencies in various industrial fields (chemical, pharmaceutical, shipbuilding, food and beverage, semiconductors, transportation etc.).

Precision Fluid Controls S.r.l., presente sul mercato dal 1997, vende su tutto il territorio italiano strumenti di misura per il controllo di livello, portata, pressione e temperatura dedicati sia al controllo di processo che ai laboratori. Grazie al supporto costante di Società leader, Precision offre soluzioni alle vostre misure di pressione, portata, livello e temperatura in vari settori industriali (chimico, farmaceutico, navale, alimentare, semiconduttori, trasporti). Dal punto di vista commerciale Precision vanta una rete di vendita che copre tutto il territorio nazionale e organizza la propria attività tramite la rappresentanza di aziende estere specializzate su specifiche linee di prodotto.

McPhy energy

McPhy Energy is a leading developer of hydrogen-based solutions for industry and energy markets.

The company draws on its exclusive technique for storing hydrogen in solid form and its years of experience in producing hydrogen through water electrolysis to design and manufacture flexible production, storage and distribution equipment.

In the fight against climate change, hydrogen mobility is powerful tool for helping to reduce greenhouse gases and stem global warming.

As an energy transition player, McPhy Energy provides expertise in the field of zero emission mobility and is deploying an infrastructure of hydrogen refuelling stations: McFilling.

McFilling is a compact and modular system that allows:

- to produce a renewable hydrogen (completely carbon-free hydrogen), using green electricity from renewable energy
- to add modules as the fleet of hydrogen vehicles enlarges
- to implement an onsite electrolysis equipment, to dispense with the transmission and distribution of hydrogen and thus removing the carbon footprint related to these stages
- to feed the hydrogen vehicles with a green - or renewable - hydrogen

EXHIBITORS



FCLAB





investiamo nel vostro futuro

The research project "Fuel Cell Lab" (FCLAB) is part of the Cluster "Energy, Environment and Green Chemistry" funded by the National Operational Programme for "Research and Competitiveness" 2007-2013, and aims to support the development of innovative technologies for energy conversion, with the aim of creating complex energy systems that combine the needs of the cheap energy availability and environmental sustainability.

The research activities of the FCLAB project are oriented to:

- Development of innovative technologies for energy conversion, with the aim of creating energy systems that combine the needs of the cheap energy availability and environmental sustainability.
- Development of modular technology platforms based on fuel cells for stationary poly-generation and micro-CHP and for mobile and portable power.

Among the various kind of fuel cells, the research activities are oriented to the development of molten carbonate fuel cells (MCFC) for poly-generation, solid oxide fuel cells (SOFC) for micro-CHP and polymer electrolyte (PME) for mobile applications, microbial cells (MFC) for the direct conversion of organic waste into electricity (bio- electrolysis), also in combination with anaerobic digestion processes for the production of biofuels (bio-hydrogen and bio-methane).

The innovative energy conversion systems developed within this project and, therefore, with performance characteristics in terms of efficiency, and greenhouse-gas emissions that are not reflected in the panorama of the international technology sector, will greatly contribute to the growth of the involved companies, which will broaden their horizons far beyond current areas of business.





FUNDING FUEL CELLS AND HYDROGEN TECHNOLOGY DEVELOPMENTS ACROSS EUROPE

The Fuel Cells and Hydrogen Joint Undertaking (FCH JU) finances Research & Development (R&D) and Demonstration projects on fuel cells and hydrogen. It is a unique public-private partnership between the European Commission, Europe's fuel cell and hydrogen industry and research organisations. A public-private partnership model works as an effective way for European intervention to coordinate R&D activities by pooling financial resources together.

The European Union is committed to changing its transport and energy systems in pursuing a future low carbon economy. Fuel Cells and Hydrogen (FCH) technologies hold great promise for energy and transport applications from the perspective of meeting Europe's energy, environmental and economic challenges.

Hydrogen can be produced using renewable energy sources, offering a clean fuel for road transportation. Moreover, hydrogen offers the ability to store electricity, addressing the intermittent character of renewable energy. When coupled with highly efficient, silent and clean fuel cells as energy convertors, hydrogen opens up new horizons for decreasing Europe's dependency on imported fossil fuels.

The aim of the FCH JU is to accelerate the market introduction of these technologies, realising their potential as an instrument in achieving a carbon-lean energy system.

Established in 2008, the FCH JU has supported 169 projects to date. Its second phase was approved by the Council of the European Union in May 2014 under the Horizon 2020 EU funding programme, with a total budget of €1.33 billion as FCH 2 JU. This marks Europe's continued confidence and support for fuel cells and hydrogen as key technologies for decarbonising our energy system, and creating a secure sustainable energy supply capable of generating new jobs.

The FCH JU programme is structured around two research and innovation pillars dedicated to **Transportation and Energy Systems**, complemented by a set of **Cross-Cutting** research activities.

ENERGY

- Fuel cells for power and combined heat & power generation
- Hydrogen production and distribution
- Hydrogen for renewable energy storage (incl. blending in natural gas grid)

TRANSPORT

- Road vehicles
- Non-road mobile vehicles and machinery
- Refuelling infrastructure
- Maritime, rail and aviation applications

CROSS-CUTTING ISSUES

(e.g. standards, consumer awareness, manufacturing methods, studies)

SPONSORS



The Institute for Advanced Energy Technologies "Nicola Giordano" (hereinafter ITAE) is an Italian research centre founded in 1980 and belonging to the National Research Council (CNR) that is distributed all over Italy through a network of institutes aiming at promoting a wide diffusion of its competences throughout the national territory and at facilitating contacts and cooperation with local firms and organizations.

ITAE is one of European leading research centre in the fuel cells and renewable energy fields and a full member of the Fuel Cells and Hydrogen Joint Technology Initiative of the European Community.

The research activity is organized in 4 sectors:

- 1 – Direct production of electric energy technologies
- 2 – Hydrogen and clean fuels production
- 3 – Energy transformation and storage technologies
- 4 – Integration of new energy technologies and renewable

Beside these four lines of research, there are three support activities that cut across all research lines and are: socio-economic impact analysis of cutting-edge energy technologies; study about the regulations governing the application and use of energy technologies; technology transfer and exploitation of R&D results.

The institute is provided with 19 equipped laboratories for preparative and characterization of materials and components, energy systems and for the construction and testing of devices and prototypes.

These laboratories are located in a building which is on three levels with a total area of 4800 square meters, and includes laboratories, offices, a conference room, a library, a guest quarters and the canteen.

Moreover, the ITAE has, in an area close to its headquarters, a "Center for new energetic technology testing, innovation and industrial promotion", that is a testing center supplying technical and scientific support to companies operating in the production of innovative energy systems



RITMARE Flagship Project is one of the National Research Programmes funded by the Italian Ministry of University and Research.

RITMARE

is the leading national marine research project for the period 2012-2016; the overall project budget amount to 250 million euros, co-funded by public and private resources. It is coordinated by the National Research Council and involves an integrated effort of most of the scientific community working on marine and maritime issues, as well as some major industrial groups.

RITMARE is divided into 7 sub-projects:

1. Maritime Technologies
2. Technologies for Sustainable Fishing
3. Planning of the Maritime Space in Coastal Waters
4. Planning of the Deep Marine Environment and the Open Sea
5. Observation System for the Marine Mediterranean Environment
6. Research, Training and Dissemination Structures
7. Interoperable Infrastructure for the Observation Network and Marine Data

RITMARE

- Supports training of a new generation of researchers, through the funding of innovative projects selected through call for proposal
- Strengthens the strategic presence of Italian research in Europe and in the Mediterranean
- Promotes the establishment of a permanent forum between researchers, decision makers and stakeholders in both the public and private sector, with the aim of fostering the integration and transfer of research results and thus place the knowledge as a reference starting point for strategies and management decisions



SPONSORS

HIDEN ANALYTICAL

30 years of design, development and manufacture of quadrupole mass spectrometers

We design, develop and manufacture quadrupole mass spectrometers for advanced research applications and specialist process monitoring.

Our product range includes: Systems for precision gas analysis for real time, multiple gas/vapour analysis with dynamic range from PPB to 100%.

Plasma diagnostics by direct measurement of plasma ions and ion energies.

SIMS probes for UHV surface science, and etch end point detection. Integrated complete surface analysis SIMS systems with automated analysis.

A range of micro furnace reactors for catalyst research for making temperature programmed analysis with techniques including TPO/TPD/TPR and TPRx.

Our bespoke design service provides for client interactive development of solutions to meet specific requirements.



Società Chimica Italiana

DIVISIONE DI ELETTROCHIMICA

The Electrochemistry Division of the Italian Society of Chemistry (SCI) – founded on 1974 and according to the objectives undertaken by the SCI – aims at the research advancement in its specific field, as well as to promote teaching and to develop strategic relationships with Industry. At this purpose the Electrochemistry Division

organizes, promote and sponsors different initiatives such as congresses, workshops and schools. Moreover it is very attentive to education, and to the enhancement of young people, through Degree and PhD Awards and supporting Conference participation. For further information please visit www.soc.chim.it/it/divisioni/elettrochimica/HOME



ROAD SHOW

18th December



MEDIA PARTNERS

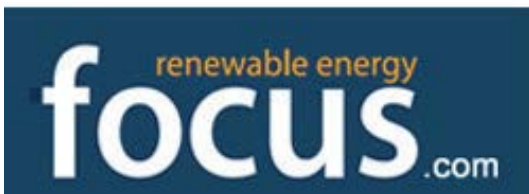


Fuel Cell &
Hydrogen Energy
Association

Fuel Cell & Hydrogen Energy Association (FCHEA) is the trade association for the fuel cell and hydrogen energy industry, dedicated to the commercialization of fuel cells and hydrogen energy technologies. FCHEA members represent the full global supply chain, including fuel cell materials, components and systems manufacturers, hydrogen producers and fuel distributors, government laboratories and agencies, trade associations, utilities, and other end users.



Fuel Cells Bulletin is the leading monthly newsletter dedicated to reporting and analysing business and technology developments in the global fuel cell sector. The newsletter – published as a Digital Edition – contains a mix of news on automotive and mobile, small and large stationary, portable and micro, hydrogen fuelling and energy storage, commercialisation and research activities and demonstrations. Each issue has a feature article on a specific company, project, technology or topic of interest, as well as an extensive summary of new US patents, and a comprehensive events calendar.



Renewable Energy Focus magazine and its website provide a forum for debate and dialogue between research, industry, financial organisations and government bodies worldwide. With in-depth coverage and incisive editorial on all areas of renewable energy, Renewable Energy Focus takes an objective look at bioenergy, energy efficiency, energy infrastructure, energy storage (including fuel cells), geothermal, green buildings, hydro power, photovoltaic (PV), solar heating and cooling, solar thermal, wave and tidal energy, and wind power.



Shmuel De-Leon Energy, Ltd. is a leading company in the field of power sources knowledge. The company provides comprehensive collection of power sources knowledge tools and services:

- Consulting services
- Market research reports
- Batteries , Fuel cells and EV seminars and conferences
- Batteries, FC & EV Weekly newsletter
- Energy Sources On-Line web DataBase (batteries, fuel cells, capacitors and more...)
- Power sources solutions
- Representing Energy Storage testing and research equipment companies in Israel



MEDIA PARTNERS



AltEnergyMag is an eMagazine full of News, Articles and Interviews covering the trends and breakthroughs in the Alternative Energy Industry, with an emphasis on the state of the art and on the horizon technologies that have strong prospects of commercialization. Since 2002 our philosophy has been to create an outlet where the industry can collaborate and report on itself. We offer those of you who work or have a passion for the Alternative Energy to contribute articles, news and product information for your peers to read and discover.



American Elements is the world leader in the industrial application of materials science. It has also been a key source for academic and corporate research, advancement and new product development in SOFC and PEM fuel cell materials and has been a decade long participant in the materials development component of the U.S. Dept. of Energy's SECA program. Our fundamental expertise in the properties, applications and cost-effective manufacturing of advanced and engineered materials, including ultra high purity refining (99,9999%) and nanotechnology (Mono Atomic Elements) scales allows us to meet the needs of thousands of global manufacturers (including over 30% of the Fortune 50), all U.S. and many foreign national laboratories, universities throughout the world, and our customers in a wide variety of industry groups, including energy, electronics, aerospace, defense, automotive, optics/photovoltaics, green technologies and pharma/cosmetics. The company provides both technical guidance and manufactured products in its 10,850 page online catalogue which includes over 3,000 elemental metal, metallic compound, ceramic and crystalline stock items. American Elements also produces numerous customer proprietary formulations from our network of production facilities strategically placed throughout the world.



Fast a not for profit private organization founded in 1897, represents 32 Italian scientific and technical associations covering the most important and priority European industrial sectors. Thanks to the competencies and expertise of the associations belonging to FAST network, the Federation is able to address significant stakeholders at regional and national level and to guarantee a permanent liaison with the most relevant EU industrial and research networks. FAST has a long standing relationship with different regional and local authorities providing them support in shaping and programming their policies with regards to innovation, research (FAST is a member of the Enterprise Europe Network, manages the Hyer secretariat -HYER - in Brussels), education and training and technical assistance to SMES.



H2IT is an independent and non-profit organization, launched in 2004 to formalize the activities of the working groups of the Italian Hydrogen Taskforce and promote the creation of an infrastructure for the use of hydrogen. The goal is to stimulate and develop the market for the use of hydrogen, to create a strong industry voice of companies and institutes involved in the sector, and to secure a leading role for Italy in the world market.





ABSTRACTS

THE INFLUENCE OF ELECTROLYTE TYPE ON DYNAMIC RESPONSE OF 1 KW-SIZE SOFC STACK

Jarosław Milewski, Arkadiusz Szczniak, Rafał Bernat

Institute of Heat Engineering
Faculty of Power and Aeronautical Engineering
Warsaw University of Technology Warsaw,
Poland
Email: milewski@itc.pw.edu.pl

Jakub Kupecki, Konrad Motyliski

Institute of Power Engineering
Warsaw, Poland
Email: milewski@itc.pw.edu.pl

ABSTRACT

This paper describes the experimental validation of transient model of 1.3 kW integrated stack module (ISM). A developed dynamic Solid Oxide Fuel Cell (SOFC) model is used and based on it, various electrolyte materials were simulated in viewpoint of their influence of dynamic behavior of the system. The YSZ as the reference case was analyzed providing also the model validation.

An adequate simulator of the SOFC stack was made and described. Based on this simulator, the dynamic response of this two-stacks compound with different electrolyte materials and thicknesses is shown, and some characteristics are given and described. The advantages and disadvantages of different electrolyte types from a transient point of view are indicated.

Introduction

Electricity is currently generated by large stationary power plants and distributed to customers through a grid. In the future, energy distribution will probably take a radically different form—it will comprise many small units connected in a network—a system called distributed generation (DG).

Fuel cells, especially Solid Oxide Fuel Cells [1] are predicted to be power and heat sources in future oriented DG. The motivation of this work was to build an SOFC dynamic model which can be used for power plant simulations. Elements of power plants other than fuel cells (turbines, compressors, pumps,

heat exchangers) are mainly modeled as 0-D models. The models available in the open literature are mostly oriented to specific purposes and very rarely validated on the experimental data—thus utilization of them for system modeling purposes is difficult and produces uncertainties. This paper describes the dynamic behavior of a single planar solid oxide fuel cell obtained by a 0-D model. Based on the model, an attempt is made to develop a control strategy for the safe and reliable operation of the SOFC. A few cases are investigated: start-up, shutdown, changes in power and some accidental behaviors.

The mathematical model of SOFC for steady state calculations was presented in a few previous papers [2–4].

The electrolyte material influence is modeled by adequate conductivity values and presented in Table 1.

Influence of electrolyte material on Solid Oxide Fuel Cell performance during dynamic operation

The 1.3 kW Integrated Stack Module (ISM) supplied by Staxera converts chemical potential energy into electricity and heat through electrochemical processes. It consists of two separated stacks, each of 30 cells operating at temperatures between 700°C and 850°C. The stacks are constructed of multiple layers of ferritic steel sheets and ceramic foils that are bound by glass. The



TABLE 1. Analyzed materials and adequate factors

Case	Electrolyte materials	Composi- tion	σ_0 , S/cm	E_{act} , kJ/mol
ZrY	ZrO ₂ /Y ₂ O ₃	0.90/0.10	390.95	-87.806
ZrCa	ZrO ₂ /CaO	0.87/0.13	399.75	-94.595
ZrSc	Zr ₂ /Sc ₂ O ₃	0.90/0.10	73.479	-60.192
BiY	Bi ₂ O ₂ /Y ₂ O ₃	0.75/0.25	350.97	-62.097
CeGd	Ce ₂ /GdO _{0.5}	0.80/0.20	25.931	-48.112

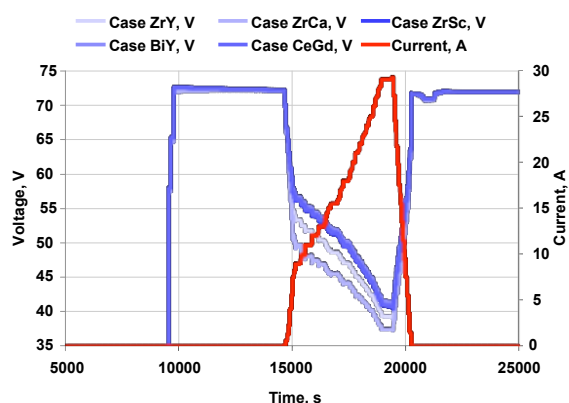


FIGURE 1. The influence of electrolyte material on dynamic response of SOFC—stack voltage

Staxera's Mk200 stack contains 30 cells, which are commercially available from H.C. Starck. The anode is porous NiO/GDC, the electrolyte is dense 3YSZ and the cathode is double layered 8YSZ/LSM–LSM. The total cell thickness is 160 μm and its active area 127.8 cm^2 per cell. The interconnectors are stamped metal sheets of Crofer22 APU, and nickel foam is used as anode contact.

The Staxera SOFC stack was analyzed with five different electrolyte materials. The compositions of these materials are listed in Table 1.

The solid electrolyte is quite thin layer, thus its influence of the thermal behavior of the entire stack can be neglected. The differences for various electrolyte materials are visible during stack load changes, and they expressed by various voltage levels for the same electric currents. The results of the simulation are shown in Fig. 1, the best performances are obtained for ZrSc, BiY, and CeGd, but the differences are very small between them. The worst performances are obtained for the reference case (ZrY)

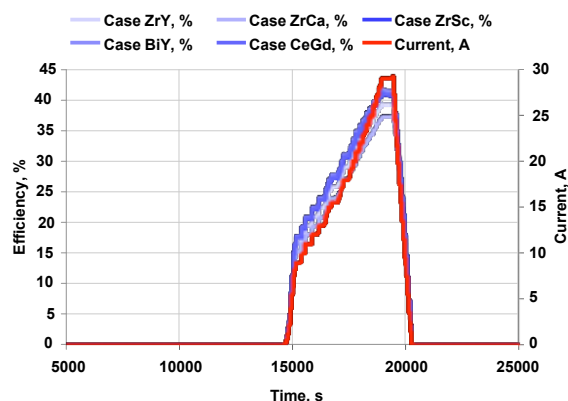


FIGURE 2. The influence of electrolyte material on dynamic response of SOFC—stack efficiency

and ZrCa, for which the voltages drop below 40 V during nominal conditions.

By changing electrolyte material the stack efficiency can be raised from 40 to 42% (by 5%)—see Fig. 2 for details.

Acknowledgments

Authors would like to acknowledge support from EU through ONSITE project (grant agreement 325325) and National Centre for Research and Development under the strategic project Advanced Technologies for Energy Generation, Task 4: Developing integrated technologies of fuel and energy production from biomass, agricultural wastes and other resources. Marek Skrzypkiewicz, Michal Wierzbicki and Michal Stepień from IEN are acknowledged for supplying experimental data for the stack.

REFERENCES

- [1] Kupecki, J., and Badyda, K., 2011. "SOFC-based micro-CHP system as an example of efficient power generation unit". *Archives of Thermodynamics*, **32**(3), pp. 33–43.
- [2] Milewski, J., Świrski, K., Santarelli, M., and Leone, P., 2011. *Advanced Methods of Solid Oxide Fuel Cell Modeling*, 1 ed. Springer-Verlag London Ltd., March.
- [3] Milewski, J., 2010. "Simultaneously modelling the influence of thermal-flow and architecture parameters on solid oxide fuel cell voltage". In *ASME Fuel Cell Science and Technology*.
- [4] Milewski, J., 2010. "Advanced model of solid oxide fuel cell". In *Fuel Cell Science, Engineering & Technology Conference*, no. FuelCell2010-33042, ASME.



CONTROL STRATEGIES TO MINIMIZE DEGRADATION IN FUEL CELL GAS TURBINE HYBRIDS

V. Zaccaria*, D. Tucker*, and A. Traverso**

*U.S. Department of Energy, NETL, 3610 Collins Ferry Rd, Morgantown WV, (USA)

**University of Genoa, TPG, via Montallegro 1, Genova, (Italy)

Abstract - The hybridization of solid oxide fuel cell (SOFC) and gas turbine technologies provides an increase in system efficiency and economic performance. The latter aspect is significantly affected by fuel cell degradation, due to several mechanisms. However, hybrid systems allow different control strategies to minimize degradation effects and impact on economic performance.

A real-time distributed model of a SOFC was used to simulate fuel cell degradation in the cases of a standalone cell and a hybrid configuration, where the numerical model would be normally coupled with the hardware components of a hybrid system. The results showed how in a hybrid system it is possible, with the appropriate controller, to maintain constant voltage even if the cell is degrading, reducing degradation rate during time. Fuel cell life could be significantly extended with the control strategies allowed by coupling with a turbine (an order of magnitude longer than a standalone fuel cell), maintaining high system efficiency despite fuel cell degradation.

Index Terms – control strategy, degradation, hybrid systems, SOFC

I. INTRODUCTION

In order to study the life of a SOFC fed by syngas, a real-time, 1D model was implemented, in which voltage degradation during time is simulated using an empirical expression for the degradation rate (percentage of voltage drop per 1000 hours of operation) as function of current density i , fuel utilization FU and temperature T [1]. More details of the model can be found in previous publications [2]. Degradation rate is expressed as shown in (1).

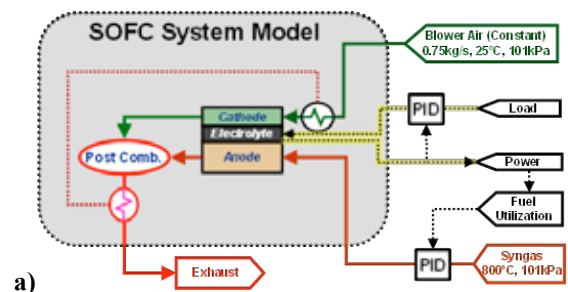
$$r_d = \frac{0.59FU + 0.74}{1 + \exp\left(\frac{T - 1087}{22.92}\right)} (e^{2.64i} - 1) \quad (1)$$

The model can simulate a standalone fuel cell or a hybrid

configuration where the waste heat from the fuel cell system is converted into electrical power by a gas turbine. In the first scenario, the power of the standalone (atmospheric) fuel cell was kept constant by increasing current as voltage degraded, with PID control of fuel to maintain constant fuel utilization. In the second scenario, two control strategies were compared, as illustrated in the following section.

II. CONTROL STRATEGIES

The different control strategies used in this work are depicted in Figure 1. In the standalone fuel cell, the only way to keep power constant as the voltage is degrading is to increase the current, which increases degradation rate with time. Fuel flow is incremented by a second controller in order to maintain fuel utilization constant (Fig. 1a). In a hybrid system the total power output can be maintained constant increasing the turbine load, i.e. the fuel flow to the system. Since the total efficiency is significantly higher than in a standalone fuel cell, there is no need to keep fuel utilization constant. The current can be let constant (Fig. 1b) or decreased by a PID in order to reduce degradation rate during time and keep constant voltage (Fig. 1c).



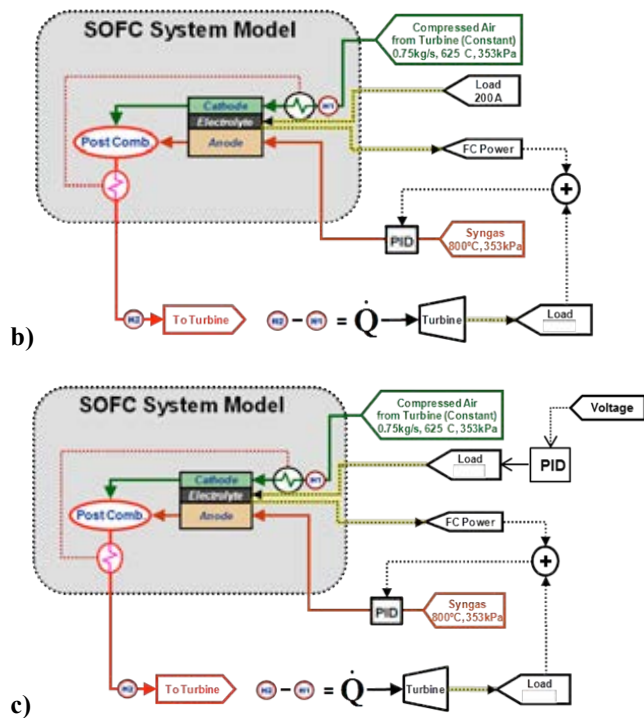


Fig. 1. Control strategies for standalone configuration (a), and hybrid configuration with constant current (b) and constant voltage (c)

III. RESULTS

Figure 2 shows the comparison between the cell lifetimes in the three cases.

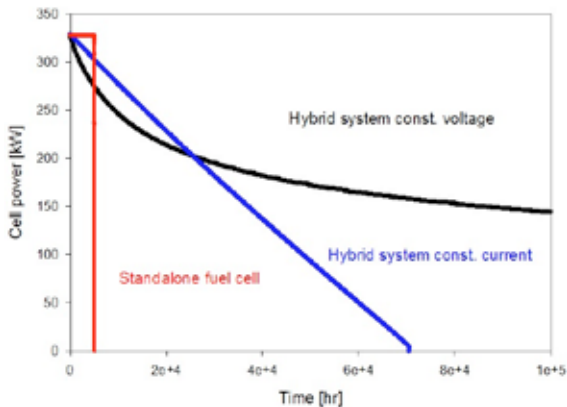


Fig. 2. Cell lifetime comparison between the three control strategies

In the standalone fuel cell, since degradation rate increased with time due to the increment in current, the voltage (and consequently the power) dropped very fast and the cell failed after about 6,000 hours. With the constant current in the hybrid configuration, degradation rate was fairly constant during time, slightly decreasing thanks to the reduction in fuel utilization, due to the increment in fuel flow. Hence, cell power gradually decreased to zero in about 75,000 hours. The second control

strategy that can be implemented in a hybrid system allowed maintaining constant voltage, reducing current load and consequently degradation rate. The cell lifetime can be thus comparable with the lifetime of the turbine, since after 100,000 hours the fuel cell power output reduced only by 60%.

The efficiencies comparison is shown in Figure 3.

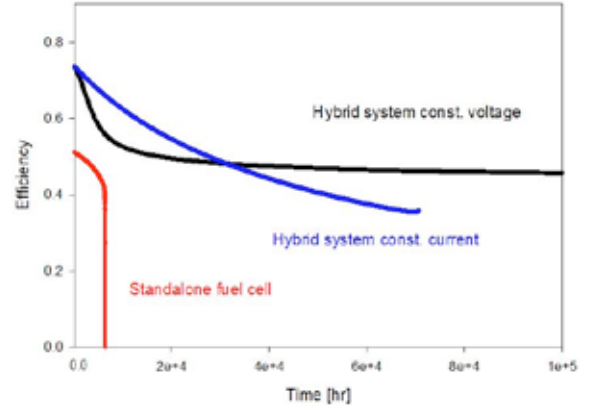


Fig. 3. System efficiency comparison between the three control strategies

The efficiency of the recuperated turbine cycle is considered constant in these simulations. However, as the cell degrades, the load needs to be shifted to the turbine, which has to be oversized at the beginning of plant life and work in off-design conditions for a considerable amount of hours. An economic analysis of the system needs to be performed in order to evaluate the cost-effectiveness of this strategy and the optimal size of the turbine to compensate cell performance degradation over time.

IV. CONCLUSIONS

Performance degradation of a SOFC was studied comparing a standalone case and a hybrid configuration where the pressurized fuel cell is coupled with a turbine. Two different control strategies were implemented in the second scenario, and compared with the standalone case. In the hybrid system it was possible to maintain the system power constant and at the same time extend the fuel cell life more than 10 times, reducing the voltage degradation rate and maintaining high system efficiency. Future works are required to analyze the effect of temperature gradients along the cell and potential mitigation actions, as long as economic feasibility of the system.

REFERENCES

- [1] Zaccaria V., Tucker D., and Traverso A., 2015, A Real-time Degradation Model for Hardware in the Loop Simulation of Fuel Cell Gas Turbine Hybrid Systems, Proceedings of ASME Turbo Expo 2015, Paper number GT2015-43604;
- [2] Hughes, D., Wepfer, W.J., Davies, K., Haynes, C., and Tucker, D., 2011, A Real-time Spatial SOFC Model for Hardware-Based Simulation of Hybrid Systems, International ASME Conference on Fuel Cell Science, Engineering and Technology.



**ROMANIA'S PARTICIPATION TO
THE EUROPEAN ASSESSMENT PROJECT TITLED HYUNDER,
MULTI-CRITERIAL ANALYSES OF SALT CAVERN LOCATIONS**

Ioan Iordache^{1,2}, Dorin Schitea^{1,2}, Adriana Marinouiu¹,
Mihaela Buga¹, Mihai Balan^{1,2}, Ioan Stefanescu¹,
Adrian Gheorghe³, Mihaela Iordache⁴

1. National Research and Development Institute for Cryogenics and Isotopic Technologies ICIT, Rm. Valcea, *Romania*
2. University POLITEHNICA of Bucharest, *Romania*
3. Old Dominion University, Norfolk, *USA*
4. National Research and Development Institute for Industrial Ecology INCD-ECOIND, Rm. Valcea, *Romania*

Abstract - The scope of the work is to assess the potential, the actors and relevant business cases for large scale storage of renewable electricity by hydrogen underground storage in Romania. This presentation intends to provide a picture of the multi-criterial analyses of salt cavern locations in Romania.

The energy sector is facing with the necessity to store large energy quantities for short to long term in order to adapt to the increasingly intermittent renewable energy. The results of this presentation have originated from an ongoing European assessment project by the name of HyUnder (FCH JU, grant 303417) regarding utilization of salt caverns for hydrogen underground storage.

Currently, main uses of salt caverns include storage of hydrocarbons or wastes disposal. Salt caverns have stirred the interest of the scientific community regarding the potential applications in hydrogen economy. Romania has active mines or caverns and others closed, many of them have the potential to be used for hydrogen storage. These facts represent an interested situation in order to initiate studies or assessments of the potential hydrogen underground storage. The salt mines, hydrogen producers, renewable energy sources and research centers with high qualified scientists, represent essentially elements for new type of studies regarding hydrogen economy. In the context of scientific community's efforts from Romania to assert active in the area of hydrogen technologies, this approach can certainly constitutes an attractive example for pan-European cooperation.

The work disclaims the technic multi-criterial analyses of salt cavern locations regarding hydrogen underground storage. The introduction of hydrogen into economy offers the possibility to provide a number of advantages: sustainable development, valorization of local resources and improvement of competitiveness. The opportunities and viabilities of salt cavern locations are analyzed.

Index Terms hydrogen storage, HyUnder, multi-criterial analyses, salt caverns

I. INTRODUCTION

The scientific literature describe the intelligent decision system as a window-based software package that has been developed on the basis of the evidential reasoning approach, that successfully is used for handling hybrid multiple criteria decision analysis (MCDA) problems with uncertainties. The approach has been developed using the concepts from several disciplines, including decision sciences, artificial intelligence, statistical analysis, fuzzy set theory, and computer technology [1].

In the situation when there is need to decide which location or sub-locations are the best choice for hydrogen underground storage placement, it is inevitable to deal with both quantitative and qualitative information under uncertainty. Evidence-based reasoning within a multiple criteria decision analysis framework provides an alternative way of handling such information systematically and consistently. In this paper, the evidential reasoning approach is used in order to analyses both quantitative and qualitative data regarding hydrogen underground storage in salt caverns in Romania. This is a part of a comprehensive study performed by the authors using data obtained from the HyUnder European project.

II. RESULTS AND DISCUSSIONS

Hydrogen storage at large scale can be expected to support the integration of intermittent renewable energy sources in the current energy system. Figure 1 provides a picture for the potential hydrogen infrastructure in Romania where four possible locations for hydrogen underground storage can be identified: Cacica, Targu Ocna, Ocnele Mari and Ocna Mures. A detailed study about these locations and afferent infrastructure was described by authors in other paper [2]. The



studies were conducted according with HyUnder project criteria, which refer to the evaluation of a set of locations, like: good geological conditions and cavern field in conservation.

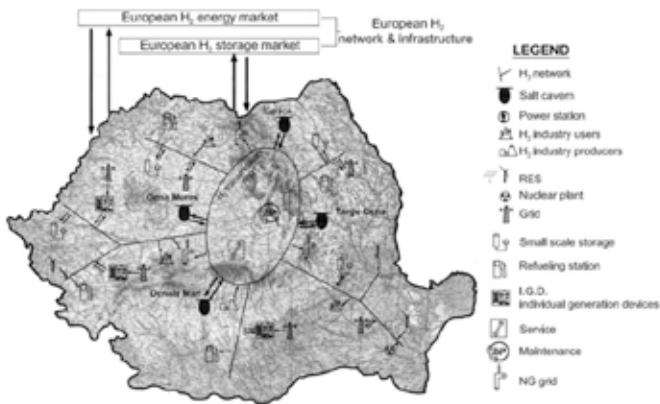


Fig. 1. Locations for hydrogen underground storage in salt cavern in Romania, source [2].

The studies were conducted according with HyUnder project criteria, which refer to the evaluation of a set of locations, like: good geological conditions and cavern field in conservation. The sites were multi-criterial analyzed. The driver for potential utilization of hydrogen underground storage in Romania is the steep gradient of introducing renewable electricity and time lagged also in other energy sectors such as mobility, chemical industry and the natural gas industry. The multiple criteria decision analysis (MCDA) of hydrogen underground storage in salt caverns offer more sensitive scenarios where more details or differences can be visualized. In Figure 2, the authors provide an example of analysis of general, geologic, geographic, industrial, grid, mobility and development aspects [3].

III. CONCLUSIONS

The extended abstract shows the collective efforts of researchers from National Research and Development Institute for Cryogenics and Isotopic Technologies - ICSI Rm.Valcea (National Hydrogen and Fuel Cell Center) to highlight potential in Romania in terms of hydrogen storage. This presentation provides a picture of the insights, perspectives and referrals for hydrogen underground storage in salts caverns in Romania, using multiple criteria decision analysis (MCDA).

Percentage Score

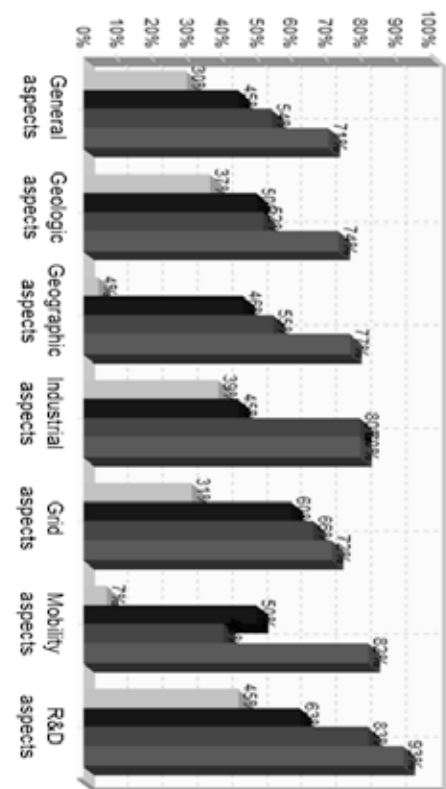


Fig. 2. Example of multiple criteria decision analysis of hydrogen underground storage in salt caverns.

ACKNOWLEDGMENT

The authors gratefully acknowledge the financial support received from the Fuel Cell and Hydrogen Joint Undertaking, Grant no. 303417 and UEFISCDI, Ministry of National Education (Romania), Contract no. JTI-09/2012.

REFERENCES

- [1] Xu Dong-Ling, Yang Jian-Bo, Intelligent decision system based on the evidential reasoning approach and its applications, J. of telecommunication and information technology, 3 (2005) 73-80.
- [2] Ioan Iordache, Dorin Schitea, Adrian Gheorghe, Mihaela Iordache, Hydrogen underground storage in Romania, potential directions of development, stakeholders and general aspects, International Journal of Hydrogen Energy, 39 (2014) 11071-11081.
- [3] Ioan Iordache, PhD Thesis, University "Politehnica" from Bucharest, Bucharest, June, 2015.



SILVER/MANGANESE DIOXIDE COMPOUNDS FOR ENHANCED OXYGEN REDUCTION CAPABILITIES IN FUEL CELL/BATTERY SYSTEM

M. Musil*, B. Choi*, and A. Tsutsumi*

* Collaborative Research Center of Energy Engineering, Institute of Industrial Science, The University of Tokyo, 4-6-1, Komaba, Meguro-ku, Tokyo 153-8505 (Japan)

Abstract – A novel silver/manganese dioxide compound was synthesized with a facile method by activating the surface of electrolytic manganese dioxide with SnCl₂ and consecutive silver deposition. The possibility of using this compound as positive electrode in a fuel cell/battery system was assessed, i.e., by electrochemical cycling and evaluating its oxygen reduction capabilities in a pressurized vessel. At electrochemical cycling, the Ag free electrode showed better performance with a higher discharge potential and capacity. However, in case of oxygen reduction, the Ag in the silver/manganese dioxide electrode had a positive effect, increasing both the potential and maximum current of the compound.

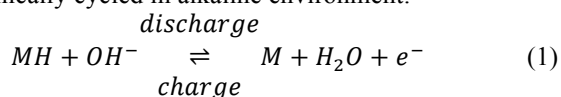
Index Terms – Fuel Cell/Battery System, Manganese Dioxide, Oxygen Reduction Reaction, Silver

I. NOMENCLATURE

CB: carbon black
EMD: electrolytic manganese dioxide
EVA: ethylene-vinyl acetate
FCB: fuel cell/battery
MH: metal hydride
PP: polypropylene

II. INTRODUCTION

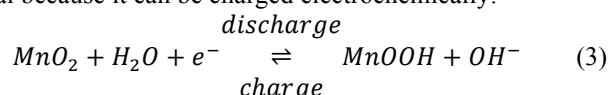
Our group has previously introduced the concept of an FCB system [1]. As a negative electrode MH is used, which can be electrochemically cycled in alkaline environment:



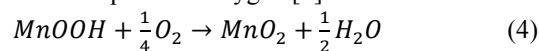
In addition to that, MH can also be charged by gaseous hydrogen:



As a positive electrode, MnO₂ was found to be a promising material because it can be charged electrochemically:



And in addition to that, discharged MnO₂, i.e., MnOOH, can be regenerated when exposed to oxygen [2]:



Furthermore, MnO₂ can work as an oxygen reduction reaction (ORR) catalyst as shown by others [3].

In previous work, it was found that the oxygen regeneration and ORR were the rate limiting steps of MnO₂ as positive electrode material in the FCB system [4]. In this work, an Ag/EMD compound has thus been synthesized and analyzed as positive electrode for an FCB because the addition of silver was expected to enhance the catalytic capabilities of the positive electrode.

III. EXPERIMENTAL

Commercially available EMD (Tosoh Japan), whose crystal structure is γ -MnO₂, was used without purification. Its surface was activated by stirring 1 g of EMD in 100 ml of 0.05 M SnCl₂ in a H₂O/Ethanol (50:50 vol.%) mixture for 1 h at room temperature. The sample was then filtered, washed with ultrapure water several times and dried for 1 h in 80°C. In the second step, the Sn-activated EMD was added into 100 ml H₂O with 0.157 g of dissolved silver nitrate. The mixture was stirred for 2 h and then filtered, washed carefully with ultrapure water and dried overnight in 80°C.

A gravimetric composition of (Ag/MnO₂):CB:EVA = 100:15:10 was mixed in ca. 100°C xylene to dissolve EVA and then grinded in a mortar. Once viscous, the slurry was pasted



on 500 μm thick nickel foam (2 cm x 4 cm) and then dried at room temperature for 24 h. The dried electrodes were pressed at 5 MPa/cm² and a half-cell was assembled with nickel foam as counter electrode and Hg/HgO in 6 M KOH as reference electrode. A 120 μm porous PP sheet and 6 M KOH were used as separator and electrolyte, respectively.

To analyze whether the silver has a positive effect, electrodes with as-received EMD – without the deposition of silver – were manufactured in the same way and used as reference.

IV. RESULTS AND DISCUSSION

The potential of the Ag/EMD to work as a secondary battery in the FCB system was analyzed in three steps and compared with and EMD electrode. First, the electrode was discharged according to reaction (3) under atmospheric condition. Then, the electrodes were regenerated by oxygen – eq. (4) – which was directly supplied to the electrodes via bubbles at an elevated pressure of 1 MPa and room temperature for 5 h. Finally, the ORR rate was assessed by continuing to supply oxygen at 50 ml/min while applying different currents. The currents were between 0.01 C and 0.1 C, whereby the C-rate is the inverse of the time in hours it takes to either fully charge or discharge the electrode. In case of MnO₂, the 1 C rate is equal to 308 mA/g.

Fig. 1 shows the discharge curve of both EMD and Ag/EMD. EMD shows both a higher potential and capacity compared to Ag/EMD. Reasons for this result may be due to the Sn modified surface area which might have a negative impact on the discharge capability of EMD. A small loss in capacity is also likely to be due to the presence of Ag, whose mass was not excluded when calculating the amount of active material.

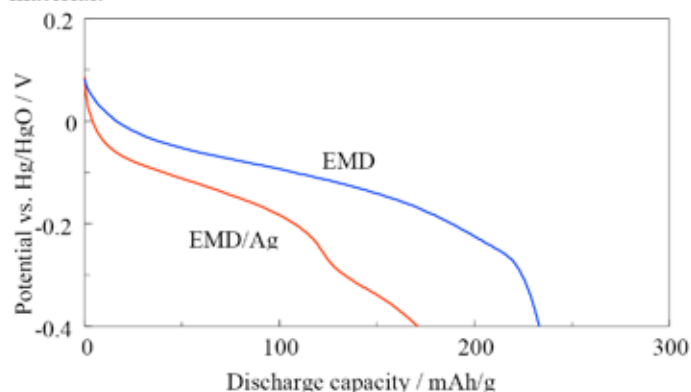


Fig. 1. Discharge curves of EMD and Ag/EMD in 6 M KOH at 0.1 C

The results of the ORR tests are shown in Fig. 2. Due to the fact that MnO₂ has an intrinsic storage capacity, all currents were applied for 1 h to see whether the potential levelled off or continued to decrease. This way, it could be assessed whether ORR was sufficiently quick or the current was drawn from discharging MnO₂.

The Ag/EMD compound showed a considerably higher potential compared to EMD. Both electrodes showed a stable potential after 1 h at 0.01 C (i.e. 3.08 mAh/g) and 0.02 C. Thereafter, a continuous decrease in voltage was observed. In case of EMD, the cut-off potential of -0.4 V vs. Hg/HgO was reached at 0.2 C and in case of Ag/EMD, the cut-off potential was hit at 0.5 C (not shown here).

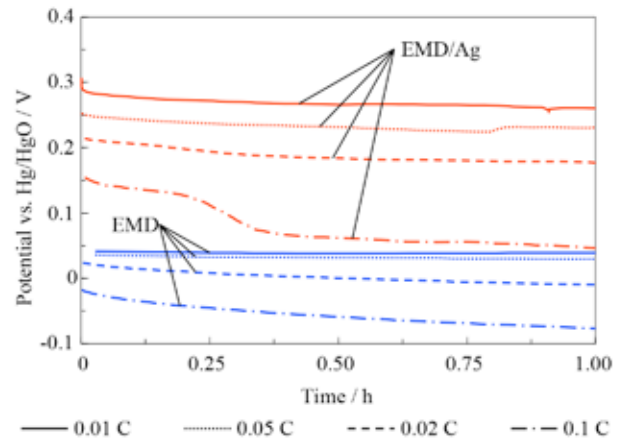


Fig. 2. Potential evolution of EMD and Ag/EMD at simultaneous oxygen supply and current application

V. CONCLUSION

A facile method to synthesize an Ag/EMD compound for the application in FCB system was introduced. The capabilities as a positive electrode in an FCB were assessed by electrochemical discharge and ORR in a pressurized vessel. As-received EMD was found to show better discharge performance (i.e., working as positive electrode in battery mode), but the Ag/EMD compound was superior for ORR (i.e., working as positive electrode in fuel cell mode).

REFERENCES

- [1] Choi, B., Lee, S., Fushimi, C., Tsutsumi, A., Development of NiMH-based Fuel Cell/Battery (FCB) system: Characterization of Ni(OH)₂/MnO₂ positive electrode for FCB, *Journal of Power Sources*, Volume 194, 2009, Pages 1150-1155
 - [2] Llompart, S., Ouboumour, H., Yu, L., Oxygen-Regeneration of Discharged Manganese Dioxide Electrode, *Journal of The Electrochemical Society*, Volume 138, Issue 3, 1991, Pages 665-669
 - [3] Cheng, F., Su, Y., Liang, J., Tao, Z., Chen, J., MnO₂-Based Nanostructures as Catalysts for Electrochemical Oxygen Reduction in Alkaline Media, *Chemistry of Materials*, Volume 22, Issue 3, 2010, Pages 898-905
- Choi, B., Lee, S., Fushimi, C., Tsutsumi, A., Power generation/energy storage by a fuel cell/battery system: Regeneration of the MnO₂ positive electrode with gaseous oxygen, *Electrochimica Acta*, Volume 55, 2010, Pages 8771-8778



OPERATION OF MICRO-TUBULAR SOLID OXIDE FUEL CELLS WITH A POROUS ZIRCONIA SUPPORT ON METHANE FUEL

D. Panthi, B. Choi, and A. Tsutsumi

Institute of Industrial Science, The University of Tokyo (Japan)

Abstract - We have proposed a novel micro-tubular SOFC design with an inert support and an integrated current collector for the anode to improve current collection efficiency and reduction-oxidation stability of the cell. The proposed design also shows potential for running on direct hydrocarbon fuels without carbon deposition because the inert support results in decreased fuel content and increased product content toward the Ni-based anode. In the present work, multi-step dip coating and cosintering methods were employed to fabricate micro-tubular SOFCs based on the proposed design. Ytria-stabilized zirconia (YSZ), Ni, Ni-scandia-stabilized zirconia (ScSZ), ScSZ, strontium-doped lanthanum manganite (LSM)-ScSZ, and LSM were used as the inert support, anode current collector, anode, electrolyte, cathode, and cathode current collector, respectively. The stability tests at 750 °C under moderate current densities indicate that the present micro-tubular SOFC can be operated satisfactorily with the direct hydrocarbon fuels.

Index Terms - Inert support, methane, micro-tubular SOFC, stability.

I. INTRODUCTION

Micro-tubular solid oxide fuel cells (SOFCs) offer a number of desirable characteristics as high-temperature fuel cells such as easy sealing, high volumetric power density, and good thermo-cycling behavior. Additionally, because of their high thermal shock resistance and low thermal mass, micro-tubular SOFCs are well-suited for rapid startup and shutdown operations. In our previous studies, we proposed a novel micro-tubular SOFC design with an inert support and an integrated current collecting layer for the inner electrode to improve current collection efficiency and reduction-oxidation (redox) stability of the cell [1-3]. The proposed micro-tubular design also shows potential for running on direct hydrocarbon fuels. Although the conventional Ni-based SOFC anodes have excellent catalytic properties for reforming of the hydrocarbon fuels, carbon deposition on the Ni surface due to pyrolysis

and/or Boudouard reactions is a serious problem leading to rapid cell degradation [4]. However, the use of an inert barrier layer to the Ni-based anode has been found to be effective for achieving stable SOFC operations with the hydrocarbon fuels such as methane and biogas [5, 6]. The barrier layer results in decreased fuel content and increased product content toward the anode, thus reducing the coking problem. Since the inert support itself serves as a diffusion barrier, the proposed micro-tubular SOFC design is expected to combine its other merits with stable performance with the hydrocarbon fuels.

In the present work, multi-step dip coating and cosintering methods were employed to fabricate micro-tubular SOFCs based on the proposed design. Ytria-stabilized zirconia (YSZ), Ni, Ni-scandia-stabilized zirconia (ScSZ), ScSZ, strontium-doped lanthanum manganite (LSM)-ScSZ, and LSM were used as the inert support, anode current collector, anode, electrolyte, cathode, and cathode current collector, respectively, as shown schematically in Fig. 1. The electrochemical performance and stability of the fabricated cells were evaluated by supplying methane saturated with water as the fuel and ambient air as the oxidant.

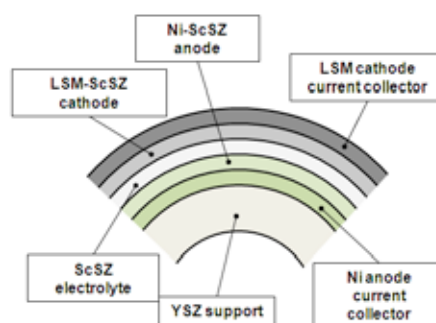


Fig. 1. Schematic of the novel micro-tubular SOFC with a porous YSZ support

II. EXPERIMENTAL

The micro-tubular SOFC samples were prepared by multi-step dip coating and cosintering methods [7, 8]. The details of the materials used for the different cell components are given in Table I. To impart desired porosity to the YSZ support, 10 wt% micro-crystalline cellulose (Avicel, Merck, Germany) and 10 wt% polymethyl methacrylate (PMMA; 2.9 μm , Soken, Japan) were used as pore formers. Similarly, 10 wt% micro-crystalline cellulose (20 μm , Sigma Aldrich, USA) was used as a pore former for the NiO anode current collector.

The electrochemical measurements were carried out with a multistat (1480, Solartron Analytical, UK). Methane humidified with 3 vol% water (20 mL min^{-1}) and ambient air (20,000 mL min^{-1}) were used as the fuel and oxidant, respectively.

TABLE I
MATERIALS USED FOR THE FABRICATION OF MICRO-TUBULAR SOFC SAMPLES

Cell component	Material	Supplier
Support	YSZ (TZ-8Y)	Tosoh, Japan
Anode current collector	NiO (NiO-AS)	Kceracell, South Korea
Anode	60 wt% NiO (NiO-AFL)	Kceracell
	40 wt% ScSZ (10Sc1CeSZ)	DKK, Japan
Electrolyte	ScSZ (10Sc1CeSZ)	DKK
Cathode	50 wt% LSM (LSM-80F)	DKK
	50 wt% ScSZ (10Sc1CeSZ)	DKK
Cathode current collector	LSM (LSM-80F)	DKK

III. RESULTS AND DISCUSSION

The current–voltage characteristic curves for a single cell operated on methane fuel in a temperature range 650–750 $^{\circ}\text{C}$ are shown in Fig. 2. The open-circuit voltages (OCVs) of the cell were 1.087, 1.074, and 1.063 V at 750, 700, and 650 $^{\circ}\text{C}$, respectively. The increasing trend of the OCV with respect to temperature is consistent with previously reported results for direct-methane SOFCs [9]. The cell delivered maximum power densities of 524, 346, and 192 mW cm^{-2} at 750, 700, and 650 $^{\circ}\text{C}$, respectively.

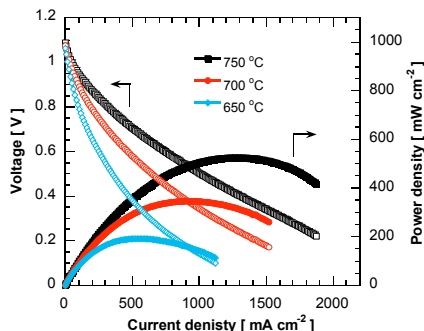


Fig. 2. Plots of cell voltage and power density versus current density at different temperatures

Figure 3 shows results obtained from the stability testing of the cell in methane at 750 $^{\circ}\text{C}$. As can be seen from Fig. 3(a), the cell operated under a load current of 500 mA cm^{-2} for the first

40 h had a stable performance. The load current was then decreased to 400 and 300 mA cm^{-2} in steps. The cell still exhibited a stable performance, as shown in Fig. 3(b). The stable cell operation suggests that the inert support plays an effective role in preventing carbon deposition on the Ni-ScSZ anode by increasing the concentration ratio of product gases (CO_2 and H_2O) to methane toward the reactive region. Additionally, the competitive power generation output of the cell indicates that there was a very small penalty on the cell performance due to the gas-transport losses. This was possible probably because of a high porosity (>40%) of the inert support.

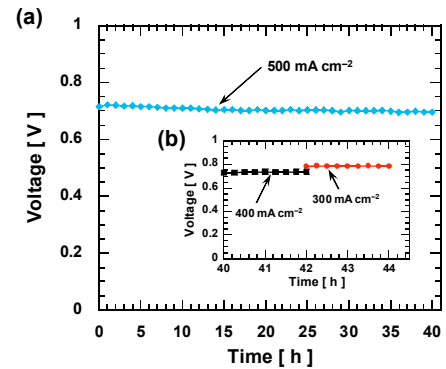


Fig. 3. Stability testing at 750 $^{\circ}\text{C}$ under different load currents: (a) 500 mA cm^{-2} ; (b) 400 and 300 mA cm^{-2}

IV. CONCLUSIONS

In this study, we fabricated a novel micro-tubular SOFC with porous YSZ as the inert support. The cell contained Ni, Ni-ScSZ, ScSZ, LSM-ScSZ, and LSM as the anode current collector, anode, electrolyte, cathode, and cathode current collector, respectively. The cell had a good electrochemical performance and operated stably with methane under moderate current densities. Our results indicate that the inert support-based micro-tubular SOFC presented here is suitable for operation with direct hydrocarbon fuels.

REFERENCES

- [1] Panthi, D., Tsutsumi, A., ECS Trans., Vol. 57, 2013, 789–798.
- [2] Panthi, D., Tsutsumi, A., Sci. Rep., Vol. 4, 2014, 5754.
- [3] Panthi, D., Choi, B., Tsutsumi, A., Int. J. Hydrogen Energy, in press (DOI:10.1016/j.ijhydene.2015.06.129).
- [4] Kendall, K., Finnerty, C.M., Saunders, G., Chung, J.T., J. Power Sources, Vol. 106, 2002, 323–327.
- [5] Lin, Y., Zhan, Z., Barnett, S.A., J. Power Sources, Vol. 158, 2006, 1313–1316.
- [6] Rosensteel, W.A., Babiniec, S.M., Storzjohann, D.D., Persky, J., Sullivan, N.P., J. Power Sources, Vol. 205, 2012, 108–113.
- [7] Panthi, D., Tsutsumi, A., J. Solid State Electrochem., Vol. 18, 2014, 1899–1905.
- [8] Panthi, D., Choi, B., Tsutsumi, A., ECS Trans., Vol. 68, 2015, 2259–2265.
- [9] Liu, J., Barnett, S.A., Solid State Ionics, Vol. 158, 2003, 11–16.



ADVANCEMENT OF GROUP 4 AND 5 METAL OXIDE BASED CATHODE FOR PEFCs

K. Ota*, K. Matsuzawa*, S. Mitsushima*,** and I. Ishihara**

Yokohama National University

*Green Hydrogen Research Center, **the Institute of Advanced Sciences
79-5 Tokiwadai, Hodogaya-ku, Yokohama, 240-8501 (Japan)

Abstract - Ti, Nb, Ta and Zr compounds were heat-treated at 800-1200°C under different flowing rate of the H₂/N₂ gas mixtures that containing small amount of oxygen to obtain oxide based specimens those contain carbon and nitrogen. These materials were evaluated as the cathode for PEFCs. An appropriate oxidation of materials is essential to have a definite catalytic activity for the ORR. The high temperature ammonia treatment after the partial oxidation was also effective to get high activity. The highest onset potential we got was 1.2 V vs. RHE for the mixture of Nb oxide and Ti oxide supported by the Ti oxide. The value is higher than that of Pt. In a single cell test using Zr oxide based cathode we obtained over 1A/cm² at 80 °C with hydrogen and oxygen. A significant cost reduction of a cathode might be possible using these oxide based materials.

Index Terms - cathode, oxygen reduction reaction, polymer electrolyte fuel cell, transition metal oxide

I. INTRODUCTION

Polymer electrolyte fuel cells are expected for the residential and transportable applications, due to their high power density and low operating temperature. The ENFARMS (home co-generation system using 1 kW PEFC system) are operating more than 120,000 units in Japan. Fuel cell vehicles are commercially available from December 2014 in Japan.

However, a significant cost reduction is needed especially for fuel cell vehicles. And the estimated amount of Pt reserve is too small to supply for the huge number of fuel cell systems. In order to commercialize the fuel cell systems widely, the development of a non-precious metal cathode is strongly required.

We think that new non-precious metal cathodes should have both high stability and high catalytic activity for the ORR. In particular, we believe that high stability in cathode condition is essentially required for the cathode catalyst. Some transition metal oxides could be used for the cathode of PEFC.

However, most of the transition metal oxides are not stable in the acidic and oxidative atmosphere.

We started this study by searching stable materials in acid and in oxygen. Group 4 and 5 metal oxides, which are well known as valve metals, are stable even in acidic and oxidative atmosphere. However, these oxides are generally insulator. In order to get some electrical conductivity, these oxides should be modified by the formation of the oxygen vacancy and/or the substitution of foreign atoms.

We have reported that partially oxidized group 4 and 5 metal carbonitrides are stable in an acid solution and have definite catalytic activity for the oxygen reduction reaction (ORR) [1-4]. We have tried to apply group 4 and 5 metal oxide-based compounds to the cathode catalyst. In this paper we will report our recent results.

II. EXPERIMENTAL

Powders of metal (Metal: Ta, Zr, Nb, Ti) compounds (carbonitride or metal complexes that contain nitrogen) were heat-treated at 800-1200°C under different flowing rate of the H₂/N₂ gas mixtures that containing small amount of oxygen to obtain specimens with different oxidation state. After heat treatment, the compounds changed to oxides that contained small amount of carbon and nitrogen. Heat treated powder was mixed with alcohol, carbon and Nafion. The mixture was dipped on a glassy carbon rod (5 mm diameter) and the working electrode was made. All electrochemical measurements were examined in 0.1 M H₂SO₄ at 30°C and 80°C under atmospheric pressure using a conventional 3-electrode cell. The RHE was used for the reference in the same solution. Slow scan voltammetry (scan rate: 5 mVs⁻¹) was performed under O₂ and N₂ atmosphere to obtain the current for the oxygen reduction reaction (ORR). Potential cycling tests were conducted by the rectangular wave between 1.0 V



and 1.5 V and by the triangular wave between 0.6 V and 1.0 V in order to check the durability of our materials. For the fuel cell test we used a 5 cm x 5 cm single cell with hydrogen and oxygen at 80°C.

III. RESULTS AND DISCUSSION

An appropriate oxidation is essential to have a definite catalytic activity for the ORR. The high temperature ammonia treatment after the partial oxidation was also effective to get high activity.

Figure 1 shows the current-potential relation on the mixed oxides supported by Ti_4O_7 . The onset potentials of partially oxidized Ti and Nb compound with the electron conductive oxide support have reached over 1.2 V vs RHE that is more than that of commercial Pt-C. The active point of our materials might have a better activity compared to Pt.

Potential cycling test was conducted between 1.0 V and 1.5 V using triangular wave, and between 0.6 V and 1.0 V using rectangular wave, respectively. We have not detected the decay of activity in both cases even at 80°C, although the current was small.

Figure 2 shows the I-E curve of a single cell test using the modified Zr oxide cathode and Pt anode. We got more than 1 A/cm² by this single cell test. These materials have great potential for PEFC cathode, especially for the cost reduction that is most important among the present PEFC technologies.

IV. CONCLUSION

Modified group 4 and 5 metal oxides have a great potential for the better activity for ORR than Pt as well as the better stability than Pt. Significant cost reduction might be possible using these materials. These materials might have great potential for a PEFC cathode.

ACKNOWLEDGEMENT

The authors wish to thank to the New Energy and Industrial Technology Development Organization (NEDO) for their financial support. The authors also thank to the effort of the members of the oxide cathode group of the NEDO project.

REFERENCES

- [1] A. Ishihara, Y. Shibata, S. Mitsushima, K. Ota, Partially Oxidized Tantalum Carbonitrides as a New Nonplatinum Cathode for PEFC, *Journal of Electrochemical Society*, volume 155, 2008, pages B400-B406.
- [2] A. Ishihara, M. Tamura, Y. Ohgi, M. Matsumoto, K. Matsuzawa, S. Mitsushima, H. Imai, K. Ota, Emergence of Oxygen Reduction Activity in Partially Oxidized Tantalum Carbonitrides: Roles of Deposited Carbon for Oxygen-Reduction-Reaction-Site Creation and Surface Electron Conduction, *Journal of Physical Chemistry, ser. C*, volume 117, 2013, pages 18837-18844.

- [3] A. Ishihara, M. Chisaka, Y. Ohgi, K. Matsuzawa, S. Mitsushima, K. Ota, Synthesis of nano-TaOx oxygen reduction reaction catalysts on multi-walled carbon nanotubes connected via a decomposition of oxy-tantalum phthalocyanine, *Physical Chemistry Chemical Physics*, volume 17, 2015, pages 7643-7647.
- [4] N Uehara, A. Ishihara, M Matsumoto, H. Imai, Y. Kohno, K. Matsuzawa, S. Mitsushima, K. Ota, Tantalum oxide-based electrocatalysts made from oxy-tantalum phthalocyanines as non-platinum cathode for polymer electrolyte fuel cell, *Electrochimica Acta*, doi:10.1016/j.electacta.2015.03.125.

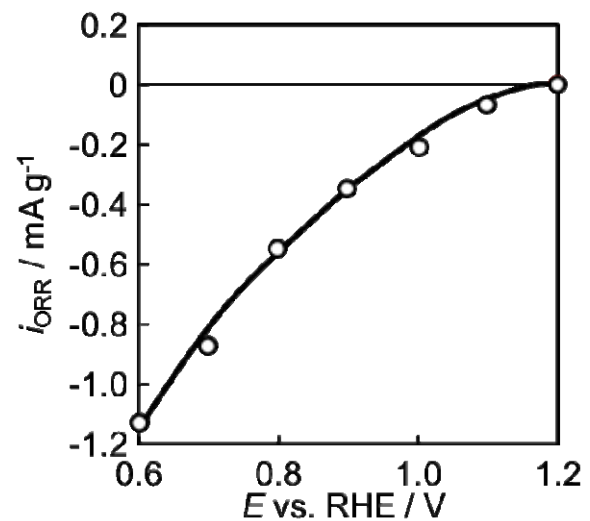


Fig. 1. Initial activities of $Ti_xNb_yO_z$ cathode supported by Ti_4O_7 in 0.1 M H_2SO_4 at 80 °C.

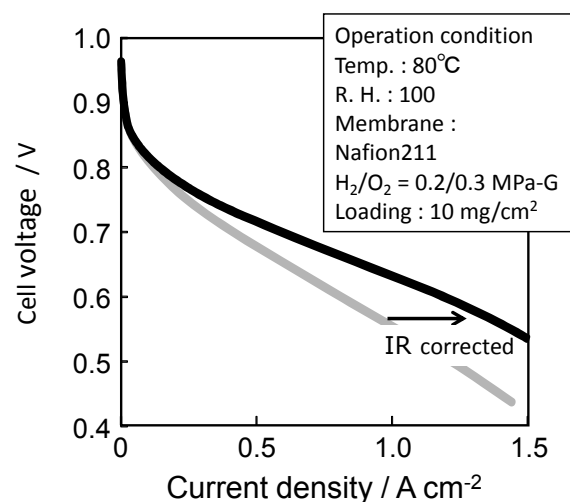


Fig. 2. Voltage- Current relation of fuel cell using modified Zr oxide cathode.



PERFORMANCE DEGRADATION STUDY ON POLYBENZIMIDAZOLE FUEL CELLS SUBJECTED TO DIFFERENT AGEING TESTS

R. Taccani⁽¹⁾, T. Chinese⁽¹⁾⁽²⁾, J.B. Obi⁽¹⁾, M. Boaro⁽³⁾

⁽¹⁾ University of Trieste, Via A. Valerio 10, 34127 Trieste, Italy

⁽²⁾ Cenergy Srl, Via della zonta 2, 34100 Trieste, Italy

⁽³⁾ University of Udine, Via del cotonificio 8, 33100 Udine, Italy

Abstract - The study presented in this paper aims to evaluate the performance degradation of Polybenzimidazole (PBI) based High Temperature PEM (HTPEM) fuel cells subjected to triangular load cycling ageing test, according to a methodology already used by the authors. A HTPEM Membrane Electrode Assembly (MEA) has been subjected to 125,000 triangular sweep cycle between Open Circuit Voltage (OCV) and 0.5 A/cm² with 2 seconds of permanence at OCV at each cycle. In order to assess the cell performance, polarization curves, Electro Impedance Spectroscopy (EIS) and Cyclic Voltammetry (CV) have been recorded during the ageing tests.

Index Terms – HTPEM, Polybenzimidazole, Degradation, Fuel Cells.

I. INTRODUCTION

Polybenzimidazole (PBI) based High Temperature Polymer Electrolyte Membrane (HTPEM) fuel cells represent a possible option to Nafion based PEM (LTPEM), especially for micro Combined Heat and Power (CHP) applications: due to their high CO tolerance HTPEMs allow fuels other than pure hydrogen to be used by means of a simplified fuel processing unit. Nevertheless, costs, performance and degradation issues still have to be overcome to achieve commercialization. Regarding performance degradation, PBI membranes demonstrated a good lifetime under steady state operation, reaching up to 20,000 hours of operational life with low voltage drop. However, higher performance degradation rates have been measured when HTPEM fuel cells operate under variable load conditions [1, 2, 3, 4]. The presented research aims to study the performance degradation of HTPEM fuel cells subjected to a triangular load cycle ageing test with 2s of permanence at OCV at each cycle.

II. METHODOLOGY

The test has been performed on a 45.6 cm² BASF Celtec-P HTPEM Membrane Electrode Assemblies (MEAs) operated with hydrogen and air. Before starting the degradation test, the MEA has been activated for 100 hours under reference conditions as suggested by the producer (T= 160°C, i=0.22A cm²). The MEA has then been subjected to 125,000 triangular sweep cycles between Open Circuit Voltage (OCV) and 0.5 A/cm². During load cycling, MEA temperature has been kept constant at 160 °C.

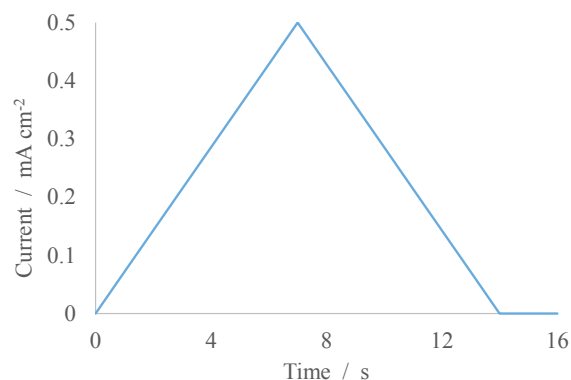


Figure 1. Load cycle profile

Figure 1 describes more in detail the current profile used during aging test. In order to measure cell performance degradation, fuel cell potential variation with time, polarization curves, Electro Impedance Spectroscopy (EIS) and Cyclic Voltammetry (CV) have been recorded.

III. EXPERIMENTAL RESULTS

A. Polarization curves

2 shows the cell voltage for different current densities after different number of ageing cycles.

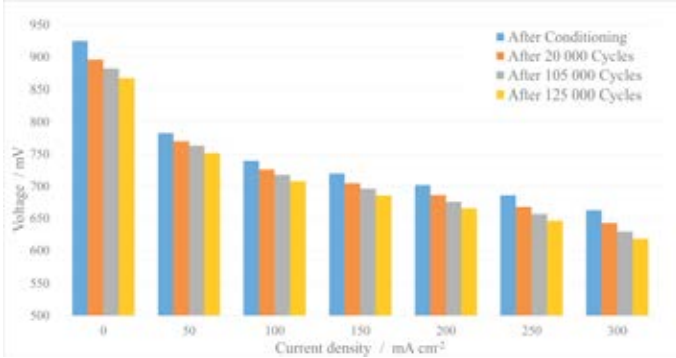


Figure 2. Cell potential at different current densities before and after ageing test.

All polarization curves have been measured at constant hydrogen flow of 0.5 l/min at 1 bar and constant air flow of 1.8 l/min at 1.05 bar.

The performance loss, in terms of potential reduction, between the beginning and the end of the 125,000 load cycling procedure, is less than 6% for all current densities which is in good agreement with the results obtained by authors in previous work [3] with the same membrane and load cycle profile. Degradation after 100 000 cycles at 220 mA/cm² has been found to be 26 mV while in the previous work, for the same current level, it has been found a degradation of 24 mV.

B. EIS

Figure 3A-B show the Electro Impedance Spectroscopy (EIS) of the MEA respectively at 220 mA/cm² and 330 mA/cm² before and after ageing test.

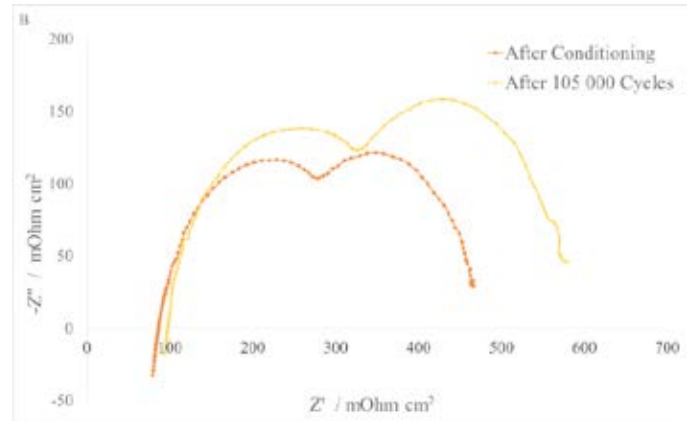
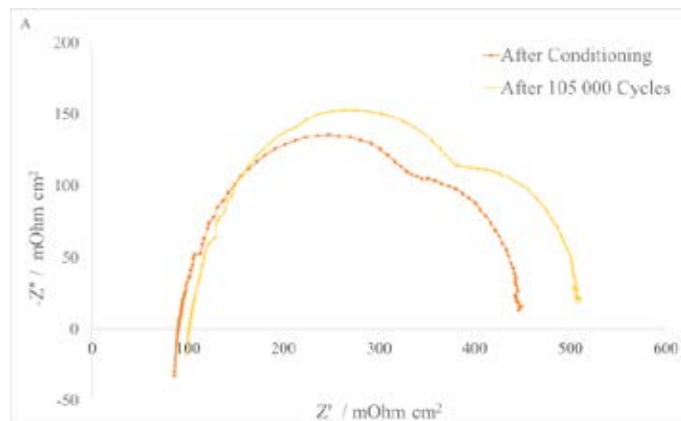


Figure 3. (A) EIS before and after ageing test at 220 mA/cm². (B) EIS before and after ageing test at 330 mA/cm².

Results in terms of dimension of the EIS spectrum and its evolution with ageing are in accordance with similar studies [2] [5], on HTPEM FC. An increase in the charge transfer resistance is observed, that can be related to the loss of catalyst active area and acid leaching.

IV. CONCLUSION

The considered load profile, after 125,000 cycle, causes a performance loss, in terms of cell potential, of less than 3% at 200 mA/cm². This value confirms the results obtained by the authors in a previous test. The effect of other load profiles will be assessed in the future, aiming at identifying stack control strategies that can be detrimental to cell performance.

REFERENCES

1. Jeon, Y., Na, H., Hwang, H., Park, J., Hwang, H., & Shul, Y. (2015). Accelerated life-time test protocols for polymer electrolyte membrane fuel cells operated at high temperature. *International Journal of Hydrogen Energy*, 40(7), 3057–3067. doi:10.1016/j.ijhydene.2015.01.010
2. Andreasen, S. J., Vang, J. R., & Kær, S. K. (2011). High temperature PEM fuel cell performance characterisation with CO and CO₂ using electrochemical impedance spectroscopy. *International Journal of Hydrogen Energy*, 36(16), 9815–9830. doi:10.1016/j.ijhydene.2011.04.076
3. Valle, F., Zuliani, N., Marmioli, B., Amenitsch, H., & Taccani, R. (2014). SAXS Analysis of Catalyst Degradation in High Temperature PEM Fuel Cells Subjected to Accelerated Ageing Tests. *Fuel Cells*, 14(6), 938–944. doi:10.1002/fuce.201300221
4. Schmidt T. J., and Baurmeister J., 2008, "Properties of high-temperature PEFC Celtec®-P 1000 MEAs in start/stop operation mode," *Journal of Power Sources*, 176(2), pp. 428–434.
5. Galbiati, S., Baricci, A., Casalegno, A., & Marchesi, R. (2013). Degradation in phosphoric acid doped polymer fuel cells: A 6000 h parametric investigation. *International Journal of Hydrogen Energy*, 38(15), 6469–6480. doi:10.1016/j.ijhydene.2013.03.012



SOFC FED WITH EUROPEAN STANDARD ROAD DIESEL BY AN ADIABATIC PRE-REFORMING FUEL PROCESSOR FOR 1000 HOURS

Nils Kleinohl*, Pedro Nehter**, Ansgar Bauschulte*, Jörg vom Schloß*, and John Bøgild Hansen***

* OWI OEL-WAERME-INSTITUT GmbH, Kaiserstrasse 100, D-52134 Herzogenrath (Germany)

** ThyssenKrupp Marine Systems AG / Operating Unit HDW, Werftstr. 112/114, D-24143 Kiel, (Germany)

*** HALDOR TOPSØE A/S, Nymøllevej 55, DK-2800 Lyngby, (Denmark)

Abstract – Power generation on board of sea-going ships need efficiency improvement in the near future. In the project SchIBZ a fuel cell system with a fuel processor for diesel fuel based on the process of adiabatic pre-reforming will be developed. A lab scale fuel processor test rig and a test rig for two SOFC modules are built for demonstration of coupled operation. As fuel processing catalyst a commercial catalyst from Haldor Topsøe A/S is used. This one showed promising results for standard European road diesel which could be processed for more than 3000 hours by the authors.

Coupled operation of both test rigs is successfully demonstrated for 1000 hours. The experiment is run with constant electric load for both SOFC modules and constant mass flow. For the complete experiment runtime no significant degradation of fuel processing catalyst and both SOFC modules are observed.

Index Terms - Diesel, Experimental, Fuel processing, SOFC

I. INTRODUCTION

Power generation on board of sea-going ships is actually provided by generator systems powered by internal combustion engines which use either heavy bunker or diesel oil as fuel. Regulations for sulfur and particulate matter emissions changed from January 1st, 2015 so that new concepts for lowering emissions of power generation systems on sea-going vessels are needed [1].

One approach for this issue is the introduction of fuel cell systems as auxiliary power units (APU) on board of ships. Overall electric efficiency can be increased from 40 %, for generator systems with internal combustion engine, to more than 50% for fuel cell systems as

mentioned by Nehter et al. [2] and the exhaust gas can be handled with fewer additional cleaning processes.

Today hydrogen storage is limited by tank technologies so that a fuel cell system cannot be operated for long times without access to a pure hydrogen supply. Fuel processing of diesel fuel with the process of adiabatic pre-reforming is one opportunity for this task. It is a steam reforming derivate with lower catalyst bed temperatures between 723 K and 873 K compared to 1023 K when using hydrocarbon feedstock. One advantage is that the exhaust gas can be heated up to 973 K without carbon depositions which was investigated by Krummrich et al. [3]. Compared to steam reforming and partial oxidation it has a relatively simple reactor design for the fuel processor because no additional heat is required for the process.

As type of fuel cell a solid oxide fuel cell (SOFC) is a choice for simple system design. Beside hydrogen a SOFC can use methane and carbon monoxide as well because of the operating temperatures above 973 K. This system concept of a SOFC fed by a adiabatic steam reforming fuel processor was investigated by Powell et al. [4] for natural gas and showed promising results for efficiency. With this type of fuel cell a simple system design can be built.

Scope of this work is a coupled operation of a fuel processor fed with standard European road diesel which feeds two SOFC modules for 1000 hours. Mainly degradation of cell voltages is considered because of their high sensitivity to catalyst poisoning.



II. EXPERIMENTAL SETUP

For experimental investigation two test-rigs are built, one for the fuel processor with all peripheral components and another one for two commercial available SOFC modules manufactured by sunfire. Each test-rig can be conditioned by itself so that optimal test parameters can be adjusted for SOFC modules and fuel processor before coupling of the anode gas supply. The schematic for coupling of both test-rigs is displayed in Figure 1.

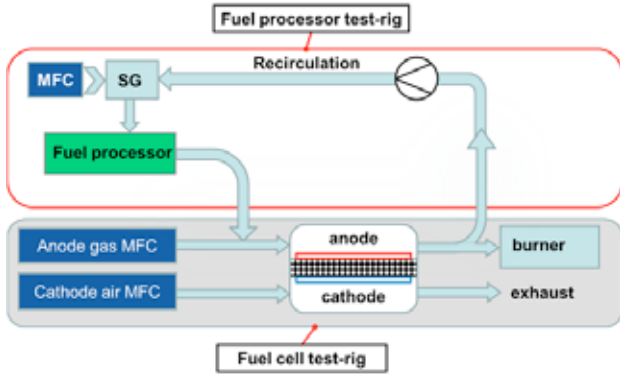


Figure 1: Schematic of coupled test-rigs

Cold anode off gas recirculation is implemented into the fuel processor test-rig for demonstration of this concept.

As catalyst a commercial available pre-reforming catalyst from Topsøe A/S is used for the fuel processor. All experiments are performed with standard European road diesel as fuel with FAME content of 3.6 % (v/v) and sulfur content of 6.4 mg/kg. Only water is added into the steam generator (SG) for steam reforming reactions. All MFCs in both test-rigs are used for system conditioning.

In each SOFC module there are two towers which are controlled independently by electronic loads for optimal operation.

III. RESULTS

In total seven experiments with identical parameters are combined for a runtime of 1000 hours. Interruptions have been caused by several maintenance interruptions for replacement of peripheral components like defect electric heaters, blown fuses and faulty fuel dosing pump. Focus in this work is on degradation of SOFC modules because this is the main issue for introduction of fuel cell systems into market.

For all experiments constant current of 14 Ampere were drawn from each SOFC module. Overall power output of both SOFC modules is 3869 ± 26 Watt with a fuel utilization of 50 % (LHV).

From the start of the experiments up till 385 hours runtime 8 kW (LHV) diesel fuel is introduced into the fuel processor and a voltage degradation (Γ) of -0.66% is estimated when using Eq. 1

$$\Gamma = \left(1 - \left(\frac{U_{11}^{\text{End}}}{U_{11}^{\text{Start}}} + \frac{U_{12}^{\text{End}}}{U_{12}^{\text{Start}}} + \frac{U_{21}^{\text{End}}}{U_{21}^{\text{Start}}} + \frac{U_{22}^{\text{End}}}{U_{22}^{\text{Start}}} \right) \frac{1}{4} \right) 100\% \quad (1)$$

At 385 hours until 1000 hours the fuel input is increased to 10 kW (LHV) diesel fuel and the estimated voltage degradation is -0.49% during this period of 615 hours.

In Fig. 2 the development of current, power output and voltages is presented as a function of runtime. No significant voltage degradation is visible for the complete experiment runtime. This indicates a suitable feedstock is provided by the applied fuel processor.

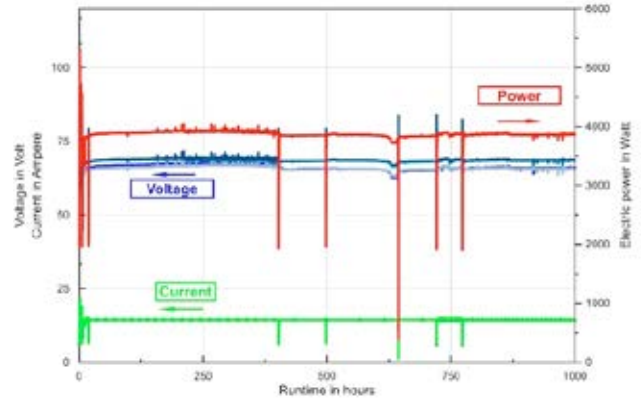


Figure 2: SOFC tower voltages, current and electric power output

IV. CONCLUSION

Coupled operation of the fuel processor and SOFC modules is demonstrated for 1000 hours with standard European road diesel. No significant degradation is observed for fuel processing catalyst and SOFC power output. Even after maintenance shutdowns cell voltages show constant levels for both SOFC modules. These results proof this design for an APU fuel cell system. Future work will focus on demonstration of feasibility of this concept for on board usage on sea-going ships.

ACKNOWLEDGMENT

This research and development project “Nationales Innovationsprogramm Wasserstoff- und Brennstoffzellentechnologie (NIP): SchIBZ – Schiffs Integration Brennstoffzelle” is funded by the German Federal Ministry of Transport, Building and Urban Development (BMVI) (Bundesministerium für Verkehr und digitale Infrastruktur) under contract 03BI206A.

REFERENCES

- [1] MARPOL ANNEX VI, <http://www.imo.org/en/OurWork/environment/pollutionprevention/airpollution/pages/the-protocol-of-1997-%28marpol-annex-vi%29.aspx>, viewed 14.April 2015
- [2] P. Nehter, J. Bøgild Hansen, and P. Koch Larsen, “A techno-economic comparison of fuel processors utilizing diesel for solid oxide fuel cell auxiliary power units”, *J. Power Sources*, Vol. 196, 2011, pp. 7347-7354.
- [3] S. Krummrich, B. Tuinstra, G. Kraaij, J. Roes, and H. Olgun, “Diesel fuel processing for fuel cells—DESIRE”, *J. Power Sources*, Vol. 160, 2006, pp. 500-504.
- [4] M. Powell, K. Meinhardt, V. Sprenkle, L. Chick, and G. McVay, “Demonstration of a highly efficient solid oxide fuel cell power system using adiabatic steam reforming and anode gas recirculation”, *J. Power Sources*, Vol. 205, 2012, pp. 377-384.



PERFORMANCE ASSESSMENT OF MICROBIAL FUEL CELLS FED BY SOLID ORGANIC WASTE

Nicole Jannelli¹, Giacomo Falcucci², Mariagiovanna Minutillo² and Elio Jannelli²

¹A.T.E.N.A. scarl, Centro Direzionale - Isola C4, 80143 Naples (Italy)

² University of Naples "Parthenope", Centro Direzionale - Isola C4, 80143 Naples (Italy)

ABSTRACT

In this paper, we present the experimental results obtained on the direct production of electrical power through the anaerobic digestion of the organic fraction of municipal solid waste (FORSU).

The performance of ad-hoc built reactors have been monitored for a 28-day period and the results in terms of performance reproducibility and power production have been assessed for two groups of microbial fuel cells (MFC's), characterized by the adoption of fresh and salt water, respectively. The addition of salt has been done in order to stress negative conditions for the bacteria growing in the MFC.

I. INTRODUCTION

Waste management is known to be a major problem, athwart plaguing the different societies, both in the western and eastern part of the world. The adoption of Microbial Fuel Cells (MFC's) is considered as a potential solution for this problem, [1, 2], turning the cost of waste disposal into the opportunity of direct electrical power production, without the production of pollutants, typical of hydrocarbon combustions.

II. EXPERIMENTAL SETUP

In our Laboratory, we have realized mini-MFC reactors by using standard 50 ml polypropylene Falcon test tubes, supplied by BD Corning Inc. (Tewksbury, USA), sterile and suitable for biological cultures. At the ends of each each Falcon, two smaller test tubes (25 ml internal volume) provided by the same manufacturer are connected, in order to

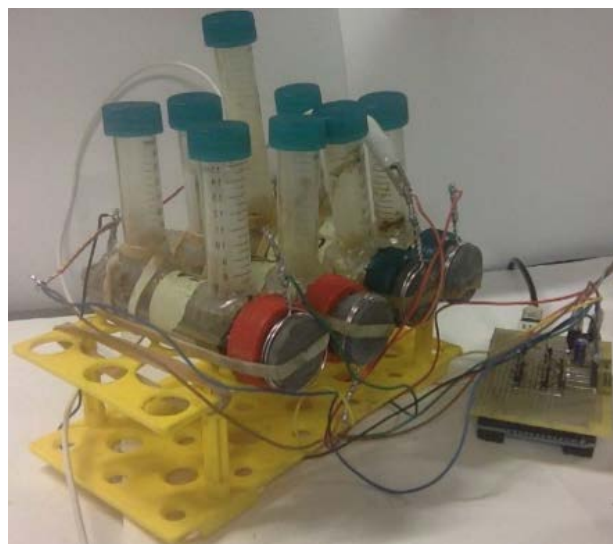


Figure 1: Layout of our experimental setup.

allow the evaluation of pH gradient along the cell longitudinal axis, see Fig. 1. The anode is realized by means of carbon fiber arranged in brush-shape, while the cathode is realized by means of an innovative material realized in our Laboratory, which is patent-pending, at the moment. The feeding substrate of our MFC's was prepared according to the composition of solid part and water reported in Tab. 1.

Twelve single-cell microbial bio-reactors have been prepared; the liquid-to-solid ratio of the substrate is reported in Tab. 2. The cells have been grouped in two classes: the first six, in which fresh water has been used, the other six in which NaCl was added in a concentration of 35 mg/l, in order to reproduce the salinity of sea water. The perfor-

Apple	100 g
Pumpkin	100 g
Chickpeas	100 g
Zucchini	100 g
pH	6.65 [-]
Electrical Conductivity (at 20°C)	420 μ S/cm
Fixed residue (at 180°C)	341 mg/l
Free CO ₂ at source	125 mg/l
Bicarbonates	254 mg/l
Potassium	26.9 mg/l
Calcium	31.5 mg/l
Magnesium	9.4 mg/l
Fluorides	1.1 mg/l
Nitrates	7 mg/l

Table 1: Solid organic substrate and water compositions.

Cell #	Fresh Water	Salt Water	FORSU	FORSU inoculum	Potentiostatic conditioning	Liquid-to-solid ratio
1	X		X			1:1
2	X		X			1:1
3	X		X		X	1:1
4	X			X		3:1
5	X			X		3:1
6	X		X			1:1
7		X	X			1:1
8		X	X			1:1
9		X	X		X	1:1
10		X		X		3:1
11		X		X		3:1
12		X	X			3:1

Table 2: Solid organic substrate and water compositions.

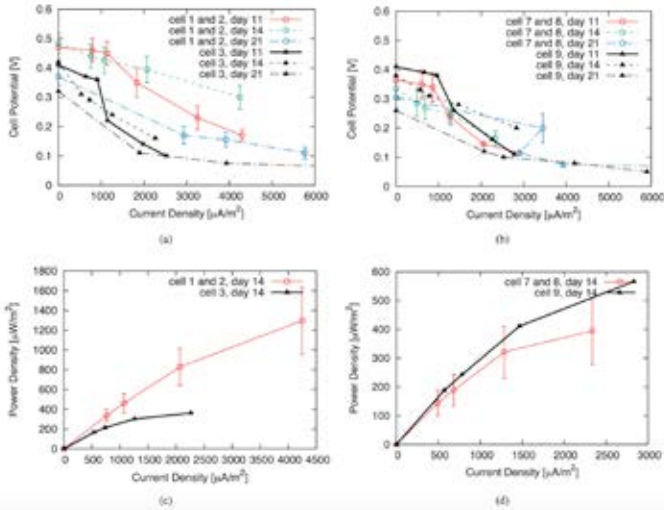


Figure 2: Comparison of MFC's performances in terms of polarization curves; (a): polarization curves of cells 1, 2 and 3 in different days; (b) polarization curves of cells 7, 8 and 9 in different days; (c) power curves of cells 1, 2 and 3 at day 14; (d) power curves of cells 7, 8 and 9 at day 14.

mance of the two groups of MFC's have been evaluated in the same environmental conditions ($T=20^{\circ}\text{C}$), for 28 days. To prevent leachate leaks through the porous structure of the cathode material, Nafion[®] 117 protonic membrane was used to seal the end of the Falcon test tube in correspondence to the cathode side.

III. RESULTS & DISCUSSION

We have assessed the performances our MFC's in terms of polarization curves, evaluated at different days. For the sake of brevity, we will focus on the comparison between cells 1, 2, 3 vs. 7, 8 and 9: the main difference between the two groups is that the first is characterized by the employment of fresh water, while the second group contains salt water. The addition of NaCl was done to assess the response of bacteria to detrimental external conditions. Finally, cells 3 and 9 have been object of potentiostatic conditioning: the analysis of their performance provides details on the suitability of such a treatment. Figure 2 reports the polarization curves for the two groups of MFC's in different days. All MFC's have worked in Open Circuit Mode

for the first 7 days; then, an external load equal to their internal resistance has been inserted. In the first 7 days, cells 3 and 9 have been connected to an external potential equal to $V_{ext} = 0.8 \text{ V}$; at the end of this phase, they have been connected to an external resistance, as the other reactors. The left panel in Fig. 2 refers to the fresh-water cells, while on the right the sea-water cell performances are reported. In the first days, the sea-water cells are characterized by a lower value of internal resistance; as the experiment goes on, however, their internal resistance increases more than in the fresh-water cells and gets even higher in the final part of the 28-day operating period. This is probably due to the adoption of pure NaCl, instead of the standard sea-water salt composition.

From Fig. 2 it is also evident that the potentiostatic conditioning provides better performance in the case of salt-water reactors only in the first half of the experiment: according to these results, the potentiostatic conditioning does not appear to be a worthy procedure for FORSU-based MFC's. The evaluation of reactor performance in the case of NaCl amendment is the object of future investigations.

IV. CONCLUSIONS

In this paper, we have assessed the performances of MFC's fed by the organic fraction of municipal solid waste according to the employment of fresh and salt water and in presence of a potentiostatic conditioning phase. The use of fresh water without a potentiostatic conditioning phase grants more even performance for the duration of the whole experiment.

ACKNOWLEDGEMENTS

This work was found by the Research Project PON03PE_00109_1 "Fuel Cell Lab".

REFERENCES

- [1] R.A. Nastro, Int. J. Perform. Eng., 10(4), 367, 2014.
- [2] V.K. Krastev, G. Falcucci, E. Jannelli, M. Minutillo and R. Cozzolino, Int. J. Hydrogen En., 39(36), 21663-21672, 2014.



RECENT RESULTS FROM THE FCH JU PROJECT CISTEM

M. Rastedt*, F.J. Pinar*, P. Wagner* and A. Dyck*

* NEXT ENERGY · EWE Research Centre for Energy Technology
at the University of Oldenburg,
Carl-von-Ossietzky Str. 15, 26129 Oldenburg, (Germany)

Abstract – In this work, recent results obtained within the FCH JU project CISTEM (Construction of improved HT-PEM MEAs and stacks for long term stable modular CHP unit) will be introduced. Various long term tests under constant load and with different reactant gas composition and diverse operation strategies like for example fuel switching and start-stop-cycling have been performed and will be presented. Degradation effects are investigated electrochemically and post-mortem by imaging procedures like micro-computed tomography.

CISTEM, HT-PEMFC, CHP system, μ -CT

I. INTRODUCTION

The vision of the European project CISTEM is the development of a new high temperature PEM fuel cell based CHP (combined heat and power) technology with an electrical output of up to 100 kW_{el}. The combination of the new modular system design with HT-PEM FC technology allows the evaluation of the CHP unit with regard to high overall efficiency, reduced costs and improved lifetime. The purpose of the CISTEM project is to show a proof of concept that HT-PEM (high temperature polymer electrolyte membrane) technology is suitable and ready for larger stationary CHP systems up to 100 kW_{el}. The CHP unit will be designed with several modules each consisting of; two fuel cell stacks with an output of 4 kW_{el} each and of a fuel processor unit, capable to be modulated between 25 and 100%. So one 8 kW_{el} module will be installed as hardware; the remaining 12 modules will be implemented as emulated modules in a hardware in the loop (HiL) test bench. With help of the modular concept the goals regarding the low production costs and higher system efficiency and increase annual operating hours will be achieved.

One key aspect in this project is the understanding of degradation effects and processes of PBI based HT-PEM fuel

cells. The improvement of the HT-PEM fuel cell can only be realized by minimizing or avoiding of conditions inducing those degradation path ways. Within CISTEM various fuel cell operation modes have been performed and investigated; a selection of these experiments is presented in the present work.

II. EXPERIMENTAL

A. Membrane Electrode Assembly (MEA)

The experiments have been carried out with Dapozol®-G55 MEAs, supplied by the project partner Danish Power Systems (Denmark). The nominal active surface area is ~25 cm². The membrane polymer electrolyte consists of phosphoric acid doped meta-PBI; the acid content is approx. 8 to 9 phosphoric acid molecules per repeat unit (monomer) of PBI [1]. Non-woven carbon cloth has been used as GDL.

B. Cell Compression Units and Fuel Cell Tests Stations

Commercially available cell compression units (CCU) from balticFuelCells (Germany) and Pragma Industries (France) [2] have been used for fuel cell test station operations. An accurately adjustable compression force is executed by either CCU via a piston onto the active surface area of the MEA. The CCU systems have been operated in constant pressure mode. The chosen nominal contact pressure was 0.75 MPa, applied on 5-fold serpentine flow fields (SFF). The balticFuelCells CCU was used in combination with the conventional test bench Evaluator C100-LT from Fuel Con AG, Germany. The second test station (Evaluator C50-LT, Fuel Con AG, Germany) operated with the CCU from Pragma Industries.

C. Fuel Cell Test Procedure

Experiments with different operation strategies and conditions have been performed. For long term tests at constant



load, a current density of 0.3 A/cm^2 was chosen while the composition of the reactant gases were varied: one test has been performed with pure H_2 and O_2 (30%) enriched air, another test has been executed with synthetic reformat and O_2 and a third test with H_2 and air, which is still under operation. The MEAs were mounted in the fixtures and placed into the CCUs. With a gas supply of nitrogen (0.3 L/min) at both sides, the fuel cell was heated up until $120 \text{ }^\circ\text{C}$. After this point, the reactant gas supply was started (as previously described) and an electrical load of 0.3 A/cm^2 was applied to the MEA. Afterwards the cell was finally heated up to $160 \text{ }^\circ\text{C}$. The following break-in period lasted $\sim 100 \text{ h}$. After this activation phase, an initial electrochemical characterization [1, 3] including polarization curves, EIS, CV and LSV has been performed, further information can be found in [4, 5].

The fuel switching test was performed with 12 h of pure H_2 followed with 12 h of synthetic reformat (78% H_2 and 22% CO_2). As oxidant O_2 enriched air (30% O_2) was used.

The duration of one cycle during the start/stop (S/S) cycling is 1 day (4 cycles per week). The break-in procedure has been performed with H_2 and was followed by an operation with 0.3 A/cm^2 for 6 h. The shut-down was under N_2/N_2 and OCV down to an idling temperature of $25 \text{ }^\circ\text{C}$, followed by an equilibration overnight.

III. RESULTS

Figure 1 shows the cell voltages and the current density as function of time for the three long term tests with different reactant gas compositions. The test operated with H_2 and O_2 enriched air reveals a degradation of $-21.9 \mu\text{V/h}$ (blue curve).

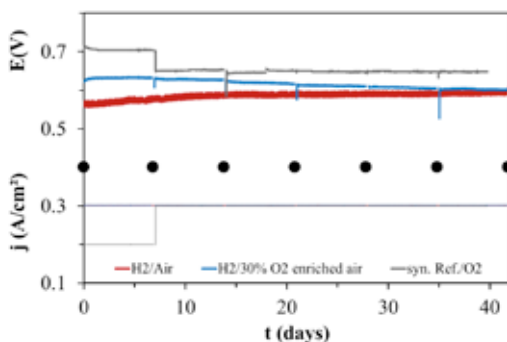


Fig. 1. Long term tests at constant current density (0.3 A/cm^2) for three different fuel/oxidant compositions.

The MEA under synthetic reformat and O_2 supply has a degradation rate of $-6.4 \mu\text{V/h}$ (grey curve); the first week of operation was performed with 0.2 A/cm^2 . For both tests an electrochemical characterization has been operated on day 0, 7, 14, 21, 28, 35 and 41. The test under H_2 and air supply (red curve) is still under operation, the electrochemical characterization has been minimized to polarizations curves at begin of life (BoL, day 0) and after 1000 and 2000 h. The MEA

shows improved fuel cell performance than BoL after 120 days of operation ($> 2500 \text{ h}$).

In Figure 2 the S/S-cycling-test with $T_{\text{idling}}=25^\circ\text{C}$ is presented; the degradation rate constitute $-12.6 \mu\text{V/h}$ and 61 S/S cycles have been performed. A voltage reduction can be observed until day 11; afterwards the voltage is almost constant.

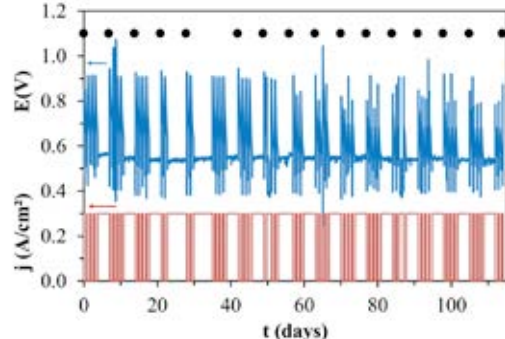


Fig. 2. Fuel cell voltage and current density as function of time during S/S cycling; MEA characterization: black dots.

IV. CONCLUSION

The results from the long term testing lead to the assumption, that fuel cell operation with air as oxidant needs a longer break-in procedure and that the electrochemical characterization accelerates the MEA degradation [4, 5]. Compared with previous tests ($T_{\text{idling}}=100 \text{ }^\circ\text{C}$, degradation rate: $-57.0 \mu\text{V/h}$ [6]), it can be stated that lower idling temperatures during S/S cycling lead to less degradation rates.

ACKNOWLEDGMENT

The authors would like to thank the European Commission as this work was supported by the Seventh Framework Programme through the project CISTEM (Grant Agreement Number 325262, 01.06.2013-31.05.2016).

REFERENCES

- [1] A. Diedrichs, M. Rastedt, F. J. Pinar and P. Wagner, Effect of compression on the performance of a HT-PEM fuel cell, *J. Appl. Electrochem.*, 43, 11, 2013, Pages 1079-1099.
- [2] Pragma Industries, Cell Compression System Version 2.0, User Guide Version 2.2a, 25.11.2009.
- [3] Q. Li, R. He, J.-A. Gao, J.O. Jensen, N.J. Bjerrum, The CO poisoning effect in PEMFCs operational at temperatures up to 200°C , *J. Electrochem. Soc.*, 150, 12, 2003, A1599-A1605
- [4] F.J. Pinar, N. Pilinski, P. Wagner, Long-term Testing of a High Temperature Polymer Electrolyte Membrane Fuel Cell: The Effect of Reactant Gases, *AIChE*, 2015, submitted.
- [5] M. Rastedt, F.J. Pinar, N. Pilinski, P. Wagner, Effects of Reactant Gases on HT-PEM Fuel Cells, *ECS Transactions*, 2015, submitted.
- [6] F.J. Pinar, A. Schlüterbusch, P. Wagner, M. Wark, A. Dyck, Start/Stop Cycling Test in a PBI based HT PEM FC, Paper presented at: 5th European PEFC and H2 Forum 2015; Lucerne.



ELECTROCHEMICAL AND MICROSTRUCTURAL STUDIES OF NI-YSZ ANODE REDOX BEHAVIOUR

D. Vladikova¹, D. Montinaro², I. Genov¹, P. Piccardo³,
Z. Stoyanov¹, Z. Wuillemin⁴, R. Spotorno³, A. Pecunia³,
V. Bongiorno³, M. Rolland², and B. Burdin¹

¹IEES-BAS, 10 Acad. G. Bonchev St., 1113 Sofia, (Bulgaria)

²SOFCpower SpA, Viale Trento 117, 38017 Mezzolombardo, (Italy)

³DCCI - Univ. Genova, via Dodecaneso 31, I-16146 Genoa, (Italy)

⁴HTceramix S.A., 26 Avenue des Sports,
CH-1400 Yverdon-les-Bains, (Switzerland)

Abstract - A new approach for *in-situ* conductivity measurements of the Ni phase in Ni/YSZ cermet anode during its formation and redox cycling, applying impedance spectroscopy, is introduced. The electrochemical testing is combined with direct gases (H₂, N₂ and their mixtures) permeability measurements. The resistance of the samples, which has inductive behavior, reaches a constant value of about 40 mΩ in the first 10-15 minutes and does not change during further reduction. The resistance decreases with about 8-10% after the first oxidation-reduction cycle. In the next cycles it does not change, or slightly increases. The permeability of the redox cycled samples is lower. Although there is a general correlation between permeability and porosity, depending on the testing conditions, for samples with the same porosity, the permeability differs due to different tortuosity.

Index Terms – YSZ/Ni anodes, Electrochemical Impedance Spectroscopy, gases permeability, redox cycling.

I. INTRODUCTION

Nickel-yttria stabilized zirconia (Ni-YSZ) cermets have been used as anode materials in solid oxide fuel cells (SOFCs) for more than 25 years. Their application as anode supports necessitates the continuous studies aiming to optimize both their electrochemical behavior and mechanical stability. Usually the final composition and microstructure are obtained by reduction of the YSZ/NiO composite to YSZ/Ni. This procedure is performed after the cell assembling, which hinders the studies of the processes that bring to the formation of a stable

electrically conductive Ni network combined with the development of a new microstructure favoring diffusive mass transfer. In addition to the initial formation of the anode, the operation of the cell is strongly influenced by two major degradation mechanisms: (i) Ni coarsening and (ii) re-oxidation of Ni to NiO due to accidental gas leaks, which influences both the Ni network and the mechanical stability of the YSZ structure. Since the electric conductivity is determined by the percolating Ni phase, its measurement may give a good indication of Ni rearrangements both during the initial reduction of NiO and the degradation of the Ni network.

Usually, the electrochemical behavior of the anode reaction is evaluated by impedance measurements carried out during operation of cells [1, 2], followed by post mortem analysis, where porosity is an important characterization parameter. The data analysis needs the application of equivalent circuit models, based on validated preliminary working hypothesis for separation of the anode contribution from the total impedance of the cell, which introduces complications and uncertainty.

This work introduces a new approach for *in-situ* conductivity measurements of the Ni phase during its formation, as well as during cyclic oxidation and reduction through Electrochemical Impedance Spectroscopy. The electrochemical testing is combined with direct gases (H₂, N₂ and their mixtures) permeability measurements performed after the reduction at room temperature.



II. EXPERIMENTAL

The reduction experiments were performed on YSZ/NiO samples with thickness about 250 μm and diameter 20 mm prepared by tape casting. The impedance measurements were carried out on “Ivium CompactStat.e” in the frequency range 100 KHz-10 Hz with density of 5 points/decade and amplitude of the AC signal 1 mA in different atmospheres and in a temperature range 25 – 800°C. Ni net was used for contact with the sample. The initial reduction was performed at 750°C and 800°C in a blend of N_2 and H_2 . The redox cycles were carried out at 730°C in a blend of N_2 and air, followed by reduction in a mixture of N_2 and H_2 . The permeability studies are based on measurements of the gas pressure P (mm H_2O) at different gas flows q_{flow} [ml/min] [3]. The SEM microstructure and porosity analysis were performed with a scanning electron microscope (SEM) Zeiss EVO 40, equipped with an energy dispersive X-ray spectroscope (EDXS Pentafet).

III. RESULTS

The experimental results performed during reduction show that the process is very fast. The resistance of the samples decreases from several $\text{k}\Omega$ down to 40 $\text{m}\Omega$ in the first 10 - 15 minutes and does not change during further reduction. As it can be seen in Fig. 1 the impedance diagrams of the Ni network formed in the YSZ matrix during reduction, has the typical for metallic wires inductive shape.

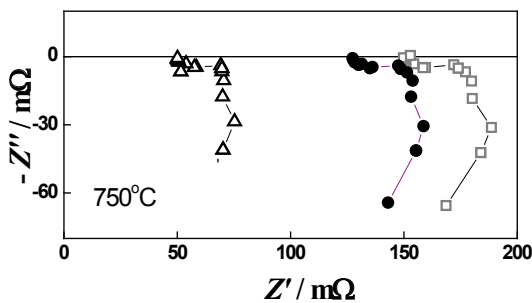


Fig. 1. Complex plane impedance diagrams measured during reduction of YSZ/NiO sample after 8,5 minutes (□), after 9,5 minutes (●) and after 10,5 minutes (▲) from the beginning of the reduction process.

Impedance diagrams of one oxidation-reduction cycle are given in Fig. 2. The value of the sample resistance decreases after the first oxidation-reduction cycle. In the next cycles it does not change, or slightly increases. The porosity analysis showed that as a result of the reduction, the average porosity increases more than two times – from 13% to 28%. Depending on the testing conditions, for samples with the same porosity, the permeability differs, obviously due to different tortuosity.

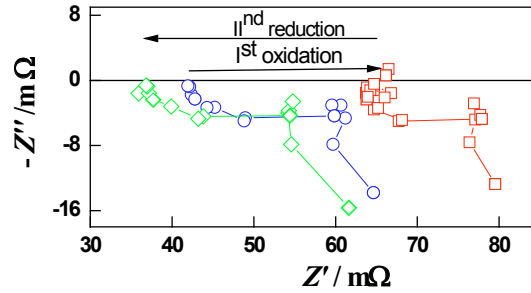


Fig. 2. Complex plane impedance diagrams measured after oxidation followed by reduction

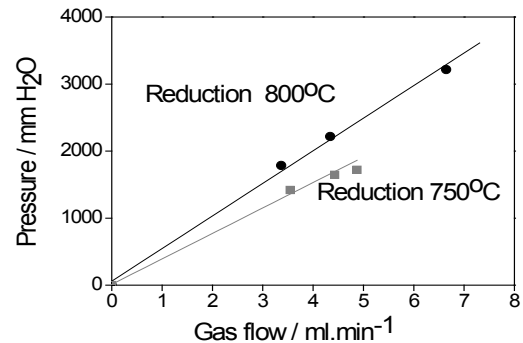


Fig. 3. Dependence of the pressure from the nitrogen gas flow for anodes with the same porosity (28%).

IV. CONCLUSIONS

In addition to providing deeper insight into the occurring phenomena, this investigation aims to develop tools and procedures for improvement of the anode quality during the initial reduction of the YSZ/NiO composite, as well as for reduction of the degradation phenomena due to oxidation.

ACKNOWLEDGMENT

The research leading to these results has received funding from the European Union's Seventh Framework Programme (FP7/2007-2013) Fuel Cells and Hydrogen Joint Undertaking (FCH-JU-2013-1) under grant agreement No 621207.

REFERENCES

- [1] Talebi, T., Sarrafi, M., Haji, M., Raissi, B., Maghsoudipour, A., Investigation on microstructures of NiO-YSZ composite and Ni-YSZ cermet for SOFCs, Internat. J. Hydrogen Economy, Volume 35, 2010, pp. 9440-9447.
- [2] Cheng, S-W., Tsai, C-H., Wu, S-H., Liu, C-K., Cheng, Y-N., Lee, R-Y., Effects of reduction process on the electrochemical and microstructural properties for electrolyte-supported SOFCs, Internat. J. Hydrogen Energy, Volume 40, 2015, pp.1534-1540.
- [3] Mladenova, E., Vladikova, D., Stoynov, Z., Chesnaud, A., Thorel A., Krapchanska, M., Gases permeability study in Dual Membrane Fuel Cell, Bulg. Chem. Commun., Volume 45, 2013, pp. 366-370.



ELECTROCATALYTIC LAYERS BASED ON REDUCED GRAPHENE OXIDE FOR PEM ELECTROCHEMICAL SYSTEMS

S.A. Grigoriev^{1*}, A.S. Pushkarev^{1,2}, I.V. Pushkareva^{1,2},
V.N. Kalinichenko³, and V.N. Fateev²

¹ National Research University "Moscow Power Engineering Institute", 14, Krasnokazarmennaya str., Moscow, 111250, Russia

² National Research Centre "Kurchatov Institute", 1, Kurchatov sq., Moscow, 123182, Russia

³ DELTARUS Limited, 2/5(B), Likhachevsky alley, Dolgoprudny, Moscow region, 141700, Russia

*E-mail: sergey.grigoriev@outlook.com

Abstract - Reduced graphene oxide (RGO) with a surface area of ca. 600 m²/g was synthesized and characterized. A series of membrane-electrode assemblies with RGO addition to electrocatalytic composition based on Pt/Vulcan XC-72 catalyst were fabricated and tested. It was shown that the optimum content of RGO in active layer is 1-5 wt % depending on MEA composition and operating conditions. At optimum RGO concentration the maximum fuel cell power density is increased by up to 30% in comparison with no-RGO containing electrocatalytic layers. An efficient method for synthesis of carbon supported Pt electrocatalysts based on magnetron-ion spraying in a pulsed mode was developed. Using this method, catalyst nano-particles with an average size of 2.7 to 6 nm and a specific surface area 47-56 m²/g were synthesized.

Index Terms - electrocatalytic layer, electrochemical system, proton exchange membrane, reduced graphene oxide.

I. INTRODUCTION

Last years a large-scale implementation of hydrogen electrochemical systems (fuel cells, water electrolyzers, and other) with proton-exchange membrane (PEM) takes place in various fields of power engineering, transport, aerospace industry, etc. A key component of PEM electrochemical systems is electrocatalytic layer. The use of different carbon nanofoms as electrocatalyst carriers aims to reducing of noble metals content and elevating of activity [1]. Graphene is attract specific attention of the scientific community because of unique properties, such as good electrical conductivity, high surface area and stability, resistance to aggressive environments [2-3].

II. EXPERIMENTAL

A. Synthesis of RGO

Graphite oxide was synthesized by modified Hummer's method [4]. Strips of dry graphite oxide were piece by piece dipped in an argon-filled vertical tube furnace with a quartz inner tube with diameter of 4 cm and a length of 100 cm warmed up to 700°C in the central zone with a minimum width of 30 cm. Thermally reduced graphene oxide is collected in the lower receiver with volume of 5 l.

B. Structural characterization of RGO

Structural characterization and chemical composition were conducted using analytical complex based on Helios NanoLab 600i (FEI, USA) scanning electron-ion microscope (SEM) with add-on device for energy dispersive X-ray analysis (EDAX, USA) with a sensitivity of elements from B to U and energy resolution of 128 eV and TitanTM 80-300 S/TEM (FEI, USA) transmission electron microscope (TEM) (80-300 kV, spatial resolution points of 0.07-0.08 nm).

C. Synthesis of Pt nano-particles on Vulcan XC-72

Platinum nano-particles on Vulcan XC-72 carbon carrier were synthesized according to the technique described in [5, 6]. However, an impulse mode has been applied. Periodically (each 20 seconds) cathode potential (-100 V) was applied to the cup with carrier to provide Pt ion acceleration and additional catalyst surface treatment with Ar ions.



D. Fabrication and testing of membrane-electrode assemblies

Nafion®-115 and Nafion®-212 membranes (Du Pont) were used as PEM in the membrane-electrode assemblies (MEAs). The catalyst Pt/Vulcan XC-72, Nafion® solution (5 wt.% D521 dispersion (DuPont)) and RGO (0-10 wt. %) were homogenized in 2-propanol in ultrasonic bath at a frequency of 22-25 kHz for 20 min. Dry weight ionomer content was 15%. The resulting catalyst ink was sprayed with intermediate drying of layers on the gas diffusion electrodes (Sigracet® 10BB carbon paper with microporous sublayer; thickness *ca.* 0.4 mm, porosity *ca.* 84%) obtained from SGL CARBON GmbH. The catalyst loading was 1.0 mg/cm².

III. RESULTS AND DISCUSSION

The RGO (fig. 1) has a specific surface area of *ca.* 600 m²/g (BET) and consisted of separate interconnected RGO nano-sheets containing an average of from 4 to 6 carbon monolayers. Both mono-layered, and multilayered nano-sheets are clearly visible on the micrographs, a direct image of the atomic planes of the crystal lattice is distinguishable.

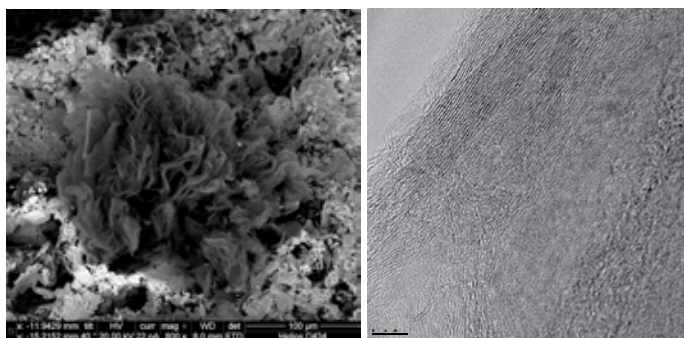


Fig 1. SEM (left) and TEM (right) micrographs of RGO nano-rosette.

The shape of current-voltage curves (fig. 2) permits to talk about reduction of the ohmic drop of potential and about possible partial reduction of transport polarization with increasing of RGO content in the electrocatalytic layers in the range of 0-5% and 0-1% for fuel cell with Nafion®-115 and Nafion®-212 membrane, respectively. The increase of RGO content more than optimal content decreasing the platinum content and the relative content of the Nafion ionomer are reduced, whereby the activity and the proton conductivity of active layer are decreased too.

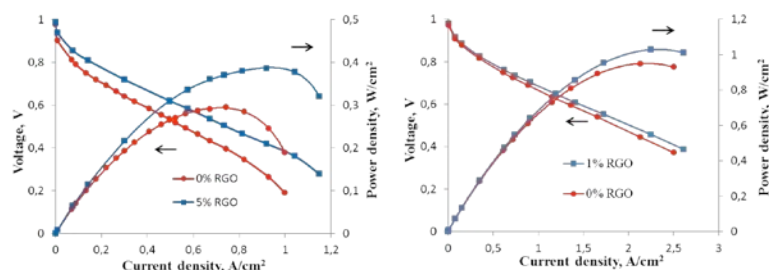


Fig 2. Current-voltage and current-power curves of PEM fuel cells based on Nafion®-115 (left) and Nafion®-212 (right). Operating conditions: 60°C, atmospheric pressure of gases (left) and 2.4 bar (right).

IV. CONCLUSION

An effective method of RGO synthesis with high specific surface area was developed. It was shown that the addition of RGO to the active layers of the fuel cell in an amount of 1-5 wt. % improves its CVC. In particular, the maximum power density increases by *ca.* 8.5-30%. Optimal RGO content in the active layer depends on the MEA composition and operation conditions (particularly, the thickness of the membrane, the operating pressure of the reactants).

ACKNOWLEDGMENT

Development of the method of reduced graphene oxide synthesis, and its characterization have been supported by the Russian Foundation for Basic Research within the framework of research project No. 14-29-04071 ofi_m. Development of pulse magnetron sputtering method of electrocatalysts synthesis, and their structural and electrochemical studies were executed at the expense of a grant of the Russian Science Foundation (project No. 14-29-00111). The tests of MEAs has been financially supported by the Ministry of Education and Science of the Russian Federation within the framework of government task No. 2014/123 (amendment No 1) for performance of the government works in scientific activities.

REFERENCES

- [1] Dai L, Chang DW, Baek J-B, Lu W. Carbon Nanomaterials for Advanced Energy Conversion and Storage. Carbon Nanomaterials, Volume 8(8), 2012, Pages 1130-66.
- [2] Geim AK, Novoselov KS. The rise of graphene. Nat Mater, Volume 6(3), 2007, Pages 183-91.
- [3] Geim AK. Graphene: Status and Prospects. Science, Volume 324, 2009, Pages 1530-4.
- [4] Hummers WS, Offman RE. Preparation of graphitic oxide. J Amer Chem Soc, Volume 80, 1958, Page 1339.
- [5] Fedotov AA, Grigoriev SA, Millet P, Fateev VN. Plasma-assisted Pt and Pt-Pd nano-particles deposition on carbon carriers for application in PEM electrochemical cells. Intern. J. Hydrogen Energy, Volume 38, 2013, Pages 8568-74.
- [6] Fedotov AA, Grigoriev SA, Lyutikova EK, Millet P, Fateev VN. Characterization of carbon-supported platinum nano-particles synthesized using magnetron sputtering for application in PEM electrochemical systems. Intern. J. Hydrogen Energy, Volume 38, 2013, Pages 426-30.



SYNCHROTRON SAXS AND GISAXS CHARACTERIZATION OF PT CATALYST NANO-MORPHOLOGY IN HIGH TEMPERATURE PEM FUEL CELLS

Benedetta Marmioli *, Francesco Valle**,
Heinz Amenitsch*, Rodolfo Tacconi**

* Institute of Inorganic Chemistry, Graz University of Technology,
Stremayrgasse 9/IV, Graz 8042, (Austria)

** Engineering and Architecture department, University of Trieste,
via A. Valerio 10, Trieste 34127, (Italy)

Abstract - In this communication an analysis of Pt catalyst morphology evolution in high temperature fuel cells subjected to different load cycles using synchrotron Small Angle X-ray Scattering (SAXS) and Grazing Incidence Small Angle X-ray Scattering (GISAXS), is presented. The measurements show the aggregation of the Pt nanoparticles (NPs) in used MEAs with respect to a reference new MEA. Moreover, the anode and cathode sides of all MEAs present different Pt NPs size whose morphological characteristics can be separately determined using GISAXS.

Index Terms – catalyst degradation, MEA, PEM Fuel Cells, synchrotron SAXS/GISAXS

NOMENCLATURE

PEM	Proton Exchange Membrane
MEA	Membrane Electrode Assembly
NPs	Nano-Particles
SAXS	Small Angle X-ray Scattering
GISAXS	Grazing Incidence SAXS

I. INTRODUCTION

Pt Catalyst degradation in PEM fuel cells is one of the main issues affecting MEA durability and performance. The catalyst deteriorates during operation through aggregation, dissolution and isolation of the nanoparticles, with the result of a lower catalytic activity [1]. We have already employed synchrotron SAXS to study both the behavior of the different constituents of the MEA and to study the difference between a not used MEA and two MEAS subjected to accelerated ageing tests [2]. In this communication we present the latest results on SAXS and GISAXS characterization of the morphology of MEAS

subjected to different load cycles.

II. THE TEST SYSTEM

Electrocatalyst evolution during long-term operation has been studied and related to performance loss. Specific stress test protocols have been developed to accelerate electrocatalyst degradation in commercial high temperature fuel cell MEAs operated in single cell configuration. On a test bench developed at the Engineering and Architecture Department of the University of Trieste, different MEAs have been subjected to load cycling and to start/stop cycling. One of the two testing protocols, regarding load cycling, included open circuit (OC) condition in each cycle with the purpose to study the effects of frequent and short OCs during operation on MEA durability and electrocatalyst evolution. Specific start-up and shutdown procedures have been used in the start/stop test in order to limit other degradation mechanisms. Cell voltage and polarization curves have been recorded to monitor cell performance during the durability tests. The electrocatalyst structural evolution induced by load cycling has been characterized with SAXS/GISAXS at the Austrian SAXS beamline at the synchrotron radiation facility Elettra-Sincrotrone Trieste [3].

III. RESULTS

The comparison between the results of the two load cycling stress tests has been useful to quantify the effect of cycle voltage range. The voltage decay rate (μVh^{-1}) at 222 mAcm^{-2} in the test in which current has been cycled between 0 and 500 mAcm^{-2} was 27% higher than in the test in which current has been cycled between 10 and 500 mAcm^{-2} . Similar results have been obtained in terms of electrocatalyst evolution: the mean



radius increased by 74% in the sample cycled between 10 and 500 mAcm⁻², while it more than doubled applying the cycle including OC condition (102% larger) [2]. Electrocatalyst load and electrochemical environment are different in cathode and anode side [4, 5, 6]. As SAXS analysis includes both the contribution of the two electrodes, it has been decided to apply Grazing Incidence SAXS (GISAXS) in order to investigate separately the two surfaces. First results show that the difference in NPs size is evident in the reference sample (new MEA), as shown in figure 2. In fact, from the scattering curves of the anode and of the cathode, it is possible to note a shoulder on each curve (indicated by the arrows). The shoulder shows the presence of the nanoparticles and its position on the q axis, the scattering vector, is inversely proportional to their mean size.

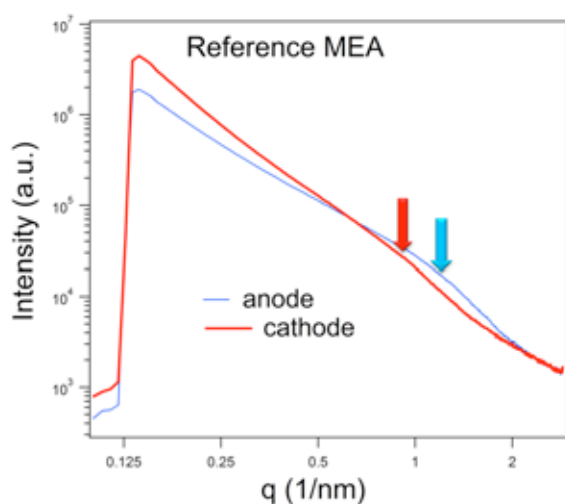


Figure 2. GISAXS pattern of the catalyst layer of the reference MEA on the anode and cathode side.

In particular, the size of the NPs in the anode is smaller than the ones in the cathode as the value of q of the shoulder is higher.

The same occurs in the MEA that has been subjected to voltage cycling including OC condition, as shown in figure 3. It appears that the cathode undergoes a larger catalyst modification than the anode, that is NPs of the cathode aggregate more than the ones in the anode.

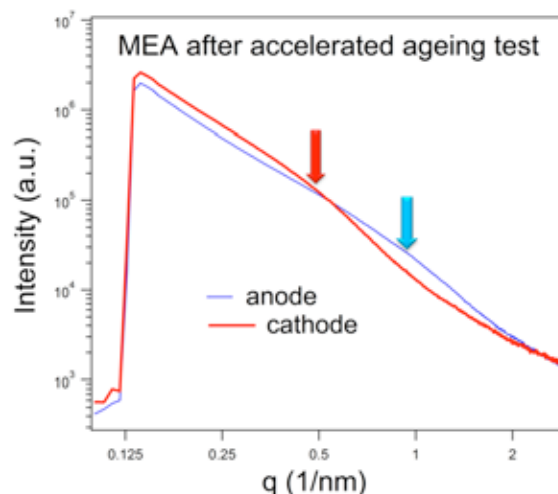


Figure 3. GISAXS pattern on the anode and cathode side of the catalyst layer of a MEA subjected to voltage cycling including OC condition.

IV. CONCLUSIONS

GISAXS technique has been used for the characterization of electrocatalyst structural properties in High Temperature PEM fuel cells. Through GISAXS measurements it has been possible to distinguish between anode and cathode catalyst morphology. Nevertheless, additional tests and measures are necessary to confirm the obtained results and to identify a direct correlational profile between the catalyst morphology and the cell operational profile.

REFERENCES

- [1] Jiujun Zhang, PEM Fuel Cell Electrocatalysts and Catalyst Layers: Fundamentals and Applications, Springer, 2008.
- [2] F. Valle, N. Zuliani, B. Marmiroli, H. Amenitsh, R. Taccani, SAXS analysis of catalyst degradation in High Temperature PEM Fuel Cells subjected to accelerated ageing tests, Fuel Cells, Volume 14, 4, pp 938-944, 2014.
- [3] H. Amenitsh, S. Bernstorff, M. Kriechbaum, D. Lombardo, H. Mio, M. Rappolt and P. Laggner, Performance and First Results of the ELETTRA High-Flux Beamline for Small-Angle X-ray Scattering, Journal of Applied Crystallography, vol. 30 (5), pp. 872-867, 1997.
- [4] Z. Qi, S. Buelte, Effect of open circuit voltage on performance and degradation of high temperature PBI-H₃PO₄ fuel cells, J. Power Sources. 161 (2006) 1126–1132.
- [5] T.J. Schmidt, J. Baurmeister, Properties of high-temperature PEFC Celtec®-P 1000 MEAs in start/stop operation mode, J. Power Sources. 176 (2008) 428–434.
- [6] J.J. Hu, H. Zhang, Y. Zhai, G. Liu, B. Yi, Performance degradation studies on PBI/H₃PO₄ high temperature PEMFC and one-dimensional numerical analysis, Electrochim. Acta. 52 (2006) 394–401.



DIRECT UTILISATION OF ETHANOL IN SOLID OXIDE FUEL CELLS USING A PROTECTIVE CATALYTIC LAYER-MODIFIED ANODE

A.S. Aricò*, M. Lo Faro*, S. C. Zignani*, R.M. Reis**,
G.G.A. Saglietti**, A.G. Sato**, and E.A. Ticianelli**
* CONSIGLIO NAZIONALE DELLE RICERCHE - CNR-ITAE,
via Salita S. Lucia sopra Contesse 5, 98126 Messina, (Italy)
** USP-IQSC, Av. Trab. São-carlense, 400 CEP 13560-970 São
Carlos, SP (Brasil)

Abstract - Electro-catalytic properties of Ni-based alloys for the conversion of ethanol in solid oxide fuel cells (SOFCs) were investigated. Electrochemical tests were carried out by utilizing a Ni-based alloy/CGO cermet as a barrier layer in a anode-supported SOFC. A comparative study was made. The aim was to efficiently convert the fuel just before the conventional anode support. The SOFC anode modified with Ni-Co/CGO showed superior performance towards the direct utilization of dry ethanol than the bare anode and that modified with Ni-Cu/CGO. A peak power of 550 mW cm⁻² was achieved for dry ethanol-fed in the Ni-Co/CGO pre-layer modified-cell at 800 °C.

Index Terms – Anode protective catalytic layer, Direct oxidation of ethanol, Ni-alloys, Solid Oxide Fuel Cells

I. NOMENCLATURE

APU: Auxiliary power units
ASC: Anode-supported cell
EIS: Electrochemical impedance spectroscopy
GCO: Gadolinia-ceria oxide
YSZ: Yttria-stabilised zirconia
YDC: Yttria-doped ceria
LSFCO: La_{0.6}Sr_{0.4}Fe_{0.8}Co_{0.2}O₃
SEM: Scanning electron microscopy
SOFC: Solid oxide fuel cells
TEM: Transmission electron microscopy

II. INTRODUCTION

H₂ is an optimal energy carrier due to its high gravimetric energy content, however, its storage on-board of transportation systems appears difficult since no efficient storage solutions have been identified yet. Ethanol may represent an attractive

alternative to H₂ especially for portable applications, auxiliary power units (APU) and distributed energy generation. Production, storage, and distribution of ethanol is well established; these aspects together with the relative low cost of ethanol make such renewable fuel promising for power generation in fuel cells.

The main risk associated to the utilization of pure (dry) ethanol in SOFCs is represented by the formation of carbon deposits on the Ni-YSZ anode that may damage the cell rapidly. A possible solution to this drawback is the utilization of an internal reforming process with a steam to carbon ratio of about 2.5. However, the utilization of water vapour causes a dilution of the energy content of the fuel stream. Water vapour also causes lower voltage and efficiency as well as an increase of the complexity of the SOFC-based system. Another possibility is represented by the use of an external pre-reforming processor for the conversion of ethanol to syngas. However, also the external reformer increases the complexity of the SOFC-based system. Therefore, a practical solution to this issue may be the utilization of a protective catalytic layer applied to the anode. This catalytic layer acts as protective substrate for the supporting anode structure by avoiding carbon deposition. In this work, we have focused our efforts on a novel Ni-Co/CGO combination for the electro-catalytic anode pre-layer in a SOFC directly fed with ethanol and we have compared the performance of this formulation to a baseline Ni-Cu/CGO catalyst.

III. RESULTS AND DISCUSSION

The SOFC cell consisted of Ni/YSZ supporting anode, YSZ/YDC electrolyte bilayer, and LSFCO cathode. The



modified cell was characterised by an additional protective catalytic layer of about 5 microns at the anode side based on a cermet consisting of a Ni-alloy and CGO. Fig. 1 shows the TEM image for the Ni–Co/CGO catalyst used at the protective anode layer. The morphology is similar to that of a supported catalyst and different than that of the conventional supporting SOFC anode (Fig 2).

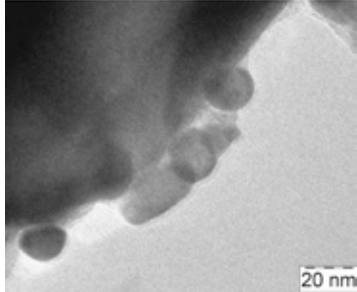


Fig. 1. TEM of the Ni–Co/CGO pre-layer

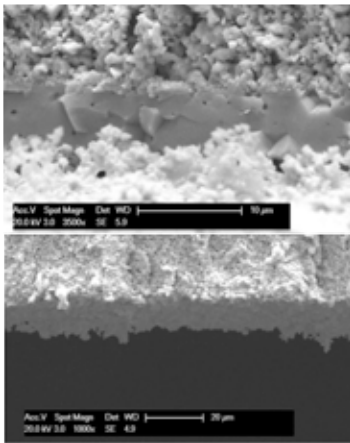


Fig. 2. SEM of the Ni–Co/CGO pre-layer (bottom) and electrocatalysts-electrolyte interface in the SOFC

The electrochemical behaviour in the presence of a pure ethanol stream at the anode is shown in Fig. 3. The OCV of the bare cell (1.1 V) and that of the NiCo/CGO modified cell (1.12 V) was significantly higher compared to the NiCu/CGO modified cell (0.97 V). The impedance spectra collected under OCV (Fig. 3a) are strongly affected by the different OCV values and cannot be compared properly in terms of the total resistance. The EIS spectra at 0.8 V shows similar profiles for the bare and NiCu/CGO modified cells (Fig. 3b), whereas the cell modified with NiCo/CGO appeared different with clear evidence of different relaxation times. Polarization curves in Fig. 3c show significantly higher performance for the cell modified with NiCo/CGO compared to the other cells under investigation. This behaviour coupled with the higher OCV indicates that the direct oxidation of ethanol in SOFCs is favoured at the NiCo/CGO electrocatalyst-based protective anode layer.

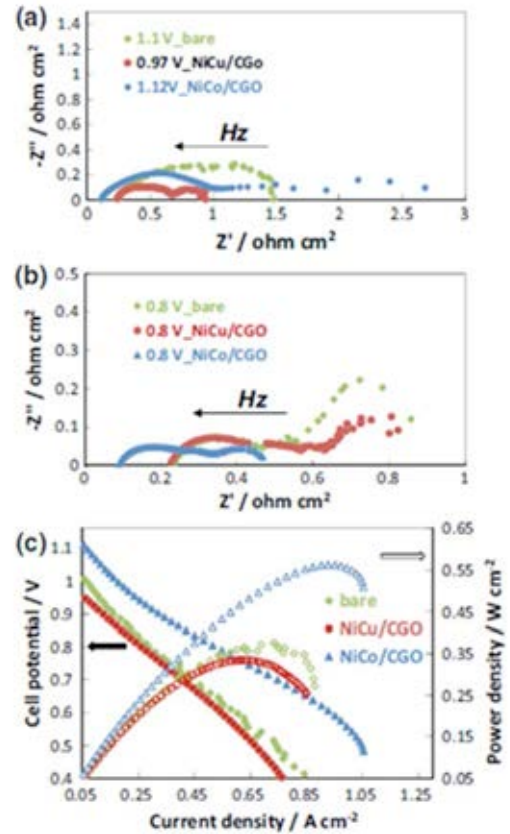


Fig. 3. EIS and polarisations of the SOFC cells

IV. CONCLUSION

The utilization of a protective layer applied to the anode of a conventional cell appears useful for the direct utilization of ethanol in SOFCs. Our study shows that the oxidation of dry ethanol appears conveniently promoted by the NiCo/CGO pre-layer catalyst. The performance of the SOFC cell based on the NiCo/CGO pre-layer is significantly higher than that of the benchmark cell with a peak power density of about 550 mW cm⁻² for the direct oxidation of ethanol. Durability tests have also shown appropriate stability for the NiCo/CGO based cell.

ACKNOWLEDGMENT

CNR-ITAE acknowledges the MIUR for the BIOITSOFC project "PROGRAMMI DI RICERCA SCIENTIFICA DI RILEVANTE INTERESSE NAZIONALE- PRIN PROGRAMMA DI RICERCA - Anno 2010-2011 - prot. 2010KHLKFC". USP-IQSC acknowledges the Research Program promoted by the Brazilian "Conselho Nacional de Desenvolvimento Científico e Tecnológico" entitled "Ciência sem Fronteiras" processo nº 402180/2012-7.



ENHANCED PERFORMANCE AND COST-EFFECTIVE MATERIALS FOR LONG-TERM OPERATION OF PEM WATER ELECTROLYSERS COUPLED TO RENEWABLE POWER SOURCES

A. S. Aricò

CNR-ITAE Institute, Via Salita S. Lucia sopra Contesse 5, 98126
S. Lucia, Messina, (Italy)

Abstract - The objective of the ELECTROHYPEM project was to develop cost-effective components for PEM electrolysis with enhanced activity and stability in order to reduce stack and system costs and to improve efficiency, performance and durability. The focus of the project was on low-cost electrocatalyst, low-noble metal loading electrodes and membrane development. The project addressed the development of PEM electrolyzers for residential applications for a suitable integration with renewable power sources. The aim is to contribute to the road-map addressing the achievement of a wide scale decentralised hydrogen production infrastructure. In the framework of this project, innovative membranes with enhanced conductivity and reduced hydrogen cross over for wide temperature operation have been developed, enhanced nanosized solid solution mixed oxide electro-catalysts have been demonstrated, membrane-electrode assembly (MEA) performance of 1.8 V at 3 A cm⁻² has been achieved. A 1.2 Nm³/h H₂ production capacity system has been demonstrated with good characteristics for coupling to renewable power sources.

Index Terms - Electro-catalysts, Membranes, PEM electrolysis, Renewable power sources.

I. NOMENCLATURE

HER: Hydrogen evolution reaction
MEA: Membrane electrode assembly
OER: Oxygen evolution reaction
PEM: Polymer electrolyte membrane
R&D: Research and demonstration

II. INTRODUCTION

R&D in innovative hydrogen production from renewable energy sources is reported among the priority topics for the application area dealing with hydrogen production and distribution. Innovative materials and components for PEM electrolyzers are needed to improve efficiency, performance and

durability of the electrolysis process in order to compete with hydrogen production processes from fossil fuels. This requires systematic materials research to reduce the total life cycle costs related to current PEM electrolyzers by replacing current commercial materials for membranes, catalysts and bipolar plates with low cost materials. The Electrohypem project entirely fulfilled these aims and expected impacts. The project specifically concerned with research on functional materials and technology for PEM electrolyzers as well as their direct coupling to renewable energy sources. The research approaches in the project were oriented towards both short and long term innovation [1, 2].

III. RESULTS AND DISCUSSION

Specifications and protocols for assessing PEM water electrolyser components and devices have been delivered and made available to the public through the project web-site (<http://www.electrohypem.eu>).

Extruded and reinforced membranes comprising short side chain perfluorinated ionomer (Aquivion) have been developed by Solvay. Proton conductivity better than 200 mS cm⁻¹ at 80 °C has been obtained. In parallel, hydrocarbon-based, cross-linked polymers have been developed by ITM with proton conductivity meeting the target of 200 mS cm⁻¹.

CNRS has focused on reinforcing Aquivion membranes for high temperature applications (up to 140 °C) and on the development of sulfonated polyheterocyclic polymers as a low-cost alternative to PFSA. Hydrogen cross-over for these polymer electrolytes was lower than 1 mA cm⁻² equivalent current density.

Nanosized Pt and Pd (supported on carbon black) and IrRu-oxide electrocatalysts with enhanced mass activity have been developed at CNR-ITAE for hydrogen and oxygen evolution reactions, respectively. Overpotentials for the OER vs. the

thermoneutral potential (1.48 V) at 1 and 2 A cm⁻² of 40 and 83 mV have been recorded at CNR-ITAE. The achieved value at 1 A cm⁻² represents a 60% improvement over the project target regarding anode performance. Whereas for the HER, the recorded overpotential at 1 A cm⁻² with a noble metal loading <0.2 mg cm⁻² was about 50 mV vs. the reversible hydrogen potential that is comparable to the project target for the cathode.

Solid solution of nanosized Ir oxide have been prepared at CNRS, and Ir and Ru oxides at ITM resulting in excellent performance at low temperatures (55 °C) and suitable stability, whereas IrOx catalysts show best characteristics at high temperature (> 80 °C).

Non-noble metal oxygen evolution catalysts have been prepared at CNRS and evaluated at CNR-ITAE for oxygen evolution.

The catalysts and membranes have been validated in MEAs. CNR-ITAE nanosized IrRuOx catalysts have provided, in combination with Aquivion short-side chain perfluorosulfonic ionomer membranes, performances of 3 A cm⁻² at 1.8 V terminal cell voltage at 90 °C (Fig. 1) with hydrogen cross-over lower than 1 mA cm⁻² and total PGM loading of 0.5 mg cm⁻². The achieved performance represents a 40% improvement over the project milestone regarding MEA performance.

Performance exceeding the project targets have been achieved at CNRS at 140 °C with reinforced Aquivion membrane.

Both ITM and CNR-ITAE have shown stable performance for MEAs based on ITM and Aquivion membranes equipped with conventional (> 1200 hrs, 8 μV/h, 1 A cm⁻²) and low noble metal loading (0.5 mg cm⁻²).

Novel stack architectures and cost-effective bipolar plate configurations have been developed.

Characterisation of 1.2 Nm³ H₂/h production capacity water electrolyser, based on the novel components, has shown a power consumption of 3.53 kWh/Nm³ during operation at 1 A cm⁻².

Two prototypes of micro wind turbine (1.5 and 7 kW) developed at TRE were selected for evaluating renewable energy source (RES) coupling of the PEM electrolyser. The dynamic behavior of the PEM electrolyser was assessed using simulated current profiles from renewable power sources.

Fig. 1. Nanostructured Electrohypem electro-catalysts and water splitting polarization curves

IV. CONCLUSION

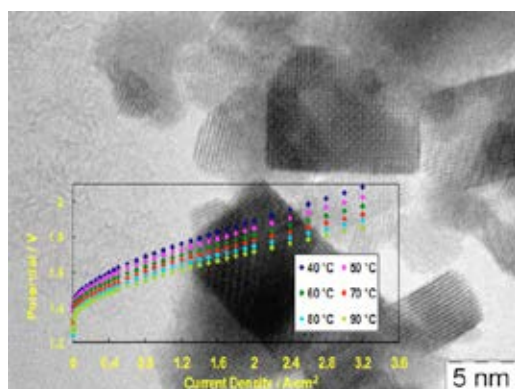
The main results achieved in Electrohypem were regarding a membrane conductivity better than 200 mS/cm and a H₂ permeation rate in the oxygen stream at high (30 bar) differential pressure <1%, low overpotentials for anode/cathode reactions (OER overpotential < 0.1 V vs. E thermoneutral, HER overpotential < 0.05 V vs. RHE at 1 A cm⁻²), noble metal loading <0.5 mg cm⁻². Large area (130 cm²) MEAs were characterized by current densities better than 1 A cm⁻² @ 1.6 V/cell and 3 A cm⁻² @ 1.8 V/cell with degradation <10 μV/h. A novel stack with low energy consumption ~3.5 kWh/Nm³ H₂ at a hydrogen production rate > 1.2 Nm³ h⁻¹ with efficiency better than 80 % LHV was developed. A significant aspect of the project was also dealing with the implementation of a system around the stack for assessing the dynamic behavior, in particular testing the stack under simulated renewable energy sources (RES) current profiles.

ACKNOWLEDGMENT

The research leading to these results has received funding from the European Community's Seventh Framework Programme (FP7/2011–2014) for the Fuel Cells and Hydrogen Joint Technology Initiative under grant agreement ELECTROHYPEM no. 300081.

REFERENCES

- [1] Siracusano, S., Baglio, V., Moukheiber, E., Merlo, L., Aricò, A.S., Performance of a PEM water electrolyser combining an IrRu-oxide anode electrocatalyst and a short-side chain Aquivion membrane. *Int. J. Hydrogen Energy*. In press. DOI/10.1016/j.ijhydene.2015.04.159
- [2] Siracusano, S., Van Dijk, N., Payne-Johnson E., Baglio V., Aricò, A.S., Nanosized IrOx and IrRuOx electrocatalysts for the O₂ evolution reaction in PEM water electrolyzers. *Applied Catalysis B: Environmental* Volume 164, 2015 pp. 488-495.



SURICAT, A PROJECT DEDICATED TO STABLE PEMFC CATALYST SUPPORTS

C. Beauger¹, L. Testut¹, G. Ozouf¹, S. Berthon-Fabry¹, G. Cognard², M. Chatenet², F. Maillard², S. Cavaliere³, D. Jones³, L. Guetaz⁴, P.A. Jacques⁴, A. Mosdale⁵ and R. Mosdale⁵

1 MINES ParisTech, PSL Research University, PERSEE - Centre procédés, énergies renouvelables et systèmes énergétiques, CS 10207 rue Claude Daunesse F-06904 Sophia Antipolis Cedex, (France)

2 Univ. Grenoble Alpes, UMR CNRS 5279, LEPMI, F-38402 St Martin d'Hères, (France)

3 Univ. Montpellier 2, UMR Agregats Interfaces & Mat Energie 5253, Inst. Charles Gerhardt Montpellier, CNRS, Pl. Eugene Bataillon, F-34095 Montpellier 5, (France)

4 CEA Grenoble, LITEN, DEHT, F-38054 Grenoble, (France)
5 Paxitech, F-38130 Echirolles, (France)

Abstract - Durability of current membrane electrode assemblies (MEAs) used in proton-exchange membrane fuel cells (PEMFC) is limited by the corrosion of the high surface area carbon (HSAC) supports in real operating conditions. Among the different strategies used to tackle this problem, using metal oxides as catalyst supports reveals promising. Doped TiO₂ and doped SnO₂ nanofibers (NF) or aerogels (AG) with morphologies appropriate for efficient mass-transport along with improved electronic conductivity (once doped with Nb or Sb) have been prepared. Pt nanoparticles were then successfully deposited on their surface via different routes. First results obtained on MEAs based on Pt/doped SnO₂ NF showed increased stability compared to conventional Pt/C during accelerated stress tests (AST).

Index Terms – Metal oxides, catalyst support, PEMFC, durability.

I. INTRODUCTION

Proton Exchange Membrane Fuel Cell (PEMFC) are clean and efficient energy converters, producing electricity and heat by catalytic oxido-reduction of hydrogen and oxygen. The power range accessible from watts to megawatts provides access to a wide range of applications (transport, portable or stationary). However, they still suffer from limitations that

hinder their widespread deployment and mass marketing; in particular, the durability of catalyst supports (high surface area carbon blacks) in real PEMFC operating conditions remains critical.

The SURICAT project, funded by the French National Research Agency (ANR) and supported by Capenergies and Tenerrdis, aims at developing new cathode catalyst supports based on metal oxides (MOx). The synthesized supports should meet four basic criteria: i) be electron-conducting, ii) allow the deposition of metal catalyst nanoparticles with good electrocatalytic activity for the oxygen reduction reaction (ORR), iii) be corrosion resistant in accelerated aging tests as well as under real PEMFC operating conditions and iv) have a texture suited to the preparation of efficient MEAs. The research programme focused on two matrices, TiO₂ and SnO₂, four dopants, Nb, Ta, V and Sb and two morphologies, nanofibers and aerogels.

Based on promising results, two metal oxides were selected, and doped with V, Nb, Ta or Sb. The metal oxides (MOx) were synthesized by various methods in order to evaluate the impact of i) the support on the spatial distribution of the catalyst and ii) the structure and morphology of the MOx support on the



PEMFC performance. A selection process based on the four criteria (conductivity, electrocatalytic activity for the ORR, robustness and morphology) was used throughout the development chain (support matrix synthesis, deposition of electrocatalysts, and manufacture of catalytic layers) to select the best candidates.

The selected MO_x were then used to prepare MEAs. Their electrochemical performance and their robustness were evaluated in single cell test bench. The performance of the best Pt/MO_x electrocatalysts was compared to that of a conventional carbon-supported reference catalyst (Pt/C). Finally, the MO_x support with higher performance (specific power and durability) will be implemented and evaluated in a small portable system.

II. MAJOR RESULTS

A. Support synthesis

TiO₂, SnO₂ and their doped counterparts were synthesized as nanofibers (NF) and aerogels (AG) following electrospinning and sol-gel routes, respectively (Figure 1). Initial results allowed to identify two formulations of interest for PEMFC applications: 1) titanium dioxide doped with niobium (Nb) to 10 at.% (Ti_{0.9}Nb_{0.1}O₂) and 2) tin dioxide doped with antimony (Sb) to 10 at.% (Sn_{0.9}Sb_{0.1}O₂). Doping with Sb increased the electronic conductivity of tin dioxide (SnO₂) to 1 S/cm, *i.e.* a 5 to 6 orders of magnitude increase compared to undoped SnO₂. The specific surface areas of the synthesized materials ranged from 20 m²/g (Ti_{0.9}Nb_{0.1}O₂-NF) to 80 m²/g (Sn_{0.9}Sb_{0.1}O₂-AG).

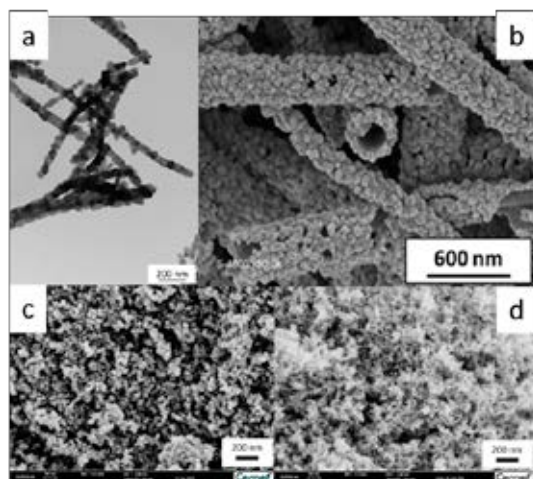


Fig. 1. Scanning electron microscopy images of TiO₂ (left) and SnO₂ (right) based materials (top: NF, bottom: AG)

B. Pt deposition and electrochemical characterization

Different procedures were used to deposit Pt nanoparticles on the MO_x surface. The synthesized Pt/MO_x featured interesting catalytic activity for the ORR [1] and improved durability compared to conventional Pt/C [2].

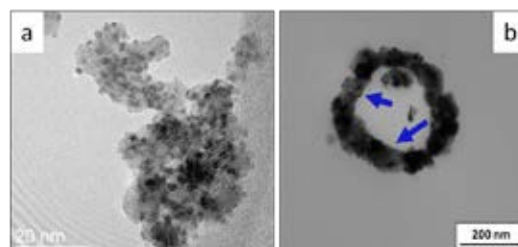


Fig. 2. Transmission electron microscopy images of a: Pt/SnO₂:Sb AG and b: Pt/SnO₂:Nb NF

C. Preliminary single cell test

Single cell tests and ASTs were made using TiO₂:Nb and SnO₂:Sb NF as supports [2]. The MEA cell voltages at $j = 1$ A/cm² are respectively 0.4 and 0.5 V and max. power densities, 0.4 and 0.6 W/cm². The durability of the synthesized Pt/MO_x and the reference Pt/C was evaluated by performing 1,200 square potential cycles between 0.9 and 1.4 V vs. RHE with a holding time of 3 s at each potential, under H₂/O₂ (1.5/2), $T = 80$ °C and 100 % relative humidity. Interestingly, although Pt/SnO₂:Sb and Pt/SnO₂:Nb-based cathodes featured lower initial performance than Pt/C, the catalytic trend is inverted after the AST. Figure 3 shows that Pt/SnO₂:Sb is much more stable than Pt/C (-0.025 V vs. 0.4 V at $j = 1$ A/cm²).

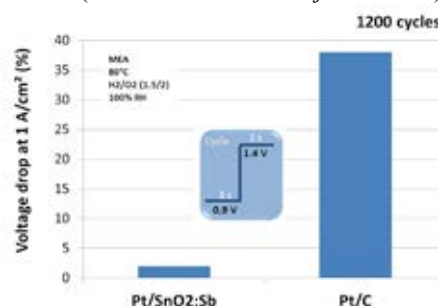


Fig. 3. Comparison of MEA voltage drop at $j = 1$ A/cm² for Pt/SnO₂:Sb and Pt/C after the AST conducted in single cell

III. CONCLUSION

TiO₂ and SnO₂, as NF or AG, are potential alternative catalyst supports to HSAC supports used in PEMFC. With adequate morphology, once doped and after Pt deposition, they show high electronic conductivity enough and appropriate catalytic activity to replace C in PEMFC. Improved durability compared to Pt/C was also demonstrated on MEA.

ACKNOWLEDGMENT

ANR PROGELEC programme (ANR-12-PRGE-007), Capenergies and Tenerrdis for funding.

REFERENCES

- [1] G. Ozouf et al., *Fall meeting ECST 2015* (accepted)
- [2] I. Savych et al. *Phys.Chem.Chem.Phys.* **2015**, *17*, 16970
- [3] S. Cavaliere et al. *ChemElectroChem* **2015**, DOI: 10.1002/celec.201500330.



WATER NUCLEATION MECHANISM IN PLANAR BREATHING FUEL CELLS

E. Coz*, J.Théry*, P.Boillat**, V.Faucheux*, D. Alincant*, I. Depatie***,
P. Capron*, G. Gébel*

*CEA, 17 rue des Martyrs, 38054 Grenoble Cedex 9 (France)

**CEA (France) and Paul Scherrer Institut -CH-5232 Villigen PSI (Switzerland)

*** Intelligent Energy, 17 rue des Martyrs, 38054 Grenoble Cedex 9 (France)

Contact : jessica.thery@cea.fr ; erwan.coz@cea.fr

Abstract – An innovative planar breathing fuel cell architecture is presented. This design offers an electron collection solution which is decoupled from water management issues. Various commercial insulating microporous materials were compared, and the importance of the thickness of the microporous layer with respect to back-diffusion and flooding occurrence was evaluated, via operando neutron radiography.

Index Terms – Neutron radiography; PEM Fuel cell; Water management;

I. INTRODUCTION

The demand for portable energy sources has dramatically increased with the development of high energy consuming mobile devices, such as smartphones and notebook computers. The autonomy of these products is of great concern, and Micro-fuel cells, especially Proton Exchange Membrane Fuel Cell (PEMFC) have been investigated as an alternative to batteries, due to their high energy densities and efficiencies.

In order to fit the current and voltage requirements of the majority of portable electronic devices, planar arrays, comprising multiple adjacent cells connected in series, have been developed [1, 2, 3, 4]. For a great majority of these planar arrays, based upon the well-known stacked fuel cell architecture, the same element acts as current collector and water management layer. The present design differs from the classical PEMFC architecture since the electron collection elements are quasi-independent from the water management layers. Understanding the mechanism for water management in fuel cell is a crucial issue, and is even more critical for breathing fuel cells in the absence of possible control on the humidity level and the temperature of the inlet air flow. Several studies [5, 6, 7, 8] proved the efficiency of neutron radiography to visualize and quantify water in an operating PEMFC, but water management optimization for in-plane connected fuel cells has been scarcely investigated. In this study, we investigate the efficiency of different cathode water management layers on a planar air-breathing fuel cell array, working in dead-end mode. Liquid water distribution is visualized thanks to neutron radiography and correlated to

performances (power at various voltages) and membrane hydration followed by Electrochemical Impedance Spectroscopy.

II. EXPERIMENTAL METHOD

A. Fuel cell array architecture

The studied planar fuel cell array is composed of in plane interconnected cells, with a breathing cathode.

A PCB support ensures the mechanical strength, current collection and cell interconnections. More precisely, a reinforced Nafion® (XL) membrane is first coated on both sides with catalyst ink, composed of C/Pt (Tanaka 70%), 5% Nafion® dispersion, solvent being a mixture of water and Isopropanol. The current collection is achieved by a 150 nm thick porous gold layer. Gold / Nickel coated copper traces ensure the interconnection of the different cells in series. Hydrogen is supplied via a laboratory-designed multi stage anodic chamber, providing a homogeneous gas feed.

On the cathode side, insulating porous water management layers are sandwiched between the electrode and the metal grid of the test fixture (see Figure 1).

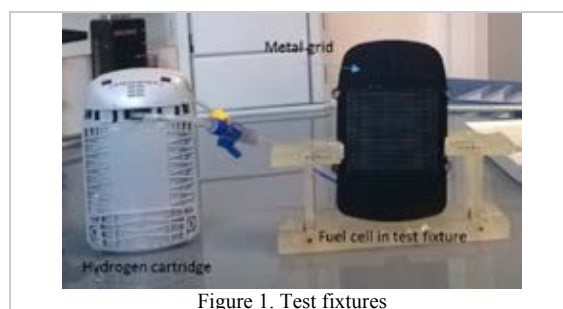


Figure 1. Test fixtures

B. Electrochemical characterizations

Voltage controlled steps were imposed via a Potentiostat (Voltalab PGZ 402 + HC Booster HCB020). Each individual cell voltage was followed thanks to a 10-channel voltage recorder and electrochemical impedance spectroscopy at high

frequency was performed after each step to measure the internal resistance of the fuel cell.

C. Water visualization

The neutron imaging experiments were carried out on G3bis-Imagine beamline at LLB Saclay, that delivers a flux of 2.10^7 neutrons/s/cm². Images of the working fuel cells were acquired, corrected (backscattered intensity, neutron source intensity), and divided by the dry reference, to visualize only water contribution. Water thickness was then calculated using Beer-Lambert's law.

III. RESULTS

Drying processes at high current density were characterized, as well as flooding behavior during long time operation. Influence of the cathode water management layer and correlation with the fuel cell design were studied. For example, it was observed that the thickness of the insulating microporous layer impacts strongly the water patterns. Using a thin hydrophobic insulating microporous (MPL) led to the water patterns shown on Figure 2-b), attributed to water condensation on the cathode water management layer, near the metal grid. In opposition, Figure 2-a) exhibits high water accumulation near the conductive paths and dramatic flooding. From the evaluation of water domains thicknesses and in correlation with the fuel cell design, we have been able to determine that for configuration 2a, the majority of liquid water accumulates at the anode side.

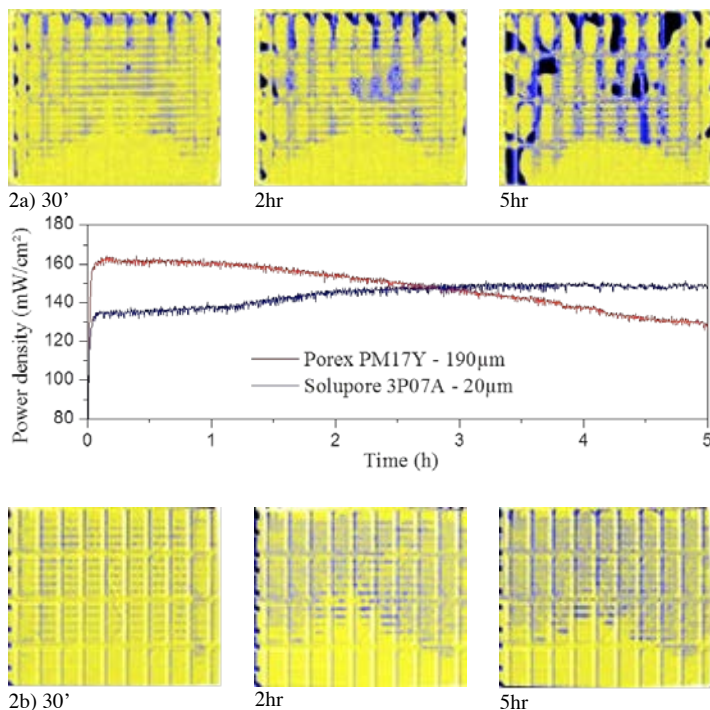


Figure 2: Water pattern during long time operation at 0.7V/cell with a) thick MPL (Porex PM17Y) b) thin MPL (Solupore 3P07A)

In the present case, the coverage of the electrode by the microporous layer and its thickness are suspected to control the repartition of water. This study led to the development of an innovative porous material which shows promising results.

IV. CONCLUSION

Different microporous layers were placed on the cathode current collector of an air-breathing PEM fuel cell array. The role of thickness and conformation was found to be crucial for the nucleation of liquid water domains. Preferential condensation zones which are design dependent were depicted. We observed that back-diffusion occurrence is correlated with the formation of liquid domain on the cathode side.

ACKNOWLEDGMENT

The authors would like to thank Frederic Ott and Camille Loupiac working on the Imagine beamline of Laboratoire Leon Brillouin (LLB Saclay, France) [9], for their support and availability.

REFERENCES

- [1] N. Bussayajarn, H. Ming, K.K. Hoong, W.Y. M. Stephen, C.S. Hwa, Planar air breathing PEMFC with self-humidifying MEA and open cathode geometry design for portable applications, *International journal of hydrogen energy* 34 (2009) 7761-7767
- [2] S-S. Hsieh, C-F. Huang, Design, fabrication and performance test of a planar array module-type micro fuel cell stack, *Energy Conversion and Management* 76 (2013) 971-979
- [3] R. Hahn, S. Wagner, A. Schmitz, H. Reichl, Development of a planar micro fuel cell with thin film and micro patterning technologies, *Journal of Power Sources* 131 (2004) 73-78
- [4] X. Zhang, D. Zheng, T. Wang, C. Chen, J. Cao, J. Yan, A preliminary study of a miniature planar 6-cell PEMFC stack combined with a small hydrogen storage canister, *Journal of Power Sources* 166 (2007) 441-444
- [5] D. Kramer, J. Zhang, R. Shimoï, E. Lehmann, A. Wokaun, K. Shinohara, G. G. Scherer, In situ diagnostic of two-phase flow phenomena in polymer electrolyte fuel cells by neutron imaging. Part A. Experimental, data treatment, and quantification, *Electrochimica Acta* 50 (2005) 2603-2614
- [6] M. A. Hickner, N. P. Siegel, K. S. Chen, D. N. McBrayer, D. S. Hussey, D. L. Jacobson, M. Arif, Real-Time Imaging of Liquid Water in an Operating Proton Exchange Membrane Fuel Cell, *Journal of The Electrochemical Society*, 153 (5)902-A908 (2006)
- [7] R. Satija, D.L. Jacobson, M. Arif, S.A. Werner, In situ neutron imaging technique for evaluation of water management systems in operating PEM fuel cells, *Journal of Power Sources* 129 (2004) 238-245
- [8] D.S. Hussey, D.L. Jacobson, M. Arif, J.P. Owejan, J.J. Gagliardo, T.A. Trabold, Neutron images of the through-plane water distribution of an operating PEM fuel cell, *Journal of Power Sources* 172 (2007) 225-228
- [9] F. Ott, C. Loupiac, S. Désert, A. Hélarly, P. Lavie, IMAGINE: a cold neutron imaging station at the Laboratoire Léon Brillouin, *Physics Procedia* (2015)



ASSESSMENT OF THE TECHNICAL AND ECONOMICAL PERFORMANCES OF A CHCP SYSTEM BASED ON SOFCs

L. Lipardi*, A.L. Facci**, E. Jannelli* and S. Ubertini**

*University of Naples “Parthenope”, Engineering Department,
Napoli (Italy)

**University of Tuscia, Industrial Engineering School -
DEIM, Viterbo (Italy)

Abstract - We here present the technical and economical performances of a small scale trigeneration plant based on solid oxide fuel cells and a double effect absorption chiller. The plant performances are assessed following an optimal control strategy, as a function of energy demands and prices, and of rated and part load efficiencies of each energy converter.

Index Terms - Combined Heat, Cooling and Power, Double Effect Absorption Chiller, Optimal Management, SOFC.

I. INTRODUCTION

While several large scale applications (i.e. up to Mega-Watts of electrical power) of CHCP plants with absorption chillers exist, there is still little experience on small scale plants [1]. In the last decade some researchers have studied the possible use of SOFCs for trigeneration [2-8]. Most of them focused on large power applications [2,4-7], given the typical sizes of absorption chillers. Moreover, to the best of our knowledge, nobody have studied such a system within an integrated energy-consumption environment, typical of distributed power generation, that allows studying the behavior in regulated power conditions of SOFCs (i.e. electrical efficiency increases with decreasing loads) could be evaluated for CHCP applications.

The purpose of this paper is to design and assess the technical and economical performances of a small scale trigeneration plant based on solid oxide fuel cells. Specifically, we envisage the possibility to realize a 30 kW plant that will be utilized to satisfy a residential energy demand of electrical, thermal and chilling energy. The design of each subsystem is optimized to minimize the energy losses.

II. DESIGN OF THE ENERGY SYSTEM

The studied power plant (fig. 1) features:

- n 24 stacks SOFC systems of 1.25 kW net AC

- nominal power operating (700 °C – 750 °C) [9];
- an absorption chiller of 23 kW of chilling power;
- a fuel boiler of 200 kW of thermal power able to satisfy the peak thermal demand;
- a mechanical chiller of 80 kW of chilling power able to satisfy the peak chilling demand.

The system is fed by methane which is internally reformed into a H₂-rich fuel gas. The fuel utilisation factor is set to 80% and the excess of fuel from the anode is burned in a combustor.

The system allows to recover heat from the exhaust flow at about 180°C, resulting in an overall first-law efficiency of 90%. Figure 2 shows the electric and thermal efficiencies of the energy system for different values of the input power.

The exhaust gases of the SOFC can be also used to directly feed a double effect absorption chiller. The coefficient of performance (COP) of the chiller is depicted as a function of its load in fig. 2, which also reports its main characteristics.

A. Primary Energy Saving

The PES is calculated considering the energy demand of 10 domestic users and reference electrical ($\eta_e = 0.45$), thermal ($\eta_t = 0.90$) and chilling efficiencies ($\eta_{AHP} = 0.46$, $COP_{rif} = 3.0$).

$$PES = 1 - \frac{F_{CHP}}{\frac{E_{CHP}}{\eta_e} + \frac{E_{fCHP}}{COP_{rif} \cdot \eta_{AHP}} + \frac{Q_{CHP}}{\eta_t}}$$

which results 36%, 29% and 33% when the system operates as CHP, CCP and CHCP, respectively.

III. OPTIMAL MANAGEMENT

The energy system is modeled through a phenomenological approach, that accounts for each equipment rated and off design performances, as well as their integration issues [10-13]. The optimal management that minimizes the total daily cost, is determined using backward dynamic programming through a



weighted and oriented graph [11,12].

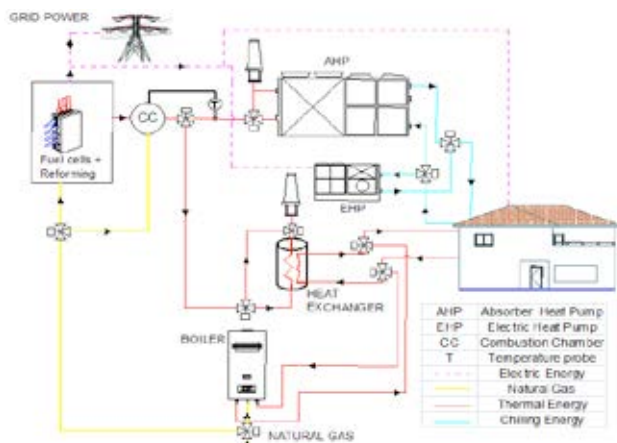


Fig. 1 – Schematic of the power plant.

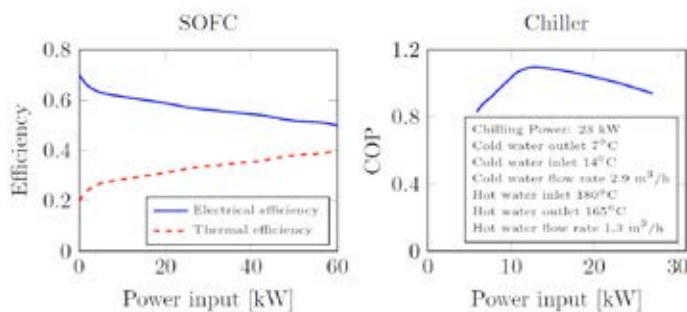


Fig. 2 - Electric and thermal efficiencies of the system and main characteristics of the chiller.

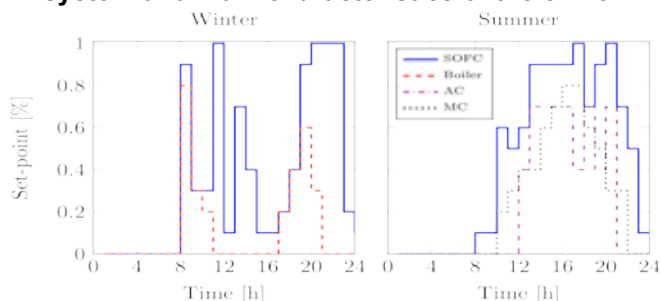


Fig. 3 – Optimal set-points of the power plant components.

The trigeneration plant is compared to separate production in terms of total energy cost and primary energy consumption. The inputs are the typical winter and summer energy demand, as well as fuel and electricity prices, for a residential application. Cogeneration reduces the total energy cost by 85% for the summer case and by 89% for the winter case, with respect to separate production. Primary energy saving is comprised between 21% (summer) and 31% (winter).

IV. CONCLUSION

In this work we present a possible application of a novel

CHCP plant based on the combination of pre-commercial SOFCs and a commercial small size double effect absorption chiller. Such a system allows a PES between 29% and 36% in nominal operating conditions. When the system is combined in a residential power plant, with optimal operation, the PES is in the range 21% - 31% and the economical benefit reaches 89%.

ACKNOWLEDGMENT

This research is supported by the Ministry of Education, Universities and Research Grant PON_03_PE_00109_1 “Fuel Cell Lab”.

REFERENCES

- [1] E. Jannelli, M. Minutillo, R. Cozzolino, G. Falcucci, Thermodynamic performance assessment of small size CCHP system unit numerical models, *Energy*, 65, 2014, 240–249.
- [2] M. Burer, K. Tanaka, D. Favrat, K. Yamada, Multi-criteria optimization of a district cogeneration plant integrating a solid oxide fuel cell-gas turbine combined cycle, heat pumps and chillers, *Energy*, 66, 1 2014, 387–400.
- [3] Z. Yu, J. Han, X. Cao, W. Chen, B. Zhang, Analysis of total energy system based on solid oxide fuel cell for combined cooling and power applications, *Int J Hydrogen Energy*, 35, 7, 2010, 2703–2707.
- [4] F. A. Al-Sulaiman, I. Dincer, F. Hamdullahpur, Energy analysis of a trigeneration plant based on solid oxide fuel cell and organic Rankine cycle, *Int J Hydrogen Energy*, 35, 10 2010, 5104–5113 2010.
- [5] F. A. Al-Sulaiman, I. Dincer, F. Hamdullahpur, Exergy analysis of an integrated solid oxide fuel cell and organic Rankine cycle for cooling, heating and power production, *J Power Sources*, 195, 8, 2010, 2346–2354.
- [6] F. Ranjbar, A. Chitsaz, S.M.S. Mahmoudi, S. Khalilarya, M. A. Rosen, Energy and exergy assessments of a novel trigeneration system based on a solid oxide fuel cell, *Energy Conversion and Management*, 87, 318–327, 2014.
- [7] A. Al-Qattan, A. El Sherbini, K. Al-Ajmi, Solid oxide fuel cell application in district cooling, *J Power Sources*, 257, 2014, 21–26.
- [8] Y. Wang, Y. Shi, M. Ni, N. Cai, A micro tri-generation system based on direct flame fuel cells for residential applications, *Int J Hydrogen Energy*, 39, 11, 2014, 5996–6005.
- [9] T. Pfeifer, L. Nusch, D. Lieftink, S. Modena, System design and process layout for a SOFC micro-CHP unit with reduced operating temperatures, *Int J of Hydrogen Energy*, 38, 1, 2013, 431–439.
- [10] D. Chiappini, A. L. Facci, L. Tribioli, S. Ubertini, SOFC Management in distributed Energy Systems *J. Fuel Cell Sci. Technol*, 8 (3), 031015, 2011.
- [11] A. L. Facci, L. Andreassi, S. Ubertini. Optimization of CHCP systems Operation Strategy Using Dynamic Programming, *Energy*, Volume 66, 1 2014, 387–400.
- [12] A. L. Facci, L. Andreassi, F. Martini, S. Ubertini, Comparing Energy and Cost Optimization in Distributed Energy Systems Management, *Journal of Energy Resources Technology*, 136 (3), 032001, 2014.
- [13] F. Cappa, A. Facci, S. Ubertini, Proton exchange membrane fuel cell for cooperating households: A convenient combined heat and power solution for residential applications, *Energy*, doi:10.1016/j.energy.2015.06.092, 2015.



DETERMINATION OF REVERSIBLE AND IRREVERSIBLE VOLTAGE LOSSES IN PEM FUEL CELLS

K.A. Friedrich, P. Gazdzicki, M. Schulze
German Aerospace Center, Institute of Engineering
Thermodynamics, Pfaffenwaldring 38-40, 70569 Stuttgart
(Germany)

Abstract – This contribution focuses on a detailed description of voltage loss rates of PEM fuel cells and particularly on the discrimination between reversible degradation that can be recovered by a specific change of operation conditions and irreversible voltage losses. A major motivation of our work is the lack of common description procedures and determination approaches of voltage losses in durability tests of fuel cell; this issue leads to severe difficulties in the comparison of results obtained by different institutions or within different projects especially if only one value for a degradation rate is reported.

Index Terms – reversible degradation, irreversible degradation, performance recovery, automotive, PEMFC

I. INTRODUCTION

To provide a reliable prediction of fuel cell life time it is necessary to distinguish between reversible degradation, that leads to a temporary loss of performance, and irreversible degradation that leads to permanent voltage losses and is the limiting factor of fuel cell life time. Examples for reversible degradation are contaminations of the catalyst by gas impurities or the flooding of gas diffusion media by water. Irreversible degradation can be caused by critical events or harsh conditions such as fuel starvation or prolonged OCV leading to chemical and physical changes of different MEA components (carbon support, catalyst layer, membrane) [1–3]. Moreover, irreversible degradation may be linked to reversible effects. For instance, flooding of electrodes leading to immediate, but recoverable losses is known to promote catalyst dissolution being a permanent degradation effect [4]. Generally, poor water management is recognized to be a major reason for degradation phenomena in PEM fuel cells [5].

In our presentation we provide a comparison and assessment of various approaches to determine voltage decay rates in durability test of PEM fuel cells. In particular, we address the

problem of the discrimination between reversible and irreversible voltage loss rates. It is generally observed that a soak time interruption or a shutdown of a cell or stack leads to considerable recovery of voltage losses; in the following the soak time is considered to recover 100% of reversible losses since, within this study, the recovery by all other tested procedures was less than the one due to soak time. In this context we systematically assess various voltage recovery procedures such as cell shutdown, potential sweeping, OCV, or N₂ purging to better understand the reason of voltage recovery upon soak time interruption.

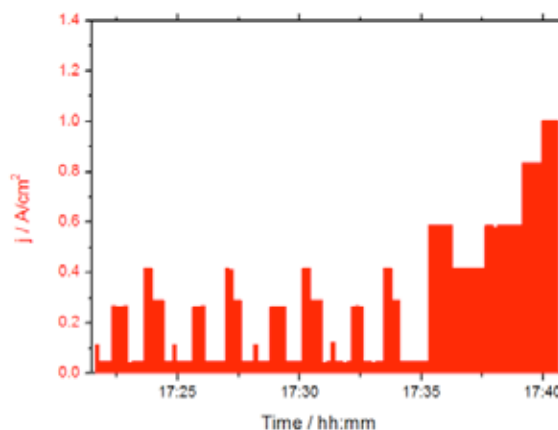


Fig. 1. The dynamic load profile used in this study.

II. EXPERIMENTAL

For the degradation tests 25 cm² single cells with single channel serpentine were used. As samples conventional 5-layer MEAs were used with PFSA membranes, Pt-based catalysts and

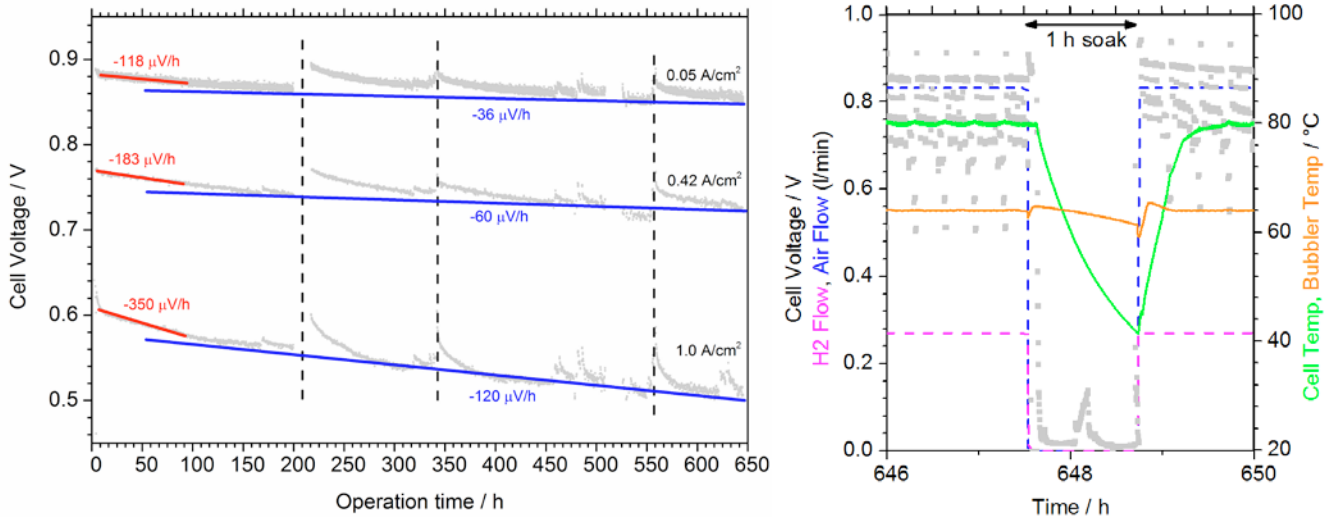


Fig. 2. LEFT: Single cell FC-DLC durability test with refresh interruptions discriminating reversible and irreversible degradation. Soak times are labelled by the dashed lines. RIGHT: Cell voltage, gas flows, cell and bubbler temperatures during a refresh.

hydrophobized carbon fiber substrates with micro porous layers as GDLs. The applied test protocol provided by the FCH JU project StackTest, is based on the European Fuel Cell Dynamic Load Cycle (FC-DLC), see Figure 1. The test contains systematic interruptions for refresh and diagnostics by means of polarization curves, cyclic voltammetry (CV), and impedance spectroscopy (EIS). The electrochemical tests were performed using a homemade test bench and an electrochemical impedance station from Zahner.

III. SELECTED RESULTS

A single cell durability test performed in cycling conditions with regular interruption by soak time is presented in Figure 2 (left). Apparently the initial degradation rates before the first refresh (red) exhibit degradation rates that are three times higher than those corresponding to irreversible degradation (blue). Hence, durability test without discrimination between permanent and recoverable losses are not suitable to predict cell durability since the observed degradation rate corresponds to the reversible one. Moreover, the reversible degradation may be sensitive to specific flow fields, gas quality etc. In the case of the irreversible decay rate the effect of these influences are reduced.

The behavior of the cell during soak time for recovery of reversible losses is provided in Figure 2 (right); the changes of each parameter (voltage, flows, temperatures, ...) are considered as being possibly responsible for the recovery effect and have been analyzed accordingly. Thereby, voltage recovery due to specific refresh procedures, are different at different current densities, e.g. potential sweep recovers 25% and 15% of reversible losses at 0.2 and 0.8 A/cm², respectively. Changing

the humidity, being reported to be a key factor regarding degradation [3], leads to corresponding improvements by 60% and 70%. Possible explanation of this effect would be a reduction of H₂ cross over due to membrane swelling or filling of pinholes or an increase of ionic conductivity of the ionomer.

An open question is the recovery of voltage losses at very low loads of < 0.2 A/cm² that are recovered by soak time but could not be recovered by any of the other tested approaches.

ACKNOWLEDGMENT

The research leading to these results has received funding from the European Union's Seventh Framework Programme (FP7/2007-2013) for Fuel Cell and Hydrogen Joint Technology Initiative under Grant No. 303452 (Impact).

REFERENCES

- [1] M. Kim, N. Jung, K. Eom, S.J. Yoo, J.Y. Kim, J.H. Jang, H.J. Kim, B.K. Hong, E. Cho, *J. Power Sources* 266 (2014) 332.
- [2] S. Helmly, B. Ohnmacht, P. Gazdzicki, R. Hiesgen, E. Gulzow, K.A. Friedrich, *J. Electrochem. Soc.* 161 (2014) F1416.
- [3] S. Kundu, M. Fowler, L.C. Simon, R. Abouatallah, *J. Power Sources* 182 (2008) 254.
- [4] T. Ous, C. Arcoumanis, *J. Power Sources* 240 (2013) 558.
- [5] N. Yousfi-Steiner, P. Moçotéguy, D. Candusso, D. Hissel, A. Hernandez, A. Aslanides, *J. Power Sources* 183 (2008) 260.



INFLUENCE OF LITHIUM ON THE SINTERING BEHAVIOR AND ON ELECTRICAL PROPERTIES OF GD-DOPED CERIA ELECTROLYTE FOR IT-SOFC

G. Accardo,* C. Ferone,* R. Cioffi,* E. Di Bartolomeo**, S. Licoccia**

* Department of Engineering and INSTM Research Unit, University of Naples "Parthenope", Centro Direzionale Isola C4, 80143, Naples, Italy

**Department of Chemical Science and Technology, University of Rome "Tor Vergata", Via della Ricerca Scientifica, 1, 00133 Rome, Italy

Abstract - The main purpose of this work is to verify the influence of lithium, as sintering aid, on the densification and electrical conductivity of gadolinium-doped ceria electrolytes. LiGDC pellets, containing 1 and 2 mol% of lithium, have been prepared from powders synthesized by sol gel combustion reaction. A control sample, without lithium addition was also prepared as reference benchmark. Pellets were sintered at 1250° and 1500°C with a dwell time of 3h. During sintering, lithium forms a thin liquid film at grain boundary which improves densification. A high dense electrolyte has been obtained at 1250°C, compared to the conventional sintering temperature of 1500°C. Over 97% of relative density was found. A small amount of lithium not only promoted densification but as well ionic mechanism in the temperature range of 500-800°C with a maximum at 800°C of $5.2 \cdot 10^{-2}$ S/cm².

Index Terms – gadolinium-doped ceria, ionic conductivity, sintering, sol gel synthesis, solid oxide electrolyte, solid oxide fuel cell.

I. INTRODUCTION

Cerium oxide, pure or doped, is the most studied solid conductor of oxygen ions in solid electrolyte fuel cells that operate at intermediate temperatures (500-800°C). Gadolinium is the most effective dopant for ceria solid solutions for its ionic properties [1-2]. Its ionic conductivity is influenced by purity of raw materials used, presence of sintering additives and processing operations as grinding and thermal treatments (calcination, sintering and aging), which determine the microstructure of the sintered material. Among process parameters, sintering temperature has the most relevant impact on electrolyte performance and fabrication costs. A way to lower the sintering temperature is to use some additives such as Cu, Co, Fe, Mn, Li and Zn as sintering aids. This method can effectively reduce the sintering temperature while ensuring the proper densification of the material. In order to develop intermediate temperature electrolyte material for solid oxide fuel cell, Gd³⁺ and Li⁺ co-doped ceria based materials have

been synthesized and characterized. Lithium was added in nitrate form during a sol gel synthesis. The advantages of this procedure are: simple preparation, high energy efficiency, short time-to-product, low processing cost, and the possibility to reduce operating temperature [3].

II. MATERIALS AND METHODS

Crystalline ceria electrolyte, doped with 20 mol% of gadolinia (Ce_{0.8}Gd_{0.2}O_{1.9}) was synthesized by a modified sol-gel technique involving cerium nitrate as oxidizer and citric acid as fuel, with a molar ratio of 1:1. During sol gel synthesis lithium was added to mixture, in nitrate form, to obtain a final powder with a lithium content of 1 and 2 mol%. A pure gadolinium-doped ceria electrolyte was also prepared as reference. After drying at 250°C and calcination at 600°C pellets were prepared in the shape of disks. Sintering was performed using different rates for heating and cooling, 3°C/min and 10°C/min respectively, with a dwell at 1250°C or 1500°C for 3h.

The sintered pellets microstructure was determined by Scanning Electron Microscopy and Energy Dispersive x-ray Scanning analysis. Electrical conductivity was evaluated by Impedance Spectroscopy.

III. RESULTS AND DISCUSSION

SEM micrographs and relative density values of gadolinium-doped ceria, pure and co-doped at different sintering temperature, are reported in Figure 1. Pure GDC sintered at 1250°C has the lowest density. In fact, as envisaged by Figure 1a), the morphology obtained is inadequate to enhance transport properties, due to the clear presence of discontinuous microstructural elements like fractures, large pores and unshaped grains, as result of the low temperature sintering process. In fact, by increasing the sintering temperature, pure GDC pellets (Figure 1d) exhibit a continuous and dense morphology, with a smaller average grain size (700 nm) and relative density of 96%. By adding 1%mol of lithium, pellets



sintered at 1250°C (Figure 1b) have similar morphology and a comparable grain size of pure GDC sintered at 1500°C. The average grain size was observed to increase with an increase in sintering temperatures while it seems not influenced by lithium content.

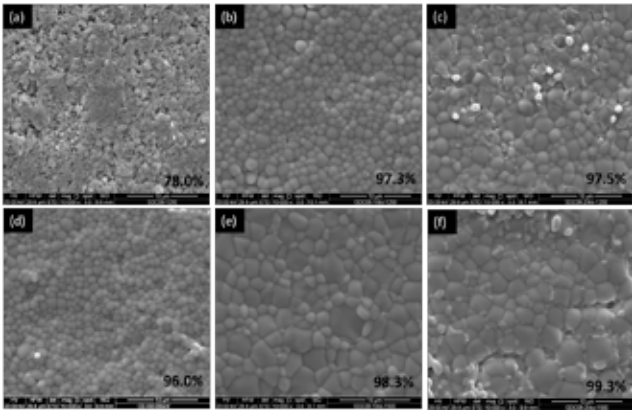


Fig. 1. SEM micrograph and relative density of pellets co-doped with 0 mol % (a), 1 mol % (b), 2 mol % (c), of Lithium sintered at 1250°C and 0 mol % (d), 1 mol % (e), 2 mol % (f), of Lithium sintered at 1500°C.

The role of lithium is to promote densification with a slight effect on grain size. Lithium, within the compacted powders, acts as melting agent and facilitates the formation of a thin liquid film at the grains boundaries during sintering. As the grains grow, the presence of such film aids the complete adhesion, stabilizes the shape of the grains and reduces the voids throughout the pellet. The lithium layer effect is proofed in the micrographs of Figure 1d) and 1e) where dopant is in excess in the system and, as result of rearrangement, although it promotes densification, an amorphous phase is formed on the surface of the grains filling the voids but an irregular morphology arises.

The temperature dependence of the ionic conductivity of different LiGDC pellets is illustrated in the Arrhenius plots of Figure 2. They cannot be fitted by a single straight line. This implies that the conduction mechanism changes at a transition temperature. According to the Arrhenius plots of all samples, we can define two parts, related to a low temperature and a high temperature regime, in which the linearity of the plots change. Thus, also the activation energy changes with temperature. The change in slope, observed around 500°C, can be explained by changes in the behavior of the defects in the GDC material. At low temperature range, the oxygen vacancies, limit the total ionic conductivity. In our study, the grain-boundary conductivities are roughly 4 orders of magnitude lower than the electrolyte conductivities for all samples. The high resistances associated to the small grain boundary conductivity imply that the grain boundary plays an important role in limiting the oxygen ionic transport.

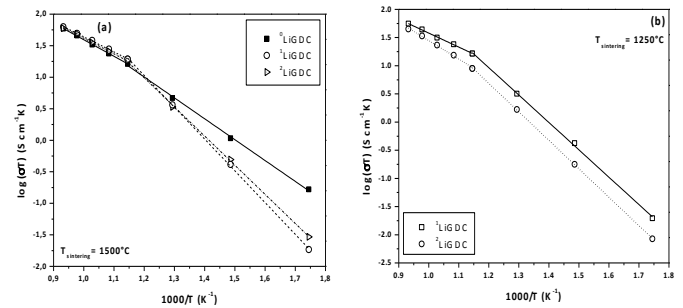


Fig. 2. Arrhenius plot for LiGDC pellets sintered (a) at 1500°C and (b) 1250°C.

Electrical behavior of ⁰LiGDC sintered at 1250°C was not studied. Its densification is inadequate to enhance ionic conductivity. Total ionic conductivity of ¹LiGDC sintered at 1250°C, at 800°C, is 5.2·10⁻² S/cm². This value is very close to the total ionic conductivity of ⁰LiGDC sintered at 1500°C (5.5·10⁻² S/cm²). This can be attributed to their similar morphology and grain size. In this study 1mol% of lithium is sufficient to improve the total conductivity. In fact, by increasing sintering temperature ¹LiGDC has a maximum value in ionic conductivity of 6.0·10⁻² S/cm². ²LiGDC sintered at 1250°C has a lower total ionic conductivity of ⁰LiGDC sintered at 1500°C and, increasing sintering temperature electrolyte has its maximum value of 5.6·10⁻² S/cm². This result is comparable to value of pure GDC but it is lower than the total ionic conductivity calculated for ¹LiGDC at the same sintering temperature.

IV. CONCLUSION

In this work lithium-gadolinium doped ceria electrolytes have been successfully synthesized through sol-gel process. A high dense electrolyte has been obtained at 1250°C, compared to the conventional sintering temperature of 1500°C. The results indicate that even a small amount of lithium has a fundamental microstructural effect that can remarkably promote the densification and affects surface and electrical properties morphology also at a sintering temperature of 1250°C.

REFERENCES

- [1] Esposito, V., Traversa E., Design of electroceramics for solid oxides fuel cell applications: Playing with ceria, Journal of American Ceramic Society 2008; 91(4), pp. 1037–1051.
- [2] Sato, K., Grain-Boundary Structures Associated with Ionic Transport in Gd-Doped Ceria Nanostructured Electrolyte, Journal of Physical Chemical C, 119 (10), 2015, pp. 5734–5738.
- [3] Ferone, C., Accardo, G., Dell’Agli, G., Cioffi, R., Sol-gel Synthesis of gadolinium doped Ceria (Gd–CeO) for intermediate Temperature SOFC Electrolyte, Proceedings of the 5th European Fuel Cell Piero Lunghi Conference, At Rome, Italy



STUDY OF MICROSTRUCTURAL PROPERTIES OF DURABLE ELECTRODES FOR MCFC AND CORRELATION TO LONG-TERM OPERATION OF SINGLE CELLS

D. Frattini*, G. Accardo*, V. Cigolotti**, R. Cioffi*, C. Ferone*, S.P. Yoon*** and J. Han***

*Department of Engineering, University of Naples Parthenope & UdR INSTM of Naples Parthenope, Centro Direzionale di Napoli Is. C4, 80143 Naples (Italy)

** Italian National Agency for New Technologies ENEA Portici Research Center, P.le E. Fermi, 80055 Portici, Naples (Italy)

*** Fuel Cell Research Center, Korea Institute of Science and Technology, Hwarang-ro 14-gil 5, Seongbuk-gu, Seoul (South Korea)

Abstract - Molten Carbonate Fuel Cell (MCFC) is considered as a clean power generation technology and it is in the early stage of market diffusion. However, the lifetime of MCFC is not long enough, namely 4 years of operation, and this short lifetime causes high maintenance costs and a limited diffusion. The development of durable components of MCFC is very important to compete in the power generation market. In this work, Ni-Al anodes, doped with ZrO₂ and TiO₂ have been successfully prepared for the first time. The addition of these oxides induced microstructural modifications which improved creep resistance and bending strength in MCFC operating conditions. Results showed that creep strain is less than 3-4%, after 100h, under 100psi and 650°C, compared to the 5-7% of commercial anodes currently used. Thus, these new materials are eligible candidates for durable anodes in MCFC applications.

Index Terms – anodes, creep resistance, microstructure, molten carbonate fuel cell

I. INTRODUCTION

State-of-the-art anodes for Molten Carbonate Fuel Cell (MCFC) are represented by Ni alloys, based on Chromium, Aluminum or both, to obtain a sintered and porous material with high performance [1]. The major causes of short lifetime and cell's performance decay are related to microstructural instability, electrolyte loss, gas crossover, poisoning due to sulfur compounds, creep and micro-cracks formation [2]. In particular, mechanical properties can be enhanced by crystal structure imperfection strengthening techniques, using alien atoms or hard oxide particles to block dislocation movements [3,4]. In this work, the use of TiO₂ and ZrO₂ as strengthening oxides for mechanical properties has been carried out for the first time. Samples with different amounts of TiO₂ and ZrO₂ have been fabricated for microstructural and mechanical characterizations. Performances of the new anodes have also been investigated in single cell tests.

II. MATERIALS AND METHODS

A. Fabrication of Ni-Al-ZrO₂/TiO₂ green sheet

Ni-Al alloy anodes, with the addition of different amounts of ZrO₂ or TiO₂, have been prepared using a commercial Ni-Al

alloy powder (Chang Sung Co., Al 5.0% wt, 5 μm), ZrO₂ powder (Alfa Caesar, >99.0%, <1 μm) and TiO₂ powder (Daejung Co., >98%, <1 μm). The fabrication steps for green sheet preparation are illustrated in Fig. 1.

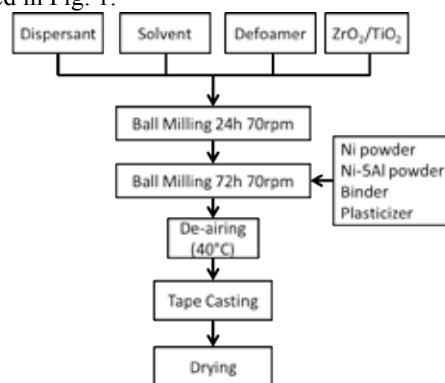


Fig. 1. Fabrication of Ni-5Al-ZrO₂/TiO₂ anodes

At first, ZrO₂ or TiO₂ were mixed with dispersant, solvent and defoamer, and then ball milled for one day. After, Ni-5Al powder, binder and plasticizer were added and ball milled for two days. A small amount of Ni powder was also added as sintering aid. A de-airing step was used to remove trapped air to avoid bubbles formation during drying. Finally, the slurry was tape casted with a doctor blade, and dried in an oven for 3 hours. For each oxide, four different compositions, ranging from 1% to 10% wt., have been prepared and characterized.

B. Characterization techniques

Microstructure of sintered samples has been determined by SEM-EDS (InspectF50, FEI Co.) microanalyses before and after creep test. Further, crystal structure and the modifications induced by oxide insertion have been investigated by means of XRD powder diffraction (Miniflex II, Rigaku Co.). Creep resistance evaluation, of the new anode materials developed, has been carried out on a green sheet specimen of 1×1×0.06 cm³. Creep test system layout and test conditions have been described in details elsewhere [5]. The bending strength was determined according to the ASTM E855-90 standard, after ex-situ sintering

at 650°C. Single cell tests have been carried out to compare performances of modified anodes. The effective area of cells was 100cm² and operating temperature was 650°C. Standard NiO cathode, α -LiAlO₂ matrix and (Li_{0.7},K_{0.3})₂CO₃ electrolyte sheets were used. The inlet gases were a mixture of Air:CO₂=70:30 at cathode and H₂:CO₂:H₂O=72:18:10 at anode. Polarization and ohmic resistance were analyzed by means of EIS (S11287, Solartron).

III. RESULTS AND DISCUSSION

In Fig. 2, diffraction spectra of Ni-Al sintered anodes, doped with ZrO₂, are compared to standard Ni-5% wt Al anodes, i.e. ZrO₂ 0%, and raw Ni-Al powders.

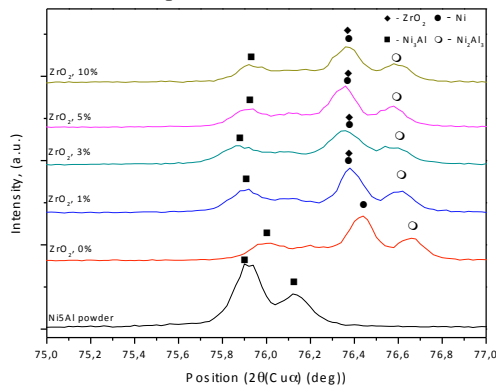


Fig. 2. XRD spectra of Ni-5Al-ZrO₂/TiO₂ anodes

In these spectra, a remarkable peak shift corresponding to the (2,2,0) and (3,0,0) planes, in the Ni-Al alloy crystal structure, is visible. These planes correspond to the crystallographic position of octahedral and tetrahedral vacancies of the Face-Centered Cubic (FCC) structure of Ni-Al alloy, where alien interstitials can be accommodated. The same result is achieved for TiO₂-doped samples. The shift can be ascribed to the interaction between the FCC structure of alloy and the Face-Centered Monoclinic (FCM) structure of ZrO₂. In addition, these planes intersect the (1,1,1) plane of the FCC structure, thus blocking dislocation movement due to creep [5]. The bending strength mean value and standard deviation, on the basis of five measurements, are shown in Fig. 3.

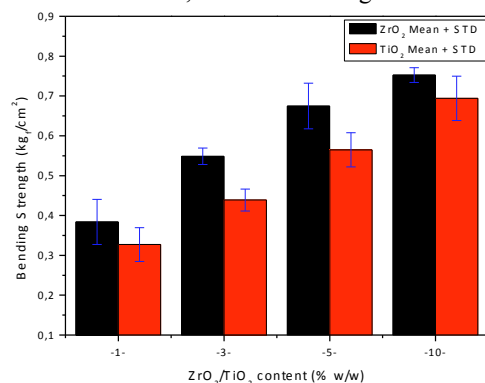


Fig. 3. Bending strength results

For both oxides, the bending strength increases when their content increases. The addition of ZrO₂ seems to be more effective than TiO₂ due to the less brittle nature of ZrO₂ compared to TiO₂. The effect on creep resistance is quantified in a decrease of the creep strain from the value of 6.5%, for Ni-5Al alloy, to values below 3% for samples reinforced with 10% of ZrO₂ and TiO₂. The polarization curves of Ni-5Al anode and anodes doped with 5% of ZrO₂ or TiO₂ are compared in Fig. 4.

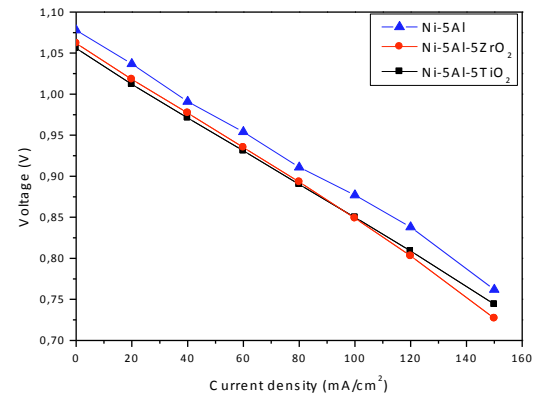


Fig. 4. Polarization curves with different Ni-5Al anodes

Single cell tests showed that performances of doped anodes are close to that of simple Ni-5Al anode, in terms of polarization. The two oxides used show similar performances, but a little gap from standard Ni-5Al anodes is visible.

IV. CONCLUSION

In this work, ZrO₂ and TiO₂ have been used during fabrication of standard Ni-5Al. The insertion of these oxides caused a structural modification, in the preferred direction for creep of FCC anode structure, which reduced creep to 3% or less, and enhanced the strength in bending for MCFC application. Single cell test showed promising results for improving the issues related to microstructural instability of conventional anode and MCFC durability. These results suggest that Ni-5Al alloys doped with 5-10% wt. of ZrO₂ or TiO₂ are good candidates for anodes in MCFCs.

REFERENCES

- [1] Antolini, E., The stability of molten carbonate fuel cell electrodes: A review of recent improvements, *Applied Energy*, Volume 88, 2011, pp. 4274-4293.
- [2] Kulkarni, A., Giddey, S., Materials issues and recent developments in molten carbonate fuel cells, *Journal of Solid State Electrochemistry*, 2012, Volume 16, pp 3123-3146.
- [3] Kim, Y.S., Lim, J.K., Chun, H.S., Creep Mechanism of Porous MCFC Ni Anodes Strengthened by Ni₃Al American Institute of Chemical Engineers 2006, 52, pp. 359-365.
- [4] Jang, S.C., Lee, B.Y., Nam, S.W., Ham, C.H., Han, J., Yoon, S.P., Oh, S.G., New method for low temperature fabrication of Ni-Al alloy powder for molten carbonate fuel cell applications, *International Journal of Hydrogen Energy* 2014, 39 (23), pp. 12259-12265.
- [5] Nguyen, H.V.P., Song, S.A., Seo, D., Park, D.N., Ham, C.H., Oh, S.G., Yoon, S.P., Han, J., Kim, J., Fabrication of Ni-Al-Cr alloy anode for molten carbonate fuel cells, *Materials Chemistry and Physics* 2012, 136, pp. 910-916.



A COMPARATIVE STUDY OF MICROSTRUCTURE AND IONIC CONDUCTION PROPERTIES OF GDC SOLID ELECTROLYTES PREPARED WITH DIFFERENT SYNTHESIS ROUTES

G. Accardo,* C. Ferone,* R. Cioffi,* L. Spiridigliozzi**, G. Dell'Agli**

* Department of Engineering and INSTM Research Unit, University of Naples "Parthenope", Centro Direzionale Isola C4, 80143, Naples, Italy

** Department of Civil and Mechanical Engineering and INSTM Research Unit, University of Cassino and Southern Lazio, Via G. Di Biasio 43, 03043 Cassino (FR) Italy

Abstract – Gadolinium doped ceria solid electrolyte prepared by different methods under the same sintering profile were examined in terms of microstructure and ionic conduction performance. The GDC powders were synthesized by a modified sol gel combustion synthesis and hydrothermal treatment. X-ray diffraction (XRD) and transmission electron microscopy (TEM) results revealed that the crystal structures of the powders synthesized by the two methods developed differently. After sintering, they showed different grain morphologies. Consequently, the electrolyte prepared from the two kinds of powders demonstrated different microstructures and different ionic conductivity. The electrolyte synthesized by sol gel methodology showed the highest ionic conductivity.

Index Terms – gadolinium-doped ceria, ionic conductivity, sintering, sol gel synthesis, hydrothermal treatment, solid oxide fuel cell.

I. INTRODUCTION

Gadolinium doped ceria electrolytes (GDC) have been studied widely for different application including solid oxide fuel cell (SOFCs). In case of SOFC operating at intermediate temperatures, GDC materials provide appreciable ionic conductivity and they have also been successfully used as part of anodes, especially when light hydrocarbons are fed. The performance of solid electrolytes can be affected by many factors such as doped composition material, thickness, microstructure and temperature at which the electrolytes are to be used [1]. The microstructure of a sintered material depends mainly on the synthesis methods and conditions used. Usually, the procedure for preparing gadolinium doped ceria consists of three steps: powder synthesis, shaping and sintering. The sintering profile (atmosphere, heating/cooling rate, highest sintering temperature and dwell time) can obviously affect the microstructure [2]. The shaping process is also a factor. For example, the pellet prepared by isostatic pressing is denser than that by extruding [3]. The first step plays a critical role in the final particle size and, consequently has an influence on the microstructure of the electrolyte as well ionic conduction

mechanism. In this work we compared the microstructure and ionic conductivity properties of $\text{Ce}_{0.9}\text{Gd}_{0.1}\text{O}_{0.195}$ ceramic electrolytes prepared by sol gel combustion synthesis and hydrothermal treatment.

II. MATERIALS AND METHODS

In sol gel combustion synthesis commercial cerium nitrate hexahydrate and gadolinium nitrate hexahydrate were used as precursors. Citric acid monohydrate was added to a mixture of nitrates and distilled water in a molar ratio with nitrates 1:1. The reaction occurred under continuous stirring and heating at 80°C for 2 hours. Powders were dried and calcined at 250°C for 1 hour and at 600°C for 3 hours respectively. In hydrothermal synthesis ceramic powders were prepared using a hydrous cerium-gadolinium oxide coprecipitate as a precursor with deionized water as mineralizer. The solution containing dissolved cerium and gadolinium salts was slowly added to an excess ammonia solution. The hydrothermal synthesis was carried out at 145 °C for 1 day. After the hydrothermal treatment, the products were filtered, washed repeatedly with deionized water and finally dried overnight at 60 °C. All the samples were characterized by X-ray powder diffraction (XRD) and transmission electron microscopy (TEM). Sintering was performed using different rates for heating and cooling, 3°C/min and 10°C/min respectively, with a dwell at 1500°C for 3h. The sintered pellets microstructure was determined by Scanning Electron Microscopy and Energy Dispersive x-ray Scanning analysis. Electrical conductivity was evaluated by Impedance Spectroscopy.

III. RESULTS AND DISCUSSION

XRD pattern (not reported) showed that only the cubic fluorite phase was present. The characteristic peaks were in agreement to the peaks of the face-centered cubic CeO_2 . Crystal size is lower for sample prepared by sol gel route, as confirmed by TEM micrographs in Figure 1. Morphology of the powder depends on concentration of citric acid and on the



fast expulsion of gases during combustion. Extremely small particles are clearly visible (10 nm). By conventional hydrothermal treatments individual single-crystal particles of GDC are formed whose size is around 20 nm. Nanoparticles have relatively uniform shapes with narrow size distribution.

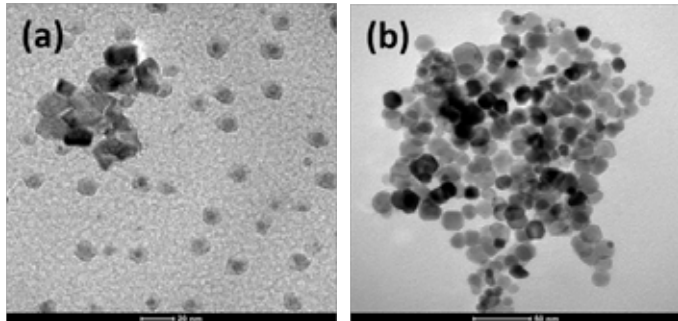


Fig. 1. TEM micrographs for GDC powders prepared by sol gel combustion route (a) and hydrothermal treatment (b)

By comparing SEM micrographs and relative density of gadolinium-doped ceria, prepared with the investigated methodology (Figure 2), powders have a distinct morphology. It is well known that grain size can greatly affect the microstructure of electrolytes. For comparison, pellets synthesized by sol gel synthesis are denser with a higher average grain size than the others prepared by hydrothermal synthesis. Much bigger particles than the electrolyte surface are found in the SEM micrographs of GDC prepared by sol gel synthesis.

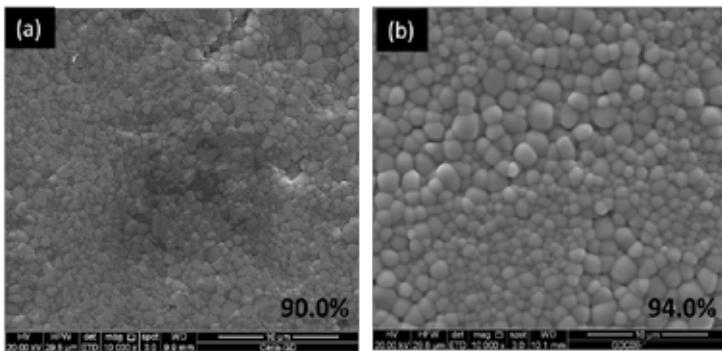


Fig. 2. SEM micrographs for GDC pellets prepared by hydrothermal treatment (a) and sol gel combustion route (b)

Because these materials are prepared under the same sintering conditions, the caused difference in the microstructure is thought to be the different characteristics of the powders, which resulted from the different powders synthesis methods.

Arrhenius plot in the temperature range 600-800°C is reported in Figure 3. Total ionic conductivities values for each sample are in agreement with literature but GDC prepared by sol gel synthesis have the higher ionic conductivity for all

temperature with a maximum of $3.2 \cdot 10^{-2}$ Sm/cm recorded at 800°C. The difference in the electrical properties depends on the different microstructure and density and is a consequence of the synthesis methods.

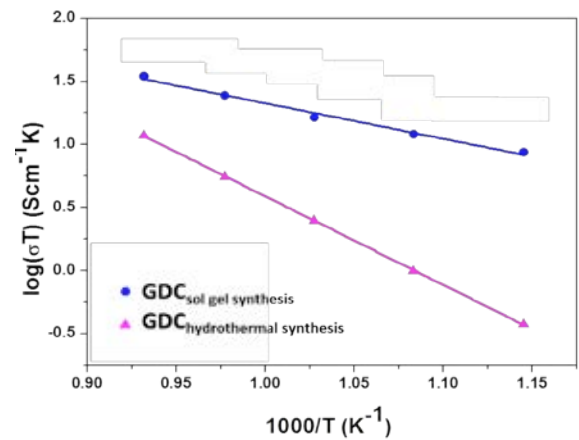


Fig. 3. Arrhenius plot for GDC pellets

IV. CONCLUSION

In this work $\text{Ce}_{0.9}\text{Gd}_{0.1}\text{O}_{0.195}$ powders were synthesized by two different methods, namely hydrothermal method and sol gel combustion synthesis. Except for the powder synthesis method, all other actors were controlled under the same conditions including pellets preparation and electrochemical characterization. Powders synthesized by different methods can produce different grain morphologies although the crystal structure is nearly the same. The electrolytes have different microstructures, which influence their ionic conduction performance. The GDC electrolyte synthesized by sol gel method showed the highest ionic conductivity for all the temperature investigated.

REFERENCES

- [1] Xu, Y., Tsumori, F., Osada, T., Miura H., Improvement of solid oxide fuel cell by imprinted micropatterns on electrolyte, *Micro & Nano Letters* 2013, 8, (10), pp. 571-574.
- [2] Mori, M., Sammes, N.M., Tompsett, G.A., Fabrication processing condition for dense sintered $\text{La}_{0.6}\text{AE}_{0.4}\text{MnO}_3$ perovskite synthesized by the coprecipitation method (AE= Ca and Sr), *Journal of Power Sources* 2000, 96, pp.395-400.
- [3] Li, S.G., Qi, H., Xu, N.P., Shi, J., Tubular dense perovskite type membrane. Preparing, sealing, and oxygen permeation properties, *Industrial & Engineering Chemistry Research* 1999, 38, pp. 5029-5033.



KINETICS OF WATER SORPTION AND DESORPTION IN NAFION[®] MEMBRANE: INFLUENCE OF THE INTERFACIAL MASS TRANSFER

S. Didierjean, J. C. Perrin, F. Xu, G. Maranzana, J. Mainka,
O. Lottin

LEMTA UMR 7563 CNRS-Université de Lorraine, 2, avenue de la
Forêt de Haye, TSA 60604, Vandoeuvre-Lès-Nancy, (France)

Abstract – A model for dynamic water sorption and desorption in Nafion[®]117 membrane is proposed allowing to calculate the water content variations induced by steps in relative humidity. It is based on the assumption that the water content of the membrane remains uniform at all times, and it takes into account a mass transfer coefficient at the interface between the membrane and the surrounding humid gas. The model allows to show in the case of large steps in relative humidity that the kinetics of desorption is faster than the kinetics of sorption.

Index Terms - Membrane, Sorption, Desorption, Interfacial Mass Transfer

I. INTRODUCTION

Nafion[®] membranes are widely used as electrolyte in PEM fuel cells. As their proton conductivity mostly depends on their water content, water transport in such materials is a crucial issue. Therefore, water sorption and desorption are frequently studied, and dynamic variations in the water content of the membrane are observed by varying the relative humidity of the gas phase. Difference in the kinetics of sorption and desorption are reported in the literature [1, 2] and the influence of the interfacial mass transfer is often presented [2]. However, the related model is not clearly established. The objective of this study is to present a model that can explain the difference in the kinetics of sorption and desorption.

II. MODEL

Starting with a membrane sample in equilibrium with a humid gas of relative humidity RH_0 , the relative humidity is modified to RH_∞ . According to the boundary layer theory applied to mass transfer, the instantaneous water flux density in the external medium at the interface with the membrane is

given by the following relation:

$$\varphi_{ext}(t) = h \left[C_{int}^{ext}(t) - C_\infty^{ext} \right], \quad (1)$$

where $C_{int}^{ext}(t)$ is the instantaneous water concentration in the gas phase at the interface with the membrane, C_∞^{ext} the water concentration in the bulk and h is the mass transfer coefficient ($m\ s^{-1}$). Assuming that the humid gas behaves like an ideal gas, the water flux can be written in the following form:

$$\varphi_{ext}(t) = h \frac{P_{sat}(T)}{RT} [RH_{int}(t) - RH_\infty], \quad (2)$$

where $RH_{int}(t)$ and RH_∞ are the relative humidities in the gas at the interface with the membrane and in the bulk, $RH_{int}(t)$ varying between RH_0 and RH_∞ during sorption or desorption. R is the ideal gas constant and T the temperature.

Assuming that the water concentration C (mole m^{-3}) in the membrane is uniform, its variation in a sample of ($2e$) thickness initially in equilibrium with the surrounding medium is given by the solution of the following equation:

$$2eS \frac{dC}{dt} = -2S \varphi_{ext}(t), \quad (3)$$

S is the membrane surface area in contact with the surrounding gas. The water content λ (number of water molecules per sulfonate ion) and the water concentration are related by:

$$C = C_{SO_3H} \lambda. \quad (4)$$

The concentration in sulfonate ions C_{SO_3H} being assumed constant and uniform, equation (3) can be rewritten as:

$$e C_{SO_3H} \frac{d\lambda}{dt} = -h \frac{P_{sat}(T)}{RT} (RH_{int}(t) - RH_\infty). \quad (5)$$



Equation (5) is solved numerically, assuming the temperature constant and uniform, and with the initial condition $\lambda_0 = f(RH_0)$. Knowing λ_i the water content at the time t_i , the water content λ_{i+1} at the time $t_{i+1} = t_i + \Delta t$ is given by:

$$\lambda_{i+1} = \lambda_i - \frac{\Delta t}{e} \frac{h}{C_{SO_3H}} \frac{P_{sat}(T)}{RT} (RH_i - RH_\infty). \quad (6)$$

Since the membrane remains permanently in equilibrium with the humid gas located at the interface, λ_i and RH_i are related by $\lambda_i = f(RH_i)$ according to the water sorption isotherm. The calculation is repeated until the steady state is reached.

III. RESULTS

In order to carry out the calculations for N-117 membrane, the relation $\lambda = f(RH)$ must be known. Figure 1 presents the sorption isotherm data measured at $T = 25^\circ\text{C}$ together with the best fit obtained using a polynomial relation.

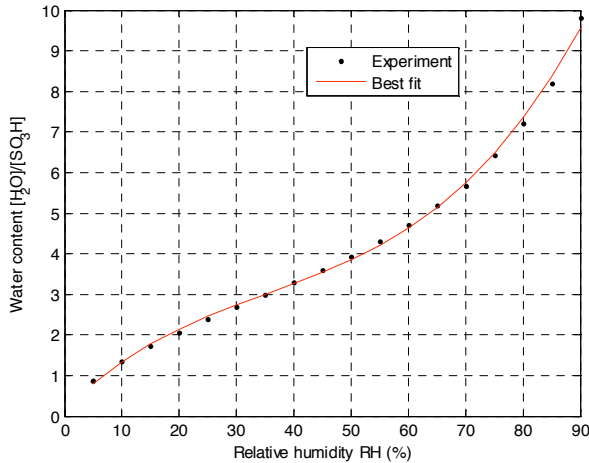


Fig. 1. Water uptake isotherm of N-117 at $T = 25^\circ\text{C}$. Best fit: $\lambda = 0.165 + 13.86 RH - 24.51 RH^2 + 23.01 RH^3$.

For the calculation, the following parameters were used: The saturated pressure $P_{sat}(T)$ is given by the Rankine relation, the half thickness of N-117 is equal to $89 \mu\text{m}$, C_{SO_3H} is equal to 1838 mole m^{-3} and h is fixed to $4 \cdot 10^{-3} \text{ m s}^{-1}$ for both sorption and desorption. The time variations of the membrane water content calculated for RH steps of 60%, between 20% and 80% are presented in Figure 2 for $T = 25^\circ\text{C}$ and 50°C .

It clearly appears that for a given temperature, the kinetic of water desorption is about 5 times faster than that of water sorption, which is in good agreement with the experimental results obtained by Satterfield and Benziger [2]. The explanation of such a difference between sorption and desorption kinetics obtained for the same value of the exchange coefficient comes from the water fluxes exchanged between the

membrane and the humid gas. As given by equation (2), the water flux which varies linearly with the difference in gas relative humidity between the membrane interface is then related to the slope of water uptake isotherm which is higher at high than at low RH .

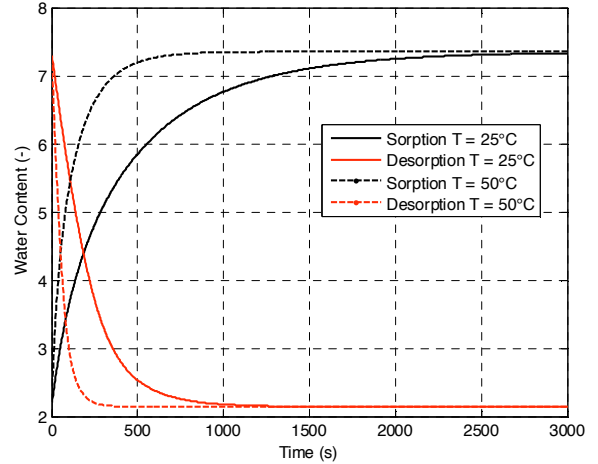


Fig. 2. Model results: water content variations during sorption (black) and desorption (red) due to step in RH between 20% and 80% calculated for $T = 25^\circ\text{C}$ (dash lines) and $T = 50^\circ\text{C}$ (solid lines). $h = 4 \cdot 10^{-3} \text{ m s}^{-1}$ for both sorption and desorption.

Figure 2 also shows the influence of temperature. For a fixed value of h , the water flux being proportional to $P_{sat}(T)/T$, it increases with T which explains (among other phenomena and physical parameters depending on temperature) why the kinetics in sorption and desorption are faster at high temperature, as presented by Satterfield and Benziger [2].

IV. CONCLUSION

Kinetics of water sorption and desorption in Nafion[®] was studied theoretically and experimentally by taking into account a mass transfer coefficient at the interface between the membrane and the surrounding medium. Considering that the water content of the membrane is uniform, the calculated variations of the water content demonstrate that for a fixed value of the mass transfer coefficient, desorption is faster than sorption due to the variations in the slope of the water sorption isotherm.

REFERENCES

- [1] Shanhai Ge, Xuguang Li, Baolian Yi and I-Ming Hsing, Absorption, Desorption, and Transport of Water in Polymer Electrolyte Membranes for Fuel Cells, *Journal of The Electrochemical Society*, 152 (6), 2005, A1149-A1157.
- [2] M. Barclay Satterfield and J. B. Benziger, Non-Fickian Water Vapor Sorption Dynamics by Nafion Membranes, *J. Phys. Chem. B* 2008, 112, 3693-3704.



Alessandra Perna*, Simona Scarfogliero**, Mariagiovanna Minutillo**, Antonio Lubrano Lavadera**,
Elio Jannelli**

* Dep.t of Civil and Mechanical Engineering, University of Cassino and Southern Lazio, Via G. di Biasio 43, 03043 Cassino, Italy

** Dep.t of Engineering, University of Naples "Parthenope", Centro Direzionale, Isola C4, Naples, Italy

ELECTROCHEMICAL MODELS DEVELOPMENT FOR THE PREDICTION OF SOFC AND SOEC BEHAVIORS AND PERFORMANCE

Abstract - The chemical storage of electricity realized by hydrogen-based systems is an interesting option that, recently, has received great attention. A promising storage technology is based on a reversible solid oxide cell (ReSOC), that can operate reversibly either as a fuel cell (SOFC) or as an electrolyser (SOEC). In this paper a numerical model to predict the behavior of ReSOC in both operating modes is proposed. The model, based on a system-level SOFC model calculates the system losses (activation, ohmic and concentration overpotentials) by means of electrochemical equations. The model, developed by using the Aspen Plus code, is based on fundamental electrochemical and physical relationships, such as the Butler-Volmer (BV) equation and Fick's law. In order to estimate the calibration parameters of the model equations a fitting procedure is carried out by using the available experimental data.

Index Terms - Reversible solid oxide fuel cells, Mathematical modeling, Solid Oxide electrolysis, Experimental validation

I. INTRODUCTION

Electric energy storage systems have a very important role in the future development of the electric network, because they allow a best management of the electric energy produced by renewable power plants. In these systems the electric energy is stored as hydrogen by water electrolysis and the stored hydrogen is used as fuel to produce electric energy by a fuel cell system upon demand. A promising storage technology is based on a reversible solid oxide cell (ReSOC), that can operate reversibly either as a fuel cell (SOFC) or as an electrolyser (SOEC). In particular, the ReSOC is an electrochemical energy conversion device that operates at high temperature (600-1000°C) and, recent studies, suggest that it is capable of working as a highly efficient (>70% roundtrip) and potentially cost-effective energy storage device [1]. The fundamental mechanisms of a ReSOC are illustrated in Fig. 1.

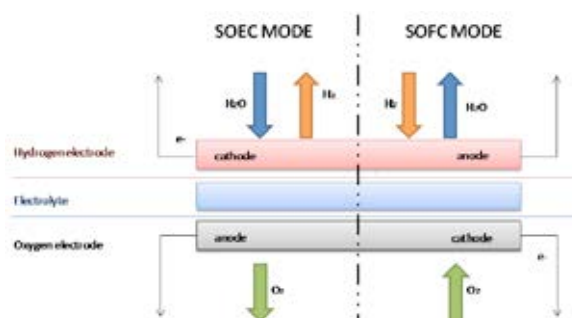


Figure 1 ReSOC working principle

II. MODELLING

The ReSOC model that can readily switch between the operational modes has been designed by integrating a one-dimensional SOFC model, previously developed by the authors and detailed in [2], with a SOEC model which considers the electrochemical equations and parameters as in ref. [3]. The cell design is planar with counter-flow arrangement. The basic assumptions are: i) steady-state, ii) isothermal conditions, iii) ideal gas mixtures, iv) equilibrium in the gas reactions, v) negligible pressure drop. The unit cell is discretized in N-elements along the flow direction and each J-element consists of fuel electrode, oxidant electrode and electrolyte.

The model flowsheet of the J element is depicted in Figure 2. It comprises an oxidant electrode (labelled C), in which the oxygen (SOFC mode) reacts producing the negatively charged ions or O^{2-} ions (SOEC mode) oxidize to O_2 and a fuel electrode (labelled A) in which the electro-oxidation reaction (SOFC mode) or the electro-reduction reaction (SOEC mode) occur. The oxidant electrode is modelled as a separator block (SOFC mode) or a mixer block (SOEC mode), whereas the fuel electrode is simulated as a stoichiometric reactor.

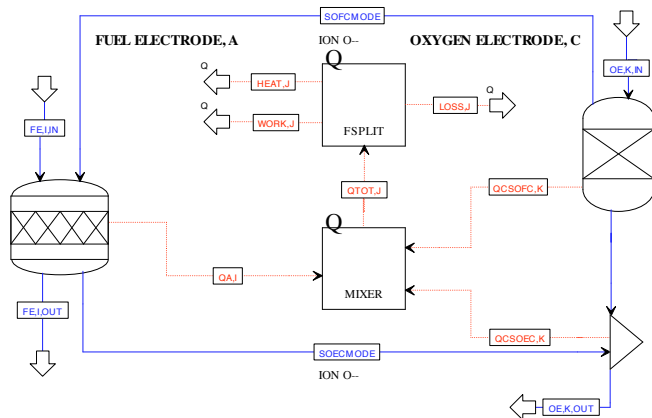


Figure 2. Flowsheet of the J-th element

The energy balance of the J-element takes into account: a) the heat of chemical reactions, b) the enthalpy change of each species at the fuel electrode and the oxidant electrode, c) the heat losses due to the convective and radiative thermal fluxes, d) the produced/consumed electric power, e) the net thermal power. Moreover, the energy balance is solved by using two specific block calculators (the energy fluxes can be positive or negative according to the cell operating mode):

- a Thermal Mixer block (QMIXER) used to perform the thermal balance of the J-element. The term $QTOT,J$ represents the net thermal power;
- a Thermal Splitter block (QFSPLIT) used to separate the energy output streams of the J-element, in terms of $WORK,J$, $HEAT,J$ and $LOSS,J$.

In order to estimate the terms $WORK,J$ and $LOSS,J$ a Fortran block calculator, in which the SOFC and SOEC electrochemical equations [2, 3] are implemented, is used.

The $WORK,J$ is defined, as known, once the voltage is determined. The voltage of the J-element at different current values is calculated by subtracting (in SOFC operation mode) or adding (in SOEC operation mode) to the Nernst potential the overvoltages terms related to the activation, ohmic, and concentration losses:

$$V_{A,C_K} = (E_{Nernst} \mp \eta_{act,a} \mp \eta_{act,c} \mp \eta_{ohmic} \mp \eta_{conc,a} \mp \eta_{conc,c})_{I,K} \quad (1)$$

where E_{Nernst} is the thermodynamic potential, $\eta_{act,a}$ and $\eta_{act,c}$ are the activation overpotentials at the fuel and oxidant electrodes respectively, η_{ohmic} is the ohmic overpotential, and $\eta_{conc,a}$ and $\eta_{conc,c}$ are the concentration overpotentials at the fuel and oxidant electrodes due to the mass transfer limitations. The cell voltage (V_{cell}) is calculated as:

$$V_{cell} = \sum_{j=1}^N \frac{V_j}{N} \quad (2)$$

The $LOSS,J$, that considers the heat losses from the cell external surface by natural convection and radiation, is evaluated as in ref.[2].

III. RESOC MODEL VALIDATION

The electrochemical coefficients used for the overpotentials calculation and the main cell design data are listed in table 1.

In figure 3 the comparison between the polarization curve obtained from the model and the available data [4] is depicted. This comparison shows good agreement.

Table 1. Design data and electrochemical coefficients

Operating temperature, T (°C)	1000
Operating pressure, P (bar)	1
Cell active area, A _{cell} (m ²)	0.016
Electrolyte thickness, (μm)	50
FE thickness, (μm)	50
OE thickness, (μm)	500
Electrode porosity, n	0.48
Electrode tortuosity, ζ	5.4
Electronic transfer coefficient, α _{FE} /α _{OE}	0.5/0.5
Number of electrons, n _{FE} /n _{OE}	2/4
FE activation energy, E _{act} , kJ/mol	120
OE activation energy, E _{act} , kJ/mol	100

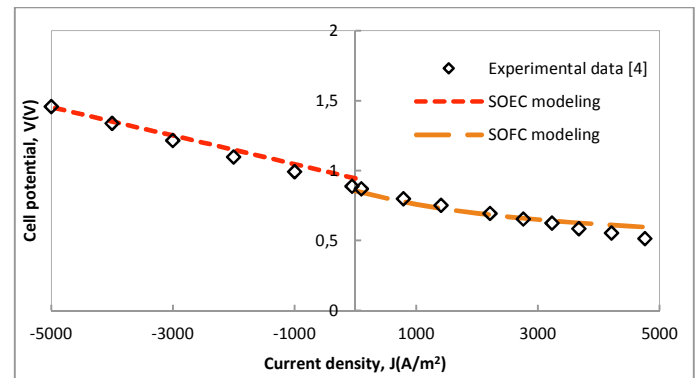


Figure 3 Comparison between SOEC/SOFC modelling and experimental data T 1273 K

IV. CONCLUSION

The model presented in this paper is capable of predicting the performance of the ReSOC with a good accuracy.

REFERENCES

- [1] C.H. Wendel, P. Kazempoor, R.J. Braun, Novel electrical energy storage system based on reversible solid oxide cells: System design and operating conditions, Journal of Power Sources 276 (2015) 133-144.
- [2] Minutillo M, Perna A, Jannelli E, SOFC and MCFC system level modeling for hybrid plants performance prediction. Int J Hydrogen Energy 2014;39(36):21688-9
- [3] M. Ni, M. K. H. Leung, D. Y. C. Leung, A modeling study on concentration overpotentials of a reversible solid oxide fuel cell, Journal of Power Sources 163 (2006) 460-466
- [4] Momma A, Kato T, Kaga Y, Nagata S. Polarization behaviour of high temperature solid oxide electrolysis cells (SOEC). J Ceram Soc Jpn 1997;105(5):369-73.



CONTROL STRATEGY OPTIMIZATION FOR A MICRO-COGENERATION POWER SYSTEM BASED ON SOLID OXIDE FUEL CELL

M. Minutillo*, F. Radunanza*, V. Cigolotti**, A. Pontecorvo** and A. Perna***

* Department of Engineering, University of Naples "Parthenope", Centro Direzionale, Naples, Italy;

**ENEA, Portici Research Center, P.le Enrico Fermi, 1 - 80055 Portici Naples, (Italy);

*** Department of Civil and Mechanical Engineering, University of Cassino and Southern Lazio Via G. Di Biasio, 43, Cassino, (Italy)

Abstract - Micro-cogeneration systems have received increasing attention in recent years because, by providing both useful electricity and heat with high efficiency, they can have a strategic role in the reduction of greenhouse gas emissions according to the European Union targets. The European Union directive 2004/8/EC introduces a performance parameter (PES, Primary Energy Saving) that allows to define the performance of the cogeneration systems. Cogeneration applications in buildings have to satisfy either both electrical and thermal demands, or satisfy the thermal demand and part of the electrical demand, or satisfy the electrical demand and part of the thermal demand. Therefore, depending on the electrical and thermal loads and on the operating strategy, a cogeneration system can be run at different conditions.

In this paper, a micro-cogenerator (μ CHP) based on the Solid Oxide Fuel Cells (SOFC) technology working under different control strategies is investigated and its overall performances have been evaluated.

Index Terms – Control strategy, Primary Energy Saving, Residential Micro combined heat and power cogeneration, Solid Oxide Fuel Cell

I. INTRODUCTION

The CHP (combined heat and power) plant is considered widely as the major alternative to traditional generation systems. For this reason, European Union by Directive 2004/8/EC [1] promoted officially the CHP diffusion and development.

Micro-cogeneration systems (micro-CHP) based on solid oxide fuel cell (SOFC) represent an interesting alternative to traditional CHP technologies to efficiently meet heating and electricity needs of residential household (Figure 1) [2].

An SOFC operates at high temperature, ranging from 700 to 1000°C, so the electrochemical conversion takes place with relatively low thermodynamic losses. Furthermore, the high-temperature heat available can be utilized both for thermal energy recovery and for additional power generation.

In this paper the assessment of the system control strategy on the primary energy saving (PES) has been evaluated. The electrical load following scenario and the thermal load following scenario (two typical strategies, usually employed to manage cogeneration systems [3]) have been considered.

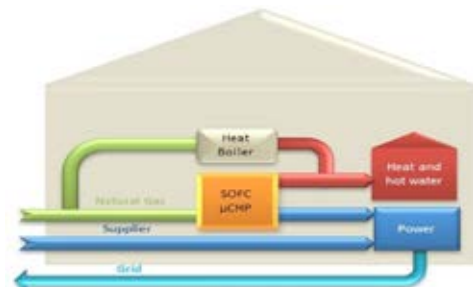


Figure 1. μ CHP system for residential household

II. METODOLOGY

A. Load Profiles

For the energy requirements a family living in Milan has been considered as utility [4]. For the thermal energy two different profiles are taken into account: (i) a cold season profile (Figure 2), which covers the space heating and the hot water production and (ii) a warm season profile (Figure 3), which only considers the hot water production. The variations in the thermal energy demand that can occur between working days and holidays are neglected. A similar procedure is used for the electric demand for both electric devices and air conditioning. The demand for summer air conditioning was converted into electricity requirements by using the energy efficiency ratio (EER).

B. System CHP

In this paper a pre-commercial micro-cogeneration system (μ -CHP) based on the Solid Oxide Fuel Cells (SOFC) technology

has been studied. In Table I the main technical specifications and operational are summarized [5].

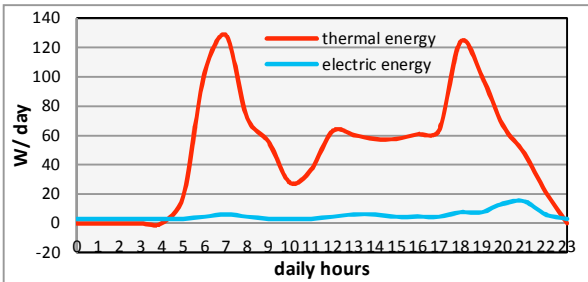


Figure 2. Daily electric and thermal energy demands-cold season

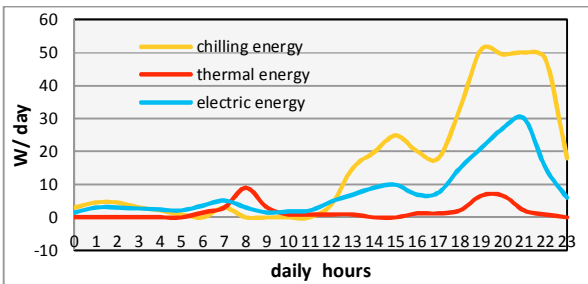


Figure 3. Daily electric, chilling and thermal energy demands-warm season

Table I: DATA SHEET OF ENGEN 2500 [5]

	40	100	%
Modulation range	40	100	%
Fuel input (natural gas)	2800	5000	W
Nominal electric power (NET AC)	1000	2500	W
Thermal power	1400	2000	W
Electrical efficiency (NET AC, LHV)	36	50	%
Thermal efficiency	50	40	%

Figure 4 shows the expected μ -CHP performance in terms of electric and thermal power and fuel input.

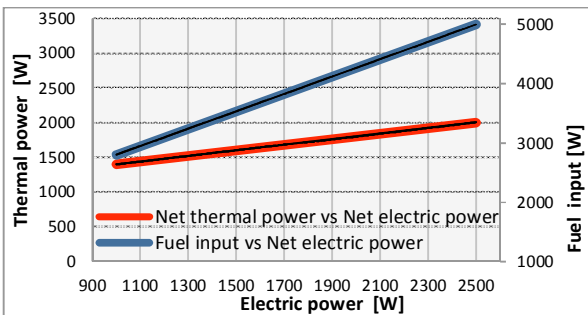


Figure 4. Performance of μ -CHP

III. RESULT

A. Electric load following

Table II shows the annual electric energy demand compared to the electric energy produced by the μ -CHP in the case of the electric load following scenario. It can be noted that the overall electric energy produced by the power system (during the year) is higher than the electric energy required by utility because the μ -CHP does not operate at a load lower than 40%.

As a consequence, the electric energy surplus is sent to grid. However, in the warm season, there are some power requirements that are higher than 2.5 kW, so that the electric power is satisfied by the grid (about 10%). The thermal energy in the cold season must be integrated with a boiler, while the more heat produced is wasted.

Table II: COMPARISON ANNUAL ELECTRIC AND THERMAL: ENERGY ELECTRICAL LOAD FOLLOWING SCENARIO

Energy (kWh/y)	Demand	Production	Sent to grid	From grid/Auxiliary boiler	Not used
Electric	7237	10505	3268	788	-
Thermal	19766	12962	-	11932	5128

B. Thermal load following

Table III shows the annual electric energy demand compared to the electric energy produced by the μ -CHP in the case of the thermal load following scenario.

Table III: COMPARISON ANNUAL ELECTRIC AND THERMAL: ENERGY THERMAL LOAD FOLLOWING SCENARIO

Energy (kWh/y)	Demand	Production	Sent to grid	From grid/Auxiliary boiler	Not used
Electric	7237	13484	6911	2421	-
Thermal	19766	14154	-	10192	4579

IV. CONCLUSION

In this paper different control strategies have been considered and compared in terms of annual efficiencies and PES (that is calculated as illustrated in [1]) as shown in Table IV. The highest overall performances are obtained considering a thermal load following operating mode.

TABLE IV: COMPARISON PERFORMANCES PES ACCORDING TO THE CHOSEN CONTROL STRATEGIES

Strategy	η_{ele}	η_{ter}	η_{cog}	PES
Thermal following	0.41	0.30	0.71	0.23
Electric following	0.37	0.29	0.66	0.20

ACKNOWLEDGMENT

This research has been funded by the Italian Government, with the PON project "Fuel Cell Lab – Innovative systems and high efficient technologies for polygeneration – PON03PE_00109_1/F12".

REFERENCES

- [1] Directive 2004/08/EC of the European Parliament and of the council. Official J Eur Union 21.2.2004: 50 e 60.
- [2] Zabalza I, Aranda A, de Gracia MD. Feasibility analysis of fuel cells for combined heat and power systems in the tertiary sector. International Journal of Hydrogen Energy 2007;32:1396 e 403.
- [3] M. Minutillo, A. Perna, Energy Analysis of a Residential CHP System based on a PEM Fuel Cell, Journal of Fuel Cell Science and Technology, Vol. 6, February 2009.
- [4] Macchi E, Campanari S, Silva P. La microgenerazione a gas naturale. Milano Italy (in Italian): Polipress; 2005
- [5] <http://www.solidpower.com>



ELECTRICAL ENERGY STORAGE SYSTEMS BASED ON RESOC TECHNOLOGY: A NOVEL APPROACH FOR THE GRID INTEGRATION OF RENEWABLE ENERGY SOURCES

R. Atochero Velasco*, A. Lubrano Lavadera* , S. Scarfogliero*, G. Cinti**, G. Bidini**,
V. Cigolotti***, M. Minutillo*

*University of Naples "Parthenope", Department of Engineering, Naples (Italy)

** University of Perugia, Department of Engineering, Perugia (Italy)

*** ENEA, Portici Research Center, P.le Enrico Fermi, 1 - Portici Naples, (Italy)

Abstract - The aim of this study is to analyze the behavior and the performance of an integrated power plant in which a renewable energy system, based on photovoltaic and wind power units, is coupled with a hydrogen energy storage system. The storage system is based on the ReSOC (Reversible Solid Oxide Cell) technology, that is an electrochemical device able to work both as fuel cell and as electrolyzer.

The role of the storage unit is to permit a constant power grid feeding. Thus, the integrated power system has to be managed in order to feed into the grid the electric energy that the renewable power plant is able to produce during its annual operation, but with a power supplying that is constant in time. This operation mode implies that if the stored hydrogen is not available to assure a constant power feeding, an auxiliary power system is used for satisfying the power requirement.

Index Terms – Hydrogen, Renewable energy storage, Reversible operation, Solid oxide cell.

I. INTRODUCTION

Today electricity generation is primarily based on fossil fuels creating serious economic and environmental difficulties. Renewable energy technologies have the potential to undercut the cost of electricity generation and have attracted great interest due to global warming issues recently arisen.

A fundamental problem associated with renewable energy sources, such as solar energy and wind energy, is the intermittence and stochastic character of these energy sources, so make them more difficult to manage it. Moreover, the

fluctuating nature of renewable energies causes an extensive strain on the grid infrastructure. One of the key objectives of European energy policy is a substantial increase in the use of renewable energy sources, coupled with a massive increase in energy efficiency.

The aim of this study is to analyze the behaviour of a renewable power system that, thanks to an energy storage system and an auxiliary power unit, is able to provide a constant power to the electric grid. The storage system is based on the ReSOC (Reversible Solid Oxide Cell) technology, that means a reverse process operation; thus, when abundant renewable energy is available it can operate as solid oxide electrolyzer cell (SOEC) mode to produce hydrogen and later the same, when renewable energy is lack, can consume the hydrogen to generate electricity in the fuel cell (SOFC) operating mode [1,2,3]. The capability of dual functions makes ReSOCs economically sound.

II. PLANT DESCRIPTION

The study is based on a novel approach in the management of renewable power plants that consists in providing a constant power to the electric grid thanks to the utilization of an energy storage system.

The proposed power plant configuration is illustrated in Figure 1. It consists of: a photovoltaic unit (100 kWp), a wind unit (Size 100 kWp), a ReSOC unit, an auxiliary power system, hydrogen and water storage tanks, and electrical devices (charge controller, inverter, buffer battery, etc.). Moreover, an Electric Control Unit manages the energy fluxes by applying the chosen control strategy (constant power supply into the electric grid).



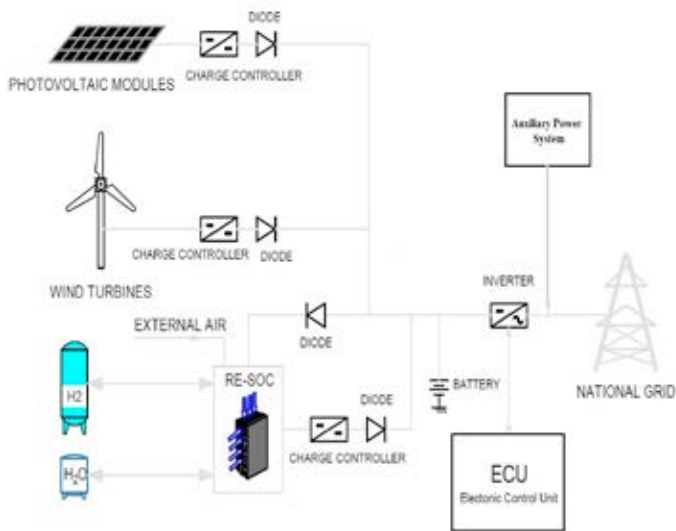


Fig.1 – Schematic of the power plant.

III. RESULT DISCUSSION

It has been assumed the plant installation in Naples. Thus, by using the program System Advisor Model [4] for the PV unit and the date of Naples Capodichino weather station [5,6] for the wind power unit, the annual energy production has been determined. Thus, it results an electric energy production equal to 160,000 kWh by the PV unit and equal to 45,000 kWh by the wind unit. Taking into account the total energy production (205,000 kWh) and considering the plant management criteria, the constant electric power is equal to 23.4 kW (it has to be supplied to network in order to guarantee the same annual electric energy as produced by the renewable power plant). By applying this plant operating mode, it is possible to avoid the fluctuations derived from the renewable energy.

By analyzing the energy fluxes during the annual plant operation the size of the ReSOC has been calculated. It results equal to 135 kW. Moreover it has been assumed that the efficiency of the ReSOC is constant with the load variation; it results equal to 50% in the SOFC mode and 70% in the SOEC mode.

Figure 2 reports the electric power produced by the renewable power plant estimated in a day of June [5,6]. In the same figure the electric power that has to be supplied to the network is shown too (23.4 kW). By comparing the curves it is possible to note that the integrated plant operates in different mode, as highlighted by the marked areas. These areas are:

- A = Energy supply by SOFC and by renewable power units
- B= Energy surplus to SOEC for hydrogen production.
- C = Energy supply by renewable power units.
- D= Energy supply by SOFC and by renewable power units.

Results have pointed out that by using only the energy storage system, a constant electric power supplying can not be guaranteed during whole year because the hydrogen, produced by the renewable power surplus, is not sufficient; thus it is needed to use the auxiliary power system that is based on the

fossil fuel consumption (i.e. reciprocating engine). The size of this power unit has to be 25 kW.

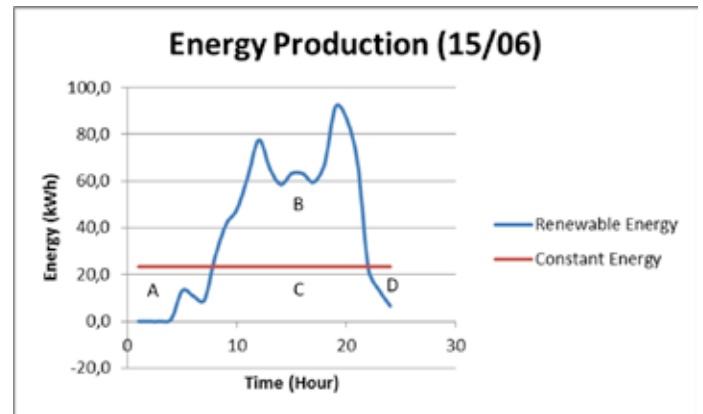


Fig.2 – Energy production in a day of June

IV. CONCLUSIONS

In this study, a novel approach in the management of renewable power plants is presented. It consists in providing, by using an integrated power plant, a constant electric power to the grid, thanks to the integration of the renewable power unit with an energy storage system and an auxiliary power unit. Moreover, the using of ReSOC as storage unit is considered as an interesting power solution from efficiency and economic (an energy system that operates in reversible mode) point of view.

ACKNOWLEDGMENT

This research has been funded by the Italian Government, with the PON project “Fuel Cell Lab – Innovative systems and high efficient technologies for polygeneration – PON03PE_00109_1/F12”.

REFERENCES

- [1] P. Kazemipoor, R.J: Braun. Model validation and performance analysis of regenerative solid oxide cells for energy storage applications : Reversible operation. International Journal of Hydrogen Energy 39 (2014).
- [2] D. Penchini, G. Cinti, G. Discepoli, U. Desideri. Theoretical study and performance by 200 W solide oxide electrolyzer stack. International Journal of Hydrogen Energy 39 (2014).
- [3] A. Lubrano Lavadera, E. Jannelli, M. Minutillo, A. Perna, S.P. Cicconardi, Investigations on an energy storage system based on high temperature fuel cells for an off-grid renewable power plant, Hypothesis XI, Toledo, Spain, September 2015.
- [4] System Advisor Model, vers. 2015.1.30 (SAM 2015.1.30) National Renewable Energy Laboratory. Golden, CO.
- [5] <http://www.tutempo.net/registros/lirn>
- [6] <http://www.northernpower.com/wp-content/uploads/2014/09/20150212-brochure-NPS-100C-24-UK.pdf>



EFC15062

MODELLING MEMBRANE HYDRATION AND WATER BALANCE OF A PEM FUEL CELL

V. Liso*, M.P. Nielsen*

*Department of Energy Technology, Aalborg University, (Denmark)

Abstract - Polymer electrolyte membrane (PEM) fuel cells requires an appropriate hydration in order to ensure high efficiency and long durability. As water is essential for promoting proton conductivity in the membrane, it is important to control membrane water hydration to avoid flooding.

In this study we propose a novel mathematical zero-dimensional model for water mass balance of a polymer electrolyte membrane. Physical and electrochemical processes occurring in the membrane electrolyte are included; water adsorption/desorption phenomena are also considered. The effect of diffusivity, surface roughness and water content driving force is considered. We validate the model against experimental data.

The water balance calculated by this model shows better fit with experimental data-points compared to other models such as the one by Springer et al. We conclude that this discrepancy is due a different rate of water transport when membrane absorption/desorption is considered in the model. The model becomes useful when studying fuel cell systems in dynamic conditions.

Index Terms – PEM fuel cells; water management; system modelling.

I. INTRODUCTION

Fuel cell based powertrain systems promise to deliver cleaner and more efficient vehicles. In order to provide a performance comparable to conventional powertrain systems, the polymer electrolyte membrane (PEM) fuel cell has to meet stringent durability requirements under demanding operating conditions encountered in automotive applications [1]. Membrane hydration can be affected by an imbalance between water production and water removal, or excessive amounts of liquid water form which can cause so-called “flooding”. To avoid flooding and still achieve good proton conductivity, it is imperative to understand the driving mechanisms behind water transport, particular inside the membrane. In this study a model of the PEM membrane hydration is developed.

II. GOVERNING PHENOMENA OF WATER TRANSPORT IN PEM-FC

In figure 1 the membrane water balance is depicted. At the anode, protons bond with one water molecule then migrate toward the cathode. At the cathode reaction sites the ions release the water molecule as they engage in the electrochemical reaction on the platinum surface. This leads to a surplus of water at cathode side.

There are kinetic barriers associated with transport such as sorption and desorption of water at membrane-GDL interface.

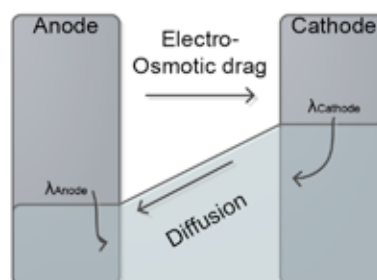


Fig. 1. Water transport between the anode and cathode.

The governing equation for the transport of water can be expressed using a non-equilibrium formulation which is dependent both on water uptake in an equilibrated and non-equilibrated membrane.

$$\mathcal{N}_{H_2O,m} = \mathcal{N}_{H_2O,m,osmotic} - \mathcal{N}_{H_2O,m,backdiff} = \frac{\rho_m}{FW} \phi k (\lambda_{equi,m} - \lambda_m) \quad (1)$$

$\mathcal{N}_{Sorption/Desorption}$

The sorption and desorption of water at the membrane/GDL interface is a function of the offset from equilibrium, where $\lambda_{equi,m}$ and λ_m are the water content at equilibrium and the actual water content in the ionomer phase.

Depending on the direction of the net membrane water flux, $\mathcal{N}_{H_2O,m}$, one side of the membrane can be either in desorption

or absorption mode. A surface roughness factor ϕ is introduced in equation to account for the difference in the specific surface area when using different types of ionomer loadings in the catalyst layer. k_a and k_d are the mass-transfer coefficients for the absorption and desorption of water, respectively.

Equation (1) can be solved depending on the membrane side is in desorption or absorption mode. The two unknowns are $\lambda^{abs.side}$ and $\lambda^{des.side}$.

$$\begin{aligned} \mathcal{R}_{H_2O,m} &= \left[1 + \lambda^{abs.side} \frac{\bar{V}_w}{\bar{V}_m} \right]^{-2} \frac{\rho_m}{EW_m} \phi k_a (\lambda_{equi}^{abs.side} - \lambda^{abs.side}) \\ \mathcal{R}_{H_2O,m} &= \left[1 + \lambda^{des.side} \frac{\bar{V}_w}{\bar{V}_m} \right]^{-2} \frac{\rho_m}{EW_m} \phi k_d (\lambda^{des.side} - \lambda_{equi}^{des.side}) \end{aligned} \quad (2)$$

Mass transport in the GDL is a porous media and each species which moves through it has a different diffusivity, so the molar fraction of the species will vary along the diffusion path. Transport in the gas diffusion layer is modeled as transport in a porous media. The gas mixture is assumed well-mixed at the molecular level, with all components sharing the same velocity, pressure, and temperature fields. When the Stefan-Maxwell expression is used, the diffusion of each gas species is linked to the other species composing the gas mixture:

$$\frac{dy_i}{dz} = \frac{RT}{p} \sum_{j=1, j \neq i}^n \frac{y_j \mathcal{R}_j - y_i \mathcal{R}_i}{D_{ij}^{eff}} \quad (3)$$

with n indicating the number of gas mixture components, and D_{ij}^{eff} is the effective pressure diffusivity product of the mixture $i - j$ in the porous medium. The diffusion coefficients (D_{ij}^{eff}) are modified to take into account the interaction with the pore walls and water saturation, s .

III. RESULTS

In this section we depict model results regarding water collection at anode and cathode outlets. We define the net drag coefficient of water through the membrane, r_d :

$$r_d = \frac{\mathcal{R}_{H_2O,an,in} - \mathcal{R}_{H_2O,an,out}}{i/F} \quad (4)$$

If $r_d > 0$, water flux across the membrane is from anode to cathode, vice-versa if $r_d < 0$, water flux is from cathode to anode.

Only the cathode water outlet mass flow rate was used for model validation due to poor measurement on the anode side. For validation purposes we consider $RH_{An,in} = 80\%$ and $RH_{Ca,in} = 100\%$. Voltage averages for each current density were calculated under stable operation and with no test

disturbance. An uncertainty for the average water mass flow rate of 0.01 g was calculated.

In the plot in figure 2 we compare the results produced when equilibrium of water activity in the membrane is assumed at the electrode/membrane interface ($\lambda_{equi,m} = \lambda_m$) (i.e. case #1) [2] to the case when adsorption/desorption is applied (i.e. case #2) [3]. In the second case $\mathcal{R}_{H_2O,Ca,Out,Stack,\#2}$ is calculated using the model of water transport with absorption/desorption. In figure 2, we see the cathode and anode outlet water mass flow rates. When equilibrium of water activity is assumed (model #1), the net drag coefficient r_d is bigger, indicating a larger water flux from anode to cathode. Vice-versa if adsorption/desorption is considered (model #2), water flux across the membrane is basically negligible, $r_d \approx 0$.

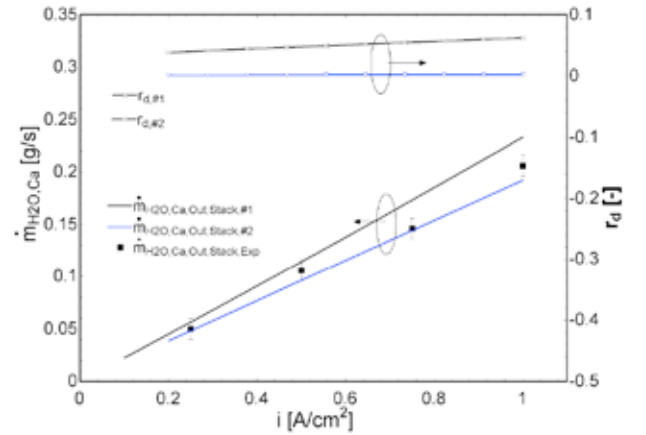


Figure 2 Cathode Outlet H_2O mass flow rate with $RH_{An,in} = 80\%$; $RH_{Ca,in} = 100\%$

From this figure we can conclude that in dynamic conditions, including adsorption/desorption phenomena in the model gives better results than considering the membrane in equilibrium condition. The water resistive effect of adsorption/desorption phenomena will reduce the water transport compared to equilibrium condition.

REFERENCES

- [1] Liso V., Nielsen M.P., Kær S.K. and Mortensen H.H., Thermal modeling and temperature control of a PEM fuel cell system for forklift applications, Int J Hydrogen Energy 39, 2014, 8410–8420.
- [2] Springer TE, Zawodzinski TA, Gottesfeld S. Polymer electrolyte fuel cell model. J Electrochem Soc 1991;138:2334–42
- [3] Liso, V., Araya, S. S., Olesen, A. C., Nielsen, M. P., Kær, S. K. Modeling and experimental validation of water mass balance in a PEM fuel cell stack: Int J of Hydrogen Energy 2015.



The effect of doping on performances of SOFCs Ni-YSZ anodes operated in carbon- and sulfur-containing fuels

M. Rolland*, D. Montinaro**, and V.M. Sglavo*

*Dipartimento di Ingegneria Industriale, Università degli Studi di Trento,
Via Sommarive, 9 – I-38123 Trento, (Italy)

** SOLIDpower S.p.A, Viale Trento 115/117, I-38017, Mezzolombardo,
(Italy)

Abstract – In this study, the tolerance of Ni/YSZ anode-supported solid oxide fuel cells to carbon deposition and sulfur poisoning has been tested by changing anode composition. Results have shown that doping the anode with small amounts of ceria allows maintaining good performances of the cell while increasing their tolerance to carbon and sulfur.

Index Terms – Carbon deposition, Ni/YSZ anodes, solid oxide fuel cells, sulfur poisoning

I. INTRODUCTION

Solid Oxide Fuel Cells (SOFCs) have been widely investigated for their high efficiency, their wide operating temperature range and their fuel flexibility. Recently, SOFCs have received more interest in operating in more realistic conditions, feeding the cell with real fuels. Even filtrated, traces of contaminants such as carbon- and sulfur-based compounds can remain in these fuels.

Due to their high catalytic activity, high conductivity and their good stability, Ni/YSZ (Yttria Stabilized Zirconia) is one of the most studied anode materials. However, Ni/YSZ is very sensitive to the aforementioned pollutants and the anode tends to degrade. Sulfur or carbon adsorption on nickel leads to anode structural damages, resulting in a reduction of cell performances, a decrease of long term stability and a loss of catalytic activity.

Many studies have been undertaken on anode materials in

order to increase the tolerance of SOFCs anodes to carbon deposition and sulfur poisoning while keeping the attractive properties of Ni/YSZ anodes. Also, those materials could be classified into two categories, Ni-based anodes and Ni-free anodes.

In this study, Ni/YSZ-based anodes containing small amounts of ceria have been electrochemically tested, before and after polarization at a constant current density, using a sulfur-containing methane gas mixture as feeding fuel. The comparison of the cell performances and the resistances obtained from the impedance data allowed us to estimate the improvement of anode tolerance to carbon deposition and sulfur poisoning.

II. EXPERIMENTAL

Reference cells of 3.14 cm^2 were prepared by deposition of (La, Sr)(Co, Fe) $\text{O}_{3.8}$ (LSCF) cathode on an 8 mol.% YSZ electrolyte supported by a Ni/YSZ anode. Anode composition of the reference cells has been modified by substituting a small YSZ amount with ceria. Cells with ceria-containing anode will be further denominated as xCe-Ni/YSZ cells, where x is the weight percentage of ceria in the anode.

Both types of cells have been characterized at 750°C , before and after polarization at 0.5 Acm^{-2} (corresponding to a fuel utilization of 16%) using sulfur-containing methane as feeding

fuel while the steam to carbon (S/C) ratio has been fixed to 2. The average concentration of sulfur-containing compounds present in the methane was 10 ppm. Electrochemical Impedance Spectroscopy (EIS) measurements have been undertaken at OCV, 900 mV and 800 mV in a frequency range of 20 kHz-0.01 Hz with a perturbation amplitude of 20 mV. SEM analyses have also been carried out.

III. RESULTS AND DISCUSSION

A. Characterization of reference cells

Previous measurements have been made on reference cells by varying the sulfur content in the gas mixture and the steam/carbon ratio in order to understand the influence of carbon and sulfur on the cell degradation. The increase of the sulfur content in the gas mixture clearly limited the electrochemical process responsible of the surface diffusion phenomena on the anode side whereas increasing the S/C ratio promoted it.

B. Influence of ceria on cell degradation

The effect of ceria on the cell performances and degradation was investigated by comparing a reference cell with a modified-anode containing 3 wt.% of ceria. Cell degradation percentage was calculated by assimilating 0% degradation to the initial voltage and 100% degradation to 660 mV, lower limit voltage to avoid degradation correlated to anode re-oxidation (Fig. 1). Besides the presence of ceria increased the anode tolerance by ca. 30%, the anode degradation started slightly later. This could probably be explained the presence of a larger number of sites for sulfur adsorption.

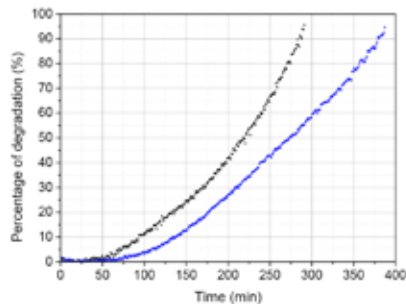


Fig. 1. Influence of the polarization time on the percentage of the voltage degradation of a reference cell (black) and a cell with a 3Ce-Ni-YSZ anode (blue). Measurements were performed at 0.5 Acm^{-2} .

Before polarization, the 3Ce-Ni/YSZ cell exhibits a slightly lower performance, which can be related to the increase of the anode resistivity due to the substitution of YSZ with ceria (Fig. 2). This result is in agreement with the increase of the Ohmic resistance values of the 3Ce-Ni/YSZ cell, obtained from the impedance data (Table I).

After polarization, both cells exhibit a drop of Ohmic resistances, consequence of deposited carbon on the anode, while a drastic increase in the polarization resistances, which

can be explained by the presence of delamination, is observed (Table II). SEM micrographs have confirmed structural damages within the cell.

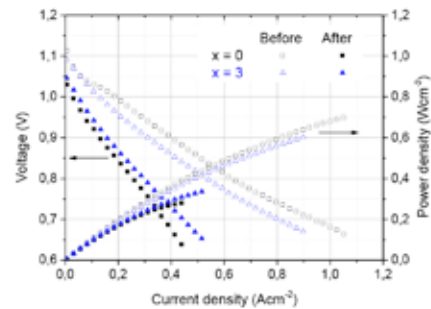


Fig. 2. Electrochemical performances of a reference cell and a cell with a 3Ce-Ni-YSZ anode before (empty symbols) and after (full symbols) polarization

If degradation is observed for both the reference cell and the 3Ce-Ni/YSZ cell, the drop of performances after the polarization as well as the increase of polarization resistances are less important for the cell with the ceria-containing anode. Such a small amount of ceria already illustrates an enhancement of the anode tolerance to carbon deposition and sulfur poisoning.

TABLE I
VALUES OF THE OHMIC RESISTANCES (IN ΩCM^{-2}) BEFORE AND AFTER POLARIZATION

Voltage	Reference cell		Cell with 3Ce-Ni-YSZ anode	
	Before	After	Before	After
OCV	0.2429	0.2360	0.2964	0.2868
900 mV	0.2637	0.2309	0.2962	0.2798
800 mV	0.2543	0.2258	0.2851	0.2735

TABLE II
VALUES OF THE POLARIZATION RESISTANCES (IN ΩCM^{-2}) BEFORE AND AFTER POLARIZATION

Voltage	Reference cell		Cell with 3Ce-Ni-YSZ anode	
	Before	After	Before	After
OCV	1.9811	1.2209	1.1402	0.9380
900 mV	0.2234	0.7249	0.2088	0.6020
800 mV	0.1713	0.7990	0.1314	0.5370

IV. CONCLUSION

This work aims to increase the SOFCs anode tolerance to carbon deposition and sulfur poisoning by doping Ni/YSZ with small amounts of ceria, maintaining the high catalytic activity of one of the most used anode material. Although the insertion of 3 wt.% of ceria slightly reduced the cell performance, the cell stability increased by ca. 30%. While the influence of carbon and sulfur compounds on the anode can be observed analysis the impedance spectra, a variation of the amount of ceria in the anode could allow us to determine the different contributions sensitive to these contaminants.



REDUCING WIND FARM FORECAST ERRORS AND PROVIDING BALANCING ENERGY WITH A FUEL CELL / ELECTROLYZER SYSTEM

F. Grueger*, F. Mochrke*

*Reiner Lemoine Institut gGmbH, Ostendstraße 25, (Germany)

Abstract - The supplementation of renewable energy sources by fuel cells (FC) and electrolyzers (ELY) is promising. This study investigates the potential of FC/ELY systems to reduce wind farm forecast errors as well as the system's capabilities of providing secondary control reserve (SCR) in Germany. Results show that both applications can be economically viable, especially when being combined. However, profitability is highly dependent on the system's configuration as well as its operating strategy.

Index Terms – Forecast Error, Fuel Cell, Electrolyzer, Secondary Control Reserve

I. INTRODUCTION

Wind farms, agglomerations of single wind turbines, are a technological option to provide electric energy based on renewable energy with a high degree of economic and technological sufficiency.

In Germany, wind farm operators (WFO) are currently able to compensate fed-in energy with a fixed tariff, which is defined in the renewable energy law (German: EEG). Additionally, it is possible for WFOs to participate in the existing energy markets, e.g. the day-ahead spot market. For day-ahead energy bidding, hourly slices of wind farm energy output have to be forecasted.

Wind forecasting is subject to error, leading to deviations of the fed-in energy from wind farm operators' market bids. Depending on the grid situation, energy deviations may result in penalty payments or profit for the WFO. Payments and profits are quantified via an imbalance energy price, which can assume positive and negative values.

Fuel cells (FC) and electrolyzers (ELY) are among the technology options which are capable to reduce the forecast error power by supplying electric energy (FC) or transforming surplus energy (ELY), thereby reducing both negative forecast deviations (FC) and positive deviations (ELY), respectively.

In Germany, Transmission System Operators (TSO) are responsible for balancing unforeseen deviations in both generation and consumption of electric energy. For this

purpose, positive and negative control reserve is required. In order to provide positive control reserve, energy has to be fed into the grid while the provision of negative control reserve implies consuming surplus energy. Primary, secondary and tertiary control reserve can be distinguished regarding call order, response time as well as compensation system.

Secondary control reserve (SCR) is organized via weekly calls for tenders. Each bid is defined by an energy price, a capacity price and the dedicated power. Positive and negative SCR is offered separately. FC and ELY operators can provide positive and negative SCR, respectively. Merit order lists of the bids are created by the TSOs, so the lowest bidder is called first when demand for positive or negative balancing energy arises. As soon as his contribution is no longer sufficient due to rising demand, the next bidder on the list is called and so on.

II. METHODOLOGY

A. Wind Farm Model and Prediction Forecast Error of Wind Farm Power

For this application study, a 100 MW wind farm in the Brandenburg region, Germany, is modeled. Both FC and ELY are considered to be operated by the WFO, assuming a single operator and a single balancing group for all components.

Simulation is conducted with quarter-hourly time steps for one year (2013). The wind farm consists of 50 wind turbines of 2 MW rated power each. 5 % for wind turbine power losses and 5 % for wind farm power losses, e.g. through shading, are taken into account.

B. Balancing Forecast Error

For modeling forecast errors, a mixed weighted normal Laplace probability distribution function (PDF) based on [1] is used. Three cases for different root mean squared errors (RMSEs) of 5 %, 10 % and 15 % are modeled. Resulting forecast error percentages are converted into the quantity of

desired time steps, i.e. 35,040 for a year in quarter-hourly resolution, and distributed on the simulated wind farm power. The distribution of forecast errors is conducted randomly with the constraint that the wind farm power with forecast error must not exceed the nominal power of the wind farm.

For FC and ELY application, scenarios with different rated electric power capacities of ELY (0.5 to 1.5 MW) and FC (0.1 to 0.75 MW) are considered. Resulting forecast error energy, hydrogen (H_2) production/consumption and cash flows are calculated. Profits or payments for reducing forecast errors are applied on resulting H_2 consumption or production, leading to H_2 production/consumption profits/costs.

C. Provision of Secondary Control Reserve

Historical data for one year (2013) is used regarding bids, their dedicated power and their power and energy prices [2]. Merit order lists are derived and minimum, maximum, average and median energy prices are identified for each week. In order to obtain an approximation of the requested balancing energy in high temporal resolution (4 s), available data of the theoretical demand is used and further processed.

Simulation is performed for different rated power capacities of ELY (0.3 MW to 0.5 MW) and FC (0.15 MW to 0.25 MW) and four bidding strategies of a FC/ELY operator are regarded. Strategies differ in energy price (minimum, maximum, average, median), but all comprise the respective median capacity price. In each time step, it is simulated whether the FC/ELY operator is called for provision of SCR. Full load hours (FLH), produced or consumed H_2 , as well as annuities and H_2 prices are determined.

D. Combination of Operation Strategies

The combination of an ELY providing SCR and a FC reducing forecast errors is analyzed as well. Different combinations are simulated and suitable configurations regarding H_2 balance are identified and evaluated.

III. RESULTS

A. Balancing Forecast Errors

In the given PDF, there is a high peak of forecast errors near the expectation value, leading to low forecast errors for most time steps. This results in high reductions of forecast error energy with even low installed power capacities of FC and ELY. For example, given a forecast RMSE of 10 %, results indicate that using a 0.7 MW ELY and a 0.2 MW FC, a total reduction of the forecast error energy by 15.2 % can be achieved. With provided data of the imbalance energy price for 2013, utilization of a FC with installed capacities of 0.1 to 0.4

MW results in profits of up to 3 €/kg H_2 while ELY operation with installed capacities between 0.5 and 1 MW results in production costs in the range of 1.6 to 2.9 €/kg H_2 .

B. Provision of Secondary Control Reserve

Results show that FLH are highly dependent on the bidding strategy. Average energy prices induce low FLH (< 600 h/a), while low prices can allow for more than 3.500 h/a (FC) and 5.000 h/a (ELY), respectively. Earnings concerning the FC are lower than 1 €/kg H_2 . Concerning the ELY, H_2 cost is 1.1 €/kg H_2 in the scenarios with FLH of more than 5.000 h/a.

C. Combination of Operation Strategies

The FC's rated power should amount for 0.2 MW to complement a 0.4 MW ELY regarding balance of H_2 production and consumption. Furthermore, low production cost of 1.1 €/kg H_2 (SCR) and relatively high earnings regarding the H_2 usage of 1.53 €/kg H_2 (forecast error reduction regarding 10 % RMSE) are achieved with this setup.

IV. CONCLUSION

FC / ELY systems are able to reduce forecast errors of wind farms. Low installed capacities of 0.7 MW FC and 0.2 MW ELY can reduce the forecast error energy by more than 15 % assuming a forecast RMSE of 10 %. This kind of system also is capable of participating in SCR market. Accepting low energy prices is necessary to obtain high FLH and low H_2 production costs of 1.1 €/kg H_2 . Economically, using FCs for provision of SCR is not sensible.

Combining those operating modes by reducing forecast errors with a FC and providing negative SCR with an ELY can be advantageous. The installed capacity of the ELY should be twice the FC's installed capacity in order to balance H_2 production and consumption.

ACKNOWLEDGMENT

The authors greatly acknowledge the funding of this work by research project "H2BER" (FKZ: 03BV242). It is part of the "National Innovation Programme Hydrogen and Fuel Cell Technology" funded by the Federal Ministry of Transport and Digital Infrastructure (BMVI). It is coordinated by the National Organization Hydrogen and Fuel Cell Technology (NOW).

REFERENCES

- [1] Wu, Junli, et al. "Statistical distribution for wind power forecast error and its application to determine optimal size of energy storage system." *International Journal of Electrical Power & Energy Systems* 55 (2014): 100-107.
- [2] German transmission system operators' internet platform for control reserve tendering, www.regelleistung.net



EFC1515070

EVALUATION OF LONG-TERM PERFORMANCE OF SEDIMENT MICROBIAL FUEL CELLS AND THE ROLE OF NATURAL RESOURCES

Timothy Ewing, Phuc Ha, and Haluk Beyenal

The Gene and Linda Voiland School of Chemical Engineering and Bioengineering,

Abstract - Sediment microbial fuel cells (SMFCs) suffer from long startup times and low power generation, which reduces their usefulness as an alternative power source for remote sensors. The goals of this work are to 1) shorten the startup time and increase the power generation of SMFCs by doping anodes with an electron donor, 2) test the long-term performance of SMFCs, and 3) quantify the microbial community structures and correlate them with power generation. We used electron donor doped anodes, which slowly release lactate, pyruvate, acetate and hydrogen. During our tests anode-limited SMFCs with and without electron donor-doped anodes were operated for approximately 18 months to simulate sensor operation. We found that electron donor-doped anodes generated their peak power within 42 days, while control anodes reached their peak power within 196 days. The anodes with electron donor generated a maximum of $55 \mu\text{W} \pm 2 \mu\text{W}$, while the control anodes generated $19 \mu\text{W} \pm 3 \mu\text{W}$ during the first 126 days of operation, demonstrating that the addition of electron donor critically improved startup time and initial power generation. After 173 days of operation control anodes generated more power than electron donor-doped anodes, demonstrating the undesired effects of electron donor-doped anodes. Finally, the two systems generated equal power after 504 days of operation. There were significant differences in community structure between control and electron donor-doped anodes. Surprisingly, these differences made no change in power generation. This was unexpected and demonstrates that power was limited by available substrates in natural environments other than the presence of certain microbial groups on the anode.

Index Terms - microbial fuel cell, sediment fuel cell, scale up, power density

I. INTRODUCTION

Sediment microbial fuel cells (SMFCs) are used as a renewable power source to operate remote sensors for environmental monitoring¹. They are deployed in lakes, rivers, and oceans and generate power where needed without maintenance. The organic compounds in the sediment serve as a source of renewable fuel. Electrons are generated from the oxidation of organic substrates and transferred to anode by the catalytic activity of

microorganisms present in the sediment²⁻⁴. These electrons are transferred from anode to the cathode to reduce oxygen⁵. In natural systems, organic compounds, known as natural organic matter (NOM), are renewed by sedimentation processes and provide organic flux to the anodes. The oxidation of organic carbon produces protons and electrons according to the following reaction:



The microorganism acts as a catalyst for this reaction. Therefore, an increase in the reaction rate on the anode (Equation 1) is expected to increase the power from a SFMC. The reaction rate can be increased 1) by increasing the organic compound concentration and 2) by improving the quality of the catalyst (microorganism). Generally, native organisms are used as the catalyst for the anode since they are already present in the sediment. Adding organic carbon to increase the reaction rate would also stimulate the catalytic community near the electrode^{6,7}. Therefore, many previous researches have tried to improve power production of SMFCs by introducing additional substrate to the sediment. However, the long-term performance of this improvement is poorly known. In this paper we investigate if addition of organic carbon could also help to increase long term performance of SMFCs. We also identify which factor limits the high power production from SMFC in long term run.

II. RESULTS AND DISCUSSION

In this work we doped a polylactate compound, 3D Microemulsion (3DMe™, Regenesis, San Clemente, CA 92673, USA) as an electron donor into anodes and used these anodes in SMFCs. This is known as a slow hydrogen release and have been used to improve long term performance of bioremediation. The performances of SMFCs with electron donor -doped anodes and controls were compared. We operated replicated SMFCs for approximately 18 months and present the average values with standard deviations. Finally, we investigated microbial community structure to determine whether the addition of electron donor caused any change.



Doping anodes with an electron donor improves the startup and power generation but not for long term

When soluble electron donor is doped into a porous anode, most of the electron donor will be trapped in the internal pores. We expect that for the first few days the power production will be similar since it takes a few days for the microbial population near the anode surface to increase significantly. We found that the power generations from electron donor doped system and the control system were almost identical for the first 5 days of operation. However after day 5, the power from the SMFCs with electron donor-doped anodes increased significantly compared to that of the control. We believe that this sudden increase was due to fast diffusion of the electron donor near the anode promoting microbial growth. The power generation of the SMFCs with electron donor-doped anodes remained relatively constant ($52 \pm 1 \mu\text{W}$) between days 42 and 168. During that time electron donor was slowly released out of the electrode by decomposing to lactate, pyruvate, acetate and hydrogen and their biological degradation byproducts. However after 168 days of operation, the power production was gradually decreased and reached a steady value of $18 \pm 1 \mu\text{W}$ after 252 days.

The control system which was not introduced with electron donor, it takes a long lag time of 196 days to reach to a maximum power production of $46 \pm 2 \mu\text{W}$. After that the power decreased until a new lower steady-state power was reached ($18 \pm 1 \mu\text{W}$).

Doping anodes with an electron donor improves the catalytic microbial community

On the 3DMe-doped anodes, the bacterial community structure showed significant change with respect to both the original inoculum (sediment) and the control anodes. Since the power generations were almost identical at long term operation before community structure analysis, this was unexpected. The Proteobacteria fraction increased significantly instead of being suppressed as in the control anodes. In addition, the classification at the class level shows that the most prevalent Proteobacteria belonged to the Deltaproteobacteria class, which accounted for almost 60% of the whole population. The other Proteobacteria groups, such as the Beta-, Gamma- and Alphaproteobacteria, represented a very minor percentage. Deltaproteobacteria are known to be anaerobic bacteria. They are known for potential of contributing anodic current in SMFCs^{15, 16}. It may seem desirable to improve the microbial community by doping microorganisms which can transfer electrons more efficiently. This would be expected to improve the anodic current. However, our results indicate that our SMFCs produce identical power in the long term regardless of the microbial community structure. This means that enriching the electron-transferring communities on the electrode may improve power generation temporarily but not in the long term.

III. CONCLUSION

In summary, the use of 3DMe shortened the startup time and improved the power generation. The main originality of our work is the long term operation of SMFC. If someone ran the experiments for 100 days, they could conclude that the SMFCs with electron donor-doped anodes produced three times higher power than the control. However, if we look at the data for 300 days we make the opposite conclusion: the control SMFCs generated twice as high a power. Finally, if we look at day 500 of operation we conclude that the two systems generate identical power. Therefore, our work show new information which was not available to the literature before and indicate the critical importance of long-term SMFC testing and improving the power.

ACKNOWLEDGMENT

This research was supported by NSF-CAREER award #0954186. Beyenal acknowledges additional support from Fundamental and Applied Chemical and Biological Catalysts to Minimize Climate Change, Create a Sustainable Energy Future, and Provide a Safer Food Supply (project #WNP00807). The authors would like to thank Mark R. Wildung and Derek Pouchnik for their assistance with the community analysis, which was done at the Washington State University (WSU) Sequencing Center. The authors also thank Regenesys for providing 3-D Microemulsion (3DMe)TM samples for this work.

REFERENCES

- 1 Dewan, A., Ay, S., Karim, N. & Beyenal, H. Alternative power sources for remote sensors: a review. *Journal of Power Sources* **245**, 129-143 (2014).
- 2 Aller, R. C. The Sedimentary Mn Cycle in Long-Island Sound - Its Role as Intermediate Oxidant and the Influence of Bioturbation, O₂, and C(Org) Flux on Diagenetic Reaction Balances. *J Mar Res* **52**, 259-295 (1994).
- 3 Reimers, C. E. *et al.* Microbial fuel cell energy from an ocean cold seep. *Geobiology* **4**, 123-136, doi:Doi 10.1111/J.1472-4669.2006.00071.X (2006).
- 4 Ateya, B. G. & Al-Kharafi, F. M. Anodic oxidation of sulfide ions from chloride brines. *Electrochem Commun* **4**, 231-238, doi:Pii S1388-2481(02)00254-0 Doi 10.1016/S1388-2481(02)00254-0 (2002).
- 5 Babauta, J. T. & Beyenal, H. Mass transfer studies of *Geobacter sulfurreducens* biofilms on rotating disk electrodes. *Biotechnol Bioeng*, doi:10.1002/bit.25105 (2013).
- 6 Lovley, D. R. The microbe electric: conversion of organic matter to electricity. *Current opinion in biotechnology* **19**, 564-571, doi:10.1016/j.copbio.2008.10.005 (2008).
- 7 Babauta, J. T. *et al.* Localized electron transfer rates and microelectrode-based enrichment of microbial communities within a phototrophic microbial mat. *Frontiers in microbiology* **5**, 11, doi:10.3389/fmicb.2014.00011 (2014).



ALTERNATIVE MATERIALS FOR ITSOFC: IMPLEMENTATION OF GADOLINIA-DOPED CERIA SOLID ELECTROLYTES IN A 3D CFD-FEM MODEL FOR NUMERICAL EVALUATION OF PERFORMANCE

D. Frattini, G. Accardo, M. de Pertis, C. Ferone, and R. Cioffi

Department of Engineering, University of Naples Parthenope & UdR INSTM of Naples
Parthenope, Centro Direzionale di Napoli – Is. C4, 80143 Naples (Italy)

Abstract – The reliable use of alternative solid electrolytes in an intermediate temperature range, namely 600-800°C, is desired to extend life time of employed materials, and to simplify the thermal management in solid oxide fuel cells. Actually, operations in this range are limited, mainly due to the absence of appropriate electrolytes that ensure high performance, in term of conductivity. Gadolinium-doped ceria is the most promising solid electrolyte material for intermediate temperature. The main aim of this study is to implement experimental conductivity data of gadolinium-doped ceria electrolytes in a computational model to evaluate their potentials and performances. The results suggest that these materials are better than traditional solid electrolytes, due to their improved ion conductivity.

Index Terms – electrolyte, gadolinium-doped ceria, modeling, SOFC.

I. INTRODUCTION

The intermediate temperature is the most desirable temperature range for fuel cells in most applications, and Solid Oxide Fuel Cells (SOFC) represent the most advanced technology to accomplish the goal [1]. In particular, compared to Yttria-Stabilized Zirconia (YSZ), which is the most diffused commercial electrolyte for SOFC, Gadolinia-Doped Ceria (GDC) electrolytes could provide appreciable ionic conductivity and lower ohmic resistance [2]. Computational models are extremely valuable tools for design and pre-analysis of Intermediate Temperature-SOFC (IT-SOFC), and also for characterization and performance studies of solid electrolytes [3]. In this work, experimental conductivity data of different GDC solid electrolytes, prepared with a modified sol-gel synthesis [4], have been used to perform 3D CFD simulations. These data have been implemented in ANSYS FLUENT to simulate an IT-SOFC and to compare electrolytes performance.

II. MATERIALS AND METHODS

A. YSZ and GDC conductivity data

Electrolyte conductivity as function of temperature is described by an Arrhenius-type equation [2, 3] as follows:

$$\sigma = \sigma_0 \cdot \exp\left(-\frac{E_a}{kT}\right) \quad (1)$$

Where σ is the conductivity, σ_0 is the pre-exponential factor,

k is the Stephen-Boltzmann constant, T the temperature in Kelvin and E_a is the activation energy for charge transport. An YSZ reference electrolyte and two new materials have been considered in this work [4-6]. GDC0.8 represents a 20% mol/mol Gd-doped electrolyte and GDC0.9 is a 10% mol/mol. The parameters used in the equation (1) for calculations are listed in Table I.

TABLE I ARRHENIUS PARAMETERS FOR SOFC ELECTROLYTES

Material	σ_0 [S/m]	E_a/k [K]
GDC0.8	$0,63 \cdot 10^3$	5084
GDC0.9	$0,53 \cdot 10^3$	5506
YSZ	$3,40 \cdot 10^4$	10350

B. SOFC geometry and model parameters

The geometric 3D model is based on a multilayer concentric tube layout, with a total length of 130 mm, according to the Westinghouse design [5]. The mathematical equations for the fluid dynamic and electrochemical model are reported in [5, 6]. Table II provides the dimensional details for all zones.

TABLE II SIZE OF SOFC MODEL ZONES

Zone	Dimension [mm]
Cathode channel diameter	4,00
Cathode thickness	2,00
Electrolyte thickness	0,04
Anode thickness	1,00
Anode channel outer diameter	8,00
Anode channel thickness	1,00
Anode current collector thickness	1,00
Cathode current collector thickness	2,00

In Fig. 1 the cross section of the layout is shown. The operating temperature is 700°C, fuel is humidified H₂, flow rate of $2,49 \cdot 10^{-7}$ kg/s, while dry air flow rate is $1,37 \cdot 10^{-5}$ kg/s.

C. Material properties of SOFC components

Anode is Ni-doped YSZ, cathode is a Lanthanum-Strontium-Manganese Oxide (LSM) and current collectors are made of Ferritic Chromium steel. The properties used during simulations, are listed in Table III [7].

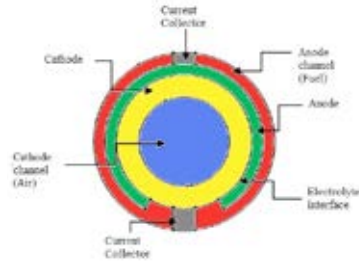


Fig. 1. Tubular IT-SOFC cross section.

Porosity and tortuosity of electrodes are assumed to be 30% and 3. Current collectors are considered impermeable [6].

TABLE III MATERIAL PROPERTIES USED FOR SOFC MODEL

Zones	Density [kg/m ³]	Thermal conductivity [W/m·K]	Specific Heat Capacity [J/kg·K]	Electrical conductivity [S/m]
Anode (Ni-YSZ)	3030	2,27	450	3,33·10 ⁵
Cathode (LSM)	4375	4,45	430	7,94·10 ³
Current collector (Steel)	8900	20,60	550	1,52·10 ⁷

III. RESULTS AND DISCUSSION

The present model has been validated by comparing polarization curves with literature [6, 8-9]. The results are shown in Fig. 2. At high current densities, the deviation is <5%.

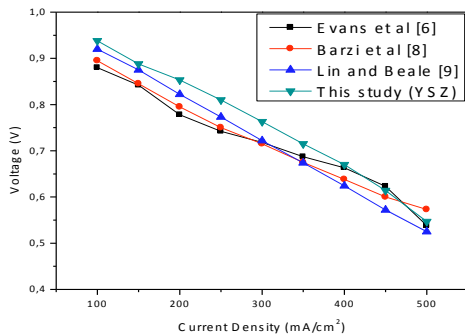


Fig. 2. Model validation with literature data.

The deviation at low current densities can be ascribed to the uncertainty on activation losses parameters used in references. In Fig.3 polarization and power curves for YSZ and the two GDC systems are compared.

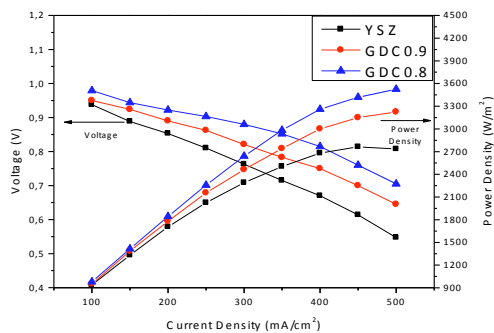


Fig. 3. Model results with different electrolytes.

A slight decrease in the linear slope is noticeable for GDC0.9 and GDC0.8 resulting in higher values of output

voltage and power density. Activation and concentration losses being the same, ohmic loss is lower due to the higher conductivity of GDC electrolytes. In Fig. 4 the spatial distribution of current density at electrolyte interface is shown. In these contours it is evident the more uniform development of the current by using GDC materials.

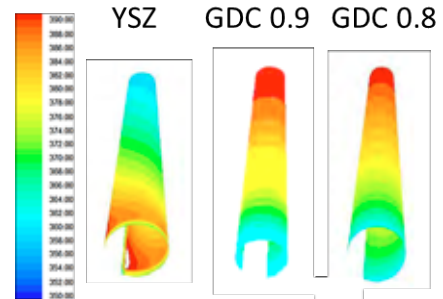


Fig. 4. Current density distribution (mA/cm²) with different electrolytes.

When conductivity increases, and ohmic loss decreases, charge transport is better, resulting also in a smoother distribution of other variables, such as temperature and molar fraction.

IV. CONCLUSION

In this work, YSZ electrolyte has been compared with GDC for IT-SOFCs application. Simulation results showed that cell with YSZ has an internal resistance higher than GDC-based cell, due to its lower conductivity. The benefit of GDC electrolytes is to enhance current density distribution at interface. In conclusion, these materials can effectively replace YSZ in IT-SOFC.

REFERENCES

- [1] Radhika, D., Nesaraj, A.S., Materials and components for low temperature solid oxide fuel cells – an overview, International Journal of Renewable Energy Development, Volume 2, 2013, pp. 87-95
- [2] Esposito, V., Traversa, E., Design of electroceramics for solid oxides fuel cell applications: playing with Ceria, Journal of the American Ceramic Society, Volume 91, 2008, pp. 1037-1051
- [3] Kakac, S., Pramuanjaroenkij, A., Zhou, X.Y., A review of numerical modeling of solid oxide fuel cells, International Journal of Hydrogen Energy, Volume 32, 2007, pp. 761-786
- [4] Ferone, C., Accardo, G., Dell'Agli, G., Cioffi, R., Sol-gel synthesis of gadolinium doped Ceria (Gd-CeO₂) for intermediate temperature SOFC electrolyte, Proceedings of the 5th European Fuel Cell Piero Lunghi Conference, 2013, pp. 391-392
- [5] Puthran, S.L., Koylu, U.O., Hosder, S., Dogan, F., Three-Dimensional CFD modeling of tubular solid oxide fuel cell with different fuels, Proceedings of the 9th ASME International Conference on Fuel Cell Science, Engineering and Technology, 2011, pp. 465-473
- [6] Evans, W.K., Rattanakornkan, K., Suksangpanomrung, A., Charojrochkul, S., The simulations of tubular solid oxide fuel cells (SOFCs), Chemical Engineering Journal, Volume 168, 2011, pp. 1301-1310
- [7] Mahato, N., Sharma, S., Keshri, A.K., Simpson, A., Agarwal, A., Balani, K., Nanomechanical properties and thermal conductivities estimation of plasma-sprayed solid-oxide fuel cell components: ceria-doped, yttria-stabilized zirconia electrolyte, Journal of Minerals, Metals & Materials Society, Volume 65, 2013, pp. 749-762
- [8] Barzi, Y.M., Ghassemi, M., Hamed, M., A 2D transient numerical model combining heat/mass transport effects in a tubular solid oxide fuel cell, Journal of Power Sources, Volume 192, 2009, pp. 200-207
- [9] Lin, Y., Beale, S.B., Performance predictions in solid oxide fuel cells, Applied Mathematical Modelling, Volume 30, 2006, pp. 1485-1496



THE EFFECTS OF OPERATING CONDITIONS ON THE PERFORMANCE OF INTERMEDIATE-TEMPERATURE SOLID OXIDE ELECTROLYSIS CELL FOR HYDROGEN PRODUCTION

Yuan Tan, Bo Chi, and Nan-Qi Duan

Center for Fuel Cell Innovation, School of Materials Science and Engineering, Huazhong University of Science and Technology, 1037 Luoyu Road Wuhan, Hubei 430074, (China)

Abstract- Solid oxide electrolysis cell provides the prospect of a cost-effective and energy efficient route to clean hydrogen production. Solution impregnated $\text{La}_{0.8}\text{Sr}_{0.2}\text{Co}_{0.8}\text{Ni}_{0.2}\text{-Gd}_{0.1}\text{Ce}_{0.9}\text{O}_2$ oxygen electrode was studied to assess the performance of the single hydrogen electrode-supported button solid oxide electrolysis cells and the electrochemical properties were evaluated and compared with the conventional pure LSCN oxygen electrode. To obtain further information for electrode design and cell performance improvement, the experiments were performed over a range of operating conditions, including the steam concentration (60-90 vol% absolute humidity), the operating temperature (650-800°C), and the applied voltage. The cell voltage decreased with increasing steam concentration, which was attributed to a decrease in the electrode polarization. Cell performances were shown continuous from the fuel-cell mode to the electrolysis mode of operation. Hydrogen production rate under the optimal conditions calculated from the Faraday' law can be up to $606 \text{ mLcm}^{-2}\text{h}^{-1}$ at 750°C.

Index Terms- anode, hydrogen production, optimal control, solid oxide electrolysis cell

I. INTRODUCTION

In recent years, there has attracted increasing interest in solid oxide electrolysis cells (SOECs) to produce hydrogen (H_2), which can be a promising effective way to achieve Zero-emission and high purity H_2 production[1]. When designing and defining the operational characteristics of the SOEC system, the control strategy used during operation is an important element which should be taken into account. However, a previous study

showed that the performance discrepancies of the cell in operation between the electrolytic and galvanic modes could be varied, depending on the electrode materials[2].

In this study, the performance and durability of a H_2 electrode-supported SOEC with a solution impregnated $\text{La}_{0.8}\text{Sr}_{0.2}\text{Co}_{0.8}\text{Ni}_{0.2}\text{-Gd}_{0.1}\text{Ce}_{0.9}\text{O}_2$ (LSCN-GDC) oxygen electrode were investigated. Ni-YSZ/YSZ/LSCN-GDC cell was studied over a range of partial pressures of $\text{H}_2\text{O}/\text{H}_2$ (60/40-90/10) and applied voltages (0.2-2 V). The durability of the cell during electrolysis was monitored, and the microstructure of the cell after the electrolysis was analyzed. Conventional pure LSCN electrode as a comparison of the electrochemical performance was also investigated.

II. EXPERIMENTS

Hydrogen electrode-supported SOECs consist of a Ni-YSZ cathode, YSZ electrolyte and LSCN oxygen electrode. NiO-YSZ and YSZ slurry were separately screen printed on the NiO-YSZ hydrogen electrode tapes fabricated by tape casting process and the tapes were co-sintered at 1390°C for 4 h. Then the GDC slurry was screen printed onto the hydrogen electrode support substrate and sintered in air at 1200°C for 2 h to form a porous GDC scaffold. A 0.5 mol L^{-1} solution for LSCN impregnation was prepared by dissolving stoichiometric amounts of $\text{La}(\text{NO}_3)_3 \cdot 6\text{H}_2\text{O}$, $\text{Sr}(\text{NO}_3)_2$, $\text{Co}(\text{NO}_3)_2 \cdot 6\text{H}_2\text{O}$, $\text{Ni}(\text{NO}_3)_2 \cdot 6\text{H}_2\text{O}$ into distilled water. The impregnated LSCN-GDC electrode was fabricated by impregnating GDC scaffold with the as-prepared LSCN solution,



followed by dried and sintered at 700°C in air for 2 h. The maximal content of impregnation treatment was achieved by repeating impregnation/drying cycles several times. For preparation of the cell with conventional LSCN anode with a GDC interlayer was screen printed and sintered at 1050°C for 2 h.

The performance of SOECs was measured at current density-voltage measurements and electrochemical impedance spectra measurements were recorded in a frequency range from 0.1 Hz to 10⁵ Hz with 10 mV amplitude at temperature between 650-800°C using an impedance/gain phase analyzer (Solartron 1260) and an electrochemical interface analyzer (Solartron 1287) at open circuit. The study was carried out over a range of SOEC operating conditions by varying the absolute humidity (AH) (60-90 vol%AH), the applied voltage (0.2-2 V) and the electrolysis current.

III. RESULTS

The performance and durability tests of the H₂ electrode-supported impregnated Ni-YSZ/YSZ/LSCN-GDC cell were performed. The variation of the SOEC performance with operating temperature was studied. The SOEC performance improved with increasing temperature, similar to the increasing SOFC performance with the operating temperature.

The effect of the steam content on the cell performance was investigated in both the SOFC and SOEC modes. Fig. 1 shows the I/V response of the impregnated LSCN-GDC cell when the absolute humidity was varied (60-90 vol%AH), and the operating temperatures were maintained at 750°C.

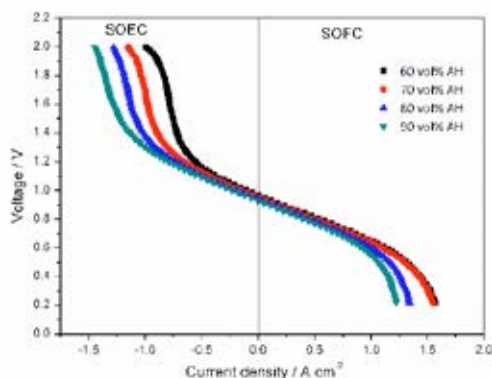


Fig. 1 I-V characteristics of H₂ electrode-supported impregnated

Ni-YSZ/YSZ/LSCN-GDC cell during the steam concentration (60-90 vol%AH) at 750°C.

The open circuit voltage was influenced by steam content and increased when the steam concentration decreased in accordance with Nernst potential. This result indicates that the increase in steam concentration in the hydrogen electrode gas stream can lead to the improvement of the cell current density values.

Durability studies on the impregnated Ni-YSZ/YSZ/LSCN-GDC cell were performed over 100 h at constant operating conditions (an electrolytic current density of 400 mA/cm², an operating temperature of 750°C, steam concentration of 60%). Compared to a conventional Ni-YSZ/YSZ/GDC/LSCN button cell under the same operating conditions, the performance durability was significantly improved.

IV. CONCLUSION

An experimental study has been completed to assess the performance of single solid oxide electrolysis cells modified by an impregnation method. Cell performances were shown to be continuous from the fuel-cell mode to the electrolysis mode of operation. For both SOEC and SOFC modes, performance improved with increasing temperature. The cell open circuit voltage decreased and performance increased with increasing steam concentration. Hydrogen production rate calculated from the Faraday' law can be up to 606 mLcm⁻²h⁻¹ at 750°C with an electrolysis voltage of 2 V and 90 vol% steam concentration. Under the optimal conditions, the cell was performed stable over 100 h.

REFERENCES

- [1] M. Keane, M. K. Mahapatra, A. Verma, and P. Singh, "LSM-YSZ interactions and anode delamination in solid oxide electrolysis cells," *Int. J. Hydrogen Energy*, vol. 37, no. 22, pp. 16776–16785, 2012.
- [2] P. Kim-Lohsoontorn, Y.-M. Kim, N. Laosiripojana, and J. Bae, "Gadolinium doped ceria-impregnated nickel-yttria stabilised zirconia cathode for solid oxide electrolysis cell," *Int. J. Hydrogen Energy*, vol. 36, no. 16, pp. 9420–9427, Aug. 2011.



FIRST-PRINCIPLES STUDY ON THE ELECTROCATALYTIC OF Pd(Zr)O AND STABILITY UNDER HIGH CATHODIC CURRENT

Ao Wang, Xiaofeng Yang, Lichao Jia, and Jian Li

School of Materials Science and Engineering, Center for Fuel Cell Innovation, Huazhong University of Science and Technology, 1037 Luoyu Road Wuhan, (China)

Abstract- The oxygen adsorption energy and formation energy of PdO (101) and Pd(Zr)O has calculated using Density Functional Theory to understand the effect of the Zr addition on the electrocatalytic of PdO. A half cell with the Pd_{0.8}Zr_{0.2}O-infiltrated LSM-YSZ cathode was polarized at the high cathodic current density of 1200 mA cm⁻² in air for 250 h at 750 °C. The result shows that the electrocatalytic has not greatly changed with the addition of Zr. The polarization resistance was decreased at the initial stage and then increased, finally reached an equilibrium since the growth of the Pd_{0.8}Zr_{0.2}O particles ceased, suggesting that the Pd_{0.8}Zr_{0.2}O particles were still stable under the high cathodic current density, which is very suitable for the operating conditions of SOFCs.

Index Terms-palladium-zirconium oxide, stability, high cathodic current, solid oxide fuel cell

I. INTRODUCTION

The improvement of Pd addition on the cathode performance has proved in previous studies [1, 2]. Considering that the poor stability of the infiltrated PdO particles, the addition of 20 mol. % Zr into PdO particles has significantly enhanced the performance and the stability of the microstructure of the cathode at 750 °C and different cathodic current densities of 400 and 800 mA cm⁻² for 250 h and 240 h in our previous study. Density Functional Theory (DFT) calculation was a power tool which allows us to gain further insight of the nature of the oxygen reduction reaction (ORR).

In this study, we attempted to gain insight into Pd_{0.8}Zr_{0.2}O catalyzed ORR by combining experimental studies and DFT calculations. And the adsorption energy

for ORR was calculated to understand the difference between the systems with or without the addition of Zr. Compared to the previous study of cathodic current densities of 400 and 800 mA cm⁻², a half cell with Pd_{0.8}Zr_{0.2}O-infiltrated LSM-YSZ cathode and YSZ electrolyte was polarized at high cathodic current density of 1200 mA cm⁻² to understand the effect of high cathodic current density on the stability of the Pd_{0.8}Zr_{0.2}O particles.

II. EXPERIMENTS

Zirconia electrolyte discs were prepared from 8 mol. % Y₂O₃-ZrO₂ (YSZ, Tosoh, Japan) by die-pressing, followed by sintering at 1550 °C in air for 4 h with ~1 mm in thick and ~20 mm in diameter. A-site deficient (La_{0.8}Sr_{0.2})_{0.95}MnO_{3- δ} (LSM, Fuel Cell) and YSZ electrode ink was prepared and applied at the center of the sintered compact YSZ electrolyte discs (1 mm* 20 mm) by slurry painting and sintered at 1200 °C for 2 h in air to form a porous cathode layer (15 μ m) with an area of ~0.5 cm².

The solution including Pd ion and Zr ion prepared by dissolving PdCl₂ and Zr(NO₃)₄·5H₂O in a hydrochloric solution under agitation at 80 °C. EDTA-NH₃·H₂O and citric acid were added to the solution in sequence at a molar ratio of EDTA: citric acid: metal ions = 1:1:2. The pH was controlled at about 8 by NH₃·H₂O. The as-prepared solution was infiltrated into the porous LSM-YSZ scaffold by sipping and dried in air and then fired at 750 °C for 2h in air. The weight gain for the optimal infiltration was about 15 wt. %. Electrochemical polarization and impedance



measurements were conducted in a three electrode set-up and a frequency range of 0.1 Hz to 10^6 Hz with 10 mV amplitude using an impedance/gain phase analyzer (Solartron 1260) and an electrochemical interface analyzer (Solartron 1287). The infiltrated cathode was polarized at cathodic current density of 1200 mA cm^{-2} in air for 250 h at 750°C to demonstrate the effect of high cathodic current density on the long-term stability of the infiltrated $\text{Pd}_{0.8}\text{Zr}_{0.2}\text{O}$ based cathode.

III. RESULTS

With the addition of Zr into PdO, the calculated adsorption energy for ORR and the formation energy by DFT calculations were both increased, suggesting that the high electrocatalytic and stability were both significantly enhanced. The electrochemical performance of $\text{Pd}_{0.8}\text{Zr}_{0.2}\text{O}$ -infiltrated LSM-YSZ cathode was polarized at high cathodic current density of 1200 mA cm^{-2} in air for 250 h at 750°C . By data fitting the impedance spectra, the initial polarization resistance before polarization was much smaller than that of the conventional LSM-YSZ cathode, suggesting the enhancement was ascribable to the high electrocatalytic $\text{Pd}_{0.8}\text{Zr}_{0.2}\text{O}$ particles. After being polarized, the polarization resistance was rapidly decreased at the first stage due to the typical activation processes of the LSM-based cathodes under polarization. Then the polarization resistance was gradually increased until it reached an equilibrium. This result demonstrated that the growth of the $\text{Pd}_{0.8}\text{Zr}_{0.2}\text{O}$ particles which resulted in the increase polarization resistance was ceased, proving that the $\text{Pd}_{0.8}\text{Zr}_{0.2}\text{O}$ particles were also stable under the high cathodic current density and high temperatures. The $\text{Pd}_{0.8}\text{Zr}_{0.2}\text{O}$ as novel high performance electrocatalyst was suitable for the application of SOFCs.

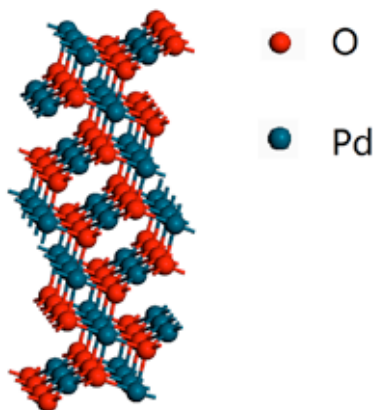


Fig. 1 Schematic representations of PdO (101) crystal structure

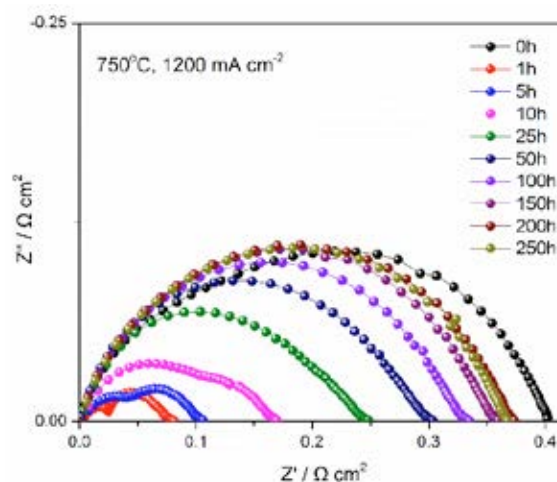


Fig. 2 Impedance curves of oxygen reduction on the $\text{Pd}_{0.8}\text{Zr}_{0.2}\text{O}$ infiltrated LSM-YSZ cathode as a function of time at 750°C and 1200 mA cm^{-2}

IV. CONCLUSION

An experimental study and theoretical calculation have been completed to assess the effect of high cathodic polarization current density on the stability of the $\text{Pd}_{0.8}\text{Zr}_{0.2}\text{O}$ electrocatalyst. The results show that the adsorption energy for ORR and formation energy were both increased. Under being polarized at the high cathodic current density of 1200 mA cm^{-2} in air for 250 h at 750°C , the change trend of the polarization resistance was similar to that of the cathodic current densities of 400 and 800 mA cm^{-2} which has been studied in previous work. The polarization resistance was finally reached an equilibrium since the growth of the $\text{Pd}_{0.8}\text{Zr}_{0.2}\text{O}$ particles ceased, suggesting the $\text{Pd}_{0.8}\text{Zr}_{0.2}\text{O}$ electrocatalyst is greatly suitable for the operating conditions of SOFC for various cathodic polarization current densities.

REFERENCES

- [1] F. Liang, J. Chen, S.P. Jiang, B. Chi, J. Pu, L. Jian, *Electrochemical and Solid-State Letters*, 11 (2008) B213.
- [2] F. Liang, J. Chen, J. Cheng, S.P. Jiang, T. He, J. Pu, J. Li, *Electrochemistry Communications*, 10 (2008) 42-46.



STRUCTURAL AND CONCEPTUAL CHALLENGES IN HIGH-TEMPERATURE FUEL CELLS

M. Cassir, A. Meléndez-Ceballos, V. Lair, A. Ringuedé

PSL Research University, Chimie ParisTech - CNRS, Institut de Recherche de Chimie
Paris, 75005, Paris, France

Abstract –We will present in this paper some of the main strategic aspects concerning structures and functionalities in two mature high temperature fuel cells: solid oxide, SOFC, and molten carbonates, MCFC. We will give a focus on the role of thin layers either as electrolyte materials (μ -SOFC, for instance) or as interfaces, insisting on high-quality Atomic Layer Deposition(ALD)-processed thin layers. We will also describe the interest of epitaxial thin films as improved catalytic layers at the anode side of SOFCs. Finally, we will depict a panorama of new concepts and applications, deriving from MCFC and SOFC: composite electrolytes, direct carbon fuel cells, CO₂ valorisation and water electrolysis.

Key words: SOFC, MCFC, hybrid fuel cells, thin layers, ALD, electrolysis

I. HIGH TEMPERATURE FUEL CELLS

High temperature fuel cells are still facing delicate problems, such as low yields, durability and costs, which mean that accelerated kinetics, degradation protection and new materials are highly required. In the case of the molten carbonate fuel cell (MCFC), the main difficulty is controlling the corrosion of the cathode and the bipolar plates and increasing power densities. The modular and compact “all solid” solid oxide fuel cell (SOFC) is the most challenging next-generation fuel cell regarding stationary power generation; however, combining solid electrodes, electrolyte and interconnects at very high temperatures requires a perfect control of interfaces. Serious developments are going on, but SOFCs should operate at lower temperatures (<650°C) without additional overpotentials at the

electrodes and with stable and efficient materials. In both SOFC and MCFC devices, thin functional layers constitute a key issue for improving interface reactions. The role of micro- or nanostructured thin films can be versatile: protective layers for MCFC (carbonate corrosion) and SOFC (diffusion or electronic barriers), bond layers between electrodes and interconnects and catalytic layers. Furthermore, in the case of SOFCs, thin-layered electrolytes can be envisaged for micro fuel cells systems as well as active electrolyte or electrode layers to improve both charge and mass transport. We are commonly using different deposition techniques: - low-cost, such as Chemical Bath Deposition (CBD) and electrodeposition; - or high-quality Atomic Layer Deposition (ALD), processing conformal, adherent and homogeneous layers [1]. Crystalline layers can be obtained by ALD at $T < 300^\circ\text{C}$ without annealing treatments. Figure 1 shows an ALD reactor with vertical flow, Picosun Sunale R200, and a homogeneous and conformal ceria deposit on a porous substrate. Cerium precursor is Ce(thd)₄ (STREM chemicals) and the oxidant ozone (70%). Ultrapure nitrogen is used as carrier gas and as purge. Deposition temperature is of 300 °C. Moreover, we have demonstrated the feasibility of epitaxial layers of ceria. Such deposits have an enhanced reductive power towards hydrogen oxidation and probably also towards the challenging direct oxidation methane. Clearly, the electrocatalytic role of these highly structured deposits has been evidenced [2,3]. In the case of MCFC, the main difficulty is the control of corrosion, particularly aggressive at the level of cathode, constituted by lithium-doped nickel oxide: Li_xNi_{1-x}O, and of the bipolar plates separating elementary cells. Among



the solutions for protecting such material, we may cite: - substituting nickel cathode by other materials more stable in carbonates; - recovering the surface of nickel by a protective coating, which allows decreasing its solubility without affecting its very good electrocatalytic properties. Several deposits have been tested (titanium, cobalt, niobium, cerium or iron oxides) by electrodeposition or by ALD [4,5]. Table 1 shows the effect of ceria, titania and cobalt oxide coatings on Ni solubility. These coatings reduce significantly Ni solubility, especially in the case of titania.

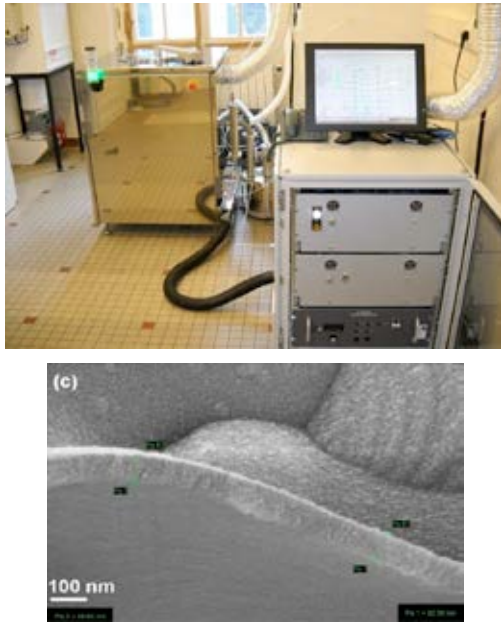


Figure 1. ALD reactor (up) and ceria deposit on a porous substrate (down).

Tableau 1. Solubility of nickel cathode as a function of the nature of the protective coating in MCFs [6].

Sample	Ni Porous	TiO ₂ 50 nm	CeO ₂ 20 nm	Co ₃ O ₄ 50 nm
Measured value (wt. ppm)	15	8	10	12

II. OTHER CONCEPTS & APPLICATIONS

Carbonate media allow highly valuable applications from the viewpoint of environment and energy, e.g. the electrochemical reduction by electrolysis of carbon dioxide producing carbon monoxide or carbon [7]. Molten carbonates, allowing a good dissolution of CO₂, appear as the best molten salts electrolytes to valorise this greenhouse effect gas.

Furthermore, the direct oxidation of carbon in a fuel cell is an old dream of electrochemists, considered during decades as

unrealistic due to the lack of knowledge on electrocatalysis and electrochemical kinetics [8]. Recently, this route is revisited successfully in hybrid systems, with a SOFC system fed on the anode side by carbon particles dispersed in molten carbonates. The molten phase acts as a fuel carrier and allows better anode oxidation kinetics.

A last application that we want to outline consists in combining two electrolytes, a solid oxide phase with a molten carbonate phase in view of associating the compactness of SOFC to a more conductive molten salt electrolyte. Very promising results are described in the literature, for example in our research group [9].

III. WATER ELECTROLYSIS

This operation is the reverse of a fuel cell and is known long time ago and already used to produce hydrogen in low temperature electrolyzers (mainly, polymer proton conductor electrolyzers). In the last ten years, there is a growing interest for high temperature electrolyzers, at atmospheric or higher pressures, which enable a significant decrease in the required expensive electrical energy, contrarily to thermal energy that tends to increase but is much cheaper. With respect to high temperatures, solid electrolyte systems are the most studied and promising ones [10]; nevertheless, the feasibility of molten carbonates electrolyzers has been recently proven and offers new prospects, in particular in the co-electrolysis of CO₂ and H₂O for producing syngas [11].

REFERENCES

- [1] M. Cassir, A. Ringuedé, L. Niinistö, J. Mater. Chem., 2010, 20, 8987
- [2] M. Cassir, S. McPhail A. Moreno, Int. J. Hydrogen Energy, 2012, 37, 19345
- [3] A. Marizy, T. Désaunay, D. Chery, P. Roussel, A. Ringuedé and M. Cassir, ECS Trans., 2013, 57, 983.
- [4] A. Marizy, P. Roussel, A. Ringuedé, J. Mater. Chem. A, 2009, 19, 760.
- [5] A. Meléndez-Ceballos, V. Albin, A. Ringuedé, S.M. Fernandez-Valverde, M. Cassir, Int. J. Hydrogen Energy, 2014, 39, 12233.
- [6] A. Meléndez-Ceballos, V. Albin, A. Ringuedé, S.M. Fernandez-Valverde, M. Cassir, Electrochim. Acta, 2014, 140, 174.
- [7] D. Chery, V. Albin, V. Lair, M. Cassir, Int. J. Hydrogen Energy, 2014, 39, 12330.
- [8] Y. Nabae, K. D. Pointon, J. T. S. Irvine, Energy Env. Sci., 2008, 1, 148.
- [9] M. Benamira, A. Ringuedé, R-N. Vannier, L. Hildebrandt, C. Lagergren, M. Cassir, Int. J. Hydrogen Energy, 2013, 37, 19371.
- [10] A. Nechache, M. Cassir, A. Ringuedé, J. Power Sources, 2014, 258, 164.
- [11] L. Hu, I. Rexed, G. Lindbergh, C. Lagergren Int. J. Hydrogen Energy, 2014, 39, 12323.



ANALYSIS OF THE EXPLOITATION OF BIOGAS FROM WASTE IN HIGH EFFICIENCY SOFC PLANTS: FROM WWTP TO AGRO-INDUSTRIAL SECTORS

M. Gandiglio ^{a*}, F. Gioelli ^b, A. Lanzini ^a, M. Santarelli ^a, P. Balsari ^b

^a Energy Department, Politecnico di Torino (Italy)

^b Waste Management Group, Department of Agricultural, Forestry and Food Sciences, Università degli Studi di Torino (Italy)

Abstract –The presented work deals with the analysis of Solid Oxide Fuel Cells (SOFCs) integration in biogas plants. Two main sections will be presented:

- The description of the DEMOSOFC EU project, related to the design and installation of an industrial size 174 kW_e SOFC in one of the SMAT Waste Water Treatment Plant in Torino (IT) [1].
- The feasibility study of the application of the same SOFC technology to other biomass local plants (agro-industrial activities) with focus on the agricultural plants with biogas from agro-wastes.

The feasibility evaluation will be performed through a techno-economic analysis of the suggested scenarios, with focus on the possible plant optimizations to yield a better energy and economic profile. Results confirm the optimal bond between the local biogas production sites and the SOFC technology.

Index Terms – Demonstration, Fuel Cells, Market, Biogas.

I. INTRODUCTION

In the context of the EU objectives for 2020, already extended through 2030 and 2050 roadmaps for climate and energy policy [1], the concepts of Renewable Energy Sources (RES), Green House Gas (GHG) Emissions reduction and Energy Efficiency (EE) are key factors for the development and the achievement of the targets. Fuel cells are a promising technology which could help the achievement of the proposed objectives.

The total demand for renewables in the EU has almost doubled in a decade and in 2012 the EU had installed about 44% of the world's renewable electricity (excluding hydro) [3]. The concept of Anaerobic Digestion (AD) from biomass has also played a central role during the last years powered by high incentives and subsidies at national level. The small and medium size biogas plants market are the core of the proposed analysis: they indeed have been found to have an optimal connection with fuel cell systems, in particular Solid Oxide Fuel Cells (SOFC). At present, in US the main SOFC producer in the medium size target is Bloom Energy [4] with several multi-MW installations either operating or planned across the US. In EU, nowadays, the only producer able to supply large size SOFC is CONVISION fuel cell [5], together with

SOLIDpower in Italy, which is enlarging its production capability.

A. Biogas

Biogas is usually produced from:

- Urban area: landfill gas, Organic Fraction of Municipal Solid Waste (OFMSW) and sewage sludges from water treatments (Waste Water Treatment Plant, WWTP).
- Agricultural area: animal manure/slurry, wastes from cereals/vegetables/fruit productions, energy crops.
- Industrial area: wastes especially from food industry (milk, beer, onion, etc...)

Throughout all EU different subsidies schemes can be found for AD plants, with incentives for the electricity production depending on the chosen substrate.

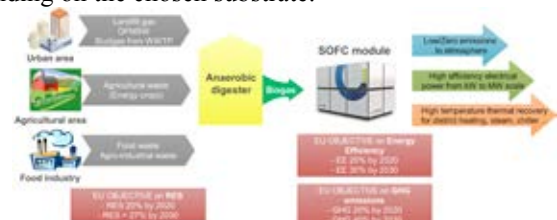


Fig. 1 . SOFC context with bio-sources.

II. SOFC PLANT INTEGRATION

A. Why biogas and fuel cells?

Depending on the chosen substrate or mix of substrates, the electrical and thermal requirements of the Anaerobic Digestion (AD) change (e.g. a more liquid feeding (high water content) will require a higher thermal contribution for heating but a lower electrical contribution for moving the stream). Biogas is usually fed to boilers for thermal-only production or Internal Combustion Engine (ICE) for Combined Heat and Power (CHP) generation.

Main disadvantages for traditional plants, which could be solved with a fuel cell installation, are related to:

- Emissions to atmosphere are often out of the limits.

- Reduced ICE electrical efficiency and higher cost at low sizes (from 43% at MW-size to 35% at kW-size).
- ICE usually operates at a fixed working point (no modulation) thus requiring a constant biogas production (and substrate) during the year.

On the other side, SOFC technology can guarantee different advantages: current modules ensure electrical efficiency >53% and total efficiency >80% [5] and the efficiency curve is almost horizontal from 100 to 50% of the nominal load. Finally, emissions to atmosphere are deleted for what concerning methane, SO_x, NO_x and VOC [5].

B. The DEMOSOFC project

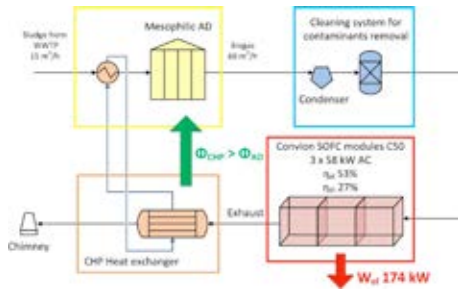


Fig. 2. The DEMOSOFC concept.

DEMOSOFC is a EU funded project which will start on September 2015, coordinated by the Energy Department of Politecnico di Torino. It will be the largest SOFC installation in Europe, and will be fed by biogas from Waste Water Treatment Plant (WWTP). The fuel cell plants will be the only and main generator of the plant, made of three modules 58 kW_e each supplied by Convion Oy [6]. Electricity will be 100% self-consumed within the plant and thermal production will be used for the digester heating. The biogas production in the WWTP is not constant during the year, depending on the availability of inlet waste water to the plant, thus requiring a system for which by-fueling or modulation is feasible.

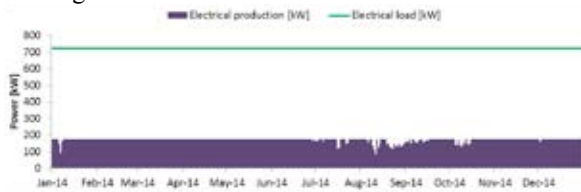


Fig. 3. Electrical production and load.

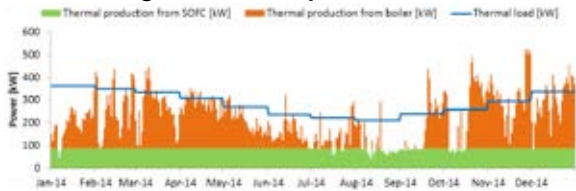


Fig. 4. Thermal production and load.

Dynamic analysis on available data for 2014 have been performed determining the expected electrical and thermal production depending on the biogas flow rate. A general minimum of the gas availability can be seen in the summer months because of the reduced production of waste water from citizens and industries. The electrical and thermal production

from the SOFC, depending on the available biogas, has then been compared to the required loads from the WWTP plant. In case of biogas surplus, extra fuel is sent to boiler for thermal production. Furthermore, during last months a detailed biogas analysis has been performed and the sulphur content detected. Results show a low and constant value for the H₂S due to the use of ferric chloride in the water treatment. The clean-up system, under design, will be made of a lead-and-lag series of reactors.

TABLE II. BIOGAS COMPOSITION ANALYSIS.

		#1	#2	#3	#4	#5
CH ₄	[%]	65.5	64.7	63.4	63.8	63.1
CO ₂	[%]	32.2	30.4	30.1	31.6	33.3
H ₂ S	[mg/m ³]	25.2	27.2	25.9	25.5	22.7

C. Biogas fed SOFC opportunities

Furthermore, despite WWTP, many AD plants presents a high surplus of thermal power which is usually wasted during transition and summer seasons (fired). SOFC, producing more electricity and less heat, can lead to a better exploitation of the biogas heating value. Agricultural waste AD plants are a wide potential market for fuel cells: trying to move from centralized large AD plants to local production, thus reducing the environmental and economic costs, the need for a < 500 kW efficient generator such as fuel cell is increasing.

TABLE II. AGRICULTURAL AD PLANTS ANALYSIS.

	Plant 1	Plant 2
Substrate	Corn crops 3 tons/day	Corn and other crops 53 tons/day
	Cow manure 30 tons/day	Rice straw 2 tons/day
ICE Size [kW]	250	1000
SOFC size [kW]	320	1320
Electricity self-consumption [%]	10%	8%
Heat self-consumption [%]	15%	10%

As can be seen from Table I, using clean and high efficiency systems as SOFCs can lead to a higher electrical production while avoiding problems related to emissions. These advantages, if subsidies for electrical production are considered, are turned into economic operational advantages.

III. CONCLUSION

SOFC systems have been found to be an optimal answer to the current limits of traditional ICE. Main barriers to the commercialization are now related to their high investment cost per kW compared to ICE and to the need for a challenging cleaning system to remove biogas impurities such as sulphur, halogens and siloxanes.

REFERENCES

- [1] Società Metropolitana Acque Torino - <http://www.smatorino.it/>
- [2] 2030 Climate and Energy Policy Framework
- [3] ESTAT SIRENE V2, Final Report May 2014
- [4] Bloomenergy - <http://www.bloomenergy.com/>
- [5] Fuel Cell Today 2013
- [6] Convion Fuel Cell Systems - <http://www.convion.fi/>



CROSSING EFFECTS OF CONTAMINANTS ON SOFC SINGLE CELLS FED BY BIOGAS

Davide Papurello*, Andrea Lanzini, Massimo Santarelli
Energy Department, Politecnico di Torino, C.so Duca degli Abruzzi
24, 10129, Torino - ITALY

Abstract - Biogas from biological treatments, as could be the anaerobic digestion of organic waste or of sewage sludge, generally contains a wide range of trace impurities (e.g., sulfurs, siloxanes, halogens, tar compounds, etc.). In this context, the paper describes an experimental analysis performed single cells fed by a reformat mixture, in order to detect the threshold tolerance limit towards different trace compounds. Results showed how the H₂S traces act mainly on the polarization losses especially on the mass transport resistance, due to the nickel sulfide starting formation. The HCl acts mainly on the electrochemical processes limitation. D4, acts already at ppb(v) levels on SOFC performance: 78ppb(v) to 178 ppb(v), are able to form silicon dioxide to block the anode porous sites. H₂S, introduced with other contaminants causes a variation of the dynamic of deterioration of SOFC performance, fasting the degradation.

Index Terms – SOFC, biogas, trace compounds, EIS.

I. INTRODUCTION

Among fuel cells, Solid Oxide Fuel Cells (SOFCs) can be regarded as the most flexible energy generator in term of fuel selections [1]. Various types of fuels can be adopted, from fossil fuels origin to biogenous ones [2]. Biogenous fuels respect to fossil ones allow to reduce the global warming potential impact in order to meet EU 20-20-20 requirements. These practical fuels, however, contain minor constituents as impurities. Among trace compounds Sasaki et al., (2011) investigated on the H₂S, PH₃, Cl₂ and D5 effect on NiScSz anode based fuel cell. The most detrimental compound on SOFCs performance, considered in literature works are H₂S and chlorine [3][4][5]. As reported by Haga et al., (2008) D5 was selected as model compound for siloxanes, 10 ppm(v) were demonstrated to be fatal on SOFCs performance [3]. No studies were accomplished on siloxanes at ultra-low concentration, even if they seem to strongly influence the cell performance at ppm(v) level [6]. Our goal is to investigate on the cell performance losses related to the different trace compounds concentration contained in a biogenous fuel.

II. MATERIAL AND METHODS

Simulated gas mixture concerning different fuel conditions are considered for the tests with trace compounds. Experiments were performed with anode supported solid oxide fuel cells

(ASC) - nickel based. Three planar circular type seal-less anode supported cells, with a diameter of 80 mm and a screen printed cathode of 78 mm, were used:

- ASC700 (SOLIDpower, Italy);
- ASC4 (H.C. Starck, Germany);
- TOFC (Topsoe fuel cell, Denmark).

The electrochemical characterization of the fuel cell was carried out with an electronic load (Kikusui Electronics Corp., Japan) in conjunction with an additional power supply in current-following mode (Delta Elektronica, The Netherlands). Electrochemical impedance spectroscopy analysis were performed through a GAMRY FC350 in the range of 10 Hz to 300 kHz. The oven temperature was kept constant at 750 °C.

III. RESULTS

Hydrogen sulfide influence on SOFC performance

The test was accomplished in order to investigate the H₂S impact on cell performance with a concentration ranging from 0,8 to 6,4 ppm(v), with a mixture that simulates a syngas produced from a wood gasifier, for example. Figure 1 depicts the nyquist diagram for ASC700 cell with a variable H₂S concentration.

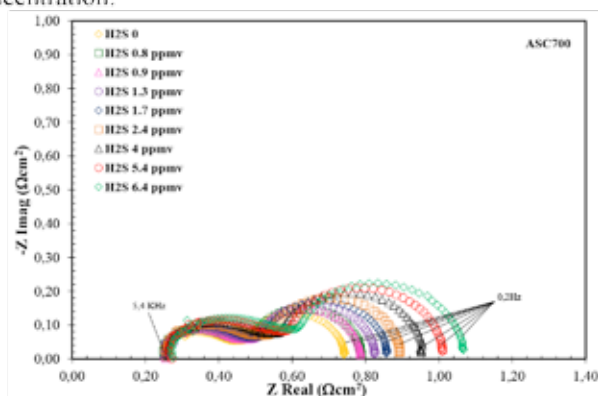


Figure 1 – Nyquist diagram varying the H₂S concentration – ASC700.

The ohmic contribution to the ASR value depicts the materials and interfaces resistances due to the transport of ions and electrons through the materials. This value is almost independent of the fuel composition and it is nearly not affected by the H₂S concentration value. Increasing the H₂S

concentration increase the low frequency circle amplitude respect to the high frequency circle, see figure 1. This is due to the mass transport resistance through the electrodes caused by the sulfur blocking sites.

Hydrogen chloride influence on SOFC performance

The hydrogen chloride dependence on the limiting factors on an anode supported fuel cell are investigated, adding to the gas reformate mixture a variable concentration of HCl that ranges from 1 ppm(v) up to 1000 ppm(v). Increasing the HCl content even at 100, 500 up to 1000 ppm(v) a strong ASR increase is not evident. Above 40 ppm(v) HCl concentration acts on the electrochemical processes that occur at the electrodes.

Octamethylcyclotetrasiloxane influence on SOFC performance

D4 concentration ranges from 111 ppb(v) to 1,92 ppm(v). This concentration range has been selected to get closer to the possible biogas mixture produced from a real plant. Figure 2 depicts the nyquist diagram for the TOFC cell fed by a variable D4 concentration range. Figure 2 in the upper right part shows how the cell performance are irreversibly affected by the D4 test. This is due to the silica precipitation that may cause a decrease in the active triple phase boundary (TPB) areas.

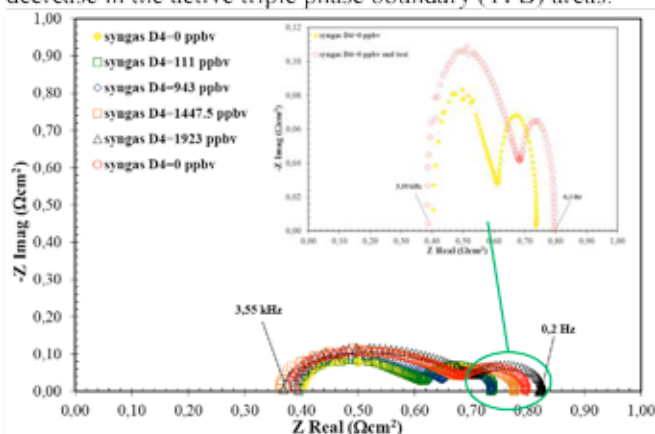


Figure 2 – Nyquist diagram varying the D4 concentration – TOFC.

Multi concentration influence on SOFC performance

Considering the H₂S concentration as the most dangerous compound for SOFCs, the contemporary presence with another detrimental compound is studied.

H₂S + C₂Cl₄

As previously reported, H₂S is the most detrimental compound and the chlorine addition is studied. Tetrachloroethylene (TCE) is a possible chloro compound detectable in a biogenous fuel, especially from waste water sludge. Possible implications on SOFC performance are studied in this section with a concentration variable from 0,62 to 1,67 ppm(v) of TCE and 4 to 0 ppm(v) of H₂S. The ohmic contribution remains constant in the double contaminant case. The C₂Cl₄ acts mainly on the high frequency polarization term, the electrochemical processes caused by the adsorption desorption behavior of chlorine. The term related to the transport phenomena instead, is greater influenced by the sulfur compound.

IV. CONCLUSION

This paper investigates the performance of an anode supported solid oxide fuel cell under a wide range of trace compounds. These compounds are found in biogenous fuels as biogas from OFMSW or from sewage sludge: H₂S, HCl, D4, C₂Cl₄. The different sources of performance limitation were shown from fuel cell impedance by the action of different trace compounds.

In particular:

The ohmic contribution is almost independent of the fuel composition and it is nearly not affected by the H₂S concentration value. The H₂S concentration acts mainly on the polarization losses, especially on the mass transport resistance through the electrodes caused by the sulfur blocking sites. The three phase boundary decrease as a consequence of the sulfur action on nickel active sites.

The HCl influence on SOFC performance is mainly due to the electrochemical processes that occur at the electrodes. Below 40 ppm(v) the HCl concentration slightly influence the SOFC performance.

D4, as model compound for siloxanes, acts already at ppb(v) levels on SOFC performance. D4 reduce the porosity and the fuel flow to reach the active sites, limiting the SOFC energy generation.

H₂S, introduced with other contaminants (C₂Cl₄) caused the instantaneous deterioration increased and the more types of contaminants included the larger the initial deterioration.

ACKNOWLEDGMENT

This work has been partly funded by the European Union under the SOFCOM project (www.sofcom.eu, contract number 278798).

REFERENCES

- [1] Sasaki K, Watanabe K and Teraoka Y. Direct-alcohol SOFCs: Current-voltage characteristics and fuel gas compositions. *J. Electrochem. Soc.* 2004; 151 (7): A965 - A970.
- [2] Sasaki K, Hlaga K, Yoshizumi T, Minematsu D, Yuki E, Liu RR, Uryu C, Oshima T, Ogura T, Shiratori Y, Ito K, Koyama M, Yokomoto K. Chemical durability of Solid Oxide Fuel Cells: Influence of impurities on long-term performance, *J. Power Sources.* 2011; 196: 9130 - 9140.
- [3] Hlaga K, Adachi S, Shiratori Y, Itoh K, Sasaki K. Poisoning of SOFC anodes by various fuel impurities, *Solid State Ionics.* 2008; 179: 1427 - 1431.
- [4] Bao J, Krishnan NG, Jayaweera P, Sanjurjo A. Effect of various coal gas contaminants on the performance of solid oxide fuel cells. Part III. Synergistic effects. *J. Power Sources.* 2010; 195: 1316 - 1324.
- [5] Rasmussen JFB, Hlaga A, Thyden K. Durability of solid oxide fuel cells using sulfur containing fuels. *J. Power Sources.* 2011; 196: 7271 - 7276.
- [6] Arnold M, Kajojinna T. Development of on-line measurement techniques for siloxanes and other trace compounds in biogas. *Waste manage.* 2010; 30: 1011 - 1017.



HARVESTING ENERGY FROM WASTEWATER: THE SOFCOM POLYGENERATION PLANT

A. Lanzini, M. Gandiglio, D. Papurello, M. Santarelli
Energy Department (DENERG), Politecnico di Torino
Corso Duca degli Abruzzi 24 – 10129 Torino, Italy

Abstract – Local renewable fuels like digester gas from various organic substrates can be efficiently exploited in high temperature fuel cell generators to co-produce electricity and heat. CO₂ capture from the anode exhaust is also feasible and can be relatively straightforward in these plants depending on the fuel cell type. This work presents the EU-funded SOFCOM project [1] which has a solid oxide fuel cell (SOFC) running on biogas from the anaerobic digestion of sludge collected from mixed urban and industrial wastewater. Results from the SOFCOM prototype plant are presented. The 2 kW_e SOFC is able to produce electricity while delivering an exhaust of pure and dry CO₂ effluent from the anode side. The captured CO₂ is recycled to a photobioreactor (PBR) to grow microalgae thus providing the benefit of enhanced water purification in term of nitrates and phosphates removal.

Index Terms – fuel cell, biogas, SOFC, algae, CO₂ capture, wastewater.

I. INTRODUCTION

The core component of the SOFCOM plant is the fuel cell stack reactor where biogas is transformed to electricity through efficient electrochemical reactions instead of combustion reactions that take place in less efficient internal combustion engines (ICEs) (see Fig. 1).



Fig. 1. The SOFCOM plant in the SMAT WWTP of Torino (IT) (the fuel cell section of the plant is shown with BoP, gas clean-up unit, reformer, oxycombustor and anode exhaust condenser).

The overall fuel cell electrical efficiency is >50% when running on biogas and the only exhausts of the plant are pure CO₂ and water. Compared to ICEs, the efficiency is 10-20 percentage points higher and with virtually zero emissions. From an energy strategy point of view, the demo plant aims at demonstrating how smart fuel cell based systems are key-enabling technologies that run on renewable fuels with best-in-class electric conversion efficiency and the potential for a closed-loop cycle on C-H-O atoms (carbon, hydrogen and oxygen). Such paradigm is that of new poly-generating systems for co-production of electricity, heat, fuels and chemicals. The as-received biogas is first cleaned to remove harmful contaminants (mostly H₂S and siloxanes), partially steam-reformed in an external fuel processor and then fed to a 2 kW_e SOFC stack (Sunfire, Germany). The anode exhaust is oxy-combusted to yield a stream that contains only H₂O and CO₂ (with only traces of H₂ and CO; N₂ is also found depending on the initial concentration in biogas). A water condensation/drying process is finally implemented to produce pipeline quality CO₂. The process layout of the fuel cell is shown in Fig. 2.

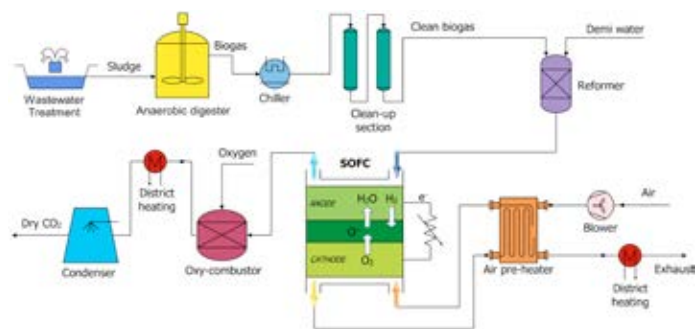


Fig. 2. SOFCOM process: biogas fuel cell plant.

In the SOFCOM plant, CO₂ is recovered and converted into a fuel stream through a photosynthetic process, which occurs in a closed tubular photobioreactor (see Fig. 3).

The photobioreactor (shown in Fig. 4) converts CO_2 into algae biomass through solar radiation and nutrients (nitrates and phosphates) found in the SMAT filtered water. The algae production leads to a high nutrients removal from filtered water generating two products: a potential fuel (algae) and a purified water stream.

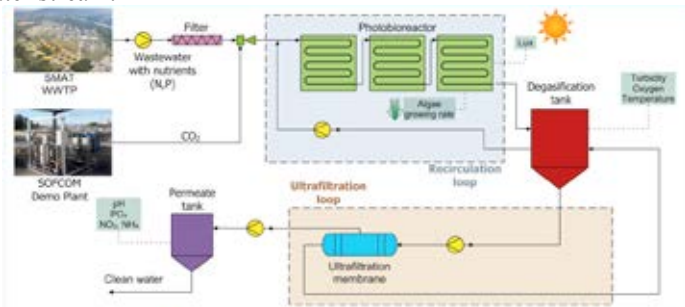


Fig. 3. SOFCOM process: photobioreactor (plant with ultrafiltration loop for clean water separation from algae).



Fig. 4. SOFCOM process: photobioreactor arrays.

II. EXPERIMENTAL

The performances of the various plant components have been tested from tens to hundreds of hours to demonstrate the technical feasibility of the proposed plant concept. The dynamic behavior of the SOFC has been assessed with respect to the thermal management of the SOFC stack during fast load transients, fluctuations in biogas composition and different anode/cathode flow conditions. Relevant parameters monitored in the PBR are the oxygen dissolved in the water stream, turbidity, chemical oxygen demand (COD) and total suspended solid (TSS) fraction.

III. RESULTS

The SOFC performances are stable during operation with biogas fuel (see Fig. 5). In Fig. 6 the performance of the photobioreactor (PBR) is presented. The diurnal profile of oxygen dissolved in the degasification tank is strictly connected to solar radiation. This clearly suggests enhanced photosynthetic activity when illuminance is high. In Fig. 7 the removal of nitrates is monitored through measurements performed every five days.

Fig. 5. Long-run biogas SOFC operation.

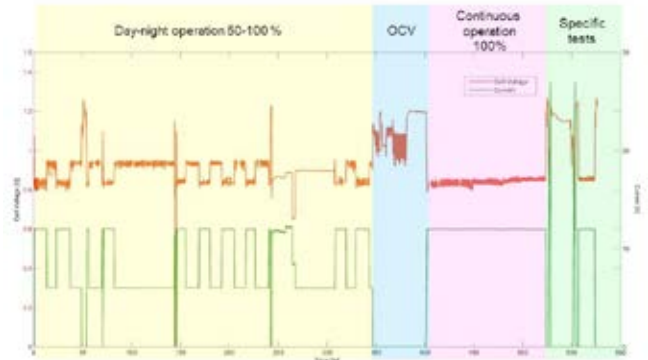


Fig. 6. Daily profiles of the PBR unit showing solar radiation, O_2

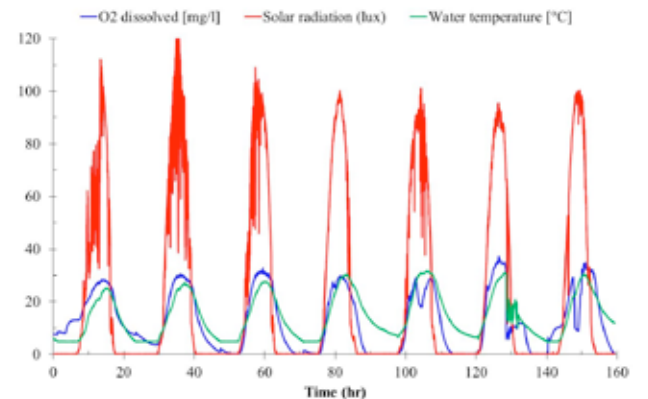
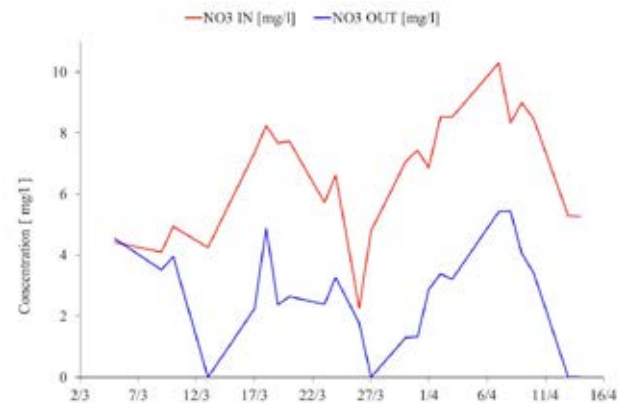


Fig. 7. Nitrates removal in the PBR.



IV. CONCLUSION

The fuel cell can be a key technology in the framework integrated in polygenerating plants whose goal is to maximize the use of inlet feeds in order to proceed further toward the development of highly energy and environmental efficient plants.

V. ACKNOWLEDGMENTS

The research leading to these results has received funding from the European Union's Seventh Framework Program (FP7/2007-2013) for the Fuel Cells and Hydrogen Joint Technology Initiative under grant agreement number 278798 'SOFCOM'.



MASS TRANSPORT ISSUES IN LOW PLATINUM LOADING CATALYST LAYERS FOR POLYMER FUEL CELLS

A. Baricci¹, M. Zago¹, H. Yu², R. Maric² and A. Casalegno¹

¹ Politecnico di Milano, Dipartimento di Energia, via Lambruschini 4, Milano 20156 (Italia)

² University of Connecticut, Department of Chemical and Biomolecular Engineering, Storrs CT (USA)

Abstract – State of art cathode catalyst layers for polymer electrolyte fuel cells require the use of Platinum based catalysts to promote the sluggish oxygen reduction reaction, with a Platinum loading of approximately 0.2 mg cm^{-2} . The main goal of research in long term deals with the necessity to reduce the Platinum loading that still impacts the cost of the system. Even though this topic has been researched intensively, low Platinum catalyst layers present mass transport limitations that strongly affect performance.

In the present work mass transport overpotential in low Platinum polymer fuel cells is investigated with the aid of a quasi 2D single cell continuum based model.

Index Terms – PEMFC, low Platinum, impedance spectroscopy, model.

I. INTRODUCTION

Polymer electrolyte fuel cells (PEMFC) are a promising candidate for automotive transportation thanks to their unique features: high power density, high efficiency, zero local emission of pollutants and fast startup. Nevertheless, PEMFC technology must overcome several issues to reach competitiveness, among which the cost and the durability that, at the state of art, do not meet the expected targets [1]. In particular, a large share of the cost of the stack is attributed to the cathode catalyst layer, because of the adoption of Platinum as electro-catalyst that significantly impacts the cost. A cost effective strategy should consist in the reduction of Platinum loading, but any attempt in this sense is challenging: low Platinum catalyst layers show important mass transport limitations. Furthermore, this mass transport loss increases during ageing, affecting stability of low Platinum PEMFC. A relevant quote of this mass transport loss has been attributed in previous works [2] to sluggish oxygen transport inside the ionomer that covers the catalyst at the agglomerate scale.

In the present work, mass transport overpotential in low

Platinum fuel cells is investigated. A theoretical approach is adopted to interpret the experimental results in the literature.

II. METHODOLOGY

The study has been carried out with an isothermal quasi 2D model of PEMFC [3]. The model solves mass conservation equation along the channel and couples this 1D channel model with a 1D model of the membrane electrode assembly (MEA). Stefan Maxwell law of diffusion is adopted in the backing layer and in the catalyst layer, where also proton conservation and Ohm's law are solved. Mass transport effect ionomer at the catalyst agglomerate level has been included according to [2] and spherical geometry has been selected. The output of the model consists in polarization curves and impedance spectra in different operating conditions, the latter performed according to the methodology reported in [4]. The effect of low Platinum has been simulated by changing physical properties, according to hypotheses discussed in Section III.

III. RESULTS AND DISCUSSION

Two approaches are identified that are used to reduce Platinum loading at the cathode side of PEMFC [2,5-6]:

- a) By using the same catalyst ink. Carbon and ionomer loading are thus reduced since same Pt/C and I/C ratio are maintained. As a consequence, catalyst layer thickness is decreased. Several experimental works in the literature adopt this approach and it is generally reported that mass transport limiting current moves toward low current density [5].
- b) By changing Pt/C in order to keep same catalyst layer thickness. In this case carbon and ionomer loading are maintained unchanged. This

methodology is seldom used in experimental works, but few works report that mass transport issues become evident while reducing Platinum loading in this case [6].

Simulations have been carried out to study case a). The results indicate that:

- 1) Oxygen and ionic transport across the CL improve at low Platinum loading as a consequence of the reduced thickness. The intensity of the improvement depends on the CL properties, *e.g.* if low values of Pt/C are implemented, a significant improvement is reported.
- 2) Additional mass transport loss becomes evident at the level of catalyst agglomerates. At low Platinum loadings the number of agglomerates is reduced and thus the reaction rate increases. Oxygen starvation occurs in the inner part of the agglomerate, where sluggish oxygen transport occurs.

Simulations have been carried out also to study case b), but the implemented model is not able to reproduce the effects reported in experimental works. If same catalyst layer and agglomerate properties are used, the model predicts that the polarization curve should basically shift at lower potential in the Tafel region, but no mass transport limitations should appear. Model limitations are identified in the onset of local effects of oxygen starvation at the agglomerate scale that are not included in the model [2].

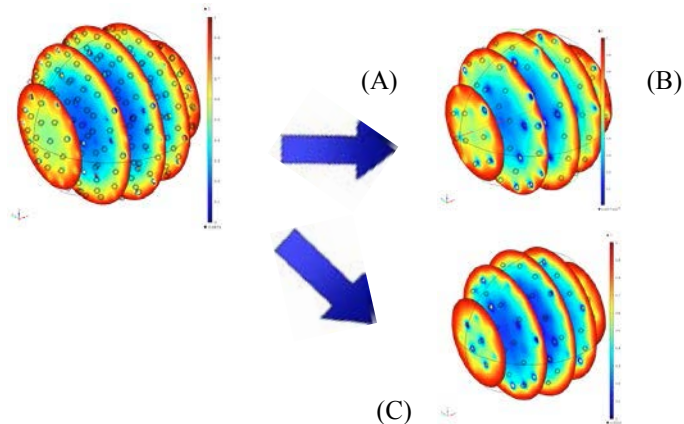


Fig. 1. Concentration of oxygen in catalyst agglomerate for different simulations. (A) High Platinum case (B) Low Platinum case with homogeneous loading dispersion (C) Low Platinum with heterogeneous catalyst distribution.

Model improvement is achieved by simulating oxygen transport at the agglomerate level with Comsol Multiphysics®, as reported in Fig. 1. Platinum catalyst nanoparticles are discretized as spheres of average particle radius (Platinum dispersion is not considered for simplicity). Special efforts are

required to guarantee uniform distribution in space and spherical symmetry. Low Platinum case is studied by maintaining same agglomerate structure.

The results indicate that the hypothesis of space homogeneity inside the agglomerate structure becomes critical for small agglomerates (~100 nm as typical for PEMFC) and low density of Pt nanoparticles or low Pt/C. The result is that the agglomerate effectiveness drops at high current density, indicating the onset of limitations in oxygen transport. It is also observed that the hypotheses regarding the distribution of Platinum in the external shell of the agglomerate strongly affect the results, demonstrating that the hypothesis of homogeneity does not hold. The simulation of impedance spectra shows that the feature related to ORR is expected to increase at low Platinum loading and this is an element for future model validation.

IV. CONCLUSIONS

The origin of mass transport limitations in low Platinum samples has been investigated in the present work. Samples produced by reducing catalyst layer thickness present mass transport limitations at the agglomerate level that may balance transport across the catalyst layer.

Low Platinum samples produced by reducing Pt/C at constant catalyst layer thickness suggest the onset of mass transport limitations due to non-uniform Platinum distribution inside the agglomerate, giving rise to local oxygen starvation.

REFERENCES

- [1] U.S. DRIVE, Fuel Cell Technical Team Roadmap (2013)
- [2] W. Yoon, A. Z. Weber, Modeling Low-Platinum-Loading Effects in Fuel-Cell Catalyst Layers, *Journal of The Electrochemical Society*, Volume 158, 2011, Pages B1007-1018.
- [3] Baricci A., Zago M., Casalegno A., A Quasi 2D Model of a High Temperature Polymer Fuel Cell for the Interpretation of Impedance Spectra, *Fuel Cells*, Volume 14, 2014, Pages 926-937.
- [4] Baricci A., Casalegno A., A simple analytical approach to simulate electrochemical impedance response of flooded agglomerates in polymer fuel cells, *Electrochimica Acta*, Volume 157, 2015, Pages 324-332.
- [5] Nonoyama N., Okazaki S., Weber A. Z., Ikogi Y., Yoshida T. Analysis of Oxygen-Transport Diffusion Resistance in Proton-Exchange-Membrane Fuel Cells, *Journal of The Electrochemical Society*, Volume 158, 2011, Pages B416-B423.
- [6] Qi Z., Kaufman A., Low Pt loading high performance cathodes for PEM fuel cells, *Journal of Power Sources*, Volume 113, Pages 47-53.



SOFC'S ANODE PROTECTION BY BIAS CURRENT APPLICATION: FIRST EXPERIMENTAL RESULTS ON A SHORT STACK.

G. Brunaccini, M. Ferraro, G. Squadrito, L. Di Giovanni, V. Antonucci

CNR- Istituto di Tecnologie Avanzate per l'Energia "Nicola Giordano" (CNR - ITAE)
Salita Santa Lucia Sopra Contesse 5, 98126 Messina (Italy)

Abstract - Solid Oxide Fuel Cells (SOFCs) are exposed to failures due to thermal cycles and to unexpected shut downs. Effects of thermal cycles related to controlled startup and shutdown can be mitigated by appropriate start/stop strategies, but unpredictable shut down strongly damages the system, especially in anode supported cells where anode's nickel oxidation arising at fast rate over 250°C usually breaks the cell, and very fast cooling of the SOFC stack down to 250° has as consequence the thermal shock break. Recently, reverse bias current application has been proposed to protect the anode from re-oxidation. In the present work the reverse bias current approach has been applied on SOFC stacks to assess the technique.

Index Terms – Solid Oxide Fuel Cells, Anode protection, Anode supported SOFC, Reverse bias current protection.

I. INTRODUCTION

Solid oxide fuel cells (SOFCs) have attracting increasing interest as highly efficient and clean energy conversion systems, due to the good electrochemical performance in the temperature range of 700-800 °C and the possibility of operating using also not pure hydrogen and simple hydrocarbons. Among these, anode supported Ni-YSZ SOFCs are now the focus of most R&D's, due to the reduction of the cell ohmic resistivity obtained because the high resistivity components (the electrolyte and the cathode) can be made very thin, while the most conductive component (the Ni-YSZ anode) can be relatively thick. The use of Ni-YSZ cermet anodes also has the advantages of high porosity, simple fabrication, chemical and physical stability in reducing environments, and good electro-catalytic activity for hydrogen oxidation. The anode structure comes from the reduction of a NiO-YSZ ceramic at the cell conditioning (first run) and it is particularly sensitive to Ni re-oxidations, due to any reason, that usually leads to a cell breaking. Under real operating conditions, redox cycling of the Ni-YSZ cermet anodes unavoidably occurs when the cells undergo run and shutdown repeatedly, which can cause some destructive stress to the thin electrolyte films due to thermo-mechanical variations in the

Ni-YSZ anodes, as well as the exposure of an anode to an oxidizing atmospheres at 800 °C due to hydrogen supply failure. This is because the re-oxidation of the Ni-YSZ anode can lead to mechanical mismatch of the anode and the electrolyte. The effects of thermal cycles related to controlled startup and shutdown can be mitigated with appropriate start/stop strategies. Recently, an alternative technique has been proposed [1-3] for unexpected shut down, it consists in the application of a reverse bias current to prevent the anodic catalyst from oxidation. This approach has been tested in half cell [3], but little information is currently available in more complex devices. Looking at the possibility to protect the SOFC stack using this technique, a series of test has been carried out on a commercially available SOFC short stack. First experimental results are here exposed and discussed.

II. EXPERIMENTAL

Tests were carried out on two short stacks (a 6 cells) by applying an external voltage through a potentiostat/galvanostat to reverse the electrical current flow by a very low current value (i.e. 0.035A/cm²). This procedure was applied with different selected reversal voltage values. For each short stack, the preliminary characterization was accomplished by an initial thermal conditioning up to 750°C supplying H₂/N₂ 5/95% mixture at anode side, and a polarization test to verify the stack integrity and the actual power generation. After this, the stack was made to work at nominal current (0.4 A/cm²) for a day and brought back at the OCV. Unexpected shut-down events were simulated by stopping the gas (hydrogen and air) flows. Since the stack voltage slowly dropped from the OCV at full gas flows to lower values (due to the internal gas consumption), once the read OCV reached the trigger value for each test iteration, the selected reversal voltage was applied, and the single cell voltages monitored. The desired time to satisfyingly complete the test was set to 30 minutes. This is due to the necessity of holding each cell voltage within a band limited by the maximum sustainable voltage (i.e. about 1.3V, as specified by the cell manufacturer) and the Ni oxidation potential (about 0.74V@750°C). This critical condition was the reason to stop some test iterations earlier than the desired time.



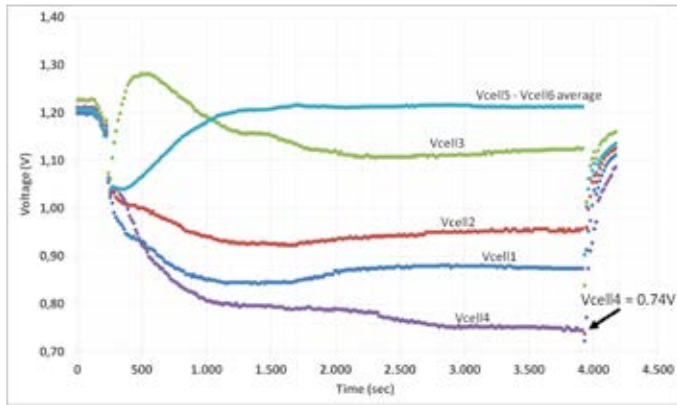


Fig. 1: Typical behavior of cell voltages under reverse bias current application.

III. RESULTS AND DISCUSSION

For each iteration of the reverse bias operations, the single cell voltages were monitored to stop the test if any cell voltage came out of the permitted band. In figure 1 a monitoring data plot is reported: a 7.35V was applied to the stack (i.e. an average cell voltage of 1.05V), and the experiment was suspended as soon as the lowest voltage reached 0.74V. Indeed, once imposed a stack voltage, each cell showed a different voltage due to the different internal impedances among cells. For this reason, depending on the applied stack voltage, the highest or the lowest cell impedance were the limiting factor for the test iteration run. In fact imposing the reverse voltage, the current is defined by the stack impedance and, consequently, the voltage of each cell will depend by its own impedance. In our tests only the reverse bias of 6.3V (1.05 V per cell) allowed a sufficiently long test, while at 1.12 and 1.1 V per cell the tests were stopped after few minutes. Figure 2 shows the electrochemical impedance spectra at OCV (1MHz - 0.1Hz; 0.1A) for 4 different reverse bias tests, compared with the reference curve. As can be seen, short tests at 1.1 and 1.12 V per cell did not affect the impedance spectra. On the other hand, at 1.05 V per cell reverse bias, the impedance showed a reduction at low frequencies. However, a slight impedance increment was detected after a second run (carried out after 48 operating hours) of the ICCP procedure at same voltage.

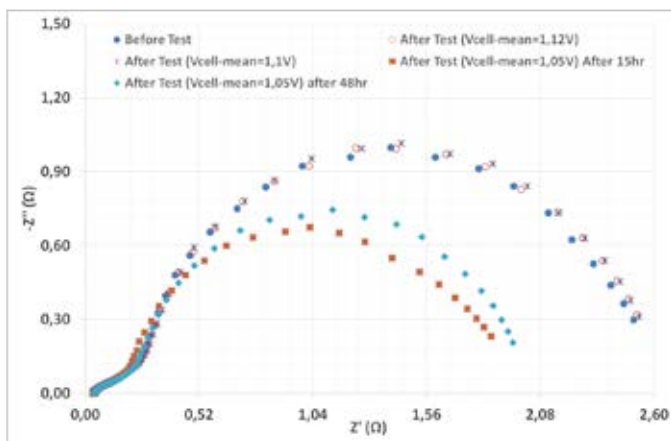


Fig. 2: EIS spectra before and after each of 4 reverse bias tests.

IV. CONCLUSION

Looking at the protection of SOFC stack anodes against Ni oxidation due to unexpected fuel supply shut down, reverse bias current method has been applied. Using this approach, a series of tests have been carried out on commercially available SOFC 6 cell stacks by single point bias control. The results show that probably this protection method could be used, but it is necessary that all the cells of the stack have the same impedance. Alternatively, a cell by cell bias application is necessary for controlling the cell voltage. This last approach would be more complex and expensive.

ACKNOWLEDGMENT

The reported results has been carried out in the framework of the EU project ASTERIX 3 (Grant Agreement n. 256764) financed by FCH-JU under the EU-FP7.

REFERENCES

- [1] D. Predinger, D. Ghosh – U.S. Patent 2002/0028362 A1 (2002)
- [2] M. J. G. Subhasish Mukerjee and B. Pieraggi, U.S. Patent 6,620,535 (2003)
- [3] J. L. Young, V. Vedharathinam, and V. I. Birss, “Reverse Cell Bias for the Prevention of Ni Oxidation During Air Exposure”, ECS Transactions, 35 (2011) 1697-1706

**Proceedings of EFC2015
European Fuel Cell Technology & Applications Conference - Piero
Lunghi Conference
December 16-18, 2015, Naples, Italy**

EFC15079

RESPONSE TO REFEREES.

The authors are grateful to the referees for their suggestions. About the addressed point.

1) Both figure 1 and 2 results difficult to read. They need to be expanded in order to appreciate axis scales and text. The suggestion is to reduce the writing, possibly shrinking and summarizing the paragraph "A. Background" into the paragraph "I. Introduction".

The two sections have been merged and the figures has been re-edited and changed according to indications to be more readable.

2) Figure 2 is not clear. Would it be possible to use different symbols for groups of two impedance spectra? This would make the comparison easier (i.e. use the same symbol and colour for the two EIS spectra of a couple, using void and filled symbol).

Figure 2 was changed and consequently also the related comments, this was done also to answer to the point 4.

3) Correct IES with EIS in sentence "Fig. 2: IES spectra before and after each of 4 reverse bias tests".

Done

4) Please spend few more words to explain better why the differences in cells impedance may affect the applicability of the reverse bias current protection method.

A more detailed description has been inserted, moreover fig. 2 was changed to better show the results. To avoid confusion a reduced set of EIS data has been reported, more data will be reported in oral presentation.



PHYSICAL MODELLING OF CATHODE IMPEDANCE IN LOW TEMPERATURE FUEL CELLS

M. Zago, A. Baricci, and A. Casalegno

Politecnico di Milano, Department of Energy, Via Lambruschini 4, 20156, Milano (Italy)

Abstract - Low temperature Polymer Electrolyte Membrane (PEM) fuel cells are a promising energy source for stationary and automotive applications, mainly due to high efficiency and low emissions. However the widely use of this technology is still hindered by some technological issues, among which severe cathode flooding and degradation. The most common technique to monitor system internal losses during real operation is the Electrochemical Impedance Spectroscopy (EIS). Despite the potentiality of this in-situ measurement technique, the interpretation of impedance data is still object of discussion in the literature and physical modelling becomes crucial to analyze experiments.

In this work, the development of a physically based model of cathode impedance is described and validated with respect to Direct Methanol Fuel Cell (DMFC) technology. The presented approach will be also applied to simulate cathode behavior in hydrogen fed PEM.

Index Terms – DMFC, EIS, PEM, model.

I. INTRODUCTION

EIS is a powerful *in-situ* measurement technique that permits to evaluate the kinetic and transport phenomena of an electrochemical system [1]. It consists in perturbing the fuel cell operation with a small AC current signal over a wide range of frequencies and in measuring the voltage response.

In the literature, the interpretation of EIS experiments is often carried out by means of equivalent circuit method (ECM). Even though simple and fast, this method is not reliable and provides only few qualitative information. In contrast, this work proposes the development and experimental validation of a physically based cathode impedance model, whose results are not related to the choice of a suitable equivalent circuit, but only depend on the governing equations of the system. In this work, the presented approach is applied to DMFC technology, since crossover and flooding phenomena are more pronounced.

II. MODEL DEVELOPMENT

The previously developed 1D (along the channel) + 1D (through the MEA) DMFC model [2] has been firstly integrated with a catalyst layer (CL) of finite thickness, which is composed by spherical flooded agglomerates [3] and the kinetic follows a direct catalytic methanol-oxygen reaction. The electrochemical mechanism of methanol oxidation reaction (MOR) generates protons and electrons, which are locally neutralized by the oxygen reduction: in this way, a proton current is generated in the CL due to the electrochemical MOR.

Subsequently, considering the same mathematical approach presented in [1], a physically based DMFC cathode impedance model has been developed. After obtaining the stationary solution, the transient perturbation solution can be obtained linearizing the system about a steady-state value and substituting each of the variables with a sufficiently low sinusoidal disturbance. The oscillating oxygen concentration at the CL-GDL interface is calculated by means of analytical solution of Fick's law in the frequency domain [4]. Because of the mass exchange with the GDL, the oscillation of oxygen concentration is produced and transported along the channel. This oscillation propagates along the channel while the channel volume dampens it. This effect is included in the impedance model, leading to the presence of an impedance feature in the low frequency region [4].

Moreover, since DMFCs are fed with a liquid mixture composed by water and methanol, the water as well as the methanol flow through the membrane from the anode to the cathode. The enhanced water crossover through the membrane may cause severe cathode flooding and its effect is considered in the model as a reduction of diffusion layers diffusivity proportional to both liquid permeation flux and water concentration at GDL-channel interface, as described in [5].

In the following, the main interesting results after model calibration on the experiments reported in [6] are presented. A systematic model validation on a wide range of operating conditions is currently in progress.

III. RESULTS

Fig. 1 reports the current density distribution across the cathode CL in OCV condition. It is interesting to note that, despite no useful current is drawn from the system, a proton current is generated in the CL due to the electrochemical MOR. This internal current is greater at channel inlet, where the methanol crossover through the membrane is higher.

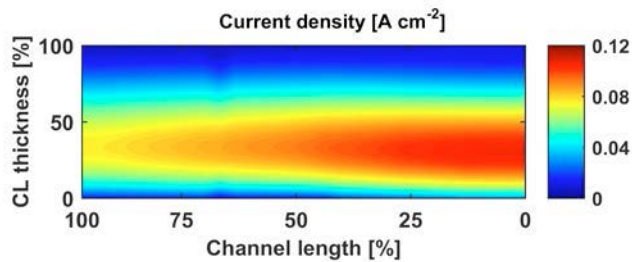


Fig.1 - Simulated current density profiles in OCV (348 K, met 3.25%).

Fig. 2 reports impedance simulations along channel length with and without the oscillations of oxygen concentration in the channel (i.e. channel impedance). It is interesting to notice that at channel inlet the two models are nearly superimposed, while toward channel end a second low frequency impedance feature appears considering channel impedance. Moreover, the difference between the two models increases with channel length. The effect of channel impedance is dampened increasing the cathode airflow or the oxygen concentration.

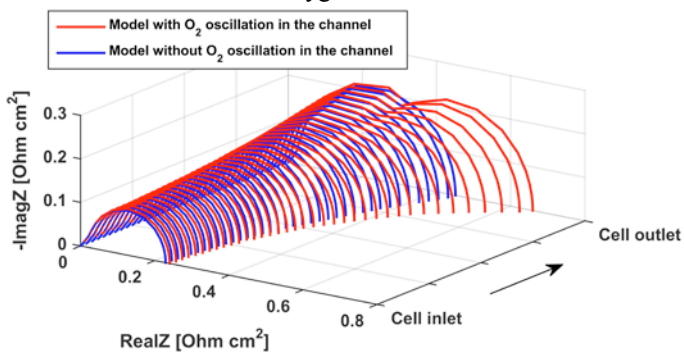


Fig.2 - Simulated cathode impedance with and without oxygen oscillation in the channel (348 K, met 3.25%, λ_a 6, λ_c 3, 0.25 A cm⁻²).

Fig.3 illustrates cathode impedance for a DMFC with anode MPL (MEA MM) and without anode MPL (MEA GM). As reported in [6], at 0.25 A cm⁻² MEA GM suffers from severe cathode flooding: this is confirmed analyzing water transport measurements and also impedance spectra, which highlight an increase of the low frequency impedance feature, related to mass transport losses. The developed model qualitatively reproduces the effect of flooding on cathode impedance,

coherently with the data reported in [6]. A rigorous model validation is still in progress.

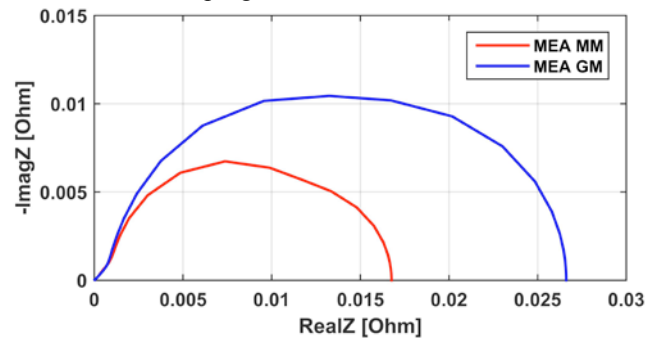


Fig.3 - Simulated cathode impedance of MEA MM and GM (348 K, met 3.25%, λ_a 6, λ_c 3, 0.25 A cm⁻²).

IV. CONCLUSION

From this work the following conclusions can be drawn:

- the electrochemical oxidation of methanol cross-over turns out in a generation of a proton current in the cathode CL;
- the oscillation of oxygen concentration in the channel implies a low frequency impedance feature, particularly evident toward channel end;
- flooding onset strongly affects the low frequency cathode impedance feature, related to mass transport phenomena.

Finally, after a systematic model validation, the developed model will be used as a diagnostic tool for the interpretation of impedance spectra measured during a degradation test.

ACKNOWLEDGMENT

This work has been performed in the frame of the FCH-JU FP7 project Second Act (EC Grant Agreement 621216).

REFERENCES

- [1] M. Zago, A. Casalegno, A physical model of Direct Methanol Fuel Cell anode impedance, *Journal of Power Sources*, Volume 248, 2014, Pages 1181-1190.
- [2] M. Zago, A. Casalegno, F. Bresciani, R. Marchesi, Effect of anode MPL on water and methanol transport in DMFC: Experimental and modeling analyses, *International Journal of Hydrogen Energy*, Volume 39, 2014, Pages 21620-21630.
- [3] A. Baricci, A. Casalegno, A simple analytical approach to simulate the electrochemical impedance response of flooded agglomerates in polymer fuel cells, *Electrochimica Acta*, Volume 157, 2015, Pages 324-332.
- [4] A. Baricci, M. Zago, A. Casalegno, A quasi 2D model of a high temperature polymer fuel cell for the interpretation of impedance spectra, *Fuel Cells*, Volume 14, 2014, Pages 926-937.
- [5] M. Zago, A. Casalegno, C. Santoro, R. Marchesi, Water transport and flooding in DMFC: experimental and modeling analyses, *Journal of Power Sources*, Volume 217, 2012, Pages 381-391.
- [6] F. Bresciani, C. Rabissi, M. Zago, R. Marchesi, A. Casalegno, On the effect of gas diffusion layers hydrophobicity on direct methanol fuel cell performance and degradation, *Journal of Power Sources*, Volume 273, 2015, 680-687



CO₂ TO METHANOL THROUGH DIRECT CATALYTIC CONVERSION BY STRUCTURED PROMOTED CeO₂ BASED CATALYSTS

A. Palella*, L. Spadaro*, M. Santoro**, A. Vita*, and F. Arena**.

* CNR Institute of Advanced Technology for Energy "Nicola Giordano", Via S. Lucia 5 98126, Messina, (Italy)

** Dipartimento di Chimica Industriale e Ingegneria dei Materiali, Università degli Studi di Messina, Salita Sperone 31 c.p. 29, I-98166 S. Agata, Messina, (Italy)

Abstract - The use of CO₂ as "reagent" looks very attractive for producing chemicals and fuels like methanol which can be directly fed to DMFC (direct methanol fuel cell) systems. Therefore, a series of Cu-ZnO based catalysts with a Cu/Zn atomic ratio of ca. 3 were prepared varying the carrier composition through the addition of ZrO₂ and tested in the CO₂ hydrogenation process. The increase of ZrO₂ content in the carrier composition improves the catalytic activity, in term of CO₂ conversion, in the whole range of operative pressures investigated.

Index Terms - CO₂ utilization, methanol, Cu-ZnO catalysts

I. INTRODUCTION

During the last century, the increasing level of the CO₂ in the atmosphere has been the principal responsible of global warming. Since the protocol of Kyoto, the major developed countries have devoted oneself to both a remarkable cut of CO₂ emission from industrial plants and to the adoption of new technologies either at low "environmental impact" or that can provide to the CO₂ recycling [1]. In particular, the use of CO₂ as "reagent" looks very attractive for producing bulk chemicals and fuels like methanol which can be directly fed to direct methanol fuel cell (DMFC) systems. Conversion of CO₂ into liquid hydrocarbons requires substantial amounts of hydrogen, which can be obtained from a renewable hydrogen source. On the other hands, methanol can represent a suitable and renewable energy sources for the hydrogen manufacturing, also being able to be used as vehicle for the "chemical storage" of the same hydrogen since it is inexpensive but has a relatively high energy density and can be easily transported and stored. It can be supplied to the fuel cell unit from a liquid reservoir which can be kept topped up, or in cartridges which can be quickly changed out when spent. Worldwide, methanol synthesis is still commercially produced by conversion of fossil-syngas (CO₂/CO/H₂) employing almost exclusively alumina supported copper-zinc catalysts, in reason of their positive cost/activity factor. In spite of this, more active catalyst

formulations have been recently proposed [2].

Thus, this work is aimed to improve the texture and metal surface exposure of CeO₂ supported Cu-ZnO catalysts through the utilization of ZrO₂ as a structure promoter, evaluating the catalytic performance of the new systems in the CO₂ hydrogenation process.

II. EXPERIMENTAL

A series of Cu-ZnO based catalysts with a Cu/Zn atomic ratio of ca. 3 were prepared by reverse co-precipitation under ultrasound irradiation route [3-4], varying the carrier composition through the addition of ZrO₂ as structure promoter (i.e. Zr_xCe_(1-x)O₂; 0.2 < x < 0.95). Catalysts were characterized by the means of XRF, XPS, XRD analysis, H₂-TPR measurements, N₂ isothermal physisorption and gas probe (H₂, N₂O) chemisorptions. The main properties of catalysts are summarized in Table I.

TABLE I. LIST OF CATALYSTS TESTED

Sample		Chemical Composition (wt.%)				Physical Properties		
		CuO	ZnO	ZrO ₂	CeO ₂	SA (m ² /g)	PV (cm ³ /g)	APD ^b (nm)
CeZr-100	calcined	44.2	13.4	42.1	0.00	154.0	0.34	9.0
	reduced ^a					132.0	0.28	8.0
CeZr-95	calcined	42.8	13.2	38.9	4.2	125.0	0.40	11.2
	reduced					62.0	0.20	12.9
CeZr-90	calcined	42.6	12.8	34.0	8.3	114.0	0.60	18.7
	reduced					56.0	0.21	10.8
CeZr-50	calcined	39.0	12.3	15.6	31.8	79.6	0.89	48.6
	reduced	39.0	12.3	15.6	31.8	40.0	0.20	15.7
CeZr-20	calcined	40.1	13.0	5.8	40.3	67.7	0.32	20.8
	reduced	40.1	13.0	5.8	40.3	36.0	0.20	21.0
CeZr-0.0	calcined	38.7	12.2	0.0	48.8	47.0	0.24	20.0
	reduced	38.7	12.2	0.0	48.8	34.0	0.17	20.0

^asamples reduced at 573K (1h) in flowing H₂ and then passivated at 293K in a 2% O₂/He flow ; ^bAverage Pore Diameter (APD, 4PV/SA)

The catalytic tests in the CO₂ hydrogenation were performed in the range of 453-513K and at 0.1-5.0 MPa using a semi-



automated LAB-micro-plant, fed with a CO₂/H₂/N₂ (3/9/1) mixture at a rate of 80 STP mL/min (GHSV, 8.800NL·kg⁻¹_{cat}·h⁻¹), while reactants and products were on-line analyzed by GC.

III. RESULTS

A. Characterization

As shown in Fig. 1, the addition of ZrO₂ in the carrier composition strongly improves the textural properties of Cu-ZnO catalysts, increasing both the total surface area, the metal surface (MSA) exposure and the resistance to sintering phenomena due to the reduction process.

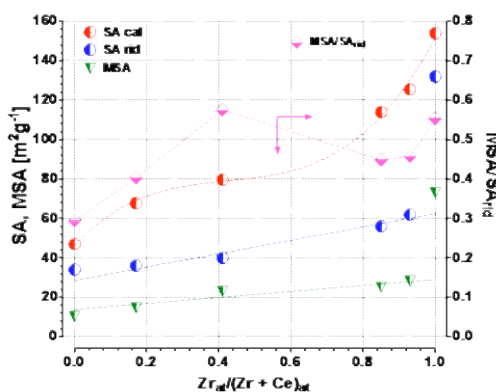


Fig. 1. Influence of carrier composition on the textural properties of catalysts

B. Catalytic Activity Measurements

Almost independently to chemical composition, at low pressure (0.1MPa) all catalytic systems show a progressive increase of CO₂ conversion with temperature and a corresponding decrease in selectivity to methanol. Namely, the increase in ZrO₂ content in the catalyst formulation drives to a positive increase in the reactivity in term of CO₂ conversion, while the selectivity to methanol tends to be reduced. In addition, catalytic data at 3.0MPa and 5.0 MPa clearly show the positive influence of pressure on the catalytic activity of all the sample tested.

Thereafter, the activity pattern of the studied catalysts in the CO₂-hydrogenation reaction is compared in Fig. 2. Namely, at low pressure the three families of catalyst exhibit a different catalytic behavior, showing a decrease in selectivity with the progressive addition of ZrO₂. On the contrary, at high pressure, all the systems show the same reactivity pattern, irrespectively to chemical composition of the catalysts and operative pressure.

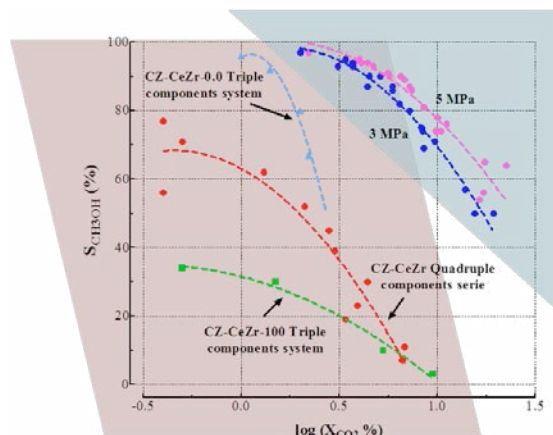


Fig. 2. Activity pattern in the CO₂ hydrogenation reaction

IV. CONCLUSION

The effects of temperature, pressure and carrier composition on the activity–selectivity patterns of ZrO₂/CeO₂-supported Cu–ZnO systems (i.e. Zr_xCe_(1-x)O₂; 0.2 < x < 0.95) in the synthesis of methanol via CO₂ hydrogenation have been thoroughly assessed. The addition of ZrO₂ in the carrier composition strongly improves the textural properties of Cu-ZnO catalysts and the catalyst reactivity in CO₂ hydrogenation process, especially at high pressure. The following reactivity scale has been recorded:

$$\text{CeZr-100} > \text{CeZr-95} \approx \text{CeZr-90} > \text{CeZr-20} > \text{CeZr-0.}$$

REFERENCES

- [1] Saeidi, S., Amin, N.A.S., Rahimpour, M.R., Hydrogenation of CO₂ to value-added products - A review and potential future developments, *Journal of CO₂ Utilization*, Volume 5, 2014, Pages 66–81.
- [2] Arena, F., Mezzatesta, G., Zafarana, G., Trunfio, G., Frusteri, F., Spadaro, L., Effects of oxide carriers on surface functionality and process performance of the Cu–ZnO system in the synthesis of methanol via CO₂ hydrogenation, *Journal of Catalysis*, Volume 300, 2013, Pages 141–151.
- [3] Arena, F., Italiano, G., Barbera, K., Bonura, G., Spadaro, L., Frusteri, F., Basic evidences for methanol-synthesis catalyst design, *Catalysis Today*, Volume 143, 2009, Pages 80-85.
- [4] Spadaro, L., Arena, F., Granados, M., Ojeda, M., Fierro, J.L.G., Frusteri, F., Metal–support interactions and reactivity of Co/CeO₂ catalysts in the Fischer–Tropsch synthesis reaction, *Journal of Catalysis*, Volume 234, 2005, Pages 451-462.



FUEL PRODUCTION BY PHOTOCATALYTIC CONVERSION OF CO₂ AND WATER FROM THE CEMENT WORKS EMISSIONS

A. Palella*, F. Arena**, P. Negro***, and L. Spadaro*

* CNR Institute of Advanced Technology for Energy “Nicola Giordano”, Via S. Lucia 5, 98126 Messina, (Italy)

** Dipartimento di Chimica Industriale e Ingegneria dei Materiali, Università degli Studi di Messina, Salita Sperone 31 c.p. 29, 98166 S. Agata Messina, (Italy)

*** Italcementi Group, Laboratorio di Brindisi, S.S. 7 per Mesagne, Km 7+300, 72100 Brindisi, (Italy)

Abstract - Anthropogenic emissions of CO₂ are one of the mainly responsible of the Planet warming, due to the greenhouse effect. In particular, it is noteworthy that the cement industry alone accounts for around the 5% of global carbon dioxide emissions, since the production of a ton of cement generates nearly a ton of CO₂. Therefore the present work aims to shed light on the behavior of several oxides and sulfured semiconductors for the direct photoreduction of CO₂ into methanol. Then, the results of research were used for the realization of an integrated pilot plant placed in a cement factory of Italcementi group in Bergamo.

Index Terms - CO₂ Photoreduction, TiO₂ based catalysts, pilot plant, exhaust fumes

I. INTRODUCTION

The increase in CO₂ emissions arguably contributes to the increase in global temperatures and climate change due to the "greenhouse effect" [1]. In particular, it is noteworthy that the cement industry alone accounts for around the 5% of global carbon dioxide emissions, since the production of a ton of cement generates nearly a ton of CO₂. Then, due to the high emissions impact, several technologies have been developed to mitigate both the production and the emission of CO₂ from cement plant, such as switching to alternative and more sustainable fuels (i.e. natural gas or biomasses), enhancing the efficiency of the whole process or capturing the CO₂ emissions after they are produced through carbon capture, use and storage technologies (CCUS). In this context, the CO₂ utilization as raw material to produce liquid and gaseous fuels, mainly methane and methanol, that could be used as energy vectors for the industrial electrical facilities, has been considered in many catalytic processes. However, all indirect approaches potentially available in the CO₂ conversion are energetically less effective than the direct photocatalytic reduction of CO₂ with water into hydrocarbons such as formic acid, formaldehyde, methanol and methane, by using of semiconductor (i.e. TiO₂, ZnO, CdS, SiC, WO₃) [2-3]. Therefore the present work aims to shed light on the behavior of several oxides and sulfured semiconductors,

doped with different metals (i.e. Cu, Zn, Co, Mn, Ni) for the direct conversion of CO₂ into methanol. Then, the results of research were used for the realization of an integrated pilot plant placed in a cement factory of Italcementi group in Bergamo.

II. EXPERIMENTAL

The diverse TiO₂ based photocatalysts were prepared by either incipient wetness impregnation (iw) or reverse coprecipitation (rc) route, according to the procedures elsewhere described [4-5]. In particular, reference TiO₂ semiconductor (TiO₂M211) was doped with CuO (CT_{iw}) or with Cu, Ce, Zn and Mn oxides (i.e. CCMZT_{iw} and CCMZT_{rc}). Besides, CdS/TiO₂ photocatalytic system was prepared by preformed TiO₂ impregnation with Cd solution and subsequent sulfiding under H₂S at 350°C for 6h. The list of photocatalysts with related chemical composition and physical properties is shown in Table I.

TABLE I. LIST OF CATALYSTS WITH CHEMICAL COMPOSITION AND PHYSICAL PROPERTIES

Code	Chemical Composition %wt					Physical Properties	
	TiO ₂ Based Photocatalysts					SA (m ² /g)	PV (cm ³ /g)
	CuO	CeO ₂	ZnO	MnO	TiO ₂		
TiO ₂ M211					85.0	297	0.37
CT _{iw}	1.0				84.0	297	0.38
CCMZT _{iw}	1.0	1.0	1.0	1.0	81.0	295	0.36
CCMZT _{rc}	5.0	5.0	5.0	5.0	80.0	155	0.21
	S-TiO ₂ Based Photocatalyst					SA (m ² /g)	PV (cm ³ /g)
	Cd		S		TiO ₂		
CdS/TiO ₂	1.1		0.9		82.0	267	0.36

All the photocatalytic systems were characterized by the means of XRD, XRF and XPS analysis, physisorptions and



chemisorptions measurements and temperature programmed reduction (TPR). Photocatalytic tests were performed both in a laboratory by using a mixture of $\text{CO}_2/\text{H}_2\text{O}$, and in the Italcementi pilot plant, using pre-treated exhaust gas evolved during the emission of cement industry furnaces. The LAB micro-plant is equipped with a continuously fed gas phase tubular quartz reactor and a UV high-pressure lamp model OSRAM ULTRA-VITALUX (300 W, AM 1.5). While, the photocatalytic reactor in the pilot plant is a shell and tube coated with a thin layer of catalyst and continuously fed with the gas phase.

III. RESULTS

A. Catalytic Activity Measurements

The results of catalytic tests carried out in the LAB micro-plant are summarized in Figure 1A-B. As can be easily seen, the reduction of CO_2 in gas/vapor phase leads to the formation of different reaction products, the main of which are formaldehyde, formic acid, acetaldehyde, methanol, methyl formate and acetals, Figure 1A. As a rule, the formation of acids, aldehydes and alcohols is probably due to direct photoreduction of CO_2 , while the production of esters and acetals is mainly linked to the occurrence of secondary condensation reactions between the first products.

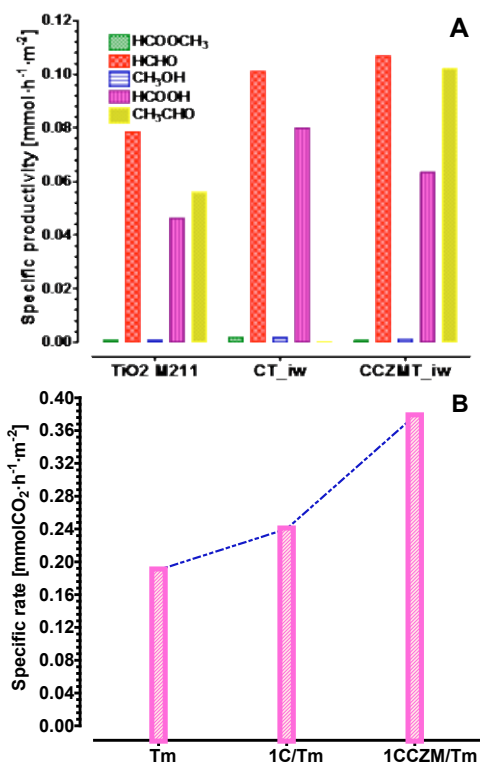


Fig. 1. Photocatalytic results of TiO_2 based catalysts.

Besides, as shown in Figure 1B, the best catalytic performance has been achieved with sample CCMZT_iw, reporting the

higher specific CO_2 conversion rate of ca. $0.4 \text{ mmol} \cdot \text{m}^{-2} \cdot \text{cat} \cdot \text{h}^{-1}$ and the higher productivity of formaldehyde (ca. $0.118 \text{ mmol} \cdot \text{m}^{-2} \cdot \text{cat} \cdot \text{h}^{-1}$), acetaldehyde (ca. $0.015 \text{ mmol} \cdot \text{m}^{-2} \cdot \text{cat} \cdot \text{h}^{-1}$) and formic acid (ca. $0.062 \text{ mmol} \cdot \text{m}^{-2} \cdot \text{cat} \cdot \text{h}^{-1}$). Then, the sample CT_iw has been selected for the scale-up phase, in reason of its good activity and the reasonably lower cost. The main products detected by using this photocatalyst in the pilot plant unit, Figure 2, were CH_4 and CO , reaching a productivity of ca. $10 \mu\text{mol} \cdot \text{g}^{-1} \cdot \text{cat} \cdot \text{h}^{-1}$.



Fig. 2 Integrated pilot plant placed in a cement factory of Italcementi group in Bergamo

IV. CONCLUSION

Photocatalytic approaches for CO_2 reduction have been exploited and the feasibility for the direct photo-conversion of CO_2 into hydrocarbons in a continuous gas phase system has been assessed. The co-presence of Cu, Mn, Ce and Zn improves the performance of TiO_2 photocatalysts, driving to higher specific productivity. Acetal aldehyde, formic acid and formaldehyde are the main products of CO_2 photoreduction in gas phase. A new integrated industrial pilot plant have been realized on the basis of the results of this study.

REFERENCES

- [1] Morton, O., Eating the sun: How Plants Power the Place, Harper, New York, 2008.
- [2] Tseng, I.H., Chang, W., Wu, J.C.S., Photoreduction of CO_2 using sol-gel derived titania and titania-supported copper catalysts, Applied Catalysis B: Environmental, Volume 37, 2002, Pages 37-48
- [3] Li, Y., Wang, W., Woo, M., Wu, C., Biswas, P., Photocatalytic reduction of CO_2 with H_2O on mesoporous silica supported Cu/ TiO_2 catalysts, Applied Catalysis B: Environmental, Volume 100, 2010, Pages 386-392.
- [4] Arena, F., Italiano, G., Barbera, K., Bonura, G., Spadaro, L., Frusteri, F., Basic evidences for methanol-synthesis catalyst design, Catalysis Today, Volume 143, 2009, Pages 80-85.
- [5] Spadaro, L., Arena, F., Granados, M., Ojeda, M., Fierro, J.L.G., Frusteri, F., Metal-support interactions and reactivity of Co/ CeO_2 catalysts in the Fischer-Tropsch synthesis reaction, Journal of Catalysis, Volume 234, 2005, Pages 451-462.



Novel macro-Segmented Fuel Cell approach to investigation of localized degradation in PEMFCs

C. Rabissi¹, J. L. Bonde², E. Brightman³, G. Hinds³ and A. Casalegno¹

¹Politecnico di Milano, Department of Energy, via Lambruschini 4, 20156 Milano (Italy)

²IRD Fuel Cell A/S, Emil Neckelmanns Vej 15 A&B, DK-5220 Odense (Denmark)

³National Physical Laboratory, Teddington, Middlesex TW11 0LW (United Kingdom)

Abstract - Here we present a novel concept of a segmented fuel cell, developed to fully and independently characterize four macro-segments of a single cell without introducing any modification to the MEA structure itself. This permits complete characterization of local electrochemical performance (using polarization curves, impedance spectra, cyclic and linear voltammetry) and mass composition (via gas-chromatography) during durability tests. Moreover, each of the four segments is fitted with an innovative reference electrode using an external, through-plane array configuration, enabling separation of anode and cathode contributions and their spatial evolution. This setup has been firstly applied to generate unprecedented insights into the evolution of local performance during DMFC operation. The variation of anode and cathode potential as a function of location within the cell and the correlation with heterogeneous current density distribution are discussed.

Index Terms - DMFC, degradation, heterogeneities, reference electrode.

I. NOMENCLATURE

DMFC – Direct Methanol Fuel Cell
EIS – Electrochemical Impedance Spectroscopy
MEA – Membrane Electrode Assembly
mSFC – macro-Segmented Fuel Cell
PEMFC – Polymer Electrolyte Membrane Fuel Cell
RHE – Reversible Hydrogen Electrode

II. INTRODUCTION

Recent research activities on PEMFC technology have indicated that local heterogeneities in operating conditions play a key role in early aging of cell components. Design optimization requires a deeper understanding of such degradation phenomena and their correlation with local conditions. It is also critical to distinguish anode and cathode contributions to the cell potential, particularly for technologies such as the direct methanol fuel cell (DMFC) or reformat PEMFC, where the anode overpotential can be non-negligible compared to that of the cathode.

In order to obtain more detailed information on localized degradation across the cell surface driven by inhomogeneous operating conditions, a novel setup has been developed, based on a segmented cell approach. The so-called macro-Segmented Fuel Cell (mSFC) is characterized by a lower current-density spatial resolution compared to existing approaches based on

S++ or resistor matrices [1], while permitting instead a full electrochemical and mass-transport characterization of each cell segment, having negligible “parasitic” in-plane currents between segments in comparison to thru-plane ones. This permits to avoid the necessity of modification on the MEA itself, while being able to determine the contribution of each segment to overall cell performance via polarization curves, impedance spectra and cyclic or linear voltammetry, enabling mass sampling analysis on each segment’s exhaust. This work aims to improve understanding of localized PEMFC degradation through the development of a novel macro-Segmented cell setup, coupled with a reference electrodes array.

III. EXPERIMENTAL SETUP

The mSFC design has been realized using materials and geometries as close as possible to the previous single cell standard [2], in order to facilitate direct comparison of the measurements.

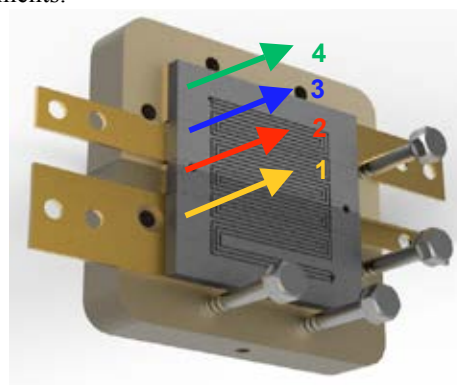


FIG 1. 25 cm² 4-segments m-SFC setup

The prototype mSFC, reported in figure 1, has 4 segments at both cathode and anode on a triple channel serpentine flow field, suitable for square 25 cm² MEAs, on which no modification is required. The graphite flowplate segments, built by IRD Fuel Cells A/S, were glued together with a 0.1 mm thick inert epoxy resin layer before machining of the flowfield pattern. The mSFC reference operating mode is galvanostatic: total current is imposed, which is divided by a multi-channel electronic load between the segments, aiming to maintain their

ΔV s at the same value. Such a configuration permits identification of the instantaneous contribution of each segment to the (constant) overall current density in the cell.

In order to provide further insight into the factors affecting localized degradation, an array of 3 reference electrodes (inlet-center-outlet configuration) has also been applied to the mSFC setup. This facilitates isolation of the anode contribution during performance and durability testing (which is of particular interest for DMFC systems due to the relatively slow kinetics of methanol oxidation) and its distribution across the segmented cell surface. The NPL reference electrode configuration [3], is based on the direct connection of a saturated Nafion[®]-salt bridge through the GDL (across which a proton-conductive path is realized via Nafion[®] solution impregnation) to measure the electrode potential. The salt bridge connects the MEA to a 0.5 M H₂SO₄ electrolytic solution in which a Gaskatel Hydroflex RHE is immersed. This through-plate configuration allows point measurements of local electrode potential across the active area of the cell, for the first time applied on a DMFC.

IV. EXPERIMENTAL RESULTS

The setup has been demonstrated on a 25 cm² commercial DMFC MEA (IRD A/S) by investigating the influence of flow orientation on local performance in short durability tests, using EIS and cyclic voltammetry.

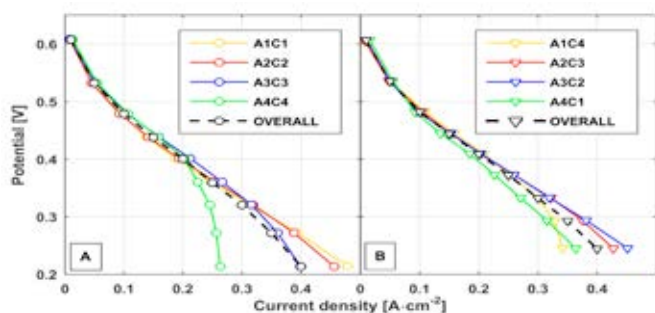


FIG 1. (A) Co and (B) Counter flow polarization curves¹

The polarization curve measurements in the mSFC (shown in Figure 1) highlight the dramatic differences in local performance between co-flow and counter flow modes, in contrast to the slight difference observed with a regular single cell setup (10 mV gain at 0.25 A cm⁻²).

In co-flow configuration, the current density decreases dramatically from inlet to outlet at higher current densities (consistent with the decreasing concentration of both reactants), resulting in a strongly inhomogeneous current density distribution. In counter-flow orientation however, performance is significantly more homogeneous over the cell surface: A4C1¹ is the worst performing segment in the low-medium current density range, probably due to a dehydrating effect of the air flow at the cathode inlet. In contrast, the worst performing segment at high current is A1C4¹, in which major cathode mass transport limitation is observed. Local EIS analysis further supports this interpretation, permitting to distinguish from the

overall cell impedance spectra the contribution of each segment, identifying from whose phenomena performance is locally decreasing. The local inhomogeneities identified in these measurements can have a major detrimental influence on DMFC lifetime.

Moreover, the reference electrode measurements reveal major differences in the local anode and cathode potentials in each case, as shown in Figure 2, for a degraded MEA in reference galvanostatic operation.

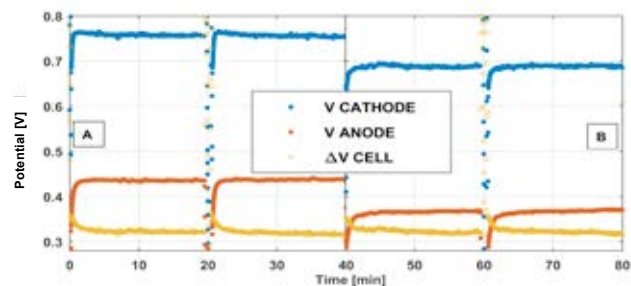


FIG 2. Counter-flow orientation: (A) A1C4¹ vs (B) A4C1¹ anode/cathode potentials vs time (@ 0.25 A cm⁻²)

Being near the cathode outlet, the A1C4 cathode segment (B) operates with an oxygen-depleted, high water content air flow while suffering from high methanol crossover rates from the anode inlet segment, conditions that result in a relatively low cathode potential (< 0.7 V). Interestingly, the cathode potential in this segment is relatively stable with time. In contrast, the A1C4 cathode segment (A) operates at over 0.85 V (i-R drop corrected value) for the opposite reasons, enhancing platinum oxide formation and thus showing a temporarily decreasing trend (though periodically recovered with each low-potential operation break [2]). These measurements highlight the value of separating the contribution of anode and cathode to the overall local potential rather than relying on measurement of the cell voltage.

V. CONCLUSION

Local current distribution and evolution of anode and cathode potential with time has been investigated for the first time in a segmented DMFC single cell. This technique shows great potential for the investigation and mitigation of critical heterogeneous degradation phenomena occurring during operation.

ACKNOWLEDGMENT

This work was supported by the FCH-JU FP7 project Second ACT (EC GA 621216) and the H2FC European Infrastructure project (EC GA 284522) under access project 2071.

- [1] L.C. Perez, L. Brandao et al., Renewable and Sustainable Energy Reviews, Volume 15(1), 2011, Pages 169-185.
- [2] F. Bresciani, C. Rabissi et al., Int. J. Hydrog. Energy, Volume 39, 2014, Pages 21647-21656.
- [3] E. Brightman, G. Hinds, J. Power Sources, Volume 267, 2014, Pages 160-170.

¹mSFC segments and RHEs are named according to their order in anode (A) and cathode (C) feeds, moving from 1 (inlet) to 4 (outlet); thus, for instance, the anode inlet segment is A1C1 and A1C4 for co-flow and



METHANOL TOLERANT PD-BASED ELECTROCATALYSTS FOR THE OXYGEN REDUCTION REACTION

V. Baglio*, C. Lo Vecchio, C. Alegre, D. Sebastian, A. Stassi
and A.S. Aricò

*CNR-ITAE, Salita S. Lucia sopra Contesse, 5 – 98126 Messina
(Italy)

Abstract - Pd nanoparticles supported on carbonaceous and non-carbonaceous supports have been synthesized and characterized, in terms of Oxygen Reduction Reaction (ORR), to evaluate their activity for direct methanol fuel cell (DMFC) applications. It appears that Pd/KB is the most active electro-catalyst in the presence of methanol in the electrolyte, thus showing promising characteristics to be used in direct methanol fuel cells fed by high methanol concentration solutions.

Index Terms - Direct methanol fuel cells, methanol tolerance, oxygen reduction reaction, Pd catalysts.

I. INTRODUCTION

The electrocatalysis of Oxygen Reduction Reaction (ORR) is a critical point due to its slow kinetics and high cost of the Pt-based catalysts commonly used. Direct Methanol Fuel Cell (DMFC) technology requires the development of a catalyst with lower cost and higher activity and selectivity than Pt/C [1]. In DMFCs, when Pt is used as the cathode catalyst, the main drawback is the methanol crossover from the anode to the cathode side through the membrane that results in a mixed potential at the cathode. To limit this effect, Pt-free catalysts with better methanol tolerance and suitable activity must be considered. Pd-based electro-catalysts are promising candidates, although their catalytic activity has to be improved [2]. Catalyst activity also depends on structural and morphological features of the support. To improve the electrochemical activity and stability of the supported catalysts, a lot of work has been done to synthesize new carbon materials with controlled and tuneable nanostructures [3]. However, the stability of carbon is not optimal for the application at the cathode of a polymer electrolyte fuel cell [4], because it is prone to corrosion, leading to a fast and significant loss of catalyst ECSA over time during fuel cell operation [5].

With the aim of improving stability, a non carbonaceous material based on Ti-suboxides is considered in the present paper as support for Pd electro-catalysts. A comparison of the Pd/Ti-suboxides (Pd/Ti_nO_{2n-1}) catalyst with Pd/C supported on commonly used carbon blacks (Ketjenblack and Vulcan) has been carried out in terms of ORR activity, tolerance to methanol poisoning and resistance to accelerated degradation tests.

II. EXPERIMENTAL

30% Pd on Ti suboxides (Ti_nO_{2n-1}, n=3-8, Ebonex® from Atraverda), on Vulcan-XC-72R (labelled as Vul, from Cabot) and on Ketjenblack (labelled as KB, from AkzoNobel) were prepared using the sulphite complex route [6]. The catalysts were physico-chemically characterized by X-ray diffraction (XRD) and transmission electron microscopy (TEM). The electrochemical characterization was performed at room temperature using a conventional three-electrode cell. The reference electrode was an Hg/Hg₂SO₄ saturated with K₂SO₄. The counter electrode was a high surface platinum wire and the working electrode was a glassy carbon (GC) disk of 5 mm where the thin film of catalysts was deposited. The 30% Pd/support catalytic inks were prepared by sonicating each catalyst in isopropyl alcohol and 30% of Nafion for half an hour and then added onto the GC disk to obtain a 50 μg cm⁻² Pd.

III. RESULTS

Figure 1a shows oxygen reduction curves for the Pd/supports catalysts in comparison with a commercial Pt/C catalyst, obtained in the base electrolyte without methanol. The commercial 30% Pt/C has a higher activity than Pd/supports in terms of onset potential and limiting current. Pd/Ti_nO_{2n-1} has an



onset potential about 90 mV more negative than Pt/C catalyst in the activation controlled region, and the limiting current density is about 2.5 mA cm^{-2} . 30% Pd/Vul and 30% Pd/KB catalysts show a similar behavior in terms of onset potential as Pd/Ti_nO_{2n-1} but the i_l reaches a value close to the commercial Pt catalyst. The lower i_l of Pd/Ti_nO_{2n-1} could be related to a lower number of electrons transferred in the ORR.

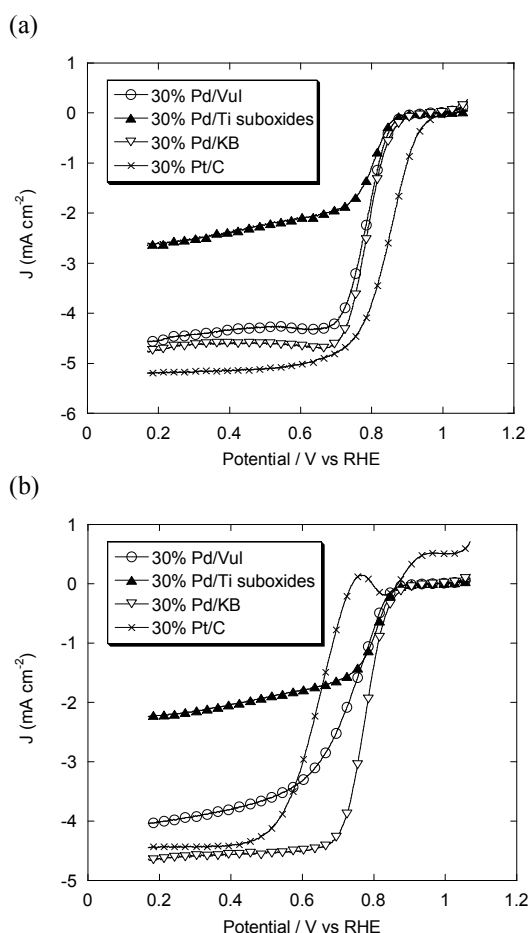


Fig. 1. Comparison of oxygen reduction voltammetric curves for the different Pd/supports catalysts and the commercial Pt/C E-TEK catalyst in the pure electrolyte (a) and in the presence of 0.1 M MeOH (b).

In Figure 1b, a comparison of oxygen reduction reactions for the different catalysts in the presence of 0.1 M methanol is presented. Under these conditions, Pd/KB catalyst shows the most positive onset potential and reaches the largest limiting current density, comparable to the one obtained with Pt/C. These results evidence the better tolerance to the presence of low methanol concentration of Pd-based catalysts compared to a benchmark Pt catalyst. Accelerated Degradation Tests

(ADTs) have been performed by sweeping (1000 cycles) the potential from 0.6 to 1.0 V vs RHE at a scan rate of 50 mV s^{-1} . The activity of Pd/Ti_nO_{2n-1} catalyst is almost unvaried, after 1000 degradation cycles, indicating the best stability of the non carbonaceous support; whereas, Pd/KB and Pd/Vul experience a significant loss of activity after 1000 potential cycles both in kinetic and diffusion-limiting current regions.

IV. CONCLUSION

30% Pd/Titanium suboxides, 30% Pd/Ketjenblack and 30% Pd/Vulcan have been synthesized and characterized, in terms of oxygen reduction reaction, to evaluate their activity for direct methanol fuel cell application. It appears that Pd/Ketjenblack is the most active electro-catalyst in the presence of methanol in the electrolyte, thus showing promising characteristics to be used in direct methanol fuel cells fed with high methanol concentration solutions. Instead, stability tests of these Pd-based catalysts indicate the best resistance to corrosion for the Ti-suboxide supported Pd catalyst compared to carbonaceous supports, pointing to good perspectives for applications in DMFC cathodes.

ACKNOWLEDGMENT

This work was supported by the PRIN 2010-11 project NAMED-PEM.

REFERENCES

- [1] Aricò, A.S., Baglio, V., Antonucci, V., Direct Methanol Fuel Cells: History, Status and Perspectives; in: H. Liu, J. Zhang (Eds.), *Electrocatalysis of Direct Methanol Fuel Cells*, WILEY-VCH Verlag GmbH & Co. KGaA, Weinheim, 2009, pp. 1-78.
- [2] Carrera-Cerritos, R., Baglio, V., Aricò, A.S., Ledesma-Garcia, J., Sgroi, M.F., Pullini, D., et al. Improved Pd electrocatalysis for oxygen reduction reaction in direct methanol fuel cell by reduced graphene oxide. *Appl. Catal. B: Environmental*, Volume 144, 2014 pp. 544–560.
- [3] Antolini, E., Carbon supports for low-temperature fuel cell catalysts, *Appl. Catal. A: General*, Volume 365, 2009, pp. 1-19.
- [4] Sebastián, D., Garcia Ruiz, A., Suelves, I., Moliner, R., Lázaro, M.J., Baglio, V., Stassi, A., Aricò, A.S. Enhanced oxygen reduction reaction activity and durability of Pt catalysts supported on carbon nanofibers. *Appl. Catal. B: Environmental*, Volume 115–116, 2012, pp. 269–275.
- [5] Ferreira, P.J., La O', G.J., Shao-Horn, Y., Morgan, D., Makharia, S., Kocha, S., Gasteiger, H.A. Instability of Pt/C electrocatalysts in proton exchange membrane fuel cells: a mechanistic investigation. *J. Electrochem. Soc.*, Volume 152, 2005, pp. A2256–A2271.
- [6] Aricò, A.S., Stassi, A., D'Urso, C., Sebastián D., Baglio, V., Synthesis of Pd₃Co₁@Pt/C Core-Shell Catalysts for Methanol-Tolerant Cathodes of Direct Methanol Fuel Cells, *Chem. Eur. J.*, Volume 20, 2014, pp. 10679-10684.



MEASUREMENT OF PROTONIC RESISTANCE OF CATALYST LAYERS

T. Gaumont^{a,b}, G. Maranzana^a, O. Lottin^a, J. Dillet^a
J. Pauchet^b, L. Guétaz^b

a) LEMTA, Université de Lorraine, 2 av. de la Forêt de Haye 54518 Vandoeuvre (France)

b) CEA, 17 avenue des Martyrs, 38000 Grenoble (France)

Abstract – In a proton exchange membrane fuel cell (PEMFC), a good catalyst layer ionic conductivity is required to ensure homogeneous current distribution within the electrode, and thus maximize the Pt utilization and minimize the over-potentials.

In a first part, the principles of the catalyst layer ionic resistance measurement by impedance spectroscopy are presented. Using a volumetric electrode model, the ionic resistance of the catalyst layer R_p , the double layer capacity C_{dl} and the high frequency resistance R_{HF} are estimated from the impedance spectra of a nitrogen inerted cathode.

In a second part, results of the degradation of a MEA submitted to three different accelerated stress tests are presented. They consist of (i) open circuit voltage (OCV) hold with air and hydrogen, (ii) 1.2V potential hold with nitrogen and hydrogen, and (iii) to a constant current operation.

Index Terms – Electrochemical impedance spectroscopy, cathode ionomer degradation, ionic resistance of active layer

I. NOMENCLATURE

R_p : cathode protonic resistance ($\Omega.cm^2$)

R_{HF} : high frequency resistance ($\Omega.cm^2$)

C_{dl} : cathode double layer capacity (F/cm²)

ρ_p : cathode protonic resistivity ($\Omega.cm$)

$\Delta\phi$: ionic phase potential perturbation (V)

ω : signal pulsation (rad/s)

L : cathode thickness (m)

ΔI : cell current density perturbation (mA/cm²)

Z : cathode impedance ($\Omega.cm^2$)

S_X : sensitivity of the impedance to the parameter X

II. INTRODUCTION

It is of prime importance for membrane electrode assemblies (MEA) manufacturers to distinguish the different contributions to the voltage losses observed in a PEMFC in regular operation, knowing that most of them originate from the cathode and the membrane: in the absence of oxygen transport limitation, they are due to oxygen reduction reaction (ORR) kinetics, ohmic drop through the membrane, and ionic resistance within the cathode. For a pristine, optimized, and well humidified

electrode, voltage drop due to proton transport within the cathode electrode must be negligible. Thus the ORR current should be almost uniform through the electrode [1]. However, little work has been done so far to characterize the ionomer degradation in the cathode and its impact on fuel cell performances [2][3].

III. MODEL AND METROLOGY

A. Model

The model is based on the charge conservation equations, assuming a negligible electronic resistance in the catalyst layer and no faradic reactions within the N₂ inerted cathode. Thus the cell operates as a supercapacitor. The electrolyte potential ϕ follows a diffusive law.

When solving in the frequency domain, for small dynamic perturbations, it yields

$$Z(\omega) = \frac{\Delta\phi}{\Delta I} = \sqrt{\frac{R_p}{iC_{dl}\omega}} \coth(\sqrt{iR_p C_{dl}\omega}) + R_{HF} \quad (\text{Eq. 1})$$

B. Estimation of the parameters and sensitivity of the model

The estimation of the parameters can be achieved provided the model is sensitive to small variations in those parameters and they are not correlated. The reduced sensitivity coefficient (fig. 1) to each parameter X can be computed as:

$$S_X = \frac{X}{|Z|} \frac{\partial |Z|}{\partial X} \quad (\text{Eq.2})$$

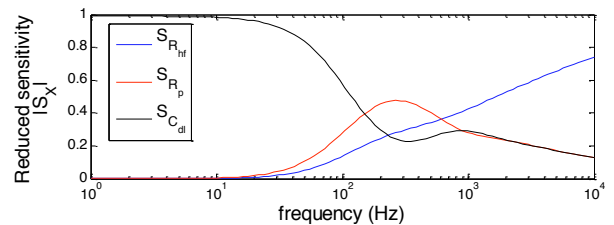


Figure 1: Reduced sensitivities of the model

A sensitivity analysis (fig. 1) shows that there is no correlation between the high frequency resistance, the ionic resistance and the double layer capacity, i. e. the set of 3 parameters yielding each individual impedance spectrum is unique. Moreover, in the selected frequency range (1Hz to 1 kHz) the sensitivity is higher than 0.1 for each parameter over more than one decade. This means that the spectra are sensitive to each of the 3 parameters.

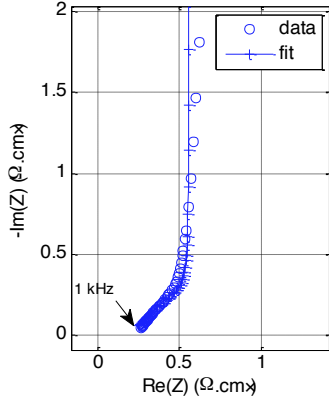


Figure 2: Nyquist impedance plot of the cell operated with cathode fed with N_2 . Cell potential is set to 0.5V

C. Sensitivity to relative humidity

Just like the protonic resistivity of the ionomer in a membrane, the protonic resistivity of the electrode decreases substantially when the relative humidity increases. Particular care has to be taken to keep the cell well humidified, during as well as before the test.

IV. DEGRADATION PROTOCOLS

A. Experimental

The cell was exposed to 3 different protocols summarized in table I. The OCV protocol (DOE membrane in Table 1) is known to degrade the ionomer in the membrane close to the cathode side [4]; holding the cell at 1.2V with a nitrogen fed cathode compartment oxidizes the carbon support (DOE carbon test in Table 1).

TABLE I
ACCELERATED STRESS TESTS APPLIED IN THIS WORK

Protocol reference	Conditions	Anode	Cathode	T, P
Constant current	0.7A/cm ² , 168h	50% RH H ₂	50% RH air	80°C, 1.5bar
DOE membrane	Open Circuit Voltage, 300h	50% RH H ₂	50% RH air	90°C, 1.5bar
DOE carbon	1.2V, 300h	50% RH H ₂	50% RH N ₂	80°C, 1.5bar

B. Results

The constant current protocol validates the stability of the estimated parameters for moderate conditions, while for the

DOE membrane protocol (OCV hold) one can observe a 65% increase of R_{HF} caused by the membrane ionomer evolution accompanied by a slight decrease of R_p . Finally, the carbon DOE protocol leads to cathode compaction and thinning due to carbon oxidation [5]. Since the estimated parameter is $R_p = \rho_p L$, with L the electrode thickness, a decrease in L leads to a decrease in R_p .

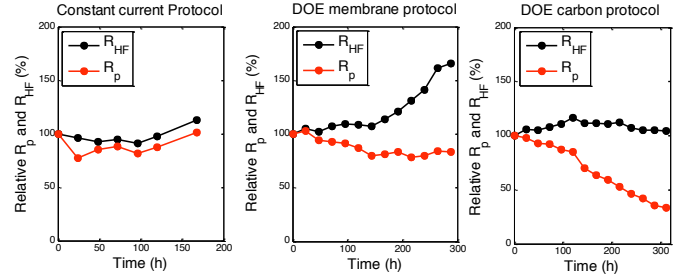


Figure 3 Evolution of the cathode protonic resistance and high frequency resistance during the 3 ageing protocol presented in table I

V. CONCLUSION

An in situ method based on electrochemical impedance spectroscopy was developed to estimate accurately membrane electrode assembly double layer capacity, the membrane resistance and the protonic resistance of the cathode catalyst layer in a PEMFC.

This work does not show any evidence of degradation of the ionomer of the cathode, though in OCV conditions the ionomer of the membrane is chemically degraded. However, our first results suggest that the decrease in the cathode thickness lead to a simultaneous decrease in the catalyst layer resistance, possibly masking the chemical degradation of the ionomer.

REFERENCES

- [1] K. C. Neyerlin *et al.*, "Cathode Catalyst Utilization for the ORR in a PEMFC," *J. Electrochem. Soc.*, vol. 154, no. 2, p. B279, 2007.
- [2] S. Park *et al.*, "Non-kinetic losses caused by electrochemical carbon corrosion in PEM fuel cells," *Int. J. Hydrog. Energy*, vol. 37, no. 10, pp. 8451–8458, May 2012.
- [3] A. P. Young *et al.*, "Ionomer Degradation in Polymer Electrolyte Membrane Fuel Cells," *J. Electrochem. Soc.*, vol. 157, no. 3, p. B425, 2010.
- [4] A. Ohma *et al.*, "Membrane degradation mechanism during open-circuit voltage hold test," *J. Power Sources*, vol. 182, no. 1, pp. 39–47, Jul. 2008.
- [5] L. Dubau *et al.*, "Carbon corrosion induced by membrane failure: The weak link of PEMFC long-term performance," *Int. J. Hydrog. Energy*, Aug. 2014.



DESIGN AND EXPERIMENTAL EVALUATION OF A NOVEL SOFC STACK CONCEPT WITH PARALLEL-CONNECTED CELLS

A. Lindermeir*, C. Szepanski*, C. Immisch*, J. Hamje**,
L. Dörner***, and U. Schmidt***

*CUTEC Institut GmbH, Leibnizstraße 21, D-38678 Clausthal-
Zellerfeld, (Germany)

** Institut für Schweißtechnik und Trennende Fertigungsverfahren,
TU Clausthal, Agricolastraße 2, D-38678 Clausthal-Zellerfeld,
(Germany)

*** Institut für Metallurgie, TU Clausthal, Robert-Koch-Straße 42,
D-38678 Clausthal-Zellerfeld, (Germany)

Abstract - A new SOFC concept based on repeating units with two electrically parallel connected cells is presented. Two alternatives were developed: an all ceramic concept with a 3YSZ cell housing and a metallic housing made of Crofer 22 APU. Reactive air brazing was used to mount the cells in the frames. Structured interconnectors were produced by hydroforming Crofer 22 APU sheets. Test units were produced and gas tightness of the joints could be confirmed. Tests with a two cell unit show good overall performance with fuel utilization above 75 %. The assembly has been operated for 1200 hours including full redox and thermal cycles. The results confirm the feasibility of the approach with potential benefits concerning durability and production cost.

Index Terms - laser welding, parallel-connected cells, reactive air brazing, SOFC

I. INTRODUCTION

Serial connection of several cells within a stack is the common method to generate user relevant voltage and power. The serial approach is accompanied with some principle drawbacks like collapse of power output in case of a serious breakdown of one cell. This is avoided in a parallel stack architecture. Besides the higher failure probability the serial approach determines the operation of single cells at the same current but at different voltages, depending on the local reaction conditions and the quality of the individual cells. If resistance of one cell is higher than that of the others, the weaker cell operates at lower voltage [1]. This accelerates degradation, especially if the cell voltage is lower than the nickel oxidation potential [2]. Cracks and failures within the cells or even complete breakdown of the cell

can be the result of the associated nickel oxidation [1, 3]. This will further intensify the degradation of the already pre-damaged cell due to the ongoing voltage decrease and the formation of hot spots. Appropriate counteractions like a lowering of the current load requires the monitoring of every single cell voltage, associated with high effort and cost.

II. RESULTS

A. Stack Concept

The proposed parallel stack concept promises lower degradation and better reliability, because all cells are operated at all time at the same voltage. A lower current load and fuel utilization for weaker cells are inherently assured by the parallel configuration. Performance differences between single cells due to variances in cell production or local operation conditions are thus being intrinsically balanced.

The presented stack is based on repeating units with two cells electrically connected in parallel (twin cell unit). The cells are arranged with their anodes face-to-face. Contacting and gas distribution is done by interconnectors that have contact either to the anode side of the cells or the cathode side. Thus, on both sides of the interconnector the gas atmosphere is identical. The internal parallel connection of the cells and power dissipation was realized by metallic current rods for the anodic and cathodic current (see Figure 1).

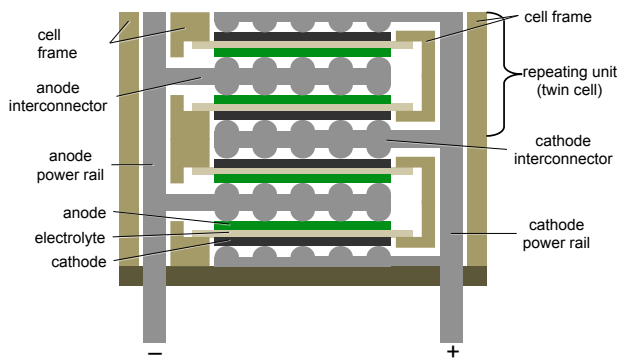


Fig. 1. Sketch of the parallel SOFC stack concept

B. Materials And Manufacturing

ESC cells (Ampergy® ESC2, H.C. Starck Ceramics GmbH, 50 mm × 50 mm, electrolyte: 3YSZ, anode: NiO/GCO, cathode: LSM) were used for the twin cell units. For the cell frame a metallic (Crofer 22 APU) and a ceramic (ZrO₂) version was developed. Issues of flow distribution and pressure drop were considered by CFD simulations. Cells have been mounted in the cell frames by reactive air brazing (RAB) using a 100 μm thick silver braze foil. The brazing was done in a furnace at 1000 °C under air atmosphere.

Knob structured interconnectors made by hydroforming of Crofer 22 APU sheets were used for the ceramic version. The produced parts show high dimensional accuracy and no cracks despite the high deformation degree. For the metallic frame concept, a 0.6 mm thick Ni-foam spot-welded on a Crofer 22 APU sheet was used as anodic interconnector while for the cathode side channels were machined directly in the frame.

For the ceramic frame concept, repeating units were produced by brazing two frames loaded with a cell. In case of the metallic frame laser welding was used instead of RAB.

Joining of cell and frame by RAB was successful for both, the metallic and the ceramic frame. No deformations were visible assuring an area-wide contacting between electrode and interconnector. The assembling of the twin cell units by RAB and laser welding could be done without severe problems.

C. Performance Tests Of Twin Cell Unit

IV curves were recorded at temperatures of 850 °C, 865 °C and 880 °C. Specific anode gas flow rates varies between 0.78 and 5.3 ml/(min cm²) with two different gas mixtures (H₂ and CO/H₂). The test stand enables the option to measure IV curves for the two parallel connected cells separately (Figure 2). OCVs were above 1100 mV for both cells showing good gas tightness. Slight deviations between the IV curves are due to small differences in the metering resistances.

Maximum power density was about 100 mW/cm² for each cell (active area: 16 cm²), so overall power output of the twin cell unit was 3.2 W, as well for pure H₂ as for H₂/CO anode gas

mixtures. Tests at low anode gas flow rate show fuel utilizations above 75 %, without accelerated degradation. Within a long term test, the unit was operated for 1200 h at 850 °C, (1000 h stationary test and 200 h thermocycle test). OCV decreases with a rate of 12 mV / 1000 h, showing enduring gas tightness of the RAB and welding seals. Voltage degradation rate under full load was about 40 mV/1000 h.

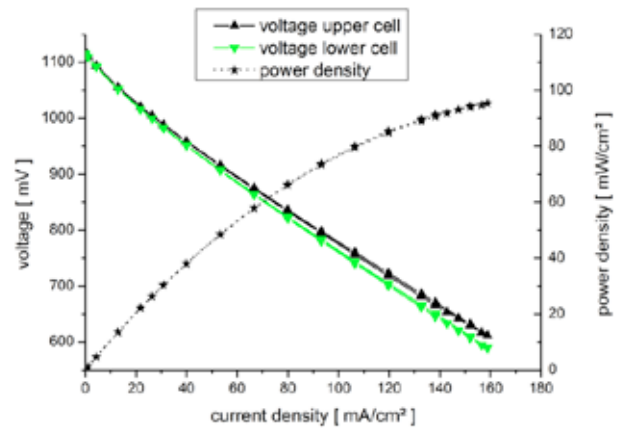


Fig. 2. IV curve for a parallel connected twin cell, both cells measured separately

III. CONCLUSIONS

A new approach for an SOFC stack architecture with parallel-connected cells have been developed. RAB and pulsed laser welding were proved to be suitable joining technologies, thus glass seals are completely avoided. Hydroforming shaped metal sheets were used as interconnectors and for gas distribution.

Good overall performance with fuel utilization above 75 % was achieved for a twin cell with a ceramic frame. Only slight cell degradation and enduring gas tightness was observed within a 1200 hour test.

ACKNOWLEDGMENT

Funding of the German “Federal Ministry of Economics and Technology” (BMWi) by the “Federation of Industrial Research Associations” (AiF) within the program of “Industrial collective research” (IGF-project no. 17598 N) and received from “DECHEMA Gesellschaft für Chemische Technik und Biotechnologie e. V.” is gratefully acknowledged.

REFERENCES

- [1] Virkar, A.V., A model for solid oxide fuel cell (SOFC) stack degradation, *Journal of Power Sources*, 172, 2007, pp. 713-724.
- [2] Nehter, P., A high fuel utilizing solid oxide fuel cell cycle with regard to the formation of nickel oxide and power density, *Journal of Power Sources*, Volume 164, 2007, pp. 252-259.
- [3] Ettler, M., Einfluss von Reoxidationszyklen auf die Betriebsfestigkeit von anodengestützten Festoxid-Brennstoffzellen, *Schriften des Forschungszentrums Jülich Reihe Energie & Umwelt*, 2009, 36



CONCEPT FOR FUEL CELL BASED MOBILITY WITH CLOSED CO₂-CYCLE

C. Immisch*, A. Lindermeir*, S. Stenger**, U. Krewer**, and
 R. Leithner**

*CUTEC Institut GmbH, Leibnizstraße 21+23, D-38678 Clausthal-
 Zellerfeld, (Germany)

**Institut für Energie- und Systemverfahrenstechnik (InES) TU-
 Braunschweig, Pockelstraße 14, D-38092 Braunschweig, (Germany)

Abstract – This paper presents an efficient fuel cell based vehicle drive system concept with a closed CO₂-cycle using compressed renewable methane as fuel. A steam reformer with integrated H₂-separation and a PEM fuel cell stack are used for power generation. The system off gas stream (mainly CO₂) is stored on-board in a pressurized two-chamber gas tank. During refueling the vehicle the captured CO₂ is passed back to the fueling station. New methane based fuel can be produced using this CO₂ together with hydrogen from water electrolysis with renewable energy, either centralized or decentralized at the fueling station. Different user scenarios were investigated for their typical fuel consumption to estimate the required plant capacities considering the available excess power in Germany.

Index Terms – CO₂-recycle, PEMFC, renewable CNG, vehicle fleet, zero emission mobility.

I. INTRODUCTION

Fuel cells are a promising technology for high efficient long distance mobility. Using compressed methane based on renewable power (here referred as renewable Compressed Natural Gas, rCNG) enables an efficient and closed CO₂-cycle. The worldwide number of vehicles using CNG fuel is steadily growing and CNG is an already common fuel.

In the presented concept an electric vehicle is driven by a fuel cell system. To fulfill the dynamic requirements of a mobile application a low temperature PEMFC was chosen as main aggregate. The concept allows the capture of the CO₂ stream. Thereby the vehicle does not release any CO₂ to the environment during its operation on the road.

During refilling at the fueling station the stored CO₂ is displaced. Together with hydrogen from an electrolysis powered by wind or photovoltaic electricity this CO₂ can be used for the synthesis of new rCNG. The required plant capacities for water electrolysis and rCNG synthesis depend on

the fuel sales of the respective fueling station and the amount of available excess renewable power. The concept is also feasible for vehicles with a battery electric drive combined with a fuel cell range extender.

II. PROCESS DESIGN

The process is divided in the fuel cell system integrated in the vehicle and the external production of new fuel, including the water electrolysis and the methanation plant (see Figure 1).

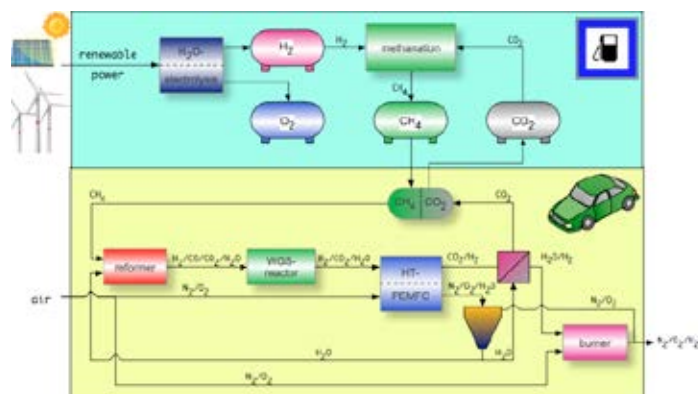


Fig. 1. Schematic flow chart of the overall system

A. Fuel Cell System In Vehicle

Figure 2 shows the flow chart and the results of stationary thermodynamic process simulations of the system in vehicle. rCNG is stored at a pressure of 20 to 25 MPa in a tank with two chambers divided by a gastight and flexible membrane. After expanding it is mixed with water from the fuel cell off gas, preheated and converted in a reformer to H₂ and CO. To increase the hydrogen content and remove harmful CO a water

gas shift (WGS) unit is used. The WGS reactor is equipped with a gas separating membrane to remove the hydrogen from the gas stream, thus shifting the chemical equilibrium in situ for maximum hydrogen yield.

The hydrogen is fed to the PEM fuel cell. To simulate the process and calculate efficiencies and gas composition a 1 kW stack with 89 cells (Serenergy A/S, type S45-90) was selected as example. The working point was set to 20 A at 50 V and a fuel utilization of 65 % [1]. Remaining hydrogen is used in a burner to produce the heat required by the endothermic steam reforming process. The offgas from the WGS reactor (mainly CO₂) is pressurized in a two-stage intercooled compressor. The water is condensed, resulting in a pure CO₂ offgas stream. The compression heat can be used for preheating the burner air and the evaporation of water for the reformer. Thereby, high heat integration was realized to assure high system efficiency.

The fuel cell system was investigated with detailed stationary process simulations and pinch analyses to predict system behavior, performance values and energy balances. The general feasibility of the concept was proved, the electrical net efficiency was 32 % considering the BoP power consumption.

efficiencies. For this study an average energy efficiency of 80 % was supposed. The methanation process was simulated with ChemCAD[®] as a three-step process similar to the TREMP[™]-process from Haldor Topsøe [2]. The calculated chemical efficiency of the methanation process was 83 %.

Considering the predicted annual load duration curve for the power production of Germany in 2030 excess power is available for about 1000 hours per annum. Combining all these data results in the required plant capacities for the fulfillment of the rCNG demand in the considered scenarios (see Table 1).

TABLE I
SCENARIOS FOR CONSUMER GROUPS: ANNUAL RCNG CONSUMPTION AS CHEMICAL ENERGY ($E_{\text{RCNG,chem}}$), REQUIRED ELECTROLYSIS POWER ($P_{\text{E,el}}$) AND CHEMICAL POWER INPUT FOR RCNG-SYNTHESIS ($P_{\text{S,chem}}$).

	public	private
large	1A: Gas station in urban area $E_{\text{rCNG,chem}}$: 75 MWh $P_{\text{E,el}}$: 123 kW $P_{\text{S,chem}}$: 91 kW	2A: large city transportation company $E_{\text{rCNG,chem}}$: 100 GWh $P_{\text{E,el}}$: 164 MW $P_{\text{S,chem}}$: 122 MW
medium		2Ba: regional transportation company $E_{\text{rCNG,chem}}$: 7 GWh $P_{\text{E,el}}$: 11,5 MW $P_{\text{S,chem}}$: 9 MW
small	1B Gas station in rural area $E_{\text{rCNG,chem}}$: 25 MWh $P_{\text{E,el}}$: 41 kW $P_{\text{S,chem}}$: 30 kW	2Bb: municipal vehicle pool $E_{\text{rCNG,chem}}$: 300 MWh $P_{\text{E,el}}$: 492 kW $P_{\text{S,chem}}$: 366 kW

The overall energy efficiency (renewable power-to-wheel) of the process is 19 %. By using high temperature electrolysis with better efficiency and beneficial effects on heat integration this value could be increased to 27 %.

III. CONCLUSION

The presented process concept implies the opportunity to generate separated gas streams in an electrically driven vehicle by combining a fuel cell with a CO₂ separation step. In this way CO₂ can be reused together with hydrogen from renewable power to produce new fuel and close the CO₂ cycle.

The concept uses rCNG as renewable fuel with an already established infrastructure and is particularly suitable for public transportation companies and municipal administration with a homogenous vehicle fleet.

The next step is a follow-up project to validate the concept by building up a 1 kW demonstration version of the system in vehicle.

ACKNOWLEDGMENT

The authors like to thank the Ministry for Science and Culture of Lower Saxony for financial support.

REFERENCES

- [1] Serenergy A/S, Product Data Sheet v2.5-0313
- [2] Haldor Topsøe A/S, Product Sheet: From solid fuels to substitute natural gas (SNG) using TREMP[™]

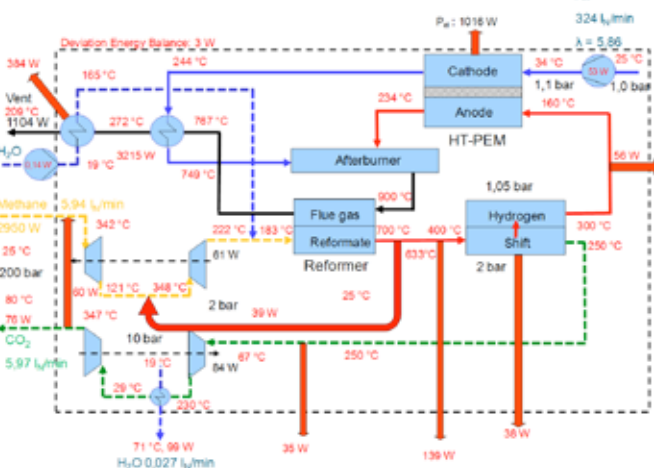


Fig. 2. Stationary process simulation

B. rCNG Production

To estimate the required plant capacities for the rCNG production different user scenarios were elaborated. In scenario 1A and 1B gas fueling stations with different catchment areas (urban and rural) were defined. The number of cars heading for these stations is calculated by using the official statistics from the German government, assuming that 0.1 % of all cars uses the presented system. Additionally, statistics for the average fuel consumption per annum and the number of fueling stations in Germany were used. For the scenarios 2A, 2Ba and 2Bb data from large and smaller public transportation companies and different local government/municipal administrations fleets were used. Various electrolysis technologies were considered with respect to their specific benefits, disadvantages, and



ANALYSIS OF THE HYDROGEN EVOLUTION REACTION MECHANISM ON MOLYBDENUM CARBIDE NANOPARTICLES BY PH METHOD

Sami Tuomi, Tanja Kallio

Aalto University, Research Group of Electrochemical Energy
Storage and Conversion, Kemistintie 1, Espoo, Finland

Abstract - The catalytic activity of molybdenum carbide nanoparticles towards hydrogen evolution reaction (HER) was analyzed in an electrochemical analysis cell. It was found that these particles are very active for catalyzing HER in acidic media and the reaction mechanism is dependent on pH and applied overpotential. The results are significant for optimizing the real application parameters and providing a method to analyze the reaction mechanism for HER.

Index Terms – Electrolysis, hydrogen production, molybdenum carbide, reaction mechanism

I. INTRODUCTION

Platinum is widely used as the catalyst for the hydrogen evolution reaction but it is highly expensive and too rare to be utilized in mass production. During the last decades different size and shape of molybdenum sulfide particles and films has been studied as a replacer for platinum as the hydrogen evolution catalyst. Molybdenum sulfide edge sites where sulfur atoms can mediate the hydrogen evolution reaction has similar properties as platinum and hydrogenase enzymes found in nature. Nevertheless, catalytic activity of the molybdenum sulfide catalysts is limited by the amount of edge sites on the surface. Molybdenum carbide (Mo_2C) is a rising challenger for molybdenum sulfide as a non-noble metal catalyst for hydrogen evolution reaction due to its catalytic activity based on the surface orientation instead of just edge sites [1]. This has resulted in a research of multiple kinds of catalyst structures from nanoparticles to nanorods.

II. BACKGROUND

According to previous theoretical calculations and measurements [2,3], if HER proceeds through Volmer reaction followed by the Tafel reaction the Tafel slope for the HER should be 30 mV per decade at low overpotentials. At high overpotentials the reaction is kinetically limited by Tafel reaction. If the reaction proceeds through Volmer reaction followed by the Heyrovsky reaction then the Tafel slope should be 40 mV per decade at low overpotentials. At high overpotentials Tafel slope of 120 mV per decade is observed.

According to the derivation of the reaction rates, the slope of $\log i$ vs. pH is around 2 for both the mechanisms at low overpotentials but at high overpotentials the slope is either 1 or 0 if the mechanism is Volmer-Heyrovsky or Volmer-Tafel, respectively. This gives another deterministic value to use for analyzing the reaction mechanism of HER.

III. EXPERIMENTAL

The electrocatalytic HER activities of the Mo_2C nanoparticles were investigated with rotating disc electrode (RDE) experiments using glassy carbon (GC) electrodes with a radius of 5 mm. The catalyst was mixed with 5 wt-% Nafion solution and ethanol to form ink which was deposited on the electrode to yield a catalyst loading of 0.56-0.60 mg/cm^2 and Nafion content of 0.42-0.46 mg/cm^2 . Platinum mesh was used as a counter electrode and reversible hydrogen electrode (RHE) as a reference electrode. All the potentials are given against RHE. Currents are normalized against the geometrical area of the GC electrode.

Electrolysis performance was measured in the pH range 0.11 to 7 at 30 °C temperature. The electrolyte solutions were made by mixing adequate amount of 1 M sulfuric acid with 1 M sodium sulfate to obtain the desired pH while maintaining electrical conductivity.

IV. RESULTS

The background corrected currents at high pH showed very little dependency on the proton concentration but there is a significant change in the behavior at pH 2, corresponding to the value where sulfate ion is protonated. At pH 2 and under (Fig. 1) the HER current is strongly dependent on pH.



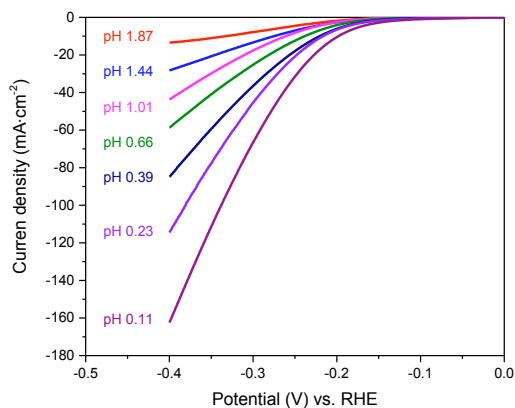


Fig. 1. The polarization curves for Mo₂C nanoparticles with low pH sulfuric acid solutions.

When logarithm of the electrolysis current is plotted as a function of pH, linear dependency is observed at pH values below 1. Our results (Fig. 2) show the expected slope of 2 with overpotential up to 50 mV at pH range 0.11 to 0.66 where linear behavior is observed. No linear relation was observed at pH higher than 0.66. When the overpotential is increased the slope starts to decrease as expected. The slope reaches value of 0.67 before it starts to slowly increase after 0.2 V overpotential. This behavior implies that the reaction proceeds with both reaction mechanisms at high overpotentials as the slope is between 0 and 1, which are the expected values for Volmer-Tafel and Volmer-Heyrovsky mechanisms at high overpotentials, respectively. The values of the slope rises closer to 1 which implies leaning towards Volmer-Heyrovsky mechanism when the potential is increased.

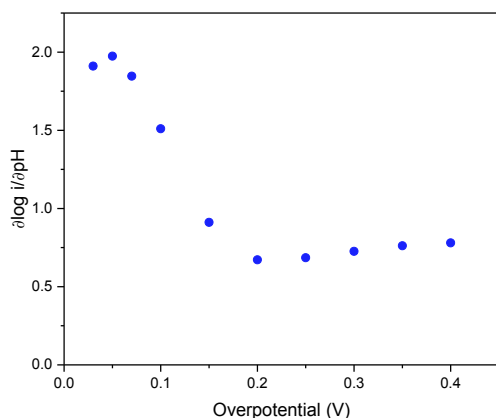


Fig. 2. The $\log i / \text{pH}$ vs. chosen overpotentials on Mo₂C nanoparticles at low pH sulfuric acid solutions.

It is also easy to observe the change in the behavior from the Tafel slopes at low pH. There is a first activation of the

hydrogen evolution reaction under 0.10 V overpotential and second activation around 0.15 V overpotential. The values of Tafel slopes at lower overpotential region is between 59 to 78 mV per decade with pH 0.39 to 1.84. The slopes increases to 111 and 117 mV per decade for pH 0.11 and 0.23, respectively. These results indicate that already 100 mV overpotential is high enough to obtain features of proton covered surface as the values close to 120 mV are representative for Volmer-Heyrovsky reaction at high surface coverage e.g. high overpotential. This results is also in line with the previous foundation that there is no single reaction mechanism close to 100 mV overpotential as the mechanism is dependent on pH at that overpotential region. For the higher overpotential region the Tafel slopes are between 60 to 71 mV per decade with pH 0.39 to 1.84 while rising only to 86 mV per decade for pH 0.11 and 0.23. These results support the previous interpretations that the reaction proceeds with both reaction mechanisms at high overpotentials. The higher Tafel slopes with lower pH are assumed to be caused by increased proton coverage due to higher proton concentration.

V. CONCLUSION

The pH analysis is easy and powerful method to gain information of the reaction mechanism of HER. Understanding the effect of pH and overpotential to the reaction mechanism is critical for the optimization of real hydrogen production systems. Molybdenum carbide nanoparticles have shown their effectiveness for catalyzing HER and replacing platinum, thus allowing significant cost savings in electrolyzer prices.

ACKNOWLEDGMENT

The authors thank the Starting Grant of Aalto University for funding this research.

REFERENCES

- [1] Q. Luo, T. Wang, G. Walther, M. Beller, H. Jiao, Molybdenum carbide catalysed hydrogen production from formic acid – A density functional theory study, *J. Power Sources*. 246 (2014) 548-555
- [2] J.O. Bockris, E.C. Potter, The Mechanism of the Cathodic Hydrogen Evolution Reaction, *J. Electrochem. Soc.* 99 (1952) 169-186.
- [3] B.E. Conway, B.V. Tilak, Interfacial processes involving electrocatalytic evolution and oxidation of H₂, and the role of chemisorbed H, *Electrochim. Acta.* 47 (2002) 3571-3594.



EXPERIMENTAL AND MODELING ANALYSES OF VANADIUM REDOX FLOW BATTERY

E. Rovera, M. Zago, and A. Casalegno

Dipartimento di Energia, Politecnico di Milano, Via Lambruschini 4, 20156, Milano (Italy)

Abstract - Vanadium redox flow battery is a promising and interesting storage technology that in a carbon-free scenario will have a key role in stabilizing the electric grid.

Experimental activity presented in this work makes use of half-cell configuration, where the working electrode is fed with Vanadium solutions, while the other works as reference hydrogen electrode. Experimental characterization of both anode and cathode electrode with flow by feeding is presented, varying flow rate and state of charge.

Moreover a 1D+1D Flow Battery model has been developed in Comsol Multiphysics, describing a single cell derived from fuel cell technology, composed by electrodes, membrane and flow field. The model includes Butler-Volmer kinetic equations, cross contamination fluxes through the membrane and mass transport phenomenon occurring in the pore of the carbon electrode. Discharge polarization curve was fitted to estimate kinetic rate constant and transfer coefficients.

Index Terms – Cross Contamination, Experimental, Migration, Vanadium Redox Flow Battery

I. NOMENCLATURE

- N – Molar Flux [$mol \cdot m^{-2} \cdot s^{-1}$]
- D – Diffusion Coefficient [$m^2 \cdot s^{-1}$]
- c – Concentration [$mol \cdot m^{-3}$]
- z – Valence [1]
- ϕ – Electrolyte Potential [V]
- F – Faraday Constant [$C \cdot mol^{-1}$]
- T – Temperature [K]

II. INTRODUCTION

A combined experimental and modeling study of a Vanadium Redox Flow Battery (VRFB) discharge operation is presented in this work.

Flow battery VRFB half-cell structure is fuel cell derived, where reactants alimentation is achieved with serpentine flow channels. Half-cell configuration has been set up to study separately anode and cathode. This system configuration is usually modeled in the literature with a 1D+1D approach [1], where a 1D channel is coupled with a 1D electrode.

Since the physical phenomena governing VRFB operation have not been completely understood, it is crucial for technology

development to investigate critical issues, among which migration influence on Vanadium ions transport. The combined experimental and modeling approach will allow to estimate the magnitude of migration phenomenon in electrolyte mass transport.

III. EXPERIMENTAL

Cell setup is the half-cell configuration described by Brandon group [2]. The working electrode is an untreated carbon GDL (Sigracet 10 AA), where Vanadium redox reactions occur. A peristaltic pump circulates Vanadium solutions through two external tanks, to keep battery state of charge (SOC) constant during measurements. The hydrogen electrode, used as a reference, is a GDE (Baltic 10707 S10CC). The membrane is Nafion 115 and the cell active area is 25 cm^2 .

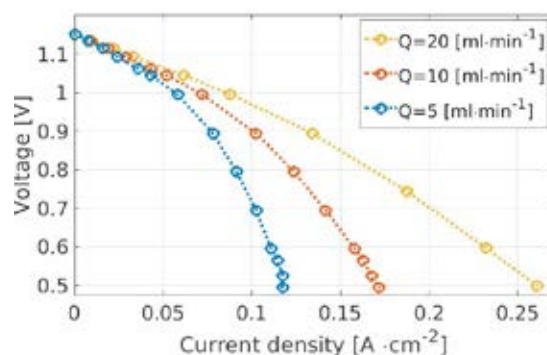


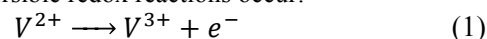
Fig.1. Cathode polarization curve for different flow rates (SOC=80%).

Cell performances are investigated in different working conditions through several electrochemical measurement, such as polarization curves (Fig.1), electrochemical impedance spectroscopy and cyclic voltammetry.

All measurements are performed at room temperature and atmospheric pressure.

IV. MODEL DEVELOPMENT

In a VRFB reversible redox reactions occur:





Main assumptions undergoing the model are the same adopted by Kumbur group [3]: steady-state, isotropic and isothermal domain, electro-neutrality of the electrolytes, dilute solution and only convective transport in flow fields. The chemical species considered are the four Vanadium oxidations states and ions from the sulfuric acid dissociation. The presence of water is neglected in all the domains due to the dilute solution assumption. The developed model accounts for cross contamination, since Nafion based membrane is not selective to only protons and allows Vanadium ions to permeate, generating reversible contamination in electrolyte and side reactions that lead to self-discharge [4]. Vanadium concentrations and fluxes are treated as continuous at the interfaces between electrodes and membrane.

The species transport in porous electrodes is described by the Nernst Planck law, which models ions transport in dilute solution approximation:

$$N_i = -D_i \Delta c_i - z_i F \frac{D_i}{RT} c_i \Delta \phi_i \quad (3)$$

It is clear the non-linearity of mass transport phenomena, that depends on both concentration and potential gradients, and on concentration itself, making fluxes interpretation rather complex.

The developed model has been firstly calibrated on the data reported by Mench group [5]. A systematic validation on a wide range of operating conditions with respect to the half-cell data is currently in progress.

V. MODELING RESULTS

In Fig.2 molar fluxes through the membrane are shown in function of the current density.

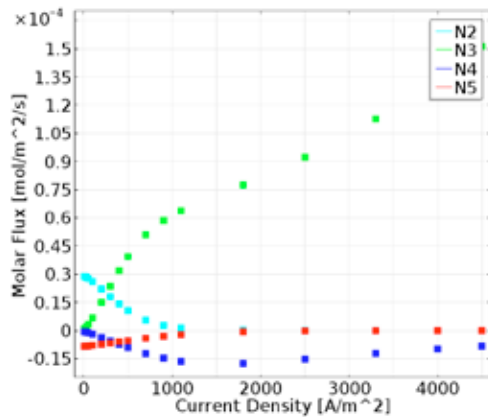


Fig.2. Relation between vanadium molar fluxes and current density in the membrane.

At high current density the V^{2+} and V^{5+} fluxes are negligible, because during discharge they are consumed and their concentrations at electrode-membrane interface is close to zero. The fluxes of V^{3+} and V^{4+} have the opposite trend, because they are reaction products and their concentration at the electrode

membrane-interface increases with the current density. Until current density is below $1500 \text{ A}\cdot\text{m}^{-2}$, diffusion across the membrane is the main transport mechanism, so total flux increases. When current density is higher than $1500 \text{ A}\cdot\text{m}^{-2}$, migration becomes predominant and have different effects on V^{3+} and V^{4+} . Total flux of the former increase, because migrative flux direction is toward the cathode, and it is the same of its diffusive flux, while for the latter the total flux starts to decrease, due to the opposite sign of V^{4+} diffusion and migration fluxes.

Fig.3 shows how total flux is conserved in the membrane, while its diffusive and migrative components have different behavior.

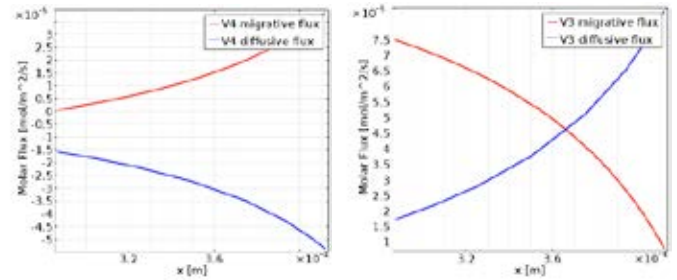


Fig.3. Vanadium diffusion and migration molar fluxes in the membrane (at $2000 \text{ A}\cdot\text{m}^{-2}$).

VI. CONCLUSION

Developed model allowed to investigate how Vanadium fluxes vary with operating conditions: at low current densities the predominant driving force for cross contamination is diffusion, while at high current density is migration.

An extended validation, considering also state of charge, flow rate and charging operations will lead to develop a diagnostic tool to minimize cross contamination.

ACKNOWLEDGMENT

Authors would like to thank ENI – Istituto Donegani for the financial support (contract n. AG35034714).

REFERENCES

- [1] M. Zago, A. Casalegno, A physical model of Direct Methanol Fuel Cell anode impedance, Journal Of Power Sources 248 (2014) 1181-1190.
- [2] V. Yufit, B. Hale, M. Matian, P. Mazur, N.P. Brandon, Development Of A Regenerative Hydrogen-Vanadium Fuel Cell For Energy Storage Applications, Journal of Electrochemical society, 160 (6) A856-A861 (2013) .
- [3] K.Knehr, E. Agar, R. Dennison, A. Kalidindi and C. Kumbur, A Transient Vanadium Flow Battery Model Incorporating Vanadium Crossover And Water Transport Through The Membrane
- [4] S. Rudolph, U. Schroder, I.M. Bayanov, On-line controlled state of charge rebalancing in vanadium redox flow battery, Journal of Electroanalytical Chemistry 703 (2013) 29-37.
- [5] D.S. Aaron, Q. Liu, Z. Tang, G.M. Grim, A.B. Papandrew, A. Turhan, T.A. Zawodzinski, M.M. Mench, Dramatic Performance Gains in Vanadium Redox Flow Batteries



SYNTHESIS OF GADOLINIUM-DOPED CERIA BY GELATION/CO-PRECIPIATION WITH UREA

L. Spiridigliozzi*, G. Dell'Agli*, C.Ferone**, R. Cioffi**, G. Accardo**, A. Marocco*

* Department of Civil and Mechanical Engineering and INSTM Research Unit, University of Cassino and Southern Lazio, Via G. Di Biasio 43, 03043 Cassino (FR), (Italy)

** Department of Engineering and INSTM Research Unit, University Parthenope of Naples, Centro Direzionale, Is. C4, 80143 Napoli, (Italy)

Abstract - Gadolinium-doped ceria, with Gd content equal to 10% and 20%, was synthesized by using urea gelation/co-precipitation method (UGC). After the co-precipitation induced by heating the solution at about 100 °C, the co-precipitate was aged in boiling water under vigorous stirring for 4 h. Thus a carbonate-based phase is formed, but with a simple calcination step at low temperature, i.e. 400°C, a single phase fluorite structure is obtained. After the calcinations step, the powders were still of nanometer size with a good sinterability. In fact, a full densification for both the samples has been obtained with a firing at 1400°C.

Index Terms – Gadolinium-doped ceria, Urea Gelation Co-precipitation, Sintering.

I. INTRODUCTION

Gadolinium-doped ceria (CGO) is an attractive electrolyte material for potential application in SOFCs operating at intermediate temperature typically with substitution of Ce^{+4} by Gd^{+3} in the range 10-20 % at. In order to improve its sinterability, chemical processes are preferred because of the better characteristics of the synthesized powder, especially the nanometric character. To synthesized ceria-based electrolytes with the desired properties, several chemical methods such as sol-gel [1], combustion, co-precipitation, hydrothermal treatment have been employed [2]. Among the chemical methods the urea gelation co-precipitation (UGC) is a good alternative for producing nanoparticles of ceria whose size is around a few nanometers and it has been applied for producing ceria for catalytic application [3,4]. In fact, it is well known that with UGC more homogeneous mixed oxides with fines

particles sizes than conventional co-precipitation are prepared [4]. In the present work UGC method is used for prepare gadolinium-doped ceria with Gd content equal to 10 % and 20 % at, as ceramic electrolytes for SOFCs. The as-synthesized powders and the calcined ones were characterized by DTA-TG and by XRD, showing that fluoritic form of CGO, for both the compositions, is easily obtained. The sintering aptitude of this powders was also ascertained with traditional sintering cycle.

II. EXPERIMENTAL

$Ce(NO_3)_3 \cdot 6H_2O$, $Gd(NO_3)_3 \cdot 6H_2O$ and $CO(NH_2)_2$ were used as starting materials for the synthesis of hydrous cerium-gadolinium oxide with Gd 10% at, indicated as CGO90 in the following, and 20 % at, indicated CGO80 in the following, by UGC. Basically the UGC method consists of the following steps: dissolution of urea and Ce-Gd nitrates in proper amount in the same solution (molar concentrations are 0.2 M and 0.05 M for urea and total metallic cations, respectively); heating of the solution at about 100 °C so that urea decomposes in ammonia and carbon dioxide with increasing the pH of the solution and so inducing the co-precipitation. The so formed co-precipitate is aged in boiling conditions under vigorous stirring for 4 h. During the last two steps a total reflux apparatus is used for avoiding the escape of the evaporated solution. The calcinations step was carried out in air at 400 °C for 2 hours. The powders were finally compacted in cylindrical pellets by cold isostatic pressing at 160 MPa. The sintering of these compacts was carried out in air at 1400 °C for 3 hours.



III. RESULTS

The white color of the co-precipitates synthesized from UGC denotes that CGO is still not formed and a carbonate-based phase is actually formed, as confirmed from the powders diffraction patterns not reported here. The relative DTA-TG thermograph of CGO90 is reported in Fig 1; a pronounced and sharp endothermic peak, related to the thermal decomposition of the carbonate-based phase, whose temperature is about 310 °C for CGO80 and about 340 °C for CGO90. The thermal decomposition is characterized by a remarkable corresponding weight loss whose value is about 20 % for both the samples.

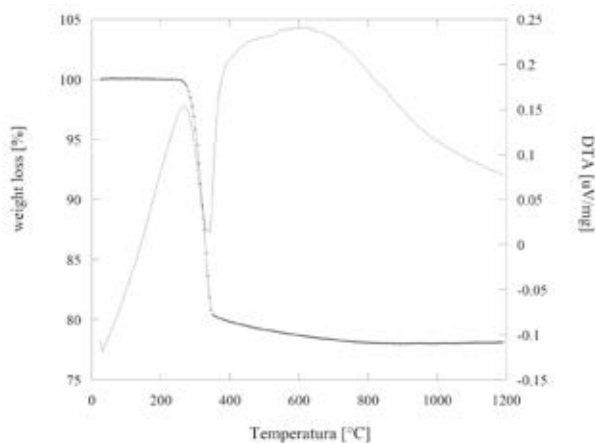


Fig. 1. DTA-TG thermograph of CGO90

Adopting the calcination step in air at 400°C, well higher than the decomposition temperature as determined in the thermographs, CGO with fluorite single phase structure is readily obtained. The relative X-Ray diffraction patterns are reported in Fig. 2 in which only the peaks of CGO in fluoritic form are present. The nanometric character of the powders is preserved also after the calcination step, as confirmed by the calculation of crystal size, carried out by the Scherrer formula on the (111) XRD peak of CGO. In particular it results that the crystal size for CGO80 and for CGO90 are respectively 15.0 nm and 15.4 nm.

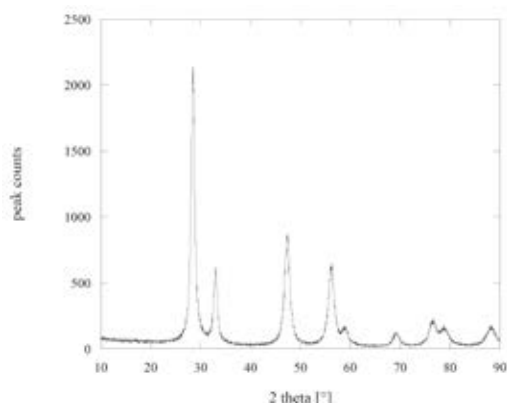


Fig. 2. XRD of calcined CGO90

The calcined powders were pressed by cold isostatic pressing and after they were fired at 1400 °C for 3 hours. The relative SEM micrograph for sample CGO90 is reported in Fig. 3 and it shows the very dense microstructure of this materials.

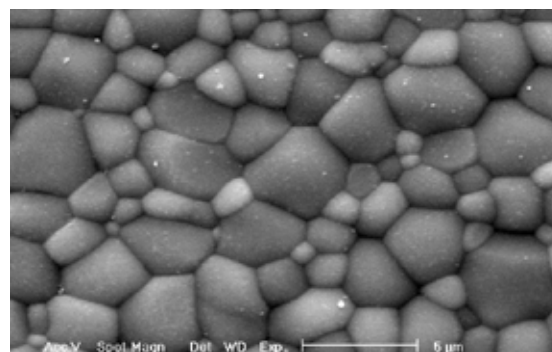


Fig.3. SEM micrograph of CGO sintered at 1400°C

IV. CONCLUSION

With UGC method it has been able to produce very fine powders of CGO with a relatively simple method and cheap raw materials. The as-synthesized powder are formed by a carbonate-based phase and a calcination step is necessary to induce the thermal decomposition and the relative formation of the single-phase fluorite structure. As clear from DTA-TG thermographs this thermal treatment can be carried out at low temperature, so preserving the nanometric character of the powders and hindering undesirable grain growth and agglomeration phenomena. Thus, the calcined powders are still very reactive so that the sintering can be carried out at 1400 °C, lower than the typical sintering temperature of ceria, attaining a nearly full densification as evident in the SEM micrographs, without using any sintering aids. In a further development the electrical behavior of these samples will be evaluated.

REFERENCES

- [1] C. Ferone, G. Accardo, G. Dell'Agli, R. Cioffi, Sol-gel synthesis of gadolinium doped ceria (Gd-CeO₂) for intermediate temperature SOFC electrolyte, EFC 2013 Proceedings of the 5th European Fuel Cell, Rome 11-13 December 2013, Pages 391-392
- [2] G. Donmez, V. Saritoba, T.B. Altincekic, M.A.F. Oksuzomer, Polyol Synthesis of Ce_{1-x}RE_xO_{2-x/2} (RE = Sm, Gd, Nd, La, 0 ≤ x ≤ 0.25) Electrolyte for IT-SOFC, Journal of the American Ceramic Society, Volume 98, 2015, Pages 501-509
- [3] F. Vindigni, M. Manzoli, T. Tabakova, V. Idakiev, F. Boccuzzi, A. Chiorino, Effect of ceria structural properties on the catalytic activity of Au-CeO₂ catalysts for WGS reaction, Phys Chem Chem Phys, Volume 15, 2013, Pages 13400-13408
- [4] X. Qi, M. Flytzani-Stephanopoulos, Activity and stability of Cu-CeO₂ catalysts in high temperature water-gas shift for fuel cell application, Industrial Engineering Chemical Research, Volume 43, 2004, Pages 3055-3062.



HYDROTHERMAL SYNTHESIS AT LOW TEMPERATURE OF GADOLINIUM-DOPED CERIA

L. Spiridigliozzi*, G. Dell'Agli*, A. Marocco*, G. Accardo**,
C. Ferone**, R. Cioffi**

* Department of Civil and Mechanical Engineering and INSTM
Research Unit, University of Cassino and Southern Lazio, Via G. Di
Biasio 43, 03043 Cassino (FR) Italy

** Department of Engineering and INSTM Research Unit,
University Parthenope of Naples, Centro Direzionale, Is. C4, 80143
Napoli, Italy

Abstract - Gadolinium-doped ceria is an attractive electrolyte material for potential application in SOFCs operating at intermediate temperature typically with 10-20 % substitution of Ce^{+4} by Gd^{+3} . Nanometric powders of Gadolinium-doped ceria have been prepared by hydrothermal treatment both with conventional method and with microwave-assisted method using co-precipitate as a precursor and in the presence of simply deionized water as a mineralizer. The obtained powders have been characterized by XRD, TEM, SEM and DTA-TG. Adopting an optimized sintering cycle very dense ceramics based on hydrothermally synthesized gadolinium-doped ceria have been obtained

Index Terms – Gadolinium-doped ceria, Hydrothermal treatment, Sintering.

I. INTRODUCTION

Conventional solid oxide fuel cells (SOFCs) must operate above 800 °C when electrolyte based on yttria-stabilized zirconia is used. Because of this it is necessary to use costly materials for other components of SOFC. Thus lowering the temperature of SOFC is one main target for recent researches [1]. From this point of view ceria-based ceramics represent promising materials. Among the various ceria-based ceramics, in particular gadolinium-doped ceria is an attractive electrolyte material for potential application in SOFCs operating at intermediate temperature typically with 10-20 % substitution of Ce^{+4} by Gd^{+3} . However, one of the main drawbacks of ceria-based materials is that high temperature is required to sinter the materials to form dense bodies [2]. Therefore for these applications it is important to obtain ultrafine powders. For

these purpose, several chemical routes have been proposed in the literature, among them the hydrothermal process has attracted a lot of attention for the direct synthesis of crystalline ceramic powders at relatively low temperatures [3]. Therefore the aim of the present work is the synthesis by hydrothermal treatment at low temperature, both conventional and microwave-assisted, of ceramic powders formed by gadolinium-doped ceria with 10% mol Gd^{+3} . Furthermore, an optimized sintering cycle is proposed.

II. EXPERIMENTAL

$Ce(NO_3)_3 \cdot 6H_2O$ and $Gd(NO_3)_3 \cdot 6H_2O$ were used as starting materials for the synthesis of hydrous cerium-gadolinium oxide by coprecipitation having the following composition in the anhydrous form: $Ce_{0.9}Gd_{0.1}O_{1.95}$. The proper amounts of cerium and gadolinium salts were dissolved in deionized water in order to have the total cationic concentration equal to 0.1 M and then the solution was vigorously stirred for 1 hour. The coprecipitation was carried out by reverse precipitation, i.e. the solution containing dissolved cerium and gadolinium salts was slowly added to an excess ammonia solution (~ 4 M) under vigorous stirring. The co-precipitate was filtered and washed repeatedly with deionized water in order to remove the undesired ions. This batch was directly used as precursor in the various hydrothermal syntheses. The conventional hydrothermal synthesis was carried out at 145 °C for 1 day. The microwave assisted hydrothermal synthesis was carried out at 160 °C for 30 minutes. The powders were compacted in cylindrical pellets by cold isostatic pressing at 160 MPa. The

sintering of these compacts was carried out in air at 1500 °C for 3 hours.

III. RESULTS

The sample obtained by conventional hydrothermal treatment using simply deionized water as mineralizer is formed by gadolinium-doped ceria in the cubic fluoritic phase as it appears in the diffraction pattern. During the hydrothermal treatment the crystallization process, started already during the co-precipitation, of gadolinium-cerium oxide into the cubic fluoritic phase continues and contemporaneously some grain growth phenomena in the nanometric powders occur. The XRD peaks are sharper than those of the precursor and the crystal size calculated by the Scherrer formula is 16.4 nm. The surface area of this sample, measured by BET method, is 52.4 m²/g which corresponds at about 16.5 nm as mean particle diameter. The morphology of these powders was observed by TEM and a micrograph is reported in Figure 1, where it clearly appears that the particles size is between 15 and 20 nm.

In order to reduce this long treatment, a microwave-assisted hydrothermal treatment was carried out on the same as-synthesized co-precipitates, using a temperature of 160 °C and a duration of 30 minutes with the same mineralizer. The XRD of this sample confirms the presence of only cubic ceria. However in this case the crystallite size, calculated by the Scherrer formula, is equal to about 10 nm and it does not significantly increase during the microwave hydrothermal treatment so confirming the results reported by Ivanov [3]. Most likely this behavior is related to the very short duration of the microwave-assisted hydrothermal treatment. These results are confirmed also by the TEM analysis of this sample. In fact the examination of its morphology shows a bimodal particle size distribution; there are particles with size around 20-30 nm and particles with size around a few nanometers.

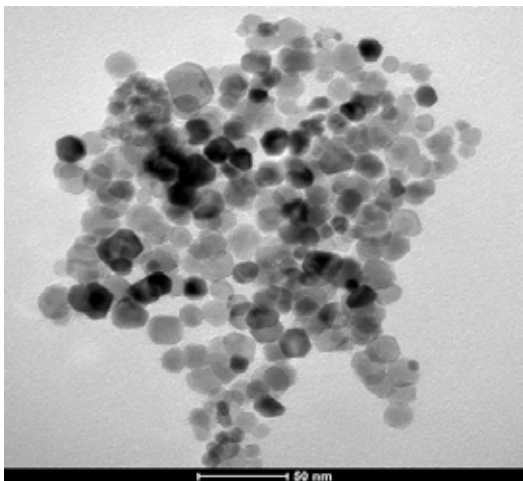


Fig. 1. TEM micrograph of powders obtained by conventional hydrothermal synthesis.

In order to obtain a full densified sample, an optimized sintering cycle, suggested by DTA thermograph of the co-precipitate, characterized by a very low heating rate in the range 300-350 °C in which water evolution occur. The sintering of these compacts was carried out in air at 1500 °C for 3 hours.

The microstructure appears as a relatively uniform (Fig. 2), dense and compact ensemble of crystalline grains whose size is in the range 1-2 μm so showing the very good densification confirmed by the relative density slightly higher than 0.97.

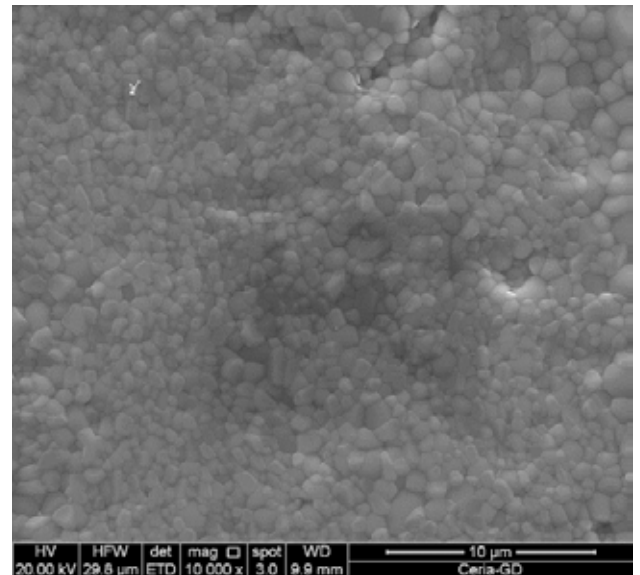


Fig. 2. SEM micrograph of sample sintered with optimized thermal cycle.

IV. CONCLUSION

By hydrothermal treatment, both conventional and MW based, directly on the as-synthesized co-precipitates, without any drying step, it results in a very positive effect on these materials which can be sintered with a high degree of densification, highlighted by the high relative density and by the SEM micrograph of their microstructure. Moreover using the microwave-assisted hydrothermal treatment it is possible to reduce significantly the duration of the treatment.

REFERENCES

- [1] X. Hao, Y. Liy, Z. Wang, J. Qiao, K. Sun, A novel sintering method to obtain fully dense gadolinia doped ceria by applying a direct current, *Journal of Power Source*, Volume 210, 2012, Pages 86-91
- [2] F. Munoz, A.Gabriela Leyva, R.T. Baker, R.O. Fuentes, Effect of preparation method on the properties of nanostructured gadolinia-doped ceria materials for IT-SOFCs, *International Journal of Hydrogen Energy*, Volume 37, 2012, Pages 14854-14863
- [3] V.K. Ivanov, G.P. Kopitsa, A.E. Baranchikov, S.V. Grigor'ev, V.V. Runov, V.M. Haramus, Hydrothermal growth of ceria nanoparticles, *Russian Journal of Inorganic Chemistry*, Volume 54, 2009, Pages 1857-1861



THE EFFECT OF PH ON THE HYDROTHERMAL SYNTHESIS OF GADOLINIUM-DOPED CERIA

L. Spiridigliozzi*, G. Dell'Agli*, G. Accardo**, E. Di Bartolomeo***, S. Licocchia***, C. Ferone**, R. Cioffi**

* Department of Civil and Mechanical Engineering and INSTM Research Unit, University of Cassino and Southern Lazio, Via G. Di Biasio 43, 03043 Cassino (FR), (Italy)

** Department of Engineering and INSTM Research Unit, University Parthenope of Naples, Centro Direzionale, Is. C4, 80143 Napoli, (Italy)

*** University of Rome Tor Vergata, Dipartimento di Scienze e Tecnologie Chimiche, Via della Ricerca Scientifica 1, 00133 Roma, (Italy)

Abstract - The effects of different mineralizer solutions, characterized by different pH, on the hydrothermal synthesis at relatively low temperature (i.e. 140 °C) of ceramic powders formed by gadolinium-doped ceria with 10% Gd doping is analyzed. Three different mineralizer solutions were used: acidic solution (with HCl) at pH 1, neutral solution (with de-ionized water) and basic solution (with KOH) at pH 13. Powders obtained from the three different pH conditions were characterized by XRD, DTA-TG, and TEM observations, and their electrical behavior was ascertained. Even if all the samples consist of a single phase fluorite cubic ceria, significant differences appear both in their thermal behavior and in their electrical behavior. In particular for IT-SOFC the best sample in terms of electrical properties appears to be the one synthesized by using basic solution as mineralizer.

Index Terms – Gadolinium-doped ceria, Hydrothermal treatment, Mineralizer.

I. INTRODUCTION

Gadolinium-doped ceria is an attractive electrolyte material for potential application in SOFCs operating at intermediate temperature typically with substitution of Ce^{+4} by Gd^{+3} in the range 10-20 % at. Owing to the difficulties for full sintering of ceria with traditional ceramic powders technology, several chemical routes have been proposed in the literature; in fact, it is well known that chemical techniques have the following advantages over the conventional ceramic processing techniques: high purity, high homogeneity and ultrafine powder

[1,2]. Among the chemical routes, the hydrothermal process has attracted a lot of attention for the direct synthesis of crystalline ceramic powders, characterized by high purity, controlled stoichiometry, high quality, narrow particle size distribution and so on, at relatively low temperatures [3].

In the present work the effect of the pH of the mineralizer solution in the hydrothermal synthesis at low temperature (i.e. 140 °C) of ceramic powders formed by gadolinium-doped ceria with 10% mol Gd^{+3} (CGO in the following) is analyzed. The ceramic precursor was a hydrous cerium-gadolinium oxide co-precipitate.

II. EXPERIMENTAL

$Ce(NO_3)_3 \cdot 6H_2O$ and $Gd(NO_3)_3 \cdot 6H_2O$ were used as starting materials for the synthesis of hydrous cerium-gadolinium oxide (with Gd 10% at) by co-precipitation. The proper amounts of cerium and gadolinium salts were dissolved in deionized water and, after one hour of vigorous stirring, the co-precipitation was carried out under vigorous stirring in reverse mode using an excess ammonia solution (~ 4 M). The co-precipitate was filtered and washed repeatedly with deionized water in order to remove the undesired ions. This batch was directly used as a precursor in the hydrothermal syntheses carried out with three different mineralizer solutions: acidic one using HCl 0.1 M (sample A), neutral one using deionized water (sample N) and basic one using KOH 0.1 M (sample B). All the hydrothermal syntheses were carried out at 140 °C for 1 day. The powders



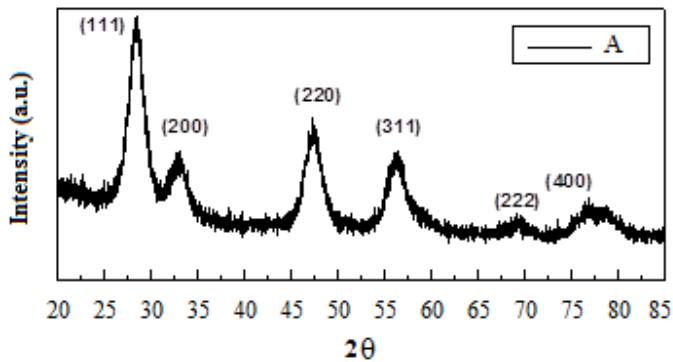
were compacted in cylindrical pellets by cold isostatic pressing at 160 MPa. The sintering of these compacts was carried out in air at 1500 °C for 3 hours.

Electrochemical impedance spectroscopy measurements were performed in order to reveal the electrical behavior of the samples.

III. RESULTS

The XRD patterns of samples A, is reported in Figure 1 and it indicate the presence of only cubic ceria in the fluoritic form; XRD patterns of samples N and B are nearly the same to this one and are not reported here. The crystallite sizes, calculated by the Scherrer formula, are roughly 16 nm for all the sample and they suggest that for CGO, in contrast to other similar ceramic systems, the hydrothermal crystal growth is almost unaffected from the pH of the mineralizer solution.

Fig. 1. XRD of sample A



However, it has been observed a different behavior by TG analysis in samples A, N and B, reported in Figure 2. In fact, as the pH of mineralizer rises, samples' total weight loss and temperature of residual amorphous phase crystallization peak rise ranging from 7.2 % to 11.1 % and from 243 °C to 349 °C respectively. All the three thermographs show very small exothermic peaks, representing the crystallization of the low residual amorphous phase after hydrothermal treatment, albeit different mineralizer affects the temperature of those peaks in a sensible manner. In particular, sample A has the lowest peak temperature and lowest associated weight loss.

Using an optimized sintering cycle, deduced from the DTA curves, and characterized by a very low heating rate in range of temperatures in which the thermal dehydration occurs, a full densification was attained with a relative density higher than 0.97 for all the three samples.

The Arrhenius plots of the three samples determined by AC impedance spectroscopy show obviously a similar behavior even if with some differences in the activation energy E_a , whose value (0.61 eV) is higher for sample N. Thus in the higher temperature range (> 650 °C) the sample N has the highest ionic conductivity while in the lower temperature range the sample B has the highest ionic conductivity.

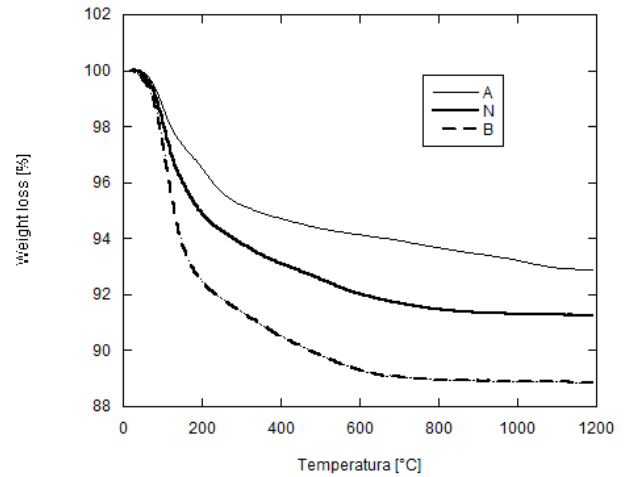


Fig. 2. TG of samples A, N and B

IV. CONCLUSION

Using a hydrothermal treatment directly on the as-synthesized gadolinium-doped ceria co-precipitates, without any drying step, it results a crystallization of GCO in the fluorite structure with nanometric crystal size. Furthermore the hydrothermal treatment causes a very positive effect on the powders, reducing substantially agglomeration phenomena, which can be sintered with a high degree of densification. The electrical characterization of the sample A, N and B has showed that even if their electrical behavior is very similar some differences appear in the Arrhenius plots and in particular the sample N is characterized by the highest value of E_a . Thus this sample has the highest electrical conductivity at higher temperatures and on the contrary has the lowest electrical conductivity at lower temperature and this change of behavior occurs at about 650 °C. However in the range of lower temperature the samples B has the highest ionic conductivity and this sample appears to be the more interesting for IT_SOFC application.

REFERENCES

- [1] Lee and H. Komarneni (Eds.), Chemical processing of ceramics Second Edition, Taylor & Francis, 2005.
- [2] G. Donmez, V. Saritoba, T.B. Altincekic, M.A.F. Oksuzomer, Polyol Synthesis of $Ce_{1-x}RE_xO_{2-x/2}$ (RE = Sm, Gd, Nd, La, $0 \leq x \leq 0.25$) Electrolyte for IT-SOFC, Journal of the American Ceramic Society, Volume 98, 2015, Pages 501-509
- [3] M. Yoshimura, Hydrothermal processing of materials: past, present and future, Journal of Materials Science, Volume 43, 2008, Pages 2085-2103



VERY LOW Pt-Pd BASED ELECTROCATALYSTS FOR OXYGEN REDUCTION REACTION

A. Brouzgou¹, F. Tzorbatzoglou¹, S. Song³, E. Gorbova², P. Tsiakaras^{1,2}

¹Department of Mechanical Engineering, School of Engineering,
University of Thessaly, Pedion Areos, 38334 Volos, (Greece)

²Laboratory of Electrochemical Devices based on Solid Oxide Proton
Electrolytes, Institute of High, Temperature Electrochemistry, Ural Branch of
RAS, Akademicheskaya Str., 620990 Yekaterinburg, (Russia)

³The Key Lab of Low-carbon Chemistry & Energy Conservation of Guangdong
Province, School of Physics and Engineering, Sun Yat-sen University,
Guangzhou 510275, (China)

Abstract - In the present manuscript very low-platinum electrocatalysts, Pd₉₇Pt₃/C, Pd₉₈Pt₂/C, Pd₉₉Pt₁/C and pure Pd/C are prepared and examined for oxygen reduction reactions (ORR) with the rotating electrode technique. From the analysis of the results the addition of Pt to the pure Pd enhances significantly the ORR activity. More specifically, the Pd₉₈Pt₂/C electrocatalyst exhibits the highest intrinsic activity, with ca. 0.75 mA cm⁻² exchange current density. However, further increment of the Pt loading against Pd loading, (Pd₉₇Pt₃/C) reduces dramatically the intrinsic catalytic activity from 0.75 mA cm⁻² to 0.2 mA cm⁻². The Tafel slopes at low potential values are calculated 127, 128, 156 and 94 mV per decade for the Pd₉₇Pt₃/C, Pd₉₈Pt₂/C, Pd₉₉Pt₁/C and Pd/C, respectively, indicating one electron transfer at the rate determining step. While the calculated Tafel slope at high potential values indicates two electrons transfer at the rate determining step. The lower Tafel slope of the Pd/C shows that some OHads intermediates were involved.

Keywords: oxygen reduction reaction, palladium-based, very low platinum electrocatalysts

I. INTRODUCTION

In today ongoing research on fuel cells as far as concerns the catalytic field, the most addressed technical barriers are:

- Reduce precious metal loading of catalysts
- Increase the specific and mass activities of catalysts
- Increase the durability and stability of catalysts with cycling

In our previous review work [1] we have identified that the most active electrocatalysts (>5 mW μg_{Pt}⁻¹) for hydrogen oxidation reaction are bimetallic Pd-Pt ones. In an attempt to reduce the catalyst loading the international research community has identified Pd as the best non-precious electrocatalyst, with comparable, but lower, Pt's

electrocatalytic activity. Meanwhile, doping Pd electrocatalyst with a very little amount of Pt has been proved to enhance significantly pure Pd's electrocatalytic activity, indicating activity higher than pure Pt [2]. Antolini *et al.* [3] decreased platinum loading adopting carbon supported Pd₉₆Pt₄ and Pt as anode and cathode materials, respectively. They found that the performance of the fuel cell was only slightly lower than the conventional PEMFC with Pt/C catalysts at both electrodes. In the present work, carbon supported Pd₉₇Pt₃, Pd₉₈Pt₂, Pd₉₉Pt₁ and pure Pd electrocatalysts are prepared via a modified-pulse microwave assisted polyol method and are examined for the oxygen reduction reaction (ORR), with the rotating electrode technique.

II. EXPERIMENTAL

The examined electrocatalysts were prepared by a modified pulse-microwave assisted polyol synthesis procedure. In a beaker, the starting metal precursors (PdCl₂ and H₂PtCl₆•6H₂O) were well mixed with ethylene glycol (EG) in an ultrasonic bath, and then XC-72 R carbon black (Cabot Corporation) was added into the above mixture. After the pH value of the system was adjusted to be more than 10 by the drop-wise addition of 1.0 M NaOH/EG, a well-dispersed slurry was obtained with ultrasonic stirring for 60 min. Thereafter, the slurry was microwave-heated in the pulse form 10s-on/10s-off for several times. Then, the solution was re-acidified with a pH value of about 2-4. The resulting black solid sample was filtered, washed and dried at 80°C for 10 h in a vacuum oven. The X-ray diffraction (XRD) patterns were recorded on a D-MAX 2200 VPC diffractometer using Cu Kα radiation (30 kV, 30 mA). The transmission electron microscopy (TEM) TEM investigations were carried out on a JEOL TEM-2010 (HR) at 120 kV. Cyclic voltammetry (CV) and rotating disk electrode (RDE) studies were carried out to estimate the electrochemical active surface area and to



characterize the activity of the as-prepared electrocatalysts for the ORR.

III. RESULTS AND DISCUSSION

The diffraction peaks of $\text{Pd}_x\text{Pt}_y/\text{C}$ catalysts at about 40° , 46° , 68° and 81° are attributed to the (1 1 1), (2 0 0), (2 2 0) and (3 1 1) planes of the face center cubic (fcc) structure of the Pd–Pt alloys.

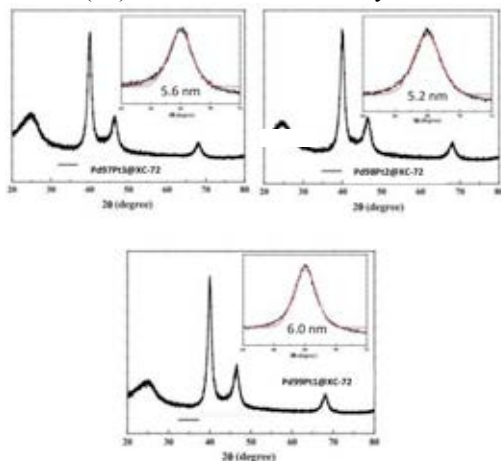


Fig. 1. XRD results, Inset: crystallite size.

From the XRD results the crystallite size is calculated (inset of Fig. 1) 5.6, 5.2 and 6.0 nm for the $\text{Pd}_{97}\text{Pt}_3/\text{C}$, $\text{Pd}_{98}\text{Pt}_2/\text{C}$ and $\text{Pd}_{99}\text{Pt}_1/\text{C}$, respectively. Moreover from the TEM images (Fig. 2), the smallest nanoparticles and the most homogeneously distributed are observed for the $\text{Pd}_{98}\text{Pt}_2/\text{C}$, ~ 5.0 nm. Then the $\text{Pd}_{97}\text{Pt}_3/\text{C}$ follows with ~ 5.5 nm nanoparticles size and finally the $\text{Pd}_{99}\text{Pt}_1/\text{C}$ with ~ 6.0 nm nanoparticles size and inhomogeneous distribution.

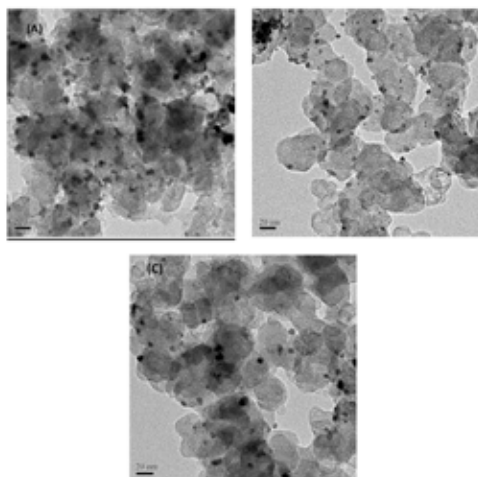


Fig. 2. TEM images of $\text{Pd}_{97}\text{Pt}_3/\text{Vulcan-XC72}$ (A), $\text{Pd}_{98}\text{Pt}_2/\text{Vulcan-XC72}$ (B), $\text{Pd}_{99}\text{Pt}_1/\text{Vulcan-XC72}$ (C).

The comparison of the kinetic analysis is depicted in Fig. 3. As it can be deduced the addition of Pt to the pure Pd enhances significantly the ORR activity. More specifically, $\text{Pd}_{98}\text{Pt}_2/\text{C}$ electrocatalyst exhibits the highest intrinsic activity, with ca. 0.75 mAcm^{-2} exchange current density. However, further increment of the Pt loading against Pd loading, ($\text{Pd}_{97}\text{Pt}_3/\text{C}$) reduces also

dramatically the intrinsic catalytic activity from 0.75 mAcm^{-2} to 0.2 mAcm^{-2} . From Fig. 3 the same volcano-type palladium loading dependence is observed for the kinetic current density values, with $\text{Pd}_{98}\text{Pt}_2/\text{C}$ to present the highest kinetic current density at all potential values.

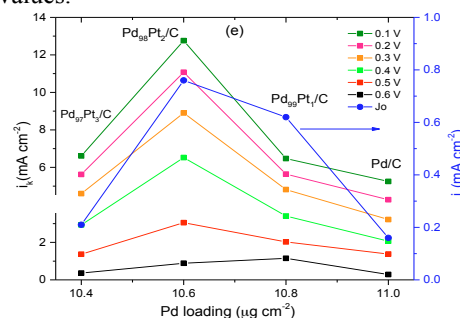


Fig. 3. Dependence of kinetic and exchange current density on palladium loading.

The total electrons that contribute to the oxygen reduction reaction are one for the $\text{Pd}_{97}\text{Pt}_3/\text{C}$ and $\text{Pd}_{98}\text{Pt}_2/\text{C}$, while their number increases to three as the palladium loading increases, at $\text{Pd}_{99}\text{Pt}_1/\text{C}$ and pure Pd/C.

IV. CONCLUSION

According to the experimental results and the kinetic analysis, the addition of a little amount of platinum to pure palladium electrocatalyst enhances electrocatalytic activity towards ORR. The exchange current density values were estimated as: $\text{Pd}_{98}\text{Pt}_2/\text{C}$ (0.76 mAcm^{-2}) > $\text{Pd}_{97}\text{Pt}_3/\text{C}$ (0.21 mA cm^{-2}) > $\text{Pd}_{99}\text{Pt}_1/\text{C}$ (0.62 mAcm^{-2}) > Pd/C (0.16 mAcm^{-2}). Among the examined electrocatalysts $\text{Pd}_{98}\text{Pt}_2/\text{C}$ and $\text{Pd}_{97}\text{Pt}_3/\text{C}$ exhibited the highest activity for ORR at room temperature.

ACKNOWLEDGMENT

The authors are grateful to the “Bilateral R&D Co-operation between Greece and China 2012–2014”, co-financed by the European Union and the Greek Ministry of Education-GSRT for financial support. Professor Tsiakaras and Dr Gorbova are also grateful for funding to the Ministry of Education and Science of the Russian Federation (contract no. 14.Z50.31.0001).

REFERENCES

- [1] Brouzgou, A., Song, S.Q., Tsiakaras, P., Low and non-platinum electrocatalysts for PEMFCs: Current status, challenges and prospects, *Applied Catalysis B: Environmental*, 127, 2012, pp. 371-388.
- [2] Xie, S., Choi, S.-I., Lu, N., Roling, L.T., Herron, J.A., Zhang, L., Park, J., Wang, J., Kim, M.J., Xie, Z., Mavrikakis, M., Xia, Y., Atomic Layer-by-Layer Deposition of Pt on Pd Nanocubes for Catalysts with Enhanced Activity and Durability toward Oxygen Reduction, *Nano Letters*, 14, 2014, pp. 3570-3576.
- [3] Antolini, E., Zignani, S.C., Santos, S.F., Gonzalez, E.R., Palladium-based electrodes: A way to reduce platinum content in polymer electrolyte membrane fuel cells, *Electrochimica Acta*, 56, 2011, pp. 2299-2305.
- [4] Ma, J., Ai, D., Xie, X., Guo, J., Novel methanol-tolerant Ir–S/C chalcogenide electrocatalysts for oxygen reduction in DMFC fuel cell, *Particuology*, 9, 2011, pp. 155-160.



AN AIR-BREATHING ENZYMATIC CATHODE WITH EXTENDED LIFETIME BY CONTINUOUS LACCASE SUPPLY

E. Kipf, D. Morse, T. Messinger, S. Sané,
and S. Kerzenmacher

Laboratory for MEMS Applications, IMTEK - Department of
Microsystems Engineering, University of Freiburg,
Georges-Koehler-Allee 103, 79110 Freiburg (Germany)

Abstract - We present a novel air-breathing enzymatic fuel cell cathode. It is continuously supplied with fresh enzyme-containing culture supernatant of the fungus *T. versicolor* to achieve an extended lifetime, independent of enzyme degradation. The new cathode design enables passive oxygen supply and circumvents the need for energy-intensive aeration. The results are an important step towards the realization of hybrid microbial-enzymatic fuel cells with extended lifetime and improved performance.

Index Terms – Microbial fuel cell, oxygen reduction, cathode, laccase.

I. INTRODUCTION

Microbial biofuel cells are a promising technology to generate renewable electricity, for instance from wastewater or similar biomass resources [1]. Often the cathode reaction limits the microbial fuel cell's overall performance [2]. In this respect, enzymes such as laccase or bilirubin oxidase, which exhibit high electrocatalytic activity for oxygen reduction, are considered to be promising alternatives to the currently used expensive noble metal catalysts. However, due to enzyme degradation the lifetime of enzymatic electrodes is typically in the range of days and weeks, which is in stark contrast to the years of operation reported for microbial fuel cell anodes. In a previous experiment we have shown that the limited lifetime of a submerged laccase cathode can be extended by a periodic exchange of the enzyme solution against fresh enzymes. Thereto the laccase-containing crude culture supernatant of the white-rot fungus *Trametes versicolor* was used and an at least five-fold extended lifetime of up to 120 days was achieved [3].

Now, we present the first results of a corresponding air-breathing cathode, which enables passive operation without energy-intensive aeration of the catholyte.

II. EXPERIMENTAL

A. Preparation of laccase-containing culture supernatant

The white-rot fungus *T. versicolor* was cultivated following the procedure described elsewhere [3]. In short, each week a new batch of culture supernatant was prepared. Thereto 3 pieces (0.5 x 0.5 cm²) of mycelium grown on YPD plates were transferred onto the surface of 150 mL of sterile SCL medium (pH 5) in a 250 mL Erlenmeyer flask. These were then cultured for two weeks in the dark under quiescent (non-shaking) conditions at 30°C. After this period the laccase-containing culture supernatant was harvested, sterile filtered, and supplied to the cathodes as described below. The enzyme activity of the different batches of culture supernatant used in this work is listed in Table 1. The activity was quantified through photometry as described elsewhere [3]. One unit (U) of enzyme activity was defined as the amount of enzyme required to oxidize 1 mmol of ABTS per minute at pH 5 and 30°C.

B. Electrode preparation & electrochemical characterization

As air-breathing cathode a buckypaper electrode made from carbon nanotubes, fabricated as described elsewhere [4], was equipped with a 0.5 mm thin silicone membrane as diffusion layer which enables sufficient oxygen supply and prevents salt crust formation and electrolyte leakage [5]. The cathode was operated as half-cell against a platinum mesh counter electrode, separated by a Nafion membrane. Through a cavity between the Nafion membrane and the porous backside of the buckypaper cathode, the laccase-containing culture supernatant was continuously supplied at a hydraulic retention time (HRT) of either 2.4 h or 1.2 h, as indicated in Fig. 1. Different



supernatant batches with differing enzyme activities (expressed as units U per ml) in were used throughout the experiment, as indicated in Fig. 1. A constant current density of $50 \mu\text{A cm}^{-2}$ was applied and the cathode potential against a saturated calomel reference electrode (SCE; KE 11, Sensortechnik Meinsberg, Germany) was recorded every 5 minutes. All experiments were performed under sterile conditions at 30°C .

III. RESULTS AND DISCUSSION

The evolution of the cathode potential over time is shown in Fig.1. Starting from an initial value of 557 mV vs. SCE, the electrode potential could be kept at values above 430 mV vs. SCE for up to 33 days before irreversible clogging of the supernatant supply tubes occurred and the experiment was eventually stopped. Therefore, theoretically a longer lifetime could be achievable. For comparison, in the previous experiment without re-supply of laccase the electrode potential already dropped to less than -50 mV vs. SCE already after 23 days [3].

Several times throughout the experiment, an interruption or disturbance of the supernatant supply occurred. This was mainly caused by air bubbles entrapped within the supply tubes, by leakage, and by fouling. In particular at the exit of the supply tubes, which were protected with sterile filters, fouling frequently led to a complete blockage. In contrast, the enzyme activity of the supernatant had no noticeable effect on the cathode potential under load within the investigated range.

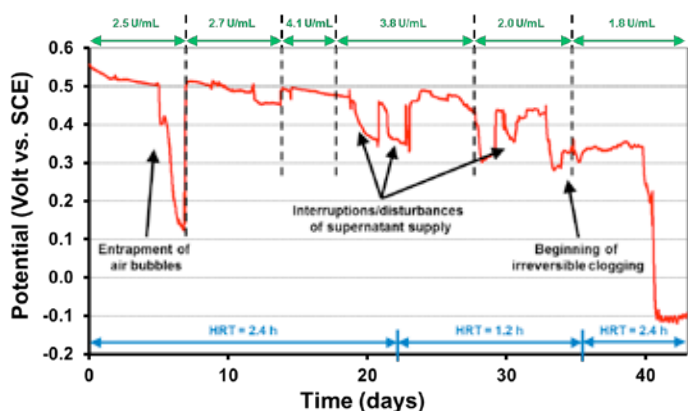


Fig. 1. Evolution of cathode potential over time at a constant current density of $50 \mu\text{A/cm}^2$. Over the course of the experiment different supernatant batches had to be used. Their enzyme activity ranged from 1.8 U/mL to 4.1 U/mL, as indicated.

IV. CONCLUSION

We successfully demonstrate an air-breathing laccase cathode that is continuously supplied with fresh enzyme to achieve an extended lifetime, independent of enzyme degradation and thus limited long-term stability. In contrast to our previous work [3], the air-breathing cathode now enables

passive operation without energy-intensive aeration of the catholyte. This is particularly relevant for practical application of the new concept.

The results are an important step towards the realization of hybrid microbial-enzymatic fuel cells with extended lifetime, in which the new enzymatic cathode is combined with a conventional microbial anode.

Currently the main challenge of our system is to sustain a stable supply of laccase-containing culture supernatant over extended periods of time. Future work will thus be focused on an optimized construction to alleviate leakage, fouling, and clogging of the supply tubes and to achieve longer operational time.

ACKNOWLEDGMENT

Financial support by the German Research Foundation (DFG) through the PhD program “Micro Energy Harvesting” (GRK 1322) and the Federal Ministry of Education and Research (BMBF) through the program “BioProFi” (FKZ: 03SF0424) is gratefully acknowledged. We also thank Claude Jolivald for providing the *T. versicolor* strain used in this study.

REFERENCES

- [1] Logan, B. E.: Simultaneous wastewater treatment and biological electricity generation, *Water Sci. Technol.* 52, 2005, pp. 31–37.
- [2] Harnisch, F.; Schröder, U.: From MFC to MXC: chemical and biological cathodes and their potential for microbial bioelectrochemical systems, *Chem.Soc.Rev.* 39, 2010, pp. 4433–4448.
- [3] Sané, S.; Jolivald, C.; Mittler, G.; Nielsen, P. J.; Rubenwolf, S.; Zengerle, R.; Kerzenmacher, S.: Overcoming Bottlenecks of Enzymatic Biofuel Cell Cathodes: Crude Fungal Culture Supernatant Can Help to Extend Lifetime and Reduce Cost, *ChemSusChem* 6, 2013, pp. 1209–1215.
- [4] Hussein, L.; Urban, G.; Krüger, M.: Fabrication and characterization of buckypaper-based nanostructured electrodes as a novel material for biofuel cell applications, *Phys.Chem.Chem.Phys.* 13, 2011, pp. 5831–5839.
- [5] Kipf, E.; Messinger, T.; Sané, S.; Kerzenmacher, S.: An air-breathing cathode based on buckypaper electrodes with reversibly adsorbed laccase, *Proceedings of the 2nd EU-ISMET Meeting*, 2014, Alcalá, Spain.



MICROBIAL FUEL CELL - A SELF-POWERED WASTEWATER ELECTROLYSER FOR ELECTROCOAGULATION

I. Gajda*, A. Stinchcombe*, J. Greenman***, C. Melhuish* and Ioannis Ieropoulos***

* Bristol BioEnergy Centre, Bristol Robotics Laboratory, University of the West of England, BS16 1QY, (UK)

** Biological, Biomedical and Analytical Sciences, University of the West of England, BS16 1QY, (UK)

Abstract - This abstract describes the suitability of the Microbial Fuel Cell (MFC) for generation of electrical power with a simultaneous synthesis of active catholyte in the form of caustic solution. The active solution was a product of self-powered electrolysis inside a MFC reactor, utilizing wastewater with a sodium acetate as a carbon source. Catholyte solution that has been actively synthesized was harvested and used for precipitation of heavy metals showing its suitability for use in electro-coagulation (electro-flocculation).

Index Terms – Microbial Fuel Cell, electrolysis, electro-flocculation, metal recovery.

I. INTRODUCTION

There is an increasing need for more cost-effective methods of treating metal polluted waste streams. The development of electrochemical processes for wastewater treatment, remediation and disinfection has become a viable option in the past two decades. Electro-coagulation (EC) is a rapidly growing area in wastewater treatment, where the conventional electrolytic treatment produces electroactive coagulants (flocculants) such as hydroxide ion (OH⁻), which precipitate heavy metals via the reaction: $M^{+n} + nOH^- \rightarrow M(OH)_n$. In recent years it has been demonstrated that hydroxide compounds such as caustic soda can be produced using Microbial Electrolysis Cells (MECs), where the proposed systems require the input of electrical energy [1]. The current study describes a Microbial Fuel Cell (MFC) system, which produces hydroxide coagulant in the form of catholyte but with the important advantage of generating - rather than using electricity. The self-powered electro-coagulation can be used to precipitate heavy metals from a range of solutions. This work presents for the first time a MFC-driven electrolysis of wastewater to produce electricity and coagulant in the form of catholyte, and proposes innovative self-powered electro-coagulation systems for practical implementation.

II. MATERIALS AND METHODS

MFCs were assembled using 10 cm long, 3.6 inside diameter terracotta caves (Weston Mills Pottery, UK) which were sealed at one end forming a hollow chamber. Figure 1 shows one MFC reactor assembled with an outer anode and inner cathode configuration, where a carbon fibre veil anode was wrapped around the ceramic cylinder and activated carbon cathode was inserted inside the inner chamber. Activated carbon paste was prepared as previously described [2] and applied on hydrophobically treated carbon fibre veil substratum. The MFCs were placed in plastic containers (210 mL) and were inoculated with activated sewage sludge (Wessex Water, UK). The MFCs were further supplemented with a mixture of sludge and 0.1M sodium acetate and kept in batch mode. The MFC reactors were tested in triplicates under 100 Ω resistor load.



Fig.1 MFC reactor

A. Data analysis

MFC performance has been monitored using a multi-channel Agilent 34972A DAQ unit, recording output in Volts. The quality of wastewater and formed catholyte has been analysed

using a 8424 pH meter (Hanna Inst., UK) and Jenway conductivity meter (Camlab, UK).

B. Precipitation analysis

Catholyte has been used for precipitation of water soluble salts such as iron chloride, copper sulphate and zinc chloride. 0.1 g of the subject salts has been dissolved in 20 mL of tested catholyte and deionized water (control).

III. RESULTS

A. MFC power performance

The polarisation experiment showed that all three tested MFCs have reached a power performance above 1 mW per MFC (actual power) with the maximum performance for MFC3 at 1.71 mW, 1.47 mW for MFC1 and 1.37 for MFC2 (Figure 2). The fluctuations in power curve during 30 second sampling intervals shows the genuine MFC behaviour during the experiment.

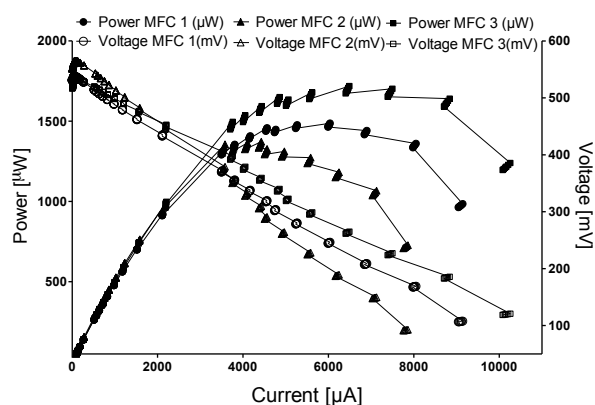


Fig. 2 Power and polarisation curves from the 3 MFCs

The MFCs have been kept under closed circuit conditions producing electricity. The MFCs produced on average 0.89 mW of electricity over a 7-day period while the formation and accumulation of catholyte has been observed in the cathode chamber. The catholyte (11.23 pH) has been collected and used as the coagulant to precipitate iron chloride, copper sulphate and zinc chloride from the solution in comparison with deionized water, for the same period of time, as shown in Fig.3; precipitation (shown on the left hand side universal bottles), which suggests flocculation, is clearly evident.

Hydroxide precipitation makes use of the fact that the solubility of many metal compounds diminishes with an increasing pH. Therefore, a very common precipitant for this process is caustic soda (NaOH). Wastewater that contains dissolved pollutants can be treated with OH⁻ ions that react with metal ion to form insoluble hydroxide compounds. Industrial wastewater can contain toxic compounds such as heavy metals, which are normally present in the form of ions and can be removed from the wastewater by ion exchange. These terracotta cylinders have demonstrated that they could be employed as cost effective MFC membranes [3].

This paper reports on the innovative MFC driven electro-coagulation that can be used for removing metal pollutants, such as copper, zinc and iron from aqueous solutions. A chemical reaction between the catholyte may produce a solid that can be easily collected. This could give an important advantage of self-driven MFCs treating polluted wastewater and removing heavy metals *in situ*. Furthermore, the production of such value added chemicals will support the sustainable production of renewable materials, which is one of the most promising biotechnological approaches.



Fig. 3 Precipitation of heavy metals from the exposure of samples to MFC-generated catholyte

IV. CONCLUSION

This work presents a Microbial Fuel Cell that is generating electricity and at the same time produces active electrolyte in this process as a product of wastewater electrolysis. The produced *in situ* active solution is highly caustic and can be used for flocculation and precipitation of heavy metals.

ACKNOWLEDGMENT

The authors would like to thank the Engineering and Physical Sciences Research Council (EPSRC) UK for funding this work through the project with grant no. EP/I004653/1 and Bill and Melinda Gates Foundation, grant number OPP1094890.

REFERENCES

- [1] Rabaey K, Bützer S, Brown S, Keller J, Rozendal R a. High current generation coupled to caustic production using a lamellar bioelectrochemical system. *Environ Sci Technol* 2010;44:4315–21.
- [2] Gajda I, Greenman J, Melhuish C, Ieropoulos I. Simultaneous electricity generation and microbially-assisted electrosynthesis in ceramic MFCs. *Bioelectrochemistry* 2015;104:58–64.
- [3] Winfield J, Greenman J, Huson D, Ieropoulos I. Comparing terracotta and earthenware for multiple functionalities in microbial fuel cells. *Bioprocess Biosyst Eng* 2013;36:1913–21.



EFFECT OF POLLUTANTS ON BIOGAS STEAM REFORMING

Chiodo, V.*, Zafarana, G.*, Maisano, S.*, Urbani, F.*, Mondello, N.* and Freni, S.*
*Institute CNR-ITAE, Via salita s. lucia sopra contesse 5; 98126 - Messina, (Italy)

Abstract – Biogas produced by biomasses anaerobic digestion is mainly composed by CH₄ and CO₂, although pollutants, as H₂S siloxanes and hydrocarbons compounds, could be present depending on the nature of the biomass, process conditions and type of digester used. Biogas steam reforming experiments were carried out, at 1073 K and steam methane ratio=2 mol/mol, in order to investigate on the effect of biogas pollutants on the performances of a Nichel catalyst. Different biogas streams were used. In particular, both a stream exclusively composed of CH₄ and CO₂ (CH₄/CO₂= 55/45 vol.%) and a gas mixture of CH₄/CO₂ and pollutants were used. Resulted showed a stable Ni performance when a “clean” biogas stream was reformed; On the contrary, the simultaneously presence of two poisoning in to the inlet gas stream negatively affected catalytic performances promoting also the coke formation.

Index Terms – Biogas, Steam reforming, Poisoning, Coke.

I. INTRODUCTION

Currently, due to its high energy potential, biogas is used in heating and electricity production; while in this last years, it was proposed as fuel for high temperature fuel cells by the steam reforming process [1]. Biogas produced by anaerobic digestion of biomass mainly consists of CH₄ (55-65 vol%) and CO₂ (30-45 vol%), but it also contains other compounds; i.e.: H₂S, hydrocarbons and siloxanes (<1000 ppm(v)) that are difficult to completely remove. The presence of these impurities in the inlet gas stream could promote tremendous effect on the catalytic performances of the biogas steam processor. Ni-based catalysts were largely investigated in biogas steam reforming reaction [1-3], however, it highlighted a limited resistance both carbon formation and sintering at high temperatures (923-1073 K). Although the advantages and disadvantages of the use of each reforming agent (CO₂, H₂O or O₂) in the biogas reforming have been widely investigated, the determination both a suitable reforming agent, operative

conditions and catalyst when the fuel processor is fed with a *real* biogas composition is still a matter for further analysis.

In this way, our investigation was focused on performances of a Ni (21 wt%) supported (CaO-Al₂O₃) catalyst working under steam reforming conditions with different biogas compositions that take into account the presence of poisoning in the inlet reformer-gas stream.

II. EXPERIMENTAL

Experiments were performed by quartz fixed-bed reactor (i.d.=4 mm; h_{bed}=2.0-4.0 cm) at atmospheric pressure and using loading 0.02-0.2 g of Ni catalyst blended with SiC. The reactor was placed into a furnace heated to the reaction temperature (Tr=1073 K).

The feed flows rate of biogas (CH₄+CO₂=55/45 vol.%) and poisonings (H₂S, hydrocarbons and siloxane) were controlled by Brooks Instruments mass flow meters. In particular, concentrations of H₂S=0.4 ppm(v), D5 siloxane=0.5 ppm(v) and hydrocarbons mixture (composed as reported in Table I)=200 ppm(v) were used. The H₂O_{in} flow (H₂O/CH₄=2 mol/mol) was fed by an isocratic HP 1100 pump and vaporized into a stainless steel reactor held at 483 K. Experiments were carried out with a Gas Hourly Space Velocity (catalyst bed volume/volume feed rate, m³*m⁻³*h⁻¹) rate of 50,000 h⁻¹.

The reaction streams were analysed “on line” by a gas chromatography GC-HP model 6890 Plus; while the carbon deposited during experiments was evaluated by CNHS elemental analysis instruments.

TABLE I
COMPOSITION OF HYDROCARBONS MIXTURE GASEOUS SAMPLE

Hydrocarbons	Concentration [ppm(v)]
Ethane	200
Ethylene	200
Acetylene	200



Propylene	200
-----------	-----

III. RESULTS AND DISCUSSION

Preliminary biogas steam reforming experiments were carried out using separately poisoning compounds (H₂S, C₂H₄ and D5). Results revealed the boundary concentrations for each impurity in order to get an equilibrium state in terms of carbon formation on time on stream. Hence, the comparison between Ni catalyst performances in biogas steam reforming process with simultaneously presence of two different poisoning in the inlet gas stream (H₂S+Hydrocarbons and Hydrocarbons+D5) was investigated. In Fig. 1., where catalytic performances in terms of methane conversion vs time are reported, an initial conversion rate of about 86% was recorded for all tests. Nevertheless, after 25 hours of test, different behaviors have been observed. A rather stable performance was recorded using a clean biogas stream (composed exclusively by CH₄+CO₂). On the contrary, Ni performances achieved in presence of impurities depicted evident deactivation patterns. In particular, the catalytic performance obtained in presence of Hydrocarbons+D5 poisonings, was affected by a significant conversion decay, reaching 40% after about 50 hours of test. While the nickel deactivation trend was less evident (about 73%) when the couple of impurities: H₂S+Hydrocarbons, was added to the inlet gas stream.

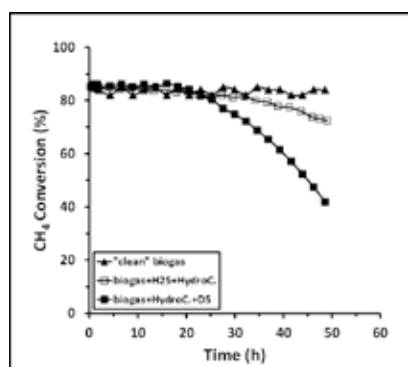


Fig. 1. Methane conversion Vs Time on stream: T=1073K; P= 1bar

Is known that, the main reason for Ni based catalysts deactivation is coke formation and/or metal sintering, hence, in order to understand the deactivation trends attention was paid to the evolution of the coke formation, therefore, CHNS analysis on all samples spent catalyst were carried out. Results, shown in Fig. 2, indicate that comparable coke formation rates occur for biogas steam reforming in presence of poisoning compounds while, the Ni sample applied in clean biogas reforming showed the lowest rate recorded (about 0.36 mgC/gcat*h).

The large amount of coke detected on catalyst samples working in presence of poisoning is attributed to equations 1-3

$$\text{CO} + \text{H}_2 = \text{C} + \text{H}_2\text{O} \quad (1)$$

$$\text{C}_n\text{H}_{2n} = n\text{C} + n\text{H}_2 \quad (2)$$


Generally, there is a tendency for cooking to increase as unsaturation (i.e. ethylene), molecular weight; thus olefins are major coke precursor. Moreover, the co-poisoning by molecules as H₂S or D5, could promote the adsorption of poisons on active site altering the Ni catalytic proprieties and probably accelerating the carbon deposition [3-5].

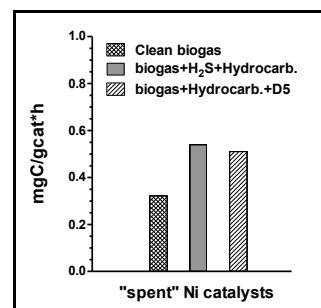


Fig. 2. Carbon formation rates: T=1073K; P= 1bar

IV. CONCLUSION

On the basis of results reported appear that the combined effect of two poisoning in the biogas stream increase the coke formation rate independently by chemical characteristics of the poisoning compounds. This is probably due to the absorption of sulphur and/or silicon oxide species on catalytic sites, even if moderate concentrations are considered (H₂S=0.4 ppm(v); Hydrocarbons=200 ppm(v); D5=0.5 ppm(v)).

ACKNOWLEDGMENT

This work was supported in the framework (FP7) of the SOFCOM Project (JTI-FCH-JU, G.A. nr. 278798).

REFERENCES

- [1] Chiodo, V., Galvagno, A., Lanzini, A., Papurello, D., Urbani, F., Santarelli, M., Freni, S., Biogas reforming process investigation for SOFC application, Energy Conversion and Management, Volume 98, 2015, pp. 252-258.
- [2] Galvagno, A., Chiodo, V., Urbani, F., Freni, S., Biogas as hydrogen source for fuel cell applications, International Journal of Hydrogen Energy, Volume 38, 2013, pp. 3913-3920.
- [3] Rostrup-Nielsen, J., Coking on nickel catalysts for steam reforming of hydrocarbons, Journal Catalysis, volume 33, 1974, pp. 184-201.
- [4] Erekson, E.J., Bartholomew, C.H., Sulfur poisoning of nickel methanation catalysts: II. Effects of H₂S concentration, CO and H₂O partial pressures and temperature on reactivation rates, Applied Catalysis, Volume 5, 1983, pp. 323-336.
- [5] Sasakia, K., et al., Chemical durability of Solid Oxide Fuel Cells: Influences of impurities on long-term performance, Journal of Power Sources, volume 196, 2011, pp. 9130-9140.



ENZYME-BASED GLUCOSE ELECTRODE FOR MFC APPLICATION

M. Grattieri*, S. Pellegrino**, F. Secundo***, M.L. Gelmi**,
P. Cristiani**** and S.P.M. Trasatti*****

*Politecnico di Milano, Department of Chemistry, Material and Chemical
Engineering, piazza L. da Vinci, 32, 20133 Milan, (Italy)

**Università degli Studi di Milano, Department of Pharmaceutical Sciences,
via Venezian 21, 20133 Milan, (Italy)

***Istituto di Chimica del Riconoscimento Molecolare, CNR, Milan, (Italy)

****RSE – Ricerca sul Sistema Energetico S.p.A, Environment and
Sustainable Development and Sources Department, via Rubattino 54, 20134
Milan, (Italy)

***** Università degli Studi di Milano, Department of Chemistry, via Golgi
19, 20133 Milan, (Italy)

Abstract - This study presents glucose oxidase-based bioelectrodes that have been developed with the aim to study the biodegradation mechanisms in glucose-fed Single Chambered Microbial Fuel Cells (SCMFC). The electrodes were tested ex-situ, in Acetate buffer solution (pH 4.8 and 5.6) and real wastewater prior to their application in the complex matrix of SCMFCs. Layer-by-layer self-assembled technique was used to prepare multilayers Osmium mediated glucose sensors. Self-assembled monolayers (SAM) of peptides were prepared to bind Glucose oxidase (GOx) for a direct electron transfer electrode.

The obtained results with both the electrodes types in the calibrating solutions (ex-situ) remarked that the matrix effect of real wastewater strongly affect the electrodes response. The enzymatic sensors placed in glucose-fed SCMFCs are currently applied to ongoing experiments.

Index Terms – Glucose oxidase, Enzyme-based Glucose sensors, Electron transfer, Microbial Fuels Cells

I. INTRODUCTION

Microbial fuel cells (MFCs) are an innovative electrochemical technology capable to produce energy from the oxidation of organic wastes and the reduction of an electron acceptor (usually oxygen) [1]. At laboratory scale sodium acetate and glucose are commonly used as substrates.

In this contest, single chamber microbial fuel cell (SCMFC) configuration has been studied due to good performances already shown with different substrates, such as acetate and urine [2], and its low cost. SCMFCs are characterized by the fact that no chemical-physical barrier between anode and cathode is provided at the startup and the cathode is exposed to the same solution of the anode. In the case of glucose fed SCMFC it has been demonstrated that a more complex bacteria community is developed at the anode, if compared to acetate fed MFC [3]. Accordingly, the study of the glucose content and degradation in the solution wetting the anode and the cathode in SCMFCs is of great interest, with the aim to clarify the biodegradation process.

Herein, the developed sensors have been applied ex-situ for calibration and matrix effect studies. Ongoing experiments in SCMFCs are aimed to study the bioelectrochemistry of the glucose oxidation process..

II. MATERIALS AND METHODS

A. Support preparation

A gold wire (45 μm \varnothing) electrically connected to a copper wire and embedded in epoxy resin inside a



micropipette tip was cleaned with Al_2O_3 ($0.5\mu\text{m}$ \O) and by 100 cyclic voltammeteries in 2 M H_2SO_4 . Following, the electrode was primed with 40mM 3-mercaptopropene sulfonate in 0.01 M H_2SO_4 and further modified depending on the desired type of bioelectrode (see below). Glucose oxidase (GOx) enzyme (Sigma-Aldrich) was used for all the electrodes preparation, with no further purification or modifications.

B. Osmium-mediated Glucose electrode

The primed surface was modified with 300 μL of 0.44 mM osmium bipyridine redox polyelectrolyte mediator (PAH-Os, pH 8) for 30 minutes via layer-by-layer (LbL) electrostatic self-assembly technique [4]. After rinsing the electrode with Milli-Q water, the following layer was deposited dunking the modified electrode in 300 μL of GOx solution ($0.5\text{mg}\cdot\text{ml}^{-1}$) in Milli-Q water for 30 minutes (figure 1). The steps were repeated until the desired number of layers. In every case the electrode structures was finished with a topmost layer of PAH-Os.

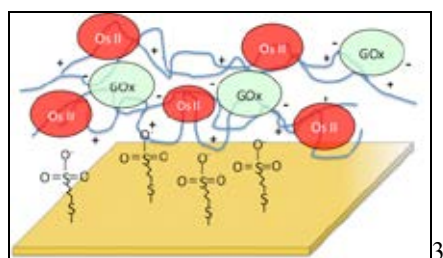


Fig. 1. Schematic representation of the Os-MET glucose oxidase-based electrode.

C. Peptide-GOx electrode

Self-assembled monolayers (SAM) of specifically synthesized peptides were prepared on the primed gold surface leaving a positive charge on the top of the chain [5]. Subsequently the GOx enzyme was electrostatically adsorbed from a GOx solution ($0.5\text{mg}\cdot\text{ml}^{-1}$) in Milli-Q water where the enzyme is negatively charged (PI 4.3), for 30 minutes. Different peptide chains were tested to investigate the influence of the chain length.

D. Electrochemical tests

The electrodes response was studied using Ag/AgCl (3M) as reference electrode and Pt wire as counter electrode. Cyclic voltammetry and chronoamperometry in 0.1M Acetate buffer a) pH 4.80 + 0.2 M KNO_3 ; b) pH 5.6 + 6mM CaCl_2 + 10mM KCl saturated with nitrogen gas were performed. D-glucose content was increased by consecutive additions of 0.4 M D-Glucose solution. The same procedure was followed to study the electrode response in real wastewater.

After calibration the electrode can be applied to glucose analysis in SCMFCs with a computer-controlled stage (Newmark System Inc., USA).

III. RESULTS

The electrochemical performances of the GOx-based electrodes were determined in optimized conditions (acetate buffer) and real medium (wastewater solution). i.e. The $(\text{GOx})_2(\text{PAH-Os})_3$ electrode response to glucose additions in acetate buffer is depicted in Figure 2 where a current increases after each glucose addition is clearly shown.

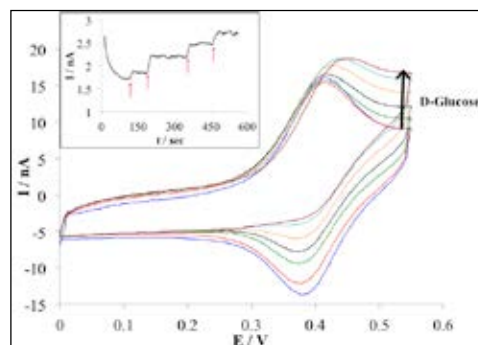


Fig. 2. Cyclic voltammeteries of $(\text{GOx})_2(\text{PAH-Os})_3$ electrode in 0.1 M acetate buffer + 0.2 M KNO_3 in oxygen free solution and increased D-glucose concentration (from 0 to 65 mM). The inset report the chronoamperometry result at 0.55 V vs Ag/AgCl (3M) with glucose addition (red arrows)

IV. CONCLUSION

GOx-based glucose sensors were developed and calibrated in different media. The matrix effect of real wastewater on the sensor response was studied.

The LbL technique allowed to obtain reproducible Os-MET electrodes. The possible application of SAM peptides as enzyme-binder to ensure direct electron transfer (DET mechanism) to the electrode was investigated.

ACKNOWLEDGMENT

MG acknowledges prof. E.J. Calvo and University of Buenos Aires to provide the PAH-Os polymer.

REFERENCES

- [1] Lovley, D.R., Microbial fuel cells: novel microbial physiologies and engineering approaches, *Current Opinion in Biotech.*, Vol. 17, 2006, pp. 327–332
- [2] Santoro, C. et al., Current generation in membraneless single chamber microbial fuel cells (MFCs) treating urine, *Journal of Power Sources*, Vol. 238, 2013, pp. 190–196.
- [3] Chae, K.-J. et al., Effect of different substrates on the performance, bacterial diversity, and bacterial viability in microbial fuel cells, *Bioresour. Technol.*, Vol. 100, 2009, pp. 3518–3525.
- [4] Grattieri, M. et al. Non-Competitive Reversible Inhibition of Laccase by H_2O_2 in Osmium Mediated Layer-By-Layer Multilayer O_2 Biocathodes *Journal of The Electrochemical Society*, Vol.162,(9), 2015, pp. G82–G86.
- [5] Juhaniwicz, J. and Sek, S., Peptide molecular junctions: Distance dependent electron transmission through oligoprolines, *Bioelectrochem*, Vol. 87, 2012, pp. 21–27.



Use of active carbon for the removal of Sulphur Impurities from a biogas stream for SOFC application.

F.Santoni^{a,b}, D. Pumiglia^{b,c}, P.Gislon^b, G.Monteleone^b, S.Mcphail^b, S.Dumontet^c

^a Department of Science and Technology, Parthenope University, Naples 80143, Italy

^b DTE-PCU-SPCT Dipartimento Tecnologie Energetiche, Laboratorio Sviluppo Processi Chimici e Termofluidodinamici per l'Energia, ENEA C.R. Casaccia, Via Anguillarese 301, Rome 00123, Italy

^c DAFNE, Università degli Studi della Tuscia, Via S. Camilo de Lellis snc, Viterbo 01100, Italy

Abstract: An interesting application of solid oxide fuel cell (SOFC) technology is the micro-cogeneration (μ -CHP) in the residential area fed with a sustainable (renewable) source such as biogas produced from anaerobic digestion (AD) of organic waste. Even though the major components of biogas are CH₄ and CO₂, several contaminants can be inside the biogas and have to be removed before entering the cell. Sulphur compounds are the most harmful for SOFC systems. The aim of this work is to study the removal of sulphur compounds using activated carbon adsorption trapping and test the obtained results in a SOFC single cell. Two different carbon filters were tested under the following sulphur contaminants: H₂S, THT, COS, DMS and single cells were performed with a simulated biogas enriched with a selected small amounts of the contaminants in order to evaluate tolerance and degradation process.

Keywords: Biogas, cleaning sorbent material, sulphur compound, SOFC

I. Introduction Nowadays, much research efforts on the fuel cell is devoted to the development of multi-fuel systems with particular emphasis on the potential use of non-traditional fuels. The value of these activities is strategic to promote power generators using renewable fuels for distributed applications. In this direction, a significant effort has been carried out from several research institutions in terms of investigation and development of processes, materials and demonstrative plants featured to treat raw fuels of different chemical characteristics. The target is to produce hydrogen-rich gas mixtures, suitable for supplying fuel cell based electricity generators. Actually, biogas is considered a very promising raw fuel to be used as syngas source for SOFC applications because of its availability and renewability. The main issue of the direct usage of biogas is the presence of different kind of contaminants, such as halogens, siloxanes and sulphur compounds. When these impurities are supplied to SOFC systems, it is likely for them to cause degradation of cell performance and to overall system durability [1]. To improve fuel cell performance (and lifetime), the implementation of a cleaning section is needed in order to reduce the presence of pollutant compound at ultra-low levels. To achieve such stringent requirements, commercial sorbent materials were investigated in laboratory condition.

II. Objective of work: The main goal of this work was to investigate on efficiency of two commercial activated carbons on the removal of different sulphur contaminants: COS, DMS, H₂S and THT. The work will focus on:

- The research of the best operational parameters to improve the adsorbent capacity of these carbons for each contaminant studied
- Understand the chemical and/or physical adsorption mechanism between the adsorbent material and the different sulphur species.
- Testing a Single Cells with a synthetic biogas stream with selected small amounts of the contaminants in order to evaluate tolerance and degradation processes (work in progress).

III. Experimental Section: The activated carbons selected for this work are two commercial carbons (RGM3 by Norit and Desotec Ultra DS by Airpel) with elevated specific surface and designed for the removal of low concentrations of sulphur compounds. The AC, originally pellet-shaped were ground and sieved, obtaining homogeneous powder with particle size in the range 250-355 μ m.

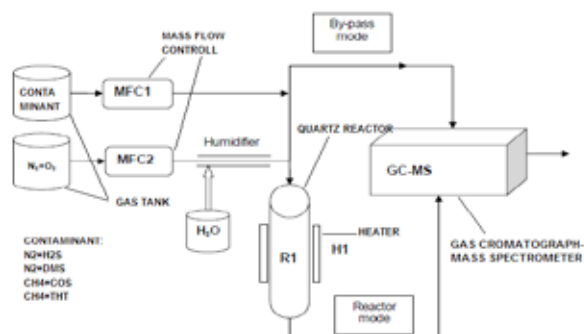
Catalytic experiments are carried

Commercial Adsorbent	RGM3	Desotec Ultra DS
Shape/size(mm)	Pellet-3 mm	Pellet-4 mm
Activation Metals	Cu, Fe, Cr	K,Ca, Fe, Mn
Superficial area surface (m ² /g)	963,24 +/- 1%	823,5 +/-1%



out at a laboratory-scale, fix-bed reactor system. The polluted gas flows through an AC bed in the reactor at controlled temperature, mass flow rate and concentration.

The outlet contaminant concentration is monitored
Fig. 1 – Test facility for sulphur compounds adsorption on AC measurements



by gas Chromatograph- Mass Spectrometer (Perkin-Elmer). A Schematic representation of the reaction system is shown in Fig.1

The pollutant adsorption capacity (C_{ads}) is calculated from breakthrough curves using the following equation [2]:

$$C_{ads} = \frac{Q_{tot} \times M_w \times [C_{in} \times t_1 - (t_1 - t_0) \times 0,5]}{V_m \times m \times 1000}$$

Where:

Q_{tot} is the total gas flow rate (l/h)

M_w is the Molecular weight

C_{in} is the inlet pollutant concentration (ppmv)

t_1 breakthrough time, when the outlet pollutant concentration is 1 ppmv

t_0 breakthrough time, when the outlet pollutant concentration is 0 ppmv

V_m molar volume (24,414 nl/mol)

m mass of adsorbent material (g)

IV. Result and Discussion: Breakthrough curves are obtained for each material and pollutant in different operating condition:

- Gas hourly Space Velocity (GHSV), defined as Q_{tot}/V_{filter} [h⁻¹]
- Effect of oxygen (0,5%)
- Gas matrix (N₂, CH₄, CO₂,CH₄+CO₂)
- Temperature
- Inlet contaminants concentration

Effect of reaction temperature: The pollutant removal efficiency of the carbons is enhanced significantly when increasing the reaction temperature, showing that the optimum temperature is 120°C for H₂S and COS. The DMS has a different behaviour for this parameter, showing an optimum temperature at 30°C.

Effect of GSHV (1000---20000 h⁻¹): The capacity of adsorption increased decreasing the GSHV values.

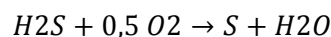
Effect of oxygen: The effect of the oxygen depends on the pollutant studied. It shows a negative effect on RGM3 capacity of removal of COS while in the removal of other sulphur compound such as H₂S and DMS the present of small amount of oxygen lead to an improvement of absorption capacity.

Effect of gas matrix: The use of N₂ as carrier gas lead to highest adsorption capacity. The adsorption capacity decrease using a mixture composed of 65% CH₄ and 35 % CO₂ (simulating a biogas).

Inlet contaminant concentration: There is a linear correlation between AC capacity and pollutant concentration, increasing concentration also increase the capacity of adsorption material.

VI. Conclusion: The adsorption capacity of commercial adsorbent materials studied depends both test condition and pollutant used. They achieve the best performance for the adsorption of H₂S, while for the other contaminants studied like COS and DMS the adsorption is not well favoured, showing low values of C_{ads} .

Selectivity toward the pollutant is in all cases negatively affected in a biogas matrix, but the effect of oxygen and of the reaction temperature affected the adsorption differently proving different mechanisms characterizing their clean-up process. In the case of H₂S the presence in the gas stream of oxygen and the reaction temperature enhance the partial oxidation reaction of this compound:



The sulphur released, chemically link the metals present on the carbon surface.

About DMS and COS the principal adsorption mechanism seems to be the physisorption. These results have been confirmed by TGA analysis.

Both the THT and the single cells SOFC testing are in progress, and the results will be presented at the conference.

V. Reference:

[1]Sasaki K., Haga K., Yoshizumi T., Minematsu D., Yuki E., Liu R.R., Uryu C., Oshima T., Ogura T., Shiratori Y., (2011),Chemical durability of Solid Oxide Fuel Cells: Influence of impurities on long-term performance, *Journal of Power Sources*,**196**, 9130-9140.

[2] G.Montealeone, M.Cerewska, R.Ciccoli, P.Gislon Abbattimento dell'H₂S e upgrading di un biogas provenienti da digestione anaerobica degli scarti di una mensa aziendale, Report RDS/par 2013/248.



LONG TERM PERFORMANCE OPTIMIZATION OF A HIGH TEMPERATURE PEM FUEL CELL BASED COGENERATION SYSTEM

B. Najafi*, A. Haghghat Mamaghani*, A. Baricci*, A. Casalegno*, F. Rinaldi*

*Dipartimento di Energia, Politecnico di Milano, Via Lambruschini 4, 20156, Milano, Italy

Abstract - In the present study, multi-objective optimization method has been employed to optimize the long term performance of an HT-PEM fuel cell based cogeneration system. In order to have a proper estimation of the long term performance of the plant, the degradation within the fuel cell stack and the fuel processor, has been taken into account. Steam to carbon ratio, auxiliary to process fuel ratio, anodic stoichiometric ratio and fuel partialization factor are considered as the design parameters. In order to investigate the feasibility of addressing an intermittent demand, thermal generation of the plant has been considered as one of the objectives while the electrical efficiency, as an indicator of the system's performance, is considered as the second one. Taking into account the degradation trends, the optimization procedure is carried out in certain time steps, therefore a series of Pareto fronts are obtained and the system design parameters are adaptively optimized.

Index Terms: high temperature PEM fuel cell, fuel processor, cogeneration, degradation, multi-objective optimization

I. INTRODUCTION

Application of PBI based high temperature PEM fuel cells, owing to their higher operation temperature range (120-200 °C), results in many advantages compared to conventional low temperature PEM fuel cells including higher efficiency, less CO poisoning issues and no water management problems [1]. Therefore, utilizing HT-PEM fuel cells in residential micro cogeneration system can be a promising alternative. Nevertheless, these types of fuel cells suffer from a considerable degradation through their lifetime. Similarly, the fuel processor (and specifically the steam reformer) employed in the plant undergoes a significant degradation. Hence, in order to have a proper estimation of the long term performance of the plant, the corresponding degradation effects should be taken into account [2].

Accordingly, in the present article, mathematical model of an HT-PEM fuel based micro-cogeneration system is developed. Next, employing the available experimental data, empirical models are employed to estimate the degradation within the fuel cell stack and the steam methane reformer.

In the next step, multi-objective optimization method is

utilized to optimize the long term performance of the system. In order to study the feasibility of employing the unit for addressing an intermittent residential thermal load, the thermal generation of the system is chosen as an objective function while the electrical efficiency, indicating the system's performance, is selected as the second objective. The steam to carbon ratio, auxiliary to process fuel ratio, anodic stoichiometric ratio and fuel partialization factor are considered as the design parameters to be optimized. Taking into account the degradation trend, the optimization procedure is carried out in different time intervals in order to optimize the system in an adaptive manner considering the plant's degradation. By utilizing the employed method, for each of the investigated intervals, a set of optimal solutions is determined each of which includes the design parameters resulting in the highest possible electrical efficiency for a specific thermal generation.

II. PLANT DESCRIPTION

The investigated plant, shown in Fig. 1, is composed of a fuel processor, an HT-PEM fuel cell stack, low and high pressure water circuits and other auxiliary components. In the first step, the mixture of natural gas and superheated steam enters the steam reformer where it undergoes the steam methane reforming reaction producing hydrogen and CO. The generated syngas subsequently passes through the WGS reactor in which the shift reaction takes place and a fraction of the CO is converted into CO₂. The processed syngas afterwards enters the anodic side of the HTPEM fuel cell where the hydrogen is consumed, through the electrochemical reaction, generating electricity and water. The anodic outlet, which includes unconsumed amounts of hydrogen and methane, is directed to the burner and burned with the auxiliary methane generating combustion products which provides the required energy of the SMR reactor and subsequently produce the steam and warm water in the superheater and economizer respectively. In the other side, the compressed air is fed to the cathodic side providing the required oxygen. Two recuperators are also employed for warming up the fuel cell inlet streams.

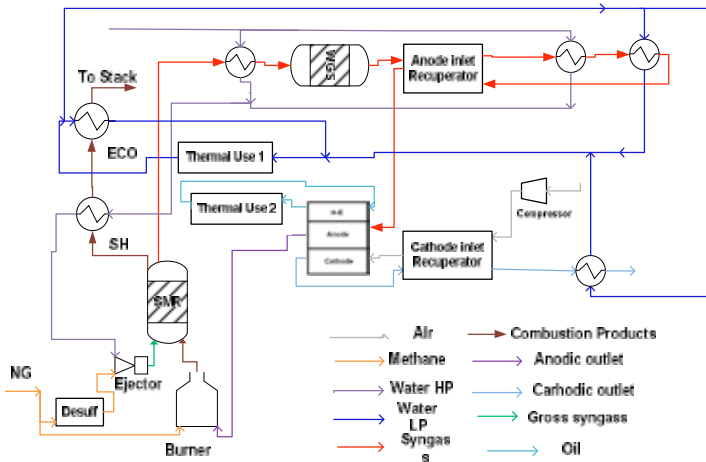


Fig. 1. Plant Description

III. MODEL DESCRIPTION

A. HT PEM fuel cell stack

A 1D+1D model has been developed in order to simulate the diffusion of reactants through the MEA and the concentration distribution through the channel. The developed model is validated using the available data in the literature as well as the provided experimental data. The details of the developed model and the validation procedure along with the employed degradation models are given in [1, 3] and [2] respectively.

B. Fuel Processor

1-D homogenous models are employed to simulate the kinetic behavior of the fuel processor components. Experimental data from "Sidera30", an already operating plant, are used for validating the model [1]. Furthermore, long term performance data obtained from the same plant, via an empirical model, is used to simulate the degradation within the steam reformer [3].

IV. RESULTS AND DISCUSSION

Fig. 2 demonstrates the obtained Pareto frontiers for different time steps. For each interval a set of optimal design parameters are provided each of which leads to the maximum possible electrical efficiency for a specific thermal generation; the fact which guarantees operating at maximum performance while addressing an intermittent load profile. Despite the fact that the optimization procedure attempts to optimize the electrical efficiency, the negative effect of degradation on the performance of the system cannot be completely alleviated and, for a specific thermal generation, value of optimal electrical efficiency at different investigated periods is continuously decreasing. The mentioned descending trend in the values of maximum electrical efficiency, while producing the same thermal output as that of the normal operation (50 kW), can be vividly seen in Table I. In order to give a more clarified idea of the obtained results, the corresponding obtained optimal design parameters of these optimal points are also given in Table I.

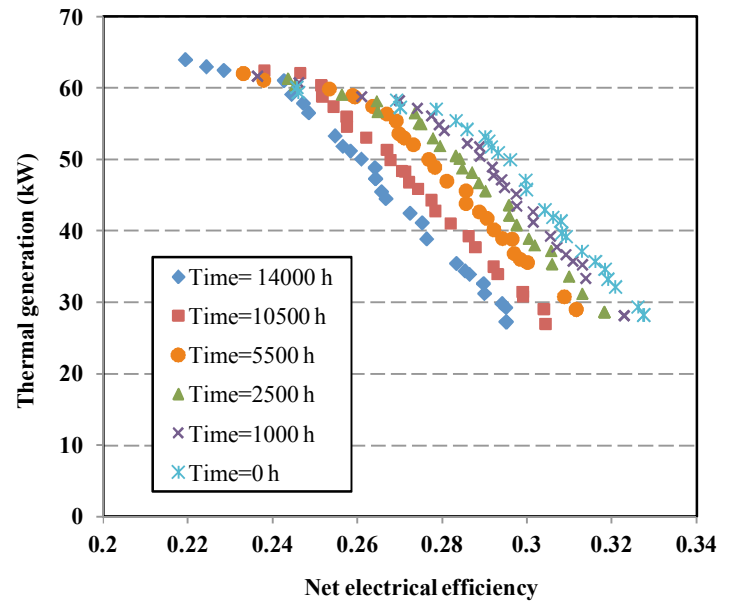


Fig. 2. Obtained Pareto fronts

Table I Parameters and efficiency of the chosen points

Time step (h)	0	1000	2500	5500	10500	14000
Steam to carbon ratio	4.55	4.69	4.66	4.60	4.52	4.58
Auxiliary to process ratio	0.164	0.189	0.147	0.157	0.159	0.141
Anodic stoichiometric ratio	1.210	1.207	1.210	1.204	1.225	1.213
Partialization factor	0.953	0.927	0.955	0.924	0.904	0.912
Electrical efficiency (%)	29.6	28.8	28.4	27.7	26.8	26.1

V. CONCLUSION

Employing the obtained results and design parameters provided in Pareto fronts enables the designer to adaptively maximize the performance of the system to mitigate the effect of degradation. Furthermore, the achieved results provide the possibility of guaranteeing the maximum possible performance while addressing intermittent load profiles.

VI. ACKNOWLEDGMENT

This work was carried out in the framework of the project Microgen30 (EE01_00013) funded by Italian Ministry of Economic Development with the program Industria2015.

REFERENCES

- [1] Najafi B, Mamaghani AH, Baricci A, Rinaldi F, Casalegno A, Mathematical modelling and parametric study on a 30 kWel high temperature PEM fuel cell based residential micro cogeneration plant, Int J Hydrogen Energy, 40 (2015) 1569-1583.
- [2] Kim M, Kang T, Kim J, Sohn Y-J. One-dimensional modeling and analysis for performance degradation of high temperature proton exchange membrane fuel cell using PA doped PBI membrane. Solid State Ionics. 2014;262:319-23.
- [3] Najafi B, Mamaghani AH, Rinaldi F, Casalegno A Long-term performance analysis of an HT-PEM fuel cell based micro-CHP system: Operational strategies. Applied Energy.2015;147:582-92.



EXPERIMENTATION OF MICROBIAL FUEL CELLS IN PROGRESS AT MILANO-NOSEDO WASTEWATER TREATMENT PLANT

F. Pizza*, E. Martinucci*, D. Porrino**, S.P.M. Trasatti**, P. Cristiani***

*Milano Depur SpA, WWTP of Milano-Nosedo, via San Dionigi 90, 20139 Milan (Italy)

** Università degli Studi di Milano, Department of Chemistry, via C. Golgi 19, 20133 Milan (Italy)

***RSE - Ricerca sul Sistema Energetico S.p.A., Environment and Sustainable Development Department, via Rubattino 54, 20134 Milan (Italy)

Abstract - A scaling trial of MFC technology, from laboratory to real plant conditions, is in progress in the denitrification pools of the wastewater treatment plant Milano-Nosedo in Milan (I). This is a first step of the integration of MFCs in industrial processes. The performances of several MFCs, having different geometry, were monitored and correlated to weather conditions and water parameters. The results of more than six months experiment, reported here, indicated a scalability inversely proportional to the electrode surface and a strict correlation between power and dissolved COD in the water.

Index Terms – Microbial fuel cells, wastewater, dissolved organics, denitrification pool.

I. NOMENCLATURE

MFC: Microbial fuel cell

WWTP: wastewater treatment plant

COD: Chemical Oxygen Demand

II. INTRODUCTION

The Wastewater Treatment Plant of Milano-Nosedo is the last phase of a complex sewerage system that collects wastewater from the central and eastern part of the city of Milan [1].

Due to its processing capacity of 1,250,000 population equivalents, it is one of the largest WWTP in Italy.

A scaling trial of MFC technology, from laboratory to real plant conditions, is in progress in the denitrification pools at this plant. This is a first step of the integration of MFCs in the industrial process.

Suitable MFCs were built and placed in operation into different tanks of the plant.

The performances of several MFCs having different geometry were monitored for more than six months [2] and the experimentation is still continuing.

The investigations presented here are focused in particular on the analysis of the MFCs power output, in relation to dissolved organics and flow of the raw wastewater incoming the plant.

III. MATERIALS AND METHODS

Performances of thirty MFCs with three different sizes (20 x 15 cm, 30 x 20 cm, 40 x 30 cm) were monitored. Each MFC consists in a floating polystyrene frame, holding identical plane electrodes made of carbon cloth (SAATI P10) separated by an insulating polypropylene felt (1 cm thick), stitched and fixed to the frame by nylon thread (Figure 1).

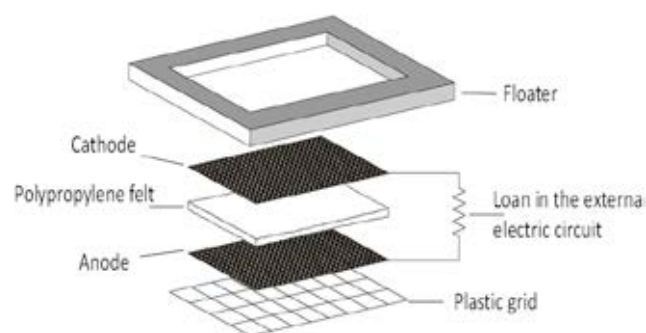


Fig. 1. Scheme of the tested MFCs

Voltage (V) across the resistors was acquired once an hour for each MFC by a multichannel potentiometer (Graphtec midi

LOGGER GL820). Data were integrated with manual recording of voltage values and visual observations during the almost daily inspections at the experimentation site.

The dissolved organics concentration was measured as COD using colorimetric kits (Hach).

IV. RESULTS

A. MFC geometry

The results of more than six months experimentation, reported here, indicated an inversely proportional correlation between geometry and power density, related to the electrode projected surface.

The concentration of dissolved COD into the denitrification tank was about 13 mg/L (Table 1).

The low COD concentration and the low conductivity of the water ($\sim 600 \mu\text{S}/\text{cm}$) limited the current density produced by the single MFC. Nevertheless, a maximum of about $750 \text{ mA}/\text{m}^2$ was reached by MFCs with the lower electrode surface ($20 \times 15 \text{ cm}$).

The plane geometry of the MFC allowed and enhanced the germination of seeds spread in the water and the consequent growth of plants on the cathodes exposed to air. At the end of the experiment, several MFC were fully covered by grass and plants, including the best performing ones (Figure 2).



Fig. 2. Floating MFCs covered by spontaneous vegetation

B. Voltage correlation with water flow and dissolved COD

The chemical-physical parameters of the wastewater were subject to cyclic variations during the day and they also depend by seasonal precipitation (rain water is generally conveyed into the sewer system, thus causing a dilution of organic content in wastewater).

The highest concentration of pollutants was found in the middle of the day, and the lowest at night and during storm events, when a reduced COD enters the plant (Table 1).

The characteristic daily trend of the water flow incoming the plant is shown in Figure 3, overlapped to the trend of the MFC voltage, generated in a cell of medium size ($30 \times 20 \text{ cm}$).

Table 1. Typical values for some key process parameters

	Average	Min	Max
Wastewater flow (m^3/h - 1 treatment line)	596	455	1200
COD (mg/L)*	13	9	25
Water temperature ($^{\circ}\text{C}$)	15.6	12.5	17.3

*These values refer only to the aqueous phase of filtrated samples, they not include the COD contained into the activated sludge biomass

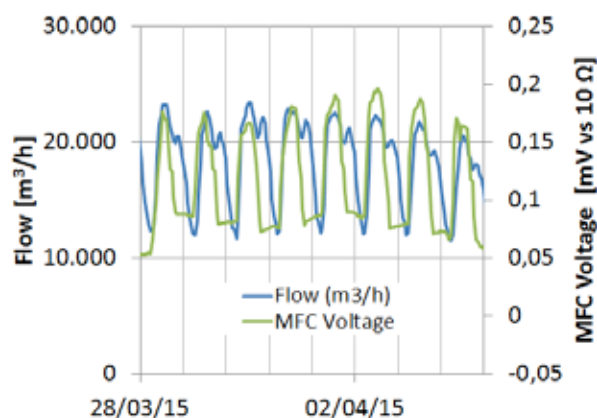


Fig. 3. Trend of the MFC output overlapped to the trend of wastewater flow

V. CONCLUSION

The results of more than six months operation indicated that all the tested MFCs were able to supply power, with a density associated to the wastewater flow and organic load, and rather inversely proportional to the electrode surface.

The harvested power generated by MFCs during the tests was low, due the low level of dissolved COD, but enough to start a step-down DC-DC converter (Linear Tech LTC3108 - Amel technology, Italy) up to 2 V to supply a remote device.

Vegetation growth on the cathodes during Spring and Summer did not inhibit the MFCs performance.

ACKNOWLEDGMENT

This work has been financed by the FSE-Lombardia, project "Luce bioelettrica" ID30166889.

References

- [1] <http://www.depuratorenosedo.eu>
- [2] E. Martinucci, F. Pizza, D. Perrino, A. Colombo, S.P.M. Trasatti, A. Lazzarini Barnabei, A. Liberale, P. Cristiani, "Energy balance and microbial fuel cells experimentation at wastewater treatment plant Milano-Nosedo", International Journal of Hydrogen Energy, 10.1016/j.ijhydene.2015.08.100 . 201



SOLID ORGANIC SUBSTRATES AS FUEL IN MICROBIAL FUEL CELLS: AN ELECTROCHEMICAL STUDY

D. Perrino*, E. Guerrini*, A. Colombo*, R. Morrone**,
P. Cristiani***, and S.P. Trasatti*

*Università degli Studi di Milano, Department of Chemistry, Via Golgi 19,
20133 Milano, (Italy)

** Istituto di Chimica Biomolecolare, Consiglio Nazionale delle Ricerche
CNR, Via P. Gaifami 18, 95126 Catania (Italy)

*** RSE – Ricerca sul Sistema Energetico S.p.A., Via Rubattino 54, 20134
Milano, (Italy)

Abstract - The capability of membraneless single-chambered microbial fuel cells to treat different solid wastes was investigated. MFCs were inoculated with anaerobic sludge of a biogas production plant. Experiments were performed with the following different organic substrates: i) organic fraction of solid urban waste, ii) whey from dairy industries, iii) residues of fish processing, iv) pulp waste from citrus juice production.

MFCs were operating for several months and with several cycles of feed. Bioanodes and biocathodes quickly developed, producing power within 3-4 days.

COD analyses were performed to follow the degradation of organic matter. The COD removal efficiency was different depending on the substrate.

Electrochemical techniques were used to monitor the development and the aging of anodic and cathodic biofilms. Polarization curves and electrochemical impedance spectroscopy tests allow correlating the power density and the electrocatalytic performances of the electrodes.

Index Terms – Microbial Fuel Cells, solid organic substrates, EIS.

I. INTRODUCTION

Several factors can influence the performances and the stability of membraneless Single-Chambered Microbial Fuel Cells (SCMFCs), especially during long-time operation. For example, the aging of the biofilm and inorganic fouling growing on the electrode [1] can affect the electron transfer resistance of electrodes. Moreover, complex organic substrates

can have low bioavailability and slow oxidation rate, resulting in low COD removal and power output.

In the present work, a long-term operation of SCMFCs has been analyzed. The aging effect of the system is discussed on the basis of electrochemical experiments. The decrease in power production and COD removal efficiency over time is correlated to the modification of the electrocatalytic properties of the electrodes.

II. MATERIALS AND METHODS

A. Materials

Lab-scale SCMFCs were inoculated with anaerobic sludge from the biogas plant site at Cremona (Italy). Four different substrates were used as organic sources:

i) dried mix of vegetal food waste; ii) dried mix of fish waste; iii) whey from dairy industries (Cremona, Italy); iv) pulp waste from citrus juice production plant (Catania, Italy).

B. Methods

The design and carbon cloth electrodes of SCMFC adopted in this work was previously described [2]. Three SCMFCs were set up for each kind of substrate. Electrodes were connected by an external circuit with a 100 Ω load. MFCs were operated at 35 $^{\circ}\text{C} \pm 1$ $^{\circ}\text{C}$ for several cycles of feeding.

Potential output of MFCs was continuously recorded by a multi channel multimeter. COD removal efficiency was

evaluated by almost daily measurements of COD using colorimetric kits (Hach). The development of biofilm on the electrodes and the aging of anodes and cathodes over time were investigated by means of quasi-stationary polarization curves and electrochemical impedance spectroscopy (EIS).

III. RESULTS AND DISCUSSIONS

All the MFCs produced power within 3-4 days and the COD continuously decreased from the first day. An example is shown in Fig. 1 for fish residues.

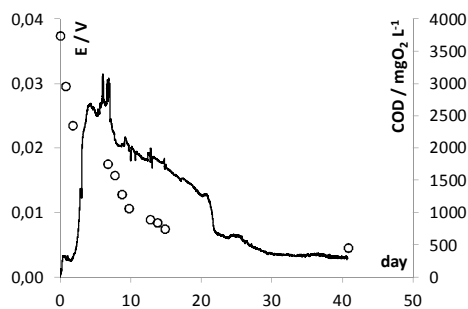


Fig. 1. Potential output (—) and COD values (○) for a MFC fed with residue of fish processing: first cycle

When COD reached an almost stable value and the potential decreased to a negligible value, a new dose of feed was added.

In Fig. 2 the power trend of an MFC fed with whey is shown together with COD values (average and standard deviation of three measurements). The maximum power output and the kinetics of COD removal decreased over each cycle. The power production of MFCs was strongly affected by long-term operation. Moreover the biodegradation process required longer time cycle after cycle. Similar results were observed for all the organic substrates. The best performance was reached for the degradation of whey, with a maximum COD removal efficiency of about 97%.

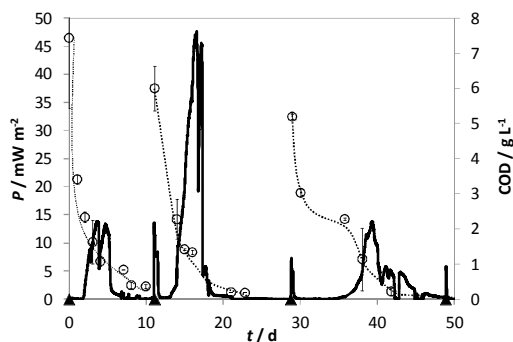


Fig. 2. Power production and COD values for an MFC fed with whey: three cycles. Triangles indicate the day of the addition of a new dose of whey.

The evolution of bioanodes and biocathodes is shown in Fig. 3 for a MFCs fed by dried mix of vegetal food waste. Anodic polarizations had similar behavior during the whole

experimentation: an anodic peak is clearly visible at -0.36 V (day 11) and at -0.3 V (days 148 and 207). These peaks can be related with the degradation processes catalyzed by the anodic biofilm. The peak position suggests that the rate determining step is the oxidation of food waste by bacteria in the biofilm, in agreement with Strycharz et al. [3]. Cathodic polarization had different catalytic activity depending on time. Performances were better for fresh electrodes (day 1 and 11), but aged electrodes showed current <0.1 mA even at very negative potentials.

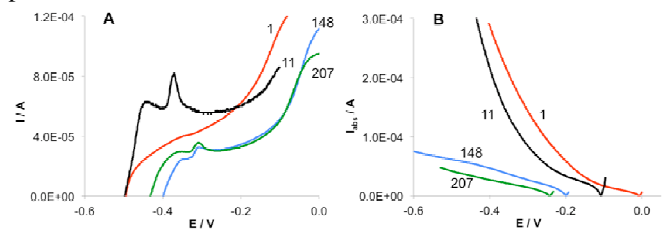


Fig. 3. Anodic (A) and cathodic (B) polarization curves recorded at different days for an MFC fed with dried mix of vegetal waste.

Moreover, EIS tests performed on cathodes showed that the charge transfer to the electrode become the rate determining step for aged electrodes. This confirms that cathodes experience a chemical modification over long-term operation.

IV. CONCLUSION

The biodegradation of complex molecules is of primary importance to guarantee bio-available organic matter to the anodic bacteria of SCMFCs operated for a more than six months. The maximum power output and the kinetics of COD removal decreased over each cycle. The best performance has been obtained for the degradation of whey. More complex substrates (dried mix of vegetal food waste, fish residues, citrus pulp) can be also degraded, even though with different efficiency. Electrochemical techniques have been applied to monitor the development and the aging of anodic and cathodic biofilms. Anodic polarization curves confirm that the food waste oxidation catalyzed by bacteria is the rate determining step. Anodes don't seem to experienced negative aging effects. The loss in performances of SCMFCs has been correlated to the chemical modification that occurs at the cathodes.

REFERENCES

- [1] M. Santini; M. Guilizzoni, M. Lorenzi, P. Atanassov, E. Marsili; S. Fest-Santini, P. Cristiani, C. Santoro. 3D X-ray Micro Computed Tomography of an operated cathode in single chamber microbial fuel cell (SCMFC). *Biointerphases*, 2015, in press
- [2] E. Guerrini, P. Cristiani, M. Grattieri, C. Santoro, B. Li, S. Trasatti, *Journal of the Electrochemical Society*, 161(3) H62-H67, 2014
- [3] S.M. Strycharz, A.P. Malanoski, R.M. Snider, H. Yi, D.R. Lovley, L.M. Tender, *Energy Environ. Sci.*, 4(2011) 896-913



FULL MULTI-SCALE MODELLING APPROACH OF PEMFC DEGRADATION MECHANISMS: UPSCALING METHOD BY A BOTTOM-UP APPROACH

M. GERARD^{*,**}, M. CHANDESRI^{*,**}, P. SCHOTT^{*,**}, M.
QUINAUD^{*,**}, R. da FONSECA^{*,**} and G. SERRE^{*,**}

^{*}Univ. Grenoble Alpes, F-38000 GRENOBLE, (France)

^{**}CEA LITEN, 17 rue des martyrs, 38000 GRENOBLE (France)

Abstract - The strong coupling between degradation mechanisms in the MEA (Membrane Electrode Assembly) (as the platinum dissolution/oxidation, Ostwald ripening, membrane degradation) and the local conditions in the MEA must be coupled to permit calculation of degradation rates function of the heterogeneities through the catalyst layer thickness and along the MEA surface.

The objective of this study is to provide a first qualitative multiscale model for catalyst degradation coupled with a semi-empirical law for membrane degradation, both of them being coupled with a performance model.

First, a mechanistic model for irreversible degradation mechanisms (platinum dissolution, Ostwald ripening) have been coupled with a local electrochemical model at the double-layer scale (EDMOND) to calculate the evolution of the active surface. The physical Ostwald ripening model has then been directly coupled with the 2D+1D fuel cell model (called PS++ model). This model is useful to calculate the local conditions along the surface of the cell. Finally, a semi empirical membrane degradation model has been added to calculate the evolution of the OCV based on the permeation current.

The different interactions between the different degradation mechanisms introduced into the 2D+1D model (evolution of the catalyst active surface, evolution of the current permeation through the membrane) and the operating conditions of the fuel cell stack, permit to calculate a global SOH (State of Health) of the fuel cell. Different mitigation strategies can be proposed.

Index Terms - PEMFC, multi-scale modeling, degradation mechanisms, Ostwald ripening, platinum dissolution, membrane degradation

I. INTRODUCTION

PEMFC lifetime prediction is a key challenge to better control the fuel cell system with durability constraints. Multi-physic modeling tools are used to couple different physico-chemical phenomena with reversible and irreversible degradation mechanisms. In this paper, a multi-scale approach,

with a bottom-up approach is developed to demonstrate the ability of coupling different degradation mechanisms in a fuel cell model to calculate and predict the fuel cell lifetime under dynamic operating conditions.

II. MODEL DESCRIPTIONS AND COUPLING

A. EDMOND model

EDMOND model is a 0D double layer model to calculate the local surface potential at the surface of the catalyst as well as the coverage of the various reaction intermediates, based on a dynamic coupling between the local operating conditions and the kinetics of the various reaction steps [1]. Both the surface potential and the coverage are involved in the mechanistic models, which makes the Edmond framework required for such a modeling approach.

B. PS++ model

PS++ model is a 2D+1D fuel cell model, based on lumped and bond graph approach. PS++ is a dynamic multi-physic model taking into account two phases flow and heat transport equations [2]. The model is used to calculate the local conditions along the surface of the cell function of dynamic operating conditions. Degradation mechanisms are added (by bottom-up or top-down approach) to calculate the fuel cell lifetime.

C. Ostwald model

The Ostwald ripening model proposed here relies on a multiscale mechanistic approach where parameters come from DFT calculations. It is able of explaining the experimental dependency of both the size of the particle, the voltage and the hydration in the degradation rate. For this, it is proposed here to decompose the total Gibbs Energy for the Ostwald ripening mechanism into 3 terms accounting for the impact of both the size of the particle via a Gibbs-Thomson formulation [3], the



local voltage via the Transition State Theory and the hydration via a dependence on the energy to extract a Pt atom from the nanoparticle. The dissolution and redeposition mechanism of Pt ($Pt \leftrightarrow Pt^{2+} + 2e^-$) with a discrete distribution of platinum particle size, compute the evolution of the number of particle for each size. The loss of the global surface area of the catalyst is so estimated. This model is found to be in good qualitative agreement with experimental results [4] and therefore provides with relevant explanations for the observed catalyst degradation.

D. Membrane degradation model

Based on specific degradation experiments to characterize membrane degradation under various operating conditions, a semi-empirical law has been demonstrated. The degradation rate has been measured given the experimental Fluoride release rate (FRR). Interestingly, the FRR was shown to depend proportionally on the cathode pressure and exponentially with the cell voltage. The first dependency is in good agreement with experiments while the second is an experimental validation of the recent model to explain the large increase of the degradation at OCV [5]. Based on the FRR law, the thinning of the membrane could be deduced and therefore the permeation current and the subsequent OCV loss. Simulated results were found in good agreement with the experimental results and thus confirms the relevance of both the mechanism and the explanation on the degradation mechanism at OCV. A semi-empirical law based on the experimental tests has been built to calculate the current permeation function of the membrane thickness:

$$I_p = 2F \cdot F_{perm}^{H_2}(e_m)$$

with $\frac{de_m}{dt} = k \cdot v_{F^{-1}}$, with k a coefficient fitted experimentally to correlate the loss of F^{-1} and the membrane thickness. The rate of F^{-1} is given by $v_{F^{-1}} = A \cdot F_{perm}^{H_2} \cdot \exp\left(-\alpha \frac{F\eta}{RT}\right) \exp\left(-\frac{E_a}{RT}\right)$. The law depends of the local temperature and potential.

E. Integration of degradation models into PS++ model

The two degradation mechanisms are introduced in PS++ model (Ostwald mechanisms and membrane degradation). The Ostwald mechanism model is directly coupled in PS++. The outputs are the evolution of the number of 2 particles size. A global degradation rate (τ_{deg}) is calculated from the ratio between the total surface of platinum and the initial surface. The active surface area of each mesh is corrected with τ_{deg} . For the degradation membrane model, the calculation of the permeation current (I_p) (from the effective membrane thickness evolution) is introduced also in the global electrochemical response of the model:

$U = E_{rev} + \eta(J, T, P_{O_2}, P_{H_2}, P_{H_2O}, \lambda) - R_m I$ with J the current density corrected by the current permeation and the loss of active surface area $J = \frac{I + I_p}{S \cdot \tau_{deg}}$.

III. RESULTS

A dynamic simulation with the WLTC automotive cycle is given as an example of the capability of PS++ model. The degradation rate of the Ostwald model is accelerated in this simulation. Fig. 1 gives the evolution the reversible (liquid water flooding effect) and irreversible degradation (Ostwald mechanism). The decrease of surface active is fast at the beginning of the cycle because the small platinum particles (radius < 0.5 nm) are dissolved and Pt^{2+} ions are redeposited on larger particle. The shape of the loss of active surface area is in good agreement with experimental tests.

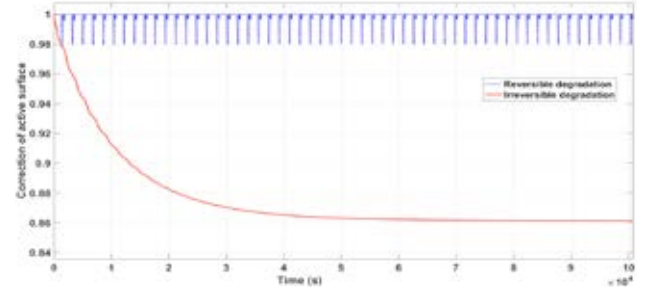


Fig. 1. Irreversible and reversible degradation mechanisms evolution

IV. CONCLUSION

The implementation by direct coupling of the Ostwald ripening mechanisms and the membrane chemical degradation into PS++ model, permits to calculate the global fuel cell lifetime. Moreover, the model captures the evolution by ageing of the distribution of the local conditions along the surface of the cell. In particular, the fast decay of performance at the beginning of life is predicted by the model.

ACKNOWLEDGMENT

The research leading to this paper has been partially supported by the European Union's Seventh Framework Program for the Fuel Cells and Hydrogen Joint Technology Initiative under the project PUMA MIND (grant agreement no 303419).

REFERENCES

- [1] A.A. Franco, S. Passot et al., Pt/Coy catalysts degradation in PEFC environments: Mechanistic insights – Part I: Multi-scale modeling, J. Electrochem. Soc., 156, B410, (2009)
- [2] C. Robin, M. Gerard, et al., Development and experimental validation of a PEM fuel cell 2D model to study heterogeneities effects along large-area cell surface, International Journal of Hydrogen Energy, 2015, 40, 10211-10230
- [3] Holby, E. F, et al., Pt nanoparticle stability in PEM fuel cells: influence of particle size distribution and crossover oxygen, Energy Environ. Sci, 2009, 2, 865-871
- [4] Ahluwalia, R.K. et al., Thermodynamics and Kinetics of Platinum Dissolution from Carbon-Supported Electrocatalysts in Aqueous Media under Potentiostatic and Potentiodynamic Conditions, Journal of The Electrochemical Society, 2013, 160, F447-F455
- [5] K. Hung-Wong and E. Kjeang, Mitigation of Chemical Membrane Degradation in Fuel Cells: Understanding the Effect of Cell Voltage and Iron Ion Redox Cycle, 2015, 8, 1072-1082



EXPERIMENTAL ANALYSIS OF DMFC CATHODE TEMPORARY DEGRADATION

A. Bisello, M. Zago, R. Marchesi and A. Casalegno

Department of Energy, Politecnico di Milano, Via Lambruschini 4, 20156 Milan (Italy)

Abstract - Dedicated OCV tests feeding the anode with a mixture of methanol and hydrogen have been performed to investigate cathode temporary degradation. There is a voltage decay of more than 20 mV between the peak voltage in OCV and the stabilized voltage value, during 20 minutes test. This voltage decay is comparable with the one occurring during nominal operation.

Different cathode electrodes have been tested in a wide range of operating conditions, varying methanol concentration, airflow rate, oxygen concentration and cell temperature.

Experiments at different methanol concentrations confirm that the recoverable voltage decay is not due to methanol crossover flux. Moreover experimental tests at different cathode humidification exhibit different membrane resistance evolution, while the voltage decay remains the same.

Instead, a strong effect of cathode potential on voltage decay is evident. This behavior suggests the possible cathode oxides formation and removal mechanism as the main cause of DMFC temporary degradation.

Index Terms – Direct Methanol Fuel Cell, Open Circuit Voltage, Platinum Oxide Formation, Temporary Degradation.

I. INTRODUCTION

Direct methanol fuel cell (DMFC) is a very promising technology as a power source for portable and automotive applications, due to the direct use of a high energy density liquid fuel, quick recharging and low operating temperature. The widely use of the DMFC technology is still hindered by some technological issues, among which the strong temporary degradation [1]. This performance loss, whose origins are not fully understood, can be partially recovered by utilizing appropriately refresh procedure, consisting in a period of continuous operation interspersed by a sequence of OCV and/or cathode air feeding interruption [2].

A systematic characterization and a complete understanding of temporary degradation phenomena are necessary to be able to effectively distinguish its effects from the permanent ones. Therefore, it is very important to improve and consolidate the understanding of DMFC operation during refresh periods.

II. EXPERIMENTAL

A. Experimental Setup

The experimental setup for single cell DMFC characterization is described in Ref. [3], where anodic temporary degradation was evaluated. Single cell DMFC of 5x5 cm² active area was manufactured by IRD Fuel Cell. Two electrode were tested: anode catalyst loading is 1.8 mg/cm² (PtRu) and cathode catalyst loading (Pt) is 1.2 mg/cm².

B. Measurements

During OCV tests, the DMFC is changed from a no air feeding state to an air feeding state. After the air is supplied, the OCV increases quickly and reaches a peak in few seconds. Rather than stabilizing at this voltage value, it declines quite rapidly and approaches a stabilized OCV value after several minutes. This initial overshoot behavior is caused by hydrogen evolution occurring in poor oxygen region and to the consequent hydrogen production at the anode [4], induced by the short circuit current. Membrane electric resistance is measured with Linear Sweep Voltammetry (LSV). The resulting value is equal to 1.1 kΩ cm², leading to a short circuit current in OCV of nearly 20 mA.

In fact, in DMFC anode sluggish kinetic implies an overpotential of nearly 0.2 V even for limited currents, but when hydrogen evolution occurs at the beginning of the OCV test the anode overpotential is negligible. In order to avoid anode dynamic behavior during the OCV, an innovative OCV test feeding the anode with a mixture of methanol and hydrogen is performed.

In order to investigate the effect of cathode potential on oxide formation/reduction, the results obtained from OCV are compared with those of Cyclic Voltammetry (CV).

Cyclic Voltammetry is a common electrochemical technique to study oxide formation and reduction on platinum [1]. Platinum oxides (PtO_x) formed at oxidation potential (UPL) after a certain period of time is measured by sweeping the

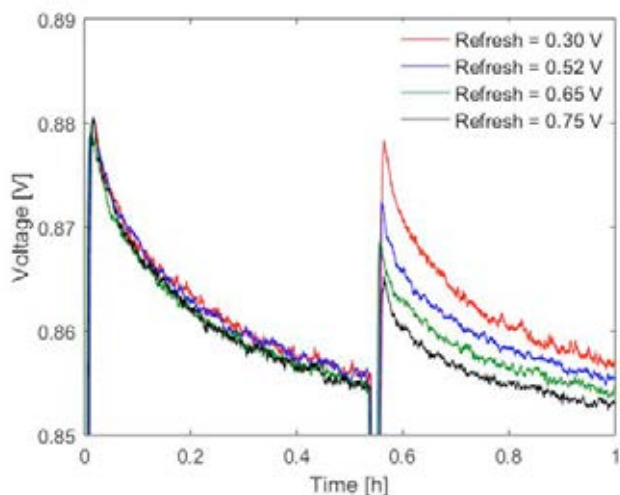


Fig. 1- Effect of refresh potential. OCV test feeding MeOH/H₂, Air 800 mL/min fully saturated, cell temperature 75°C.

potential from oxidation potential to lower potential limit (LPL) and integrating the charge under the oxide reduction peak.

The fractional coverage of platinum oxide is calculated, as is done in Ref. [6], assuming one-electron transfer, within the range DMFC cathode operates.

III. RESULT AND DISCUSSION

OCV test, as reported in Ref. [5], shows that voltage decay is not affected by the methanol concentration neither by progressive membrane dehydration.

The effect of potential has been deeply investigated: for low cathode potential no voltage decay is observable, coherently with the formation of PtO_x, which occurs only at high operating potentials.

Since the voltage recovery was observed only at low cathode potentials, the effect of refresh potential has been also investigated, feeding an appropriate airflow during the refresh. As seen in Fig. 1, it is evident that the lower is the refresh potential, the higher is the performance recovery. These results further support the theory of PtO_x formation and removal. Moreover, other experiments have been performed varying the duration of the refresh period and it turned out that just few seconds at low potential are enough for a complete performance recovery.

Fig. 2 shows CV after 1 minute at different UPL. As indicated by the data, there is threshold potential under which there is not oxide formation, compatible with OCV tests.

Different CV at same oxidation potential and time show that a progressive elevation of LPL causes an increase of the time needed for oxides reduction. Moreover, a threshold potential exists above which the recovery is not completely reversible.

The calculation of the coverage shows that oxide reduction is reversible in few second at potential lower than 0.55 V.

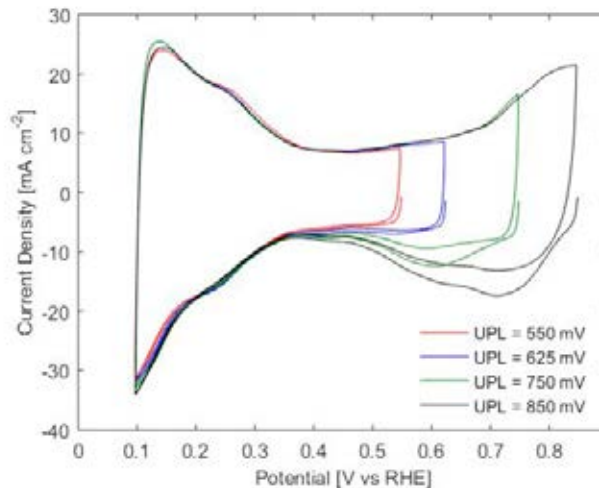


Fig. 2 - CV at different oxidation potential. RE/CE H₂ 50 mL/min RH 100%, WE N₂ 50 mL/min RH 100%, cell temperature 75°C.

IV. CONCLUSION

The presented experiments demonstrate that the temporary voltage decay occurring at the cathode of a DMFC is mainly caused by the PtO_x formation at high potentials and removal at low potentials. The results also show that the oxide reduction is faster at low potential, but the effectiveness of such mechanism is reduced at higher potential.

V. ACKNOWLEDGMENT

This work has been performed in the frame of the FCH-JU FP7 project Second Act (EC Grant Agreement 621216).

REFERENCES

- [1] C. Eickes, P. Piel, J. Davey, and P. Zelenay, Recoverable Cathode Performance Loss in Direct Methanol Fuel Cells, *J. Electrochem. Soc.*, vol. 153, no. 1, p. A171, 2006.
- [2] F. Bresciani, C. Rabissi, A. Casalegno, M. Zago, and R. Marchesi, Experimental investigation on DMFC temporary degradation, *Int. J. Hydrogen Energy*, vol. 39, no. 36, pp. 21647–21656, Dec. 2014.
- [3] F. Bresciani, a. Casalegno, M. Zago, and R. Marchesi, A Parametric Analysis on DMFC Anode Degradation, *Fuel Cells*, vol. 14, no. 3, pp. 386–394, Jun. 2014.
- [4] Q. Ye, T. S. Zhao, H. Yang, and J. Prabhuram, Electrochemical Reactions in a DMFC under Open-Circuit Conditions, *Electrochem. Solid-State Lett.*, vol. 8, no. 1, p. A52, 2005.
- [5] M. Zago, C. Rabissi, A. Baricci, and A. Casalegno, Experimental and Modelling Analyses of DMFC Temporary Degradation, 5th Eur. PEFC H₂ Forum 2015 - 30 June – 3 July 2015, Lucerne Switz., no. July, A1106 pp. 1–6, 2015.
- [6] H. Xu, R. Kunz, and J. M. Fenton, Investigation of Platinum Oxidation in PEM Fuel Cells at Various Relative Humidities, *Electrochem. Solid-State Lett.*, vol. 10, no. 1, p. B1, 2007.



INVESTIGATION OF DIFFERENT CONFIGURATIONS OF MFCs FOR TREATMENT OF OILFIELD PRODUCED WATER

A. Colombo*, P. Roustazadeh Sheikhyousefi**, M. Nasr Esfahany**,
P. Cristiani***, and S.P. Trasatti*

*Università degli Studi di Milano, Department of Chemistry, Via Golgi 19, 20133 Milano, (Italy)

**Isfahan University of Technology, Isfahan, (Iran)

*** RSE – Ricerca sul Sistema Energetico S.p.A., Via Rubattino 54, 20134 Milano, (Italy)

Abstract – Produced water is the largest waste stream in the oil production process: it contains light polar and aliphatic hydrocarbons, production process compounds, dissolved gases, anions and cations.

Disposal of produced water is subjected to strict legislations. Oil producing countries are focused on finding effective and economic methods for its treatment. Among the others, biological treatments have been proven to efficiently remove dissolved hydrocarbon compounds. Coupling of anaerobic biological treatment with electrochemical technology can lead to the production of clean water and electric energy.

In the present work, Microbial Fuel Cells (MFC) technology was applied to the treatment of produced water. Different configurations of MFCs were investigated. A first group of cells was fed by produced water from western oilfields of Iran. A second group (control) was fed by a synthetic wastewater added with sodium acetate as carbon source and with level of salinity identical to the real produced water.

Index Terms – microbial fuel cells, oilfield produced water.

I. INTRODUCTION

Produced water (or oilfield wastewater) is the largest waste stream generated in oil and gas industries. It is considered as the major source of pollution in the oil and gas fields. It is rich in oil (mainly total n-alkane (TNA), but also benzenes, phenols and polycyclic aromatic hydrocarbons (PAHs)) and contains high levels of minerals, radioactive substances and humus. Salt concentration of produced water may range from a few

mg L⁻¹ to 300 g L⁻¹. Due to the increasing volume of this waste all over the world, the effect of discharging produced water on the environment has lately become a significant issue of environmental concern [1]. To remove hydrocarbon components from produced water, some physical and chemical methods have been investigated including hydrocyclones [2], coagulation and flocculation [3] and membranes [1]. An alternative way is provided by electrochemistry. In the present paper, treatment of oilfield produced water was investigated using Microbial Fuel Cells with a simple design [4].

To test the robustness of MFCs when treating recalcitrant pollutants it is necessary to investigate the response of the system under different operating conditions. In this work, four configurations of MFCs were investigated: with or without membrane, with or without inorganic catalyst on the cathode.

II. MATERIALS AND METHODS

A. Materials and cell design

The design of MFC used in this study was previously described [4]. Anode and cathode were made of carbon cloth and a microporous layer (MPL) was applied on cathode.

The inoculum was constituted by a mixture (1:1) of sludge from a dairy plant and sludge from petrochemical plant. Bacteria from dairy plant experienced a high salinity environment, while bacteria from petrochemical



plant experienced a hydrocarbons-rich environment.

The MFCs were filled with produced water from western oilfields of Iran. Gas Chromatography-Mass Spectrometry (GC-MS) analysis was performed on fresh produced water and the results are reported in Fig. 1. The physico-chemical parameters of produced water are listed in Table 1.

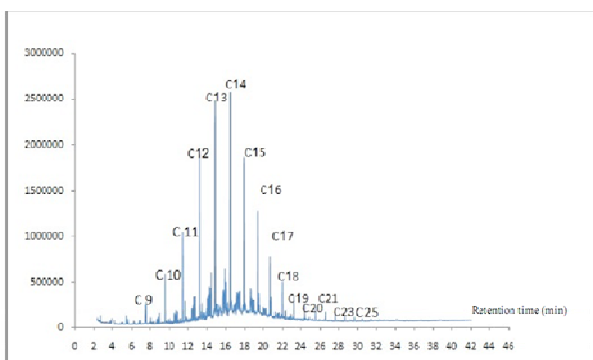


Fig. 1. GC/MS analysis of produced water

TABLE I
PHYSICO-CHEMICAL PARAMETERS OF PRODUCED WATER

Parameter	Value
pH	6-8
Turbidity (NTU)	30
Density (kg m^{-3})	1113
COD ($\text{mgO}_2 \text{L}^{-1}$)	3685 ± 100
TDS (mg L^{-1})	187300 ± 2300
Chloride (mg L^{-1})	73100
Oil & Grease (mg L^{-1})	6.85 ± 4
Conductivity (mS)	132 ± 8

Four MFC configurations have been tested: i) with membrane and Pt catalyst on cathode; ii) with membrane and without Pt catalyst; iii) without membrane and with Pt catalyst on cathode; iv) without membrane and without Pt catalyst.

MFCs were operated for several cycles of feeding.

A second group of cells were filled with synthetic produced water containing sodium acetate as reference organic substrate.

B. Methods

Performances of the system were evaluated in terms of degradation capability (COD removal efficiency) and electrical parameters. Polarization curves were recorded on both electrodes. Microbiological analyses were also performed on anode from both working and not working cells.

III. RESULTS AND DISCUSSION

Pt catalyst offered an immediate answer in terms of power output, for MFCs fed either with produced water and acetate.

COD removal efficiency higher than 90% was achieved in 20 days of operation for MFCs without Pt regardless of the membrane. Even though the power output is higher in MFCs with membrane, after the second cycle of feeding the membrane suffered clogging and the performances of MFC with membrane considerably decreased. In the case of MFCs without membrane and without Pt, there is a delay in the power output due to the time needed by biofilm to develop on the cathode (biocathode). However, after the first cycle, MFCs fed with acetate showed the best performance. MFCs fed with produced water also improved their performances cycles after cycles, almost reaching performances of MFCs with Pt (Fig. 2).

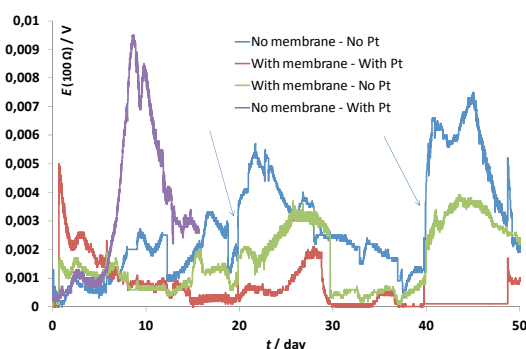


Fig. 2. Potential trend at 100Ω of MFCs fed with oil produced water. Arrows indicate produced water addition.

Microbiological analysis performed on anode of working MFCs showed the presence of a great amount of Burkholderiales able to degrade a vast array of aromatic compounds and Methylococcales that have the capability to oxidize and utilize methane.

When Clostridiales bacteria were found on anodes, MFCs didn't show any power output.

IV. CONCLUSION

The best performances were obtained by MFC without membrane and without Pt. Though sodium acetate has better bioavailability, also produced water can be degraded by bacteria. Organic compounds from produced water can be degraded with a simple system.

Electroactive bacteria are responsible for degradation.

When saprophyte bacteria (Clostridiales) development occurred, energy generation from MFCs was inhibited.

REFERENCES

- [1] A. Fakhru'l-Razi et al, J. Hazard. Mater. 170 (2009) 530–551.
- [2] S. Liu et al, SPE Asia Pacific Health, Safety and Environment Conference and Exhibition, Kuala Lumpur, Malaysia, 19-20 september 2005.
- [3] F.S. Zhou et al, Oilfield Chem. 17 (2000) 256–259.
- [4] P. Cristiani, M.L. Carvalho, E. Guerrini, M. Daghighi, C. Santoro, B. Li, Bioelectrochemistry 92 (2013) 6–13.



Battery and hydrogen-based systems to store electric energy from renewable sources: performance and comparisons

E.Jannelli¹, R.Cristofaro¹, A.Lubrano Lavadera¹,
M.Minutillo¹,G.Falcucci¹

¹Department of Engineering, University of Naples "Parthenope", Naples, Italy

Abstract – In this paper hybrid power plant configurations based on a photovoltaic power system integrated with an energy storage unit are proposed and analyzed. As storage technologies a hydrogen based system, that consists of an alkaline electrolyser (AEL) and a polymer electrolyte membrane fuel cell (PEMFC), and Li-ion battery system have been chosen.

The hybrid power plant in both configurations has been designed and sized with the aim of satisfying the energy demand of a radio base station located in a remote area.

In this study a sensitivity analysis based on the PV power system size has been performed; thus, once assigned the PV unit size, the other plant components (the PEM FC, the electrolyzer, the battery unit and reciprocating engine) have been defined and characterized.

The performances of the proposed plant configurations have been compared in order to evaluate, as each power system is able to satisfy the energy requirements during the year.

Results showed that the hybrid power system is able to operate by using only the renewable resource (solar energy) if:

- the PV power system of 17 kWp integrated with the hydrogen storage unit is installed;
- the PV power system of 15 kWp integrated with the battery system is installed;

Index Terms – energy storage system, fuel cell, battery, renewable energy source, hybrid plant

I. INTRODUCTION

The employment of hybrid energy systems based on renewable and conventional energy sources, are considered an optimal solution for off-grid power supply options in remote places or rural area.

Because of the random behavior of the renewable sources, energy storage technologies are an interesting solution for sustaining the energy production from renewable power plants; as a matter of fact, the ability of the storage systems is to accumulate the surplus of electricity produced by renewable power plants in order to return it when the power system is not able to satisfy the utility energy demand.

Different energy storage technologies, based on various processes are available. The most popular way to store electric energy is based on battery systems but, recently, the interest on hydrogen-based systems is grown rapidly.

The purpose of this study is to analyze the performance and the behaviour of renewable power plants, based on photovoltaic power modules, integrated with battery or hydrogen-based systems.

II. PLANT DESCRIPTION

The hybrid power plant configurations, as proposed and analyzed in this study, are illustrated in Figures 1 and 2.

The power plant mainly consists of: i) a PV power unit; ii) a storage system; iii) a reciprocating engine (RE); iv) electrical devices (charge controller, inverter, buffer battery, etc.).

Figure 1 shows the schematic layout of the power plant that uses the hydrogen storage technology.

The hydrogen storage system comprises: an alkaline electrolyser (AEL), metal hydride tanks for hydrogen storage and a PEM fuel cell unit.

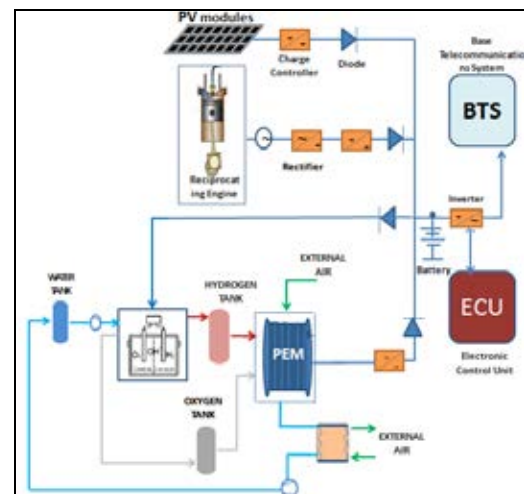


Fig. 1. The schematic layout of the hybrid hydrogen power plant

Figure 2 shows the schematic layout of the power plant that uses a battery system as storage technology. The battery system is based on Li-ion batteries.

Figure 3 predicted voltage-current in percentage relative to Maximum value for an alkaline electrolyser (AEL)[1], PEM Fuel cell [2] and Li-ion battery [3].

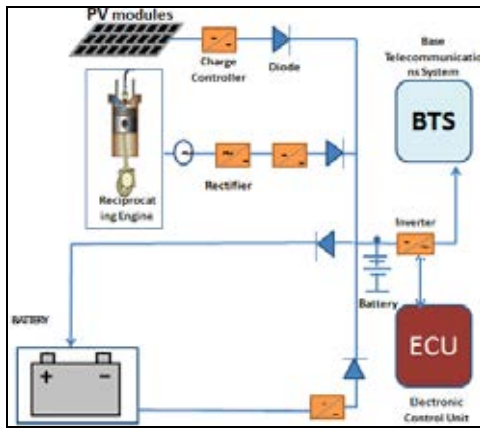


Fig. 2. The schematic layout of the hybrid battery power plant

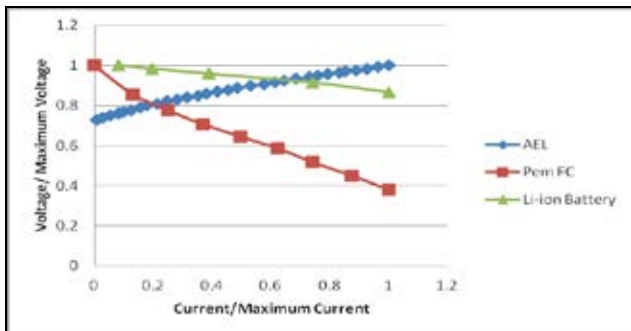


Fig.3. Voltage vs. current density for AEL, PEMFC, Li-ion battery

III. RESULTS AND DISCUSSION

In order to define the optimal size of the hybrid plant, a sensitivity analysis based on the PV power system size has been performed. The power range varies between a minimum value 1 kW_p to a maximum value that corresponds to the full renewable operation (the RE does not work). The sizing procedure has been presented in [4].

In Figure 5 the sizes of the Reciprocating Engine and of the storage system versus the PV power unit size, in both configurations, are illustrated. The PEM fuel cell and the Li-ion battery efficiencies are equal to 30% and 67%.

The sizes of the hydrogen based system components and the size of the battery system increase linearly.

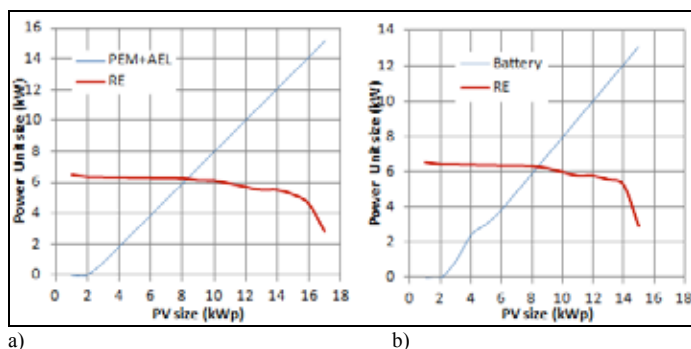


Fig. 5. Hybrid Plant components size vs. PV size; a) hydrogen storage system, b) battery storage system

The electric load is fully satisfied by the renewable source, thanks to the energy storage systems, if the sizes of the PV unit are 17 kW_p and 15 kW_p in the case of hydrogen based system and of the battery system, respectively.

In Figure 6 the fuel energy saving vs. PV size is shown. The fuel consumption in the RE decreases as the PV size increases and, using a PV power system size of 17 kW_p and 15 kW_p for hybrid hydrogen or battery power plant, it has saving about 8 tons of fossil fuel (Diesel).

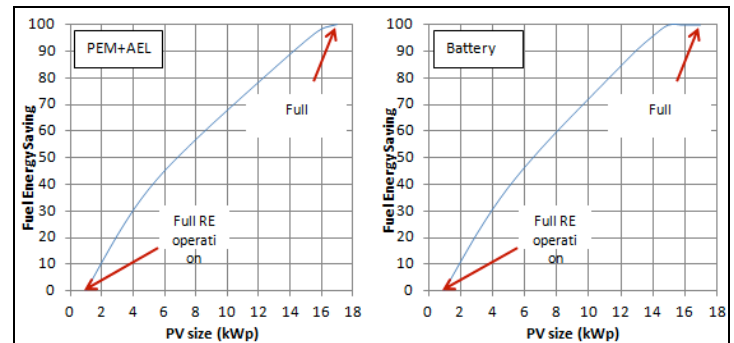


Fig. 6. Fuel Energy Saving obtained by the hybrid hydrogen and battery plant at different PV size

IV. CONCLUSION

Results showed that the hybrid power system is able to operate by using only the renewable resource (solar energy) if:

- the PV power system of 17 kW_p integrated with the hydrogen storage unit is installed;
- the PV power system of 15 kW_p integrated with the battery system is installed;

However, a good compromise it can be reached, in terms of components size and fuel consumption for PV sizes ranging from 9 to 11 kW_p for hydrogen based systems and 8 to 10 kW_p for Li-ion battery system in which the fuel energy saving varies between 60 and 70%.

ACKNOWLEDGMENT

This research has been funded by the Italian Government, with the PON project “Fuel Cell Lab – Innovative systems and high efficient technologies for polygeneration – PON03PE_00109_1/F12”.

REFERENCES

- [1] Agata Godula. Hydrogen Production: by Electrolysis.(2014) 137-138.
- [2] M.G. Santarelli, M.F. Torchio, P. Cochis. Parameters estimation of a PEM fuel cell polarization curve and analysis of their behavior with temperature. (2006) 8.
- [3] R. Lazzari, E. Micolano. Definizione e validazione di una procedura di prova per batterie al litio per applicazioni stazionarie. Installazione e sperimentazione nella test facility di GD di un filtro attivo con Supercapacitori. (2010) 22-31.
- [4] A. Lubrano Lavadera, E. Jannelli, M. Minutillo, A. Perna, S.P. Cicconardi, Investigations on an energy storage system based on high temperature fuel cells for an off-grid renewable power plant, Hypothesis XI, Toledo, Spain, 6 – 9 September 2015.



SOFC OPERATION UNDER PARTIAL DIRECT REFORMING: NUMERICAL STUDY ON THE IMPACT OF CARBON DEPOSITION ON ELECTROCHEMICAL PERFORMANCE

D. Ferrero *, E. Veglio *, A. Lanzini*, P. Leone* and M. Santarelli *
*Politecnico di Torino, C.so Duca degli Abruzzi 24, 10129, Torino, (Italy)

Abstract - The present study focuses on the modeling of an electrolyte-supported SOFC operating under partial direct methane reforming conditions. A two dimensional model that includes fuel, air channels and cell is developed and calibrated on the basis of polarization and temperature data obtained from a SOFC stack. The model is subsequently applied to the simulation of the effects of carbon deposition that can occur in case of malfunctioning of fuel processing upstream the cell. The numerical model calculates the amount of carbon deposited during time within the electrode by Boudouard and methane cracking reactions and the consequent progressive reduction of anode porosity and catalytic activity. The results show that carbon formation in the anode can lead to a significant degradation of SOFC performance. The model predicts a reduction of the stack power up to 10% after 2000 h of operation with the fuel processor in off-design conditions.

Index Terms - Carbon deposition, Degradation, Modeling, Solid Oxide Fuel Cell.

I. INTRODUCTION

Solid Oxide Fuel Cells (SOFCs) are highly flexible toward the primary fuel. Even though SOFCs run on a wide range of hydrocarbons, the conventional Ni-based anode cermet easily undergoes coking formation if operating temperature and fuel compositions are not properly controlled.

This work investigates the impact of carbon deposition on the performance of a syngas-fuelled SOFC.

A numerical model is developed to simulate the combined chemical, thermal and electrochemical processes that take place in the cell. The model is calibrated on the basis of experimental data obtained from a SOFC stack tested in the demonstration plant of the SOFCOM project (see Acknowledgments for further detail on this project). In the plant, the stack is fed with a reformat gas produced from the steam reforming of biogas that takes place in a separated fuel processor. The model is applied to the study of the carbon deposition in the case of

malfunctioning of the fuel processor upstream the cell. The amount of carbon deposited during time within the anode is calculated and the effects due to the reduction of catalyst (i.e., Nickel) activity and electrode porosity on the cell performance are assessed.

II. NUMERICAL MODEL

The numerical model includes fuel, air channels and cell. Electrodes are assumed as homogeneous porous media and the anode material is Ni/YSZ. The equations for the transfer and conservation of energy, charge, mass and momentum are imposed in the model. Laminar flow is assumed in the fuel and air channels, where Navier-Stokes equations are used. The Darcy-Brinkmann flow model is applied in the porous electrodes and the species diffusion is described by using the Fick's model. Electrochemical reactions of CO and H₂ are assumed to take place into electrode reaction layers and are modeled by using Butler-Volmer formalism. Methane steam reforming, water gas shift, methane cracking and Boudouard reactions are imposed in the anode; the reactions are described by using global rate expressions. The local thermal equilibrium approach is adopted for modeling the heat transfer in the porous domains.

The carbon deposition rate is calculated as the variation of the molar concentration of deposited carbon:

$$\frac{dc}{dt} = a \cdot (R_{cr} + R_{Bd}) \quad (1)$$

where c is the molar concentration of deposited carbon, a is the catalyst activity (i.e., value between 0 and 1, 1 if no carbon is deposited) and R_{cr} and R_{Bd} are the reaction rates of methane cracking and Boudouard reactions.

The catalyst deactivation is given by [1]:



$$\frac{da}{dt} = -k_a \cdot \left(\frac{dc}{dt}\right)^2 \cdot c \cdot a \quad (2)$$

where k_a is an attenuation constant.

The porosity variation is a function of the carbon deposition rate [2]:

$$-\frac{d\varepsilon}{dt} = \frac{\varepsilon \left(\frac{dc}{dt}\right) M_C}{\rho_C} \quad (3)$$

where M_C is the molar mass of carbon and ρ_C is the carbon density.

All the equations are solved by using COMSOL Multiphysics platform.

III. RESULTS AND DISCUSSION

The model is calibrated with the data obtained from the stack tested with H₂/N₂ and reformat mixtures (50% H₂, 20% CO, 9% CO₂, 21% H₂O), the results are shown in Figure 1.

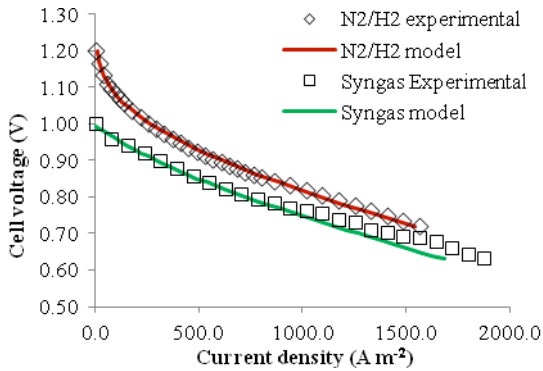


Figure 1. Model calibration.

In order to simulate the malfunctioning of the methane steam reformer, it is assumed that a fraction of the biogas flow bypasses the fuel reactor; thus, the fuel entering the cell in off-design conditions is a mixture of biogas and reformat.

The effect of carbon deposition on cell performance is shown in Figure 2.

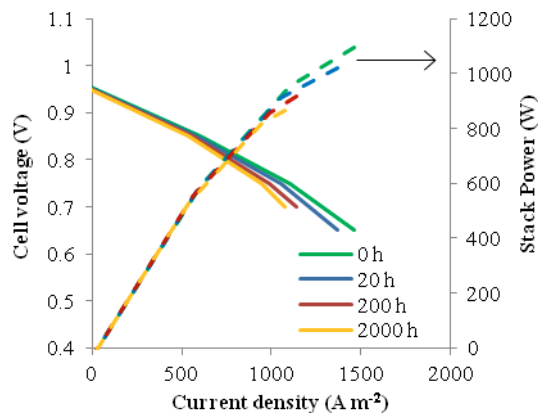


Figure 2. Effect of carbon deposition on cell performance (50% bypass rate

and 0.7 V cell voltage).

The model predicts a reduction of the stack power up to 10% (at 0.7 V) after 2000 h of operation with 50% bypass rate of the fuel processor and constant cell voltage of 0.7 V.

The degradation of cell performance is due to the progressive accumulation of carbon on the Nickel surface that reduces the porosity of the anode, as shown in Figure 3, and increases the gas diffusive losses in the electrode. The carbon coverage also reduces the catalyst activity and inhibits the methane steam reforming reaction that contributes to the conversion of CH₄ to H₂ within the cell.

However, the covered Nickel is also less active towards the methane cracking, thus also the carbon deposition rate progressively decrease with the increase of the carbon coverage, as shown in Figure 3.

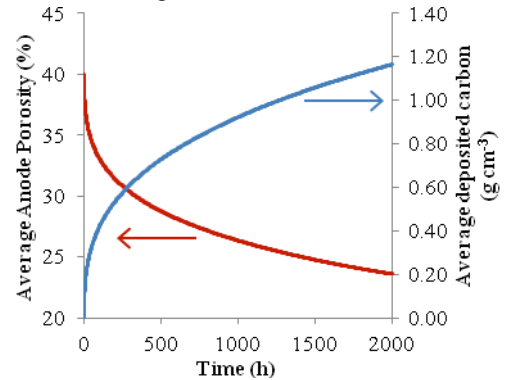


Figure 3. Average anode porosity and deposited carbon (50% bypass rate and 0.7 V cell voltage).

IV. CONCLUSION

A numerical model of an electrolyte-supported SOFC has been developed. The model simulates the combined chemical, thermal and electrochemical processes that take place in the cell and has been applied to the study of the effects of carbon deposition on cell performance. The model can be a useful tool to predict the performance degradation and analyze the off-design conditions for the study of control strategies to mitigate the carbon deposition effects.

ACKNOWLEDGMENT

This work was partly funded by the European Union (Project number 278798, <http://areeweb.polito.it/ricerca/sofcom>), with contributions from the partners involved: POLITO, SMAT, IEN, TUM, MATGAS, CNR, VTT and TOPSOE.

REFERENCES

- [1] Zavarkhin, S.G., Kuvshinov, G.G., The kinetic model of formation of nanofibrous carbon from CH₄-H₂ mixture over a high-loaded nickel catalyst with consideration for the catalyst deactivation, *Applied Catalysis*, Vol. 272, 2004, pp. 219-227.
- [2] Yan, M., Zeng, M., Chen, Q., Wang, Q., Numerical study on carbon deposition of SOFC with unsteady variation of porosity, *Applied Energy*, Vol. 97, 2012, pp. 754-762.



EFC15120

SOFC ANODES FOR THE DIRECT UTILIZATION OF ETHANOL AS FUEL

Selma A. Venâncio^{a}, Ugo Icardi^a, Gianni Bidini^b,
Giovanni Cinti^b, Paulo Emílio V. de Miranda^a*

^aThe Hydrogen Laboratory, Coppe-Federal University of Rio de Janeiro, Av. Horácio Macedo, 2030, 1-146, , Rio de Janeiro, 21941-914, Brazil.

^bFuel Cell Lab, Dipartimento Di Ingegneria, Università degli Studi di Perugia, Via G. Duranti 93, 06125 Perugia, Italy .

Abstract - The present work explores the performance of electrolyte supported solid oxide fuel cells – SOFC – that possess conventional strontium-doped lanthanum manganite cathodes and Cu-(Zr_xCe_{1-x}O₂/Al₂O₃)-based multifunctional anodes for the direct utilization of ethanol as fuel with resistance to carbon coking and clogging. Scanning electron microscopy and X ray diffraction structural characterizations have shown that the successful performance of such anodes is mainly attributed to the overall morphology and the microstructure of the Zr_xCe_{1-x}O₂ and Al₂O₃ oxides at the electrolyte/anode interface, as well as to the copper dispersion throughout the microstructure of the porous electrode. It is inferred that the enhancement of charge distribution due to the presence of copper favors the anode activity by promoting the interaction of copper with the oxides Zr_xCe_{1-x}O₂ and Al₂O₃ by increasing the amount of active sites for the electrochemical reactions of interest. Important electrical and electrochemical performances were reached by operating SOFCs at 950°C with the direct utilization of ethanol as fuel with limited occurrence of problems related to carbon deposition in tubes that give the fuel access to the SOFC anode or at the anode itself. Such material and fabrication concepts unveil new multifunctional SOFC anodes that allow the direct utilization of ethanol as fuel

Keywords: *Direct utilization of ethanol; Solid oxide fuel cell; Multifunctional anode.*

Solid oxide fuel cells – SOFCs – usually operate with hydrogen or natural gas reformat and are characterized by the converting the fuel's chemical energy into electricity with very small emissions of pollutants. Preferably, SOFCs are used for stationary energy generation with power greater than 1 kW. There is also great interest in the development of SOFCs for auxiliary power units and for portable energy generation systems. In such type of applications it is convenient to make the direct utilization of high energy density liquid fuels instead of natural gas, with additional simplification of the system by eliminating fuel reforming and purification units [1]. The

solution herein researched is the development of alternative anodes featured to be simultaneously tolerant to coking and sulfur poisoning with performance comparable to that of the conventional Ni-YSZ cermet (8%mol yttria stabilized zirconia). The Ni-YSZ cermet is not the adequate anode for the direct utilization of alcohols in SOFCs because of its inactivity for the electrochemical oxidation of CO [2] and for catalyzing carbon formation, which results on destruction of the anodic microstructure [3]. This has motivated the development of alternative anodic compositions [4-6]. The present work presents the development of two multifunctional anodes, herein named 1 and 2, which are composed with two different functional layers. Their functionalities are evaluated with respect to the microstructure, the phases that are formed and their electrochemical behavior. Table 1 presents the chemical composition of such multifunctional anodes.

Table 1. Chemical composition of the anode functional layers.

Anodes	Functional Layer 1	Functional Layer 2	Impregnation
1	YSZ (70%) + CeO ₂ -Al ₂ O ₃ (30%)	CeO ₂ -Al ₂ O ₃	Cu (20%)
2	YSZ (70%) + CeO ₂ -Al ₂ O ₃ (30%)	YSZ (50%) + CeO ₂ -Al ₂ O ₃ (50%)	Cu (20%)

As previously described [7], to obtain the anode chemical compositions depicted in Table 1, electrocatalyst ceramic powder based on CeO₂-Al₂O₃ was synthesized by the amorphous citrate method and calcined at 900°C. From there on, ceramic suspensions containing the inorganic ceramic powders indicated in Table 1 were produced by high-energy milling with compositions that additionally



included YSZ, corn starch, as pore former and a terpeneol-based vehicle. Subsequently to this process, the anodes were deposited onto YSZ electrolytes by screen-printing and sintered at 1500°C. After sintering, the anodes were impregnated with a copper nitrate solution until 20% wt. copper was reached in the anode microstructure. This allowed producing anodes that were composed by the solid solution of $Zr_xCe_{1-x}O_2$ and Al_2O_3 , as presented in the X ray diffraction patterns in Figure 1. Anodes based on the Ceria-Zirconia solid solution were developed with the objectives to improve the electrocatalytic properties, the chemical and thermal stabilities, as well as to achieve an increased capacity to store oxygen ions as compared to anodes solely based on ceria. In such a case, metallic copper was used to guarantee better electronic conductivity, while the ceramic compound acted as a mixed electronic-ionic conductor, promoting the fuel's oxidation, and Al_2O_3 plays the role of a diffusion barrier that prevents grain coarsening. It is also envisaged to facilitate the oxygen ions transfer from the electrolyte to the electrocatalytic sites and the charge transfer processes at the triple phase boundaries.

Analysis of the interactions among the anode precursor oxides was evaluated by X ray diffraction, as presented in Figure 1. It was observed for anode 1 the formation of the mixed oxides $Zr_{0.25}Ce_{0.75}O_2$, with cubic lattice and $Zr_{0.50}Ce_{0.50}O_2$, with tetragonal lattice. However, anode 2 presents only the $Zr_{0.50}Ce_{0.50}O_2$ phase. Compared to anode 1, anode 2 showed an increase on the Al_2O_3 X ray diffraction peaks, with trigonal lattice. This is due to the fact that the functional layer 2 in anode 1 is uniquely composed by the electrocatalyst $CeO_2-Al_2O_3$.

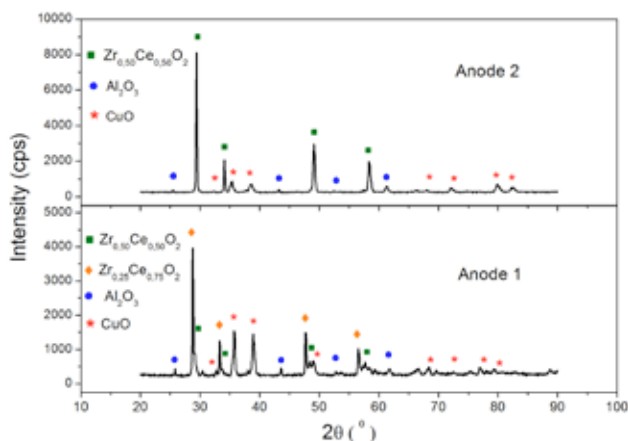


Fig. 1. X Ray Diffraction Patterns for Anodes 1 and 2.

The effect of the different anode compositions was evaluated by the electrochemical performance of single SOFCs with active areas of 16 cm², with a conventional $La_{0.8}Sr_{0.2}MnO_3$ cathode and tested with the direct utilization of ethanol as fuel at 950°C. The electrochemical performance results for SOFCs with the two anodes developed are presented in Figure 2. It indicates that better result was achieved by the SOFC that contained anode 2. Both SOFC types, with anodes 1 or 2, contain the same amount of copper in their anodes. It is inferred

that the improved performance of the SOFC containing anode 2 is related to the predominant presence of the $Zr_{0.50}Ce_{0.50}O_2$ phase, while the SOFC containing anode 1 is predominantly composed of the $Zr_{0.25}Ce_{0.75}O_2$ phase.

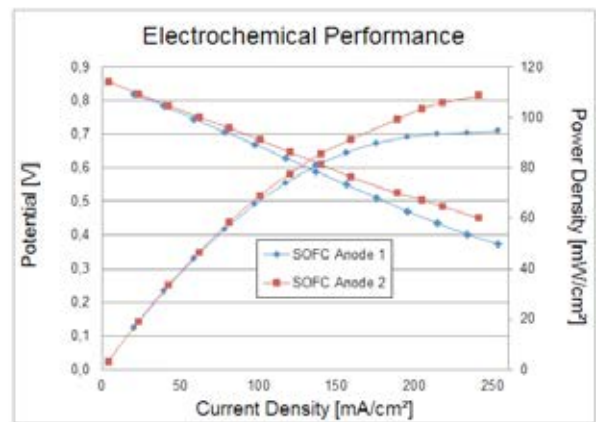


Fig. 2. Electrochemical performance for SOFCs fabricated with anodes 1 and 2, presenting potential versus current density and power density versus current density curves for the direct utilization of ethanol at 950°C.

CONCLUSION

Important electrochemical performances were reached by operating SOFCs with the direct utilization of ethanol as fuel with limited occurrence of problems related to carbon deposition in tubes that give the fuel access to the SOFC anode or at the anode itself.

REFERENCES

- [1] Badwal, S.P.S., Giddey, S., Kulkarni, A., Goel, J., Basu, S, Direct ethanol fuel cells for transport and stationary applications – A Comprehensive review, Applied Energy, volume 145, 2015, pages 80-103.
- [2] Holtappels, P., De Haart, L.G.J., U. Stimming, Vinke, I.C., Mogensen, M, Journal of Applied Electrochemistry, volume 29, 1999, pages 561-568.
- [3] Toebe, M.L., Bitter, J.H., van Dillen, A.J., de Jong, K.P., Impact of the structure and reactivity of nickel particles on the catalytic growth of carbon nanofibers, Catalysis Today, volume 76, 2002, pages 33-42.
- [4] Atkinson, A., Barnett, S. t, Gorte, R.J., Irvine, J.T.S., McEvoy, A.J., Mogensen, M., Singhal, S.C., Vohs, J, Advanced anodes for high-temperature fuel cells, Nature Materials, volume 3, 2004, pages 17-27.
- [5] McIntosh, S., Gorte, R.J, Direct Hydrocarbon Solid Oxide Fuel Cells, Chemical Reviews, volume 104, 2004, pages 4845-4865.
- [6] Gross, M.D., Vohs, J.M. Gorte, R.J, Recent progress in SOFC anodes for direct utilization of hydrocarbons, Journal of Materials Chemistry, volume 17, pages 3071-3077.
- [7] Venâncio, S.A., de Miranda, P.E.V, Synthesis of $CeAlO_3/CeO_2-Al_2O_3$ for use as a solid oxide fuel cell functional anode material, Ceramics International, volume 37, 2011, pages 3139-3152.



USE OF MFC SYSTEMS AS BIOSENSORS OF ORGANICS

Andrea Franzetti*, Matteo Daglio*, Tommaso Truppi*, Giuseppina Bestetti*,
Edoardo Guerrini**, Davide Perrino** and Pierangela Cristiani***

*Dept. of Earth and Environmental Sciences – University of Milano-Bicocca, Piazza
dellaScienza 1, 20126 Milan, Italy

**Dept. of Chemistry, University of Milano, Via Golgi 19, 20133, Milan, Italy

***RSE — Ricerca sul Sistema Elettrico S.p.A., Environment and Sustainable
Development Department, Via Rubattino 54, 20134 Milan, Italy

Abstract - Microbial fuel cells (MFCs) are attracting considerable attention as innovative systems for energy production from renewable residual biomass and biomass-derived wastes. Current produced by a microbial fuel cell can also be used to quantify the rate of specific metabolic processes and the substrate concentration in real time. Aim of this work is to develop a MFC based biosensor for real time quantification of organic biodegradable substrates at low concentration, in the range of 0 – 100 mg/L COD. In a continuous flow membraneless MFC, a concentration-dependent current output was achieved using sodium acetate as organic substrate. Furthermore, Monod kinetics was observed as the best-fitting model.

Index Terms – BES, monitoring, acetate, Monod

I. INTRODUCTION

A bioelectrochemical system (BES) is a device that makes use of microorganisms or enzymes to catalyze redox reactions on or near electrodes. Initial applications of this technology have been directed towards conversion of chemical energy into electrical energy [1]. This can be achieved by biologically catalyzed oxidation of organic carbon or sulfides in anaerobic environments on the anode [2]. The released electrons are transferred from the anode via an electrical circuit to a cathode where a reduction takes place. This reduction can be chemically or biologically catalyzed. If the redox potential of the oxidation reaction is lower compared to the potential of the reduction reaction at the cathode, a net energy gain can be achieved. Recently, some studies tried to assess a correlation between the electrical output and the bioelectrochemical degradation of organic matter as a measure of the substrate concentration available for microbial degradation. The rationale behind this

possible application is that electrical current is proportional to the electrons that flow into the electrochemical system per time unit. The current is therefore proportional to the extent at which the electrons are transferred to the electrode by the oxidation reaction (anodic process) and diverted by the reduction reaction (cathodic process). The electron exchanged can thus be used as effective parameter to quantify the rate of specific metabolic processes in real time [3, 4]. Several studies already investigated the correlation between the current and the oxidation of specific organics and more complex organic matrix like wastewater [5, 6]. Mostly focalizing the attention on high electrical signal and high organic concentration, such as in the range of 500 – 3000 mg/L COD [7]. Nevertheless, further studies about the degradation kinetics will be required to apply BES based biosensors for measuring the concentration of the high number of relevant chemicals polluting waters. In this work, Single Chamber and mediatorless MFCs (SCMFCs) were investigated to monitoring low level of COD concentration, in the range of 0 – 100 mg/L, by adding sodium acetate in wastewater media. This is the COD range allowed at the discharge of the wastewater plants by the Italian rule.

II. BIOSENSOR SET UP AND MONITORING

A. Biosensor set up

The biosensor was set up with three connected SCisMFC (solution volume: 50 mL) operated with an external resistor (R_{ext}) of 100 Ω , at a temperature of 28 ± 2 °C. A Pt-free cathode (10 cm² projected area) was made with carbon cloth (60 wt.% PTFE, FuelCellEarth) and a Micro-Porous Layer (MPL) of 30–



50 μm thickness was applied since it was found to enhance oxygen exchange and facilitate the biofilm growth [8]. Untreated carbon cloth (SEAL, Legnano, Italy) was used as anode. The biosensor was operated in continuous flow with the single SCMFC connected in series (Figure 1). The cells were inoculated with raw wastewater from waste water treatment plant. After inoculation, sodium acetate was added as sole carbon source.

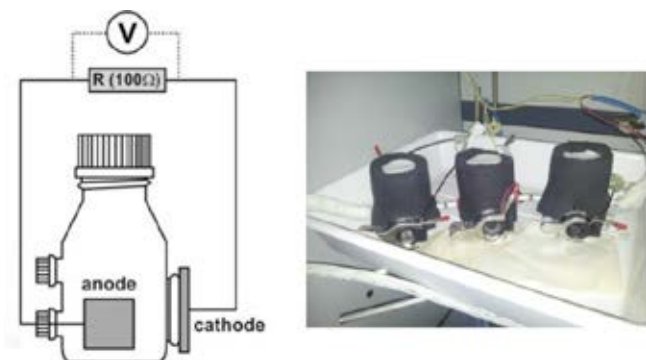


Fig. 1. Scheme and picture of the biosensor

Orders in the anodic biofilm. Conversely, *Xanthomonadales*, *Rhodocyclales* and *Bacillales* were the dominant bacterial populations on the cathode.

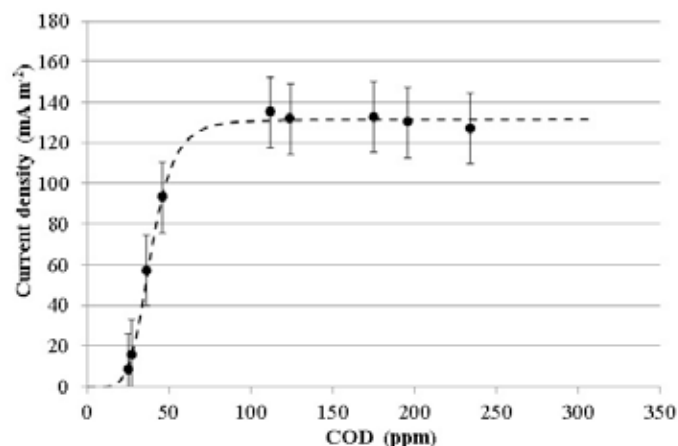


Fig. 2. Relationship between CD and COD and best-fitting model.

B. Monitoring

The electric current was monitored over time. Residual concentration of acetate was estimated by COD analyses. Anodic and cathodic biofilm samples were aseptically collected during biosensor operation in order to describe in detail the communities by 16S rRNA gene sequencing. Amplification of the V5-V6 hypervariable regions of the 16S rRNA gene, sequencing and sequence elaboration were carried out as previously described [9].

III. BIOSENSOR PERFORMANCES AND OPERATING BIOMASS

Figure 2 shows the relationship between current density (CD) and COD values obtained after 80 days of continuous feeding of the cells. Data has been fitted with different kinetics models and showed the best fitting ($R^2=0.997$) with a modified Monod model (equation 1).

$$\mu = \mu_{\text{MAX}} \frac{[S]^n}{K_s + [S]^n} \quad (1)$$

Best fitting parameters of the models were: $K_s = 38.47$; $\mu_{\text{max}} = 131.23$; $n = 5.49$.

In the tested condition the biosensor is, therefore, suitable for monitoring COD less than 100 ppm.

Anodic and cathodic microbial communities operating in the biosensor differed substantially. *Actinomycetales*, *Ignavibacteriales* and *Burkholderiales* were the most abundant

REFERENCES

- [1] Arends JB a, Verstraete W. 100 years of microbial electricity production: Three concepts for the future. *Microb Biotechnol* 2012;5:333–46.
- [2] Rabaey K, Van de Soempel K, Maignien L, Boon N, Aelterman P, Clauwaert P, et al. Microbial fuel cells for sulfide removal. *Environ Sci Technol* 2006;40:5218–24.
- [3] PrévotEAU A, Geirnaert A, Arends JBA, Lannebère S, Van de Wiele T, Rabaey K. Hydrodynamic chronoamperometry for probing kinetics of anaerobic microbial metabolism - case study of *Faecalibacterium prausnitzii*. *Sci Rep* 2015; Article in.
- [4] Kumlanghan A, Liu J, Thavarungkul P, Kanatharana P, Mattiasson B. Microbial fuel cell-based biosensor for fast analysis of biodegradable organic matter. *Biosens Bioelectron* 2007;22:2939–44.
- [5] Tront JM, Fortner JD, Plötze M, Hughes JB, Puzrin a M. Microbial fuel cell technology for measurement of microbial respiration of lactate as an example of bioremediation amendment. *Biotechnol Lett* 2008;30:1385–90.
- [6] Kim BH, Chang IS, Gil GC, Park HS, Kim HJ. Novel BOD (biological oxygen demand) sensor using mediator-less microbial fuel cell. *Biotechnol Lett* 2003;25:541–5.
- [7] P. Cristiani, M.L. Carvalho, E. Guerrini, M. Daghigho; C. Santoro, B. Li, Cathodic and anodic biofilms in single chamber microbial fuel cells. *Bioelectrochemistry*. 92 (2013) 6–13.
- [8] E. Guerrini, M. Grattieri, A. Faggianelli, P. Cristiani, S. Trasatti. PTFE effect on the electrocatalysis of the oxygen reduction reaction in membraneless microbial fuel cells. *Bioelectrochemistry* on line.
- [9] Daghigho, M, Tatangelo, V, Franzetti, A et al. Hydrocarbon degrading microbial communities in bench scale aerobic biobarriers for gasoline contaminated groundwater treatment. *Chemosphere*; 130:34:39.



FRONTIERS AND RECENT DEVELOPMENTS IN NANOMATERIALS FOR FUEL CELL APPLICATIONS: AN OVERVIEW OF PERFORMANCES AND PERSPECTIVES

D. Frattini, F.M. De Rosa, G. Accardo, G. Roviello, L. Cimino, C. Ferone and R. Cioffi
Department of Engineering, University of Naples Parthenope & UdR INSTM of Naples Parthenope,
Centro Direzionale di Napoli – Is. C4, 80143 Naples (Italy)

Abstract - In actual nanotechnology field, the development of new materials with tailored structures, from molecular to the nanometric scale, is very fast and many improvements have been made. In the last decades a remarkable progress in fuel cells performance has been due to the use of advanced nanocomposites. In this work, an overview of the transversal role of nanomaterials and actual trends in research, with updated performances, are analysed and compared to show potentials and barriers of these materials. The principal result is that electrochemical activity, transport properties and durability are enhanced in components with nanomaterials. This aspect is of fundamental importance for fuel cell technologies to compete with traditional energy systems.

Index Terms – fuel cell, materials, nanoparticle, performances.

I. INTRODUCTION

Fuel cell technology is based on different operating principles and system design to obtain the electrochemical conversion of a fuel, but the common trend is to introduce nanomaterials as a key factor to open a door to new perspectives for their application [1,2]. In fact, nanomaterials are extensively used in Proton Exchange Membrane Fuel Cells (PEMFC), Solid Oxide Fuel Cells (SOFC) and Microbial Fuel Cells (MFC) [3-5]. In particular, non-Nafion polymeric membranes, based on Sulfonated Poly(Ether Ether Ketone) (SPEEK), and organic/inorganic hybrid membranes are treated for PEMFCs; Gadolinium-doped Ceria (GDC), Lanthanum-Strontium-Gallate-Magnesium (LSGM) and other perovskite oxides solid electrolytes are analyzed and compared for SOFCs; performances of Graphene Oxide (GO) and Carbon Nanotubes (CNT) are briefly described for MFC applications.

II. APPLICATION OF NANOMATERIALS IN FUEL CELL TECHNOLOGY

A. Proton Exchange Membranes based on Nanomaterials

In PEMFC, the most important component is Membrane Electrode Assembly (MEA) for the proton conduction. Actual trend is to add nanoadditives in Nafion or substitute it with low-cost functionalized materials. Some interesting materials, recently proposed in literature, are compared in Table I.

TABLE I. EMERGING PEMFC MATERIALS AND THEIR PROPERTIES

Material	Type	Nano component	Proton Conductivity (S·cm ⁻¹)	Ref.
Nafion/TiO ₂	Organic/Inorganic	Nano TiO ₂	0.11	[6]
Sulfonated poly(arylene ether sulfone)	Organic	Thionyl Chloride	0.08	[7]
Nafion/Clay	Organic/Inorganic	Nano Clay	0.09	[8]
Nafion/Ni-CNT	Organic//Inorganic	Carbon Nanotube	0.12	[9]

Other very interesting nanocomposites, based on SPEEK/Pt-Cs_{2.5}H_{0.5}PW₁₂O₄₀ nano-complexes [10] and inorganic Nb-P-Si nanopowders [11,12] have shown enhanced chemical stability and thermal properties for PEMFC application. The robust nanostructures of these emerging materials do not collapse or sinter at high temperature. They can tolerate temperature of 140-150°C, compared to the standard 120-130°C of PEMFC, leading to a theoretical increment in efficiency of about 6-8%.

B. Advanced Nanoceramic Electrolytes Materials for SOFCs

SOFCs are actually considered the most reliable fuel cells for power production due to the stability, durability and versatility of their ceramic electrolytes. Table II shows a list of the most promising ceramic materials for SOFCs.

TABLE II. ADVANCED CERAMIC ELECTROLYTES PROPERTIES FOR SOFCs

Name (Abbreviation)	Formula	Particle size (nm)	Ion conduc. @T (S·m ⁻¹)	Sint. T (°C)	Ref.
Gadolinium-doped Ceria (GDC)	Ce _{0.8} Gd _{0.2} O _{1.9}	20.3	5.5 @800°C	1500	[13]
Lanthanum-doped Strontium Gallate Magnesium (LSGM)	La _{0.8} Sr _{0.2} Ga _{0.8} Mg _{3.5}	500*	0.2 @600°C	1500	[14]
Niobium-doped Barium Cerate Yttria (BCYN)	BaCe _{0.84} Y _{0.1} Nb _{0.06} O _{2.9}	<1000	1.02 @700°C	1450	[15]
Yttrium-doped Barium Zirconate Cerate (BZCY)	BaZr _{0.1} Ce _{0.7} Y _{0.2} O _{3-δ}	75	5.0 @750°C	1400	[16]

*film thickness

Their structure is based on the insertion of nanodopants which



fill vacancies, enhancing sinterability. The final densification can easily be >98%. The dense structure at nanoscale is the cause of improved ion conductivity, by hopping mechanism [15, 16]. When nanodopants are inserted in perovskite oxides, the local structure is coordinated by them and the electronic state is altered. These modifications at nanostructure level can lead to an increment in power generation of about 20%

C. Carbon-based Nanomaterials as Electrodes for MFCs

MFCs operate bio-electrochemical conversion of an organic substrate at near-room temperature and reactions kinetics at electrodes is limited. Nanotechnology gives an important help in mass and electrical transport enhancement at electrodes [4, 17]. The actual cutting edge technology is the use of CNT and GO nanocomposites due to their biocompatibility, porous structure and electrical conductivity. These materials allow longer operation and high power density, as 1000-1300 mW·m⁻² using Activated Carbon (AC) and GO nanocomposites [18], 500 mW·m⁻² with MnO₂/CNT composite [19] and 300-600 mW·m⁻² with graphite nanoflakes [4]. The increment of power density is mainly due to the combined nanoporous and conductive nanostructure of carbon nanomaterials because, as emerge from [17, 19], the conductive porous nanostructure reduces diffusion and ohmic resistances of about 20-25% compared to plain electrodes without nanoadditives.

III. POTENTIALS AND BARRIERS OF NANOMATERIALS

The distinguishing potential of these materials is based on their highly-ordered structures (Nanotubes, nanowires, nanosheets, nanoceramic particles, ultrathin films, etc.) [2]. In fuel cell applications, these structures can increase the electrochemical active area by ensuring a truly effective contact between reactants at the nano level in MFCs or can drive charge carriers through nano pathways, as take place in SOFCs. The use of nanomaterials exhibits a strong enhancement of transport properties and new interface functionalities [1-5]. However, effects of human exposition and their potential environmental impact, including recycling and disposal, represent the major issue to their safe use on large scale [2, 20].

IV. CONCLUSION

The greater functions offered by nanomaterials should push their utilization in fuel cells to contribute to efficiency improvement and profitability of such technology and more studies on scale-up for industrial production are required. The material properties reported in this work are a proof of the enabling and cross-cutting role of nanotechnology for fuel cell components development. The clear advantage of nanomaterials, as pointed out by literature overview, is that new phenomena and principles can be exploited to achieve high performance, not accessible to conventional materials.

REFERENCES

[1] Kelarakis, A., Functional nanomaterials for energy and sustainability, *Advanced Materials Letters*, Volume 5, 2014, pp. 236-241.

[2] Osada, M., Nanoscale materials, in *Materials outlook for energy and environment*, 2013, pp. 64-65.

[3] Aricò, A.S., Baglio, V., Antonucci, V., *Nanomaterials for fuel cell technologies*, in *Nanotechnology for the energy challenge*, 2013, pp. 171-211.

[4] Venkata Mohan, S., Velvizhi, G., Modestra, J.A., Srikanth, S., *Microbial fuel cell: critical factors regulating bio-catalyzed electrochemical process and recent advancements*, *Renewable and Sustainable Energy Review*, Volume 40, 2014, pp. 779-797.

[5] Zhu, B., *Solid Oxide Fuel Cell (SOFC) technical challenges and solutions from nano-aspects*, *International Journal of Energy Research*, Volume 33, 2009, pp. 1126-1137.

[6] De Bonis, C., Cozzi, D., Mecheri, B., D'Epifanio, A., Rainer, A., De Porcellinis, D., Licoccia, S., *Effect of filler surface functionalization on the performance of Nafion/Titanium Oxide composite membranes*, *Electrochimica Acta*, Volume 147, pp. 418-425.

[7] Kwon, Y., Lee, S.Y., Hong, S., Jang, J.H., Henkensmeier, D., Yoo, S.J., Kim, H.J., Kim, S.H., *Novel sulfonated poly(arylene ether sulfone) containing hydroxyl groups for enhanced proton exchange membrane properties*, *Polymer Chemistry*, Volume 6, 2015, pp. 233-239.

[8] Alonso, R.H., Estevez, L., Lian, H., Kelarakis, A., Giannelis, E.P., *Nafion-clay nanocomposite membranes: morphology and properties*, *Polymer*, Volume 50, 2009, pp. 2402-2410.

[9] Tran, P.D., Morozan, A., Archambault, S., Heidkamp, J., Chenevier, P., Dau, H., Fontecave, M., Martinet, A., Jusselme, B., Artero, A., *A noble metal-free proton-exchange membrane fuel cell based on bio-inspired molecular catalysts*, *Chemical Science*, Volume 6, 2015, pp. 2050-2053.

[10] Rowshanzamir, S., Peighambaroust, S.J., Parnian, M.J., Amirizhanlou, G.R., Rahnavard, A., *Effect of Pt-Cs2.5H0.5PW12O40 catalyst addition on durability of self-humidifying nanocomposite membranes based on sulfonated poly(ether ether ketone) for proton exchange membrane fuel cell applications*, *International Journal of Hydrogen Energy*, Volume 40, 2015, pp. 549-560.

[11] Clayden, N.J., Accardo, G., Mazzei, P., Piccolo, A., Pernice, P., Vergara, A., Ferone, C., Aronne, A., *Phosphorus stably bonded to a silica gel matrix through niobium bridges*, *Journal of Material Chemistry A*, Volume 31, 2015, pp. 15968-15995.

[12] Accardo, G., Ferone, C., Aronne, A., Pernice, P., Cioffi, R., *Synthesis of Nb2O5-P2O5-SiO2 materials for proton exchange membranes fuel cell (PEMFC) applications*, *Proceedings of the 5th European Fuel Cell Piero Lunghi Conference*, 2013, pp. 393-394.

[13] Ferone, C., Accardo, G., Dell'Agli, G., Cioffi, R., *Sol-gel synthesis of gadolinium doped Ceria (Gd-CeO2) for intermediate temperature SOFC electrolyte*, *Proceedings of the 5th European Fuel Cell Piero Lunghi Conference*, 2013, pp. 391-392.

[14] Yang, N., D'Epifanio A., Di Bartolomeo, E., Pugalini C., Tebano, A., Balestrino, G., Licoccia, S., *La0.8Sr0.2Ga0.8Mg0.2O3 thin films for IT-SOFCs: Microstructure and transport properties correlation*, *Journal of Power Sources*, Volume 222, 2013, pp.10-14.

[15] Di Bartolomeo, E., D'Epifanio, A., Pugalini, C., Giannici, F., Longo, A., Martorana, A., Licoccia, S., *Structural analysis, phase stability and electrochemical characterization of Nb doped BaCe0.9Y0.1O3 electrolyte for IT-SOFCs*, *Journal of Power Sources*, 2012, Volume 199, pp. 201-206.

[16] Konwar, D., Nguyen, N.T.Q., Yoon, H.H., *Evaluation of BaZr0.1Ce0.7Y0.2O3 electrolyte prepared by carbonate precipitation for a mixed ion-conducting SOFC*, *International Journal of Hydrogen Energy*, Volume 35, 2015, pp. 11651-11658.

[17] Liew, K.B., Daud, W.R.W., Ghasemi, M., Leong, J.X., Lim, S.S., Ismail, M., *Non-Pt catalyst as oxygen reduction reaction in microbial fuel cell: a review*, *International Journal of Hydrogen Energy*, Volume 39, 2014, pp. 4870-4883.

[18] Zhang, X., Xia, X., Ivamov, I., Huang, X., Logan, B.E., *Enhanced activated carbon cathode performance for microbial fuel cell by blending carbon black*, *Environmental Science and Technology*, Volume 48, 2014, pp. 2075-2081.

[19] Liew, K.B., Daud, W.R.W., Ghasemi, M., Loh, K.S., Ismail, M., Lim, S.S., Leong, J.X., *Manganese oxide/functionalised carbon nanotubes nanocomposite as catalyst for oxygen reduction reaction in microbial fuel cell*, *International Journal of Hydrogen Energy*, 2015, DOI:10.1016/j.ijhydene.2015.04.030.

[20] Pereira, S.R., Coelho, M.C., *Can nanomaterials be a solution for application on alternative vehicles? – A review paper on life cycle assessment and risk analysis*, *International Journal of Hydrogen Energy*, Volume 40, pp. 4969-4979.



TRANSIENT SIMULATION OF A SOEC SYSTEM FOR WIND ENERGY STORAGE

G.Botta*, F. Mangia**, P. Leone** and P.V. Aravind*

* Process and Energy laboratory, Technische Universiteit Delft,
TuDelft, Leeghwaterstraat 39, 2628 CB, Delft, Netherlands.

** Energy Department, Politecnico di Torino, Corso Duca Degli
Abruzzi 24, 10129, Torino.

Abstract - This paper describes the dynamic behaviour of a high temperature electrolysis system through a transient model. The system is based on solid oxide electrolysis cells (SOECs), coupled with a wind farm in a power-to-gas configuration. The model takes into account mass and energy balances for the SOEC stack as well as for the different balance of plant components. A 1D approach has been implemented to study the system behaviour along the flow direction. The model is able to capture the physical behaviour of the SOEC system under transient operation including shifts in thermal regimes (e.g., endothermic versus exothermic), consumption of reactants and hydrogen production. Dynamics of pressurized SOEC systems are reported.

The model is used to evaluate the storage option of energy produced from a wind farm in Italy. The evaluation includes the incorporation of the model with daily curves of an Italian wind farm and power consumption of local users.

Index Terms – Energy storage, High temperature electrolysis, Solid Oxide Electrolysis, Transient model.

I. INTRODUCTION

This work presents the transient behavior of an electrolyser system fed with current coming from an eolic plant.

A dynamic model can help in understanding parameter variations occurring in real systems, taking into account electrochemical and thermo-mechanical features that otherwise can not be captured in stationary simulations.

It gives a more accurate description of the system, considering inertial phenomena related for eg. to physical structure of the system, helping to understand how to preserve the integrity of the stack. It is essential, therefore, to build and study dynamic models as well as the stationary ones.

Modeling all relevant physics in a SOEC system requires a flexible tool capable of including several physical domains in the same model. For this reason the system is implemented in

Dymola and several simulations of systems and individual components have been performed.

II. IMPLEMENTATION

The cell models are based on a template model containing common parts in all fuel cell models, modified ad hoc to be able to work in the electrolyser mode. This includes connectors for mass flow, heat transfer and electrical current. Also a temperature state is introduced and energy balance is defined. The complete stack is modeled by connecting 10 substack models in parallel, while every substack is modeled connecting electrically and thermally 100 cells in series.

This stack model is applied in a complete electrolyser system including the BOP: compression, heating and fuel treatment elements.

The inlet mass flow rate is varied in order to maintain a constant Utilization Factor equal to 70% for avoiding structural damages to the stack and to its integrity. The system has been studied at three different pressures: 1.2 bar, 12 and 30 bar respectively. After a sensitivity analysis the inlet fuel temperature has been fixed at 800 C°. The cell voltage has been chosen as 1.35 V in order to work in exothermic regime.

III. SIMULATIONS AND RESULTS

The electrolyser system is coupled with an eolic plant and several simulations of the complete system and individual components have been carried out in order to understand their operation.

The evaluation includes the incorporation of the model with daily curves of an Italian wind farm.

Figure 1 displays the trend of the current that is supplied to the single substack.

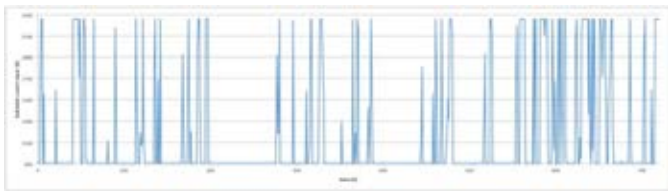


Fig. 1. Current that is supplied to the substack

The flow rate entering in the system has been varied according to the availability of the current to maintain a constant utilization factor within the limits recommended.

The heat power produced at ambient pressure by the stack, has the same trend as the current and it settles at an average value of 1.2 MW.

Similar to the stack, imposing physical and geometrical characteristics, the dynamic response of each auxiliary components present in the balance of plant has been evaluated.

The daily efficiency of the ambient pressure system is 50%.

It is also very important to examine how temperature of the stack changes with time. The peculiarity of this program allows us the possibility to analyze the real performance taking into account the effective mass of the stack and the thermal inertia. The results are shown in Figure 2.

Comparing this graph with Figure 1 we note the higher pulses of current corresponds to the considerable increasing in temperature.

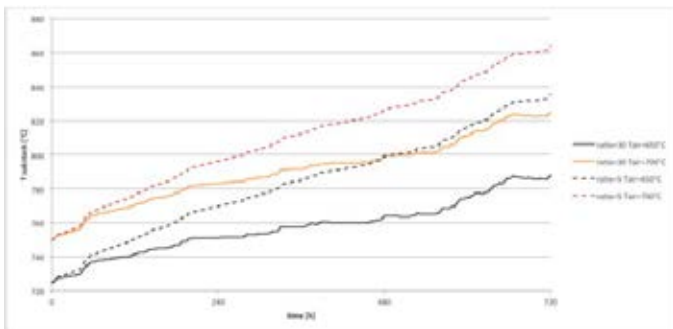


Fig. 2. Stack trend temperature in 1 month

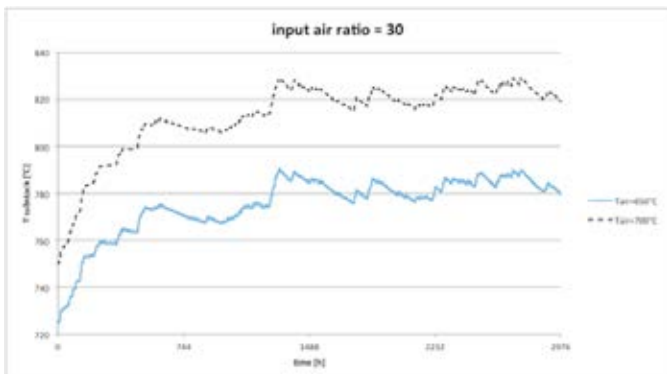


Fig. 3. Stack trend temperature in 4 months

Different anode inlet temperature has been analyzed.

The Area Specific Resistance (ASR) varies inversely to the temperature.

For avoiding integrity issues of the stack related to the very high temperature, and for maintaining the ASR almost constant, the amount of air that acts as a cooler has been changed from a ratio of fuel-air equal to 5 to a ratio equal to 30.

Nevertheless the temperature variation still seems to increase fast, reaching a highest value of 820 C° instead of 860 C° when the air flow temperature is 700 C°. We notice in both cases a dramatically increase in the first 720 hours, this is very unlikely in practical cases and can be due to the attempt of extrapolating the time simulation from seconds to hours. Looking at Figure 3 we notice that the temperature increase in four months is slower, approaching an asymptote, despite the current trend is similar to the one obtained during the first 720 hours.

In 4 months the control of the temperature seems satisfactory and the final level is in a safe region reaching its peak at 780 C° when the inlet air temperature is equal to 650 C°. If we change the inlet air temperature to 700 C°, the outlet temperature reaches 820 C°. Based on this observation, we can conclude that the value of current has a great impact on the reached temperature; nevertheless, the temperature trend is mostly influenced by the time of the simulations that is lower than the time the system would need to reach the steady state, especially in the first hours.

The same analysis have been carried out for 12 bar and 30 bar cases. The pressurized system resulted in slightly lower efficiency with a daily efficiency equal to 49.2 for the 12 bar system and 48.6 for the 30 bar system.

IV. CONCLUSIONS

The transient behavior of an electrolyser system coupled with an eolic plant has been analyzed. All the developed components have been studied at first individually. After having verified by running several simulations of the developed components under various boundary conditions and studying their influence on the results it can be concluded that the model responds properly and that Dymola and Modelica are tools well suited for simulations of the transient electrolyser system behavior. The model is able to capture the physical behaviour of the SOEC system under transient operation including shifts in thermal regimes consumption of reactants and hydrogen production. Despite the attempting of adjusting the time simulation with real period of analysis it can be conclude that system reaches steady state and maintains conditions (in safe operational region) for remaining observation period.



Enhancement of microbial fuel cell anode through conductive polymer

Y.L. Kang*, S. Ibrahim*, and P. Saravanan*

*Environmental Engineering Laboratory, Department of Civil Engineering,
Faculty of Engineering, University of Malaya, 50603, Kuala Lumpur,
(Malaysia)

Abstract - The current study focuses on the viability of a conductive polymer, poly(3,4 ethylenedioxythiophene) (PEDOT) as an anode synergist. The PEDOT was prepared through a facile chemical polymerization method and coated on graphite felt (GF). Electrochemical studies showed the PEDOT coating drastically improved the electrochemical activity and reduced the charge transfer resistance of the anodes. The current density increased to 3.50 A/m² for GF-P from 0.48 A/m² and further inclined to 4.57 A/m² with subsequent increase in PEDOT loading. The maximum power density of the modified anodes ranged from 1.56 W/m² to 1.62 W/m² while the GF anode recorded a much lower power density of 0.52 W/m². In conclusion, the performance of the anodes improved significantly even with the minimal addition of PEDOT.

Index Terms - anode, conductive polymer, microbial fuel cell, PEDOT.

I. INTRODUCTION

Numerous limitations of microbial fuel cell (MFC) are hampering the commercial viability of this sustainable application. Anode is one of the major constraints in MFC as they are the performance controlling factor. Various approach of enhancement has been experimented and one such is using conductive polymer as an additive for anode. Conductive polymers such as polypyrrole, polyaniline and their composite have been extensively studied as potential additives. However, limited research has focused on exploring the candidature of poly(3,4-ethylenedioxythiophene) (PEDOT) towards MFC applications.

II. METHODOLOGY

A. PEDOT and anode synthesis

PEDOT was synthesized through chemical polymerization where the oxidant, FeCl₃·6H₂O (10.0

mmol) and EDOT monomer (5.0 mmol) in 100 mL acetonitrile were stirred for 4 h. PEDOT particles were filtered and washed until the filtrate was colorless. It was then dried at 80°C for 24 h. PEDOT ink was prepared by dispersing appropriate amount of PEDOT powder with 1% sodium dodecylbenzenesulfonate (SDBS) by sonication. Graphite felt (GF) (4×4 cm) was dipped into the PEDOT ink and dried at 80°C. The dip-dry process was repeated until all the ink was consumed. The loading rates were adjusted to 2.5, 5.0 and 7.5 mg/cm² by varying the quantity of PEDOT powder and are referred to as GF-P, GF-2P and GF-3P respectively. GF without PEDOT attachment was used as a control sample.

B. Characterization and Application of Anodes

The cyclic voltammetry (CV) and electrochemical impedance spectroscopy (EIS) were performed using AUTOLAB PGSTAT128N (Metrohm, Netherlands) in three-electrode mode. The anode electrode, Pt wire and Ag/AgCl were used as working, counter and reference electrode respectively. The electrolyte used was 1mM ferricyanide ([Fe(CN)₆]³⁻) in 0.5M potassium nitrate (KNO₃) as supporting electrolyte. The synthesized anodes were applied in a dual chamber MFC cell with 1k Ω external resistor and acetate as carbon source. Polarization curves and power density were obtained by linear scanning voltammetry at a scan rate of 1mV/s.

III. RESULT AND DISCUSSION

A. Electrochemical Analysis

CV analysis (Fig. 1) showed the peak current and area under the graph of the tested anode increase with increasing PEDOT loading. This demonstrates the role of PEDOT in amplifying the electrochemical reactivity and conductivity of the materials [1]. Additionally, a shift in redox peaks among the tested anodes was observed.



These shifts are characteristic of decreasing rate constant owing to the delay in current response to the applied voltage [2]. This phenomenon suggests that the presence of PEDOT particles obstructs the diffusion of the electrolyte to the inner section of the felts and the effect is more prominent with the increase in PEDOT loading rate.

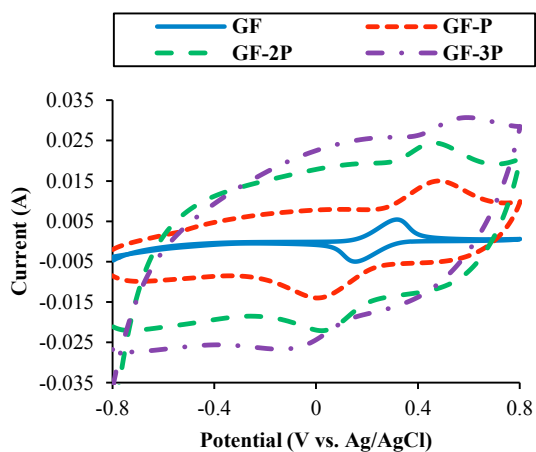


Fig. 1. CV analysis of the tested anodes

EIS analysis was performed to evaluate the internal resistance components of the anodes. Nyquist plot were presented in Fig. 2 and were fitted into a modified Randle's equivalent circuit. The GF anode has the highest charge-transfer resistance, R_{ct} (16.5Ω) while GF-P and GF-2P both recorded a significant reduction of R_{ct} to 10.6Ω and 4.9Ω respectively. This improvement is evidently brought about by the addition of PEDOT onto the anodes. The R_{ct} of GF-3P was 5.3Ω which is slightly higher than that of GF-2P. Hence, the lowest R_{ct} was achieved by GF-2P and further increase in PEDOT loading (GF-3P) does not influence the internal resistance.

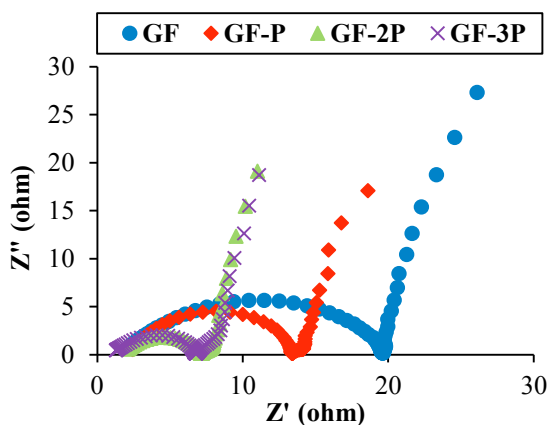


Fig. 2. Nyquist plots of all the tested anodes

B. Application of tested anodes in MFC system

Polarization and power density curves were computed and are presented in Fig. 3. The control anode, GF recorded maximum current density of 0.48 A/m^2 . The GF-P recorded a 7.3 times higher current density to 3.50

A/m^2 . Subsequent increase of PEDOT loading pushed the current density up to 4.11 A/m^2 and 4.57 A/m^2 for GF-2P and GF-3P respectively. The maximum power density achieved by all the modified anodes (GF-P, GF-2P and GF-3P) ranged from 1.56 W/m^2 to 1.62 W/m^2 , which is a vast improvement compared to GF anode which recorded a maximum power density of 0.52 W/m^2 . The substantial increase in anode performance establishes the role of PEDOT additive in improving the electrocatalytic activity and conductivity of the anodes. The modification also facilitates the formation of stable biofilm due to the electrostatic attraction between the PEDOT polymer backbone and microbial cell wall [3].

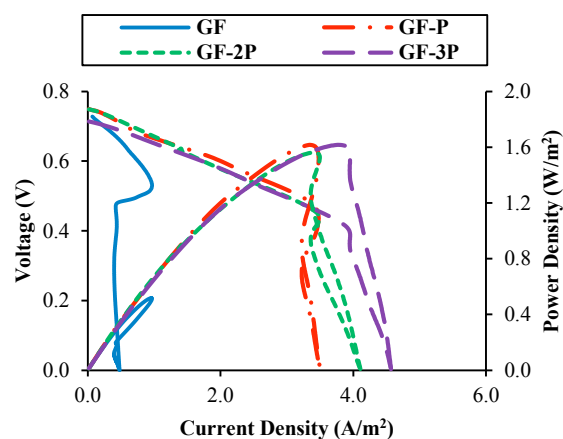


Fig. 3. Polarization curve and power density of the tested anodes.

IV. CONCLUSION

The present study verified the applicability of PEDOT as an anode synergist for MFC system. The addition of PEDOT significantly improves the electrochemical activities and conductivity of the anodes. Both the current density and power density demonstrate substantial improvement compared to the control anode even with the least PEDOT loading. Further investigations with wastewater would capitalize the efficiency of these anodes and furnish a comprehensive analysis on the performance of these modified anodes.

ACKNOWLEDGEMENT

This work was supported by High Impact Research Grant (UM.C/625/1/HIR/053/2) and Postgraduate Research Grant (PG022-2013A), University of Malaya.

REFERENCES

- [1] Hou, J., Liu, Z., Zhang, P., A new method for fabrication of graphene/polyaniline nanocomplex modified microbial fuel cell anodes, *Journal of Power Sources*, Volume 224, 2013, pp. 139-144.
- [2] Bard, A. J., Faulkner, L. R., *Electrochemical methods: fundamentals and applications*, 2nd ed., Wiley, New York, 2001.
- [3] Wang, Y., Zhao, C., Sun, D., Zhang, J.-R., Zhu, J.-J., A Graphene/Poly(3,4-ethylenedioxythiophene) Hybrid as an Anode for High-Performance Microbial Fuel Cells, *ChemPlusChem*, Volume 78, 2013, pp. 823-829.



DYNAMIC MODELING OF SOLID OXIDE FUEL CELL-ENGINE HYBRID SYSTEM

Sanggyu Kang*, Kanghun Lee*, Youngduk Lee*, and Kook-Young Ahn*

*Korea Institute of Machinery and Materials, Daejeon 34103,
(Republic of Korea)

Abstract - Novel hybrid system composed of solid oxide fuel cell (SOFC) and engine has been introduced by our previous study. The fuel contents remained in the anode tail gas from the SOFC is reutilized in the engine to improve the system electrical efficiency. Our previous research has proved the electrical efficiency of the hybrid system can be enhanced by about 5% compared to the stand alone system. Although the hybrid system has higher efficiency than the stand alone system, higher elaboration for the system operation should be necessary due to higher system complication. The objectives of the present study is to develop the dynamic modeling of the SOFC-engine hybrid system. The component dynamic modeling of SOFC, engine, steam reformer, blower, pump, and heat exchangers are developed and integrated into a system. The system dynamic behavior and correlation among each components during transients is investigated.

Index Terms – Solid Oxide Fuel Cell (SOFC); Engine; Hybrid System; Dynamic Modeling

I. INTRODUCTION

High temperature fuel cell system has been regarded as a promising power generation for the stationary application due to high fuel flexibility, high efficiency, low emission, and high capability for combined heat and power (CHP) [1-2]. Our previous research presented the solid oxide fuel cell (SOFC)-engine hybrid system. In order to increase the system efficiency, anode-tail gas is reutilized in the engine. Due to complexity of the hybrid system, system control logic should be developed. The objectives of the work is to develop the dynamic modeling of the SOFC-engine hybrid system. The SOFC component model is validated by comparison with the experimental data. The system dynamic behavior is captured during transients. The present study provides the basic insight to establish the optimal control strategy for the SOFC-engine hybrid system.

II. MODEL DESCRIPTION

A. SOFC-Engine Hybrid System

The schematics of the SOFC-Engine hybrid system is shown in Fig. 1. The natural gas is partially reformed by flowing through the external reformer. The partially reformed gas enters the SOFC stack for the electrochemical reaction. After the SOFC stack, anode-tail gas flows into the condenser to remove the water to increase the fuel concentration. Engine exhaust gas transfers the heat for the external reforming reaction by flowing through the heat exchanger. The dynamic modeling of the SOFC-engine hybrid system is composed of the SOFC stack, Engine, air blower, and heat exchangers. The engine model developed by Matlab® is integrated with SOFC system model developed by Matlab-Simulink® by using the S-function.

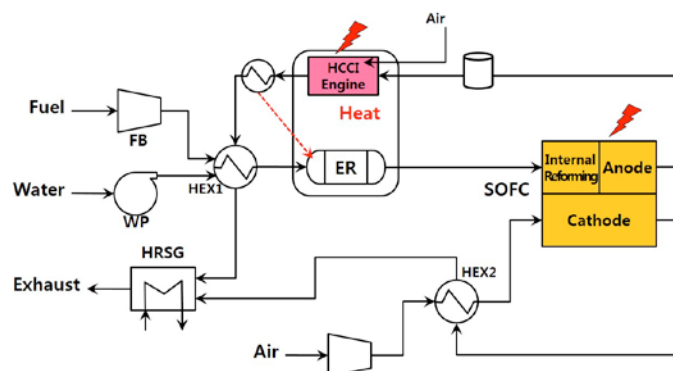


Fig. 1. Schematics of the SOFC-Engine hybrid system

B. SOFC stack

The three-dimensional dynamic model of SOFC stack is developed by Matlab-Simulink®. To resolve the mass and energy conservation, the model was discretized into five and

seven control volumes in the flow perpendicular direction. The model is also discretized into 25 control volumes in the flow parallel direction to capture the characteristic distribution of the SOFC stack. The direct internal reforming reaction is considered in the anode electrode control volume. The electrochemical reaction of H_2O and CO_2 are considered to predict the SOFC performance accurately [3].

C. Engine

Since the anode tail gas of the SOFC stack is lean condition, the homogenous charge compression ignition (HCCI) engine is selected for the combustion of the anode exhaust gas. To predict the combustion timing, GRI-Mech 3.0, containing 53 species and 325 reactions is employed [4].

D. Balance of Plant (BOP)

All the BOP components model is developed by Matlab-Simulink[®]. The steam reformer and heat exchanger is two-dimensionally discretized to resolve the heat transfer in the flow perpendicular direction and capture the characteristic distribution in the flow parallel direction. The lumped dynamic model of air blower is developed by considering the motor-blower inertia.

III. SIMULATION RESULTS

In order to verify the SOFC stack model, the current-voltage polarization curve is compared between experiment and simulation, as shown in Fig. 1. The simulation results are in good agreement with the experimental data within an error of $\pm 1.2V$.

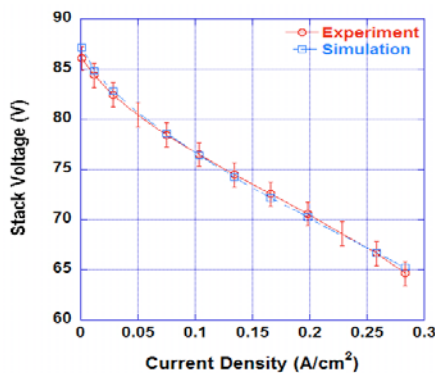


Fig. 1. Comparison of current-voltage polarization curve between experiment and simulation

The system model was simulated at the step change of stack demand power from 50 kW to 100 kW at 2000 s. The dynamic behavior of the SOFC stack power and overvoltage of activation and ohmic are presented in Fig. 3. Due to the dynamic characteristic of the species mole fraction and temperature in the SOFC, the overshoot behavior is appeared in the activation and ohmic overvoltage during demand power increase, which results in the overshoot of the stack power.

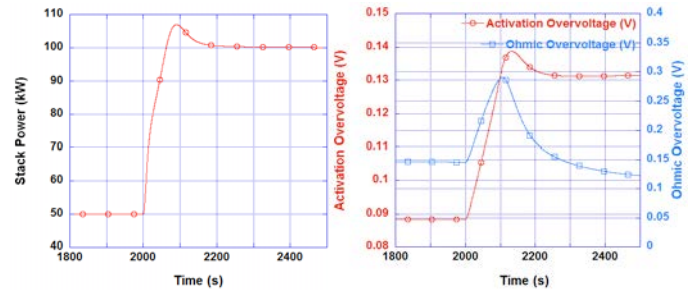


Fig. 3. Dynamic behavior of stack power and overvoltage of activation and ohmic at the step change of demand power from 50 kW to 100 kW.

The dynamic behavior of air blower and fuel temperature is captured at the step change of demand power from 50 kW to 100 kW.

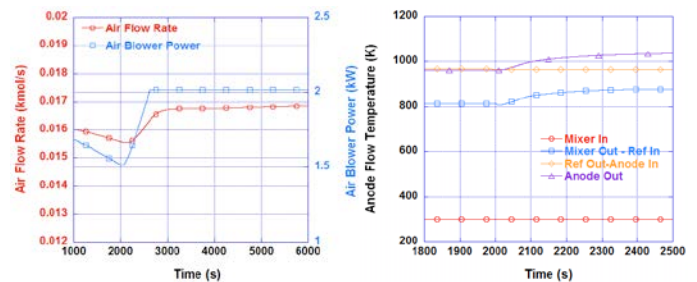


Fig. 4. Dynamic behavior of air blower and temperature between BOP at the step change of demand power from 50 kW to 100 kW.

IV. CONCLUSION

The dynamic modeling of SOFC-engine hybrid system has been developed in this study. SOFC model is validated by comparing the current-voltage polarization curve between experiment and simulation. The system model is simulated at the step change of demand power increase to capture the system dynamic behavior. This model is useful to develop the optimal control strategy of the SOFC-engine hybrid system during transients.

ACKNOWLEDGMENT

This work was supported by the Industrial Strategic technology development program (10049010, The Development of Engineering Technology for 100kW-class High Temperature Fuel Cell-Engine Hybrid System) funded By the Ministry of Trade, industry & Energy (MI, Korea).

REFERENCES

- [1] R.J.Braun, S.A.Klein, D.T.Reindl, Evaluation of system configurations for solid oxide fuel cell-based micro-combined heat and power generation in residential applications, *J. Power Source*, 2006;158:1290-1306.
- [2] M.Hlinen, O.Thomann, J.Kiviaho, Effect of anode off-gas recycling on reforming of natural gas for solid oxide fuel cell systems, *Fuel Cells*,2012;12:754-760.
- [3] M.Andersson, J.Yuan, B.Sunden, SOFC modeling considering hydrogen and carbon monoxide as electrochemical reactants, 2013;232:42-54.
- [4] GRI-MechTM [Internet]. Chicago : gas research institute; c200



DEVELOPMENT OF COMPONENTS FOR SPE ELECTROLYSERS – LAB SCALE TO PILOT SCALE MANUFACTURING

V. Linkov, S Pasupathi, H Su, B Bladergroen
South African Institute for Advanced Materials Chemistry,
University of the Western Cape, Robert Sobukwe Road, Bellville
7535, Cape Town (South Africa)

Abstract - The commercialization of SPE electrolyzers are hindered by its high cost. Two crucial components expected to address this issue are the catalyst and the catalyst coated membrane (CCM). In this study we present the development of these two crucial components, prepared and tested, at lab scale first and then at a pilot scale.

Index Terms –Catalysts, Catalyst coated membranes, Pilot scale, SPE Electrolyser.

I. INTRODUCTION

Catalyst Development

The commercialization of SPE electrolyzers are hindered due to its high cost. Unsupported catalysts are employed so far due to the stability issues of the supports under the operating conditions of the electrolyser. Iridium (Ir) and Iridium (IV) oxide (IrO_2), are well known for their electrocatalytic properties due to their low overpotential for oxygen evolution reaction (OER) but account for a significant part of the electrolyser cost. The study deals with the development of IrO_2 based catalysts with better mass specific activity in order to address part of the cost issue.

CCM development

CCM/MEA (Membrane Electrode Assemblies) is the key component of a SPE water electrolyser with electrochemical reaction taking place at 'triple-phase boundaries', where reactant, electrolyte and electrons are brought together. A high performance MEA for SPE water electrolysis should possess the following characteristics: (1) good adhesion of the catalyst to the membrane; (2) ample triple-phase boundaries where reaction materials, electrolyte and electrically conducted catalysts contact each other; (3) minimum resistivity between the catalyst layer (CL) and the membrane; (4) a structure that allows easy transport of water and gas to and from the

catalytically active zone; (5) a certain percolation path to obtain high electrical conductivity of the layer; (6) easy release of gas bubbles. This study deals with the preparation of the MEA in a novel way to address the various issues mentioned above.

II. RESULTS AND DISCUSSION

A. Catalyst Development

In this study binary metal oxides based on IrO_2 were developed and optimized as anode catalysts for the SPE electrolyser and compared to the 'state-of-art' commercial IrO_2 catalyst. The Adams fusion method was adapted and used to synthesize the catalysts. The activities of the catalysts were determined using half-cell studies. Optimum conditions for the preparation of unsupported IrO_2 catalysts were found to be 350 °C and 2 hours. The resulting catalysts had twice the activity of the 'state-of-art' commercial IrO_2 catalyst. Secondary metals were carefully selected, after carrying out both a literature study and an experimental study. Binary metal oxides were then developed using the optimum synthesis conditions. Four binary metal oxides were studied to identify the best/most efficient catalyst for electrolysis.

The catalysts were characterized using XRD, TEM, SEM and EDS analyses, in efforts to understand and correlate the activity of the catalysts to its physical properties and obtain information that could be useful for the further development of efficient catalysts. Although all the binary metal oxides studied showed improved activity compared to IrO_2 , the catalytic activity of $\text{Ir}_{0.7}\text{Ru}_{0.3}\text{O}_2$ was found to be significantly better (Figure 1) than the commercial catalyst: it was over 5 times more active than the 'state-of-art' commercial IrO_2 catalyst. Ir-Pd mixed oxides also proved to be highly efficient as anode catalysts for SPE electrolyzers.



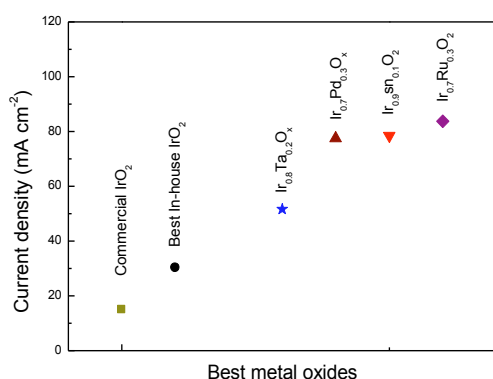


Fig. 1. Peak catalytic activity of the best metal oxide catalysts at 1.8V.

B. CCM Development

MEA is the key component of a SPE water electrolyser with electrochemical reaction taking place at ‘triple-phase boundaries’, where reactant, electrolyte and electrons are brought together. A high performance MEA for SPE water electrolysis should possess the following characteristics: (1) good adhesion of the catalyst to the membrane; (2) ample triple-phase boundaries where reaction materials, electrolyte and electrically conducted catalysts contact each other; (3) minimum resistivity between the catalyst layer (CL) and the membrane; (4) a structure that allows easy transport of water and gas to and from the catalytically active zone; (5) a certain percolation path to obtain high electrical conductivity of the layer; (6) easy release of gas bubbles. A novel CCM method, namely CSMUI [1], was developed to prepare the MEAs for PEMFC, whereby the swelling and distorting of the membrane was greatly reduced during spraying by simultaneously evaporating the solvent under the infrared light.

It is clear from Figure 2 that the MEA prepared by CSMUI method (MEA-1) yields much better performance than the MEA prepared by ordinary catalyst sprayed membrane method (MEA-2) in all regions of the polarization curve. MEA-1 shows lower voltage rise than does MEA-2, which means that the catalyst layer structure of MEA-1 is more effective to enhance the kinetics of OER than that of MEA-2. This is mainly attributable to the instantaneous evaporation of the solvent during MEA-1 preparation, which results in closer adherence of

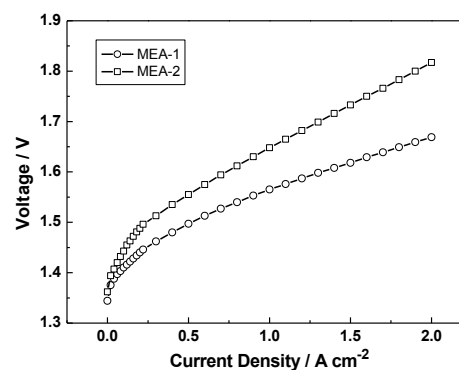


Fig. 2. Performance of MEA-1 as compared to MEA-2.

The ohmic resistance of the SPE cell with MEA-1 is smaller than that of the SPE cell with MEA-2. At the current of 1 A cm^{-2} , the cell voltage of MEA-1 can be as low as 1.564 V, 84 mV lower than that of the MEA-2 (1.648 V). The terminal voltage of MEA-1 is 1.669 V at 2 A cm^{-2} , 148 mV lower than that of the MEA-2 (1.817 V). These values are among the best results yet reported for SPE water electrolysis with IrO_2 catalyst. The MEA performance did not noticeably decline even when the anode IrO_2 loading was decreased from 4 to 1.5 mg cm^{-2} , i.e., the increase in cell voltage at 1 A cm^{-2} was less than 0.7%, but when the IrO_2 loading was decreased from 1.5 to 0.5 mg cm^{-2} , the cell voltage at 1 A cm^{-2} increased sharply from 1.586 to 1.673 V, an increase of 5.5%. This result implies that by using CSMUI method, the anode IrO_2 loading of the MEA could be lowered to as little as $1\sim 1.5 \text{ mg cm}^{-2}$, just one-third of the current $3\sim 5 \text{ mg cm}^{-2}$ loading used by many companies and research institute.

III. CONCLUSION

Catalysts and CCMs with activity and performance on par or better than reported values have been developed and were upscaled from lab to a pilot scale and prototype/s were demonstrated.

ACKNOWLEDGMENT

This work was supported by the South African department of Science and Technology through the Technology Implementation Agency (TIA) project number T70600 (SPE Electrolyser).

REFERENCES

- [1] Xu LM, Liao SJ, Yang LJ, Liang ZX. “Investigation of a Novel Catalyst Coated Membrane Method to Prepare Low-Platinum-Loading Membrane Electrode Assemblies for PEMFCs”. *Fuel Cells* 2009;9(2):101-5.



ENERGY ANALYSIS OF A COGENERATION SYSTEM BASED ON MOLTEN CARBONATE FUEL CELL

D. Chianese*, V. Cigolotti**, M. Minutillo*, E. Graditi**, E. Jannelli*

* Department of Engineering, University of Naples "Parthenope", Centro Direzionale, Naples, Italy;

**ENEA, Portici Research Center, P.le Enrico Fermi, 1 - 80055 Portici Naples, (Italy).

Abstract - In recent years, countries around the world are trying to use high efficiency plants to produce energy with low fuel consumption and consequently low operation costs. The molten carbonate fuel cell (MCFC) power plant is an emerging high efficiency, ultra-clean power generator utilizing a variety of gaseous, liquid and solid carbonaceous fuels for commercial and industrial applications with an electrical efficiency exceeding 45%. Therefore, the high temperature of the exhaust gas exiting from cathode side makes MCFC suited for co-generation. The co-generation system includes processes of production of combined heating and power (CHP) from a single fuel source. This combined solution allows high levels of overall energy efficiency, lower emissions and security of supply. As well as, this solution privileges the reduction of CO₂ emission compared with traditional systems. In this study, either energy or economic (SPB, VAN, TIR) analysis of a co-generation plant based on MCFC technology fed with natural gas is conducted.

Index Terms – Combined Heat and Power generation, Molten Carbonate Fuel Cell, Hospital, Primary Energy Saving, CO₂ reduction.

I. INTRODUCTION

The CHP (combined heat and power) plant is widely considered as the major alternative to traditional generation systems. For this reason, European Union by Directive 2004/8/EC [1] promoted officially the CHP diffusion and development.

Cogeneration systems (CHP) based on molten carbonate fuel cell (MCFC) represent an interesting alternative to traditional CHP technologies to supply efficiently heating and electricity required by an hospital (Figure 1) [2].

A MCFC operates at high temperature, ranging from 550 to 650 °C, so the electrochemical conversion takes place with relatively low thermodynamic losses. Furthermore, the high-temperature heat available could be applied both for thermal energy recovery for additional power.

In this paper, the strategy of control system is thermal load following. The primary energy saving (PES) and the CO₂

emission reduction have been evaluated. The economic analysis has assessed the SPB, VAN and TIR.

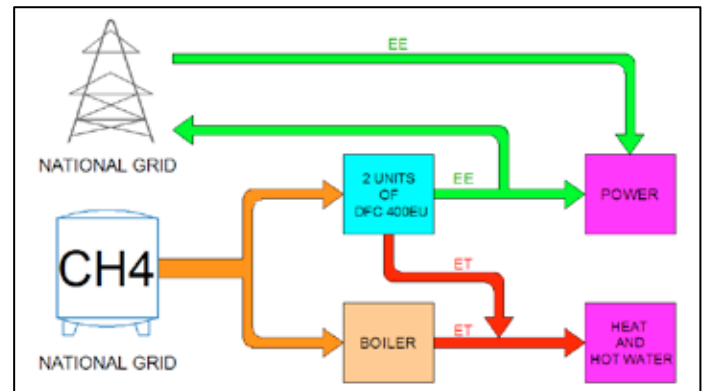


Figure 1: CHP system for a hospital

II. METODOLOGY

A. Load Profiles

The energy demand of a hospital in Naples is the case of study of this paper. The thermal energy takes into account the annual hot water production and the heat for space heating during the cold season. The cooling demand has been converted into electric requirements by using the energy efficiency ratio (EER).

B. System CHP

In this paper, two units of the commercial cogeneration system (CHP) based on the MCFC technology have been analysed. In Table I the main technical and operational CHP specifications are summarized. It has been supposed the temperature of exhaust gas is around 130 °C and the thermal power recovered at this temperature by n.2 MCFC is around 500 kW. Furthermore, the DFC 400EU utilization factor is estimated around 95% out of 8760 hour per year.

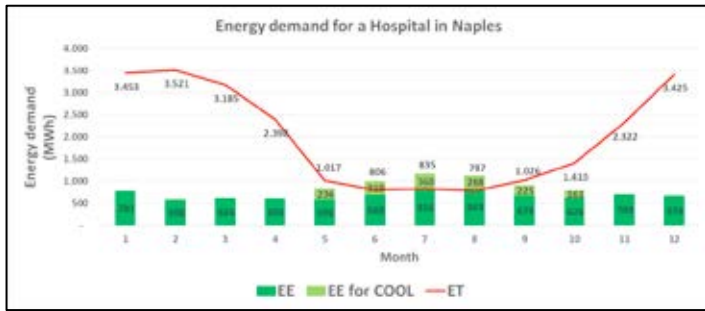


Figure 2: Annual electric and thermal energy demands by the hospital

Table I: DATA SHEET OF MCFC

Temp. Exh (°C)	DFC 400 (kW)	
	Elec. Pow. (kW)	Therm. Pow. (kW)
90	442	280
100	442	275
110	442	265
120	442	260
130	442	250
140	442	240
150	442	237
160	442	230
170	442	220
180	442	210
190	442	200
200	442	190

III. RESULT

A. Energy analysis

Table II shows the annual electric energy demand compared to the electric energy produced by the CHP. It can be noted that the overall electric energy produced by the power system (during the year) is lower than the electric energy required by utility because the CHP operates approximately at maximum load for whole the year.

The electric energy surplus is very low and it is sent to the national grid. The thermal energy demand has to be integrated with a boiler for all year long, while no heat is wasted during whole year.

The following diagram depicts the forecast of CO₂ emission reduction after the DFC 400EU installation, about 38%.

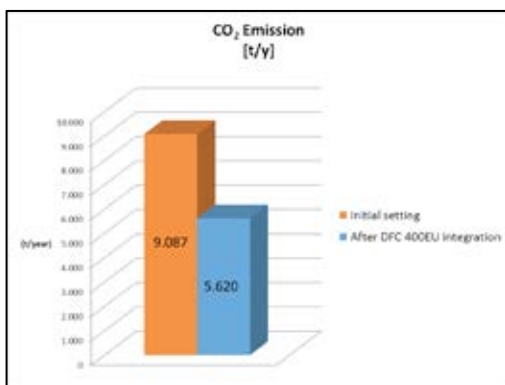


Figure 3: CO₂ emission reduction after the DFC 400EU installation

Table II: electrical and thermal energy balance

Energy	Hospital Demand	x2 DFC 400EU Production	Sent to grid	From grid/Auxiliary boiler	x2 DFC 400EU Dissipated Energy
Electric [MWh/y]	9,813.0	7,356.6	8.4	2,464.8	-
Thermal [MWh/y]	24,184.0	4,161.0	-	20,023.0	-

B. Economic Analysis

The result of the economic analysis is summarized in the table below (Table III).

Table III: economic analysis

Economic Analysis					
Investment [k€]	Annual Saving [k€/year]	Discount Rate [%]	VAN [k€]	IP [%]	SPB [years]
3,735	For the first three years	4%	8,346,5	2,23	8,3
	For the rest of the years				

The Figure 4 shows the cumulative discounted cash flows.

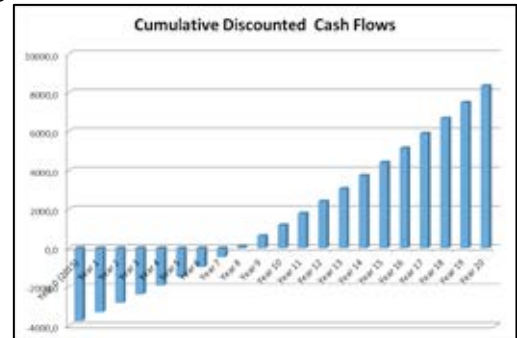


Figure 4: cumulative discounted cash flows

IV. CONCLUSIONS

A confluence of economic factors, including low natural gas prices, government and utility incentives, and low interest rates, are causing an upsurge in the use of CHP applications. A number of conventional and emerging technologies are available for CHP systems. Among them, it is envisioned that fuel cells will serve a variety of CHP applications in the future. This paper presents the analysis of a cogeneration system, using a MCFC system, which meets the energetic demands of a hospital for electricity, heating and hot water. One of the main challenges that MCFC has to face to reach full commercialization is costs reduction and strategic niche management to trial new approaches.

ACKNOWLEDGMENT

This research is supported by the Ministry of Education, Universities and Research Grant PON_03_PE_00109_1 "Fuel Cell Lab"

REFERENCES

- [1] Directive 2004/08/EC of the European Parliament and of the council. Official J Eur Union 21.2.2004: 50 e 60.
- [2] Zabalza I, Aranda A, de Gracia MD. Feasibility analysis of fuel cells for combined heat and power systems in the tertiary sector. International Journal of Hydrogen Energy 2007;32:1396 e 403.



MODELING OF A MW SCALE PEM FUEL CELL POWER PLANT INTEGRATED IN INDUSTRIAL CHLOR-ALKALI PROCESS

G. Guandalini*, S. Foresti*, S. Campanari*, J. Coolegem^o, J. ten Have[^]

*Politecnico di Milano, Energy department, Milano (Italy)

^o Nedstack fuel cell technology B.V., Arnhem (The Netherlands)

[^] MTSA Technopower B.V., Arnhem (The Netherlands)

Abstract - As part of DEMCOPEM-2MW FP7 EU Project, we developed a model of a large scale PEM system coupled with a chlor-alkali plant. Mass and energy balances are performed for the fuel cell and auxiliaries, in order to assess efficiency and streams' conditions at partial load or changing operating parameters. Preliminary results are in agreement with data from reference plants and show the effectiveness of the model.

Index Terms - chlor-alkali plant, DEMCOPEM-2MW, hydrogen recovery, PEM fuel cell

I. NOMENCLATURE

BOL	Beginning of Life
EOL	End of Life
PEM FC	Polymeric Electrolyte Membrane Fuel Cell

II. INTRODUCTION

Scale up of stationary power plants based on PEM fuel cells is an ongoing process with many open challenges. This work presents the modeling of a 1 MW PEM fuel cell power plant. Model validation is based on data from existing plants, and will be used for the scale-up of the plant to 2MW, following the expected design developed within the European project *DEMCOPEM-2MW*. The final goal of the project is the construction of a demonstration plant, coupled with a chlor-alkali process, receiving hydrogen (a process byproduct) at site conditions and cogenerating heat for the chemical plant. A model is developed in order to optimize the operating point of the plant and to assess the effectiveness in recovering heat and in converting hydrogen into electricity.

The simulation is developed with ASPEN Plus[®], with particular attention to incorporate the physical processes of the PEM fuel cell and predicting the behavior of the stacks depending on the operating parameters and stream conditions.

The model is calibrated and validated based on available data from (i) a 70 kW PEM installation operating in AkzoNobel's

plant in Delfzijl [1], where Nedstack PEM fuel cell stacks of the same class used in the projected plant are being tested; and from (ii) a 1 MW PEM plant in Lillo (Belgium), developed by Nedstack and MTSA with a layout similar to the design of DEMCOPEM-2MW plant.

III. PLANT MODELING

The model considers the plant layout with all main auxiliaries (e.g. saturators, heat exchangers, blowers, pumps), as summarized by Fig. 1.

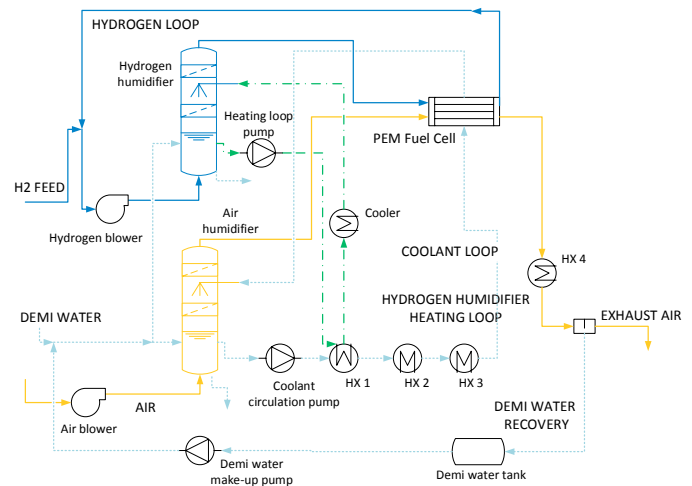


Fig. 1 - Simplified plant layout (1MW)

Blower performance curves are included in the model, as well as lumped descriptions of heat exchangers. Feeding and recirculated flows are controlled to maintain desired reactants stoichiometry in the fuel cell, while coolant flow controls the temperature. Fuel cell section is arranged in groups of stacks operated in parallel (feed streams and electrical connections) in order to reach the desired total power. General mass and energy

balances are calculated and expected efficiencies, auxiliaries consumption, pressure drops and components operating conditions are calculated.

IV. FUEL CELL MODELING

A lumped customized model of the fuel cell is developed for the purpose, reflecting both modular characteristics and differences in operating conditions among the modules. The model is designed also to analyze the off-design operation, taking into account variations in the cell stoichiometry as well as the influence of cell performance decay. The analytical formulation of the polarization curve [2] adopted for single cells can be summarized in the voltage (V) vs. current density (i , A/cm²) expression:

$$V(i, x_H, x_O) = A + B \ln\left(\frac{x_{H_2}}{x_{H_2, st}}\right) + C \ln\left(\frac{x_{O_2}}{x_{O_2, st}}\right) + Di + E \ln\left(\frac{i}{i_0} + 1\right) + F \ln\left(1 - \frac{i}{i_L}\right) \quad (1)$$

Where stoichiometry effects are taken into account through species molar fractions x_i . Coefficients A , B , C , D and E , as well as exchange and limiting current densities i_0 and i_L are regressed on experimental data. An example is presented in Fig. 2.

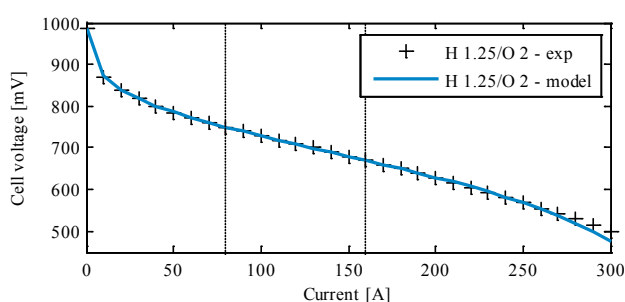


Fig. 2 - Example of regressed polarization curve for a given stoichiometry at BOL

Because of a dependence of exchange and limiting current on stoichiometry when going towards EOL, they are calculated as linear functions of reactants molar fractions.

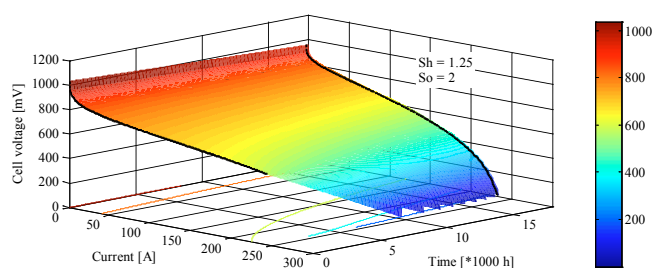


Fig. 3 - Regressed polarization curves as function of current and time

Moreover, linear decay of cell performance is considered between the available dataset; Fig. 3 shows the resulting operating map for a given stoichiometry. Accordingly, it is possible to evaluate the performances and optimize the plant

operating point during lifetime, while maintaining the required electric output.

V. RESULTS

Stack performances at BOL are estimated within a 1% tolerance with respect to available experimental data. Tables 1 and 2 report stream results and general performances of the simulated 1MW plant.

TABLE 1
SIMULATED STREAMS CONDITIONS

	T °C	Flow rate Nm ³ /hr
Hydrogen to stacks (dry)	50	1200
Recirculated hydrogen (dry)	65	600
Air to stacks (dry)	63	3450
Coolant (FC inlet/outlet)	60/65	165
Water loop (Hum inlet)	50	60

TABLE 2
MODELING RESULTS

Gross DC electric power	kW	1040
Gross DC efficiency (H ₂ LHV basis)	%	57.7
Recovered heat	kW	522
Auxiliaries consumption	kW	67

Humidified hydrogen and air are fed to the stacks in a quantity higher than the stoichiometric (2.0 and 2.4 respectively). Heat recovery from FCs to the chlor-alkali plant is about 500kW. Gross efficiency of the FCs is close to 60% on H₂ LHV. Main auxiliaries total consumption is ~67 kW, mostly concentrated on air and hydrogen blowers, followed by coolant pumps and inverter systems.

VI. CONCLUSION

Simulation results confirm the general validity and physical coherence of the plant model, supporting a further extension to long-term performance evaluation and optimization of balance of plant design and set points. The modelling process evidenced relevant parameters that influence costs and performances, useful for next step decisions related to the technology deployment and further scale-up.

ACKNOWLEDGEMENTS

This work was carried out in the framework of the FP7-FCH-JU project "DEMCOPEM-2MW", cofounded by the FCH JU under grant agreement n° 621256.

REFERENCES

- [1] Verhage A., Coolegem J. *et al.*, "30,000 h operation of a 70 kW stationary PEM fuel cell system using hydrogen from a chlorine factory", *Int J of Hydrogen Energy*, 38(11), 2013
- [2] Anon. "Fuel cell handbook", 7th ed., EG&G Services, Inc., U.S. Department of Energy, Nov. 2004.



VANADIUM-CERIA CATALYSTS FOR H₂S ABATEMENT FROM BIOGAS TO FEED TO MCFC

V. Palma, D. Barba

University of Salerno, Giovanni Paolo II 132, Fisciano, (Italy)

Abstract –

Vanadium-based catalysts supported on ceria were studied for the direct and selective oxidation of H₂S to sulfur and water at low temperature. Catalysts with different vanadium loading (2.55-50wt%) were prepared, characterized and tested at temperature of 150-200°C. The most promising catalyst was the sample with the highest Vanadium oxide load (20 wt%) that showed 99% of sulfur selectivity and equilibrium conversion at 150°C.

The effect of the components of a typical biogas stream (CH₄, CO₂ and H₂O) was studied at 150°C in order to investigate the possible formation of secondary products such COS, CS₂.

No significant effect was observed in terms of H₂S conversion (99%) and selectivity to SO₂ (<1%) by adding CH₄ and CO₂ to the feed stream.

A slight increase of the SO₂ selectivity (>1%) was obtained by adding water to the feed stream.

Index Terms -Biogas Clean-Up, H₂S catalytic oxidation, Vanadium-based catalysts.

I. INTRODUCTION

Biogas is produced by the anaerobic digestion fermentation of biodegradable materials such as biomass, manure, sludge. It comprises primarily methane, carbon dioxide and small amounts of hydrogen sulfide (H₂S).

Today it can be used for energy production in unconventional systems as the molten carbonate fuel cells (MCFC) but the removal of H₂S from biogas is needed [1].

The main limitation to the utilization of the biogas as fuel for MCFC is represented by the poisoning of the anode, of the electrolyte by sulfur based compounds (H₂S, COS) that are always present in biogas [1].

H₂S can be removed by different traditional physical-chemical treatments, characterized by high costs and a limited overall efficiency [2].

The selective catalytic oxidation of H₂S to elemental sulfur may be an interesting alternative to the traditional processes if a good catalyst is allowable. In our previous works vanadium-based catalysts supported on different metal oxides were investigated in the temperature range of 50–250°C [3]. Among the others, the ceria supported catalyst showed the best catalytic

performances at 150–250°C with a moderate selectivity to SO₂ (13%).

In addition, the effect of the vanadium loading between 2.55-50 wt% was also studied in order to minimize the SO₂ selectivity [4]. The most promising catalyst was the sample with the Vanadium oxide load of 20 wt% that showed 99% of sulfur selectivity and equilibrium conversion at 150°C.

The aim of this work is to investigate the influence of the components of a typical biogas stream (CH₄, CO₂ and H₂O saturated at room temperature) on the reaction mechanism at 150°C, evaluating also the possible formation of undesired products such COS, CS₂.

II. EXPERIMENTAL RESULTS

A. Materials and Methods

The catalyst with a V₂O₅ loading of 20 wt% supported on cerium oxide was prepared by wet impregnation of the salt precursor (NH₄VO₃) on CeO₂.

The catalyst was dried at 120 °C overnight, and finally calcined in a muffle furnace at 400 °C for 3 h.

Catalytic tests were carried out using the experimental setup shown in our previous works to which have been added the feed streams of CH₄, CO₂ and H₂O [5].

Experimental tests were carried out at atmospheric pressure and GHSV of 98,000 h⁻¹ (~40 ms), at temperature of 150°C, with 500 ppm of H₂S, 250 ppm of O₂, 37.4 vol% CH₄ and CO₂, N₂ to balance. The elemental Sulphur produced during the reaction mainly remains on the surface of the catalyst; the small residual in gas phase is separated from the stream by condensation at the reactor outlet.

The H₂S conversion (xH₂S) and the SO₂ selectivity (ySO₂) were calculated by using the following equations (Eq. 1-2), by considering negligible the gas phase volume change:

$$x_{H_2S}, \% = ((H_2S_{IN} - H_2S_{OUT}) / H_2S_{IN}) \cdot 100 \quad (\text{Eq. 1})$$

$$y_{SO_2}, \% = SO_{2OUT} / (H_2S_{IN} - H_2S_{OUT}) \cdot 100 \quad (\text{Eq. 2})$$

B. Catalytic Activity Test

The effect of the CO₂ concentration on the catalytic activity is shown in Figure 1.

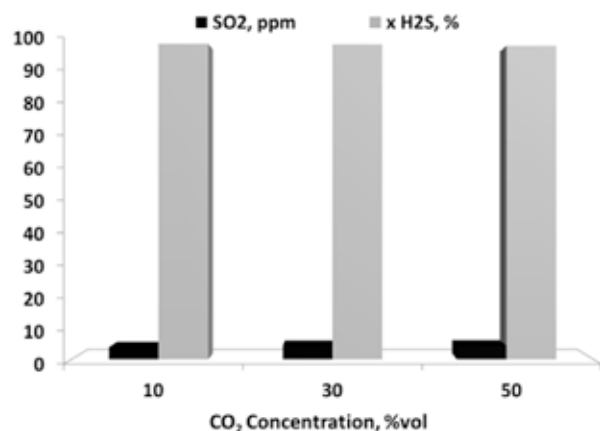


Fig.1: Influence of the CO₂ concentration on H₂S conversion and SO₂ formation at 150°C (H₂S=500 ppm, O₂/H₂S=0.5).

It is possible to observe no significant variation of the H₂S conversion (99%) and SO₂ concentration (2 ppm) by varying the CO₂ concentration in the feed stream between 10 vol% and 50 vol%.

The joint effect of the CH₄ and CO₂ is reported in Figure 2, where the concentration profiles of H₂S, SO₂, are reported as function of time.

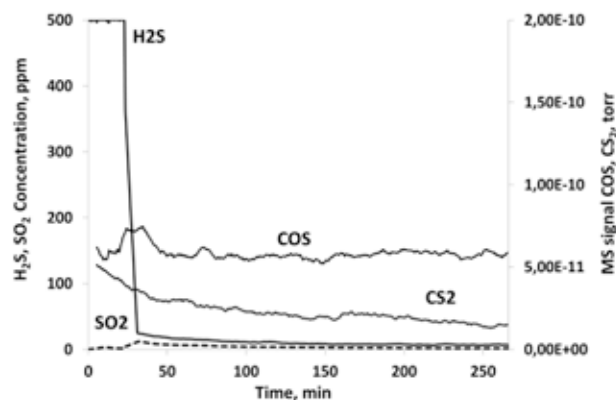


Fig.2: Catalytic activity test in presence of CH₄ (37.4vol%), CO₂ (37.4vol%) at 150°C (H₂S=500 ppm, O₂/H₂S=0.5).

The feed stream, after 30 minutes in by pass position, is sent to the reactor. The concentration values of H₂S and SO₂ reach a stationary value after 10 minutes of time on stream. The final H₂S conversion value was 99% with a SO₂ selectivity very low (<1%). The low intensity of the MS signal ascribable to COS, CS₂ evidence no formation of these undesired compounds.

In Figure 3 is showed the catalytic activity test in presence of H₂O.

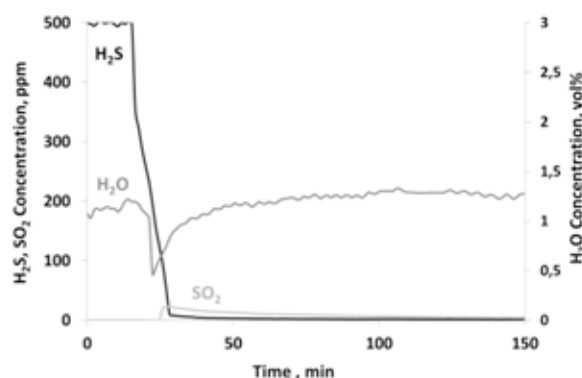


Fig.3: Catalytic activity test in presence of H₂O (1.3vol%) at 150°C (H₂S=500 ppm, O₂/H₂S=0.5).

From the results obtained, it was observed only a slight increase of the SO₂ concentration (4 ppm), corresponding to the selectivity value greater of 1%.

III. CONCLUSION

The 20% V₂O₅/CeO₂ catalysts was prepared, characterized and tested for the H₂S oxidation reaction at low temperature.

The influence of the components of a typical biogas stream on the reaction mechanism was studied at 150°C.

No formation of undesired products such COS, CS₂ was observed in presence of CH₄ and CO₂ in the feed stream, obtaining a almost total sulfur selectivity (99%) and equilibrium H₂S conversion.

The presence of the water as moisture has slightly influenced the SO₂ formation, likely due to the possible oxidizing effect of the H₂O.

ACKNOWLEDGMENT

This work was performed and financed in the framework of the Italian MSE-ENEA research agreement "Sviluppo di sistemi per la produzione di energia elettrica da biomasse e l'upgrading dei biocombustibili" (Piano Annuale di Realizzazione 2014).

REFERENCES

- [1] Ciccoli, R. Cigolotti, V., Molten carbonate fuel cells fed with biogas: combating H₂S, Waste Management, Volume 30, 2010, pp. 1018-1024.
- [2] Abatzoglou, N., Boivin, S., A review of biogas purification processes, Biofuels, Bioprod. Bioref., Volume 3, 2009, pp. 42-71.
- [3] Barba D., Palma V., Ciambelli P., Screening of catalysts for H₂S abatement from biogas to feed molten carbonate fuel cells, Int. Hydrogen Energy, Volume 38, 2013, pp. 328-335.
- [4] Palma, V., Barba, D., Ciambelli, P., Selective oxidation of H₂S to sulphur from biogas on V₂O₅/CeO₂ catalysts, Chem Eng Trans, Volume 32, 2013, pp. 631-636.
- [5] Palma, V., Barba, D., H₂S purification from biogas by direct selective oxidation to sulfur on V₂O₅-CeO₂ structured catalysts, Fuel, Volume 135, 2014, pp. 99-104.



COUPLING SOLID OXIDE ELECTROLYSER (SOE) AND AMMONIA PRODUCTION PLANT

G. Cinti*, D. Frattini**, U. Desideri***, E. Jannelli**, R. Cioffi**, G. Bidini*

*Università degli Studi di Perugia, via Duranti 66, 06125 Perugia, (Italy)

** University of Naples 'Parthenope', Centro Direzionale Napoli, Isola C4, 80143 Naples, (Italy)

*** Department of Energy, Systems and Constructions Engineering, University of Pisa, Largo L. Lazzarino, 56122 Pisa (Italy)

Abstract - Solid Oxide Electrolyser (SOE), can operate with high efficiency as hydrogen produce using renewable energy coming from renewable energy source (RES). This technology can be integrated in many industrial plant reducing the requirement of traditional fossil sources and increasing the sustainability of the process. In addition, if an heat source is available at high temperature, SOE get additional advantage in terms of efficiency. This study presents the integration of a SOE in an ammonia synthesis plant evaluating the advantages that can be achieved in terms of environmental benefits.

Index Terms – Ammonia synthesis, Energy storage, Solid Oxide Electrolyzer, sustainable production

I. INTRODUCTION

Recent development of Solid Oxide Fuel Cells (SOFCs) brought novel interest on high temperature Solid Oxide Electrolyser (SOE), based on the same materials and design [1,2]. SOEs, compared to traditional electrolyser, operate with high power density and efficiency, especially if fed with high temperature waste heat, because the electrochemical conversion of water permits to store both heat and electricity in the produced hydrogen (H_2) [3]. Such application is currently under study in industrial processes where waste heat recovery at high temperature is possible. For example, the coupling is possible with nuclear power plants [4], where heat is usually a by-product, or with solar field panel collectors in solar thermal power plants, where renewable heat comes from the sun. The coupling of SOE and ammonia (NH_3) production plants concept is presented in this study. Ammonia is one of the most produced chemical of the world and is usually based on natural gas as

primary feedstock causing CO_2 emission and fossil source consumption. The NH_3 synthesis is an exothermic chemical reaction at relative high temperature and pressure, thus in the energy balance of the plant, a large amount of heat is available for recovery. Moreover, this integration has a potential double-sided advantage by the fact that the produced H_2 can be used as feed for NH_3 production, if mixed with a proper amount of nitrogen, without consuming fossil hydrocarbons. A thermodynamic simulation of a system integrating a SOE and an NH_3 plant, operated at high pressure (250-300 bar) and temperature (550-600°C) have been carried out. The effect of coupling on the global efficiency, and on avoided CO_2 emissions are evaluated. The feasibility of ammonia production from renewable energy via electrolysis of water is of fundamental importance to pursue sustainable chemistry with the respect to the environment. This work can enhance the development of green ammonia concept and can offer, at the same time, an interesting application for SOE technology and relative market diffusion.

II. THEORY

Ammonia synthesis is realized, at industrial level, mainly with the design developed by Haber and Bosh (HB). In such loop ammonia reactor operates at 650°C and 250 atm. Selected temperature is the highest that can be accepted and, at the same time, is the lowest that is possible to consider in a SOE at present stage of development. Figure 1 depicts the HB loop as designed in Aspen.



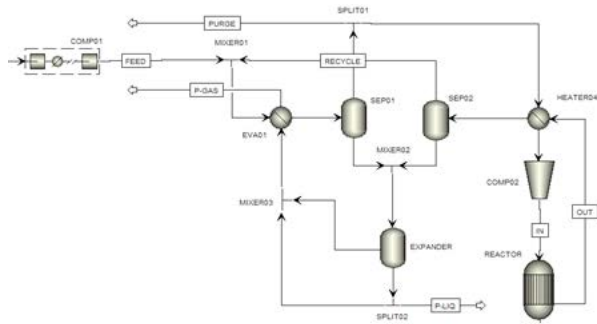
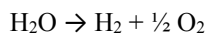
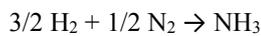


Figure 1 Haber Bosh loop simulated in Aspen

Electrolysis reaction is the following;



While ammonia synthesis is:



Thermodynamic values at 650°C are reported in Table 1.

	ΔH [Kj/mol]	$T\Delta S$ [Kj/mol]	ΔG [Kj/mol]
Electrolysis	247,03	49,57	197,46
Ammonia	-63,841	-136,24	72,40

Table 1 Thermodynamic values of involved reactions

Results show how ammonia reaction can supply even more than the energy required by electrolysis reaction considering that for each ammonia synthesis, 1,5 moles of hydrogen are required. To perform a complete study of energy flows a simple linear model for the SOEC unit can be realized using an area specific resistance of 0.57 ohm cm². Typical SOE energy flows are reported in Figure 2 where PH2 is the enthalpy flow of produced hydrogen, Pe the electrical power input and Eff the efficiency calculated as the ratio between the two values. Thermoneutral point (PH2=Pe) is obtained at $j_m=450$ mA/cm².

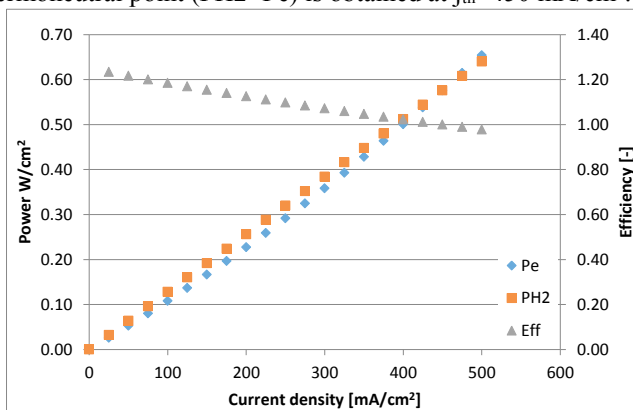


Figure 2 Energy flows in a SOE

In detail in Figure 3 are reported: the heat duty (DH=PH2-Pe) necessary to get thermal stability of the SOE and the heat

available from ammonia synthesis reaction enthalpy (DHNH3). The values of DHNH3 are normalized for the relative moles of produced H₂ (each mole of hydrogen produced participates to 2/3 of NH₃ synthesis). The results confirm that ammonia can supply all the heat required to operate SOE, even before thermoneutral point.

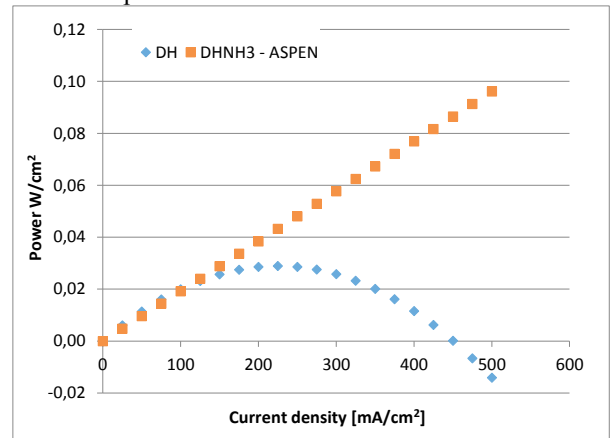


Figure 3 Energy balance of electrolysis and ammonia synthesis

III. CONCLUSION

The preliminary evaluations show that the heat production of HB process can be used to feed SOE process increasing electrical efficiency above 100% with direct transformation of heat into chemical energy.

REFERENCES

- [1] Ferrero D, Lanzini A, Santarelli M, Leone P. A comparative assessment on hydrogen production from low- and high-temperature electrolysis. *Int J Hydrogen Energy* 2013;38:3523–36.
- [2] Laguna-Bercero M a. Recent advances in high temperature electrolysis using solid oxide fuel cells: A review. *J Power Sources* 2012;203:4–16.
- [3] Penchini D, Cinti G, Discepoli G, Desideri U. Theoretical study and performance evaluation of hydrogen production by 200 W solid oxide electrolyzer stack. *Int J Hydrogen Energy* 2014;39:9457–66.
- [4] O'Brien JE, McKellar MG, Harvego E a., Stoots CM. High-temperature electrolysis for large-scale hydrogen and syngas production from nuclear energy – summary of system simulation and economic analyses. *Int J Hydrogen Energy* 2010;35:4808–19.



EFFECT OF FLOW CHANNEL SIZE ON CARBON DIOXIDE AND PRODUCT WATER EXHAUSTS IN A SMALL DIRECT METHANOL FUEL CELL

Kohei Nakashima*, Hirokazu Shimizu*, and Ryuta Inagaki *

*Meijo University, 1-501 Shiogamaguchi, Tempaku-ku, Nagoya, Aichi 468-8502, (Japan)

Abstract - This study visualized carbon dioxide and product water exhausts from a transparent direct methanol fuel cell (DMFC) with an active area of 4 cm² and serpentine through-channels. We tested separators with a fixed channel width but two different channel depths in both the anode and the cathode of the DMFC, investigating the effect of flow channel size on the cell's exhausts and power performance. Results indicate that a shallower anode channel facilitated the ejection of bubbles of carbon dioxide, increasing power performance. Similarly, a shallower cathode channel emitted more droplets of product water, but hardly changed power performance. Finally, shallower anode and cathode channels together increased exhaust of both carbon dioxide and product water, thus increasing power performance.

Index Terms – Carbon Dioxide Exhaust, Direct Methanol Fuel Cell, Flow Channel Size, Product Water Exhaust

I. INTRODUCTION

When a direct methanol fuel cell (DMFC) generates electricity by electrochemical reaction, it produces carbon dioxide in the anode and water in the cathode. To generate electricity stably, a DMFC must effectively exhaust this carbon dioxide and product water. Despite extensive research on DMFCs [1], no full reports have observed these exhausts in a transparent DMFC with smaller flow rates of methanol solution and air, applicable to powering portable electronic devices. This study visualized carbon dioxide and product water exhausts, by first constructing a transparent DMFC, with serpentine through-channels, and an active area of 4 cm². For our experiments, we then installed separators with two different channel depths (1.2 and 2.0 mm) and a fixed channel width (2.0 mm) in both the anode and the cathode of our DMFC. We finally examined the exhausts of carbon dioxide from the anode channel and product

water from the cathode channel, as well as power performance, all as functions of the flow channels size and the flow rates of methanol-water solution and air.

II. EXPERIMENT

The transparent DMFC (with an active area of 4cm²) comprised a membrane electrode assembly (MEA), gaskets, separators, gaskets with serpentine channels, and end plates. In the MEA, a solid polymer electrolyte membrane (Nafion 112) with a thickness of 50μm was coated on either side with catalyzed electrodes which were supported with gas diffusion layers made of carbon paper (Toray TGP-H-120) with a thickness of 0.37mm. For the anode catalyst layer, loading of platinum/ruthenium was 3mg/cm², and for the cathode catalyst layer, loading of platinum was 1mg/cm². The separator was made of carbon, and had a serpentine through-channel with a width of 2.0mm and a thickness (channel depth) of either 1.2mm or 2.0mm. The anode end plate was made of vinyl chloride; the cathode end plate, acrylic.

Cell temperature was set at 60°C. Methanol solution (3wt%) successively supplied at ratios of 1 and 2, and air at ratios of 1, 2, and 5 (times the stoichiometric flow rates at 250mA/cm²). The methanol solution was supplied in an upward flow, and air in a downward flow. During our experiments, we plotted polarization curves by measuring the DMFC voltage while increasing the current density in increments of 1.25mA/cm². When the DMFC voltage dropped below 0.4V, we then used a video camera to observe carbon dioxide in the anode channel and product water in the cathode channel, as we continued to increase the current density in increments of 1.25mA/cm² every five minutes.

III. RESULTS AND CONSIDERATION

Figure 1 shows the effect of anode channel depth on carbon dioxide exhaust, with a cathode channel depth of 2.0 mm, a methanol solution supply ratio of 1, and an air supply ratio of 5. With the deeper anode channel of 2.0 mm, bubbles of carbon dioxide more frequently coalesced in the channel near the inlet, these bubbles enlarged, and then tended to grow stagnant. In contrast, with a shallower anode channel of 1.2 mm, bubbles of carbon dioxide did not coalesce in the channel near the inlet, but instead were more frequently ejected, increasing power performance at a methanol solution supply ratio of 1.

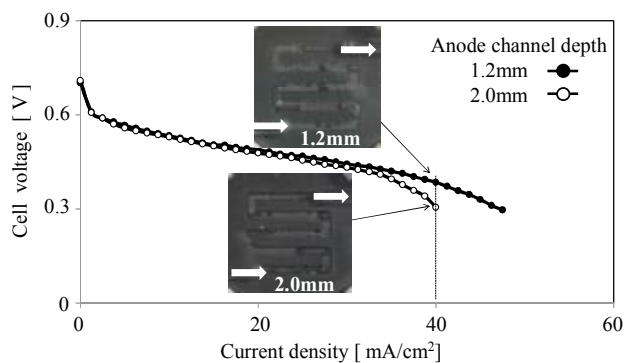


Fig.1 Effect of anode channel depth on carbon dioxide exhaust, with a cathode channel depth of 2.0 mm, a methanol solution supply ratio of 1, and an air supply ratio of 5

However, not shown in a figure, in the combination of anode channel depth of 1.2mm and cathode channel depth of 2.0mm, as methanol solution supply ratio increased, smaller bubbles appeared in the anode channel, suggesting improved exhaust, yet power performance decreased. It seems in this combination of a shallower anode channel with a deeper cathode channel, when the methanol solution supply ratio increased, excess methanol is supplied against air, and then crossover occurs, decreasing power performance.

Figure 2 shows the effect of cathode channel depth on product water exhaust, with an anode channel depth of 2.0 mm, a methanol solution supply ratio of 1, and an air supply ratio of 2. As the cathode channel depth decreased, droplets of product water were more frequently emitted, yet power performance hardly changed. Evidently, with a deeper anode channel, the methanol solution supply ratio has a minimum effect on power performance.

Finally, Fig. 3 shows the effect of cathode channel depth on product water exhaust, with an anode channel depth of 1.2 mm, a methanol solution supply ratio of 1, and an air supply ratio of 2. Again, when the cathode channel depth decreased, droplets of product water were more frequently emitted, yet power performance hardly changed, with a methanol solution supply ratio of 1. Evidently, product water exhaust has minimal effect on power performance.

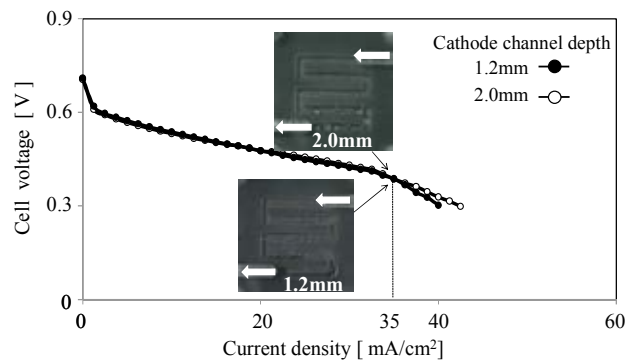


Fig.2 Effect of cathode channel depth on product water exhaust, with an anode channel depth of 2.0 mm, a methanol solution supply ratio of 1, and an air supply ratio of 2

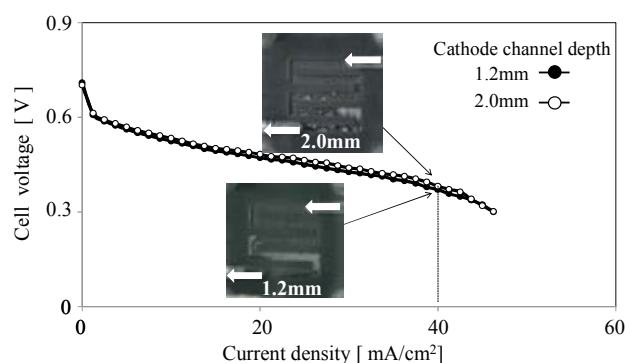


Fig.3 Effect of cathode channel depth on product water exhaust, with an anode channel depth of 1.2 mm, a methanol solution supply ratio of 1, and an air supply ratio of 2

Therefore, shallower channel depths in both anode and cathode increased exhausts of both carbon dioxide and product water, and so increased power performance with both methanol solution supply ratios.

IV. CONCLUSION

Utilizing a small transparent DMFC with different channel depths of separators, we investigated the effect of flow channel size on carbon dioxide and product water exhausts as well as power performance. Our major results follow:

(1) A shallower channel depth in the anode increased carbon dioxide exhaust and power performance. But the combination of a shallower anode channel depth with a deeper cathode channel depth decreased power performance at a higher methanol solution ratio.

(2) A shallower channel depth in the cathode increased product water exhaust, but hardly changed power performance.

REFERENCES

- [1] Argyropoulos, P., Scott, K., Taama, W. M., Gas Evolution and Power Performance in Direct Methanol Fuel Cells, Journal of Applied Electrochemistry, 29, 1999, pp. 661-669.



PERFORMANCE CHARACTERIZATION OF A NOVEL SORBENT FOR ANAEROBIC GAS DESULFURIZATION FINALIZED TO HIGH TEMPERATURE FUEL CELL APPLICATIONS

L. Barelli*, G. Bidini*, E. Hernández Balada**, J. Mata Álvarez**, E. Sisani*

* Department of Engineering, University of Perugia, via Duranti 93, 06125, Perugia (Italy)

**UCL, University of Barcelona, Martí i Franquès 1,08028, Barcelona (Spain)

Abstract - A novel sorbent (SCX) composed of mixed iron oxides and hydroxides was studied to assess its suitability for H₂S removal from biogas finalized to high temperature fuel cell systems. From an industrial point of view, the potential usage of this product would have a beneficial impact on operational costs, since it is less expensive than activated carbons, and on environment, because of its non-hazardous and landfilled spent product.

Sorbent SCX was tested in different operative conditions, evaluating the influence on adsorption capacity of gas hourly space velocity (GHSV), gas composition (inlet H₂S concentration, gas matrix, humidity), reactor temperature and filter geometry. As main outcomes, the experimentation highlighted a hyperbolic increase of adsorption capacity at GHSV decreasing, its parabolic enhance with temperature and a negative effect of humidity. Moreover, a H₂S adsorption capacity higher than the ones obtained for alkali or metal impregnated activated carbons was estimated for GHSV < 330 h⁻¹.

Index Terms – Desulphurization, Biogas, Iron oxide, Fuel cells.

I. NOMENCLATURE

ACs activated carbons; C_{ads} adsorption capacity; D filter diameter; GHSV gas hourly space velocity; h filter height; ID reactor inner diameter; R.H. relative humidity; T temperature.

II. INTRODUCTION

High temperature fuel cells represent an attractive opportunity for energy production, due to their high efficiency, low environmental impact and fuel flexibility. The possibility to use biogas as renewable energy source leads to enormous advantages in terms of fossil fuels saving and lower carbon emissions. However, biogas contains many sulfur impurities, mainly constituted by hydrogen sulfide (typically 100-1000 ppmv), that are detrimental for high temperature fuel cell anode, causing nickel sulfide formation and consequently fuel

cells long term degradation (tolerance limit < 1 ppmv) [1]. Among the existing desulfurization methods, adsorbent materials are unique in achieving outlet H₂S concentrations below 1 ppmv, using simple reactors with very high removal efficiency [2].

SCX, a novel sorbent constituted by mixed iron oxides and hydroxides, was tested in different operative conditions, evaluating the effect on adsorption capacity of the following parameters: GHSV in the range 250-20,000 h⁻¹, inlet H₂S concentration (200, 1000 ppmv), temperature (16-90°C), humidity (R.H. up to 90%), gas matrix composition (N₂, CH₄/CO₂) and filter geometry (in terms of h/D). SCX performance was also compared with the activity of impregnated (Cu-Cr or KOH) activated carbons, in order to identify the optimal GHSV values for a superior adsorption capacity.

III. EXPERIMENTAL

Breakthrough tests were carried out in a fixed bed flow reactor made of quartz (ID 18 mm, length 200 mm) provided with temperature control up to 300°C. Outlet H₂S concentration was detected using an electrochemical sensor. Breakthrough times t₀ and t₁, related to the last detection of 0 ppmv and to 1 ppmv of outlet H₂S concentration respectively, were used to calculate filter adsorption capacity, in terms of mg of H₂S removed for g of used sorbent material.

SCX pellets (bulk density 850 g/dm³) were ground and sieved in the range 250-355 μm. SCX virgin sample was characterized through nitrogen adsorption-desorption measurements at 77K (B.E.T. method), evidencing a low B.E.T. surface area (21 m²/g) and the absence of micropores.

The inlet gases were N₂ or CH₄/CO₂ containing H₂S in concentration from 100 to 1000 ppmv. To evaluate the effect of humidity, wet inlet mixtures (R.H. 50% or 90%) were fed to the



filter. Two reactor geometries were considered, characterized by h/D equal to 0.32 ($h/D < 1$) and 1.32 ($h/D > 1$) respectively; in the first case, 1.25 g of sorbent was used for the adsorption runs.

IV. RESULTS AND DISCUSSION

The variation of sorption capacity as function of GHSV was studied in the range 1000-20,000 h^{-1} for an inlet H_2S concentration of 200 ppmv and in the range 250-1875 h^{-1} for 1000 ppmv H_2S (operating conditions: N_2 dry matrix, T 30°C, h/D 0.32). In both cases, the experimental results showed a significant increase of sorption capacity as GHSV decreased, following hyperbolic behaviors, whose explicit functions were calculated using the least squares method (Fig. 1).

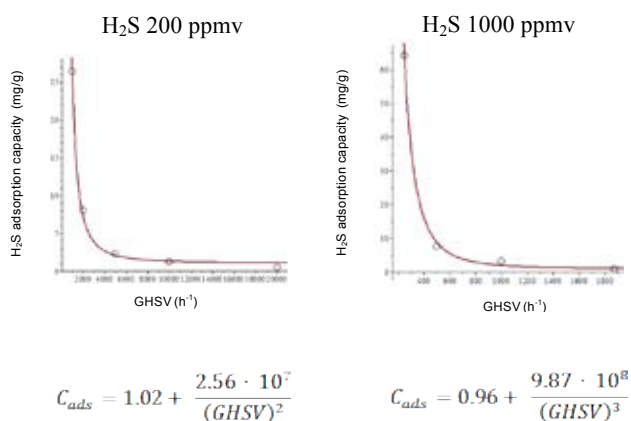


Fig. 1. Effect of GHSV on H_2S sorption capacity: experimental points and hyperbolic curves obtained using the least squares method

A significant increase in sorption capacity was registered for GHSV lower than 1000 h^{-1} (H_2S 1000 ppmv): in particular, for GHSV equal to 250 h^{-1} , the sorption capacity reached the value of 64.27 mg/g. SCX performance (H_2S 200 ppmv) was compared with two commercial Cu-Cr and KOH treated activated carbons (ACs), whose behavior in terms of GHSV variation was studied using the least squares method. Intersecting the corresponding hyperbolic curves obtained in the same operative conditions, it may be predictable that SCX sorption capacity will be higher than those of ACs for GHSV values lower than 330 h^{-1} (corresponding to an expected sorption capacity of 240 mg/g).

Reactor temperature significantly affected filter performance: SCX sorption capacity increased going from room temperature (about 16°C) to 90°C revealing a parabolic behavior, due to an enhancement of the involved chemical reactions (Fig. 2).

The presence of humidity in the inlet gas mixture had a negative effect on SCX performance (Tab. 1), while, simulating a biogas matrix composed of CH_4 60% and CO_2 40%, a three times sorption capacity improvement was observed (Tab. 2).

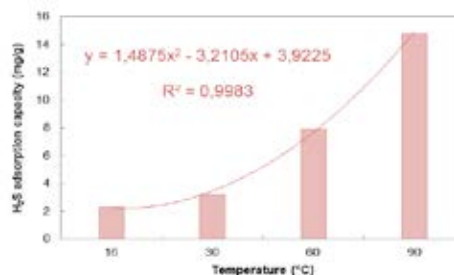


Fig. 2. Effect of temperature on H_2S sorption capacity (N_2 dry matrix, H_2S 1000 ppmv, GHSV 1000 h^{-1} , h/D 0.32)

Tab. 1. H_2S sorption capacity variation as function of R.H. (N_2 matrix, T 45°C, H_2S 100 ppmv, GHSV 10,000 h^{-1} , h/D 0.32)

R.H. (%)	t_0 (h)	t_1 (h)	C_{ads} (mg/g)
0	1.167	1.467	2.62
50	0.383	0.483	0.86
90	0.267	0.300	0.54

Tab. 2. H_2S sorption capacities calculated for N_2 and simulated biogas matrix (T 45°C, H_2S 100 ppmv, GHSV 10,000 h^{-1} , R.H. 0%, h/D 0.32)

Gas matrix	t_0 (h)	t_1 (h)	C_{ads} (mg/g)
N_2	1.167	1.467	2.62
CH_4 (60%)/ CO_2 (40%)	3.767	4.483	8.00

Regarding filter geometry (N_2 dry matrix, T 30°C, H_2S 1000 ppmv, GHSV 1000 h^{-1}), the configuration characterized by h/D 1.32 presented higher sorption capacity (7.11 mg/g) than for h/D 0.32 (3.18 mg/g). This behavior can be attributed to a better gas distribution inside the filter for geometries $h/D > 1$. Different shapes of the related breakthrough curves were also observed (higher slope for $h/D > 1$ configuration).

V. CONCLUSIONS

The experimentation highlighted that SCX activity can be enhanced lowering space velocity, increasing reactor temperature, diminishing humidity content and using a filter geometry characterized by $h/D > 1$. In particular, for GHSV lower than 330 h^{-1} (H_2S 200 ppmv), SCX performance is greater than the ones of modified ACs typically used for the same purpose. The expected SCX sorption mechanisms is the reaction between iron oxides/hydroxides and H_2S leading to iron sulfide formation and resulting, for the spent samples, in a marked color change, from orange to black.

ACKNOWLEDGMENT

This work was carried out with the financial support of H2FC project (FP7, Grant Agreement N° 284522).

REFERENCES

- [1] S. Hernández, L. Solarino, G. Orsello, N. Russo, D. Fino, G. Saracco et al.: Desulfurization processes for fuel cells systems; Int. J. Hydrogen Energy 33 (2008) 3209–3214.
- [2] D. Shekhawat, J.J. Spivey, D.A. Berry eds.: Fuel cells: technologies for fuel processing (2011).



OXIDATIVE STEAM REFORMING OF ETHANOL ON MESOPOROUS SILICA SUPPORTED PT-NI/CEO₂ CATALYSTS

V. Palma, C. Ruocco, E. Meloni, A. Ricca

Department of Industrial Engineering, University of Salerno, Via
Giovanni Paolo II 132, 84084 Fisciano (SA), Italy

Abstract - The activity and stability of bimetallic Pt-Ni/CeO₂ catalysts supported over mesoporous silica, for steam (ESR) and oxidative steam reforming (OSR) of ethanol in the low-temperature range (300-600°C) was studied. The influence of temperature and gas hourly space velocity (GHSV between 10000 and 30000 h⁻¹) on product gas distribution was investigated, showing that at T>480 °C the system reached thermodynamic equilibrium in both the scenarios, independently from the contact time values. During time-on-stream (TOS) tests at 500°C, oxygen co-feeding strongly improved catalyst durability, depressing coke formation and also resulting in lower CO selectivity.

I. INTRODUCTION

The increasing world energy demand, in combination with environmental concerns, requires the urgent development of alternative technologies for power generation. To that end, hydrogen fuel cells offer an advantageous alternative, due to the absence of hazardous waste products. Moreover, a powder system incorporating H₂ from renewables and fuel cells devices is truly sustainable. In this scenario, biomass-derived ethanol provides a viable solution [1], due to its low toxicity, wide availability, easy storage and handling safety. Bioethanol can be catalytically converted to H₂ through steam reforming and the main interest towards this process arises from the benefit of combining a mature technology to a clean source. However, due to the reaction endothermicity, an external heat supply is required. On the contrary, ethanol oxidative steam reforming, being a combination of the steam reforming and the partial oxidation reactions, assures a reasonable balance between energy efficiency and hydrogen yield. Moreover, the oxygen feeding is expected to facilitate coke deposits removal from catalyst surface and the oxidation of dangerous CO to CO₂ [2].

This study focuses on the performances evaluation of Pt-Ni/CeO₂ catalysts supported over SiO₂ for both steam and oxidative steam reforming at T=300-600°C and H₂O/C₂H₅OH

molar ratio equal to 4. In particular, the influence of contact time on products selectivities as well as the impact of oxygen co-feeding on catalyst durability was investigated.

II. EXPERIMENTAL

The supported catalysts were prepared by wet impregnation. Silica gel was calcined at T=600°C for 3 h and added to an aqueous solution containing CeO₂ salt precursor. The next step involved active species deposition, carried out by impregnating Ni earlier than Pt on CeO₂/SiO₂ surface. An impregnation-drying-calcination cycle was repeated to reach 3wt% Pt-10wt% Ni/CeO₂; the CeO₂ content was 20wt % with respect to SiO₂.

For activity and stability tests, a fixed-bed stainless steel reactor, placed in an electrical oven, was employed. The catalytic bed is located in the reactor annular section and the powder catalyst (180÷355 μm) is sandwiched between quartz flakes; process temperature is monitored by a thermocouple placed at the middle of the catalytic outer section. The liquid ethanol/water mixture, prepared at a fixed molar ratio, is stored in a tank and sent to the vaporization section after premixing with a N₂ dilution stream. For OSR text, air can be feed directly to the reactor through an independent line. The products at the reactor outlet can be detected through an online FT-IR multi-gas analyzer: as diatomic molecules do not adsorb infrared radiation, the H₂ and O₂ concentrations are measured by a thermoconductivity and paramagnetic analyzers, respectively, which are also supplied with a sample gas conditioning system. To avoid water condensation, all connections from feed section to FT-IR gas analyzer were heated at 140°C.

Catalytic tests between 300 and 600°C were performed at 10000, 20000 and 30000 h⁻¹ at H₂O/C₂H₅OH (r.a.) molar ratio equal to 4 and O₂/C₂H₅OH (r.o.) molar ratio equal to 0 or 0.4 under a total follow rate of 550 Ncm³/min and the results were also compared in terms of products selectivity. The catalysts



stability for ESR and OSR was investigated at $T=500^{\circ}\text{C}$ and $\text{GHSV}=20000\text{ h}^{-1}$.

III. RESULTS & DISCUSSION

Table I summarizes the evolution of $\text{C}_2\text{H}_5\text{OH}$ conversion (X) as a function of temperature and space velocity for catalytic steam and oxidative steam reforming tests. Ethanol was completely converted at $T>480^{\circ}\text{C}$ for all the operative conditions investigated. However, at lower temperatures, the increase of space velocity negatively affected ethanol conversion. It is also worthwhile noting that, at $T<480^{\circ}\text{C}$ the X values recorded in the presence of oxygen are higher than those observed during ESR tests. O_2 co-feeding, in fact, increases the rate of C-C bonds cleavage and of the oxidation reactions, thus producing more C1 products, which can be converted to CO_2 [3]. Moreover, a total conversion of oxygen was recorded in the whole interval of contact time investigated.

TABLE I

Ethanol conversion as a function of T and GHSV for ESR and OSR; r.a.=4, r.o.=0,0.5.

Test	T ($^{\circ}\text{C}$)	10000 h^{-1}	20000 h^{-1}	30000 h^{-1}
ESR	600	100 %	100 %	100 %
	480	100 %	100 %	100 %
	360	100 %	96.2 %	77.5 %
	300	83.5 %	42.5 %	24.7 %
OSR	600	100 %	100 %	100 %
	480	100 %	100 %	100 %
	360	100 %	98.9 %	79.5 %
	300	100 %	62.1 %	40.8 %

The catalyst, during ESR as well as OSR, assured a good agreement between experimental selectivities and thermodynamic predictions at $T > 480^{\circ}\text{C}$; moreover, at high temperatures, no influence of space velocity on products gas distribution was observed. Fig. 1 shows H_2 and CO selectivities as a function of temperature at an intermediate value of GHSV.

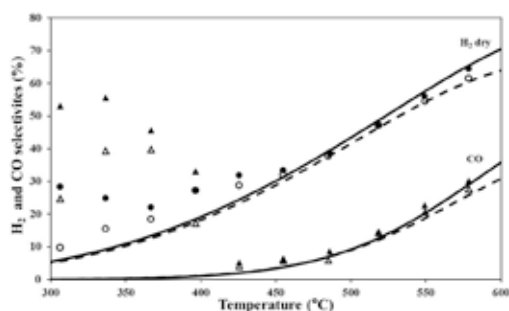


Fig. 1. H_2 (circle) and CO (triangle) selectivities in comparison with equilibrium data (continues and dotted lines for ESR and OSR, respectively); filled and empty symbols for ESR and OSR, respectively. $\text{GHSV}=20000\text{ h}^{-1}$, r.a.=4, r.o.=0,0.5.

The strongest variation, in terms of both H_2 and CO selectivity, between ESR and OSR tests was recorded at $T<350^{\circ}\text{C}$: in these conditions, a significant reduction of CO selectivity was reached (25% against 53% at 305°C) during oxygen co-feeding. The addition of O_2 promotes CO oxidation reaction, which is highly desirable for fuel cells applications. However, slightly lower hydrogen selectivities for OSR were observed especially at $T<370^{\circ}\text{C}$, which can be justified by both the lower carbon selectivity and the higher CO_2 concentration generated under OSR. In fact, the addition of O_2 contributed to minimize ethanol decomposition to C_xH_y products, which can be easily converted to H_2 and carbon, as well as enhance CO_2 formation, which may promote the reverse water gas shift, thus consuming a fraction of H_2 . Further tests (not reported) were performed at 500°C and 20000 h^{-1} in order to investigate the impact of oxygen co-feeding on catalyst stability. The presence of O_2 strongly improved coke resistance, as total ethanol conversion was recorded for 17 h more than the ESR case, in which the system was stable for almost 40 h.

IV. CONCLUSIONS

The activity of $\text{Pt-Ni/CeO}_2/\text{SiO}_2$ catalysts was investigated for steam and oxidative reforming of ethanol between 300 and 600°C at different space velocity (10000, 20000 and 30000 h^{-1}): the agreement of product gas distribution with equilibrium data was not affected by contact time decrease at $T>480^{\circ}\text{C}$ in both the scenarios. Moreover, O_2 co-feeding assured a relevant improvement of catalyst stability, due to the higher extent of coke gasification reaction which resulted in total ethanol conversion for almost 57 h at 500°C and $\text{GHSV} = 20000\text{ h}^{-1}$.

ACKNOWLEDGMENTS

The research leading to these results has received funding from the European Union's Seventh Framework Programme (FP7/2007-2013) for the Fuel Cells and Hydrogen Joint Technology Initiative under grant agreement n° 621196. The present publication reflects only the author's views and the FCH JU and the Union are not liable for any use that may be made of the information contained therein.

REFERENCES

- [1] Rao Peela, N., Kunzru, D., Oxidative steam reforming of ethanol over Rh based catalysts in a micro-channel reactor, International Journal of Hydrogen Energy, Volume 36, 2011, Pages 3384-3396.
- [2] Han, X., Yu, Y., He, H., Shan, W., Hydrogen production from oxidative steam reforming of ethanol over rhodium catalysts supported on Ce-La solid solution, International Journal of Hydrogen Energy, Volume 38, 2013, Pages 10293-10304.
- [3] Hung C.-C., Chen S.-L., Liao Y.-K., Chen C.-H., Wang J.-H., Oxidative steam reforming of ethanol for hydrogen production on $\text{M/Al}_2\text{O}_3$, International Journal of Hydrogen Energy, Volume 37, 2012, Pages 4955-4966.



HYDROGEN PRODUCTION IN A COMPACT ATR-BASED KW-SCALE FUEL PROCESSOR

V. Palma*, A. Ricca*, B. Addeo*, M. Rea** and G. Paolillo**

*Department of Industrial Engineering, University of Salerno, via
Giovanni Paolo II, 132 – 84084 Fisciano (SA), (Italy)

**SOL Spa, via Borgazzi, 27 – 20052 Monza (MI), (Italy)

Abstract – In the present work, a very compact reaction system thermally integrated for the distributed hydrogen production by natural gas reforming is reported. The system is based on hydrocarbon Auto-Thermal Reforming, followed by a Water-Gas Shift module. A compact heat exchanger was placed between the two catalytic stages, in order to assure an appropriate thermal integration that avoid any other external heat duties. Experimental results demonstrated that the integrated configuration allowed short start-up time, since the system reached the thermal regime in less than 3 minutes, and assuring a relevant hydrogen production in very short time. Preliminary tests showed very impressive performances of the system. Despite a quite slow WGS stage, the processor was able to produce up to 10 Nm³/h of hydrogen, with a thermal efficiency higher than traditional systems.

Index Terms – Auto-thermal reforming, Fuel processor, Hydrogen distributed production, Process intensification.

I. INTRODUCTION

Fuel cells were highlighted as the most amazing route against the well-known problems linked to the depletion of fossil fuels and to the growing energy demand. In particular, hydrogen – fuel cell combination appeared the favored “green” solution, since energy was obtained in a process having water as the only side-product. On the other hand hydrogen production through hydrocarbon reforming still appears as the most viable solution in a transition period towards a hydrogen based economy. Since one of the main limitation connected to the hydrogen-based technologies is linked to economic issues related to the H₂ transport and storage, distributed hydrogen production appeared an optimal solution, both for the stationary and mobile fuel cell installations. Auto-thermal reforming (ATR) combines SR and POX, since hydrocarbon reacts both with steam and oxygen, and the endothermicity of the reforming process is sustained by the oxidation reactions inside the catalytic volume. As a result, a hydrogen production not too far

from the SR may be achieved in a fast and versatile process. From this point of view, hydrocarbons catalytic Auto-Thermal Reforming (ATR) appears the best candidate process [1]. Anyway the high carbon monoxide content of the produced stream require a further catalytic stage, the Water-Gas Shift (WGS) in which CO reacts with steam to produce further hydrogen. The very different operating temperature of ATR and WGS stages resulted in the necessity of a heat exchange system, with a consequent increasing in plant size and operating costs. Aim of this work was to design and test a thermally integrated fuel processor based on natural gas ATR, aimed to the hydrogen production intensification and to the external duty minimization.

II. EXPERIMENTAL

A compact fuel processor based on Auto-Thermal Reforming process for natural gas conversion was designed and configured aimed to the production of 10 Nm³/h of H₂. The process was carried out by using water, air and hydrocarbons (methane or natural gas (NG)) as reactant. In the system, 2 catalytic volumes were designed, to host the ATR and the WGS reactions. In the ATR module a 1 L commercial (Johnson Matthey) honeycomb catalyst noble metals based was loaded, while in the WGS 7.5 L of commercial (JM) pellets catalyst was employed. Both modules have a cylindrical shape. Due to the very different temperature in the two stages, a compact and optimized heat exchange module was designed and placed between the two reaction volumes. The module appeared as a tube-shell like exchanger, in which cold reactants flow tube-side and exhaust gas from ATR flows shell side. In this way, sensible heat of effluent gas from ATR volume was exploited to pre-heat reactants before feeding to it; moreover, effluent gas were cooled to a temperature consistent to the WGS stage [2]. Such configuration allowed to feed all reactants at room temperature, without external heat exchangers; moreover, the thermal integration



was able to reduce system start-up transient times.

Preliminary studies were carried out on the system, in order to evaluate the effect of feed ratios (H_2O/C and O_2/C). Tests were carried out on both methane and natural gas, to understand the reforming catalyst tolerance to the impurity contained in NG. Finally, the feed rate effect was evaluated on NG-ATR.

III. RESULTS AND DISCUSSION

Preliminary tests confirmed that the designed system was characterized by very short start-up times, being able to produce up to $5 \text{ Nm}^3/\text{h}$ of hydrogen (27% $_{\text{vol}}$) in less than 3 minutes. The transitory phases were strictly related to the overall gas rate, since higher stream rate resulted in faster system response. Experimental tests on methane (Table I) showed the very good performances of the system, since the ATR module well approach thermodynamic equilibrium. On the other hand, WGS stage seems to suffer the operating conditions of the module, due to the too low temperature and H_2O/CO ratio, that in turn affected WGS performances for both thermodynamic and kinetic issues. The increasing in O_2/C ratio assured a higher methane conversion in the ATR stage, anyway also promoting total oxidation reactions since the H_2 yield did not showed any improvement. On the other hand, to increase S/C ratio did not led to any benefit to the ATR module, while weakly increased the CO conversion in the WGS stage, so resulting in a sensible increasing in hydrogen yield.

TABLE I
METHANE PROCESSING: EXPERIMENTAL ACHIEVEMENTS (GHSV = $14,000 \text{ H}^{-1}$)

GHSV h^{-1}	$H_2O:O_2:C$	ATR			H_2O/CO	WGS			Q_{H_2} Nm^3/h	η
		T in	Tout	X_{CH_4}		Tin	Tout	X_{CO}		
15,000	0.49:0.6:1	297	694	96.7%	0.74	298	300	36.7%	6.98	64.5%
15,000	0.60:0.65:1	326	737	99.0%	0.70	311	327	52.1%	7.02	70.2%
15,000	0.65:0.65:1	350	764	99.5%	0.70	323	366	51.1%	7.27	72.9%
15,000	0.75:0.65:1	358	767	99.5%	0.84	307	372	52.5%	7.38	73.8%

Tests carried out on NG (Table II) showed a sensible reduction in ATR catalyst performances, probably due to some poisoning compound in the gas. Despite the observed effect, no reduction of catalytic performances were observed in the time (not reported), to suggest a reversible catalyst deactivation. Once again, the O_2/NG ratio enhanced the hydrocarbons conversion but reduced the H_2 yield, while the steam-to-NG ratio increasing in a first range improved performances in WGS module, in a further range, caused a decreasing in WGS module temperature, that in turn affected the catalyst kinetics, so reducing the CO conversion. Once defined the optimal operating conditions ($H_2O:O_2:NG = 0.8:0.6:1$), the effect of reactants rate was evaluated.

By increasing gas rate, no clear effects were observed on ATR module, but the kinetic issues on WGS catalytic volume were highlighted, since the decreasing residence time resulted in the depletion in WGS performances. On the other hand, the higher process rate reduced the system heat loss, so increasing

temperature of the reactor, more evident in the WGS module.

TABLE II
NATURAL GAS PROCESSING: EXPERIMENTAL ACHIEVEMENTS

GHSV h^{-1}	$H_2O:O_2:NG$	ATR			H_2O/CO	WGS			Q_{H_2} Nm^3/h	η
		T in	Tout	X_{CH_4}		Tin	Tout	X_{CO}		
15000	0.7:0.55:1	244	646	83.9%	1.67	207	186	1.4%	7.35	60.3%
15000	0.7:0.6:1	337	759	91.5%	0.78	268	278	39.7%	7.11	61.5%
15000	0.8:0.6:1	359	775	95.0%	0.85	280	316	58.0%	7.67	67.9%
15000	0.9:0.6:1	363	775	94.2%	1.17	258	297	59.0%	7.29	65.9%
15000	1.0:0.6:1	366	775	94.2%	1.30	237	294	58.0%	7.26	67.0%
17500	0.8:0.6:1	362	782	94.2%	0.97	285	330	48.4%	8.84	67.0%
20000	0.8:0.6:1	368	789	94.2%	0.96	285	332	46.2%	9.50	63.0%
22500	0.8:0.6:1	358	791	93.8%	1.03	286	348	50.6%	10.75	63.4%

IV. CONCLUSIONS

An ATR-based fuel processor thermally integrated was realized. Preliminary tests evidenced the promising performances of the system, able to self-sustain the hosted processes without external heat sources. The ATR module was characterized by excellent performances in methane processing, while the weak reduction in performances with NG may be devoted to competitive adsorption of some compounds of the fuel on the catalytic surface. On the contrary, the WGS module seems to suffer the operating conditions, apparently due to a too high activation temperature not easy to reach due to the system thermal integration. If in one hand a more appropriate formulation for the WGS catalyst appeared mandatory, in the other hand the WGS module performances should be clearly improved by increasing H_2O/CO feed ratio. Such condition may be achieved by feeding more steam directly to the WGS module, to be produced by exploiting sensible heat of WGS exhaust stream. Anyway, despite the low CO conversion, the system was able to produce up to $10 \text{ Nm}^3/\text{h}$ of hydrogen, assuring a thermal efficiency of 68% (that could increase up to 71% by optimizing WGS catalyst), significantly higher than reported efficiency (63%) of conventional distributed hydrogen production plants [3].

REFERENCES

- [1] Chen W-H, Lin M-R, Lu J-J, Chao Y, Leu T-S. Thermodynamic analysis of hydrogen production from methane via autothermal reforming and partial oxidation followed by water gas shift reaction. *International Journal of Hydrogen Energy*. 2010;35:11787-97.
- [2] Palma V, Ricca A, Ciambelli P. Fuel cell feed system based on H_2 production by a compact multi-fuel catalytic ATR reactor. *International Journal of Hydrogen Energy*. 2013;38:406-16.
- [3] Lee DK, Koo KY, Seo DJ, Yoon WL. Analysis of design variables for an efficient natural gas steam reforming process comprised in a small scale hydrogen fueling station. *Renewable Energy*. 2012;42:234-42.



METHANE STEAM REFORMING INTENSIFICATION BY INNOVATIVE STRUCTURED CATALYSTS CONFIGURATION

V. Palma, A. Ricca, M. Martino, E. Meloni

Department of Industrial Engineering, University of Salerno, via
Giovanni Paolo II, 132 – 84084 Fisciano (SA), (Italy)

Abstract – In the present work, structured catalysts were investigated for the methane steam reforming reaction. By selecting nickel based catalyst, the effect of the deposition of active metal on highly thermal conductive support was evaluated. The SiC carrier enhanced heat transfer from the heating medium to the catalytic volume, resulting in higher reaction rate. Moreover, flux geometry configuration able to force the reaction stream to cross structure porous walls increased mass transfer rate between gaseous and solid phases, further enhancing catalytic performances. Finally, the development of a Ceria based washcoat as chemical support played a crucial role in the catalytic mechanism, resulting in improved performances in particular in low temperature range and low contact time.

Index Terms – Methane reforming, Hydrogen production, Structured catalysts, Process intensification.

I. INTRODUCTION

The depletion of fossil fuels and the growing energy demand of the recent years shifted research attention toward alternative energy sources. Between them, hydrogen–fuel cells combination attracts the greatest interest in scientific research and technology innovation for hydrogen production intensification. Despite the amazing target to exploit renewable sources for energy, hydrogen production by fossil fuels reforming still remain the most viable solution in a transition phase toward an hydrogen based economy. Actually, the main technique to produce hydrogen is methane steam reforming (SR), a catalytic endothermic process in which the hydrocarbon reacts with steam to produce hydrogen and carbon monoxide. Due to its endothermicity, very high reaction temperature and heat flux towards the reaction system are required to achieve high methane conversion [1]. In the process intensification direction, the combination of these requirements up to now results the main limiting step of the process. Previous studies demonstrated that high thermal conductivity supports (foams, honeycomb monoliths) allow a flatter thermal profile along the

catalytic bed, so resulting in a higher average temperature at the outlet section of the catalytic bed, and consequently in higher hydrocarbon conversion [2]. Furthermore, the highly conductive supports helps to flat the radial temperature profile, so reducing hot-spot phenomena, and mainly minimizing the heat transfer resistance from the heating medium to the catalytic volume. Moreover, the use of structured catalysis allows to reduce pressure drops and to minimize mass transfer limitation in the catalytic volume. In this aim, the thermal advantages achieved by using highly thermal conductive honeycomb monoliths as catalytic support may be further enhanced by forcing the flux to cross the monolithic walls. In this aim the use of Wall-Flow monoliths appear a viable solution towards the methane steam reforming intensification [3].

II. EXPERIMENTAL

Structured catalysts were prepared by starting from Silicon Carbide (SiC) porous walls monoliths (Pirelli Eco-technology, 150 cpsi), activated by nickel. Several aspects were investigated in this work: the nickel loading, the effect of a preliminary CeO₂ based slurry deposition on the support, and the flux geometry. The Ni loaded SiC monolith was prepared by repeated impregnation phases in 1M nickel acetate solution (C₄H₆O₄Ni·4H₂O), drying (120°C, 30min) and calcination (600°C, 2hr), in order to obtain a Ni loading of 30%wt. This procedure allows realizing a uniform and homogeneous distribution of the nickel oxide on the monolith walls and inside the porosity. For the washcoated samples, the support was preliminarily dipped in a CeO₂ based slurry (2:1wt ceria : pseudo-bohemite) several times (dipping-drying-calcination cycles) up to reach a washcoat loading of 20%wt; then Ni was deposited by the impregnation steps reported above up to reach a Ni loading of 20%wt. Finally, some samples were converted in



Wall-Flow configuration, by alternately plugging channels in the inlet and outlet sections, so forcing the process gas to cross the porous walls. The prepared samples were characterized by X-Ray Diffraction (XRD), Scanning Electron Microscopy (SEM) and Energy Dispersive Spectroscopy (EDAX), Surface area evaluation (BET) and Hg penetration porosimetry.

The experimental tests were carried out in a tubular lab scale catalytic reactor in isothermal conditions. The activity tests were performed on the catalytic monoliths in the Flow-Through (FT) and Wall Flow (WF) configurations, by feeding steam and methane to the system ($H_2O:CH_4 = 3:1$) and by varying reaction temperature and GHSV (Q/V_{cat}) values.

III. RESULTS AND DISCUSSION

XRD analysis showed that the increase in the Ni load results in the increase of the characteristic NiO signals. SEM and EDAX images proved a uniform distribution of the active species and the washcoat (if present) over the SiC surface, thus confirming the effectiveness of the preparation procedure. Moreover, the porosimetric analyses confirmed that slurry was deposited inside the pores, as the mean pores diameter was reduced. The activity tests results, summarized in Figures 1 and 2, highlighted the better performances of the WF configuration than the FT, in terms of hydrogen yields and methane conversion. The WF configuration enhancement was more evident in the more extreme conditions, at the lowest operating temperatures and at highest reactants flow rate. The same behavior was observed in the washcoated samples, since a marked improvement in catalytic performances was observed by using the WF configuration. The washcoated FT configuration showed excellent performances, by approaching thermodynamic equilibrium in the whole temperature range, resulting in an appreciable H_2 yield also at low temperature.

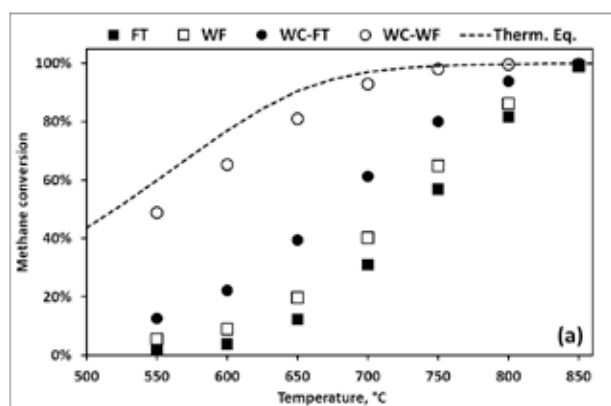


Fig. 1 Methane conversion for the selected catalyst configurations

Moreover, the comparison between hydrogen production on non-washcoated and washcoated samples confirmed the strong role of ceria on the steam reforming reaction trend: the oxygen-storage capacity, proper to the cerium oxide, accelerates the

migration of oxygen from steam to the carbon [4], so resulting in a clear increasing in catalytic system performances.

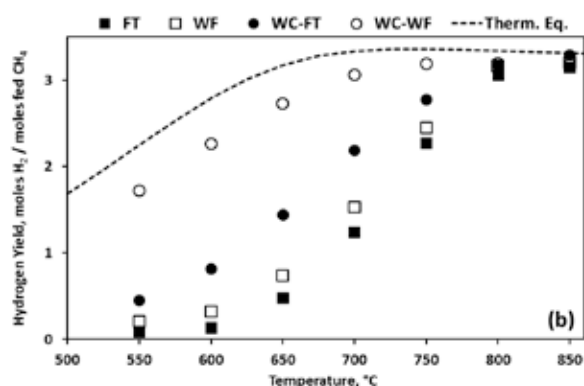


Fig. 2 Hydrogen yield for the selected catalyst configurations

IV. CONCLUSIONS

In the direction of process intensification for hydrogen production for fuel cell feeding, innovative structured catalysts were proposed for reforming process. Specific experimental tests were carried out in order to evaluate the influence of flux geometry of Nickel based monolithic catalyst on methane SR reaction. The activity tests highlighted the improvements due to the WF configuration with respect to the FT, in terms of hydrogen yields. By forcing gas to cross the monolith catalytic porous walls, heat and mass transfer mechanisms between gas and solid phases were enhanced, so resulting in faster reaction kinetics. The role of ceria as catalytic support was also investigated, highlighting that the Ni-CeO₂ interactions and the OSC properties linked to the ceria clearly improves catalyst performances.

REFERENCES

- [1] Yan, Y., Zhang, Z., Zhang, L., Wang, X., Liu, K., Yang, Z., Investigation of autothermal reforming of methane for hydrogen production in a spiral multi-cylinder micro-reactor used for mobile fuel cell, *International Journal of Hydrogen energy*, vol 40, 2015, Pages 1886-1893.
- [2] Palma, V., Ricca, A., Ciambelli, P., Monolith and foam catalysts performances in ATR of liquid and gaseous fuels, *Chemical Engineering Journal*, vol. 207, 2012, pages 577-586.
- [3] Palma, V., Miccio, M., Ricca, A., Meloni, E., Ciambelli, P., Monolithic catalysts for methane steam reforming intensification: Experimental and numerical investigations, *Fuel*. Vol. 138, 2014, pages 80-90.
- [4] K. Polychronopoulou, K., Kalamaras, C.M., Efstathiou A.M., Ceria-Based Materials for Hydrogen Production Via Hydrocarbon Steam Reforming and Water-Gas Shift Reactions, *Recent Patents on Materials Science* vol. 4, 2011, pages 122-145



CHARACTERIZATION OF PLATINUM-FREE ELECTROCATALYSTS AND ANION EXCHANGE MEMBRANES FOR DIRECT ETHANOL FUEL CELL

B. Cermenek*, B. Feketeföldi**, R. Zacharias*, V. Ribitsch*** and V. Hacker*

*Institute of Chemical Engineering and Environmental Technology, Graz University of Technology, NAWI Graz, Inffeldgasse 25C, 8010 Graz, (Austria)

**Institute for Surface Technologies and Photonics, JOANNEUM RESEARCH Forschungsgesellschaft mbH/Materials, Franz-Pichler-Straße, 8160 Weiz, (Austria)

***Institute of Chemistry, University of Graz, Heinrichstraße 28, 8010 Graz, (Austria)

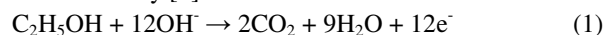
Abstract – Nickel dimethylglyoxime (Ni(II)(DMG)₂) complex was synthesized with precipitation method and the electrochemical properties were characterized by means of cyclic voltammetry and chronoamperometry. This catalyst exhibits superior long-term stability. A series of membranes based on quaternized chitosan (HTCC) and quaternized poly(vinyl alcohol) (QPVA) with various degrees of silica content were synthesized using a mixture of tetraethoxysilane / methyltriethoxysilane (TEOS/MTES) by sol-gel method. The chemical properties of the organic/inorganic hybrids were characterized by means of electrochemical impedance spectroscopy (EIS) method and permeability-cell method. These membranes show an ion conductivity between $4.1 \cdot 10^{-3}$ and $5.3 \cdot 10^{-3}$ S·cm⁻¹ and low ethanol permeability from $1.5 \cdot 10^{-7}$ to $7.3 \cdot 10^{-7}$ cm²·s⁻¹ at 60 °C.

Index Terms – Anion Exchange Membrane, EtOH-permeability, Pt-free electrocatalyst, long-term stability.

I. INTRODUCTION

The alkaline direct ethanol fuel cell (DEFC) is a promising energy technology for portable applications [1]. Main challenges are their low power density and high costs of the components. Hence, the optimization of the membrane and the electrocatalyst is very important. Ethanol as renewable fuel is converted directly into electricity without reforming within fuel cells. However, the whole Gibbs free energy of this oxidation reaction may not be converted into electric energy so far, since the C-C bond is thermodynamically stable. Therefore, the great challenge is to develop a highly active catalyst for breaking the C-C bond of ethanol to achieve the complete oxidation to carbon dioxide and water releasing 12 electrons (see Eq. 1) [2]. Different reaction intermediate products, which are generated during ethanol oxidation reaction (EOR) in alkaline medium

(see Eq. 2), deactivate the catalyst resulting in only 33.3% of Faradic efficiency [2].



Various nickel-complexes [3-5] were established as catalysts for EOR in alkaline medium in order to substitute noble metal containing catalysts (for example: Pt, Pd, Au etc.) and enhance their long-term stability, respectively. Anion exchange membranes (AEMs) are used in DEFCs to transport the OH⁻ ions from the cathode to the anode and to reduce the so-called ethanol crossover due the reversed ion direction [6].

In this study, the catalytic activity and stability of the synthesized Ni(II)(DMG)₂ complex are compared to Pd/C and Pd₈₀Ni₂₀/C catalyst as references [7]. Furthermore, HTCC/QPVA membranes are prepared by blending and chemical cross-linking with ethylene glycol diglycidyl ether (EGDE) for chitosan and glutaraldehyde (GA) for QPVA. Nanoscale particles are introduced into the blend matrix leading to a hybrid system of organic/inorganic membranes. A sol-gel process with tetraethoxysilane (TEOS) as precursor and couple agent, such as methyltriethoxysilane (MTES), is chosen and hydrolysis and condensation reactions cause polymerization of nano-silicon dioxide particles [8, 9].

II. EXPERIMENTAL

A. Synthesis of anion exchange membranes

All reagents were supplied by Sigma-Aldrich Handels GmbH, Austria. QPVA and HTCC were dissolved in water and cross-linking reagents and quantitative amount of TEOS/MTES solution were added. The solutions were poured into plastic Petri dishes and dried.

B. Synthesis of Pt-free electrocatalysts

Ni(II)(DMG)₂ complex was synthesized by a precipitation method [4,5]. An appropriate amount of (NH₄)₂SO₄ and NiSO₄·6H₂O in the ratio of 1:1 was dissolved in 14 ml HCl (2.5 M) and filled up to 200 ml with ultra-pure water. The solution was vigorously stirred at 70-80 °C. Then dimethylglyoxime (DMG) in 20 ml EtOH (99.9%) was added to the solution under stirring at 70-80 °C for approx. 1-1.5 h. After that 6.0 M KOH was added to the solution until pH = 8 was reached resulting a red-rose complex. After 24 h reaction time the Ni(II)(DMG)₂-complex was centrifuged and washed several times and dried at 70 °C.

C. Characterization of anion exchange membranes

The OH⁻-conductivity was determined using EIS [10] and the ethanol permeability was measured by the permeability-cell method.

D. Characterization of Pt-free electrocatalysts

The catalytic activity and stability of Ni(II)(DMG)₂ complex (without carbon as support material) toward EOR in alkaline medium were analyzed using cyclic voltammetry (CV) and chronoamperometry (CA) technique using Rotating Disc Electrode (RDE).

III. RESULTS AND DISCUSSION

A limiting factor in operation of DEFC is the transport of ethanol through the membrane from anode to cathode. In Table I the ethanol permeability of the synthesized hybrid membranes at a temperature of 60 °C in 1.0 M ethanol mixture is presented. The addition of silica into the blend membranes changed the ethanol transport properties. The silica content led to the increase of aggregate pores, thus to a higher mass/ethanol transport [9].

TABLE I: SiO₂-CONTENT AND ETHANOL PERMEABILITY (P) FOR MEMBRANES

Membrane	HM-0	HM-5	HM-10	HM-15	HM-20	HM-25
SiO ₂ (wt %)	0	5	10	15	20	25
Px10 ⁻⁷ (cm ² s ⁻¹), 60°C	1.46	2.56	3.50	4.70	5.90	7.32

Fig. 1. shows the OH⁻-conductivity of the hybrid membranes. The ion conductivity increases with higher SiO₂ contents. The ion conductivity of these hybrid membranes depends on water uptake and quaternization degree of chitosan (88%) and QPVA (15%). The addition of silica facilitated the formation of small ion channels for OH⁻-transfer, resulting in a higher conductivity.

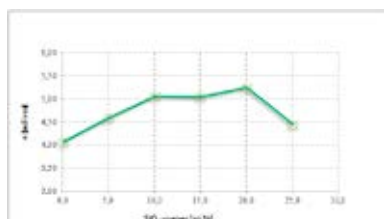


Fig. 1. Effect of SiO₂ content on OH⁻-conductivity.

The drawbacks of alkaline DEFC catalysis are on the one hand the sluggish kinetics of EOR on standard materials and on the other hand the insufficient long-term stability under operating conditions of these standard catalysts. Fig. 2a. shows that Ni(II)(DMG)₂ complex possesses a dissatisfactory catalytic activity toward EOR, due to high onset-potential and large anodic overpotential. However, the Ni(II)(DMG)₂ complex exhibits the highest stability in comparison with Pd-based catalysts due to the ligand (see Fig. 2b) [4].

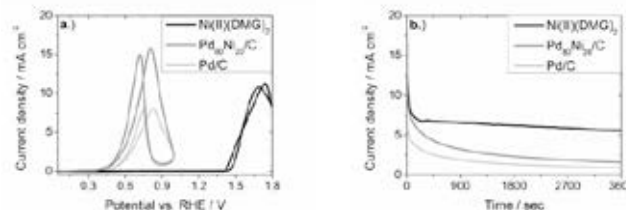


Fig. 2a.) CV and b.) CA measurement of Ni(II)(DMG)₂ complex (0.1 M KOH + 1.0 EtOH) compared with Pd-based electrocatalysts (1.0 M KOH + 1.0 M EtOH) [7].

IV. CONCLUSION

Hybrid AEMs were successfully prepared with HTCC/QPVA and TEOS/MTES by sol-gel method. Membrane properties were highly dependent on SiO₂ content. The highlight of the electrochemical investigation of Ni(II)(DMG)₂ complex was their superior long-term stability.

The components as Ni(II)(DMG)₂ complex as well as Pd-based electrocatalysts and HM-20 will be further processed to membrane electrode assemblies (MEAs) and operated in single cell DEFC.

ACKNOWLEDGMENT

Financial support by the Austrian Federal Ministry of Transport, Innovation and Technology (BMVIT), The Austrian Research Promotion Agency (FFG) and the IEA research cooperation is gratefully acknowledged.

REFERENCES

- [1] An, T.S. Zhao, Y.S. Li, *Renew. Sustain. Energy Rev.* 50 (2015) 1462–1468.
- [2] M.Z.F. Kamarudin, S.K. Kamarudin, M.S. Masdar, W.R.W. Daud, *Int. J. Hydrogen Energy* (2012) 1.
- [3] M. Revenga-Parra, T. García, E. Lorenzo, F. Pariente, *Sens. Actuators B Chem.* 130 (2008) 730.
- [4] W.S. Cardoso, V.L.N. Dias, W.M. Costa, I. de Araujo Rodrigues, E.P. Marques, A.G. Sousa, J. Boaventura, C.W.B. Bezerra, C. Song, H. Liu, J. Zhang, A.L.B. Marques, *J. Appl. Electrochem.* 39 (2008) 55–64.
- [5] M.A. Malati, *Experimental Inorganic/Physical Chemistry*, 1999.
- [6] E.H. Yu, U. Krewer, K. Scott, *Energies* 3 (2010) 1499.
- [7] B. Cermenek, R. Zacharias, M. Grandi, C. Grimmer, A. Schenk, V. Hacker, 1st International Workshop on Hydrogen and Fuel Cells, Yokohama National University, Japan, 2015.
- [8] Y. Xiong, Q.L. Liu, Q.G. Zhang, A.M. Zhu, *J. Power Sources* 183 (2008) 447–453.
- [9] B.P. Tripathi, M. Kumar, V.K. Shahi, *J. Memb. Sci.* 360 (2010) 90–101.
- [10] C. Ranacher, R. Resel, P. Moni, B. Cermenek, V. Hacker, A.M. Coclite, *Macromolecules* (2015).



EXPERIMENTAL AND MODELING INVESTIGATION OF IT-SOFC FOR USE WITH BIOGAS AND SYNGAS MIXTURES

A. Donazzi*, M. Rahmanipour*, M. Maestri*, G. Groppi*, L. Bardini**, A. Pappacena**, M. Boaro**

*Politecnico di Milano, Dipartimento di Energia, Via Lambruschini 4, 20156, Milano

**Università degli Studi di Udine, Dipartimento di Chimica, Fisica e Ambiente, Via Cotonificio 108, 33100, Udine

Abstract – SDC electrolyte-supported IT-SOFCs with Cu-Pd-CZ80 composite anodes and LSCF cathodes were tested under a wide range of operating conditions. Polarization and EIS measurements were collected at 650°C and 600°C with syngas mixtures (2.3-0.4 H₂/CO ratio), H₂/N₂ mixtures (97-30% H₂ v/v) and CO/CO₂ mixtures (97-50% CO v/v). In the presence of syngas, a co-oxidation route was active, wherein H₂ and CO were electro-oxidized in parallel and contemporarily. A 1D, dynamic and heterogeneous model of the cell was applied to analyze the polarization and the EIS curves. The kinetics of the reactions of H₂ electro-oxidation, CO electro-oxidation and O₂ reduction were individually investigated and global power law rates were derived. The syngas experiments were simulated on a fully predictive basis, confirming that the polarization behavior could be reproduced exclusively by assuming the presence of the co-oxidative route. The cell was also exposed to biogas, revealing that dry-reforming was active.

Index Terms - IT-SOFC; ceria; kinetics; co-oxidation.

I. INTRODUCTION

Applications based on Solid Oxide Fuel Cells (SOFC) for the distributed production of energy require the cell to operate with both traditional hydrocarbon fuels (CH₄ and LPG) and biomass derived fuels (biogas, ethanol). Several benefits in terms of lifetime and thermo-mechanical resistance are also achieved by decreasing the operating temperature to 500-700°C (IT-SOFC). On the one hand, the use of hydrocarbons leads the traditional Ni-based anodic materials to deactivate due to coke formation; on the other hand, lower temperatures ask for electrolytes different from YSZ, such as those based on Ce oxides. Novel cells and materials are thus required, whose development must be accompanied by numerical model analysis to rationalize chemical and physical phenomena. In this work, IT-SOFCs based on Samaria doped Ceria electrolytes (Sm_{0.1}Ce_{0.9}O_{1.95}, SDC) and Cu-Pd-CZ80 anodes are tested with syngas (H₂/CO) and biogas (CO₂/CH₄). Polarization and EIS experiments were performed at varying the reactants concentration. A numerical model of the cell was applied to analyze the experimental results and kinetic equations were derived for the electro-chemical reactions of the process.

II. MATERIALS AND METHODS

SDC electrolyte supported cells (2 cm Ø) with Cu-Pd-CZ80 (20 wt% CeO₂, 80 wt% ZrO₂) with composite anodes and LSCF cathodes were prepared by die-pressing. Graphite-containing SDC powder was uniaxially pressed with pure SDC powder. This bilayer was calcined in air (1400°C for 3 h) producing a porous 150 µm thick SDC scaffold supported on a dense 380 µm thick SDC electrolyte. After forming the anode and the electrolyte, the LSCF cathode (40 µm) was applied. The porous SDC scaffold was then impregnated with Cu- and Pd-CZ80 nitric solutions, repeating the steps of impregnation and calcination (600°C) until the desired amounts were loaded [1]. The resulting cell was calcined at 700°C for 3 h. Polarization and EIS experiments were carried out between 600 and 650°C with H₂/N₂, CO/CO₂, H₂/CO and CH₄/CO₂ mixtures, at different concentration of the reactants. The EIS tests (0.1 Hz – 1 kHz, 50 mV amplitude) were performed at the OCV. SEM micrographs allowed to access the morphologic characteristics of the cells. A 1D, dynamic and heterogeneous model was applied to analyze both the EIS spectra and the polarization curves. The model allows to predict the cell voltage as a function of the current density, the temperature, the pressure and the composition of the anodic and cathodic gas streams. The model includes a molecular kinetic equations for the WGS reaction, and the for the electrocatalytic reactions of H₂ and CO electro-oxidation at the anode, O₂ reduction at the cathode.

III. RESULTS AND DISCUSSION

The IT-SOFCs were first tested in syngas mixtures at varying the H₂/CO ratio (Fig. 1): no variation was found passing from a ratio of 2.3 to a ratio of 0.4. The OCV values maintained constant, so as the slope and the current extracted at 0.5 V. Analogous observations were done with the EIS spectra. These results were significant since they suggested that both the H₂ electro-oxidation and the CO electro-oxidation were occurring in parallel in the presence of syngas.

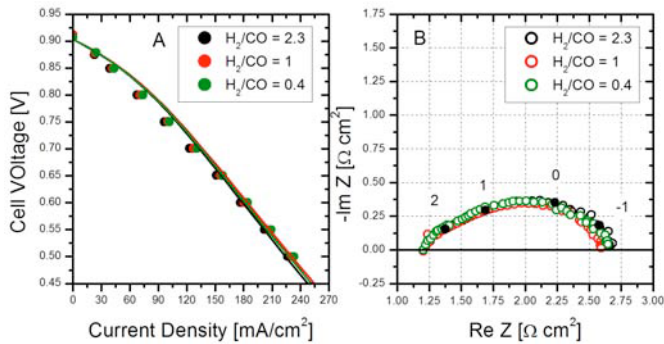


Figure 1 – Test with syngas mixtures, $T = 650^{\circ}\text{C}$, $P_{\text{H}_2} = 70\text{--}30\%$ v/v, balance CO. Lines are simulations, symbols are data.

A numerical model analysis of the polarization curves was carried out to prove the activation of the co-oxidative route for CO and H_2 . Along with this task, the IT-SOFCs were tested in H_2/N_2 mixtures at varying the H_2 partial pressure, to derive a power-law kinetic equation for the rate of the electro-oxidation of H_2 . The polarization curves (Fig. 2a) showed a decrease of the extracted current at decreasing the partial pressure of H_2 . As well, an increase of the polarization resistance at decreasing H_2 content was observed in the EIS tests (Fig. 2b). Coherently with the use of SDC, which is a MIEC electrolyte and activates a leakage current, the measured OCVs were always lower than those expected from the Nernst equation. The leakage current decreased at decreasing the H_2 partial pressure as well as at increasing the total current density (Fig. 2a insert). An effect related to the leakage current was also observed in the EIS, wherein the ohmic resistance increased at decreasing the H_2 partial pressure. To complete the kinetic investigation, EIS and polarization experiments with CO/CO_2 mixtures were carried out to derive a power-law rate for the CO electro-oxidation reaction. A picture similar to that of the H_2/N_2 tests was observed.

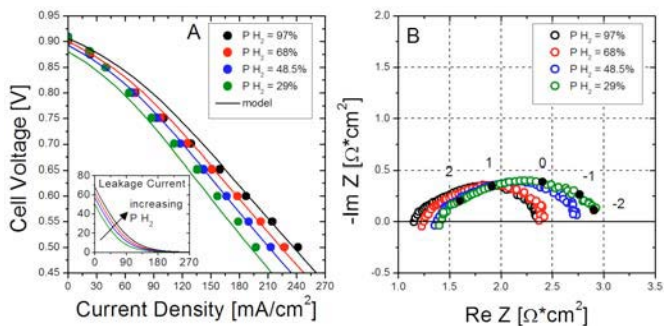


Figure 2 – Test with H_2/N_2 mixtures, $T = 650^{\circ}\text{C}$, $P_{\text{H}_2} = 97\text{--}30\%$ v/v. Lines are simulations, symbols are data.

The rate equations and their kinetic parameters were derived based on the best simulation of the polarization resistances (Fig. 3, R_{Pol}) obtained in the EIS tests. Indeed the modeling approach adopted [2] allowed to rigorously predict the real part

of the spectra, but not the imaginary part (Fig. 3a). In the case of the electro-oxidation of H_2 , the model predictions well agreed with the experiments by assuming that the H_2 order was equal to 0.5 in the rate. In the case of the electro-oxidation of CO, the rate was first order in CO and zeroth order in CO_2 . The order of O_2 in the reduction rate was found to be equal to 0.33.

Once the rates of the oxidation processes were derived, the experiments with syngas mixtures (Fig. 1) were simulated on a fully predictive basis. The close match of the simulations allowed to verify that the co-oxidative scheme was able to rationalize the data. Simulations based on different reactive schemes (H_2 oxidation + WGS, CO oxidation + RWGS) failed in achieving a satisfactory description, confirming that the parallel oxidation of H_2 and CO was the only adequate scheme.

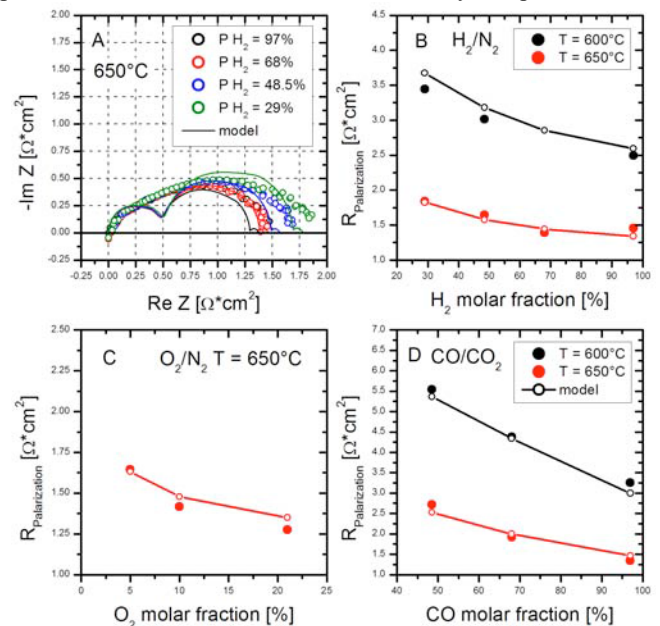


Figure 3 – A) EIS, 650°C , $P_{\text{H}_2} = 97\text{--}30\%$ v/v. R_{Pol} vs. molar fraction for EIS tests with: B) H_2/N_2 ; C) O_2/N_2 ; D) CO/CO_2 . Lines are simulations, symbols are data.

IV. CONCLUSION

In this work, a 1D, dynamic, MEA model was applied to rationalize polarization and impedance behavior of SDC electrolyte supported IT-SOFCs, tested over a wide range of conditions, including syngas mixtures and biogas. The cell was active in the combustion of syngas at varying H_2 to CO ratio, and the activation of a co-oxidative route could be envisaged, wherein H_2 and CO were electro-oxidized in parallel and contemporarily. Rate equations were derived for the oxidation reactions and the co-oxidative scheme could be quantitatively rationalized.

REFERENCES

- [1] J.M. Vohs, R.J. Gorte, *Advanced Materials*, 21 (2009) 943–956
- [2] H. Zhou and R.J. Kee, *J. Electrochem. Soc.* 153 (2006) A1765



ELECTROCHEMICAL IMPEDANCE SPECTROSCOPY FOR PEM FUEL CELL DEGRADATION DIAGNOSTICS

I. Pivac, D. Bezmalinovic, and F. Barbir

FESB University of Split, R. Boskovicica 32, 21000 Split, (Croatia)

Abstract - An accelerated stress test for catalyst degradation, that involves voltage cycling, was conducted on a single PEM fuel cell. Diagnostic tests, such as polarization curves, electrochemical impedance spectroscopy, cyclic voltammetry, and linear sweep voltammetry were conducted periodically to monitor performance degradation. A novel equivalent circuit model is suggested by adding a couple additional resonance loops comprising of resistance, capacitance and inductance in parallel, one for the anode and one for the cathode. The model was then used to fit the results of the electrochemical impedance spectroscopy measurements taken during the accelerated stress test. The results confirmed the findings from diagnostic tests, namely that the cathode catalyst layer parameters, resistance and inductance increased significantly during the accelerated stress test.

Index Terms - degradation, electrochemical impedance spectroscopy, equivalent circuit model, impedance model, inductance

I. EQUIVALENT CIRCUIT MODEL DESCRIPTION

A standard, simple representation of the fuel cell processes by equivalent circuits involves resistance/capacitance loops, representing charge transfer resistance and double layer capacitance on both anode and cathode, in series with a resistance, representing both ionic and electrical resistance in the membrane and cell hardware. What is missing in such a model is representation of other processes in the catalyst layers.

A novel impedance model of a PEM fuel cell is suggested, represented by a modified equivalent circuit in Fig. 1. This model has additional loops, one for the cathode and one for the anode, comprising of a resistance, capacitance and inductance in parallel (the so called resonant loop). These resonant loops represent the mass transport and resistive losses within the catalyst layer (CL). In this case, the physical processes preceding the catalytic reaction that take place in a complex structure of the fuel cell catalyst layer are represented by their electrical equivalents. Namely, inductance represents inertia of

reactant gas (oxygen on the cathode and hydrogen on the anode) to dissolve in water, and water adsorption/desorption in the CL ionomer; resistance represents protonic resistance through ionomer within the CL; and capacitance represents stored (dissolved) quantity of gas within the water/ionomer in the CL.

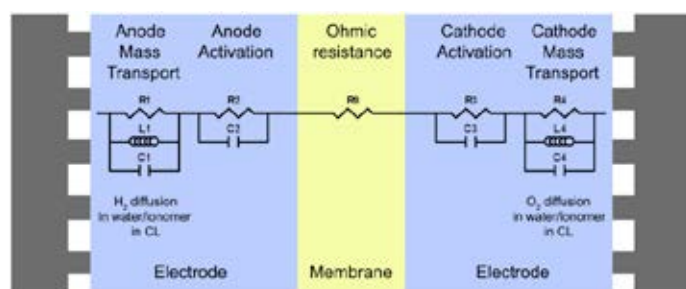


Fig. 1. A novel equivalent circuit model

II. APPLICATION OF MODEL TO FUEL CELL DEGRADATION STUDY

The model was applied to the EIS spectra obtained on a degrading hydrogen/air fuel cell operated at 65°C, 0.5 bar(g) and 0.1 A/cm², with reactants inlet relative humidities (RH) of 83.4% (dew point of 61 °C) and constant stoichiometry of 4.0/2.0. A single cell with a 50 cm² active area MEA was exposed to an accelerated stress test designed to target electrocatalyst degradation. The cell was exposed to voltage cycling between 0.6 V and 0.9 V in a non-operating mode, i.e. nitrogen was used on the cathode and hydrogen on the anode side. As a part of degradation diagnostics, the EIS tests were conducted at the beginning of life (BOL), after 1000, 3000, and 5000 cycles. The resulting Nyquist plots are shown in Fig. 2.

The diagram clearly shows performance deterioration with time (i.e. number of cycles): the semicircles are distorted at high-frequencies, indicating an increase in the CL ionic resistance, while the low-frequency loops, representing mass

transport losses, are getting bigger and in the end it is difficult to tell the two semicircles apart. As a result, the total resistance of the cell increased dramatically (the low frequency intercept). At the same time the high-frequency intercept, indicating ohmic losses, increased only in the first 1000 cycles (by ~30%), while it remained unchanged for the remainder of the degradation test. This concurs with the findings of the other diagnostic tests (polarization curves and cyclic voltammetry), which also indicated a significant loss of the cathode electrochemical active surface area (ECSA), almost 80% by the end of the test. The loss of the ECSA apparently resulted in big structural changes within the CL, which resulted in increased CL resistance and increased of mass transport losses.

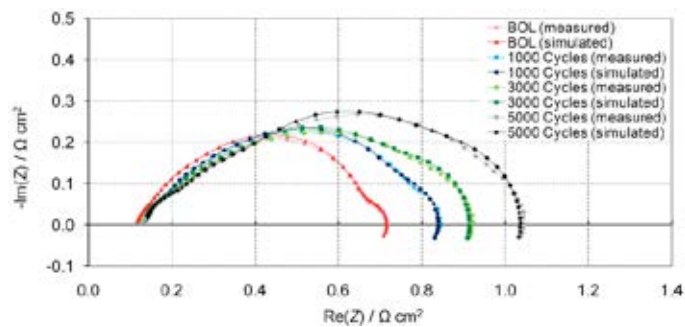


Fig. 2. Comparison of Nyquist plots of measured and simulated impedance data at 0.1 A cm^{-2} at different steps of the accelerated stress test.

The previously described model was fitted to the obtained EIS spectra, using Z Fit numerical tool from Bio-Logic EC-Lab[®] software, in order to give more insight into cell's degradation. As shown in Fig. 2, a very good agreement between simulation and measured data was achieved. This enabled quantification of individual model components and the change of their values during the degradation experiment.

The model results indicated that both, the anode and cathode activation (charge transfer) resistances, R2 and R3 respectively, did not change significantly during the degradation test.

Fig. 3 shows the resulting CL resistances during the accelerated degradation test. The cathode CL resistance (R4) increased several times.

Similarly, the cathode CL inductance, L4, also increased dramatically during the degradation, much more than the anode CL inductance, L1, as shown in Fig. 4.

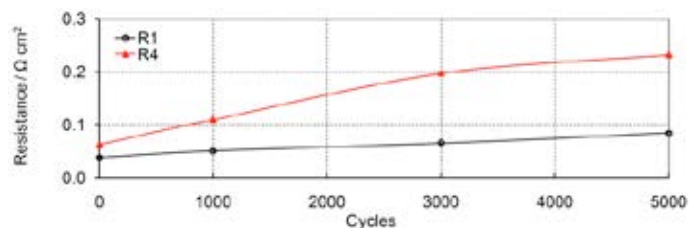


Fig. 3. CL resistances (R1 = anode and R4 = cathode) during the accelerated degradation test.

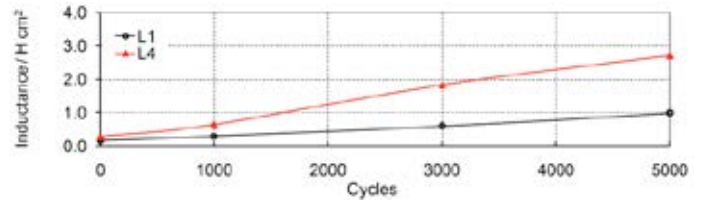


Fig. 4. CL inductances (L1 = anode and L4 = cathode) during the accelerated degradation test.

The catalyst layer capacitances (double layer capacitances), C2 (representing the anode) and C3 (representing the cathode), did not change significantly during the degradation test, as shown in Fig. 5. However, the cathode catalyst layer capacitance, C4, representing capacitance of oxygen dissolved in water/ionomer in the cathode catalyst layer, decreased by an order of magnitude over the duration of the degradation test.

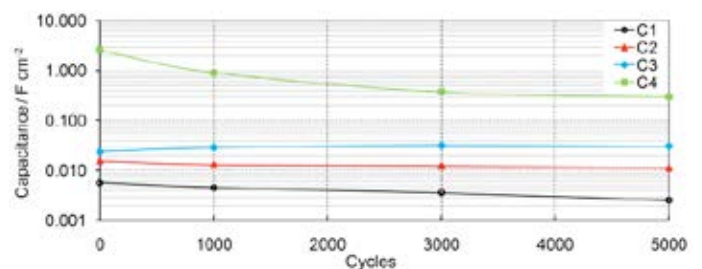


Fig. 5. Capacitances during the accelerated degradation test.

III. CONCLUSIONS

A novel equivalent circuit model, that attempts to include the processes in the catalyst layers represented by the two resonant loops, was applied as a tool for diagnostic of PEM fuel cell degradation. A fuel cell exposed to an accelerated degradation test degraded very fast. The periodic diagnostic tests (polarization curve, EIS, CV, LSV) confirmed that it was the cathode catalyst layer that degraded, as intended by frequent voltage cycling. The model managed to extract contributions of different phenomena responsible for the cell degradation. The cathode catalyst layer resistance and the cathode inductance both increased several times during the accelerated degradation test, while the catalyst layer capacitance decreased by an order of magnitude. This coincides with almost 80% of the electrochemical surface area loss during the accelerated stress test. The loss of electrochemical surface area caused by the accelerated stress test was probably the result of morphological changes within the catalyst layer, which in turn resulted in increase in catalyst layer resistance and capacitance and decrease of catalyst layer capacitance.

It appears that electrochemical impedance spectroscopy accompanied by the presented novel equivalent circuit model may be used for diagnostics of PEM fuel cell degradation.



HYDROGEN PRODUCTION VIA STEAM REFORMING OF A “MODEL” BIOETHANOL: STUDY OF COKE FORMATION OVER PT-NI/CEO₂-ZRO₂

V. Palma, C. Ruocco, and A. Ricca

Department of Industrial Engineering, University of Salerno, Via
Giovanni Paolo II 132, 84084 Fisciano (SA), Italy

Abstract - In this paper, the impact of the main contaminants of bioethanol (C₂H₄O, C₃H₇OH, C₄H₉OH and C₅H₁₁OH) on the performances of a bimetallic (Pt-Ni) catalyst supported on CeO₂-ZrO₂, in the form of powder as well as deposited on a SiC foam containing SiO₂ or γ -AlO(OH) binders, for ethanol steam reforming in the low-temperature range was investigated. Preliminary tests were carried out on powder samples, showing that the increase of impurities carbon content caused a quasi-linear growth of carbon formation rate. Moreover, the stability tests under a model mixture, containing 1 mol% of every impurity, at 450°C and a H₂O/C₂H₅OH ratio of 6 showed the highest resistance to deactivation of boehmite-based foam catalyst which assured total ethanol conversion for more than 1 day of time-on-stream.

Index Terms –bioethanol, foam, impurities, hydrogen.

I. INTRODUCTION

The massive consumption of fossil fuels as energy sources implies several global issues and the development of new production technologies is highly desired. In the last decades, hydrogen has been considered as a very promising energetic carrier, suitable for power generation through fuel cells with no pollutant emissions. However, only when renewable feedstocks are employed as H₂ sources, harmless energy supply can be provided. In this context, the way of converting ethanol from biomass through reforming reaction is regarded as an excellent H₂ source. Bioethanol mixtures contain ethanol and water as major components, combined with organic impurities, including higher alcohols and aldehydes. In order to avoid the costly steps for water and impurities separation, the direct feed of bioethanol mixtures to the reformer appears very interesting. As a drawback, contaminants may enhance deactivation phenomena due to carbon formation and deposition [1].

The present work is focused on the coke resistance evaluation of Pt-Ni/CeO₂-ZrO₂ powders and structured catalysts (ceramic foams) in the presence of the main

bioethanol impurities. The effect of such species on product distribution during ethanol steam reforming (ESR) reaction as well as the comparison between powders and foams stability at T=450°C and a H₂O/C₂H₅OH ratio (r.a.) of 6 at different space velocities were the main issues of this study.

II. EXPERIMENTAL

Foam and powder catalysts were prepared by wet impregnation. 10wt% Ni was deposited on the support (CeO₂-ZrO₂) calcined at 600°C as well as on coated foams earlier than Pt (3wt%) at University of Salerno. The CeO₂-ZrO₂ washcoat deposition on ceramic (SiC) foams was carried out at the Fraunhofer Institute (IKTS, Germany); SiO₂ and γ -AlO(OH) were employed as binders. Powders catalysts were tested in an annular reactor while the tubular configuration was employed for foams. After H₂ reduction in situ, the water/ethanol mixture, stored in a tank under N₂ pressure, was diluted with nitrogen, vaporized and fed to the reactor, which was placed in an electrical oven. 5 heated solenoids allowed the reaction mixture to be sent to the reactor or to the analysis section. All the lines downstream the boiler were heated at 140 °C in order to avoid condensation. The products distribution was continuously monitored through a FT-IR spectrophotometer, paramagnetic and thermoconductivity analyzers.

Preliminary tests in the presence of impurities (1 mol % with respect to ethanol) were carried out at T=450°C and under a gas hourly space velocity (GHSV) of 15000 h⁻¹ over powders (m_{cat}=6 g); the mixture had the following composition: 5% C₂H₅OH/30% H₂O/65% N₂. Further tests were performed over powders and foams at lower contact times and m_{cat} was reduced to 0.6 g. Carbon formation rate (CFR) was evaluated through Temperature Programmed Oxidation (5% O₂/N₂ from room T to 600°C @10°C/min), which allowed the calculation of coke mass (g_C), and starting from the mass of carbon fed during the test (g_{C,T}) as well as the time-on-stream (TOS).



III. RESULTS & DISCUSSION

The stability tests with model bioethanol mixtures, prepared by adding individually 1 mol % of every impurity, were carried out for 5 hours. Whatever was the impurity added, total ethanol conversion was assured. However, the product gas distribution was affected during TOS for all the tests: the higher variation was observed at $t > 100$ min, when CH_4 selectivity started to decrease. It is generally known [2] that one of the roles of Pt during reforming reaction would be to hydrogenate reaction intermediates to CH_4 . Therefore, it was supposed that, during ESR, impurities adsorb on Pt sites, thus partially reducing its hydrogenation capability and leading to lessened CH_4 selectivity. The results of TPO analysis carried out over the exhaust samples showed slightly higher carbon formation rates with respect to the ones observed by feeding pure mixtures (Fig. 1); an increase in H_2 selectivity with the carbon content of the impurity was also recorded (not shown). This last finding was probably due to the reforming contribution of these species and to the increase in carbon selectivity from C_3 to C_5 iso-alcohols. In fact, CH_4 decomposition or intermediates condensation/polymerization reactions may enhance both H_2 production and coke deposits formation on catalyst surface.

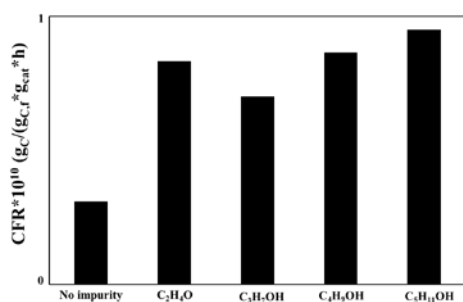


Fig. 1. CFR as a function of the impurity (1 mol% with respect to $\text{C}_2\text{H}_5\text{OH}$); $T=450^\circ\text{C}$, $\text{GHSV}=15000 \text{ h}^{-1}$, $r.a.=6$.

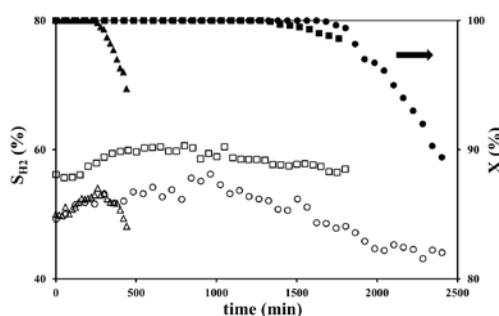


Fig. 2. S_{H_2} (empty) and X (filled symbols) vs TOS for powder (square), foam-containing silica (triangle) and boehmite (circle); $T=450^\circ\text{C}$, $\text{GHSV}=50000 \text{ h}^{-1}$, $r.a.=6$.

No catalyst deactivation was observed for almost 1 day even when a model bioethanol mixture, containing 1 mol % of all the impurities, was fed to the reformer at 15000 h^{-1} . Therefore, in

order to test catalyst stability in more stressful conditions, space velocity was increased to 50000 h^{-1} and the performances of powders and foams, containing boehmite or SiO_2 as binder, were compared. The results, in terms of H_2 selectivity (S_{H_2}) and $\text{C}_2\text{H}_5\text{OH}$ conversion (X), are summarized in Fig. 2. The foam catalyst prepared using boehmite allowed total ethanol conversion for more than 27 h and a better catalytic behavior than powder sample, which deactivated in 21 h, was observed. In the same conditions, worst performances were reached over the silica-containing foam: total ethanol conversion was recorded only for little more than 4 h of TOS. In terms of H_2 selectivity, the two foam samples reached very close results, while slightly higher values were recorded over the powder. In order to investigate the deactivation over the three catalysts, the carbon formation rate data (not reported) were compared. The foam catalyst, prepared employing the silica binder, despite showed a very fast deactivation, was characterized by a CFR data similar to the one observed for the catalytic powder. Therefore, coke deposition was not the main mechanism of its deactivation. Conversely, this phenomenon was explained considering that, during reforming reactions, steam can attack Si atoms [3], causing SiO_2 structural changes and wrapping Ni and/or Pt within silica: such covered metal particles become inactive for the desired reaction.

IV. CONCLUSIONS

In this work, the influence of the main bioethanol contaminants ($\text{C}_2\text{H}_4\text{O}$ and C_3 - C_5 iso-alcohols) on the stability of Pt-Ni/ CeO_2 - ZrO_2 powder and structured catalysts for ESR at 450°C was studied. Despite total $\text{C}_2\text{H}_5\text{OH}$ conversion was recorded for 5 h over powders, an increasing trend of CFR with impurity carbon content was observed. Moreover, structured catalysts containing boehmite as binder showed more promising results at 50000 h^{-1} and $\text{H}_2\text{O}/\text{C}_2\text{H}_5\text{OH}$ ratio of 6, in terms of durability, than powders and SiO_2 -based foam under a model mixture containing 1 mol% of all the impurities.

ACKNOWLEDGMENTS

The authors thank Fraunhofer Institute for supplying ceramic foams and Comethy project for financial assistance.

REFERENCES

- [1] Rass-Hansen, J., Johansson, R., Møller, M., Christensen C.H., Steam reforming of technical bioethanol for hydrogen production. International Journal of Hydrogen Energy Volume 33, 2008, pp. 4547-4554.
- [2] Jacobs, G., Keogh, R. A., Davis, B. H., Steam reforming of ethanol over Pt/ceria with co-fed hydrogen, Journal of Catalysis, Volume 245, 2007, pp. 326-337.
- [3] Takahashi, R., Sato, S., Sodesawa, T., Yoshida, M., Tomiyama, S., Addition of zirconia in Ni/ SiO_2 catalyst for improvement of steam resistance, Applied Catalysis A: General, Volume 273, 2005, pp. 211-215.



A NOVEL PLANAR SOLID OXIDE FUEL CELL CONFIGURATION FOR INDIRECT INTERNAL REFORMING

R. Cañas-Vargas*, F. Elizalde-Blancas*, I. R. Galindo-Esquivel*, J. M. Riesco-Avila*, A. Gallegos-Muñoz*

*University of Guanajuato, Lascaráin de Retana No. 5, Guanajuato, Guanajuato (Mexico)

Abstract - The performance of a planar solid oxide fuel cell with indirect internal reforming (IIR-SOFC) is analyzed by means of computational fluid dynamics. The cell operates with a fuel consisting mainly of methane and steam. Coflow and counterflow configurations with direct and indirect internal reforming were analyzed in order to determine the feasibility of planar IIR-SOFC configurations, since there are no works on planar IIR-SOFC in the available scientific literature. The set of equations such as continuity, momentum, heat, mass and charge transfer are coupled along with the correlations for reforming and electrochemical reactions. The set of equations was solved by using a commercial CFD software. The results show a better performance of the IIR-SOFC configurations due to lower diffusion losses, having a higher hydrogen concentration near to the anode.

Index Terms – Numerical analysis, solid oxide fuel cell, fuel processing.

I. INTRODUCTION

Due to their high operating temperature SOFC's can operate with fossil fuels because of the possibility to realize internal reforming. For a methane based operation of a SOFC, there are two approaches for internal reforming, direct internal (DIR-SOFC), or indirect internal (IIR-SOFC). Most of the works on modeling of IIR-SOFC focus on tubular cells, [1]. At this moment, no works on planar IIR-SOFC have been found. The purpose of this work is primarily to determine the feasibility of a planar IIR-SOFC comparing the performance of this configuration with the DIR-SOFC configuration at two different operating temperatures and secondly, to study how the flow configuration affects the temperature distribution in the cell.

II. PLANAR IIR-SOFC MODEL

A. Cell Geometry

A design for a planar IIR-SOFC is proposed based on the geometry used by Achenbach [2] and Li & Powers [3]. In this design, the reformer channel is located on the anode side and is connected to the anode fuel channel. On the cathode side the air flows in co-flow or counter-flow to the fuel stream as shown schematically in Figure 1.

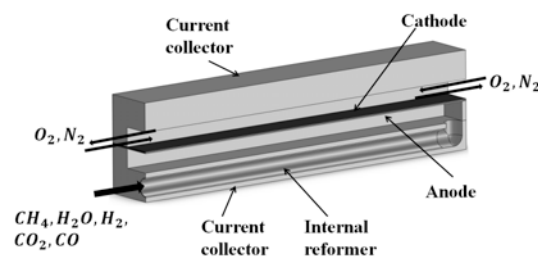


Fig. 1. Proposed IIR-SOFC geometry.

The reforming reaction takes place in a porous structure in the reformer channel and directly in the anode. The electrochemical reactions occur at the electrode-electrolyte interfaces.

B. 3D Model

A three-dimensional steady state model coupling the electrochemical reactions, chemical kinetics with fluid dynamics was used to simulate heat, mass and charge transfer. This model has been described previously in the work of De la Peña et al. [4]. For the present work, the

chemical kinetics of the reforming reactions in the anode are modeled by the global homogeneous catalyzed mechanism described in [4]. For the reforming reactions in the internal reformer the expressions proposed by Haberman & Young [5] for the porous material $MgAl_2O_4$ are used. Regarding the electrochemical model, the information for the exchange current density is taken from [6] considering that this is a function of the mean temperature in the electrode-electrolyte layer and is uniform in the electrode-electrolyte interface.

III. MODEL VERIFICATION

The model was verified using the planar SOFC modeling “benchmark 2” developed by the IEA [1], where a DIR-SOFC with steam reforming of CH_4 and air is modeled. The operating conditions for the planar IIR-SOFC were also taken from “benchmark 2”. A summary of the model verification is presented in Table 1.

TABLE I
MODEL VERIFICATION

Parameter	Benchmark 2	This work
Voltage (V)	High/low 0.649/0.633	0.647
Current density ($A\ m^{-2}$)	High/low 3665/3040	3118
Min	2508/1748	2895
PEN temperature (K)	High/low 1307/1294	1278
Min	1135/1120	1184
Outlet gas temperature (K)	High/low	
Air	1299/1289	1273
Fuel	1299/1294	1273

In this work more uniform temperatures and current densities are observed, this is because of the consideration of a constant exchange current density in the electrode electrolyte interface.

IV. RESULTS

A. Polarization Curves

Figure 2 shows the performance comparison between the DIR-SOFC and IIR-SOFC at two different operating temperatures, 1073 K and 1173 K. It can be observed that the co-flow DIR-SOFC delivers the lowest performance at the two operating temperatures. The counter-flow DIR-SOFC and both IIR-SOFC have in general a similar performance with a slightly higher performance for the counter-flow arrangement in the IIR-SOFC.

B. Temperature Distribution

Results indicate that IIR-SOFC configurations reach lower mean temperatures in the cell when this operates at the operating conditions in [2] (1173 K and $3000\ A/m^2$). In co-flow arrangement, the average cell temperatures for DIR-SOFC and IIR-SOFC are 1256 K and 1262 K, respectively. The average temperatures in the

counterflow arrangement are 1270K and 1254 K for the DIR-SOFC and IIR-SOFC, respectively.

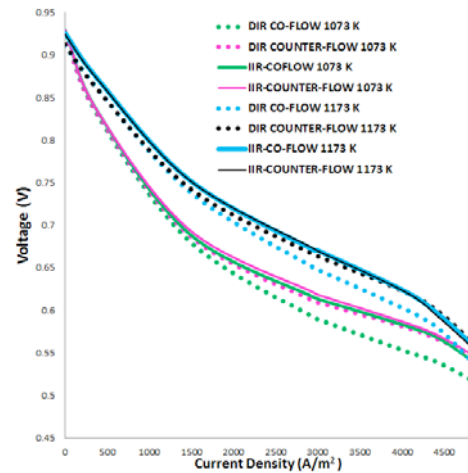


Fig. 2. Polarization curves for DIR and IIR.

V. CONCLUSIONS

A novel planar IIR-SOFC has been proposed to determine the feasibility of this configuration. The results indicate a better performance of the two flow configurations for the IIR-SOFC when compared with the DIR-SOFC co-flow, and a similar performance than counter-flow DIR-SOFC. The temperature distribution is slightly more uniform in IIR-SOFC. In general the planar IIR-SOFCs are feasible for performance improvement.

REFERENCES

- [1] Ahmad Hajimolana, S., Azlan Hussain M., Ashri Wan Daud, W. M., Soroush M., Shamiri A., Mathematical modeling of solid oxide fuel cells: A review, *Renewable and Sustainable Energy Reviews*, Volume 15, Issue 4, 2011, pp. 1893-1917.
- [2] Achenbach, E., 1996, SOFC Stack Modeling, Final Report of Activity A2, Annex II: Modeling and Evaluation of Advanced Solid Oxide Fuel Cells, International Energy Agency, Juelich, Germany.
- [3] Li, M. Powers, J. D., A Finite Volume SOFC Model for Coal-Based Integrated Gasification Fuel Cell Systems Analysis, *Journal of Fuel Cell Science and Technology*, Volume 7, 4, 2009, p. 041017
- [4] De La Pena-Cortes, E., Elizalde-Blancas, F. Hernandez-Guerrero, A., Gallegos-Muñoz, A., Belman-Flore, J. M., Numerical Analysis of the Internal Fuel Processing in Solid Oxide Fuel Cells, ASME 2013 International Mechanical Engineering Congress and Exposition.
- [5] Haberman, B. A., Young J. B., Three-dimensional simulation of chemically reacting gas flows in the porous support structure of an integrated-planar solid oxide fuel cell, *International Journal of Heat and Mass Transfer*, Volume 47, 2004, pp. 3617-3629.
- [6] Costamagna, P., Selimovic, A., Del Borghi, M., Agnew, G., Electrochemical model of the integrated planar solid oxide fuel cell (IP-SOFC), *Chemical Engineering Journal*, Volume 102, 2004, pp. 61-69.



EXPERIMENTAL INVESTIGATION OF SUPPLYING DUST-CONTAMINATED GAS TO THE CATHODE OF A MOLTEN CARBONATE FUEL CELL

R. Bernat*, J. Milewski*

*Warsaw University of Technology, Institute of Heat Engineering,
ul. Nowowiejska 21/25, 00-665 Warszawa, (Poland)

Abstract - The paper presents initial research on processes present on the cathode side of Molten Carbonate Fuel Cells (MCFC). The main goal of the investigation was to check the influence of solid particles, which could possibly be present in the gases fed to the MCFC cathode, on the alteration in properties of porous layers of the fuel cell. The research is based on experiments conducted at the Institute of Heat Engineering of Warsaw University of Technology.

The main task was to determine whether and to what extent solid particles disable or hinder the operation of a molten carbonate fuel cell. It is thought that they might change the features of porous layers. Investigation on the sizes and amount of solid particles significantly changing the processes occurring on the triple phase was done.

Experimental investigation was done that determines the change in operational parameters due to dust contamination.

Index Terms – contaminations, dust, molten carbonate fuel cells, solid particles

I. INTRODUCTION

Due to environmental reasons more and more pressure, even despite the economic crisis, is put on carbon dioxide emissions. For carbon intensive economies, e.g. Poland (90% of electricity generated from hard coal and lignite), an reasonable option could be to develop carbon capture and storage or carbon capture and utilization technologies. Therefore some scientific attention was focused on the research of novel technologies allowing to separate carbon dioxide from the flue gases stream without losing much of the nominal coal combustion plant efficiency. Molten Carbonate Fuel Cells were already proven both mathematically and experimentally to be capable of separating carbon dioxide and some modelling research results have shown that such operation could keep the plants efficiency at nominal levels or, in some cases, increase the whole system fuel efficacy. None of these works however

take into account the solid particle contamination of flue gases (and therefore feeding to the cathode chamber of the cell) though and this probably would be the case if an MCFC installation would have to be installed in an already existing plant that is subject to current (and even future) emission standards. In this work the results of an experimental work focused on fuel cell dust contamination is presented. In Fuel Cell Handbook (Seventh Edition) [1] allowable contaminant levels for molten carbonate fuel cells are mentioned. The dust contamination levels are based on research results presented in [2] and [3]. There are however significant differences. The authors analyzed the anode of the fuel cells – their focus was on solid particles present in the anode flow that could be present due to coal gasification process. Another aspect is the fact that in the last 30 years the materials for MCFC changed dramatically including electrode porosity, their chemical composition and mean pore diameters. In result of the experimental work a reaction took place due to the dust contaminant – zinc oxide. In results the influence of the particle size and physical phenomena were not investigated at the end.

II. EXPERIMENTAL EQUIPMENT

The apparatus used for experiments was a tailored made test rig for molten carbonate fuel cell investigation. The test bench had however to be modified in order to allow for dust contamination. As little research was done on solid particle contamination before innovative experimental methods had to be applied. A generator of solid aerosol was combined with the existing fuel cell experimental set-up (fig. 1). Additional measurements had to be taken to make sure that the composition of gases was appropriate.





Fig. 1. Test rig connected with an aerosol generator

III. THE CONTAMINANT

Regular industrial talc powder (finntalc) was used for contamination of the cathode porous structures of the fuel cell. The main goal was to assess, whether the porous structure of the cathode will not be clogged with the small solid particles with diameters below the pore diameters of the cell. It contains about 60% of silica and 32% of magnesia and traces of other oxides. The main parameter – median size of the powder – was equal to about 5 microns.

IV. EXPERIMENTAL RESULTS

As it was expected that the dust contamination test would terminate the fuel cell, usually experiments were done already after other experiments have been performed previously. Nevertheless, before every solid particle contamination there was a polarization curve drawn in order to define the performance of each tested cell (Fig. 3).

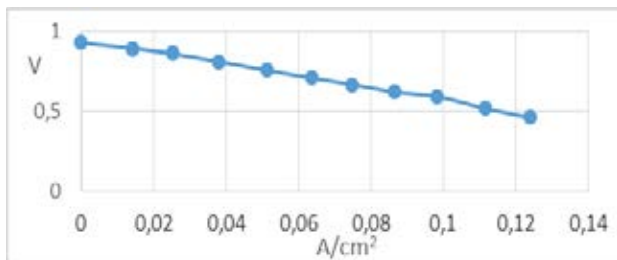


Fig. 3. Polarization curve of the cell used for testing

The cell was supplied with regular operation gas flows for its normal functioning. It was loaded with 1.5 A, what corresponds to 0.074 A/cm² at 700 mV. 1.68 g of dust was fed to the cathode in 2.5 hrs. The experimental results of the tests are shown in the figure 4. The green graph is the voltage of the cell. There are two sudden voltage drops. The first one corresponds to loading the cell with the current, the second one is due to disconnection of gas supply caused by disattaching the aerosol generator and reattaching the supply pipe to the test bench system. A post mortem picture of the cell cathode side was shown in the figure 5.

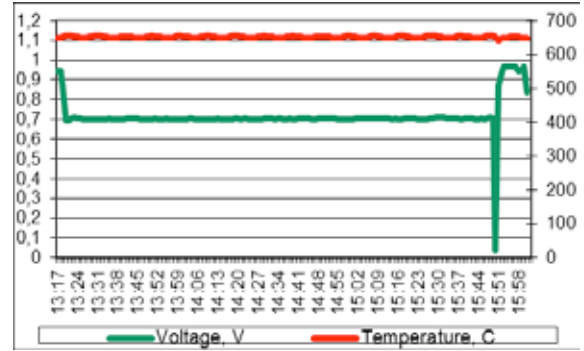


Fig. 4. Experimental results of the solid particles influence on the cathode of an MCFC



Fig. 5. Post-mortem picture of the cell used for experiments

V. CONCLUSION

Solid particles suspended in the cathode inlet flow did not cause any disturbance in cell operation. No voltage drop was observed during 2.5 hours of operation with amount of dust highly exceeding the limits enforced on power plant flue gases. This probably shows a high potential for MCFC as a CO₂ separator. However, more experimental work should be performed including other types of dust (also real coal fired boiler dust) and longer exposure periods. Nevertheless, it is proved that MCFCs are not highly sensitive to dust contamination.

ACKNOWLEDGMENT

We would like to thank the National Centre for Research for financing this work within a Preludium Grant.

REFERENCES

- [1] EG&G Technical Services, I. (Ed.) Fuel Cell Handbook (Seventh Edition) U.S. Department of Energy Office of Fossil Energy National Energy Technology Laboratory, 2004
- [2] Pigeaud, A. & Klinger, J. Study of the effects of soot, particulate and other contaminants on molten carbonate fuel cells fueled by coal gas Energy Research Corporation, 3 Great Pasture Road, Danbury, CT 06813, 1986
- [3] Pigeaud, A.; Klinger, J. & Kennedy, H. Study of the effects of soot, particulates and other contaminants on molten carbonate fuel cells fueled by coal Energy Research Corporation, 3 Great Pasture Road, Danbury, CT 06813, 1987



COMPLETE RELAXATION OF RESIDUAL STRESSES DURING REDUCTION OF SOLID OXIDE FUEL CELLS

H. L. Frandsen, C. Chatzichristodoulou, P. V. Hendriksen
Technical University of Denmark, Department of Energy
Conversion and Storage, Frederiksborgvej 399, 4000 Roskilde,
(Denmark)

Abstract - To assess the reliability of solid oxide fuel cell (SOFC) stacks during operation, the stress field in the stack must be known. During operation the stress field will depend on time as creep processes relax stresses. This work reports further details on a newly discovered creep phenomenon, *accelerated creep*, taking place during the reduction of the anode. This relaxes stresses at a much higher rate ($\sim 10^4$) than creep during operation. The phenomenon has previously been studied by simultaneous loading and reduction. With the recorded high creep rates, the stresses at the time of reduction should reduce significantly over minutes. In this work the stresses are measured in-situ before and after the reduction by use of XRD. The phenomenon of accelerated creep has to be considered both in the production of stacks and in the analysis of the stress field in a stack based on anode supported SOFCs.

I. INTRODUCTION

Ensuring mechanical stability of SOFC stacks is a key challenge for the commercialization of the technology. To evaluate the reliability of the SOFC stacks during operation, the stress field in the stack must be known. The stresses in a stack evolve over time depending on the operational conditions, external pressures, thermal expansions, elastic and creep properties of the various stack components. Knowing these, it is possible to estimate the stress evolution over time by a thermo-mechanical model. It is however essential that the *initial* stress field generated through the assembly of the SOFC stack is accurately determined.

To determine the initial stress field, the creep through the assembly of all the stack components is of key importance, as the stress development depends on the mutual relaxation of stresses. In this study we focus on the creep and relaxation of the stresses of the anode and anode support of the SOFC as this, for many cell designs, constitutes the main structural component. The anode/anode-support is typically made from nickel (Ni) and zirconia with 3 or 8 mol % yttrium doping.

Recently a phenomenon, so-called *accelerated creep* of SOFC Ni(O)-YSZ anodes occurring on the reduction of the

NiO, has been discovered [1]. The creep phenomenon was studied by measuring macroscopic deflections/extensions of composite samples on different sequences of loading and reduction. Different creep rates were found in bending and uniaxial tension. The reason for this was speculated to be due to a chemo-mechanical interaction, i.e. mechanical stress nucleates the chemical reduction, which as a consequence occurs faster on stressed zones. A hypothesis for the mechanisms behind the accelerated creep was also proposed, i.e. it is due to a fast softening of the Ni(O) phase during reduction, which provides; 1) increased creep rate of the relatively porous YSZ backbone, 2) a significant decrease of the elastic modulus (by a factor of 10), 3) an expansion due to release of compressive residual stresses in the YSZ phase. The latter is contradicting previous literature but is confirmed by measurements. It also implies that the internal residual stress between the Ni(O) and YSZ phases, arising from the cool down after sintering, are completely released upon reduction (see Fig. 2).

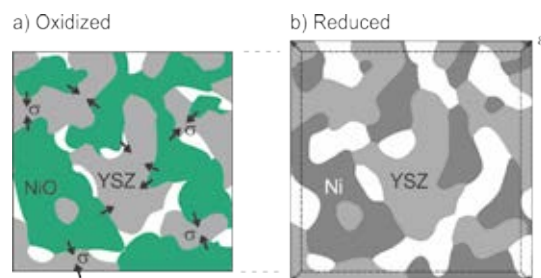


Fig. 1. Expansion of microstructure during reduction due to release of residual stresses.

Residual stresses in NiO-YSZ half cells have been measured by X-ray diffraction by following the Bragg edges for different reflection angles at room temperature, see e.g. [2–4], from the curvature of half-cells and by modelling it by creep deformations from the sintering temperature [3,5].

In this work the residual stresses (/elastic strains) are measured by *in-situ* XRD as a function of temperature in oxidized (as sintered) condition and through reduction.

II. EXPERIMENTAL

Samples were tape-cast and sintered half-cells consisting of a ~ 300 μm anode support of NiO-3YSZ, ~ 40 μm anode of NiO-8YSZ anode, and 10 μm electrolyte.

The *in-situ* X-ray diffraction measurements were carried out in a Rigaku SmartLab diffractometer with Cu $K\alpha$ radiation, using an Anton Paar HTK 1200N high temperature oven chamber with atmosphere control. The XRD patterns were recorded in the 2θ range $25 - 150^\circ$ with a step of 0.01° . The software package PDXL was employed for the Whole Powder Pattern Fitting of the diffractograms and for the microstrain analysis based on the Halder-Wagner method [6].

III. RESULTS

In Fig. 1 the elastic microstrain in both phases of the composite measured through the heat up of the oxidized (as sintered) anode support and during cooling after reduction is plotted. The elastic strain is directly proportional to the stress (with elastic modulus as proportionality factor). Through the reduction the stress drops in both material phases and goes to zero in the Ni phase. Some stress remains in the YSZ phase.

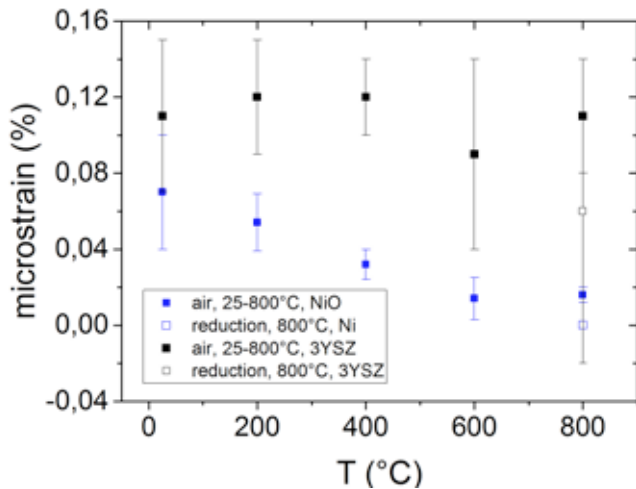


Fig. 2. Microstrain of the individual phases of the Ni(O)-3YSZ composite through temperature and reduction.

IV. DISCUSSION

That the stress in Ni(O) phase goes to zero at reduction is consistent with the hypothesis for the expansion during reduction in [1] (see Fig. 1). That the stress in the YSZ phase in the anode support does not go to zero at reduction could be ascribed to the small TEC difference between 3YSZ and 8YSZ in the different half-cell layers. Further work is under way to record XRD data with improved signal to noise ratio in an attempt to reproduce these results and reduce the uncertainty of the estimated microstrain values.

The measured elastic strain is related to the previous estimates of expansion of the YSZ backbone through reduction (0.04 % at 800°C), as the expansion at this point is exactly due to the release of residual stresses (according to the hypothesis

in [1]. By extrapolating this residual strain linearly to room temperature given a reference temperature of $\sim 1100^\circ\text{C}$ results in a strain of 0.11 % ($0.04 \% \times 800^\circ\text{C} / 300^\circ\text{C}$), which is in very good agreement with these measurements (see Fig. 2).

This means that for a SOFC constrained in a stack the elastic expansion of the YSZ during reduction will be balanced by the other stack components through the seals. If a particular stack design has problems with durability of the seals, reduction of the SOFC stack should be considered immediately after sealing the stack, as the seals might at this point be ductile and compliant to release the compressive residual stresses in the YSZ phase (in electrolyte and anode).

In general the observed phenomenon complicates a thermo-mechanical simulation of a SOFC stack considerably, as the phases of Ni-YSZ layers in principle must be considered individually. However, in many cases it is reasonable to assume that all stress goes to zero in the SOFC stack at the point of reduction (see above discussion), which simplifies the thermo-mechanical analysis.

V. CONCLUSION

In this work the elastic microstrain was measured up through temperature in oxidized condition, through reduction at 800°C. The stress in the Ni phase goes to zero during reduction, which is consistent with previously reported macroscopic expansions on reduction of Ni(O)/YSZ-composites. These expansions are one of the contributions of the large distortions occurring during reduction of the composite, referred to as accelerated creep.

Furthermore, the amount of residual microstrain in the YSZ was found to be in the order of 0.11 % at room temperature, which is in very good agreement with the observed expansion on reduction in the previous work [1]. The consequence of this is that the stress in many cases can be considered to go to zero at the point of reduction in SOFC stacks.

ACKNOWLEDGMENTS

The European Union's Seventh Framework Programme (FP7/2007-2013), FCH-JTI, grant agreement n° 325278 and from Energinet.dk, ForskEL contract 2014-1-12236.

REFERENCES

- [1] Frandsen HL, Makowska M, Chatzichristodoulou C, Greco F, Ni DW, Curran DJ, et al. Accelerated creep in solid oxide fuel cell Ni-YSZ anode supports during reduction
- [2] Sun B, Rudkin R., Atkinson A., Fuel Cells 2009;9:805–13.
- [3] Charlas B, Chatzichristodoulou C, et al. 11th Eur. SOFC SOE Forum 2014, Lucerne: 2014, p. B1107.
- [4] Fischer W, Malzbender J, Blass G, Steinbrech RW. J Power Sources 2005;150:73–7.
- [5] Greco F, Frandsen HL, Nakajo A, Madsen MF, Van herle J. J Eur Ceram Soc 2014, 34(11), p. 2695–2704.
- [6] Halder N. C. and Wagner C. N. J., Acta Cryst 1966, 20, p. 312-313.



SYNERGIC INTERACTION BETWEEN CERIA AND TIN IN SOFC ANODES

L Bardini*, A. Pappacena*, M. Boaro* and A. Trovarelli*

*University of Udine, Department of Chemistry, Physics and
Environment, Via Cotonificio 108, 33100 Udine, (Italy)

Abstract - Ceria and tin oxide were infiltrated in samaria-doped ceria (SDC) anodes for use in intermediate-temperature solid oxide fuel cells (IT-SOFCs). It was found that ceria is able to stabilize tin as a molten metal in a reducing atmosphere up to 973 K, by preventing its coalescence and segregation. Moreover, electrochemical tests showed that the addition of tin significantly improves the performance of ceria towards the oxidation of hydrogen and methane. Impedance spectra suggested that the addition of tin affects conduction as well as reaction kinetics in the anode.

Index Terms - Ceria based anode, IT-SOFC, Molten-metal catalyst, Tin.

I. INTRODUCTION

Cerium oxide has received considerable attention in the development of IT-SOFC anodes [1]. Ceria, in fact, possesses a relatively high ionic conductivity at temperatures as low as 873 K, nevertheless its conductivity and catalytic properties must be improved. This means that a metal co-catalyst needs to be added in order to achieve good fuel conversion rates and to increase electronic conductivity in the anode compartment at the same time. In this regard, tin has not been investigated yet, despite its low cost and its demonstrated catalytic activity towards CO and H₂ oxidation when combined with ceria [2].

In this work the effect of tin on cell performance of ceria-infiltrated SOFC anodes at intermediate temperature in both hydrogen and methane is studied, and a synergistic interaction between ceria and tin is highlighted.

II. EXPERIMENTAL SECTION

Fuel cells were prepared by uniaxially pressing 600 mg of commercial samaria-doped ceria (Nextech, FuelCell Materials) for the electrolyte and 150 mg of samaria-doped ceria mixed with 30% w/w commercial starch (Mantovani) as the pore former for the anode. The two

layers were co-sintered at 1673 K for 3h. The LSCF/GCD cathode (Nextech, FuelCell Materials) was applied by painting with 5% w/w vulcan carbon as the pore former, and sintered at 1473 K for 3h. The anode was then infiltrated with the catalyst using a proper solution of its precursor. Ceria was infiltrated and calcined at 873 K before infiltrating tin oxide.

Electrochemical impedance spectroscopy (EIS) measurements were conducted in the frequency range 1 MHz-100 mHz with a signal amplitude of 30 mV at open circuit potential. Materials and cells were characterized with conventional techniques (XRD, SEM, XPS, HRTEM).

III. RESULTS

The cell has an electrolyte of 380 μm thick, while the SDC anode and the cathode have a thickness of 150 μm and 20 μm respectively. Porosity measured via Archimede's technique for the anodes is ca. 40%, which is low when compared to other examples present in the literature. SEM images of the anode cross-section (not shown) reveal that the anode microstructure is not optimized.

Figure 1 shows the Current-Voltage/Power density curves (left) and the corresponding Nyquist plots (right) of cells whose anode has been infiltrated with ceria only, tin only and with ceria and tin in Ce/Sn molar ratios 0.8 (CeSn0.8) and 1.5 (CeSn1.5).

Overall performance remains relatively low for all materials due to the anode morphology: its low porosity and high thickness pose an a priori limit to the performance of the cells. An analysis of the relative power output of the cells is more informative. It can be seen that the addition of tin significantly increases the power and current output. Cells infiltrated with tin oxide alone, on the other hand, give a maximum power output of 20 mW/cm² (not shown). This result was explained by a post-mortem analysis of cells. Cells infiltrated with tin alone showed a distinct grey halo on top of the anode



(results not shown), indicating that tin is reduced to a metal and segregates. Interestingly, no such effect is observed when ceria and tin are both present, which means that ceria is effectively able to stabilize tin in operational conditions.

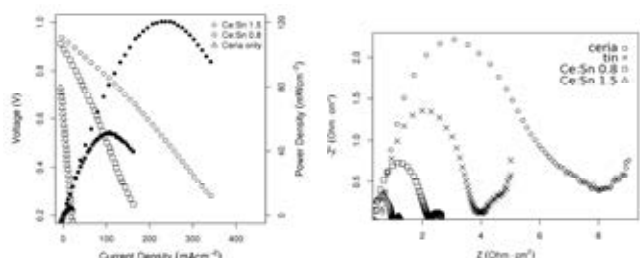


Fig. 1. Left: Power and current density curves of fuel cells tested in 100% hydrogen at 873 K, Right: Corresponding EIS spectra.

EIS spectra show that the addition of tin has an important impact on the conductivity in the anode. This can be seen from the considerable decrease in the reactance and resistance of the high frequency semicircle in the Nyquist plots (right). The fact that even tin alone generates a lower impedance than ceria means that an important contribution comes from an increase in electronic conductivity. The conductivity of cells infiltrated with both tin and ceria increases further with respect to the separate components, reaching a maximum for the cell CeSn1.5. An increase of the ionic conductivity is also probable in this case, as tin can effectively reduce ceria [3]. The low frequency region of the Nyquist plots also decreases significantly with the addition of tin, indicating that tin also positively affects catalytic performance by acting on charge transfer, oxygen transfer or on hydrogen adsorption [4].

The effect of the co-presence of ceria and tin on cell performance was also tested in methane (Fig. 2).

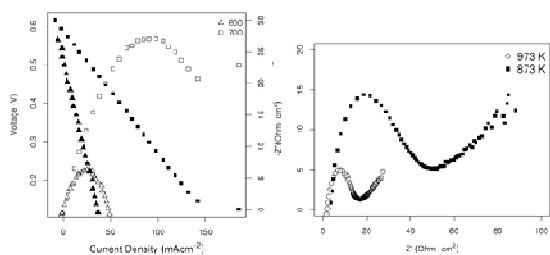


Fig. 2. Left: Power and current density curves of CeSn 1.5 fuel cell, tested in 100% methane at different temperatures, Right: Corresponding EIS spectra.

Cells containing ceria alone have an extremely low power (not shown). The improvement upon addition of tin is striking, especially when the temperature increases, confirming improved catalytic activity and stability of the infiltrated tin even under CH_4 flow. The high impedance values recorded suggest that the catalyst can be further improved.

Open circuit voltage (OCV) values (Table 1) are in agreement with the above results. While the deviation from the theoretical value for all cells is to be ascribed to large losses due to the faulty anode morphology and to a possible partial reduction of the electrolyte, the increase in OCV with the co-presence of tin and ceria is likely due to reduced activation losses, which supports an active role of the tin-ceria interface in the oxidation reaction.

No significant differences were found between the performance in H_2 for CeSn1.5 cells previously tested in methane. This indicates that carbon deposition, if present, is not significant on short time scales (< 20 hours).

TABLE I. Open circuit voltage (OCV) values in hydrogen and methane at various temperatures. All OCV values are reported in Volts.

Hydrogen	873 K	903 K	936 K	973 K
Ceria	0.88	0.88	0.89	0.88
Tin	0.78	-	-	-
Ce:Sn 0.8	0.90	0.88	0.88	0.87
Ce:Sn 1.5	0.92	0.91	0.91	0.90
Methane				
Ce:Sn 1.5	0.57	-	-	0.63

Structural characterization of the infiltrated anodes and of ceria powder shows that, upon exposure to hydrogen at 873 K, SnO_2 is reduced to molten metallic tin, which is stabilized at temperatures as high as 873 K by ceria. The stabilization is possible thanks to the formation of a nanometric amorphous layer of oxidized tin encapsulating molten Sn^0 nanoparticles [5]. This layer would have the effect of creating a synergistic interaction between tin and cerium oxide: Sn is anchored on ceria thanks to oxygen transfer from the CeO_2 , at the same time, the reduction of ceria is favored improving oxygen conduction and exchange. Further study are in progress to get insight into the stability and activity of this structure with other fuels.

IV. CONCLUSION

The system Ce-Sn results a promising composition for the development of IT-SOFC anodes and further studies are in progress to implement compositions suitable for biogas and alternative fuels.

V. REFERENCES

- [1] Chatzichristodoulou, C.; Blennow, P.; Sogaard, M.; Hendriksen, P.; Mogensen, M. In *Catalysis by ceria and related materials*; Trovarelli, A., Fornasiero, P., Eds.; Imperial College Press: London, 2013.
- [2] Iglesias-González, A.; Ayastuy, J.; González-Marcos, M.; Gutiérrez-Ortiz, M. $\text{CuO/Ce}_x\text{Sn}_{1-x}\text{O}_2$ catalysts with low tin content for CO removal from H_2 -rich streams, *Int. J. Hydrogen Energy* 39, 2014, 5213-5224.
- [3] Matolin, V., et.al. Sn interaction with the CeO_2 (1 1 1) system: bimetallic bonding and ceria reduction., *Surf. Inter. Analysis*, 40, 2008, 225-230.
- [4] Huang, Q.-A., Hui, R., Wang, B., Zhang, J. A review of AC impedance modeling and validation in SOFC diagnosis, *Electrochimica Acta*, 52, 2007, 8144-8164.
- [5] Bardini, L. et al., manuscript in preparation.



ELECTRICITY GENERATION FROM NOPAL BIOGAS WASTE BIOMASS USING CLAY CUP (CANTARITO) MODIFIED MICROBIAL FUEL CELL

Sathish-Kumar Kamaraj *, Alejandro Esqueda Rivera *,
Selvasankar Murugesan **, Jaime García-Mena **, Claudio
Frausto Reyes*** and José Tapia-Ramírez**

* Universidad Politécnica de Aguascalientes, Ingeniería en Energía
Calle Paseo San Gerardo No. 207. Fracc. San Gerardo.

Aguascalientes, Ags. México, 20342, (Mexico)

** Departamento de Genética y Biología Molecular, Cinvestav-IPN,
México DF, México. D.F. 07360. (Mexico)

*** Centro de Investigaciones en Óptica, A.C. Prol. Constitución
607, Fracc. Reserva Loma Bonita Aguascalientes, 20200, (Mexico)

Abstract - We designed the clay cup (cantarito) modified microbial fuel cell (CCM-MFCs) for digest the Nopal biogas effluent (NPE). Further, we painted the commercial Acrylic varnish on the clay cup, in order to study the impact of power generation in CCM-MFCs. In this context, we performed the three experiments, which follows the order: 1) Painting of commercial varnish on both side of clay cup (CCM-MFC:BS) 2) painting of commercial varnish on inside of clay cup (CCM-MFC:IS) and 3) painting of commercial varnish on outside of clay cup (CCM-MFC:OS). The maximum volumetric power densities as follows: CCM-MFC:BS (1841.99 mW/m^3) > CCM-MFC: IS (1023.74 mW/m^3) > CCM-MFC:OS (448.90 mW/m^3). The Closed circuit (3000Ω) operational maximum volumetric power densities as follows: CCM-MFC:BS (205.03 mW/m^3) > CCM-MFC:OS (140.83 mW/m^3) > CCM-MFC: IS (74.91 mW/m^3). The control experiment without varnish doesn't show the stable potential. Hence, Acryloyl group in varnish could favors the cationic ion conduction and favor the performance. Finally, we powered the 4digital clock with the CCM-MFC:BS of 2-cell connected in series .

Index Terms –Clay Cup, Microbial fuel cell, Nopal biogass effluent, Prototype

I. NOMENCLATURE

CCM-MFCs	Clay cup modified microbial fuel cells
NPE	Nopal biogas effluent
P_V	Volumetric power density
I_V	Volumetric current density

II. INTRODUCTION

In Microbial fuel cells (MFCs), electricity is extracting it from the wastewater, where biocatalysts oxidize complex organic material. There are many different types of wastewaters have been used to produce electricity in MFCs, performance has substantially varied depending on the specific wastewater and reactor configuration. In this study, power production and

organics removal of a NPE exploited in CCM-MFCs. Where, we used the clay cup as a separator, and the NPE used in anodic compartment for generating electricity. Further, we painted the commercial varnish on the clay cup, in order to improve the power generation in CCM-MFCs. Later we found the interesting microbial communities through metagenomics. In the final stage, we developed prototype to power the 4digital clock by the 2 CCM-MFCs connected in series.

III. MATERIALS AND METHODS

A. Collection of NPE

NPE was collected from the Nopal biogas plant situated at Calvillo, Aguascalientes, in Mexico, and stored in refrigerator at 4°C .

B. Construction of clay cup based MFC, characterization and operation

We purchased the clay cup from the local market of Aguascalientes and used Ultra color commercial varnish for painting. Graphite felt used as anode and cathodic current collector. Inside of the clay cup filled with the potassium ferricyanide (100 mM) solution, and outside of the clay cup contains the NPE, which is served as inoculum in anode and also as medium to be treated (Mexican Patent No: submitted). Further, the CCM-MFCs were characterized by linear sweep voltammetry (LSV) at 0.1 mV s^{-1} using Gamry Interface 1000 Potentiostat/Galvanostat/ZRA (Kamaraj et al., 2015). Finally two of the CCM-MFC-BS in series connection used for power the digital clock operated for 1008 hrs of batch operations. We analyzed the Bacterial Genomic DNA from the CCM-MFCs, 16S rDNA libraries of V3 region was prepared and sequenced through Ion semi-conductor sequencing. Sequenced data were analyzed using QIIME-V.1.9.0 pipeline.



IV. RESULTS AND DISCUSSION

The initial parameters for the nopal biogas waste biomass were as follows: 3.45 g/l of COD, 7.4 of pH, 4.66 g/l of TDS, 9.32 mS/cm of conductivity and 1.909 % of transmittance at 750 nm. We performed the each CCM-MFC, for intermittent characterization (every four days) and closed circuit (3000 Ω) operation for 29 days. During the intermittent characterization, CCM-MFC:IS exhibited the maximum OCP of 1.358 V. CCM-MFC:OS shows the 1.075 V maximum OCP, CCM-MFC:BS display the maximum OCP of 0.923 V. Nevertheless, with respect to the stability time of maximum OCP as follows the order: CCM-MFC:BS for 27.75 hrs > CCM-MFC:OS for 15 hrs > CCM-MFC:IS for 7.5 hrs. The maximum volumetric power densities as follows: CCM-MFC:BS (1841.99 mW/m³) > CCM-MFC: IS (1023.74 mW/m³) > CCM-MFC:OS (448.90 mW/m³). The Closed circuit (3000 Ω) operational maximum volumetric power densities as follows: CCM-MFC:BS (205.04 mW/m³) > CCM-MFC:OS (140.83 mW/m³) > CCM-MFC: IS (74.91 mW/m³) (Fig 1.). The control experiment without varnish painting doesn't show the stable potential.

Both side painted varnish (CCM-MFC:BS) shows a superior performance in the characterization and closed circuit operation. Which infer the Acryloyl group in varnish on both sides could favor the cationic movement (Jiayin and Markas 2011), which improve the performance of CCM-MFC:BS. Moreover, The COD removal % of CCM-MFC:BS cell demonstrate the 72.88 % for characterization and 75.01% for closed circuit operation. This was higher than other cells. Finally, we connected series of two CCM-MFC:BS powered the digital clock for 1008 hrs of batch operation. It shows the average potential of 1.21 V and 76.01 % of COD removal in NPE (Table 1. And Fig 2.). More interestingly, in our system we didn't use any external power required systems (agitation, incubator and etc.).

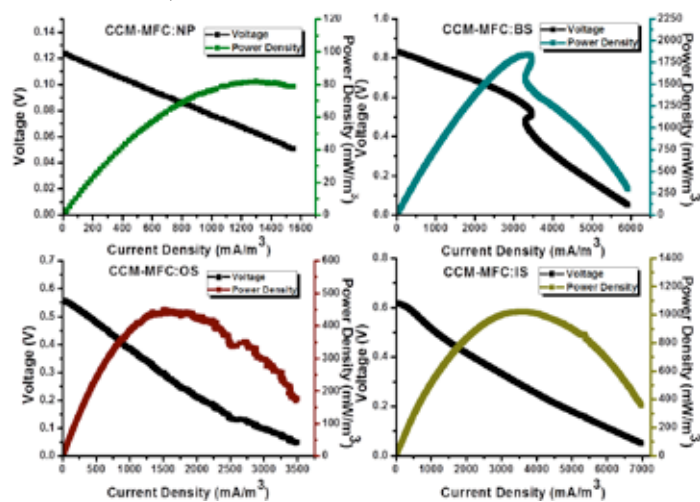


Fig. 1. Polarization cure of CCM-MFCs

In metagenomic analysis of CCM-MFCs:BS anode, most abundant phyla were Bacteroidetes, Firmicutes, TM7, and

Proteobacteria. The abundance of TM7 decreased upon Nopal wastewater treatment using Cantarito based MFC-Varnish painted in and out 3K ohm and Graphite Felt 3K ohm connected. But TM7 recovered to its initial state abundance at final state (Fig 3.).

TABLE I
AVERAGE VALUES OF PARAMETERS IN BATCH OPERATION OF CCM-MFC:BS WITH DIGITAL CLOCK.

Parameters	CCM-MFC:BS:CLK-SERIE
P_v (mW m ⁻³)	263.57
P (mW m ⁻²)	2.50
I_v (mA m ⁻³)	216.90
I (mA m ⁻²)	2.06
Potential (V)	1.21
COD %	76.01



Fig. 2. Prototype developed from CCM-MFC:BS:CLK (2 cell- serie) to power the Digital clock

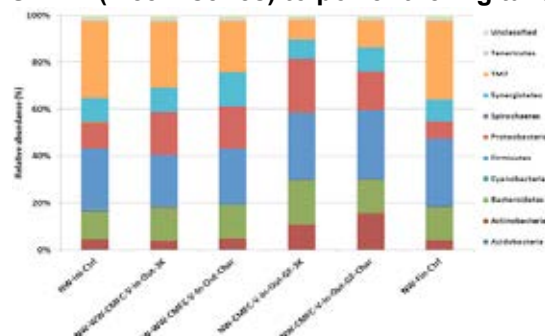


Fig. 3. Metagenomic analysis of the NPE

V. CONCLUSION

We designed and optimized the CCM-MFCs for powered the 4 digital clocks upto 1008 hrs in a batch operation. Interestingly, Bacteroidetes, Firmicutes, TM7, and Proteobacteria were identified in CCM-MFCs:BS.

ACKNOWLEDGMENT

The author KSK thanks the SEP for the grant of PRODEP 2014 project No. DSA/103.5/14/10671, UPA and CONACYT.

REFERENCES

- [1] Kamaraj, S.-K., Romano, S.M., Moreno, V.C., Poggi-Varaldo, H.M., Solorza-Feria, O, Use of Novel Reinforced Cation Exchange Membranes for Microbial Fuel Cells. *Electrochimica Acta*, Volume 176, 2015, Pages 555-566.



FACILE MICROBIAL FUEL CELL FROM PENCIL UTILIZING SUSTAINABLE CATHODE AS OF USED BATTERY

Angel Rodrigo Montes Ochoa *, K. Sathish-Kumar *, O.
Solarza-Feria**, Manuel Sanchez Cardenas*, Fernando Trejo
Zarraga*** and J. Tapia-Ramírez****

* Universidad Politécnica de Aguascalientes, Ingeniería en Energía
Calle Paseo San Gerardo No. 207. Fracc. San Gerardo.

Aguascalientes, Ags. México, 20342, (Mexico)

** CINVESTAV-IPN, Departamento de Química, México D.F.

***Centro de Investigación en Ciencia Aplicada y Tecnología

Avanzada del IPN, Unidad Legaria, 11500 (Mexico)

****CINVESTAV-IPN, Departamento de Genéticas y Biología
Molecular (Mexico)

Abstract - In our work, we proposed the novel simplified pencil-based integrated microbial fuel cells (P-MFCs). In a pencil, the graphite rod could act as anode with a wooden portion submerged into the raw wastewater solution, whereas the remained wooden portion is exposed to air and bound with carbon cloth containing the Pt electrocatalysts for oxygen reduction reaction. P-MFC showed a volumetric power density of 3.61 mW m^{-3} and current density of 9 mA m^{-3} at 0.403 V . Further, the pencil was treated with sulphuric acid solution and exhibited the lignosulfonate peaks at 1032 cm^{-1} and 872 cm^{-1} in the FT-IR spectroscopy. Later, 6M sulfuric acid-treated pencil standard cell exhibited a volumetric power density of 956 mW m^{-3} (as standard P-MFCs) Then, we took the cathode of an alkaline battery to be used as cathode for P-MFCs. Interestingly, this arrangement exhibit a volumetric power density of 936.12 mW m^{-3} . Finally, we developed a prototype for powering a digital clock. Thus, we avoided using noble metal catalyst and our simplified MFC design greatly decreased the cost.

Index Terms –Microbial fuel cell, Pencil, Prototype, Wastewater

I. NOMENCLATURE

P-MFCs Pencil based integrated Microbial fuel cells.

II. INTRODUCTION

Microbial fuel cells are a promising renewable energy technology, especially in wastewater treatment, where bacteria oxidize complex organic or inorganic material to generate electricity, while at the same time the wastewater is treated. MFCs power production has been increased over the years by several orders of magnitude and showed a promising trend. However, further power increases are desirable to improve the economic feasibility of MFCs technologies for practical real-world applications (Kamaraj et al., 2015). Improved MFCs performance is likely a result from the optimized component

such as anode, cathode, separator and reactor configurations. In this context, we proposed the simplified integrated MFC design from a pencil. Further, we improved the performance of P-MFC by treating the pencil with sulfuric acid solution. Later, we introduced the cathodic catalyst of used alkaline battery as cathode instant of standard Pt/C carbon cloth for P-MFCs. Moreover, this type of integrated system will have the possibility to scale up the MFC for conventional wastewater treatment.

III. MATERIAL AND METHODS

A. Collection of Inoculum

Wastewater was collected from Universidad Politécnica de Aguascalientes (UPA) and stored under refrigeration at 4°C . The wastewater served as inoculum in anode and medium to be treated as well.

B. Construction of P-MFC, characterization and operation

We used a Koh-i-Noor Hardtmuth pencil, which was peeled off to remove the protective layer of softwood (up to 4.2 cm). The remaining graphite could act as anode with a wooden portion submerged (4.2 cm) into the wastewater. The remaining wooden portion (4.2 cm) is bound with Pt/Carbon cloth (0.5 mg cm^{-2}) as standard cell (alkaline battery cathode - 31.25 mg cm^{-2}) exposed to air, in order to reduce the oxygen in air (Fig 1.) (Mexican Patent No: MX/E/2015/008636). Further, the pencil materials were treated with 6M sulphuric acid solution for overnight and analyzed by FT-IR spectroscopy. P-MFC was characterized by LSV at 0.1 mV s^{-1} using Gamry Interface 1000 (Kamaraj et al., 2015). Finally two of the P-MFCs (each one of the standard cell and used alkaline battery cathode cell) in series connection was used to powering a digital clock for batch operation during 350 hrs.



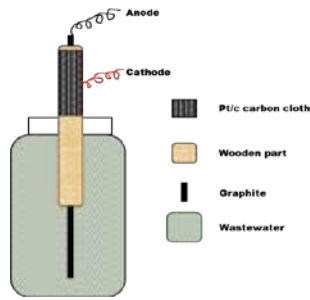


Fig. 1. Schematic representation of P-MFC

IV. RESULTS AND DISCUSSION

P-MFC showed the volumetric power density of 3.61 mW m^{-3} and current density of 9 mA m^{-3} at 0.403 V . Later 6M sulfuric acid treated pencil standard cell exhibit a power density of 956.21 mW m^{-3} and current density of $2511.21 \text{ mA m}^{-3}$ at 0.380 V (Fig 2). It confirms the presence of lignosulfonate on the sulphuric acid treated softwood in the 1032 cm^{-1} and 872 cm^{-1} regions of FT-IR spectrum (Fig 3). Lee 2013), would facilitate the vertical proton hooping via proton transfer could enhance the power production in P-MFC.

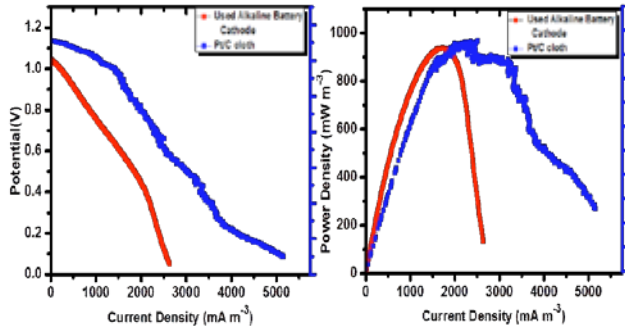


Fig. 2. Polarization curve of P-MFC

Further, we concentrated the cathodic side, and introduced the used alkaline battery cathodic catalyst applied for the cathode of P-MFC showed the volumetric power density of 936.83 mW m^{-3} and current density of $1723.49 \text{ mA m}^{-3}$ at 0.540 V (Fig 3.). This could be an alternative cathodic catalyst for MFCs. Later we connected two P-MFCs in series with Pt/C and used alkaline battery cathode catalyst used for power the digital clock operated for 350 h of batch operation (Fig 4a and Table D). Interestingly, the alternative cathode from used alkaline battery exhibits the constant power production of 61.68 mW m^{-3} for 350 h and 92 % of COD removal (Table 1.)

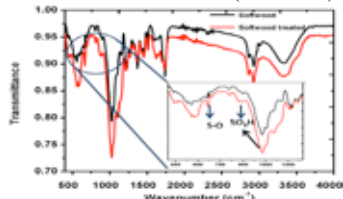


Fig. 3. FT-IR Spectrum of the Pencil

TABLE I

AVERAGE VALUES OF PARAMETERS IN BATCH OPERATION OF P-MFCs WITH A DIGITAL CLOCK.

Parameters	Pt/C as cathode	Used alkaline battery cathode
$P_v(\text{mW m}^{-3})$	64.74 ± 8.86	61.68 ± 9.76
$P(\text{mW m}^{-2})$	15.89 ± 2.17	11.69 ± 1.85
$I_v(\text{mA m}^{-3})$	47.67 ± 3.38	65.44 ± 4.94
$I(\text{mA m}^{-2})$	11.7 ± 0.83	12.41 ± 0.94
Potential (V)	1.35 ± 0.095	0.94 ± 0.07
COD %	82.65	92
Columbic efficiency	19	18



Fig. 4. P-MFCs prototype powered Digital clock

V. CONCLUSION

6M sulphuric acid treated P-MFC with Pt/C carbon cloth as cathode (956.21 mW m^{-3}) was served as standard Cell, This can compare with cathode catalyst of used alkaline battery as cathode (936.83 mW m^{-3}). In both the case Pencil led graphite as anode. Standard cell with Pt catalyst superior in volumetric Power density. However, the cost per power production can be higher, when use of noble metal catalyst. Since it could be recommendable to use other sustainable catalyst from the recycle process.

ACKNOWLEDGMENT

The author KSK thanks to SEP for the grant of PRODEP 2014 project No. DSA/103.5/14/10671, Conacyt and UPA.

REFERENCES

- [1] Kamaraj, S.-K., Romano, S.M., Moreno, V.C., Poggi-Varaldo, H.M., Solorza-Feria, O, Use of Novel Reinforced Cation Exchange Membranes for Microbial Fuel Cells. *Electrochimica Acta*, Volume 176, 2015, Pages 555-566.
- [2] Lee, D, Preparation of a Sulfonated Carbonaceous Material from Lignosulfonate and Its Usefulness as an Esterification Catalyst. *Molecules*, Volume 18, 2013, Pages 8168-8180.



AUTOSTACK – CORE – INDUSTRY LED EUROPEAN CONSORTIUM TO DEVELOP NEXT GENERATION AUTOMOTIVE STACK HARDWARE

A. Martin*, L. Jörissen**

* AMC, Taubenberg 94, D-65510 Idstein, (Germany)

**Zentrum für Sonnenenergie- und Wasserstoff-Forschung Baden-
Württemberg, Helmholtzstrasse 8, D-89081 Ulm, (Germany)

High power density stack technology is a key enabler for use of fuel cells in automotive applications. AutoStack-CORE is a collaborative project establishing a coalition from component manufacturers, OEMs and research organizations to develop automotive stack technology with superior power density and performance while using components manufactured at an industrial scale meeting commercial target cost. The stack design is based on a joint specification including a packaging constraint analysis developed in a previous project. Within the project 2 evolutions of stack hardware will be built. A final evolution will be realized as a design only. In this paper the key achievements of the evolution 1 design will be shown. The stack is based on metallic bipolar plates to achieve high power density (2.7 kW/l) and specific power (2.0 kW/kg). A cost engineering study according to automotive standards revealed specific cost of 47.83 €/kW when using the same parameters and aggregated to the same level as the 2013 update of the cost study by Strategic Analysis. The stack has been thoroughly tested on short stack and full stack level. Robust operation within the limits of the specification as well as freeze-start capability down to -20 °C could be demonstrated. The consortium completed a design review identifying the necessary steps for the evolution 2 design phase.

Index Terms – automotive PEM fuel cell stack, .

I. INTRODUCTION

Recent announcements for the commercialization of fuel cell vehicles in the next years is a clear signal for the functional readiness of fuel cell technology in automotive application. However, several aspects need further advancements and in some cases substantial improvement in years to come.

“Auto-Stack Core” is a European funded collaborative project establishing a coalition with the objective to develop best-of-its-class automotive stack hardware with superior power density and performance while using components manufactured in an industrial scale and meeting commercial target cost.

II. THE CONSORTIUM

The project consortium combines the collective expertise of European automotive OEMs, component suppliers, system integrators and research institutes as shown in TABLE 1.

TABLE 1
MEMBERS OF THE CONSORTIUM

OEMs	Component and system suppliers	Research organizations
BMW Volvo VW	Belenos DANA Freudenberg	CEA Fraunhofer ISE Joint Research Centre, Institute for Energy Paul Scherrer Institute ZSW
	Powercell Solvicore SymbioFCCell	

III. TECHNICAL APPROACH

The technical concept is based on the **Auto-Stack** assessments carried out under an FCH JU Grant Agreement from 2010 to 2012 and reflects the system requirements of major OEMs. It suggests a stack platform concept with the aim to substantially improve economies of scale and reduce critical investment cost for individual OEMs. The viability of the platform approach has been proven by an in depth analysis of fuel cell power system integration space available in three different vehicles from three manufacturers.

One of the key features of this project is the use of mature components which already were manufactured on an industrial scale allowing an easy transfer of the results obtained in the research phase into industrial manufacturing. The stack platform can be scaled in the power range from 10 kW to 95 kW thus providing the opportunity to use the stack in non-automotive applications.



Stack development is arranged in three development cycles: Prototype (stack evolution 1), A-sample (stack evolution 2), and B-sample (stack evolution 3). This approach is based on the typical development cycle in the automotive industry.

Stack evolutions 1 and 2 will be tested extensively with respect to performance, endurance, and reaction to environmental conditions to demonstrate the achievement of objectives and identify potential for further improvement.

The project also includes benchmark analyses of state-of-the-art stack development including innovative materials and component solutions. The technical development work is accompanied by a detailed cost analysis using established tools of the automotive industry.

After a development time of 18 months, a total of 20 short stacks with 10 or 20 cells as well as a full sized stack having a cell count of 331 have been built and subject to validation testing. Qualification testing has been finalized successfully after 23 months.

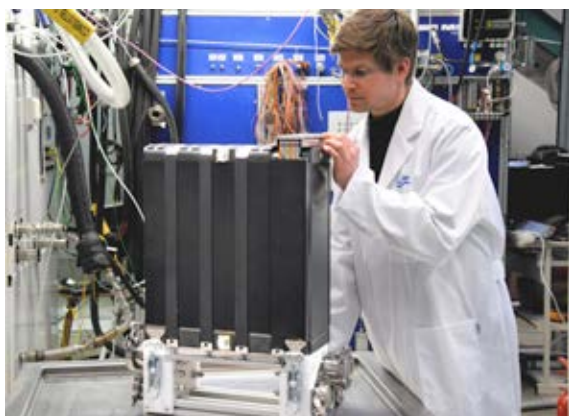


Figure 1: Stack on the test bench (Evolution 1)

Performance tests showed excellent agreement of operation characteristics at short stack and full size stack level as shown in Figure 2. Further increase in specific stack power could be achieved by a slight increase in operating pressure (**Figure 3**).

Stack cost for future series production has been analyzed by external experts and demonstrates that the final objectives are almost met already in the early prototype phase.

Direct exchange of information in combination with a joint assessment of critical development tasks enabled the optimization of cell and stack design as well as fast and efficient achievement of technical and economic objectives. Close interaction with automotive manufacturers provides immediate feedback on design approaches allowing achievement of key results at much lower budget compared to typical development programs in the automotive industry.

TABLE 2
OBJECTIVES AND ACHIEVEMENTS IN EVOLUTION 1

Objective	Specification	Achieved in Evolution 1
Power	95kW (continuous), 118kW (peak for 30 sec)	94 kW (continuous), 99 kW (peak for 30sec)
Stack-power density	2,8 kW/l (continuous), 3,4 kW/l (peak)	2.7 kW·l ⁻¹ (continuous), 2.9 kW·l ⁻¹ (peak)
Nominal power density	1 W·cm ⁻² @ 1.5 A·cm ⁻²	0.947 W·cm ⁻² @ 1.5 A·cm ⁻²
Maximum operating temperature	95 °C	95°C
Cathode humidity	< 50 % RH	50 % RH
Operating pressure	2.2 ... 2.4 bar (continuous) 2.7 bar (peak)	2.2 bar (continuous) 3 bar (peak)
Degradation rate	< 12 μV·h ⁻¹	50 μV·h ⁻¹
Freeze-start	From -25°C	Demonstrated -20 °C
Specific stack cost corresponding to DoE-study ¹	< 40,00 €·kW ⁻¹	47.83 €·kW ⁻¹

¹ Brian D. James, Jennie M. Moton, Whitney G. Colella, "Mass Production Cost Estimation of Direct H₂ PEM Fuel Cell Systems for Transport Applications 2013 Update"; Strategic Analysis Inc., Arlington VA (2014)

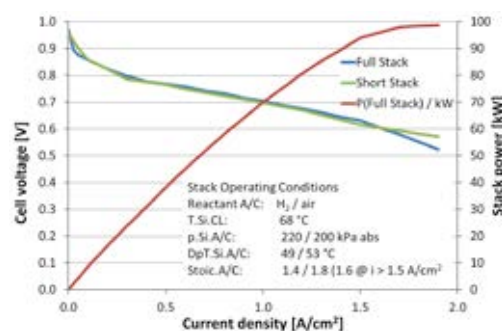


Figure 2: Comparison of I/V curves of short and full sized stacks in hydrogen – air operation.

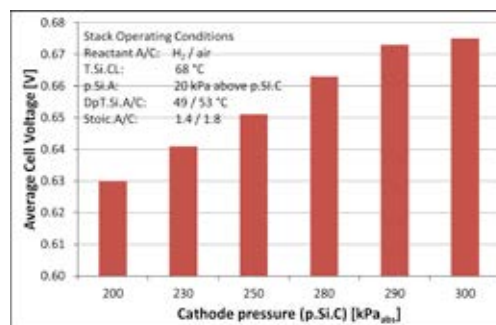


Figure 3: evolution of average stack voltage at a current density of 1.5 A·cm⁻².

CONCLUSIONS

In 18 months, the consortium has delivered a comprehensive stack design with the potential for technology leadership.

ACKNOWLEDGMENT

The work reported has been supported by the Fuel Cell and Hydrogen Joint Undertaking under Grant Agreement 325335.



STACK – TEST – DEVELOPMENT OF PEM FUEL CELL STACK REFERENCE TEST PROCEDURES FOR INDUSTRY

A. Kabza, J. Hunger, L. Jörissen

Zentrum für Sonnenenergie- und Wasserstoff-Forschung Baden-
Württemberg, Helmholtzstrasse 8, D-89081 Ulm, (Germany)

Fuel cell systems are becoming more and more industrial reality. Many interfaces are being established along the value chain, where consistent and comparable data are required for detailed understanding and identification of fuel cell stack parameters.

Development of test procedures for PEM fuel cell stacks was started at the end of the FCTESQA-project, however left significant gaps to be filled.

Within the project Stack-Test, a structured approach to testing PEM fuel cell stacks with respect to performance, endurance and safety issues has been developed.

The general approach has been described in a series of test modules and test programs addressing relevant performance, endurance and safety parameters. A harmonized nomenclature for all test input and output parameters enables data exchange and independent data evaluation. Application of specific parametrization of the test input data allows the acquisition of relevant data supporting system integration and modelling work. All test modules and test programs have been validated experimentally using short stacks provided by the project partners.

Overall the project has contributed to pre-normative research with the potential to transfer the findings into international standardization..

Index Terms –PEM fuel cell stack, Test Procedures.

I. INTRODUCTION

In the Stack-Test proposal, industry wide harmonized test procedures for PEFC stacks will be developed and validated. The proposal builds on experiences gained in the FCTESTNET, FCSTEQA series of projects taking up the methodology developed there and expanding it to the test of PEFC stacks. Furthermore, individual consortium members have long time experience in international standardization. Performance / functional, durability and safety outputs for vehicle propulsion, stationary and portable applications will be addressed.

Generic test modules addressing the effects of outputs to the variation of a single test parameter will be defined and experimentally validated on a stack level. From these building blocks, selected application oriented test programs shall be derived and validated as well. A two phase approach is pursued starting with an initial selection and definition phase followed by experimental validation. Subsequently, a review is carried out followed by a second validation phase.

II. THE CONSORTIUM

The consortium mainly consists of experienced research organizations, all working in close contact with and providing testing services to industry. The test modules and test programs are expected to be methodologically sound and independent. Contact to industrial practice will be established by the implementation of an industrial advisory group consisting of selected key stakeholders along the value chain of the fuel cell industry. The consortium will liaise with international standardization activities and contribute to the improvement of existing standards by pre-normative research and – if deemed necessary – initiate new work item proposals on performance and endurance testing of PEFC stacks.

III. TECHNICAL APPROACH

The work carried out in this project aims at the development of harmonized, industrially relevant test procedures allowing an assessment of PEM fuel cell stacks with respect to

- Performance
- Endurance, and
- Safety related issues

The tests developed within this project are written in a common format allowing sufficient flexibility to adopt specific requirements of fuel cell applications. Typical application areas identified for PEM fuel cells are: vehicle propulsion where the fuel cell can act either as the prime mover or as an range



extender; stationary applications such as combined heat and power generation (CHP); uninterruptible and backup power supply as well as portable power generators. It is evident that PEM fuel cell stacks will be operated under significantly different operating conditions in each of these applications.

The particular challenge is to find a common methodology for testing which still is flexible enough to cover the application areas mentioned above while clearly defining requirements to the test equipment, the in- and output parameters and the points of control for the parameters defining the operating conditions. **Figure 1** shows the approach taken within the project to address complex test tasks.

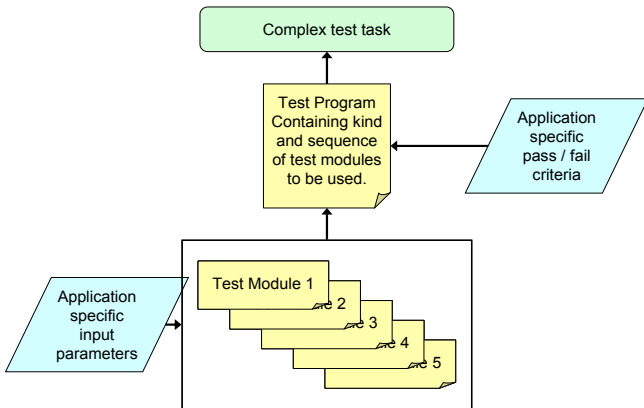


Figure 1: Interaction of test programs and test modules for complex testing tasks.

Within the project, a master document defining salient features of PEM fuel cell stack testing, requirements on parameter stability and test benches as well as a data reporting format and a nomenclature for input and output parameters has been proposed. **Figure 2** shows an example of the nomenclature for test input conditions and test output conditions as well as sensors.

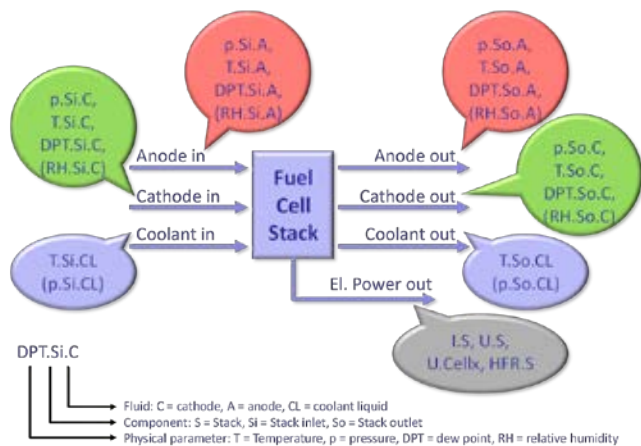


Figure 2: Stack-Test nomenclature.

Subsequently, a series of test modules each addressing the assessment of the impact of a single input parameter to the stack has been defined, experimentally validated, reviewed and finally validated. Furthermore, sets of input parameters

characteristic for different applications such as automotive propulsion, CHP, portable systems etc. have been proposed. To address complex test challenges individual test modules can be combined to test programs. A few characteristic test programs have been proposed and also been subject to a validation, revision and final validation sequence.

Two types of short stacks were used to carry out the validation experiments as showed in **Figure 3**: one stack using metallic bipolar plates representing automotive applications, another using graphite composite bipolar plates more characteristic for stationary and portable applications

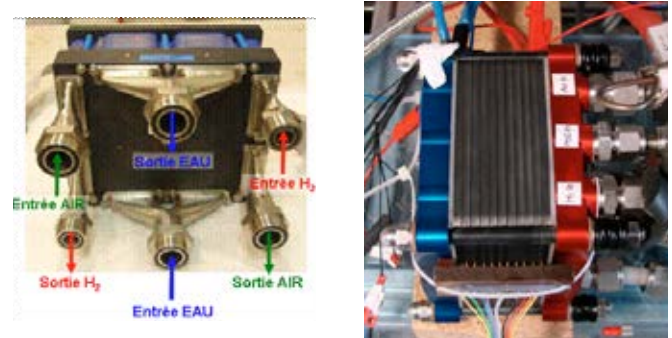


Figure 3: Stacks used for test module and test program validation.

Key achievements of the project are:

- Definition and validation of test modules concerning sensitivity to operating parameters, endurance, and safety;
- Definition of an easily implemented load cycle for endurance testing;
- Definition of relevant safety tests and working out of safety tests proposed in the IEC 62282-2 standard;
- Preparation of a new work item proposal for PEM fuel cell stack testing.

The collection of test modules and test programs developed during the project is available in the project web page: <http://Stacktest.zsw-bw.de>.

CONCLUSIONS ARE MISSING

ACKNOWLEDGMENT

The work reported has been supported by the Fuel Cell and Hydrogen Joint Undertaking under Grant Agreement 303445.



PREPARATION AND CHARACTERIZATION OF Y-DOPED CaZrO_3 ELECTROLYTE FILM ON A POROUS $\text{SrTi}_{0.8}\text{Fe}_{0.2}\text{O}_{3-\Delta}$ SUBSTRATE

L.A. Dunyushkina*, V.M. Kuimov*, A.A. Pankratov*,

A. Brouzgou**, V.P. Gorelov*, P.Tsiakaras*,**

*Laboratory of Electrochemical Devices Based on Solid Oxide Proton Electrolytes, Institute of High Temperature Electrochemistry, Yekaterinburg 620137, (Russia)

**Department of Mechanical Engineering, School of Engineering, University of Thessaly,

Pedion Areos, Volos 383 34, (Greece)

E-mail: tsiak@uth.gr (P.Tsiakaras), lidung@list.ru (L. Dunyushkina)

Abstract - Fabrication, characterization and electrochemical performance of a dense Y-doped CaZrO_3 electrolyte film deposited on a porous $\text{SrTi}_{0.8}\text{Fe}_{0.2}\text{O}_{3-\delta}$ substrate is investigated in the present work. The film is prepared by a multi-step chemical solution deposition using ethanol-based solution of precursors. The applied deposition technique allows continuous obtaining electrolyte films on the porous electrodes. Low viscosity and high wetting ability of the precursor solution promote formation of a composite layer, with interpenetrating networks of electrode and electrolyte phases, at the film/substrate interface that should enhance the electrochemical performance of the cell. Interdiffusion between the film and substrate materials is revealed.

Keywords: chemical solution deposition, electrode-supported SOFC, ionic transport number, Y-doped CaZrO_3 film

I. INTRODUCTION

The oxygen-ion and proton conducting materials have been studied for various applications such as solid oxide fuel cells (SOFCs), sensors, separating membranes and other kinds of electrochemical devices. Calcium zirconate based oxides exhibit mixed oxygen-ion, proton and electronic conduction [1-3], extremely high chemical stability, high density, good strength, and good tolerance against thermal shock [4, 5]. Combination of these properties makes the oxides attractive for application as a film electrolyte since high chemical stability and inertness of the components become very important in the film based SOFCs. Reducing the electrolyte thickness results in reduction of the ohmic losses across the electrolyte and enhances SOFC efficiency. That is why thin film technologies are widely applied for fabrication of SOFCs operating at intermediate temperatures [6]. For the successful fabrication of an SOFC based on a film electrolyte, the electrolyte film must be gas-tight to avoid fuel leakage, while the supporting electrode must be porous enough in order to facilitate gas transport. Deposition of a thin gas-tight film on a porous substrate with high surface roughness is one of challenges which are to be solved for thin film SOFC development. This problem is often solved by forming of a dense layer over a porous electrode surface [7, 8].

In this research a multi-step chemical solution deposition was applied for fabrication of a dense electrolyte film on a porous supporting electrode.

This technique is suggested to be a promising method to optimize the microstructure of the electrode/electrolyte interface and thus enhance performance of the electrode-supported SOFCs. A low-viscous liquid precursor solution impregnates a porous electrode to a considerable depth forming a composite layer, with interpenetrating networks of electrode and electrolyte phases. Multi-step deposition of the precursor solution is expected to result in the gradual densifying of the substrate surface layer and finally in formation of a thin dense film of the electrolyte.

II. RESULTS & DISCUSSION

Phase purity and microstructure of the films are tested by means of X-ray diffraction (Fig. 1), energy-dispersive X-ray spectroscopy and scanning electron microscopy (Fig.2). For the study of the electrochemical performance of the film, a gas concentration cell Pt/STF/CZY-film/Pt is fabricated. OCV, impedance spectra and current-voltage characteristic curves are measured in the oxygen concentration cell, in the temperature range from 500 to 600°C. The ionic transport numbers in CZY under various $p\text{O}_2$ gradients are presented in Fig. 3a. As can be seen the transport numbers determined with the aid of the Liu approach which uses the data of the impedance- and OCV-measurements on a gas concentration cell are close to those determined using only the results of fitting of the impedance spectra for the concentration cell.

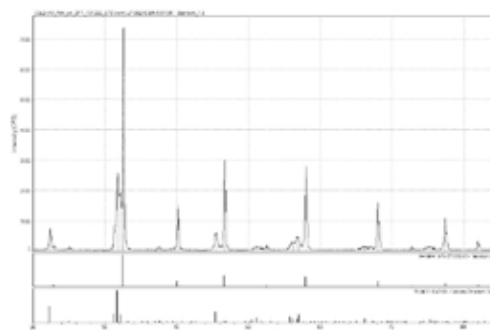


Fig. 1. XRD pattern for CZY film deposited on STF substrate.

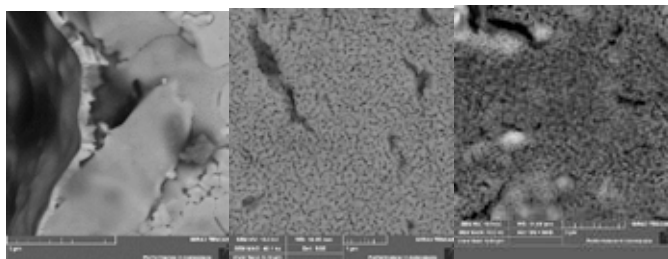


Fig. 2. SEM micrographs. (a) After 5-fold deposition of the solution, SEM tests showed formation of a film. b & c) The film surface exhibited fine-grained microstructure with nano- and micropores and cracks observed on the irregularities of the substrate surface.

Both sets of the transport numbers vary within 0.90 – 0.96 interval which is significantly higher than E_m/E_N ratios which determine the average transport number of ions for the case of non-polarizable electrodes (Fig. 3a). The difference is apparently caused by the processes occurring in the supporting STF electrode.

Liu [9] approach allows determination of the electrolyte ionic resistance, electrode polarization resistance and ionic transport number of the electrolyte using the data of impedance and OCV measurements. On the other hand the values of ionic and electronic resistance, R_i and R_e , of the electrolyte under applied gradient of electrochemically active gas can be extracted by fitting of the impedance spectrum (from impedance measurements) for the concentration cell using an equivalent circuit which includes a shorting electronic resistance of an electrolyte. High polarization resistance in the pO_2^1 , Pt/STF/CZY-film/Pt, pO_2^2 cell has crucial influence on its performance. Cell voltage and power density as a function of current density for the cell under $\text{Log } pO_2^1 = -20.3$ and $pO_2^2 = 0.21$ atm at 500 and 600°C are shown in Fig.3b. Maximum power densities of 0.24 and 0.08 mW/cm² and the open-circuit voltage values of 0.486 and 0.470 V were obtained at 600 and 500°C, respectively.

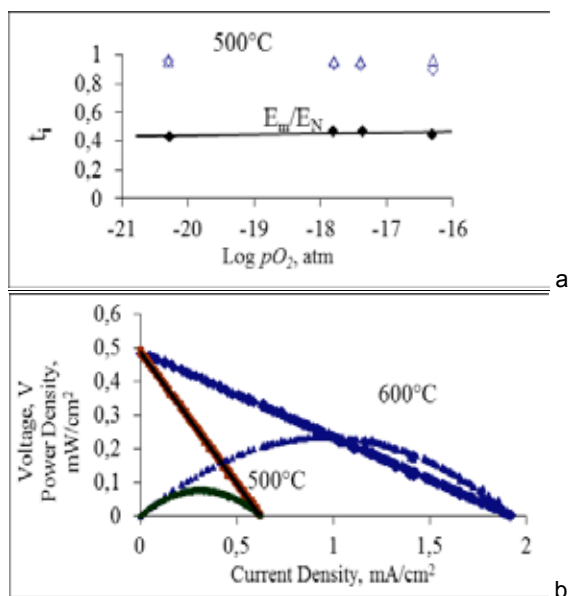


Fig. 3. (a) The ionic transport numbers in CZY under various pO_2 gradients. (b) Cell voltage and power density as a function of current density for the cell under $\text{Log } pO_2^1 = -20.3$ and $pO_2^2 = 0.21$ atm at 500 and 600°C.

In spite of high values of ionic transport number in CZY-film and enhanced microstructure of the electrolyte/electrode interface which should promote charge transfer, STF-supported CZY film has shown poor performance under applied pO_2 gradient because of high polarization resistance.

III. CONCLUSION

Against our expectations, the electrochemical performance of STF-supported CZY-film under applied pO_2 gradient is found to be very poor, due to high polarization resistance of the cell. The ionic transport numbers, determined using the results of OCV- and EIS measurements on a gas concentration cell, are found to vary within 0.90 – 0.96, which is significantly higher than E_m/E_N ratio. The difference is apparently caused by the high cell's polarization resistance.

ACKNOWLEDGMENT

The present work was financially supported by grant of the government of the Russian federation (no. 14.z50.31.0001) and of Russian foundation for basic research (project no. 14-29-04013).

REFERENCES

1. T. Yajima, H. Kazeoka, T.Yogo, H.Iwahara, Proton conduction in sintered oxides based on CaZrO_3 , *Solid State Ionics* **1991**, 47, P. 271-275.
2. H. Iwahara, T.Yajima, T. Hibino, K. Ozaki, H. Suzuki, Proton conduction in calcium, strontium and barium zirconates, *Solid State Ionics*, **1993**, 61, P. 65-69.
3. V. P. Gorelov, V. B. Balakireva, A. V. Kuz'min, S. V. Plaksin, Electrical Conductivity of $\text{CaZr}_{1-x}\text{Sc}_x\text{O}_{3-\alpha}$ ($x = 0.01-0.20$) in Dry and Humid Air, *Inorganic Materials* **2014**, 50, P. 495.
4. T. Murakami, H. Fukuyama, T. Kishida, M. Susa, K. Nagata, Phase diagram for the system $\text{CaO-Al}_2\text{O}_3\text{-ZrO}_2$, *Metall. Mater. Trans., B, Proc. Metall. Mater. Proc. Sci.* **2000**, 31, P. 25.
5. C. Wang, X. Xu, H. Yu, Y. Wen, K. Zhao, A study of the solid electrolyte Y_2O_3 -doped CaZrO_3 , *Solid State Ionics* **1988**, 28, P. 542.
6. D. Beckel, A. Bieberle-Hutter, A. Harvey, A. Infortuna, U.P. Muecke, M. Prestat, J.L.M. Rupp, L.J. Gauckler, Thin films for micro solid oxide fuel cells, *Journal of Power Sources* **2007**, 173, P. 325-345.
7. A.A. Soloviev, N.S. Sochugov, A.V. Shipilova, K.B. Efimova, A.E. Tumashevskaya, Mid-Temperature Solid Oxide Fuel Cells with Thin Film $\text{ZrO}_2\text{:Y}_2\text{O}_3$ Electrolyte, *Russian Journal of Electrochemistry* **2011**, 47, P. 494 – 502.
8. H. Xiao, T. Reitz, Anode-Supported Solid Oxide Fuel Cells with Thin Film Electrolyte for Operation at Reduced Temperatures, *ECS Transactions* **2006**, 1, P. 201-208.
9. M. Liu, H. Hu, Effect of Interfacial Resistance on Determination of Transport Properties of Mixed-Conducting Electrolytes, *J. Electrochem. Soc.* **1996**, 143, P. L109-L112.



**A DETAILED ANALYSIS OF THERMAL AND CHEMICAL COMPATIBILITY OF CATHODE MATERIALS
FOR BaCeO₃ AND BaZrO₃-BASED ELECTROLYTES FOR SOLID OXIDE FUEL CELL APPLICATION**

D. Medvedev^{1,2}, J. Lyagaeva¹, A. Brouzgou³, E. Pikalova^{1,2},
S. Plaksin¹, A. Demin¹, P. Tsiakaras^{1,3}

¹Laboratory of Electrochemical Devices based on Solid Oxide Proton Electrolytes, Institute of High Temperature Electrochemistry, Russian Academy of Sciences
Ural Branch, 20, Academicheskaya St. Ekaterinburg, Russia.

²Department of Environmental Economics, Ural Federal University, Yekaterinburg 620002, Russia.

³Department of Mechanical Engineering, University of Thessaly,
Pedion Areos, Volos, Greece.

E-mail: tsiak@uth.gr, dmitrymedv@F

I. ABSTRACT

The identification of suitable cathode materials, which can be successfully used in unit SOFCs based on proton-conducting electrolytes during long-term stability and thermal cycling measurements is investigated in the present work. To achieve this aim, a wide variety of materials were synthesized and their thermal and chemical compatibilities toward BaCe_{0.8}Y_{0.2}O_{3-δ} and BaZr_{0.8}Y_{0.2}O_{3-δ} are verified by means of detailed dilatometry and XRD analysis of calcined electrode/electrolyte mixtures, respectively. It is found that most of the studied cathodes are characterized by significant thermal expansion along with the tangible chemical one. Moreover, some of them react to a different degree with selected electrolytes. It is also found that, LaNi_{0.6}Fe_{0.4}O_{3-δ} and La₂NiO_{4+δ} oxides can be considered as suitable cathode materials for BaCe_{0.8}Y_{0.2}O_{3-δ} and BaZr_{0.8}Y_{0.2}O_{3-δ} proton-conducting electrolytes. Moreover, layered Y_{0.8}Ca_{0.2}BaCo₄O_{7+δ} cobaltite also possesses the required thermal properties and acceptable compatibility with BaZr_{0.8}Y_{0.2}O_{3-δ} material.

II. INTRODUCTION

The number of works appeared in international literature devoted to the development of new proton-conducting electrolytes for solid oxide fuel cells (SOFC-H⁺), is currently declining. On the contrary, many studies are devoted to applied aspects, including the enhancement of SOFC-H⁺s electrical & electrochemical characteristics, mainly by decreasing electrolyte thickness and developing new cathode materials having excellent electrocatalytic activity [1-5]. Because of the bareness of thermal and chemical compatibilities data, the present work is addressed to the investigation of thermal affinity and degree of chemical reactivity between BaCe_{0.8}Y_{0.2}O_{3-δ} and BaZr_{0.8}Y_{0.2}O_{3-δ} electrolytes (the basic materials of BCZY systems at x = 0 and 0.8) with thirteen (13) cathode materials, including simple and layered cobaltites and cobaltite-ferrites, as well as Co-free materials, which were selected on the base of recently published works [3-5].

III. RESULTS AND DISCUSSION

In the present study 12 cathode materials, except LaNi_{0.6}Fe_{0.4}O_{3-δ} (LNF), were successfully synthesized according to the solid state reaction method using oxides and carbonates of corresponding metals with purity not less

than 99% as precursors. The citrate-nitrate combustion method was used for the formation of single-phase LNF product. The designation of these materials is presented in Table 1.

Table 1. Chemical composition of the as-prepared cathode materials.

Composition	Designation
Ba _{0.5} Sr _{0.5} CoO _{3-δ}	BSC
GdBaCo ₂ O _{5+δ}	GBC
NdBaCo ₂ O _{5+δ}	NBC
Y _{0.8} Ca _{0.2} BaCo ₄ O _{7+δ}	YCBC
Ba _{0.5} Sr _{0.5} Co _{0.2} Fe _{0.8} O _{3-δ}	BSCF28
Ba _{0.5} Sr _{0.5} Co _{0.8} Fe _{0.2} O _{3-δ}	BSCF82
La _{0.6} Sr _{0.4} Co _{0.2} Fe _{0.8} O _{3-δ}	LSCF
GdBaCoFeO _{5+δ}	GBCF
NdBa _{0.5} Sr _{0.5} Co _{1.5} Fe _{0.5} O _{5+δ}	NBSCF
Ba _{0.5} Sr _{0.5} FeO _{3-δ}	BSF
La _{0.75} Sr _{0.25} MnO _{3-δ}	LSM
La ₂ NiO _{4+δ}	LN
LaNi _{0.6} Fe _{0.4} O _{3-δ}	LNF

Thermal compatibility

The nature of thermal expansion of BaCe_{0.8-x}Zr_xY_{0.2}O_{3-δ} materials was recently studied [6]. It is clear that both BaCe_{0.8}Y_{0.2}O_{3-δ} (x = 0) and BaZr_{0.8}Y_{0.2}O_{3-δ} (x = 0.8) belong to this system. As can clearly be seen (Fig. 1a) the TEC of BaCeO₃- and BaZrO₃- materials is close to those for ZrO₂-, CeO₂- and LaGaO₃-based electrolytes [7] and, theoretically, different cathode materials, showing good electrochemical results in contact with these electrolytes, can be also used for cerate and zirconate proton conductors. Simple and layered cobaltites considered as perspective cathode materials, having excellent transport properties. However, their absolute expansions (Fig. 1b) and, correspondingly, TEC values are higher by 1.5–3 times than those measured for BaCe_{0.8}Y_{0.2}O_{3-δ} and BaZr_{0.8}Y_{0.2}O_{3-δ}. At the same time, some of them (LnBaCo₂O_{5+δ} [9], Sm_{0.5}Sr_{0.5}CoO_{3-δ} [8]) already were used as cathode materials in contact with BCZY electrolytes, exhibiting a rather good electrocatalytic activity (~0.5 Ω cm² at 600°C and ~0.1 Ω cm² at 700°C). In cobaltites, the strategy of partial substitution of Co-ions by other transition metals (M = Fe, Ni, Cu) or of big cations, occupied A-site of Co-based perovskite, by lower cations is usually adopted in order to decrease



TEC values.

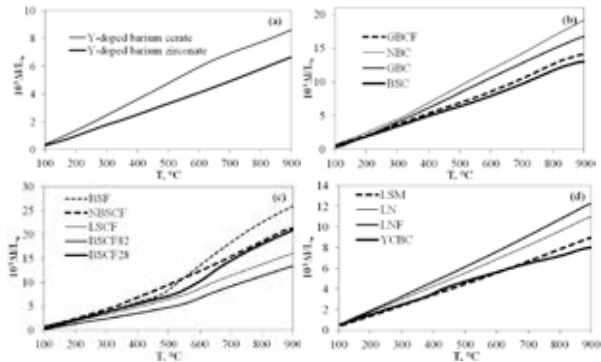


Fig. 1. Thermal expansion of $\text{BaCe}_{0.8}\text{Y}_{0.2}\text{O}_{3-\delta}$ and $\text{BaZr}_{0.8}\text{Y}_{0.2}\text{O}_{3-\delta}$ electrolyte materials (a) and cathodes with high TEC (b), with high TEC and chemical expansion (c) and relatively low TEC (d).

The comparison of thermal data for $\text{GdBaCo}_2\text{O}_{5+\delta}$ and $\text{GdBaCoFeO}_{5+\delta}$ (Fig. 1b) confirms the proposed strategy. On the other hand, for many cobaltite-ferrites (Fig. 1c) the thermal expansion behavior deviates from linearity, resulting in the intense expansion of ceramics in high-temperature range in comparison with low-temperature one. Usually, such deviation can be associated with two main factors: the realization of phase transition(s) or chemical expansion. Since the BSCF82, NBSCF and BSF materials possess the cubic structure a decisive contribution in high-temperature regions renders namely chemical expansion, caused by the presence of elements in different oxidation and spin states. For example, $\text{Ba}_{0.5}\text{Sr}_{0.5}\text{Co}_{0.8}\text{Fe}_{0.2}\text{O}_{3-\delta}$ exhibits lower absolute expansion among other cobaltite-ferrites (Fig. 1c), but average TEC for high-temperature regions remains rather high ($22.6 \cdot 10^{-6} \text{ K}^{-1}$).

Co-free cathode ceramics (LN, LNF, LSM) are characterized by practically linear behavior of thermal expansion (Fig. 1d) and lower average TEC values ($10.7\text{--}14.5 \cdot 10^{-6} \text{ K}^{-1}$). Moreover, the average TEC of YCBC oxide is also low and close to target values of electrolytes TECs. The shape of graph “TEC vs T”, presenting temperature dependences of differential TECs, show objective abnormal changes near 400 and 850°C (Fig. 2). This behavior can be associated with orthorhombic → hexagonal phase transition near 400°C coupled with the processes of oxygen adsorption at 200–400°C and oxygen desorption at 700–900°C. It is interesting to note that in Y–Ba–Co–O system another layered perovskite phase ($\text{YBaCo}_2\text{O}_{5+\delta}$ double cobaltite) with relatively low TECs ($13\text{--}15 \cdot 10^{-6} \text{ K}^{-1}$) can be formed. The temperature dependences of expansion and differential TEC of Ni- and Mn-containing materials is virtually linear without abrupt changes (Fig. 2), indicating the absence of structure phase transitions. The differential TECs for these materials slightly increase with temperature and can be associated with minor contribution of the chemical expansion.

Chemical compatibility

The 26 powders mixtures were characterized by XRD analysis for the estimation of the degree of chemical interaction between 2 electrolytes and 13 cathode materials. It was found, that the $\text{BaCe}_{0.8}\text{Y}_{0.2}\text{O}_{3-\delta}$ electrolyte possesses a low chemical stability in the contact with majority cathode compositions. Although the structures of main phases in electrolyte/cathode mixtures remain, different impurities and phases of interaction can be clearly observed:

- CeO_2 for BSC, GBC, YCBC, BSCF82, GBCF, and LSM;
- SrO for BSC and BSCF82;
- barium cobaltites for GBC, NBC, GBCF and NBSCF and strontium cobaltite for LSCF;
- BaO and SrO for GBC and BSCF82, respectively;
- $\text{BaCoNd}_2\text{O}_7$ for NBC, La_2CoO_4 for LSCF, Fe_3O_4 for GBCF, $\text{Sr}(\text{Fe},\text{Co})\text{O}_3$ for NBSCF, YMn_2O_5 for LSM and $\text{BaGd}_2\text{FeO}_7$ for GBCF.

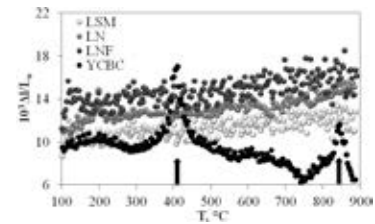


Fig. 2 Effect of temperature on TEC for $\text{Y}_{0.8}\text{Ca}_{0.2}\text{BaCo}_4\text{O}_{7+\delta}$ (YCBC), $\text{LaNi}_{0.6}\text{Fe}_{0.4}\text{O}_{3-\delta}$ (LSM), $\text{La}_2\text{NiO}_{4+\delta}$ (LN) and $\text{La}_{0.75}\text{Sr}_{0.2}\text{MnO}_{3-\delta}$ (LNF).

The $\text{Y}_{0.8}\text{Ca}_{0.2}\text{BaCo}_4\text{O}_{7+\delta}$ layered perovskite phase completely decomposes in the mixture with cerate after long-term treatment: YBaCo_2O_5 , $\text{YBa}_2\text{Co}_3\text{O}_9$ and CeO_2 phases are fixed along with main BaCeO_3 structure.

No significant interactions were observed in the calcined mixtures of $\text{BaCe}_{0.8}\text{Y}_{0.2}\text{O}_{3-\delta}$ with BSCF28, BSF, LN and LNF. The obtained data confirm previously presented results [10], showing an active Co-diffusion from cobaltites into BaCeO_3 -based electrolytes and, as a consequence, the formation of BaO, BaCo_2 and BaCo_3 impurities. The decrease in Co-ions concentration results in the some suppression of phase formation, as it is shown in the row of $\text{Ba}_{0.5}\text{Sr}_{0.5}\text{Co}_{0.8}\text{Fe}_{0.2}\text{O}_{3-\delta}$ – $\text{Ba}_{0.5}\text{Sr}_{0.5}\text{Co}_{0.8}\text{Fe}_{0.2}\text{O}_{3-\delta}$ – $\text{Ba}_{0.5}\text{Sr}_{0.5}\text{Co}_{0.2}\text{Fe}_{0.8}\text{O}_{3-\delta}$ – $\text{Ba}_{0.5}\text{Sr}_{0.5}\text{FeO}_{3-\delta}$. For example, no impurity phases were detected in the mixture of $\text{Ba}_{0.5}\text{Sr}_{0.5}\text{FeO}_{3-\delta}$ with $\text{BaCe}_{0.8}\text{Y}_{0.2}\text{O}_{3-\delta}$. The activity of the cerate electrolyte with double cobaltites seems to be higher than that with simple cobaltite, since for all the calcined mixtures, containing $\text{LnBaCo}_2\text{O}_{5+\delta}$ -based oxide, the formation of secondary phases were detected.

IV. CONCLUSION

In the present work, different cathode materials, selected on the base of their electrical and electrochemical properties, were successfully prepared and thoroughly investigated in order to find the appropriate compositions for eventual applications in SOFC- H^+ with BaCeO_3 and BaZrO_3 proton-conducting electrolytes. The main attention was paid to the comparison of thermal behaviours of cathode and electrolyte system as well as the chemical compatibility between them. Taking into account the relatively low TEC values, no significant chemical expansion and high resistance to impurity phase formation, $\text{LaNi}_{0.6}\text{Fe}_{0.4}\text{O}_{3-\delta}$ and $\text{La}_2\text{NiO}_{4+\delta}$ samples can be proposed as suitable cathodes for $\text{BaCe}_{0.8}\text{Y}_{0.2}\text{O}_{3-\delta}$ and $\text{BaZr}_{0.8}\text{Y}_{0.2}\text{O}_{3-\delta}$ electrolytes. The layered $\text{Y}_{0.8}\text{Ca}_{0.2}\text{BaCo}_4\text{O}_{7+\delta}$ cobaltite has the closest TEC value with those for cerate and zirconate ceramics, however completely decomposes after treatment of $\text{Y}_{0.8}\text{Ca}_{0.2}\text{BaCo}_4\text{O}_{7+\delta}/\text{BaCe}_{0.8}\text{Y}_{0.2}\text{O}_{3-\delta}$ mixture and is stable in contact with $\text{BaZr}_{0.8}\text{Y}_{0.2}\text{O}_{3-\delta}$.

ACKNOWLEDGMENT

Authors are grateful to *The Ministry of Education and Science of the Russian Federation* (Mega-grant contract no. 14.Z50.31.0001) and the Council of the President of the Russian Federation (grant no. CII-1885.2015.1) for financial support.

REFERENCES

1. S.M. Jamil, M.H.D. Othman, M.A. Rahman, J. Jaafar, A.F. Ismail, K. Li, J. Eur. Ceram. Soc. 35(1) (2015) 1–22.
2. E. Kendrick, P. Slater, Annu. Rep. Prog. Chem., Sect. A: Inorg. Chem. 109 (2013) 396–420.
3. D. Ding, X. Li, S. Lai, K. Gerdes, M. Liu, Energy Environ. Sci. 7 (2014) 552–575.
4. V. Lawlor, J. Power Sources 240 (2013) 421–441.
5. D. Medvedev, A. Murashkina, E. Pikalova, A. Demin, A. Podias, P. Tsiakaras, Progr. Mater. Sci. 60 (2014) 72–129.
6. Yu. Lyagaeva, D. Medvedev, A. Demin, P. Tsiakaras, O.Reznitskikh, Phys. Solid State 57(2) (2015) 285–289.
7. E.V. Tsipis, V.V. Kharton, J. Solid State Electrochem. 12(9) (2008) 1039–1060.
8. T. Wu, Y. Zhao, R. Peng, C. Xia, Electrochim. Acta 54(21) (2009) 4888–4892.
9. N. Li, Z. Lü, B. Wei, X. Huang, K. Chen, Y. Zhang, W. Su, J. Alloys Compd. 484(1–2) (2008) 274–279.
10. Y. Lin, R. Ran, C. Zhang, R. Cai, Z. Shao, J. Phys. Chem. A 114(11) (2010) 3764–3772.



THE EFFECT OF Y BY YB SUBSTITUTION IN $\text{BaCe}_{0.5}\text{Zr}_{0.3}\text{Y}_{0.2}\text{O}_{3-\Delta}$ ON THE TARGET PROPERTIES OF PROTON-CONDUCTING ELECTROLYTES

D. Medvedev*, J. Lyagaeva*, G. Vdovin*, A. Brouzgou**,
A. Demin*, P. Tsiakaras ***

*Laboratory of electrochemical devices based on solid oxide proton electrolytes, Institute of High Temperature Electrochemistry, Yekaterinburg 620990, Russia

**Laboratory of Alternative Energy Conversion Systems, Department of Mechanical Engineering, School of Engineering, University of Thessaly, Pedion Areos, Volos 383 34, Greece

Abstract – The $\text{BaCe}_{0.5}\text{Zr}_{0.3}\text{Y}_{0.2-x}\text{Yb}_x\text{O}_{3-\delta}$ ceramic materials are prepared and characterized in the present work. The impact of the partial $\text{Y}^{3+}/\text{Yb}^{3+}$ substitution on i) crystal structure, ii) microstructure (relative density, grain size), iii) thermal properties (linear expansion, thermal expansion coefficient) and iv) electrical properties (nature and value of conductivity) is identified. The $\text{BaCe}_{0.5}\text{Zr}_{0.3}\text{Y}_{0.1}\text{Yb}_{0.1}\text{O}_{3-\delta}$ possesses high density, high conductivity, but relative low thermal expansion coefficient.

Index Terms – proton-conducting electrolytes, SOFC, conductivity, thermal expansion, acceptor doping.

I. INTRODUCTION

BaCeO_3 – BaZrO_3 solid solutions are the basis of the development of advanced proton-conducting electrolytes for their applications in solid oxide fuel cells, high-temperature electrolyzes and membrane devices [1,2]. The heightened interest to mixed cerate-zirconate systems is caused by several reasons: i) enhanced transport properties in comparison with doped BaZrO_3 conductors, ii) higher chemical stability in comparison with doped BaCeO_3 representatives, and iii) optimized combination of thermomechanical characteristics in contrast to those of basic compounds. Currently, the main regularities in the changes of mentioned properties for BaCeO_3 – BaZrO_3 are establishment (Fig. 1). According to existing views, the optimal level of Ce by Zr substitution is in the range 30–50 mol.%. Due to this fact the researchers' attentions to the slightly Zr-substituted cerates (for instance, $\text{BaCe}_{0.7}\text{Zr}_{0.1}\text{Y}_{0.2}\text{O}_{3-\delta}$) gradually decreases, and a number of investigations related with Zr-enriched ones, on the contrary, grows [1].

Yttrium (Y^{3+}) is considered the most used acceptor dopant for BaCeO_3 – BaZrO_3 system from the viewpoint of transport properties [2], however there are results, showing better results for Y^{3+} and Yb^{3+} co-doped materials [3,4]. Such fact can be explained by either synergistic effect of co-doping or optimal characteristics of ytterbium as acceptor dopant. In the present work, the materials with $\text{BaCe}_{0.5}\text{Zr}_{0.3}\text{Y}_{0.2-x}\text{Yb}_x\text{O}_{3-\delta}$ compositions were successfully prepared and their structural, ceramic, thermomechanical and transport properties were thoroughly investigated in order to reveal the Yb^{3+} impact.

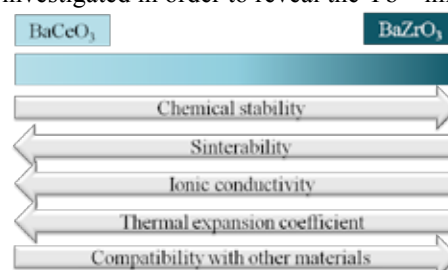


Fig. 1. Schematic representation of changing target properties for BaCeO_3 – BaZrO_3 system.

II. EXPERIMENTAL SECTION

Powders with $\text{BaCe}_{0.5}\text{Zr}_{0.3}\text{Y}_{0.2-x}\text{Yb}_x\text{O}_{3-\delta}$ compositions (BCZYYbx , $x = 0, 0.05 \dots 0.2$) were prepared by the aid of citrate-nitrate combustion synthesis. Subsequent temperature regimes included annealing of obtained powders at 700 °C (1 h), calcinations at 1050 °C (5 h) and sintering of ceramics at 1450 °C (5 h). It should be noted that the citrate-nitrate combustion synthesis method was modified by the addition of 1 wt % CuO

which effectively facilitate the ceramics densification and grain growth.

The sintered ceramics were examined by X-ray diffraction analysis (XRD, RIGAKU D/MAX-2200), scanning electron microscopy (SEM, JSM-5900 LV), dilatometry (Tesatronic TT-80 dilatometer) and 4-probe DC conductivity measurements.

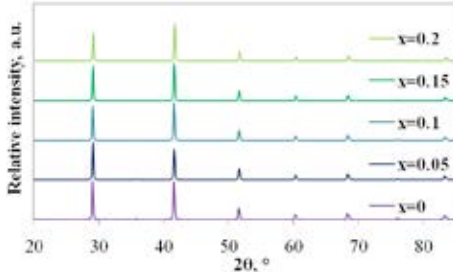


Fig. 2. XRD data of BCZYYbx ceramics.

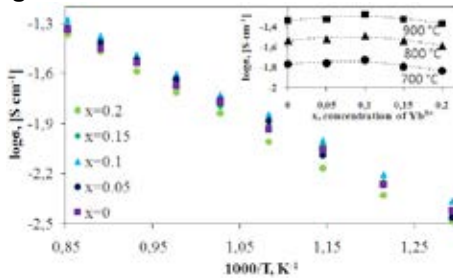


Fig. 3. Temperature and concentration dependences of conductivity for BCZYYbx ceramics in wet air.

III. RESULTS AND DISCUSSION

All the sintered BCZYYbx ceramics were identified by using XRD analysis. The obtained materials were consisted by a single-phase rhombohedral-distorted perovskite structure (R3c) indicating the formation of solid solutions over the entire investigated range of x . The unit cell parameters of sintered materials slightly decrease with increasing of Yb^{3+} concentration due to its lower ionic radius in comparison with that for Y^{3+} .

The measuring of relative density and the microstructure SEM analysis demonstrate a high density of sintered ceramics which is higher than 94% for $0 \leq x \leq 0.15$ and close to 91% for $x = 0.2$. The mean grain size (D_{av}) of BZCYYbx ceramics was calculated on the base of grain size distribution data. It was shown that the concentration dependence of D_{av} is characterized by a maximum. For example, this parameter is equal $2.5 \mu\text{m}$ for $x = 0$, $2.0 \mu\text{m}$ for $x = 0.2$ and about $4 \mu\text{m}$ for $x = 0.1$.

The thermal expansion coefficient (TEC) of sintered ceramic was evaluated by dilatometry technique. For all the samples, there is a clear inflection point on the $\Delta L/L_0 \div T$ dependences around $570 \text{ }^\circ\text{C}$. Such nonmonotonic behavior can be associated with the presence of phase transition (rhombohedral phase, R3C \rightarrow cubic phase, Pm3m). Therefore, TEC values were calculated for rhombohedral and cubic phases. TECs slightly change in low-temperature interval and decrease (from $8.5 \cdot 10^{-6} \text{ K}^{-1}$ for $x = 0$ to

from $7.6 \cdot 10^{-6} \text{ K}^{-1}$ for $x = 0.2$) in high-temperature range. This fact also can be explained by size factor caused the ionic radii difference between Y^{3+} and Yb^{3+} .

The conductivity of BCZYYbx was calculated in wide range of temperatures $500 - 900 \text{ }^\circ\text{C}$ in wet air, wet nitrogen and wet hydrogen atmospheres. It was found that the sample containing equimolar concentrations of yttrium and ytterbium exhibits the highest conductivity (Fig. 3) despite the type of atmosphere. The obtained results can be related to the lower grain boundary resistance due to highest D_{av} parameter.

IV. CONCLUSION

In this work the relationship between Y by Yb substitution on the crystal and microstructure properties as well as thermomechanical and electrical features of $\text{BaCe}_{0.5}\text{Zr}_{0.3}\text{Y}_{0.2-x}\text{Yb}_x\text{O}_{3-\delta}$ -based ceramics (BCZYYbx) were investigated. The increase of Yb concentration from 0 to 0.2 is found to decrease: i) the unit cell parameters/volume (from 490.57 to 486.80 \AA^3), ii) the TEC values (from $8.5 \cdot 10^{-6}$ to $7.6 \cdot 10^{-6} \text{ K}^{-1}$). However, the concentration dependences of mean grain size and total conductivity of BCZYYbx ceramics are similar, which allows one to conclude that grain boundary significantly affects the transport properties of these proton-conducting electrolytes.

ACKNOWLEDGMENT

This work was supported by the Ministry of Education and Science of the Russian Federation (contract no. 14.Z50.31.0001), the Russian Foundation for Basic Research (grant no. № 13-03-00065) and the Council of the President of the Russian Federation (grant no. CII-1885.2015.1).

REFERENCES

- [1] Medvedev, D., Murashkina, A., Pikalova, E., Demin, A., Podias, A., Tsiakaras, P. BaCeO₃: Materials development, properties and application. Progress in Material Science, volume 60, 2014, pp 72–129.
- [2] Medvedev, D.A., Lyagaeva, J.G., Gorbova, E.V., Demin, A.K., Tsiakaras, P. Advanced materials for SOFC applications: Strategies for the development of highly conductive and stable proton conductors. Progress in Materials Science, In press, doi: 10.1016/j.pmatsci.2015.08.001.
- [3] Yang, L., Wang, S., Blinn, K., Liu, M., Liu, Z., Cheng, Z., Liu M. Enhanced sulfur and coking tolerance of a mixed ion conductor for SOFCs: BaZr_{0.1}Ce_{0.7}Y_{0.2-x}Yb_xO_{3-δ}. Nature, volume 326, 2009, pp. 126–129.
- [4] Yang, K., Wang, J.X., Xue, Y.J., Wang, M.S., He, C.R., Wang, Q., Miao, H., Wang, W.G. Synthesis, sintering behavior and electrical properties of Ba(Zr_{0.1}Ce_{0.7}Y_{0.2})O_{3-δ} and Ba(Zr_{0.1}Ce_{0.7}Y_{0.1}Yb_{0.1})O_{3-δ} proton conductors. Ceramic International, volume 40, 2014, pp. 15073–15081.



PROTON-CONDUCTING $\text{BaCe}_{0.5}\text{Zr}_{0.3}\text{Ln}_{0.2}\text{O}_{3-\delta}$ (Ln = Yb, Gd, Sm, Nd, La or Y) CERAMICS FOR
SOLID OXIDE FUEL CELL APPLICATIONS: EFFECTS OF ACCEPTOR-DOPING ON
MICROSTRUCTURE, THERMAL AND ELECTRICAL
PROPERTIES

J. Lyagaeva*, D. Medvedev*, B. Antonov*, L.
Dunyushkina*, V. Kuimov*, A. Demin*, A. Brouzgou***,
Panagiotis Tsiakaras***

*Laboratory of Electrochemical Devices based on Solid Oxide Proton Electrolytes,
Institute of High Temperature Electrochemistry, Russian Academy of
Sciences Urals Branch, 20, Akademicheskaya St. Ekaterinburg, (Russia)

** Department of Mechanical Engineering, University of Thessaly,
Pedion Areos, Volos, (Greece)

E-mail: tsiak@uth.gr

Abstract - Six materials belonging to Ln-doped $\text{BaCeO}_3\text{-BaZrO}_3$ system (Ln = Yb, Y, Gd, Sm, Nd, La) are prepared and characterized in the present work. The impact of the type of the acceptor dopant on (i) the microstructure (relative density, size and type of grains), (ii) the thermal properties (linear expansion, thermal expansion coefficient) and (iii) the electrical properties (nature and value of conductivity) is identified. The modified citrate-nitrate combustion synthesis method is adopted in order to achieve single-phase ceramic samples with relative density higher than 94% at reduced sintering regime (1450°C for 5 h). It is found that: i) the mean grain size increases (from 1.4 to 3.8 μm), ii) the thermal expansion coefficient tends to growth (from $7.6 \cdot 10^{-6}$ to $11.3 \cdot 10^{-6}$ K^{-1} in the high temperature range), iii) the ionic conductivity decreases (from 10.2 to 0.3 mS cm^{-1} at 800°C) with increasing ionic radius of acceptor Ln-dopant. It is also found that $\text{BaCe}_{0.3}\text{Zr}_{0.3}\text{Y}_{0.2}\text{O}_{3-\delta}$ electrolyte can be considered as the most optimal one for IT-SOFC applications from the view point of electrical properties. However, in the temperature interval of 550-700°C, this sample possesses non-uniform thermal expansion.

Keywords. BaCeO_3 , BaZrO_3 , ionic conductivity, textured ceramics, thermal expansion

I. INTRODUCTION

Mixed systems based on $\text{BaCeO}_3\text{-BaZrO}_3$ are considered among the most stable proton-conducting electrolytes, which have been studied widely for solid oxide fuel cells (SOFCs) application [1]. It is widely known that high level of conductivity, including protonic conductivity, was achieved for Y-doped BaZrO_3 and Gd-doped BaCeO_3 mainly due to size factors: the closeness of ionic radii of acceptor dopant with that for Zr^{4+} or Ce^{4+} , as well as the optimal combination of tolerance factor and cell's free volume. Most of the investigations were devoted to $\text{BaCe}_{1-x}\text{Zr}_x\text{Y}_y\text{O}_{3-\delta}$ materials characterized by higher ionic conductivity

than that for $\text{Ce}_{0.9}\text{Gd}_{0.1}\text{O}_{2-\delta}$, $\text{Ce}_{0.8}\text{Sm}_{0.2}\text{O}_{2-\delta}$, YSZ and $\text{La}_{0.8}\text{Sr}_{0.2}\text{Ga}_{0.8}\text{Mg}_{0.2}\text{O}_{3-\delta}$ electrolytes in the intermediate temperature range (500–750°C) [2]. However the same oxides, doped by other acceptor elements (for example, Sm, Gd, Nd), are much less investigated [3].

The current study is devoted to identify the impact of the type of acceptor dopant on the microstructure, thermal thermomechanical and electrical properties of six materials belonging to Ln doped $\text{BaCeO}_3\text{-BaZrO}_3$ system (Ln = Yb, Y, Gd, Sm, Nd, La).

II. EXPERIMENTAL

A. Synthesis

Powders of $\text{BaCe}_{0.5}\text{Zr}_{0.3}\text{Ln}_{0.2}\text{O}_{3-\delta}$ (Ln = Yb, Y, Gd, Sm, Nd, La) were prepared by the aid of a modified version of citrate-nitrate combustion synthesis. High purity >99.5% of $\text{Ba}(\text{NO}_3)_2$, $\text{Ce}(\text{NO}_3)_3 \cdot 6\text{H}_2\text{O}$, $\text{Ln}(\text{NO}_3)_3 \cdot 6\text{H}_2\text{O}$ and a solution of $\text{ZrO}(\text{NO}_3)_2$ with known concentration of salt were used as precursors.

B. Ceramics Characterization

The sintered ceramics were examined by X-ray diffraction analysis (XRD, RIGAKU D/MAX-2200) using $\text{CuK}\alpha_1$ radiation monochromatized by Si-monocrystal 5 at room temperature in ambient air. The morphology of the sintered samples was investigated by scanning electron microscopy (SEM, JSM-5900 LV).

The conductivity of the samples was investigated by the aid of a standard four probe dc-method utilizing the microprocessor system ZIRCONIA-318 at 500–900°C at different atmospheres. Electrical conductivity of the samples doped with Y and La was studied also



by two-probe impedance spectroscopy (Parstat 2273-SVS, USA) in a frequency range of 0.1 Hz – 1 MHz and with an amplitude of 30 mV.

III. RESULTS & DISCUSSION

The materials crystallize in a rhombohedral cell in the case when Ln = Y and Yb, and a cubic cell for Ln = Gd, Sm, Nd and La (Fig.1). As it can be seen, no expected size effect of Ln³⁺ on the unit cell parameters of BaCe_{0.5}Zr_{0.3}Ln_{0.2}O_{3-δ} ceramics was observed.

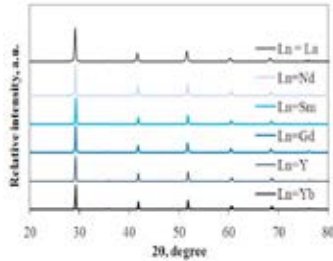


Fig. 1. XRD patterns of powders obtained by grinding of the BaCe_{0.5}Zr_{0.3}Ln_{0.2}O_{3-δ} ceramics sintered at 1450 °C for 5 h.

As it can be distinguished from Fig. 2 for the rhombohedral perovskite materials the surface morphology exhibits rectangular grains, whereas for the cubic structured samples well-connected and close-packed grains with hexahedral form can be observed. The relative density calculated on the base of theoretical and measured ones was found to be higher 94% for all the doped materials.

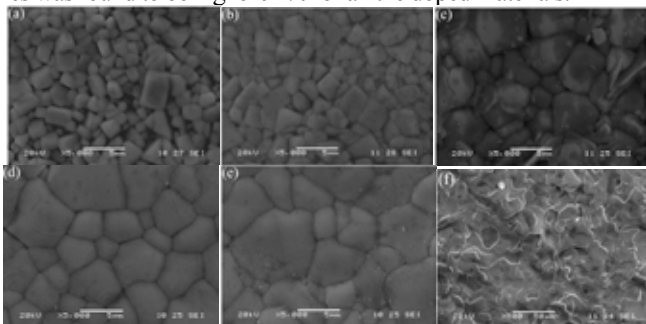


Fig. 2. SEM images of BaCe_{0.5}Zr_{0.3}Ln_{0.2}O_{3-δ} ceramics sintered at 1450 °C for 5 h: Ln = Yb (a), Ln = Y (b), Ln = Gd (c), Ln = Sm (d), Ln = Nd (e) and Ln = La (f).

From Fig. 3 it can be seen that there is a clear inflection point on the $\Delta L/L_0 \div T$ dependences for Y- and Yb-containing materials.

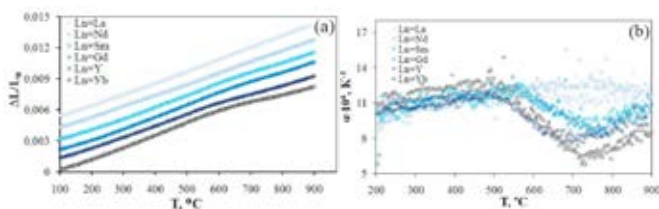


Fig. 3. Temperature dependences of linear expansion (a) and TEC (b) of the BaCe_{0.5}Zr_{0.3}Ln_{0.2}O_{3-δ} as a function of temperature in ambient air atmosphere.

Moreover, from Fig. 4 it is deduced that the total conductivity of the BaCe_{0.5}Zr_{0.3}Ln_{0.2}O_{3-δ} samples was measured by changing pO₂ and estimating the contribution of p-type electronic conductivity and the level of the ionic one. The decrease in conductivity to a constant value occurs with pO₂ drop and the following decrease of this parameter does not lead to significant changes in conductivity.

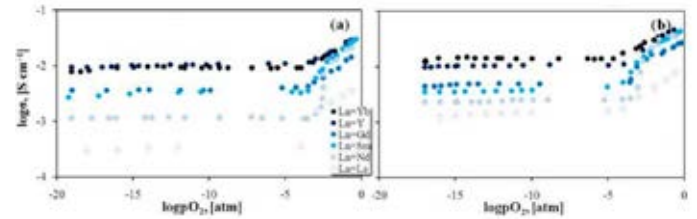


Fig. 4. Conductivity of the BaCe_{0.5}Zr_{0.3}Ln_{0.2}O_{3-δ} samples as a function of pO₂ at 800 °C (a) and 900 °C (b).

IV. CONCLUSION

For the low-temperature range no significant differences in thermal expansion coefficient value are found, whereas for the high-temperature range this parameter increases by ~40%. The ionic conductivity of BaCe_{0.5}Zr_{0.3}Ln_{0.2}O_{3-δ} ceramics tends to decrease with the transition from Y³⁺ to La³⁺, showing the predominant influence of Zr-ions on the transport properties of mixed cerate-zirconate materials; at the same time, the contribution of p-type electronic conductivity increases. On the one hand, Y-containing material is characterized by higher ionic conductivity; however, BaCe_{0.5}Zr_{0.3}Y_{0.2}O_{3-δ} possesses the uneven thermal expansion coupled with strong change in TEC values (30–35% between 500 and 750 °C).

ACKNOWLEDGMENT

The authors of the present investigation are grateful to *The Ministry of Education and Science of the Russian Federation* (Mega-grant contract no. 14.Z50.31.0001) for financial support.

REFERENCES

- [1] Medvedev, D., Murashkina, A., Pikalova, E., Demin, A., Podias, A., Tsiakaras, P., BaCeO₃: Materials development, properties and application, *Progress of Materials Science*, 60, 2014, pp. 72–129.
- [2] Bi, L., Traversa, E., Synthesis strategies for improving the performance of doped BaZrO₃ materials in solid oxide fuel cell applications, *Journal of Material Research*, 2, 2014, pp. 1–15.
- [3] Lyagaeva, Y.G., Medvedev, D.A., Demin, A.K., Yaroslavtseva, T.V., Plaksin, S.V., Porotnikova, N.M., Specific features of preparation of dense ceramic based on barium zirconate, *Semiconductors*, 48, 2014, pp. 1353–1358.



A HIGHLY ACTIVE AND STABLE PT-SKIN OVER PTCU₃/C INTERMETALLIC SHELL ORR ELECTROCATALYST

M. Bele^a, M. Gatalo^a, N. Hodnik^b, G. Dražič^a, P. Jovanovič^a, M. Zorko^a, M. Gaberšček^a and S. Hočevar^{b,c*}

^a Laboratory for Materials Chemistry, National Institute of Chemistry Hajdrihova 19, SI-1000 Ljubljana (Slovenia)

^b Laboratory of Catalysis and Chemical Reaction Engineering, National Institute of Chemistry Hajdrihova 19, SI-1000 Ljubljana (Slovenia)

^c Mebius d.o.o., Na jami 3, SI-1000, Ljubljana (Slovenia)

Abstract - We present here selected recent results on oxygen reduction reaction (ORR) activity and stability of a proprietary carbon supported Pt-skin over PtCu₃ intermetallics shell around PtCu core alloy catalyst.

The modified sol-gel synthesis method was optimized as to achieve the following major goals: the presence of Pt-skin, the presence of ordered intermetallics (Pm $\bar{3}$ m) phase, firm embedment of catalyst nanoparticles into carbon and possibility of large-scale production. The annealing step is crucial for obtaining three of the material's decisive properties: particle size distribution, formation of intermetallics shell, and Pt segregation on the surface (Pt-skin formation).

Index Terms – fuel cell, catalyst, oxygen reduction, Pt-skin.

I. INTRODUCTION

The efficiency of PEMFC is still limited by high activation overpotential in oxygen reduction reaction (ORR). Commercial ORR catalysts still possess insufficient mass activity (MA) and poor stability. Among the promising materials with highest specific (SA) and mass activities (MA) are Pt-alloyed catalysts [1]. In these catalysts the activity of Pt in ORR is enhanced due to the so-called strain and ligand effects induced by the alloyed transition elements [2]. Especially Pt-skin catalysts with subsurface non-noble transition metal (TM) layer have demonstrated high MA and stability during potential cycling at electrode catalyst loading below 0.1 mg_{PGM} cm⁻²_{geom}

The state-of-the-art Pt-based PEMFC has the working

potential of 0.67 V @ 1.5 A cm⁻² with 0.133 mg_{PGM} cm⁻² loading and 0.154 g_{PGM} kW⁻¹ PGM total content, demonstrating a significantly lower overpotential for ORR [3].

We present here recent results on ORR activity and stability of our proprietary carbon supported Pt-skin over PtCu₃ intermetallics shell around PtCu core alloy catalyst.

II. EXPERIMENTAL

A. Catalyst synthesis

The modified sol-gel synthesis method [4] was optimized so as to achieve the following major goals: the presence of Pt-skin, the presence of ordered intermetallics (Pm $\bar{3}$ m) phase, firm embedment of catalyst nanoparticles into carbon and possibility of large-scale production. The alloy annealing step in the synthesis procedure is crucial since it influences on particle size distribution, formation of intermetallics shell in nanoparticles (NP), and Pt segregation on the surface of NPs (Pt-skin formation).

B. Catalyst characterization methods

The catalyst was thoroughly characterized by several methods: structure and composition determination by powder XRD, SEM, STEM-HAADF with simultaneous EDX, HRTEM, ICP-MS; ECSA determination by CV (HUPD, CO stripping); activity determination by RDE and single cell test; stability determination by CV (ECSA stability), RDE (SA and MA stability), IL-SEM and IL-TEM (morphology and structure stability).

III. RESULTS AND DISCUSSION

Analysis of particles reveals that the ordered phase always forms a shell around the disordered core, reflecting the surface-to-core phase growth during the annealing procedure. This shell enhances the electrocatalytic activity and stability of the catalyst [5]. Furthermore, the existence of a Pt-skin can be demonstrated on the surface of particles (Fig. 1).

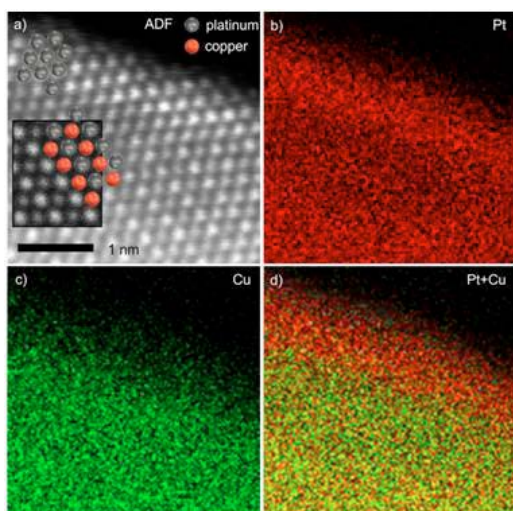


Fig. 1. a-d) Direct evidence of Pt-skin formation on the surface of catalyst particles. The atomic columns with a brighter contrast at the STEM-HAADF image (a) correspond to Pt, the insert shows a simulated PtCu₃ ordered structure. This phase was observed at the outer edge of the particle, which is terminated by a Pt-skin of a thickness of below 1nm formed at the very surface of the particle. The skin is clearly visible in EDX maps (b-d), acquired simultaneously with HAADF-STEM image.

A tight embedment of catalyst nanoparticles into carbon support was observed (Fig. 2). The latter prevents particles to detach, migrate and agglomerate.

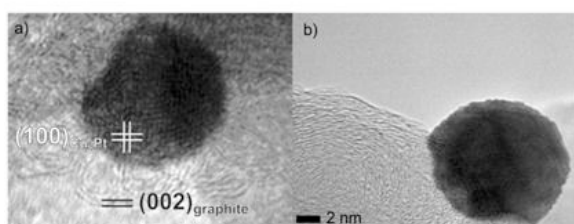


Fig.2. a,b) Semi-epitaxial growth of lacy, graphene-like bands sprouting from the 8 nm large CuPt particle oriented close to the [001] zone axis. Concave imprints on some crystals (the visibility of the imprints depends on the crystal orientation) at the original attachment point with carbon matrix are visible.

Single cell test (25 cm²) performed with Pt loading of 0.09 mg cm⁻²_{geom} gave ECSA equal to 47 m² g_{Pt}⁻¹ and beginning of life (BoL) MA (@ 0.9 V_{iR-free}) equal to 0.77 A mg_{Pt}⁻¹. The power density of 1.13 W cm⁻² (@ 1.5 A cm⁻²)

was obtained. Given 0.05 mg_{Pt} cm⁻² Pt loading at anode, the total Pt loading amounts 0.124 g_{Pt} kW⁻¹ (Fig.3).

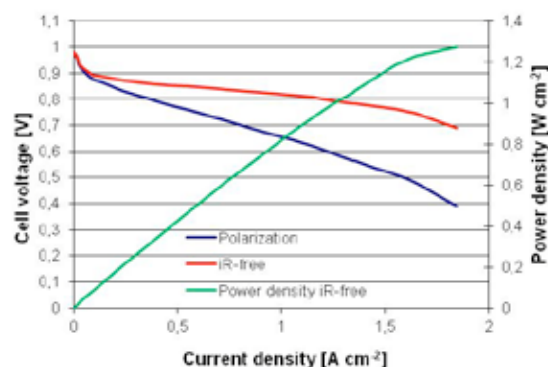


Fig.3. Single cell polarization curve at 80 °C, H₂/O₂, Φ = 1000 mL min⁻¹, P_{H₂} = 100 kPa, P_{O₂} = 200 kPa, RH = 0%.

IV. CONCLUSION

The new catalyst produced in 20 g batches highly outperforms the conventional Pt/C benchmark electrocatalyst and markedly exceeds the US Department of Energy targets for 2017. Very importantly, our catalyst exhibits a marked decrease of Pt dissolution compared to the Pt/C benchmark electrocatalyst under potentiodynamic treatment.

ACKNOWLEDGMENT

The authors kindly acknowledge grants No. P2-0152-104 and No. P2-0393-104 provided by the Slovenian Research Agency.

REFERENCES

- [1] Debe, M. K., Electrocatalyst approaches and challenges for automotive fuel cells, *Nature*, Volume 486, 2012, pp. 43-51.
- [2] Stephens, I. E. L., Bondarenko, A. S., Grønbjerg, U., Rossmeisl, J. and Chorkendorff, I., Understanding the electrocatalysis of oxygen reduction on platinum and its alloys, *Energy & Environmental Science*, Issue 5, 2012, pp. 6744-6762.
- [3] Steinbach, A. J., U.S. Department of Energy EERE FCTO Annual Merit Review (2015), Project FC104, http://www.hydrogen.energy.gov/pdfs/review15/fc104_steinbach_2015_o.pdf
- [4] Bele, M., Gaberšček, M., Kapun, G., Hodnik, N., Hočevar, S., Electrocatalytic composite(s), associated composition(s), and associated process(es), US 2013/045866 (A1); EP2735044 (A2); JP2014525829 (A); WO2013012398 (A3).
- [5] Bele, M., Jovanovič, P., Pavlišič, A., Jozinovič, B., Zorko, M., Rečnik, A., Chernyshova, E., Hočevar, S., Hodnik, N. and Gaberšček, M., A highly active PtCu₃ intermetallic core-shell, multilayered Pt-skin, carbon embedded electrocatalyst produced by a scale-up sol-gel synthesis, *Chemical Communications*, Volume 50(86), 2014, pp. 13124-13126.



NEW HIGH-TEMPERATURE PROTON CONDUCTING POLYMER NANOCOMPOSITE MEMBRANES

A. Kržan*, M. Jazbec**, J. Hočevar**, A. Lotrič**, J.
Moškon*, and S. Hočevar* **

*National Institute of Chemistry, Hajdrihova 19, 1000 Ljubljana,
(Slovenia)

**Mebius Ltd., Na jami 3, 1000 Ljubljana, (Slovenia)

Abstract - We present a general method for the synthesis of a new class of proton conducting polyoxometallate-based organic-inorganic salts, which can be characterized as high temperature ionic liquids or plastic crystals. Further, we present the method for the preparation of polymer nanocomposite membranes based on the synthesized salts as well as the preparation of membrane-electrode assemblies and the results of high temperature PEMFC single cell tests.

Index Terms - fuel cell, membrane, polymer, proton conducting.

I. INTRODUCTION

A key unresolved challenge in the development of proton exchange membrane fuel cells (PEMFC) are robust electrolyte membranes with high proton conductivity at high temperatures and negligible humidity [1].

An alternate approach to synthesis/preparation of proton conducting membranes is to combine a polymer with a proton conductive additive or filler. Among other possibilities heteropolyacids (HPA) and ionic liquids (IL) have also been explored as proton conducting polymer fillers but with only limited success [2].

We here present a general method for synthesis of HPA/IL based proton conducting organic-inorganic salts, a method for nanocomposite polymer membranes preparation, membrane-electrode assembly (MEA) and results of single cell tests of high temperature PEMFC (HT PEMFC) at 195 - 260 °C under dry gases condition.

II. EXPERIMENTAL

A. Synthesis

Organic-inorganic hybrid compounds are synthesized in a metathesis reaction between a HPA with an IL in which the

conjugate anion of the stronger acid (HPA) replaces the conjugate anion of a weaker acid (IL anion) resulting in a new salt composed of a polyoxometalate anion and a stoichiometric number of organic cations. The synthesis is extremely versatile and may be carried out through mixing of the reagents in pure form, in suspension or in solution with at least one reagent in liquid form. Using HPA in combination with a range of imidazolium based ionic liquids resulted in water insoluble salts [3].

B. Membrane preparation

A membrane was prepared from N-methylpyrrolidone solution of a polyimideamide and sulphonated polyetheretherketone (1:1) mixture with a salt prepared from BMIMCl and 1,3-MIMTf (in mixture of 1:1 molar ratio) and SiWA. The salt content in the membrane was 40 wt.%. A clear homogeneous viscous solution was used to prepare a 100 µm thick membrane on a glass support by means of a moving blade. The initially cloudy membrane became perfectly transparent, mechanically stable and flexible after curing at 150 °C indicating a nano-composite structure formation.

C. Membrane-electrode assembly (MEA)

MEA were composed of Pt/C gas diffusion electrodes and a 100 µm membrane made from N-methylpyrrolidone solution of a polyimideamide and sulphonated polyetheretherketone (1:1) mixture with a salt prepared from BMIMCl and 1,3-MIMTf (in mixture of 1:1 molar ratio) and SiWA. The salt content in the membrane was 40 wt.%.

D. Characterization

Structural: single crystal XRD, powder XRD; Thermal: TGA, DSC; Conductivity: electrochemical impedance spectroscopy (EIS); Single cell fuel cell test.



III. RESULTS AND DISCUSSION

X-ray analysis of a BMIM-SiWA salt single crystal revealed a well ordered, layered structure confirming the 4 : 1 ion ratio. Thermal gravimetric analysis (TGA) showed the salt to be stable to 380 °C.

We analyzed the powder X-ray diffractograms of the salt during the heating-cooling cycle from room temperature to 300 °C and backward. The diffractogram at room temperature coincided with a simulation based on the single crystal X ray analysis. Upon heating the crystalline structure was gradually and partially lost but would reappear upon cooling as shown in Fig. 1.

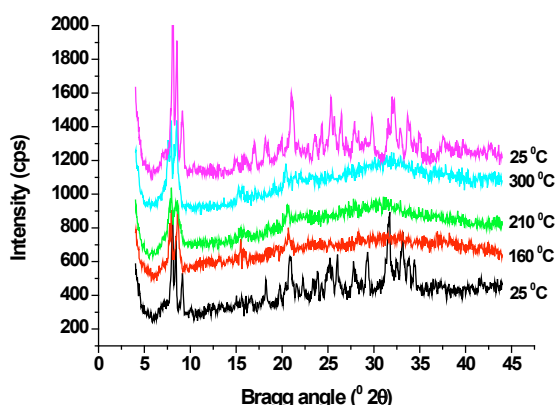


Fig. 1. Powder XRD of (BMIM)₄SiWA salt scanned at different temperatures with high-temperature XRD apparatus.

EIS of the BMIM-SiWA salt under dry conditions showed a large reversible increase / decrease in ionic conductivity by several orders of magnitude. A high ionic conductivity on the order of 10⁻³ S/cm was achieved at temperatures up to 299 °C as shown in Fig. 2.

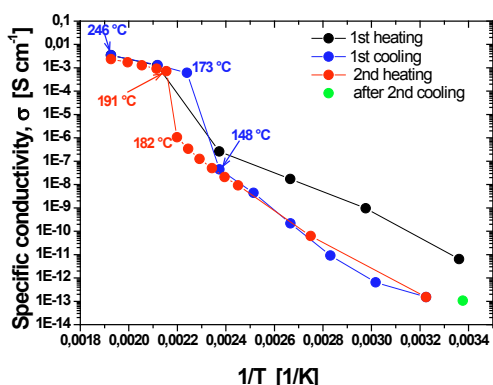


Fig. 2. Dependence of specific conductivity on inverse temperature for (BMIM)₄SiWA salt obtained with EIS with Pt foil contacts in dry Ar.

The stepwise increase/decrease in ionic conductivity coincides with an observed thermal transition seen by DSC. XRD and EIS indicate a thermally induced loosening of the ordered crystal structure (formation of plastic crystal phase)

that provides for the structural flexibility at the molecular level, which supports the drastic increase of ionic conductivity. Upon cooling the ruptured weak linkages are re-connected, reducing plasticity and causing ionic conductivity to decrease.

The polarization and power curves of the MEAs are shown in Fig. 3.

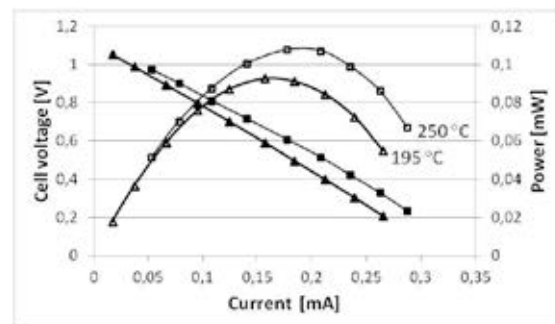


Fig. 3. Polarization curve obtained in a 12 cm² single cell with open channels on cathode side at 250 °C with dry H₂ (20 mL min⁻¹) and ambient air (> 100 mL min⁻¹), and polarization curve obtained in a 25 cm² single cell at 195 °C with dry H₂/O₂ (both 20 mL min⁻¹).

IV. CONCLUSION

The presented study illustrates a general route to a class of heteropolyacid-based organic – inorganic salts (plastic crystals) with specific structural characteristics that support proton conductivity and can be exploited to construct a functional fuel cell operating with dry gases in a temperature range between 195 and 250 °C. Due to their structural transitions the synthesized salts should be considered as a new family of plastic crystals which differs from protic (organic) ionic plastic crystals (POIPCs) [4] by higher thermal resistance.

ACKNOWLEDGMENT

Financial support by grants from Slovenian Research Agency and Ministry of Defence are kindly acknowledged.

REFERENCES

- [1] Paddison, S. J., Gasteiger, H. A., PEM Fuel Cells, Materials and Design Development Challenges, Chapter 11 in Encyclopedia of Sustainability Science and Technology (Ed.: Robert A. Meyers), Springer New York, 2013, pp. 7756-7777.
- [2] Sachdeva, S., Turner, J.A., Horan, J.L., Herring, A.M., The use of heteropoly acids in proton exchange fuel cells, in Fuel Cells and Hydrogen Storage (Eds.: Bocarsly A., Mingos D.M.P.), Struct. Bond., Vol 141, 2011, pp. 115-168.
- [3] Hočvar, S., Kržan, A., Polyoxometalate Salts, Proton Exchange Membranes and Precursors, Membrane-Electrode Assemblies, Fuel Cells and Methods, PCT/EP2014/070697
- [4] Luo, J., Conrad, O. and Vankelecom, I.F.J., Imidazolium methanesulfonate as a high temperature proton conductor, J. Mater. Chem. A, Issue 1, 2013, pp. 2238-2247.



EDEN: NOVEL POWER-TO-POWER SYSTEM FOR ENHANCED HYDROGEN STORAGE IN SOLID STATE

L. Crema*, M. Testi*, and F. Alberti*

*Fondazione Bruno Kessler, Via Sommarive 18, 38123 Trento,
(Italy)

Abstract - EDEN aims at research, development and validation of a solid-state hydrogen storage technology for specific sector of stationary applications and at support of distributed grid level applications. EDEN realizes a full-scale prototype composed by a storage tank, R-SOC (reversible-Solid Oxide Cell) and an energy recovery solution, which allows overall efficiency improvement and that, is compatible for the use with "polluted" hydrogen. The main objectives of this research project address the development of a new storage material with high hydrogen storage capacity, loaded into a specifically designed storage tank and fully integrated with R-SOC. 10 kg material has been prepared. The intermediate tests demonstrated 7.1 w/w % hydrogen density on the material. Once completed the development and lab characterization, EDEN system prototype has been installed in FBK in Trento, in order to evaluate system performances in real working condition. The demonstration of the technology will be completed in Barcelona, in a selected site controlled by the Barcelona Energy Agency

Index Terms – hydrogen storage, power to power hydrogen, reversible fuel cell

I. INTRODUCTION

The wider market penetration of renewable energy systems is leveraging the problem of the grid stability and security of supply to a critical level in several countries. Intermittent and variable sources in time and in magnitude are difficult to manage and distribute, with the proper demand response. A big effort is so dedicated in developing new storage solutions able to reduce the specific problem to a sustainable level. Different technologies have indeed important limitations in density, in cycling, in security of supply and reliability, in costs, in down- and up- scalability. Hydrogen, among other solutions, has a big potential in matching the scope on a wide range of applications and through different possible storage solutions. Among these, solid-state storage is getting a level of maturity never achieved before, where the readiness level is increasing to the demonstration of the integrated systems in real environments. Some specific developments will be illustrated on new

promising materials: Mg-based metal hydrides in several nano-composites, the innovation on integration layouts proposing new solutions to manage hydrogen storage on solid state, the coupling with bidirectional solid oxide cell and the balance of plants with auxiliaries for both thermal and fuel management.

II. METHODOLOGY

Eden project up-scaled (10kg) a new Mg-Base storage material by High Energy Ball Milling technique. Its properties were improved particularly through superficial deposition of selected metal oxide catalyst by innovative vibrating sputtering probe directly on powder. This allowed faster kinetics of hydrogen absorption and desorption reaction using a minimized quantity of catalyst. Tank layout and its main parameters are designed and optimized through analytical tool that includes a deep multi-physical modelling investigations focused on heat transfer, fluid dynamic, structural mechanical analysis. Numerical simulation allowed the identification the best design/layout for hydrogen storage tank, which was finally validated through a real comparison with a small-scale tank prototype. Finally, system integration layout was studied, including matching analysis for flows, heat transfer and temperatures tailoring auxiliary components such as: hydrogen burner, steam generator, water removal system, compressor as well as R-SOFC and hydrogen storage tank. Simulations of the whole system performances evaluated and extracted the main critical parameters for efficient system management procedure. In particular, data simulated are gathered to evaluate the connection of the storage tank with different simulated SOC behaviors, both during fuel cell mode (with hydrogen consumption) and high temperature electrolyzer (with hydrogen production and storing).

III. RESULTS

The power-to-power system has experimentally confirmed the target results for the Mg-based material, in kg-size up scaled configuration within a fully integrated and controlled tank. Below a summary on main achievements.



A. Innovative Mg-based material

The best candidate material is a nanostructured Mg-based powder. The main properties of this material are reported in the following table 1.

TABLE 1. H₂ STORAGE PROPERTIES FOR BEST CANDIDATE MATERIAL

Properties	Unit	Value
Gravimetric capacity	kgH ₂ /kg %	7,1
	kWh/kg	2,4
Volumetric capacity	kgH ₂ /l	0,13
	kWh/l	4,4
Operating temperature	°C	320
Max delivery pressure	Bar	2
Min charging pressure	Bar	3
Desorption rate*	gH ₂ /min	>1

* For 1kg of material, at 320 °C and 1.2 bar (0.2 barG)

B. Storage tank

The storage tank was realized in intermediate and full scales, as reported in Fig. 1. At the working conditions, the fuel utilization is around 90%. The pressure is self-regulating below 10 Bars. At the working temperature of 320°C and at the hydrogen flowrate of 0,5 g/min, the full load storage capacity time is 5 hours. The tank is provided of fuel and heat management and an internal design to minimize the temperature gradient. This was achieved using graphite as heat transport material in combination with heat pipes.



FIG. 1 EDEN STORAGE TANK DURING INTERMEDIATE SIZE VALIDATION AND IN FULL SIZE LAYOUT

Gravimetric storage capacity measured for material activation and cycling beginning are shown in Fig. 2 below. Dark blue for absorption step, light blue for desorption step.

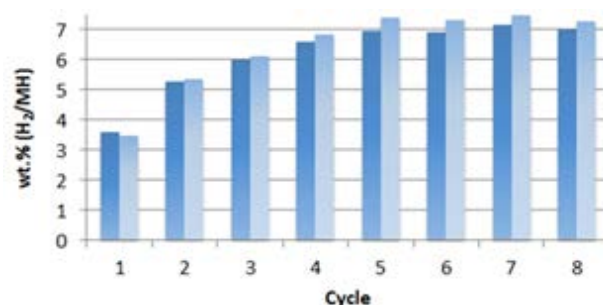


FIG. 2. INITIAL CYCLING OF EDEN MATERIAL AT FULL SCALE

C. Power-to-power prototype

The full power-to-power system is fully designed and prototyped. The components are under validation. At the present it has been demonstrated part of the integrated layout: the thermal cycles between material inside the tank, the solid oxide system and some further components such as a hydrogen burner, the heat pipes, the heat high temperature exchangers. In Fig. 3 below a picture of the prototype.



FIG. 3 FULL SCALE POWER TO POWER EDEN SYSTEM

IV. CONCLUSION

The prototypal technology is under a validation and demonstration phase. The full system has been validated in main components, such as the hydrogen storage material, the tank, the integration layout between the tank, the solid oxide cell and the main auxiliaries of the Balance of plant (BoP). Gravimetric storage capacity of the material is 7,1%, the volumetric capacity of the integrated tank is at 2%. The business case related the developed technology is looking to bring the technology at support of distributed energy generation for scales between few kW up to MW, and at support of grid services in scales from hundreds of kW up to several MW. The system will be demonstrated in Barcelona, by the Energy Agency of the city, until March 2016.

ACKNOWLEDGMENT

The research leading to these results has received funding from the European Union's Seventh Framework Programme (FP7/2007-2013) for the Fuel Cells and Hydrogen Joint Technology Initiative under grant agreement nr. 303472.

HIGH PERFORMANCE THIN FILM MIXED IONIC-ELECTRONIC CONDUCTING ELECTRODE FOR LOW TEMPERATURE SOLID OXIDE FUEL CELLS

G. Y. Cho*, Y. H. Lee*, T. Park*, Y. Lee*, J. An** and S. W. Cha*,#

*Department of mechanical and aerospace engineering, Seoul National University, 301-dong 116-ho, Gwanak-ro 1, Gwanak-gu Seoul 151-744, (Republic of Korea)

**Manufacturing Systems and Design Engineering Programme, Seoul National University of Science and Technology, 232 Gongneung-ro, Nowon-gu, Seoul 139-743, (Republic of Korea)

Abstract - NiO-GDC thin films fabricated by sputtering are used as mixed ionic electronic conducting (MIEC) anodes for ScSZ electrolyte supported low temperature solid oxide fuel cells (LT-SOFCs). Dense NiO-GDC thin film MIEC anode based LT-SOFC showed improved performance (29.5 mW/cm^2 at $500 \text{ }^\circ\text{C}$) compared with Pt only anode based LT-SOFC (23 mW/cm^2 at $500 \text{ }^\circ\text{C}$). Furthermore, LT-SOFC with porous NiO-GDC thin film MIEC anode showed much enhanced maximum performance, 36 mW/cm^2 at $500 \text{ }^\circ\text{C}$ compared with Pt only anode based LT-SOFCs. These improved performances of LT-SOFCs are caused by higher density of triple phase boundaries for hydrogen oxidation reactions in MIEC anodes than Pt only anode and increased porosity of thin film anodes.

Index Terms – anode, low-temperature solid oxide fuel cells, mixed ionic electronic conductor, thin film.

I. INTRODUCTION

Solid oxide fuel cells (SOFCs) are considered as promising next power generation devices due to high efficiency, low pollutants, and fuel flexibility. Despite of these advantages, typical SOFCs have many problems caused by excessive high operation temperature (above $800 \text{ }^\circ\text{C}$) such as thermal degradation and material durability. [1-3] Therefore, there have been many researches to lower operation temperature of SOFCs such as utilization of thin film techniques to fabricate low temperature SOFCs (LT-SOFCs). [2, 3]

Most of LT-SOFCs use Pt electrodes because of low electrical resistance and superior catalytic activity for both hydrogen oxidation reactions (HORs) and oxygen

reduction reactions (ORRs) especially at low temperature. However, in spite of these advantages, metal only electrodes have many problems such as high price, agglomeration of catalysts and limitation of triple phase boundaries (TPBs).

Mixed ionic electronic conducting (MIEC) materials such as NiO-YSZ, NiO-GDC or LSCF are composed of electronic conducting metal catalysts and ionic conducting ceramic backbones. Therefore, MIEC electrodes have 3 dimensional TPBs in whole electrodes and mitigated thermal degradation caused by agglomeration.

In this study, thin film NiO-GDC anodes were fabricated by using sputtering methods to reduce the amount of Pt and to maximize the performance of LT-SOFCs. In order to investigate effects of thin film MIEC anode, Pt only anode cell was also prepared. Also, structural effects of thin film MIEC anode were also studied. LT-SOFC with porous thin film NiO-GDC anode showed much improved performance compared with Pt only anode cells due to increased porosity and TPBs.

II. EXPERIMENTAL SECTION

$150 \mu\text{m}$ thick commercial scandia-stabilized zirconia (ScSZ, 10 mol. % Sc_2O_3 , SOFCMAN, China) pellets were used as electrolyte substrates. ScSZ substrates were cleaned in ultrasonic bath with acetone, ethanol, and deionized water for 10 minutes to remove surface impurities. In order to prepare thin film MIEC anodes, a commercial NiO-GDC (NiO 50 wt. %, RnD Korea, Korea) target was used. Anodes were deposited with



radio-frequency sputtering power 200 W at different Ar deposition pressure. For cathodes of LT-SOFCs, Pt target was used with direct-current (DC) sputtering power 100 W and 12 Pa Ar atmosphere. For a reference LT-SOFC, thin film Pt anode was fabricated by DC sputtering power 100 W and 12 Pa Ar atmosphere.

Electrochemical characterization was conducted at 500 °C with custom-made experimental set-up. [3] 30 sccm of pure H₂ was supplied to anode side and the cathode side was exposed to the ambient atmosphere. Solartron 1287/1260 (Solartron, U.K.) were used to measure open circuit voltage (OCV), current-voltage behavior, and electrochemical impedance spectroscopy (EIS).

III. RESULTS AND DISCUSSION

Table 1. summarizes composition and preparation conditions of LT-SOFCs. As seen in table 1, cell-1 was composed of porous Pt anode and porous Pt cathode. Cell-2 and cell-3 had thin film NiO-GDC anode and porous Pt cathode. Anode of cell-2 was fabricated at 0.67 Pa and anode of cell-3 was prepared at 8 Pa to investigate influence of porosity of thin film MIEC anode on performance.

TABLE I
PREPARATION CONDITIONS OF LT-SOFCs

	Cell-1	Cell-2	Cell-3
Anode	Porous Pt (12 Pa)	Dense NiO-GDC (0.67 Pa)	Porous NiO-GDC (8 Pa)
Preparation conditions	DC sputter 100W 12 Pa	RF sputter 200 W 0.67 Pa	RF sputter 200 W 8 Pa
Electrolyte	ScSZ pellet		
Cathode	Porous Pt (12 Pa)		
Preparation conditions	DC sputter 100W 12 Pa		

Before electrochemical measurement, chemical composition of NiO-GDC thin film was measured by using field emission scanning electron microscopy with energy dispersive x-ray spectroscopy (FESEM-EDX). Atomic concentration of Ni, Gd, and Ce are 32.6 at. %, 2.0 at. %, and 12.0 at. %, respectively. It means that NiO-GDC thin films prepared by RF-sputtering contain reasonable metal catalyst (Ni) and ionic conducting ceramics. (Gd₂O₃ and CeO₂)

After investigation of NiO-GDC thin films, electrochemical characterizations were conducted. Fig. 1. shows current density-voltage behavior of LT-SOFCs. As seen in Fig. 1, cell-1 (porous Pt anode and porous Pt cathode) showed the lowest maximum power density compared with cell-2 and cell-3. (23 mW/cm² at 500 °C) However, cell-2 (dense NiO-GDC anode and porous Pt cathode) presented slightly improved performance than cell-1. (29.5 mW/cm² at 500 °C) This result implied dense NiO-GDC thin film successfully acted as an anode for LT-SOFCs. Despite of low electrical conductivity of thin film NiO-GDC anode compared with thin film Pt

anode, maximum power density of cell-2 was increased because of increment of TPBs for HORs in NiO-GDC anode. Interestingly, cell-3 (porous NiO-GDC anode and porous Pt cathode) showed the highest peak power density among all cells. (36 mW/cm² at 500 °C) We believe that the highest peak power density of cell-3 caused from higher density of TPBs compared with cell-1 and increased porosity compared with cell-2.

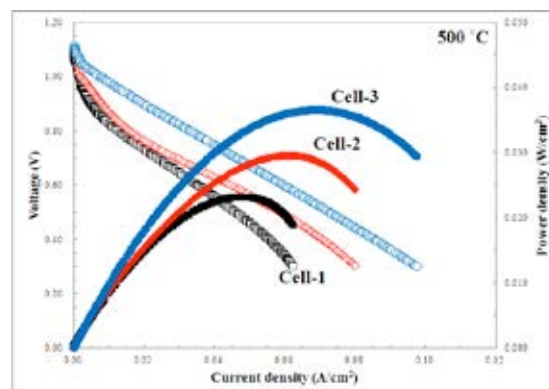


Fig. 1. Polarization curves of LT-SOFCs with different thin film anodes at 500 °C

IV. CONCLUSION

Thin film NiO-GDC MIEC anode was successfully fabricated by sputtering method and applied to ScSZ electrolyte supported LT-SOFCs. LT-SOFC with dense thin film NiO-GDC anode showed 29.5 mW/cm² at 500 °C which was higher than Pt only anode based LT-SOFCs. Moreover, LT-SOFC with porous NiO-GDC thin film anode showed the highest maximum power density. (36 mW/cm² at 500 °C) This improved performance of LT-SOFCs caused by higher density of TPBs in MIEC anode and increased porosity of NiO-GDC thin film.

ACKNOWLEDGMENT

This research was partially supported by National Research Foundation of Korea (NRF-2013R1A1A2A10065234). Brain Korea 21 plus program should be also acknowledged for their partial support.

REFERENCES

- [1] O'Hayre, R., Cha, S-W., Colella, W., Prinz, F.B., Fuel cell fundamentals, 2nd, Wiley
- [2] An, J., Kim, Y. B., Park, J., Gür, T. M., Prinz, F. B. Three-dimensional nanostructured bilayer solid oxide fuel cell with 1.3 W/cm² at 450° C. Nano letters, Volume 13, 2013, Pages 4551-4555.
- [3] Ji, S., Cho, G. Y., Yu, W., Su, P. C., Lee, M. H., Cha, S. W., Plasma-enhanced atomic layer deposition of nanoscale yttria-stabilized zirconia electrolyte for solid oxide fuel cells with porous substrate. ACS applied materials & interfaces, Volume 7, 2015, Pages 2998-3002.



COUPLING OF A HIGH TEMPERATURE ELECTROLYSER WITH CONCENTRATED SOLAR ENERGY

N. Monnerie*, A. Houaijia*, M. Romero*, H.-P. Streber*, M. Roeb* and C. Sattler*

*German Aerospace Center (DLR), Institute of Solar Research,
Linder Höhe, 51147 Cologne, (Germany)

Abstract - The coupling of pressurized high temperature steam electrolysis (HTE) with concentrated solar energy in order to produce hydrogen is studied. Flow-sheets and simulations have been carried out in MW-range. Different solar tower systems have been considered. For a production of 400 kg/d hydrogen for its use in transport and with the molten salt solar tower technology, the total thermal energy input of the solar receivers is 20.43 MWth. The total electrical power generated is about 1.687 MWe. In the case of a production of 4000 kg/d hydrogen for an industrial use and using the DSG solar tower technology, the total thermal energy input of the solar receivers is 82.4 MWth while the generating power is about 16.7 MWe. In parallel, a demonstrator is being constructed to demonstrate this concept. For this purpose, a solar receiver was developed and tested in order to provide the electrolyser with superheated steam.

Index Terms – High temperature electrolysis, hydrogen, solar energy.

I. INTRODUCTION

Climate change issues and global warming have become hard environmental challenges. In order to reduce the CO₂ emissions, an energy economy based on hydrogen has been developed and the non-fossil hydrogen production is becoming more interest. Amongst the diverse methods, high temperature steam electrolysis (HTE) is considered as a promising technology for a sustainable hydrogen production. In this process, the steam is decomposed into hydrogen and oxygen using a combination of electrical energy and high temperature heat. It has the advantage of higher hydrogen production efficiency in comparison with the conventional low temperature electrolysis [1]. In the frame of the FCH-JU project SOPHIA (Solar integrated pressurized high temperature electrolysis) the coupling of pressurized high temperature steam electrolysis in a Solid Oxide Electrolyser (SOE) with concentrated solar energy to produce

hydrogen is studied. The total energy demand of the electrolyser unit consists indeed of electricity and heat which can be both generated by solar concentrating energy systems like the solar tower.

II. DESCRIPTION OF THE TECHNOLOGY

A. Process for hydrogen production

Solar Tower technologies are composed of many large and computer-controlled sun-tracking mirrors, so-called heliostats, which concentrate the incoming solar radiation into a solar receiver placed on the top of a tower. In the solar receiver, the solar radiation is absorbed by a heat transfer fluid that flows through the tubes of the receiver to generate steam. The process design of the plant depends on the heat transfer fluid, which can be water, air or molten salts. In this study, the Direct Steam Generation (DSG) solar tower, the molten salt solar tower and the pressurized air-cooled solar tower have been considered. For these three solar tower technologies, two different scenarios have been considered: the first one concerns the production of 400 kg/d hydrogen for its use in transport. The second scenario deals with the production of 4000 kg/d hydrogen for an industrial use.

The solar tower is coupled to the HTE to which it provides the electricity and heat required. Thus, the steam coming into the HTE is preheated and evaporated by the solar receiver steam. The electrolyser operates at 750°C and 15 bars. An electrical heater is required in order to superheat the steam up to the operating temperature of the electrolyser of 750°C. A steam to hydrogen conversion of 50% is assumed as well as the use of air as sweep gas. The main specifications of the HTE unit are resumed in Table I.

TABLE I
MAIN SPECIFICATIONS OF THE HTE UNIT

Operation Mode	Thermoneutral
Sweep gas/cathode stream ratio	1:1
Steam conversion	50%
Operating pressure	15 bar
Inlet/outlet cathode temperature	750°C
Inlet/outlet anode temperature	750°C
H ₂ at cathode inlet	10%

In the HTE stack, the water steam is supplied to the cathode side and is splitted into hydrogen and oxygen ions. The oxygen ions are transferred through the electrolyte to the anode side where they combine to form oxygen. The steam supplied to the cathode side is first mixed with a part of the produced hydrogen in order to have a composition of 90%mol H₂O and 10%mol H₂. The product gas containing hydrogen and water steam is introduced to a flash unit, where the water steam is separated by condensation and then introduced again as HTE feed water.

B. Solar receiver for steam production

A demonstrator is being designed and constructed in order to demonstrate the studied concept. A solar receiver will be coupled to a 3 kWe-size pressurized high temperature steam electrolyser and operated on-sun for proof of principle. For this purpose, a solar receiver has been developed as depicted in Figure 1 in order to provide the electrolyser with superheated steam.

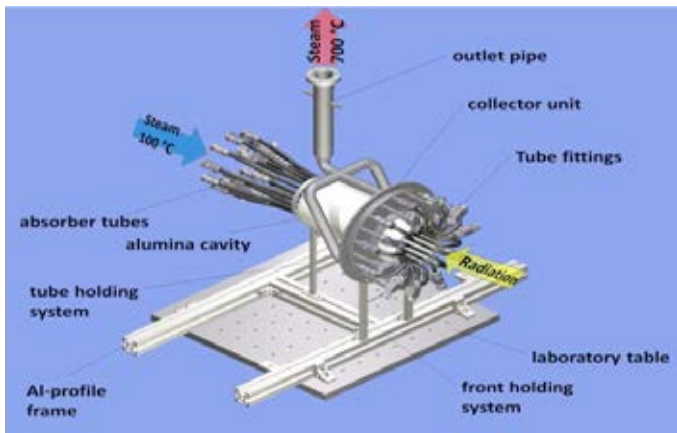


Fig. 1. Model of the solar receiver

III. RESULTS

Flow-sheets and simulations have been carried out for hydrogen production in MW-range by using the simulation tool Aspen Plus. Two different scenarios have been considered for each solar tower technology as explained in section III. A part of the total thermal energy input of the solar receiver is used to generate the superheated steam needed in the HTE while the

other part is used to generate the required electricity. Tables II and III sum up the results obtained for the 2 scenarios.

TABLE II
RESULTS OF THE SIMULATION FOR THE SCENARIO 1: 400 KG/D H₂

Solar Tower technology	Total thermal energy input [MWth]	Total electrical power generated [MWel]
DSG	8.24	1.68
Molten Salts	20.43	1.687
Pressurized air-cooled	4.85	1.67

TABLE III
RESULTS OF THE SIMULATION FOR THE SCENARIO 2: 4000 KG/D H₂

Solar Tower technology	Total thermal energy input [MWth]	Total electrical power generated [MWel]
DSG	82.4	16.7
Molten Salts	204.3	16.87
Pressurized air-cooled	48.5	16.7

The solar receiver has been tested in DLR's high flux simulator in Cologne. Saturated steam of 100 °C enters the absorber pipes from behind and is superheated by concentrated solar radiation. With a feeding mass flow of 5 kg/h of steam, the outlet temperature reaches 700°C.

IV. CONCLUSION

Flowsheets for solar high temperature electrolysis driven by different solar tower technologies was designed and the plants were simulated for two different scenarios depending on the end-use of hydrogen. Thus, for a production of 400 kg/d hydrogen, the DSG plant has a thermal energy input of 8.24 MWth and generates 1.68 MWel. In addition to this simulation works, a solar receiver has been tested in the solar simulator of DLR in cologne to provide superheated steam to the electrolyser. In a next step, this receiver will be optimized and coupled to the HTE and finally operated on-sun for proof of principle. Finally, the flowsheeting analysis will be the basis of a techno-economic study of a high temperature electrolysis process coupled with concentrated solar energy.

ACKNOWLEDGMENT

The authors of this paper gratefully acknowledge the co-funding of the project SOPHIA (Grant agreement No. 621173) by the FCH JU.

REFERENCES

1. Steinfeld, A., Solar thermochemical production of hydrogen - A review. *Solar Energy*, 2005. 78: p. 603-615.



PROTON-CONDUCTING ELECTROLYTES BASED ON Ba(Ce, Zr)O₃: THE COMPARATIVE ANALYSIS OF SYNTHESIS METHODS

D. Medvedev*, J. Lygaeva*, A. Vylkov*,
M. Gorshkov*, A. Demin*, P. Tsiakaras ***

*Laboratory of electrochemical devices based on solid oxide proton electrolytes, Institute of High Temperature Electrochemistry, Yekaterinburg 620990, *Russia*

**Laboratory of Alternative Energy Conversion Systems, Department of Mechanical Engineering, School of Engineering, University of Thessaly, Pedion Areos, Volos 383 34, *Greece*

Abstract – This work is aimed at the identifying possible synthesis ways for the formation of a proton-conducting electrolyte based on BaCeO₃ and BaZrO₃ solid solutions. Among different methods (solid-state reaction, citrate-nitrate combustion, oxalate co-precipitation) and their CuO-modified analogs, the citrate-nitrate combustion or solid-state reaction synthesis coupled with the introduction of 0.5 wt.% CuO are found to be more appropriate strategies for the development of not only single-phase, but also high-dense BaCe_{0.5}Zr_{0.3}Y_{0.2}O_{3-δ} ceramic.

Index Terms – proton-conducting electrolytes, SOFC, dilatometry, densification.

I. INTRODUCTION

High-temperature proton-conducting materials are widely proposed as electrolytes for applications in electrochemical devices, including solid oxide fuel cells (SOFCs), electrolyzers, sensors, hydrogen-permeable membranes for hydrogen production or ammonia synthesis [1]. The BaCeO₃–BaZrO₃ representatives of high-temperature proton-conducting materials possess target properties: acceptable chemical stability, high ionic conductivity, good thermal and mechanical properties. However the high sintering temperatures required for gas-tight electrolyte formation during standard solid state reaction method still impede their practical applications. This fact can be attributed to the inhibitory nature of Zr⁴⁺. The advanced chemical solution methods (combustion, co-precipitation, sol-gel and Pechini methods [2]) are widely used in order to promote the densification of different solid oxide materials at reduced temperatures, but they have a minor impact for BaCeO₃–BaZrO₃ system. The strategy of introduction of sintering aids is also considered as possible solution of poor sinterability of Zr-containing BaCeO₃-based electrolytes [3].

In present work we compare different synthesis methods and evaluate their effect on the densification, phase structure and density of BaCe_{0.5}Zr_{0.3}Y_{0.2}O_{3-δ} proton-conducting electrolyte.

II. EXPERIMENTAL SECTION

The materials with BaCe_{0.5}Zr_{0.3}Y_{0.2}O_{3-δ} composition were prepared by solid-state reaction (SSR) method, oxalate co-precipitation (OCP) and citrate-nitrate combustion (CNC) methods. Moreover, these methods were modified by introduction of 0.25, 0.5 or 1 wt % CuO. The details of synthesis methods were described in our previous work [4].

The materials synthesis was carried out at 1000 °C for 5 h and 1100 °C for 5 h. The powders obtained were pressed into pellets and initially investigated by dilatometry for the determination of optimal temperature regime for sintering.

The prepared ceramic materials were characterized by X-Ray diffraction (XRD) analysis, scanning electron microscopy (SEM) and hydrostatic weighing in kerosene.

III. RESULTS AND DISCUSSION

The dilatometry results demonstrate (Fig. 1) that the samples obtained by SSR, OCP and CNC methods possess an insignificant shrinkage (2–6% at 1550 °C). Therefore, even the use of nano-sized powders does not promote the densification of Zr-containing BaCeO₃-based ceramics. On the other hand, the introduction of small amount of CuO as a sintering aid results in the essential shrinkage of ceramics, which can exceeds more than 16% at 1450 °C (CNC+0.5 mol.% CuO).

The sintering temperature of 1450 °C (soaking time 5 h) was chosen on the base of dilatometry results. According to data of



hydrostatic weighing in kerosene, the relative density of samples sintered at 1450 °C is equal 60–65% for SSR and OCP, ~75% for CNC, ~83% for SSR+0.25 mol.% CuO and more than 93% for the rest cases. From the viewpoint of densification behavior, the most optimal method is found to be CNC modified by the introduction of 0.5 mol % CuO.

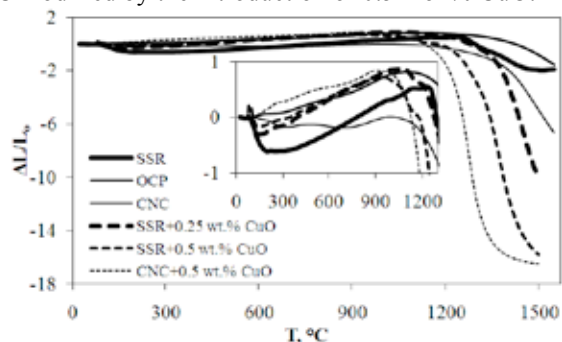


Fig. 1. Dilatometry curves of $\text{BaCe}_{0.5}\text{Zr}_{0.3}\text{Y}_{0.2}\text{O}_{3-\delta}$ samples prepared by different synthesis methods.

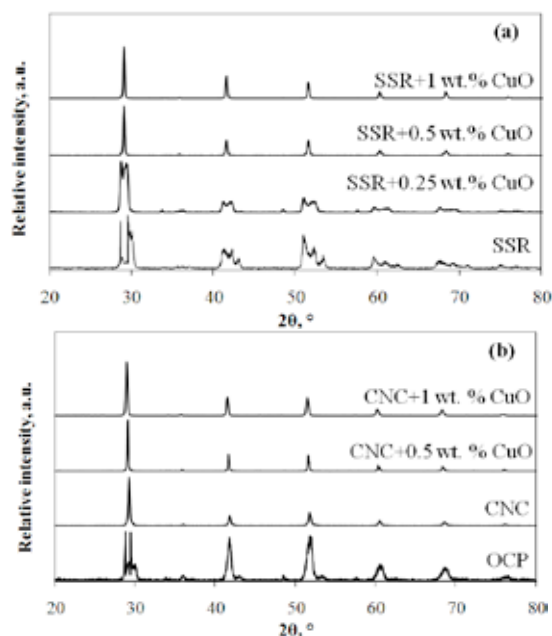


Fig. 2. XRD data of sintered $\text{BaCe}_{0.5}\text{Zr}_{0.3}\text{Y}_{0.2}\text{O}_{3-\delta}$ ceramics prepared by solid state reaction method (a) and chemical solution methods (b).

The XRD analysis was performed for all the sintered ceramics (Fig. 2). The samples prepared by SSR and OCP methods are multiphase: two perovskite impurities based on Zr-enriched $\text{Ba}(\text{Zr,Ce})\text{O}_3$ and BaZrO_3 coexist with the main Ce-enriched $\text{Ba}(\text{Ce,Zr})\text{O}_3$ phase, whereas Y_2O_3 and Zr-enriched phases $\text{Ba}(\text{Zr,Ce})\text{O}_3$ are found to be impurities for second case. The modification of SSR method by the introduction of CuO sintering aid (this method is called recently as solid-state reactive sintering [3,5]) results in a gradual decrease in the concentrations of impurity phases. More precisely, rather small concentration of CuO (0.5 wt.%) is already sufficient to form of

a single-phase product. The CNC synthesis and its modified analogs are the most appropriate methods for the preparation of ceramic material with specified composition. The SEM analysis confirms microstructure uniformity and well-developed grains for single-phase ceramic materials.

The obtained results are in a good agreement with data of Nikodemski et al. [5]. They found that the introduction of sintering aids, having stable +2 oxidation state and ionic radii close to that of Zr^{4+} , promotes i) the activation of BaCeO_3 and BaZrO_3 intermediate phases during synthesis, ii) the formation of single-phase and dense ceramics during sintering

IV. CONCLUSION

In the present work the different synthesis methods were analyzed in order to prepare the single-phase and high-dense $\text{BaCe}_{0.5}\text{Zr}_{0.3}\text{Y}_{0.2}\text{O}_{3-\delta}$ electrolyte ceramic. The XRD and SEM analyzes, dilatometry method and hydrostatic weighing were used for the estimation of quality of ceramics. The results obtained demonstrate that the use of SSR and CNC methods modified by the introduction of 0.5 wt.% CuO promotes the achievement of the necessary properties of ceramic samples (excellent densification, single-phase, high density and non-porous microstructure).

ACKNOWLEDGMENT

This work was supported by the Ministry of Education and Science of the Russian Federation (contract no. 14.Z50.31.0001), the Russian Foundation for Basic Research (grant no. № 13-03-00065) and the Council of the President of the Russian Federation (grant no. CII-1885.2015.1).

REFERENCES

- [1] Medvedev, D., Murashkina, A., Pikalova, E., Demin, A., Podias, A., Tsiakaras, P. BaCeO_3 : Materials development, properties and application. *Progress in Material Science*, volume 60, 2014, pp 72–129.
- [2] Shao, Z., Zhou, W., Zhu, Z. Advanced synthesis of materials for intermediate-temperature solid oxide fuel cells. *Progress in Material Science*, volume 57, 2012, pp 804–74.
- [3] Medvedev, D.A., Murashkina, A.A., Demin, A.K. Formation of dense electrolytes on the base of BaCeO_3 and BaZrO_3 for solid oxide fuel cells application: the role of the solid-state reactive sintering method. *Review Journal of Chemistry*, volume 5, 2015, pp. 193–213.
- [4] Lyagaeva, Yu.G., Medvedev, D.A., Demin, A.K., Yaroslavl'tseva, T.V., Plaksin, S.V., Porotnikova N.M. Preparation features of dense ceramics based on barium zirconate. *Semiconductors*, volume 48, 2014, pp. 1353–1358.
- [5] Nikodemski, S., Tong, J., O'Hayre, R. Solid-state reactive sintering mechanism for proton conducting ceramics. *Solid State Ionics*, volume 253, 2013, pp. 201–210.



NEW CONCEPT OF HIGHLY INTEGRATED MSR – HT PEMFC SYSTEM FOR SMALL PORTABLE POWER UNITS

Andrej Lotrič^{a,b}, Mihael Sekavčnik^b, Andrej Pohar^c, Stanko Hočevar^{a,c}

^a Mebius d.o.o., Na jami 3, SI-1000 Ljubljana (Slovenia)

^b Faculty of Mechanical Engineering, University of Ljubljana, Aškerčeva 6, SI-1000, Ljubljana (Slovenia)

^c Laboratory of Catalysis and Chemical Reaction Engineering, National Institute of Chemistry, Hajdrihova 19, SI-1000 Ljubljana (Slovenia)

Abstract - In a combined methanol steam reformer (MSR) and a proton exchange membrane fuel cell (PEMFC) stack system the processes are both endothermic and exothermic. Hence, proper thermal integration can help raising the system efficiency. First task was to identify possible configurations and prove the concept of such system with a numerical model. Three systems were designed based on different PEMFC stacks. Low-temperature (LT) and conventional high-temperature (cHT) PEMFC stack characteristics were based on available data from commercial suppliers. Also, a novel high-temperature (nHT) PEMFC stack was proposed because its operating temperature coincides with that of MSR. In the systems with HT PEMFC stacks the heat is produced at higher temperature levels and thus it is used more efficiently which is shown in better system efficiencies. Second task is to construct a prototype of such integrated system and experimentally define its characteristics. Also, methods of construction and suitability of materials are to be identified in relation to the operating conditions.

Index Terms - Fuel processor, Heat integrated system, Methanol steam reformer, PEM fuel cell.

I. INTRODUCTION

The main challenge of every energy system is to recuperate heat available within the system to maximize its efficiency. Since some reactors in combined MSR-PEMFC systems are exothermic (catalytic combustor, PEMFC stack) and others endothermic (vaporizer, MSR) the goal is to direct heat from sources to sinks within the system. The most obvious step that applies such action is direct thermal coupling of the MSR and the HT PEMFC stack which can be done in two ways. One is to use the conventional catalyst in the MSR which enables to attain practically full conversion of methanol between

250 - 300 °C. This however depends on geometry, flow characteristics, catalysts loading, and steam-to-carbon ratio (S/C). Typically, conversions above 95% are achieved at 250 °C with $S/C \leq 2:1$ while some researches also achieved 100% conversion with $S/C \leq 1.5:1$ [1, 2]. Since conventional PEMFCs operate at lower temperatures than the MSR there is a need for development of a nHT PEMFC that could operate at temperatures higher than 250 °C [3] and consequently enable direct thermal coupling of the nHT PEMFC stack and the MSR. Some research efforts in this direction have been published with the development of so-called solid acid fuel cell (SAFC) [4, 5]. The second way is to use cHT PEMFCs and newly developed LT catalyst [6, 7] that will allow the MSR to operate at temperatures below 200 °C and still achieve near to 100% conversions.

II. MODELING THE INTEGRATED SYSTEM

A. Proof of Concept

The objective of numerical model is to study and show the concept of compact and highly integrated system with conventional MSR (operating between 230 - 250 °C) and PEMFC stack. All fuel processing reactors have planar configuration and are stacked into a compact form and arranged in a thermal cascade. The study compares different configurations of integrated MSR-PEMFC-stack systems with:

- LT PEMFC – Nafion® membranes,
- cHT PEMFC – PBI/H₃PO₄ membranes,
- nHT PEMFC membranes that can operate up to 300 °C.

TABLE I: COMPARISON OF THE INTEGRATED SYSTEMS

Integrated system	Stack temp.	Gross electric efficiency	Gross cogeneration efficiency	Methanol consumption	Methanol conversion	Excess air	Heat losses
LT PEMFC	70 °C	39.2%	50.5%	$7.34 \cdot 10^{-5} \text{ mol s}^{-1}$ ^a $1.64 \cdot 10^{-5} \text{ mol s}^{-1}$ ^b	99.0%	9.0	16.1 W ^c 3.6 W ^d
cHT PEMFC	180 °C	35.9%	79.2%	$9.8 \cdot 10^{-5} \text{ mol s}^{-1}$	97.1%	7.4	3.4 W
nHT PEMFC	255 °C	42.2%	81.6%	$8.3 \cdot 10^{-5} \text{ mol s}^{-1}$	98.3%	4.7	3.8 W

^a used in the MSR^b used in the catalytic combustor^c uninsulated part of the system (natural convection)^d insulated part of the system

Two different pathways are used to more thoroughly examine the conceived systems. First, applies a zero-dimensional model based on mass and energy balances of the systems. This is done by using Aspen Plus® where all the modeled units of a system are studied at their operating, isothermal and stationary conditions. Second, uses COMSOL Multiphysics® to simulate physical models of the integrated systems. Here, heat transfer is studied at stationary conditions where the volume average temperature of modeled units closely corresponds to the temperatures used in mass and energy balance calculations. The two pathways are interdependent and coupled together. The calculation process, design and modeling of the systems are explained more in detail in [8] and results are shown in TABLE I.

B. Modeling the prototype

Since the development of nHT PEMFC is in its early stage we are not able yet to produce such fuel cells with sufficiently large power densities. On the other hand, the cHT PEMFCs are readily available and the LT catalyst for MSR was successfully reproduced following the procedure from researches [6, 7]. Due to these facts constructing a prototype LT MSR-cHT PEMFC-stack system that has conditions similar to MSR-nHT PEMFC-stack system is now possible.

Hence, our next goal is to characterize the kinetics of LT MSR which will allow modeling the LT MSR in Aspen Plus®. Once the kinetics is available the whole system can be modeled using the procedure described in subsection A. Materials and the shape of the system can be adapted to correspond to the new concept of LT MSR-cHT PEMFC-stack prototype that is in development.

III. BUILDING THE PROTOTYPE

Based on facts given in section II(B) and the fact that lower operating temperature increases possibilities of more conventional materials to be used in the system, the decision was made to proceed with experimental coupling of the LT MSR and the stack of cHT PEMFC. The stack of cHT PEMFC has already been designed and commercial membrane electrode assemblies (MEA) have been obtained.

First goal is to construct a small, two-cell stack with nominal power output around 10 W and to measure its characteristics separately. The second goal is to test the LT catalyst in the MSR which will be constructed according to the needs of the two-cell cHT PEMFC stack. Also, the LT MSR characteristics

will be first measured separately.

Once both units are constructed and their characteristics are known the operating point of the combined system can be predicted. The ultimate goal is to prove the concept experimentally.

IV. CONCLUSION

First steps towards the prototype of MSR-PEMFC-stack system have been taken. The concept was numerically proved on the basis of modeling and comparison of three different system designs. However, currently available materials only allow construction of the LT MSR-cHT PEMFC-stack system. Therefore, efforts for modelling and building the prototype are now focused in this direction.

REFERENCES

- [1] Pan, C., He, R., Li, Q., Jensen, J.O., Bjerrum, N.J., Hjulmand, H.A., Jensen, A.B., Integration of high temperature PEM fuel cells with a methanol reformer, *Journal of Power Sources*, Vol 145, 2005, pp. 392-398.
- [2] Morse, J.D., Upadhye, R.S., Graff, R.T., Spadaccini, C., Park, H.G., Hart, E.K., A MEMS-based reformed methanol fuel cell for portable power, *Journal of Micromechanics and Microengineering*. Vol 17, 2007, p. S237.
- [3] Hočevar, S., Kržan, A., Polyoxometalate Salts, Proton Exchange Membranes and Precursors, *Membrane-Electrode Assemblies, Fuel Cells and Methods*, Patent application PCT/EP2014/070697.
- [4] Chisholm, C.R.I., Boysen, D.A., Papandrew, A.B., Zecevic, S., Cha, S., Sasaki, K.A., Varga, A., Giapis, K.P., Haile, S.M., From Laboratory Breakthrough to Technological Realization: The Development Path for Solid Acid Fuel Cells, *Interface*, Vol 18, 2009, pp. 53-59.
- [5] Hindhede Jensen, A., Qingfeng, L., Christensen, E., Bjerrum, N.J., Intermediate Temperature Fuel Cell Using CsH₂PO₄/ZrO₂-Based Composite Electrolytes, *Journal of the Electrochemical Society*. Vol 161, 2014, p. F72.
- [6] Yu, K. M. K., Tong, W., West, Cheung, A. K., Li, T., Smith, G., Guo, Y. and Tsang, S. C. E., Non-syngas direct steam reforming of methanol to hydrogen and carbon dioxide at low temperature, *Nature Communications*, Vol 3, 2012, p. 1230.
- [7] Tong, W., Cheung, K., West, A., Yu, K.-M., Tsang, S.C.E., Direct methanol steam reforming to hydrogen over CuZnGaOx catalysts without CO post-treatment: mechanistic considerations, *Physical Chemistry Chemical Physics*. Vol 15, 2013, pp. 7240-7248.
- [8] Lotrič, A., Sekavčnik, M., Hočevar, S., Effectiveness of heat-integrated methanol steam reformer and polymer electrolyte membrane fuel cell stack systems for portable applications, *Journal of Power Sources*, Vol 270, 2014, pp. 166-182.



Effect of Mixed Torsion and Bending on Performance of Bendable Polymer Electrolyte Fuel Cell Based on PDMS Endplates

T. Park*, I. Chang**, Y. H. Lee*, G. Y. Cho*,
and S. W. Cha***

*Department of Mechanical and Aerospace Engineering, Seoul
National University, Gwanak-ro 1, Gwanak-gu, Seoul 151-744,
Republic of Korea

**Graduate School of Convergence Science and Technology, Seoul
National University, Gwanak-ro 1, Gwanak-gu, Seoul 151-742,
Republic of Korea

Abstract - Our previous bendable fuel cell was fabricated by using polydimethylsiloxane endplates coated with Ag nanowire current collectors. It was tested under only bent or twisted conditions in order to prove it can be used in real wearable applications. In this study, the bendable fuel cell at mixed bent and twisted position, closer to real circumstances, is tested. The performance of the cell is measured at specifically defined positions (flat, 10° twisted, and 10° twisted and bent by bending radius of 36.3 cm). Here, current-voltage curves, and electrochemical impedance spectra are measured to compare the performances together. The result shows that the performance is the function of both bending and twisting, but bending and twisting affected to the performance independently.

Index Terms - Bendable fuel cell, electrochemical impedance spectroscopy, flexible electronics.

I. INTRODUCTION

Fuel cell is one of the prospective candidates to be used as a portable power sources thanks to its higher energy density than current secondary lithium-ion batteries. Among various types of fuel cell, polymer electrolyte fuel cell (PEFC) is considered as a suitable fuel cell type for portable applications because it operates at low temperature, thus showing simple configuration of the system. In addition, the demand for portable power sources with high energy density is increasing because most of the electronics nowadays is turned out to be very complicated and requires power more. Accordingly, it is necessary to miniaturize PEFC in order to cope with this technological demands.

Another trend of electronics is that so-called ‘wearable electronics’ is being highlighted as many flexible electronic sub-components are realized such as flexible displays and stretchable circuits. Considering that the energy density of current state-of-the-art lithium-ion battery is confronting its theoretical maximum of energy density and wearable electronics requires higher power, it can be elicited that ‘bendable fuel cell’ should be developed.

That is why our research team has developed miniaturized bendable fuel cell based on polydimethylsiloxane (PDMS) coated with stretchable electrical conductor [1-3]. In particular the performance was tested at various bending radii and torsions [1, 4]. The performance of the bendable fuel cell showed increasing tendency of maximal power density as it was bent while it showed decreasing tendency as it was twisted.

This study investigates the variation of the performance of bendable PEFC when it is bent and twisted simultaneously. It is because real applications of wearable electronics generate internal stress not only by bending or twisting but both together. As supposed in the previous studies, because the electrochemical performance of the bendable fuel cell is strongly related to the generated compressive stress on membrane-electrode assembly (MEA), this study also compares the performances and corresponding compressive stresses generated by both bending and twisting.

II. EXPERIMENTAL

The PDMS endplates with flow channels were fabricated by using specially designed mold with the inverse patterns of channels. The PDMS and a curing agent with the weight ratio

of 10:1 were poured into the mold and heated at 70 °C for 4 hours to solidify it. The cross-sectional area of the flow-channels in anode and cathode endplates were 1 x 1 and 2 x 1 mm², respectively. An MEA (Fuel Cell Power Co., Republic of Korea) had the electrochemical reaction area of 30 x 30 mm². The Pt/C loading was 0.45 mg/cm² at both anode and cathode. The gas diffusion layers (GDLs) and Nafion™ 212 were all attached by hot-pressing. The endplates and the MEA were assembled together by using silicone sealant.

The as-fabricated bendable fuel cell was tested under variously defined positions: flat, twisted, and both twisted and bent. Each position was precisely controlled by specific bending radii and twisted angles. Dry hydrogen and air at room temperature were supplied into the cell with the volumetric flow rate of 500 and 1000 cm³/min, respectively. Before measuring the current-voltage characteristics and impedance, it was operated at 0.5 V for 12 hours to avoid the variation of the performance by activation effect.

III. RESULTS AND DISCUSSION

In-situ performance variation result by mixed bending and twisting is indicated in Fig. 1. Here, we show the power densities at three well-defined positions: flat, 10° twisted, 10° twisted and bent by 36.3 cm of bending radius. Open-circuit voltage of the fuel cell was 0.93 V (Not shown here), meaning that there is almost no fuel crossover since 0.93 V is close to the theoretical voltage derived from Nernst equation. At the time of the start of the operation, the power density is 23 mW/cm² and it is twisted at 12s. Then the performance is decreased to around 13 mW/cm². It is reasonable result because this power density corresponds with what is indicated in Fig. 3 in [4]. At 28 s, the fuel cell is twisted and bent simultaneously. Interestingly, the performance is increased to around 26 mW/cm². It means the performance of the fuel cell was enhanced by just applying bending. It is thought that the electrochemical kinetics of the cell was enhanced due to the compressive stress generated by bending. It was already supposed that bending the fuel cell generates compressive stress normal to MEA and it lowers contact resistances between each components and charge transfer loss inside the MEA [1]. Likewise, although the fuel cell was twisted, the compressive stress induced by bending would increase the performance of the bendable fuel cell. The variation of the impedance spectra and all the resistances estimated from them (Not shown here) showed same tendency of the variation, meaning that this fuel cell follows the performance behavior same as the previous result. This supposition can also be supported based on solid-mechanics that axial and torsional stresses are treated as independent vector element. The time range from 68 to 84 s, the fuel cell was released to its normal position and the corresponding power density was fully recovered. It means that the performance variation is induced not from the permanent damage or deformation. Even after that, the fuel cell was twisted and bent simultaneously to exclude the ‘memory effect’ which can occur from the order of the deformation (bending to twisting vs. twisting to

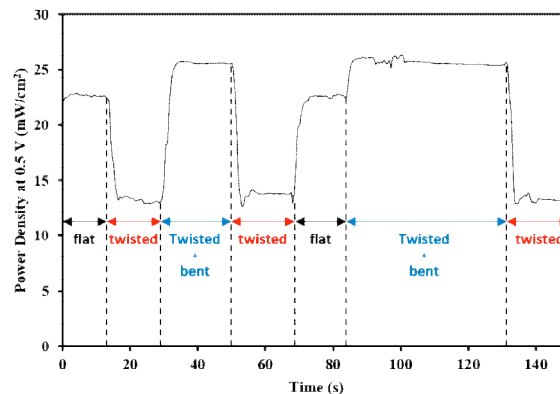


Fig. 1. Variation of the power density of bendable fuel cell at 0.5 V in accordance with deformation

bending). However, there is no difference of power densities at 40 and 100 s. It means that the power variation of the bendable fuel cell is induced from the torsion and bending independently.

IV. CONCLUSION

The bendable fuel cell was fabricated by using PDMS endplates coated with electrically conductive material. Its *in-situ* variation of the performance in accordance with the deformation defined by mixed bending and torsion was investigated. The result showed that the performance responded to both bending and twisting, but bending and twisting affected to the performance independently. This result also corresponds with the previous studies that bending of the cell increased but twisting decreased the performance by quantitatively same amount as previously.

ACKNOWLEDGMENT

This work was supported by the Global Frontier R&D Program on Center for Multiscale Energy System funded by the National Research Foundation under the Ministry of Education, Science and Technology, Korea (2011-0031569). Brain Korea 21 plus program should also be acknowledged for their partial support.

REFERENCES

- [1] Chang, I., Park, T., Lee, J., Lee, M. H., Ko, S. H., Cha, S. W., Bendable polymer electrolyte fuel cell using highly flexible Ag nanowire percolation network current collectors, *Journal of Materials Chemistry A*, Volume 1, 2013, pp. 8541-8546.
- [2] Chang, I., Park, T., Lee, J., Lee, H. B., Ji, S., Lee, M. H., Ko, S. H., Cha, S. W., Performance enhancement in bendable fuel cell using highly conductive Ag nanowires, *International Journal of Hydrogen Energy*, Volume 39, 2014, pp. 7422-7427.
- [3] Lee, P., Lee, J., Lee, H., Yeo, J., Hong, S., Nam, K. H., Lee, D., Lee, S. S., Ko, S. H., Highly Stretchable and Highly Conductive Metal Electrode by Very Long Metal Nanowire Percolation Network, Volume 24, 2012, pp. 3326-3332.
- [4] Park, T., Chang, I., Lee, J., Ko, S. H., Cha, S. W., Performance Variation of Flexible Polymer Electrolyte Fuel Cell with Ag Nanowire Current Collector under Torsion, *ECS Transactions*, Volume 64, 2014, pp. 927-934.



DURABILITY EVALUATION OF INNOVATIVE FEP-BASED GAS DIFFUSION MEDIA FOR PEM FUEL CELLS

S. Latorrata*, P. Gallo Stampino*, C. Cristiani*, G. Dotelli*

*Politecnico di Milano, Department of Chemistry, Materials and Chemical Engineering, Piazza Leonardo da Vinci 32, 20133, Milan (Italy)

Abstract – Gas diffusion medium (GDM) is a fundamental component for a PEM fuel cell because its main function is to avoid flooding of the whole device. In this work, different amounts of fluorinated ethylene propylene (FEP) and carboxymethylcellulose (CMC) were used in GDMs preparation. Ex-situ chemical and mechanical accelerated stress tests (ASTs) were developed in order to assess durability of prepared materials. The highest amount of FEP in GDMs allowed to get the best performance. Moreover, the presence of CMC allowed to reduce overall ohmic resistance. A satisfying durability can be claimed since GDMs hydrophobicity, ohmic and diffusion resistances, kept quasi-constant after the different ASTs.

Index Terms – PEM fuel cells, gas diffusion media, durability, accelerated stress test.

I. INTRODUCTION

Water management in polymer electrolyte membrane fuel cells (PEMFCs) is a crucial aspect which must be properly addressed in order to have high and constant efficiency during device operation [1]. This task is accomplished by gas diffusion medium (GDM). It is formed by a carbon cloth macro-porous substrate (gas diffusion layer, GDL) and a micro-porous layer (MPL) made from an ink and coated onto GDL [2].

Currently, MPLs are mainly prepared from inks containing carbon black particles and PTFE, the latter used as a hydrophobic agent [2]. Recently, authors proved that replacing PTFE with fluorinated ethylene propylene (FEP) is effective in improving mass transport properties and water management of the whole system. In this work different amounts of FEP were used, both for GDL and for MPL hydrophobization. Carboxymethylcellulose (CMC) was also employed both in inks preparation and in final MPL consolidation in order to have a better adhesion and durability. Durability is still a critical issue to be faced in fuel cells field in order to have a widespread commercialization of these devices. Thus, ex-situ chemical and

mechanical accelerated stress tests (ASTs) were developed. Morphological and electrochemical tests were carried out on GDMs upon different times of ASTs, up to 1000 h.

II. EXPERIMENTAL WORK

Inks containing FEP, already proven to be superior to PTFE-based ones [3], were prepared. Thus, on the basis of the preparation route described in [3], a slurry was formulated mixing a FEP-containing dispersion (55 % wt), in deionized water; then, carbon black (Vulcan XC72R) was slowly added. The mixture was vigorously stirred by a high shear mixer at 8000 rpm for 10 minutes. CMC was added as a rheology controller on the basis of a previous work [4]. First of all, performance of CMC-free samples were evaluated. The so-obtained inks were deposited onto FEP pre-treated GDL substrates via the blade coating technique to form micro-porous layers [3]. Finally, the samples were calcined up to 260 °C to remove water, alcohol and to sinter FEP [3]. The chemical AST was performed by soaking GDMs in a 20 % v/v sulfuric acid solution at pH equal to 0, far below the typical pH value (2-3) of the running cell environment, for a total time of 1000 h. The mechanical AST was carried out on the basis of a recent literature study [5], but a simpler system was developed with a dummy cell consisting of GDMs both at the anodic and cathodic side, separated by a Nafion 212 plain membrane, i.e. without any catalyst, in order to avoid any possible electrochemical stress. Only air was fed on either side at a flow rate of 2 NL/min, considerably higher than those employed during standard running (0.2 and 1.0 NL/min for hydrogen and air, respectively) for accelerating mechanical degradation. This air stream was fully humidified (RH: 100 %). Even for mechanical AST, total time was 1000 h.

Electrochemical tests were performed in a single lab-scale (25 cm²) cell at 60 °C with different relative humidities.

Electrochemical Impedance Spectroscopy (EIS) was carried out and the experimental data were analyzed and fitted using an equivalent circuit model (ZView[®] software).

III. RESULTS AND DISCUSSION

GDMs containing the maximum amount of FEP, i.e. 12 % wt, allowed to obtain the best electrochemical performance. Indeed, as it can be observed from Table I, fuel cell assembled with such samples achieved the highest output power density and the lowest diffusion resistance. Such a finding may be due to the higher hydrophobicity, resulting from static contact angle measurements. A better water-repellency should be the reason of a more efficient removal of the excess water, produced by the cathodic reduction reaction.

TABLE I

MAIN PROPERTIES OF FEP BASED GDMs AND RESULTS OF ELECTRICAL TESTS

Sample	P [$\text{W}\cdot\text{cm}^{-2}$]	R_d [$\Omega\cdot\text{cm}^2$]	C.A. [$^\circ$]	η (0 h)	η (1000 h) chem. AST	η (1000 h) mech. AST
FEP 12 %	0.42	0.143	155.4	0.382	0.372	0.369
FEP 9 %	0.40	0.19	150.1	0.365	0.332	0.319
FEP 6 %	0.39	0.25	149.2	0.359	0.316	0.294

Moreover, GDM FEP 12 % showed a better durability with respect to that one of the other samples, since global efficiency, calculated at $0.5 \text{ A}\cdot\text{cm}^{-2}$, keeps quasi-constant after 1000 h of both chemical and mechanical AST.

Then, a sample with the same composition was prepared, soaked in a 0.75 % wt CMC solution and then thermal treated at $260 \text{ }^\circ\text{C}$ for 30 min. Fig. 1 shows polarization and power density curves obtained at $60 \text{ }^\circ\text{C}$ and RH 80-80 (A-C) for fuel cells assembled with GDMs containing and non-containing CMC. Moreover, both ohmic (R_s) and diffusion resistances (R_d) are reported as a function of current density.

From Fig. 1, it is clear that the presence of a CMC upper layer improves performance, particularly in the ohmic zone of the V-I curve, i.e. a lower slope with CMC-containing samples is evident. This behavior is due to the hydrophilic nature of CMC which acts as a water reservoir leading to a better hydration of the polymeric membrane; accordingly, a higher protonic conductivity and a lower ohmic resistance are obtained. Indeed R_s trend of CMC-coated GDMs as a function of current density confirms this: it is always lower than non-containing CMC samples. As expected, R_d increases upon increasing current, due to a greater water production. However, such an increase is absolutely limited and satisfying, since lower values than conventional PTFE-based [3] GDMs were obtained for both types of GDMs.

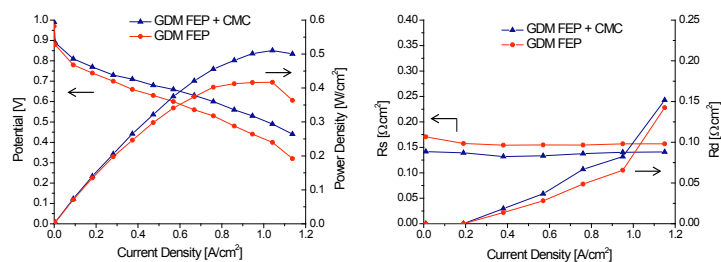


Fig. 1. Polarization and power density curves (left) and ohmic and diffusion resistances (right) as a function of current density of FEP based (12 % wt) GDMs with and without CMC.

Chemical and mechanical ASTs are in progress for CMC-based samples. Early results demonstrate that efficiency keeps constant as well as that one of no CMC samples. Anyway, final results about this part of the work will be showed during the conference.

IV. CONCLUSION

In this work FEP, which had been already demonstrated to be a better hydrophobic agent than traditionally employed PTFE, was used in different concentration in the preparation of GDMs for PEMFCs. The best performance in terms of maximum power density, fuel cell efficiency and durability, upon running the cell for 1000 h of ASTs, was achieved with the GDM with the highest FEP content (12 % wt). Then, CMC-based GDMs with the same content of FEP were also tested. CMC was effective in reducing overall ohmic resistance, thus improving the global performance of the device. Early durability tests on such samples pointed out constant electrochemical parameters and efficiency.

REFERENCES

- [1] Wang, Y., Chen, K.S., Mishler, J., Cho, S.C., Adroher, X.C. A review of polymer electrolyte membrane fuel cells: Technology, applications, and needs on fundamental research. Applied Energy, Volume 88, 2011, pp. 981-1007.
- [2] Park, S., Lee, J.W., Popov, B.N., A review of gas diffusion layer in PEM fuel cells: Materials and designs. International Journal of Hydrogen Energy, Volume 37, 2012, pp. 5850-5865.
- [3] Latorrata, S., Stampino, P.G., Cristiani, C., Dotelli, G., Novel superhydrophobic microporous layers for enhanced performance and efficient water management in PEM fuel cells. International Journal of Hydrogen Energy, Volume 39, 2014, pp. 5350-5357
- [4] Latorrata, S., Stampino, P.G., Amici, E., Pelosato, R., Cristiani, C., Dotelli, G., Effect of rheology controller agent addition to Micro-Porous Layers on PEMFC performances. Solid State Ionics, Volume 216, 2012, pp. 73-77.
- [5] Chun, J.H., Jo, D.H., Kim, S.G., Park, S.H., Lee, C.H., Kim, S.H., Improvement of the mechanical durability of microporous layer in a proton exchange membrane fuel cell by elimination of surface cracks, Renewable Energy, Volume 48, 2012, pp. 35-41.



EFFECT OF SYNTHETIC ROUTE ON PERFORMANCE OF $\text{La}_{0.8}\text{Sr}_{1.2}\text{Fe}_{0.9}\text{Cu}_{0.1}\text{O}_{4\pm\delta}$ ELECTRODES FOR SYMMETRIC SOLID OXIDES FUEL CELLS

G. Cordaro*, Chen Yu*, A. Donazzi**, R. Pelosato*, G. Dotelli*, and C. Cristiani*

* Dipartimento di Chimica, Materiali e Ingegneria Chimica "G. Natta", Politecnico di Milano, P.zza Leonardo da Vinci 32, 20133 Milano, (Italy)

** Dipartimento di Energia, Politecnico di Milano, Via Lambruschini 4, 20156 Milano, (Italy)

Abstract - The solid oxide $\text{La}_{0.8}\text{Sr}_{1.2}\text{Fe}_{0.9}\text{Cu}_{0.1}\text{O}_{4\pm\delta}$ of interest as electrode for Symmetric Solid Oxide Fuel Cells (SSOFCs) has been prepared via three different synthetic methods: solid-state reaction (SSR), melt citrate route (MC) and co-precipitation (CoP). In order to determine advantages and drawbacks of each synthesis, the materials have been characterized by X-Ray Powder Diffraction (XRD) and Scanning Electron Microscopy (SEM) analysis. Phase purity, structural and morphological characteristics of the powders have been determined. Wet chemical methods (CIT and COP) have the advantage over SSR synthesis of yielding small-sized powders ($\sim 1\mu\text{m}$); moreover, melt citrate route allows lowering the preparation temperature down to 1000 °C. Electrochemical characterization was performed by Electrochemical Impedance Spectroscopy (EIS) in air in an electrolyte supported symmetric cells configuration. Preliminary results allow to draw some conclusions on the relation between the structural and microstructural characteristics of the powders and the electrochemical performance.

Index Terms - K_2NiF_4 -type electrodes, Synthetics Route, SSOFC, Impedance Spectroscopy.

I. INTRODUCTION

In last years, the idea of Symmetric Solid Oxides Fuel Cells (SSOFC) structure proposed in literature has drawn researchers' attention [1, 2]. Using the same material as both anode and cathode in a SOFC allows overcoming some issues of SOFC technologies, like thermal mismatch among materials, carbon deposition in anode, Sulphur poisoning; moreover, this configuration can open the way to reversible operation as both SOFC and SOEC (Solid Oxide Electrolysis Cells) in a single device. However, the requirements of a SSOFC electrode are

several and strict; primarily, the material of choice should be stable in both oxidizing and reducing environment, and should show good catalytic activity for fuel (H_2 or hydrocarbons) oxidation and O_2 reduction. Among the investigated materials, K_2NiF_4 -type oxides are an interesting class, due to their electrical and physical properties. Among them, $\text{La}_x\text{Sr}_{2-x}\text{CuO}_4$ and $\text{La}_x\text{Sr}_{2-x}\text{FeO}_4$ [3, 4] show chemical stability and high oxygen diffusion coefficients in the intermediate temperature range. The compound $\text{La}_{0.8}\text{Sr}_{1.2}\text{Fe}_{0.9}\text{Cu}_{0.1}\text{O}_{4\pm\delta}$ was selected among other compositions as the most promising one [5]. In this study, three different synthetic methods are compared. The traditional solid state reaction (SSR) is compared with two wet chemical methods, namely Co-precipitation (CoP) [6] and Melt citrate route (MC) [7] to synthesize the electrode materials. Microstructural and Electrochemical methods are used to discuss the advantages and drawbacks of each route.

II. EXPERIMENTAL WORK

$\text{La}_{0.8}\text{Sr}_{1.2}\text{Fe}_{0.9}\text{Cu}_{0.1}\text{O}_{4\pm\delta}$ (LSFC) was prepared via SSR starting from La_2O_3 (99.5%, Sigma Aldrich), SrCO_3 (99%, Sigma Aldrich), Fe_2O_3 (99.8%, Sigma Aldrich) and Cu_2O (99%, Sigma Aldrich). The compounds were weighted according to the desired stoichiometry and ball-milled in ethanol for 12 h, before firing at 1000 and 1400 °C for 12 h. MC sample was prepared by the same precursors except for iron, which was added as $\text{Fe}(\text{NO}_3)_3 \cdot 9\text{H}_2\text{O}$ (99%, Sigma Aldrich). The precursors were dissolved in melt citric acid in a beaker under vigorous stirring; the obtained gel was heated in



oven to 300°C for 24 h and after calcined at 500 and 1000 °C. The co-precipitation procedure is reported in details elsewhere [6]; the obtained powders were fired at 1000 and 1200 °C. All the produced powders were characterized by X-Ray Powder Diffraction (XRPD) and Scanning Electron Microscopy (SEM). The electrical conductivity and polarization resistance were determined as a function of temperature in electrolyte supported cells (La_{0.8}Sr_{0.2}Ga_{0.8}Mg_{0.2}O₃, LSGM, Fuel cells Materials). The electrolyte pellets were realized by cold pressing at 10 MPa and the electrodes were brush painted on both sides of the electrolyte. An ink was used for the deposition, composed by a 60-40% mixture of electrode-binder (the binder is made by 76% terpineol, 20% propanol and 4% etilcellulose). A potentiostat/galvanostat (Amel 7050) equipped with a frequency response analyzer (510 V10, Materials and Mates) was used for the measurements.

III. RESULTS AND DISCUSSION

XRPD patterns of the fired samples are reported in Fig. 1. SSR sample (A) fired at 1400 °C still contains small amounts of a secondary phase identified as Sr₃Fe₂O₇, revealing that the reaction is not completed. CoP sample was multiphase at 1000°C (B) with many unreacted phases (La₂O₃, SrCO₃, Sr(OH)₂). On the contrary, sample prepared via MC route shows only the peaks belonging to the K₂NiF₄-type phase already after firing at 1000°C (C).

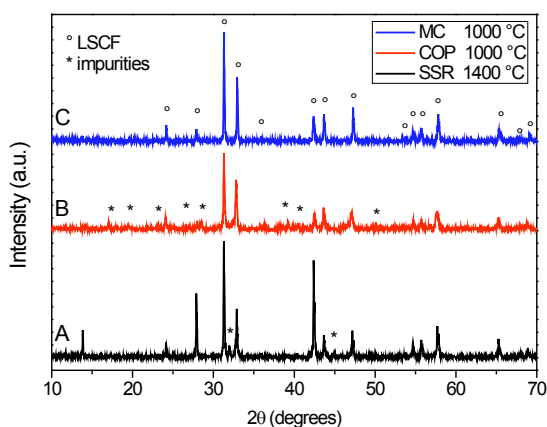


Fig. 1. XRPD pattern of SSR, CoP and MC samples.

SEM analysis (Fig.2) revealed that morphology and grain size of the powders is strongly dependent on the synthetic route and on the firing temperature. SSR sample shows large bulk grains with average size of 5-20 μm, due to the firing at 1400°C that promotes grain sintering. MC and CoP samples prepared via wet chemical routes get advantage of the dissolution of the reactants and retain small sized grains in the sub-micron range in MC sample and in the micron range in CoP material. These small-sized grains are arranged in large agglomerated particles

in the 5-10 μm size in MC and even larger in CoP.

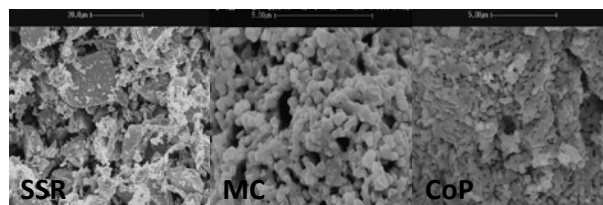


Fig. 2. SEM pictures of SSR, MC and CoP samples.

IV. CONCLUSION

K₂NiF₄-type electrodes for Symmetric solid oxide fuel cells were prepared via three different preparation routes. Sample prepared via solid state reaction requires high temperature (1400 °C) that leads to bulky grains (10-20 μm) and moreover, it retains a small amount of Sr₃Fe₂O₇ secondary phase. CoP sample developed a pure phase at 1200 °C with small grain size (5-10 μm). MC method allowed obtaining a pure phase already at 1000 °C with even smaller grain size (< 1 μm). Polarization resistance measurements in electrolyte supported button cells show that the wet chemical methods are advantageous for the preparation of electrode materials that showed improved activity when compared with those prepared by solid state reaction.

REFERENCES

- [1] Bastidas DM, Tao S, Irvine JTS. A symmetrical solid oxide fuel cell demonstrating redox stable perovskite electrodes. *J Mater Chem.* 2006;16:1603..
- [2] Ruiz-Morales JC, Canales-Vázquez J, Peña-Martínez J, López DM, Núñez P. On the simultaneous use of La_{0.75}Sr_{0.25}Cr_{0.5}Mn_{0.5}O_{3-δ} as both anode and cathode material with improved microstructure in solid oxide fuel cells. *Electrochim Acta.* 2006;52:278-84.
- [3] Yu HC, Fung KZ. La_{1-x}Sr_xCuO_{2.5-δ} as new cathode materials for intermediate temperature solid oxide fuel cells. *Materials Research Bulletin,* 2003, 38: 231-239.
- [4] Jennings A J, Skinner S J. Thermal stability and conduction properties of the La_xSr_{2-x}FeO_{4+δ} system. *Solid State Ionics,* 2002, 152-153: 663-667.
- [5] Unpublished results.
- [6] Pelosato R, Cristiani C, Dotelli G, Mariani M, Donazzi A, Natali Sora I. Co-precipitation synthesis of SOFC electrode materials. *Int J Hydrogen Energy.* 2013;38:480-91.
- [7] Karen P, Woodward PM. Liquid-Mix Disorder in Crystalline Solids: ScMnO₃. *J Solid State Chem.* 1998;141:78-88.



POROUS ELECTRODE OPTIMIZATION IN ANION-EXCHANGE MEMBRANE FUEL CELLS

Annika Carlson, Pavel Shapturenka, Göran Lindbergh, Carina Lagergren,
Rakel Wreland Lindström

Applied Electrochemistry, Department of Chemical Engineering and Technology
KTH Royal Institute of Technology, SE-100 44 Stockholm, (Sweden)

Abstract – The performance of anion-exchange membrane fuel cells is highly dependent on electrode preparation. This study has investigated the influence of water content and catalyst to ionomer ratio in the electrode ink on in-situ fuel cell performance and the electrode microstructure using SEM. It has shown that changing the solvent composition affects the electrode properties. Higher water content in ink results in a lower power density. An increase in water content from 40 to 70 vol% shows a 500 mA/cm² drop in current density. SEM analysis of newly prepared electrodes revealed an observable difference in the microstructure. This indicates that for high water volume the ionomer distribution in the electrode is very uneven. The results also indicate that lower ionomer content in the bulk of the structure lowers the cell performance, which may be explained by limited hydroxide transportation.

Index Terms – Anion exchange membranes (AEM), electrode composition, electrode ink, polymer electrolyte fuel cells (PEFC)

I. INTRODUCTION

Anion-exchange membrane fuel cells (AEMFC) have recently gained more interest as an area of research. An advantage of AEMFC is the possibility to use non-noble metal catalysts. However, one of the major drawbacks of the system is its sensitivity to carbon dioxide [1]. AEMFCs, like the proton exchange membrane fuel cells (PEMFC), make use of porous electrodes. These electrodes create a three-phase interface of polymer electrolyte, carbon supported catalyst and pores for the reacting gas. If the electrode structure does not contain sufficient three phase interfaces the reaction rate is limited. Previous studies [2,3] on the electrode structure and behavior in AEMFC have shown that the ionomer to catalyst ratio affects the power density. There is however no consensus on the preparation method. The effects of other variations, such as solvent composition, have not

been fully clarified. Related studies on PEMFC have shown that electrode morphology and preparation methods can affect the cell behavior [4]. This study aims to gain a better understanding of the effects the preparation method and ink formulation have on the final electrode structure and performance. It is aimed to explain the electrochemical characterization results by using complementing ex-situ methods for studying the morphology of the porous structure.

II. EXPERIMENTAL

Electrode inks were formulated using 36 % Pt on carbon from Tanaka Kikinzo, AS-4 ionomer solution from Tokuyama, isopropanol and Milli-Q water. The inks were alternately stirred and ultra-sonicated in 15 min periods for 1 h. Thereafter 60 µl of the ink was pipetted onto a gas diffusion layer (Sigracet BC25) and vacuum dried. The resulting electrodes had a by weight difference calculated loading of ~0.4 mg Pt/cm². The solvent composition and the ionomer content were varied. The membrane used, A201 from Tokuyama, was treated 3x20 min in 1 M KOH and 3x20 min in Milli-Q water. The membrane was mounted wet with electrodes that were not ion exchanged. The cell was heated to 50 °C with 95 % R.H. for the gas inflows. To activate the membrane electrode assembly the cell was cycled between 0.1 V and OCP at 10 mV/s until no improvement was observed. Impedance spectroscopy was performed at 0.95 V, 0.5 V and 0.2 V. Polarization curves were registered from OCP to 0.1 V at 1 mV/s.

Ex-situ analysis of the prepared electrodes was performed using SEM for comparison of the electrode microstructures.



III. RESULTS AND DISCUSSION

The main results are presented in Fig.1. The highest current density obtained was approximately 725 mA/cm^2 , which is similar to those presented by Fukuta [2]. The small deviation can be explained by different preparation methods of the electrodes. The presented results have been repeated three times.

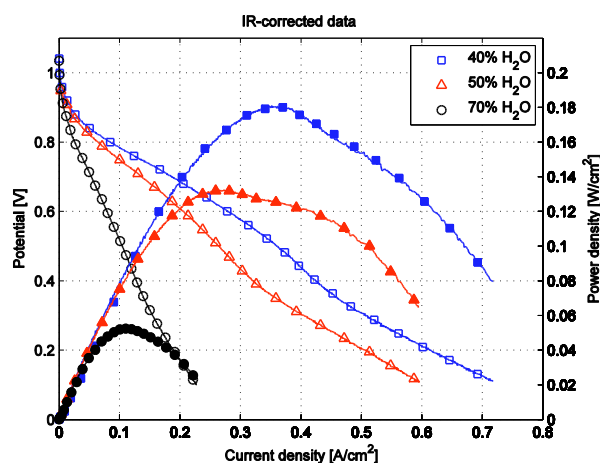


Fig. 1 – Influence of water content in the ink on the electrode performance. Power density vs. current density (■) and potential vs. current density (□). The water fraction is given in vol% and ionomer content is 37 wt%.

It is evident that the amount of water in the ink influences the performance of the porous electrodes, with the highest power density for the 40 vol% H_2O ink.

Ex-situ analysis using SEM was performed and two electrodes 70 and 40 vol% water content are shown in Fig.2. The electrode surfaces were visibly different for varying solvent compositions where lower H_2O content gave a more homogeneous surface. The electrodes prepared with a lower water content has a more porous microstructure that can be related to polymer filling the pores while the high water content show less polymer in the structure.

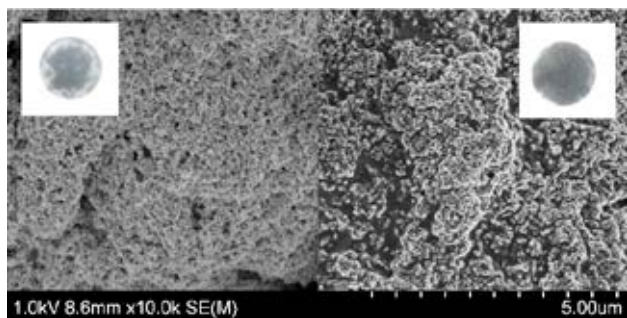


Fig. 2 – SEM image of newly prepared electrodes, 70% H_2O (left) and 40% H_2O (right). Insets: Macroscopic photo of the electrodes (11 mm diameter).

The difference in the microstructure can possibly explain the performance variations. Too high water content in the ink apparently results in an uneven ionomer distribution in the porous structure. If the ionomer is not

present throughout the electrode it may result in a limited hydroxide transport to the catalytic sites. This study shows that the ionomer content in the electrode is of importance for AEMFC and can be affected by the solvent composition in the ink. Previous studies on PEMFC by Gode et al. [4] show that the ionomer distribution and the porosity is also greatly affected by the ionomer to catalyst ratio. In a continuation of this work the ionomer ratio dependence is being analyzed where preliminary results indicate that an insufficient amount of ionomer has a negative effect on the electrode performance. Carmo et al. [3] and Fukuta [2] analysed the effect of ionomer ratio and found an optimum at 25 wt% and 30 wt% respectively. It is indicated that the system still needs to be further optimized and the influence of the preparation better understood.

IV. CONCLUSION

Solvent composition in the ink has been shown to have a large effect on the structure and performance of porous electrodes. A lower water content results in better ionomer distribution in the structure and a higher power density. Further studies are needed though to optimize the electrode composition and performance. Understanding of the influencing parameters in the preparation of porous electrodes can lead to improvements for AEMFC.

ACKNOWLEDGMENT

Thanks to Strategic Vehicle Research and Innovation, Sweden, for sponsoring this project, to Pavel Shapturenka from City College of New York for his contribution to the laboratory work and Simon Leijonmarck for the SEM pictures.

REFERENCES

- [1] J. R. Varcoe, P. Atanassov, D. R. Dekel, A. M. Herring, M. a. Hickner, P. a. Kohl, A. R. Kucernak, W. E. Mustain, K. Nijmeijer, K. Scott, T. Xu, and L. Zhuang, "Anion-exchange membranes in electrochemical energy systems," *Energy Environ. Sci.*, vol. 7, no. 10, pp. 3135–3191, Aug. 2014.
- [2] K. Fukuta, "2011 AMFC WORKSHOP Electrolyte Materials for AMFCs and AMFC Performance," 2011, pp. 1–38.
- [3] M. Carmo, G. Doubek, R. C. Sekol, M. Linardi, and A. D. Taylor, "Development and electrochemical studies of membrane electrode assemblies for polymer electrolyte alkaline fuel cells using FAA membrane and ionomer," *J. Power Sources*, vol. 230, pp. 169–175, 2013.
- [4] P. Gode, F. Jaouen, G. Lindbergh, A. Lundblad, and G. Sundholm, "Influence of the composition on the structure and electrochemical characteristics of the PEFC cathode," *Electrochim. Acta*, vol. 48, pp. 4175–4187, 2003.



EFC15187

DEGRADATION AND LIFETIME EVALUATION OF Fe-N-C BASED CATALYST IN PEMFC

Björn Eriksson*, Frédéric Jaouen**, Göran Lindbergh*, Rakel Wreland Lindström*, Carina Lagergren*

* Applied Electrochemistry, School of Chemical Science and Engineering,
KTH Royal Institute of Technology, SE-100 44 Stockholm, (Sweden)

** ICGM - UMR5253 - Equipe AIME, Université de Montpellier,
2 Place Eugène Bataillon - CC 1502, 34095 Montpellier CEDEX 5, (France)

Abstract – The restricted lifetime of Fe-N-C based catalysts is often assumed to be connected to the operating temperature. This study will investigate how the cell performance, electrode structure and composition vary over time, at different cell temperatures. At lower temperature, one may expect an increase in radical's stability, but a decrease in reactivity. Results show that the electrode degenerates over time, and that the electrochemical performance decay is similar for 40, 60, and 80° C. However, the loss of active sites is higher at higher temperature. This suggests that indirect production of radicals via H₂O₂ production during ORR is higher at higher temperatures and is a key degradation mechanism for this Fe-N-C catalyst.

Index Terms - Degradation, NPMC, proton exchange membrane fuel cell (PEMFC)

I. INTRODUCTION

Catalysts used in proton exchange membrane fuel cell (PEMFC) improve the reaction kinetics at the electrodes. Due to the sluggish kinetics of oxygen reduction reaction at the cathode, this electrode contains more platinum than the anode. It is of interest to reduce platinum content on the cathode, while maintaining the high power density. An alternative method for reducing the catalyst cost is to replace platinum with a non-noble metal catalyst. Some of these catalysts show great promise with high activity, however, they usually have short lifetime.

The Fe-N-C catalyst investigated in this study is prepared from iron acetate, phenanthroline and ZIF-8, in a dry milling method followed by Ar pyrolysis, and is labelled Fe0.5 in ref [1]. It consists of iron-ions coordinated by nitrogen ligands on a carbon support. The main mechanism for degradation of this catalyst is carbon bulk or surface corrosion. This is either caused by the

electrochemical bulk corrosion of the carbon support at high voltage, or by surface oxidation by radical species formed between hydrogen peroxide and iron [2] [4].

II. EXPERIMENTAL

A. Ink and MEA fabrication

For all the measurements the following ink formulation was used: 4 mg of the catalyst labelled Fe0.5 [1], 131 µl 5 wt. % Nafion® solution containing 15-20 % water, 62 µl ethanol, and 54 µl Milli-Q® water. The inks were sonicated and stirred, at room temperature, in 15 min intervals for a total of 1 h. Then 82 µl aliquots were pipetted onto a 0.95 cm² Sigracet 25 BC gas diffusion layer (GDL), and dried at room temperature, in vacuum for 15 min. Three aliquots were successively deposited on the GDL, reaching a total loading of 4 mg_{FeCN} cm⁻². After the last dot was deposited, the entire gas diffusion electrode (GDE) was dried for 1 h in vacuum. A Nafion® 212 membrane and a 3.8 cm² SLGDE FuelCels 0.5mg_{Pt}/cm², GDE anodes were used to complete the cell.

B. PEMFC measurements

All measurements were performed using an in-house cell house [3]. Gases were heated and humidified, to 100% relative humidity (RH) at cell temperature, prior to being fed into the cell. Lifetime evaluation was undertaken by running the cell potentiostatically at 0.5 V until 12 Ah of electric charge had passed through the cell. In this way, the cumulative number of O₂ molecules electrochemically reduced during the lifetime experiment was almost independent of the cell temperature. Polarization curves were recorded every 5 h of operation.



III. RESULTS

The surface structure of a fabricated Fe-N-C electrode is shown in **Fig 1**.

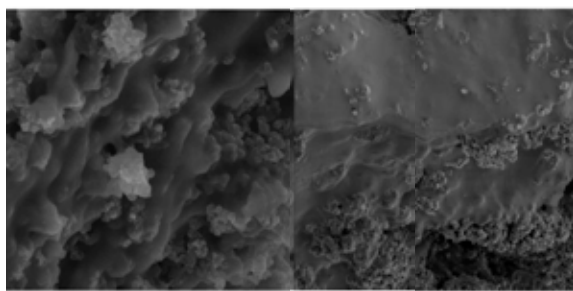


Fig 1- SEM image of electrode before (left) and after (right) fuel cell operation at 80 °C and 0.5 V, until 12 Ah/cm² electric charge was reached. For SEM analysis only one aliquot of ink was pipetted on the GDE (approximate loading 1.33 mg_{FeNC} cm⁻²). The scale bar is 5 μm.

The electrode has a non-homogeneous porous structure, which is attributed to the manufacturing method, and the inhomogeneous distribution of Nafion ionomer on the catalytic particles. The main visible structural change, after operation, is the disappearance of larger catalyst particles in the porous electrode structure after fuel cell testing. This change might be correlated to a redistribution of Nafion ionomer during fuel cell testing, Nafion covering the large catalytic particles after fuel cell testing. This redistribution might explain the increased current density at 0.5 V during the first 5 hours of operation, assigned to improved mass transport (**Fig. 2a**). In contrast, the ORR activity at 0.75 V only decreased with time (**Fig 3**).

The effects of running the cell are presented in **Fig 2**. Generally, at any given time during the stability experiment, the current density increases with increased cell temperature (**Fig. 2a**): This can be attributed to the increase in initial ORR kinetics and gas diffusivity with temperature. Considering the time evolution of any given curve, the initial increase in current density which occurs over the first 5 h, for the 80 °C case, is due to improved mass transport properties within the cathode. The subsequent linear decrease of current density with charge following this activation is due to a decrease of the ORR activity of the cathode (**Fig. 3**), possibly combined with a decrease of the mass-transport properties.

While **Fig 2a** shows the change of current density versus time, a more meaningful plot is the change of current density versus the electric charge that passed through the cell (**Fig 2b**). If the active site or electrode degradation is induced by the process of reducing O₂ molecules, then time is not the correct parameter to look at, due to large differences in current density with cell temperature. We chose to replace time by the cumulative electric charge that passed through the cell at 0.5 V (**Fig**

2b). From **Fig 2b** cell performance degradation is more consistent between the different temperatures.

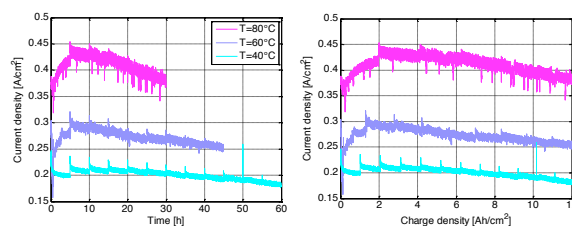


Fig 2-Influence of cell temperature on the decay of cell performance. IR-corrected potentiostatic measurement with an applied potential of 0.5 V. Decay versus time 2a (left) and charge 2b (right).

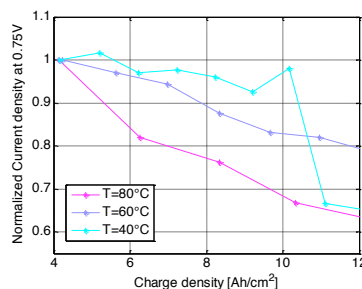


Fig 3: ORR activity at an applied potential of 0.75 V as a function of charge density. Values found by interpolation of polarization curves. Normalized at 4 Ah/cm².

CONCLUSION

Porous electrodes utilizing a Fe-C-N catalyst have been fabricated, and their structure and lifetime have been studied. Results show that the electrode degradation is more correlated to charge than time, and that the degradation is higher at higher temperatures. The main mechanism for degradation is due to loss of electrochemically active catalytic sites.

ACKNOWLEDGMENT

We acknowledge funding from Strategic Vehicle Research and Innovation (FFI), Sweden.

REFERENCES

- [1] A Zitolo, V. Goellner, V. Armel, M.-T Sougrati, T. Mineva, L. Stievano, E. Fonda, F. Jaouen, Identification of catalytic sites for oxygen reduction in iron- and nitrogen-doped graphene materials, *Nature Materials*, Volume 14, 2015, Pages 937-942
- [2] V. Goellner, C. Baldizzone, A Schuppert, M. Sougrati, K. Mayrhofer, F. Jaouen, Degredation of Fe/N/C catalyst upon high polarization in acid medium, *Physical Chemistry Chemical Physics*, Volume 16, 2014, Pages 18454-18462
- [3] P. Gode, J. Itonen, A. Strandroth, G. Lindbergh, M. Paronen, F. Sundholm, G. Sundholm, N. Walsby, Membrane Durability in a PEM Fuel Cell Studied using PVDF Based Radiation Grafted Membranes, *Fuel Cells*, Volume 3, 2003, Pages 21-27
- [4] V. Goellner, V. Armel, A. Zitolo, E. Fonda, F. Jaouen, Degradation by hydrogen peroxide of metal-nitrogen-carbon catalysts for oxygen reduction, *Journal of the Electrochemical Society*, Volume 162, 2015, Pages H403-H414



POLYACRINOLYTRILE DERIVED CARBON BASED NANOFIBER MATS AS ANODES IN MICROBIAL FUEL CELLS

Giulia Massaglia^{a,b,*}, Valeria Agostino^{a,b}, Luisa Delmondo^b, Valentina Margaria^a, Adriano Sacco^a,
Micaela Castellino^a, José A. Muñoz-Tabares^a, Gian Paolo Salvador^a, Tonia Tommasi^a, Matteo Gerosa^{a,b},
Caterina Armato^b, Angelica Chiodoni^a, Marzia Quaglio^a,

^a Center For Space Human Robotics, Istituto Italiano di Tecnologia@POLITO, C.so Trento 21, 10129 Torino, Italy

^b DISAT, Politecnico di Torino, Corso Duca Degli Abruzzi 24, 10129, Torino, Italy

Abstract – This work aims to enhance the performances of Microbial Fuel Cells. Bundled carbon nanofibers with average diameter from 100 nm to 1 µm were then prepared from polyacrylonitrile through electrospinning process. The spun nanofibers were oxidatively stabilized at 280 °C in air and thermally treated at 600 °C under inert atmosphere for 1 hour. Morphological and physical properties were measured, demonstrating the graphitic character of carbon nanofibers processed at 600 °C. In particular the electrical conductivity of the nanofiber mats is close to $2.47 \cdot 10^{-3}$ S/cm. Cytotoxicity tests were performed demonstrating the suitability of the carbon based nanofibers to host living microorganisms. The formation of a biofilm was finally evaluated through field emission scanning electron microscopy analysis, showing a very good interaction between carbon nanofibers and bacteria, and the development of a densely connected biofilm. These good results open the door to application for anodic electrode in microbial fuel cells.

Index Terms – Carbon Nanofibers, cytotoxicity, electrospinning, microbial Fuel Cells, polyacrylonitrile.

I. NOMENCLATURE

Polyacrinolytrile (PAN); Microbial Fuel Cells (MFCs); N-N dimethylformamide (DMF); commercial felt (CF); Field scanning microscopy (FESEM)

II. INTRODUCTION

MFCs are bio-electrochemical systems that convert chemical energy into electrical energy from the respiratory metabolic profit of electrochemically active bacteria. MFCs are one of the most promising technologies to produce renewable electrical energy. However, it is still necessary to enhance the device

performances in order to grant its diffusion. In particular, new anodic electrodes materials, with good electrical properties and able to support microorganisms growth, have to be investigated. For the fabrication of electrodes for energy applications carbon has been found as most promising material in its various forms like powder, fibers and mats. Porous carbon nanofibers have extremely high length to diameter ratio, nanoscale diameter and ultrahigh specific surface area as compared to other carbon materials [1,2]. To generate electricity using bacteria in MFCs, highly conductive non corrosive materials are needed; those materials must have a high specific surface area and an open structure to avoid biofouling [3]. The nanofibers have been obtained through the electrospinning technology. The eletrospinning process produces fibers as a continuous charged polymeric jet by means of an electrical potential applied between the needle of the syringe and a grounded collector. The aim of this work is to evaluate the application of bundled carbon nanofibers as anode in MFCs.

III. EXPERIMENTAL SECTIONS

A. Material and Methods

PAN (average molecular weight $M_w=150,000$ kDa) and DMF (assay 99.8%) were purchased from Sigma Aldrich. Samples were prepared by electrospinning solutions containing 12wt% PAN in DMF. The electrospinning parameters have been defined as summarized in the TABLE I. The two values of flow rate permit to obtain different morphological properties of the



mat of nanofibers and to compare the different interaction between the material and the bacteria growth.

TABLE I

Electrospinning parameters defined during the process.

Samples	Voltage (kV)	Distance (cm)	Time of process (hour)	Flow rate (mL/h)
PAN_0.2	15	15	1	0.2
PAN_0.4	15	15	1	0.4

As spun these nanofibers were stabilized at 280 °C in air and thermally treated at 600°C under inert atmosphere for 1h to obtain conductive carbon nanofibers. The resulting samples are nonwoven mats of graphitic conductive nanofibers with a high surface area. Raman spectroscopy showed the typical G-bands and D-bands of graphitic materials, confirming this feature in the nanofibers, as represented in the Fig. 1.

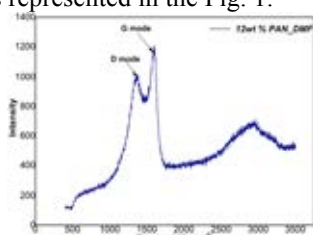


Fig. 1 Raman spectroscopy conducted on the sample PAN_0.2

The morphology of the nonwoven mats of nanofibers was characterized by FESEM: bundled carbon nanofibers were observed in all samples. In particular the mat of PAN_0.2 nanofibers have a diameter smaller, closes to 1 μm, than the diameter of the nanofibers of PAN_0.4, of about 1.5 μm, as shown in the Fig. 2.

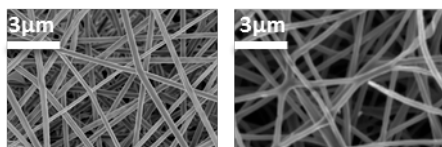


Fig. 2 Fesem characterization of the morphology of the 2 mat of nanofibers respectively PAN_0.2 on left and PAN_0.4 on the right.

Moreover it has been investigated the cytotoxicity and the biofilm interaction with the mat of nanofiber in comparison with commercial electrode material CF. The inclusion of the material within a gel made of agar, sodium acetate, peptone and the microorganism, reveals no cytotoxicity seeing as the bacteria proliferated and spread uniformly in all plates containing the nanofibers of PAN. To investigate the interaction between the bacteria and the material, the samples have been then put in a solution of sodium acetate for 1 month. The formation of biofilm has been finally investigated through a FESEM analysis, showing a very good interaction with a nanofibers of PAN. The development of a densely connected biofilm results better in the mat of PAN_0.2 than the biofilm in CF and in PAN_0.4, as represented in the Fig. 3. In the PAN_0.2 sample, it is possible evaluate the development of a densely connected biofilm.

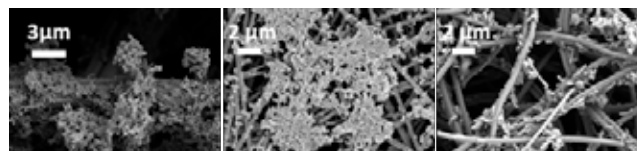


Fig. 3 The comparison of the different biofilms on CF, on left, on PAN_0.2 on the middle and on PAN_0.4 on the right.

Finally the electrical properties of the carbon nanofibers were investigated, showing a value of conductivity equal to $2.47 \cdot 10^{-3}$ S/cm. This value is defined as a function of the resistivity of the sample and its thickness of about 4 μm.

IV. CONCLUSION

In this work, we demonstrate the biocompatibility and a good conductivity, characterized the mat of carbon nanofibers, obtained from PAN as a polymeric precursor. The graphitic features of nanofibers of PAN, which are pyrolysed at 600°C under inert atmosphere, guarantees a good conductivity value that ensure the possible application of the material as an electrode in MFCs. Moreover thanks to the high surface area of nanofibers ratio to volume, we evaluated the formation of deeply connected of biofilm on nanofibers. The bacteria have a better proliferation in the sample of PAN_0.2, than the proliferation on CF, a commercial material used as a reference material. Probably the good proliferation of bacteria on PAN_0.2 is due to an higher porosity of the material and to an higher roughness of nanofibers of PAN than the fibers of CF. In particular the high porosity of nanofibers of PAN_0.2 is due to a lower distribution of diameters, while the roughness is induced by the bundled carbon nanofibers morphology. All these good results open the door to application for anodic electrode in MFCs.

ACKNOWLEDGEMENTS

The authors gratefully acknowledge the support provided by the Department of the Navy, Office of Naval Research Global, USA (Award number: N62909-14-1-N041).

REFERENCES

- [1] Kim C et al. Synthesis and characterization of porous carbon nanofibers with hollow cores through the thermal treatment of electrospun copolymeric nanofibers web. *Small* 2007;3: 91-5
- [2] Kim C et al. Self- sustained thin webs consisting of porous carbon nanofibers via electrospinning of Polyacrylonitrile solutions containing zinc chloride, *Adv materials* 2007;19:2341-6
- [3] Logan et al. Graphite Fiber Brush Anodes for Increased Power Production in Air-Cathode Microbial Fuel Cells, *Environ. Sci. Technol.* 2007, 41, 3341-3346



Comparison of enriched biofilm communities from natural environments in a single chamber microbial fuel cell with open air cathode.

Valeria Agostino^{1,2}, Giulia Massaglia^{1,2}, Valentina Margaria¹, Tonia Tommasi¹, Caterina Armato², Gian Paolo Salvador¹, Adriano Sacco¹, Matteo Gerosa^{1,2}, Angelica Chiodoni¹, Luisa Delmondo², Nadia Garino¹, José A. Muñoz-Tabares¹, Micaela Castellino¹, Marzia Quaglio¹.

¹Center for Space Human Robotics @PoliTo, Istituto Italiano di Tecnologia, Corso Trento 21, 10129, Torino, Italy

²Applied Science and Technology Department, Politecnico di Torino, Corso Duca degli Abruzzi 24, 10129, Torino, Italy

Abstract – Microbial Fuel cells (MFCs) have been deeply investigated as a key technology for wastewater treatment with simultaneous energy recovery. More recently the possibility to use of MFCs as biosensors for water quality monitoring has gained interest as new emerging application. Many studies about MFC-based biosensors have employed as inoculum source different consortia from wastewater, activated sludge, anaerobic sludge and long term operated MFCs. In this work an enriched environmental sample from freshwater sediment was used to obtain a high-current and fast developing biofilm. In particular two different enrichment methods (Geobacter medium and general anaerobic medium) were tested in a small single chamber air cathode MFC. Electroactive biofilm acclimatation was performed applying a 47 Ω external resistance. General anaerobic enrichment method exhibited an higher current density (0.6 A/m²) and a shorter start-up time of 5 days. This study shows the applicability of the use of enriched freshwater sediment samples as inoculum for MFC-based biosensor.

Index Terms – environmental inoculum source, electroactive biofilm, open-air cathode MFC biosensor.

I. INTRODUCTION

The Microbial Fuel Cell (MFC) technology have enormous potential as biosensors for water quality monitoring, being this system intrinsically sensitive to environmental conditions. The current generated by MFC directly reflects the metabolic activity of the anodophilic bacteria. Temperature, pH, the amount of nutrients present in the substrate are among the most important factors affecting the behaviour of MFCs, as they affect the activity of the biofilm. In the same way the presence of a toxicant in the feeding solution can affect the microbial metabolism with consequent changes in the current generated [1]. In particular small single-chamber air-cathode MFC is a promising device architecture to

minimise any differences in the anolyte concentration at the input phase, to enhance the detection range and to reduce the sensor response time [2]. Additionally small MFCs may be cheap to manufacture using 3D printing techniques [3]. Many studies about MFC-based biosensors for toxicant monitoring have used as inoculum source different consortia from wastewater, activated sludge, anaerobic sludge and long term operated MFCs. These inocula required long period for electroactive biofilm formation and stabilization, ranging from 25 to 80 days, under poised anode potential conditions [4] so limiting the starting time of the MFC-based biosensors. These inoculum samples, effectively, are not the preferential sources of exoelectrogens. ElectroActive microbial Biofilms (EABfs) are composed by a special kind of microorganisms capable of “exocellular” respiration, named anode-respiring bacteria (ARB). ARB are usually found in anaerobic subsurface environments, such as seawater and freshwater sediments, where the low redox potential and limited nutrient concentrations facilitate exocellular metal-reducing pathways [5]. Other microorganisms are actually present in these environments (e.g., methanogens and sulfate reducers), creating competition for the use of carbon and electron donor species [6].

The aim of this study is to achieve a high-current and fast developing anodic biofilm using freshwater sediment sample as inoculum, in a small single chamber air cathode MFC. To obtain this result we decided to introduce and test two different chemical enrichment methods, combined with a low external resistance acclimatation for fast biofilm formation. The acquirement of an high and stable baseline current output is necessary for future test of this device as biosensor for freshwater quality monitoring.



II. EXPERIMENTAL SECTION

A freshwater sediment sample (Valle D'Aosta) was enriched with two different media under anoxic conditions: a *Geobacter* medium and a general medium for selection of anaerobic bacteria. In both enrichment methods sodium acetate was used as electron donor and carbon source. *Geobacter* medium consisted in: Fe(III) citrate 13.70 g/L; NaHCO₃ 2.50 g/L; NH₄Cl 1.50 g/L; NaH₂PO₄ 0.60 g/L; KCl 0.10 g/L; Na-acetate 2.50 g/L; Wolfe's Vitamin solution 10.00 ml/L (ATCC) and Wolfe's trace mineral solution 10.00 ml/L (ATCC) (*Geobacter* medium). General anaerobic medium consisted in: NH₄Cl 1.50 g/L; NaH₂PO₄ 2.45 g/L; Na₂HPO₄ 4.28 g/L; KCl 0.10 g/L; Na-acetate 2.50 g/L; Wolfe's Vitamin solution 10.00 ml/L (ATCC) and Wolfe's trace mineral solution 10.00 ml/L (ATCC) The microbial cultures were subjected to 3 sequential enrichments for 28 days of total growth.

The enriched consortia were tested into small membrane-less single chamber MFC with open-air cathode (Fig.1). The prototype consisted of an anodic chamber of 9 cm³ and a fixed electrode spacing of 1 cm. The anode and the cathode electrodes were made of carbon felt (electrode area = 9 cm²). Stainless steel wires were threaded along the carbon felt electrodes and used for the electrical contacts. The open-air cathode consisted of a platinum catalyst and a carbon/PTFE (Polytetrafluoroethylene) diffusion layer.

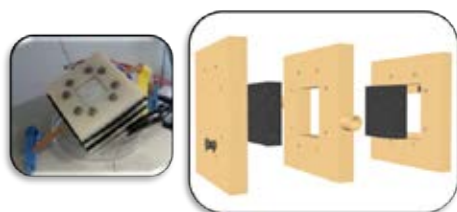


Fig. 1 Architecture of single-chamber MFC square shaped with open air cathode. The device was made through 3D-printing technology.

Experiments were conducted in duplicate, in continuous modality using Na-Acetate (1 g/L per day) as anodic substrate feeding, at a room temperature of 18-20°C. An external resistance of 47 Ω was applied to allow a faster formation of EABfs on the anode surface. The voltage of MFCs was acquired every 30 minutes by a digital multimeter (Agilent, 34972A) and the current generated was calculated with the Ohm's law ($I = V/R_{ext}$). Polarization curves and electrochemical impedance spectroscopy analysis were performed after 15 days of test in order to characterize EABfs.

The current density delivered by MFC inoculated with general anaerobic enrichment method was up to 0.55 A/m², with a short start-up time of 4 days. On the contrary *Geobacter* enrichment MFC generated a current density 3 times lower (max 0.18 A/m²), with a start-up time of 8 days. Both MFCs maintained a constant current output for two weeks (Fig. 2).

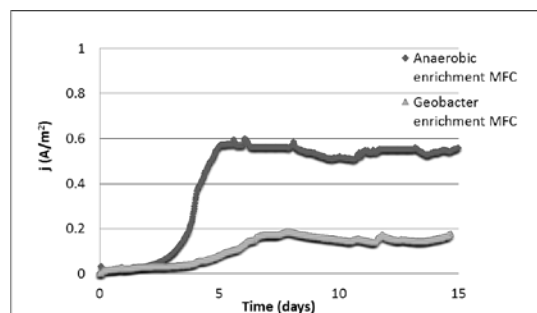


Fig.2 Current density generated by the MFCs inoculated with two different enrichment methods over time.

III. CONCLUSION

In this work, we demonstrated the effectiveness of chemical enrichment method combined with low resistance acclimatation to achieve short start-up time (4 days) and stable high-current values for MFC-based biosensor application. The good behavior of the device gives evidence of the formation of a robust and efficient biofilm from freshwater sediment. The open-air cathode MFCs inoculated by general anaerobic enrichment method showed a faster start-up time and a higher stable current output, compared to MFCs inoculated by *Geobacter* enrichment. Indeed in freshwater sediment samples *Geobacter* medium loses its specificity for ARB selection, given the presence of other microorganisms with similar metabolic pathways. In this purpose a deeper biological analysis is necessary to get a better understanding of the actual composition of both the environmental sample and the derived biofilms.

REFERENCES

- [1] Abrevaya, X.C., Sacco N.J., Bonetto, M.C., Hilding-Ohlsson, A., Cortón, E. Analytical applications of microbial fuel cells. Part II: Toxicity, microbial activity and quantification, single analyte detection and other uses. *Biosensors and Bioelectronics* Vol. 63, 2015, pages 591-601
- [2] Chouler, J. and Di Lorenzo, M., Water quality monitoring in developing countries; can microbial fuel cell be the answer? *Biosensors* Vol.5, 2015, pages 450-470
- [3] Di Lorenzo, M.; Thomson, A.R.; Schneider, K.; Cameron, P.J.; Ieropoulos, I. A small-scale air-cathode microbial fuel cell for on-line monitoring of water quality. *Biosensors & Bioelectronics* Vol. 62, 2014, pages 182-188.
- [4] Sun, J.Z., Kingori, G.P., Si, R.W., Zhai, D.D., Liao, Z.H., Sun, D.Z., Zheng, T. and Yong, Y.C. Microbial fuel cell-based biosensors for environmental monitoring: a review. *Water Science & Technology* Vol.71.6, 2015, pages 801-809
- [5] Doyle, L.E. and Marsili, E. Methods for enrichment of novel electrochemically-active microorganisms. *Bioresour. Technology* Vol. 7, 2015, pages 375-381
- [6] Lovley, D. R Organic matter mineralization with the reduction of ferric iron: review. *Geomicrobiology Journal* Vol. 5, 1987, pages 375-399



EFC15192

INVESTIGATING THE EFFECT OF WATER VAPOR AND RESIDUAL METHANOL ON THE ANODE OF HIGH TEMPERATURE PEM FUEL CELL

Sobi Thomas*, Samuel Simon Aarya*, Søren Knudsen Kær*,
and Jakob Rabjerg Vang*

*Department of Energy Technology, Pontoppidanstraede 101,
Aalborg University, Aalborg-9220, (Denmark)

Abstract - The objective is to understand the effect of methanol and water vapor separately on a high temperature PEM fuel cell. An investigation was performed with different anode fuel compositions and results in terms of performance and impedance analyzed. During the initial 1000 h, cell was tested with pure hydrogen under varying current densities of 0.2 A cm⁻² and 0.6 A cm⁻², followed by hydrogen mixed with 15 % water vapor and then with 1 % methanol. The degradation rates at two current densities 0.2 A cm⁻² and 0.6 A cm⁻² were analyzed and discussed. The degradation at higher current density is more severe than at lower current density. However, on switching from higher to lower current density, the effect is reversible and the performance is improved. This suggests that some degradation is reversible. The addition of water vapor in the feed improves the performance at high current densities, which suggest an improvement of total cell resistance also supported by the impedance comparison. There is no or minimal variation in performance with the introduction of 1 % methanol along with water vapor in the anode feed at 0.2 A cm⁻² and 0.6 A cm⁻².

Index Terms – HTPEM, EIS, Reformate Feed

I. INTRODUCTION

Fuel cells have the advantage of high energy density and lower environmental impacts, which makes them an attractive alternate power unit. Among the various kinds of PEM fuel cells, high temperature polymer electrolyte membrane (HTPEM) fuel cells have the advantages in terms of higher CO tolerance, enhanced catalytic activity and lower operational complexities [1-2]. The high CO tolerance makes them compatible with reformate gas feeds. The present study focuses on achieving a proper operational strategy for wet reformate based HTPEM fuel cells. The effect of reformate gas composition (mainly residual methanol and water vapour) on the durability and performance of the fuel cell is studied and the results discussed. In the present work, the effects of water and methanol under two different operating condition viz., 0.2 A cm⁻² and 0.6 A cm⁻² were tested. The two operating point was selected to understand the degradation mechanism under high and low current density

points. Polarization and impedance data was analysed to understand the phenomenon.

II. EXPERIMENTAL

A. Test setup

The test setup consists of integrated control system for carrying out load cycling and electrochemical impedance spectroscopy (EIS) measurements. The setup has the provision to introduce reformate composition (carbon monoxide, carbon dioxide) on the anode. It also consists of a methanol pump, connected to an evaporator before the feed enters the anode chamber. The membrane electrode assembly (MEA) is DPS-G77 with an active area of 45 cm².

B. Test Procedure

A break-in at 0.2 A cm⁻² is carried out for 100 h as recommended by the MEA manufacturer. The polarization recorded at an interval of 100 h, while the EIS recorded at an interval of 25 h. The EIS scan is carried out between a frequency of 10 KHz to 0.1 Hz, while the polarization is recorded at a scan rate of 5A/min to 50 A. The hydrogen and airflow rates were 1.5 and 4 stoichiometry respectively.

III. RESULTS AND DISCUSSION

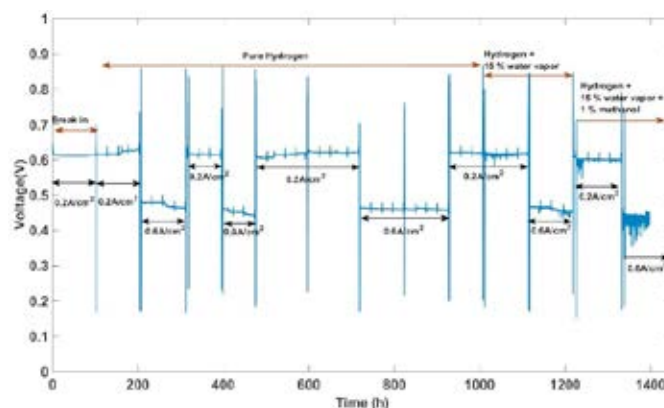


Fig. 1. Voltage profile with varying fuel composition

Copyright © 2015



The voltage variations under different fuel compositions and varying current densities is as shown in Fig.1. The break-in results, a decrease in voltage during initial 10 h then an improvement thereafter. The voltage is seen to improve during the next 100 h also but it is after a shutdown of the setup (i.e., due to hydrogen leak from the setup) for few hours. This improvement is probably attributed to some impurity removal i.e., CO sitting on the platinum sites due to sudden stop of hydrogen flow, resulting from air entering the anode chamber.

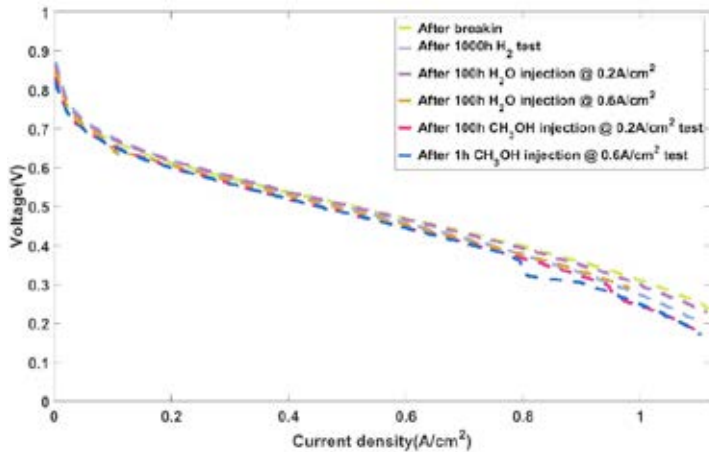


Fig.2: Performance comparison with different fuel composition and at two current densities

The performance improves with water vapour in the feed at high current density as shown in Fig.2, which suggest an improvement in the mass transport. The mass transport improves due to improved ion conduction with water vapour enhancing the ion conduction mechanism and the contact between the gas diffusion layer (GDL), membrane and catalyst layer (CL) is improved. Chen et al. [3] reported a similar observation. The decrease in performance after a test of 100 h is probably due to the combination of effects of some phosphoric acid removal by water or droplets of water accumulated on the GDL over a long time operation. The performance with methanol decreased at both low and high current density. However, the performance loss is prominently visible only at very high current densities.

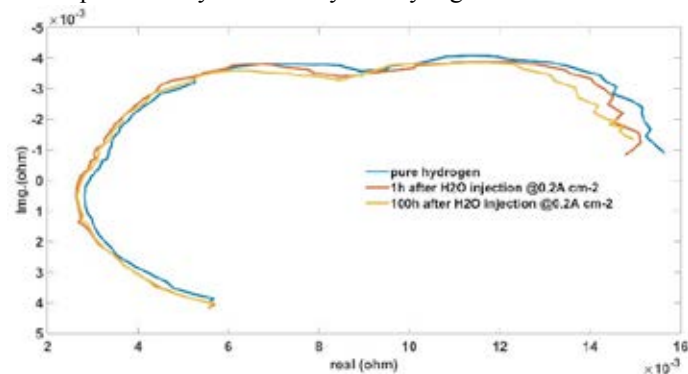


Fig.3: Impedance comparison with and without water vapour in the anode feed @ 0.2 A cm⁻²

A variation in impedance at intermediate and low frequency region imply a change in resistance at those areas with the presence of water vapor in the feed. During, the initial 1 h of water vapor the Ohmic resistance improves and no changes occur over prolonged water vapor injection, as shown in fig.3. The mass transport resistance improves with prolonged water injection on the anode feed.

IV. CONCLUSION

The test with 15% water vapor at different current densities was performed to understand the effect of water vapor in enhancing or degrading a HTPEM fuel cell. The water vapor improved the ion conduction and the contact resistance, which improved the performance at high current density. However, over a prolonged operation the improvement degraded, probably due to water droplets in the GDL leading to acid removal and higher ion transport resistance. The test with methanol at low current density suggest minimal effect with 1% methanol vapors in the anode feed in terms of performance. The minimal drop in performance in the ohmic region with water vapor and methanol vapor suggests the potential of HTPEM operation with methanol feed reformat gas.

FUTURE WORK

The test with methanol will be carried out at higher current density i.e., 0.6 A cm⁻². The feed will be changed back to water vapor alone to account for if the impedance change with methanol is reversible or irreversible.

ACKNOWLEDGMENT

The authors would like to thank 4M project for providing the funding to carry out the experiments. The authors are also thankful to Danish Power Systems for providing the MEA's used in the experiments.

REFERENCE

- [1] Qingfeng Li, Ronghuan He, Jens Oluf Jensen, and Niels J. Bjerrum. Approaches and Recent Development of Polymer Electrolyte Membranes for Fuel Cells Operating above 100 C. *Chemistry of Materials*, 15(26):4896–4915, December 2003.
- [2] Jianlu Zhang, Zhong Xie, Jiujun Zhang, Yanghua Tang, Chaojie Song, Titichai Navessin, Zhiqing Shi, Datong Song, Haijiang Wang, David P. Wilkinson, Zhong-Sheng Liu, and Steven Holdcroft. High temperature PEM fuel cells. *Journal of Power Sources*, 160(2):872–891, 2006.
- [3] Chen-Yu Chen and Wei-Hsiang Lai. Effects of temperature and humidity on the cell performance and resistance of a phosphoric acid doped polybenzimidazole fuel cell. *Journal of Power Sources*, 95(21):7152–7159, November 2010.



LOW LOADING MAGNETRON SPUTTERED Pt-Ir THIN FILM CATALYST FOR UNITIZED REGENERATIVE FUEL CELL

P. Kúš, R. Fiala, M. Václavů, M. Vorokhta, I. Khalakhan,
T. Skála and V. Matolín

Department of Surface and Plasma Science, Charles University in
Prague, V Holešovičkách 2, 18000 Prague 8 (Czech Republic)

Abstract - This work consists of complex characterization of bifunctional Pt-Ir catalyst for unitized regenerative polymer electrolyte membrane fuel cell (URFC). 70 nm Pt-Ir (1:1) thin film was magnetron sputtered onto Ti protected carbon gas diffusion layer (GDL). Performance of the catalyst was measured in “fuel cell” as well as in “electrolyzer” mode in experimental press cell, where Pt-Ir coated GDL was part of the membrane electrode assembly (MEA). Physicochemical properties were studied using scanning electron microscopy (SEM), Energy-dispersive X-ray spectroscopy (EDX) and synchrotrone radiation photoelectron spectroscopy (SRPES). Results indicate that magnetron sputtered Pt-Ir thin film is perspective catalysts for URFC, giving high performance per micro gram of noble metal.

Index Terms - Pt-Ir, SEM, SRPES, URFC

I. INTRODUCTION

Modern world is increasingly leaning towards using renewable sources for power generation. Power generated in this manner (e.g. harvested from solar or wind energy) is however intermittent and in order to be used efficiently, requires incorporation of certain buffer within the electrical grid. PEM electrolyzer for decomposition of water (PEMWE) during power overproduction and subsequent usage of hydrogen as a fuel for PEM fuel cells (PEMFC) in time of power shortage could fulfill this role. [1].

Common catalysts for oxygen evolution reaction (OER) used in PEMWE [2] differ from those for oxygen reduction reaction (ORR) in PEMFC [3, 4]. Great effort is made to find effective bifunctional catalyst capable of reversible operation, which could be used in unitized regenerative fuel cell (URFC), in order to simplify the buffer system and reduce its price. Pt-Ir proves to catalyze both ORR and OER, making it ideal candidate for such application [5]. Both Pt and Ir however belong to the least abundant elements in Earth's crust [6] and as

such their loading within the catalyst layer has to be minimized, for URFCs to be commercially available.

In the following text we present complex characterization of magnetron sputtered low loading Pt-Ir thin film from the deposition details through the physicochemical analysis to the “in cell” performance measurements.

II. EXPERIMENTAL

70 nm Pt-Ir (1:1) catalytic film was DC magnetron sputtered simultaneously from Ir and Pt metallic targets (Kurt J. Lesker) in Ar atmosphere. Layer thickness was checked by atomic force microscope (AFM) Veeco di MultiMode-V. Catalyst was deposited onto Ti coated (200 nm, DC sputtered) carbon paper (Alfa Aesar). Ti coating is essential for preventing carbon corrosion during OER in PEMWE operation.

URFC unit consisted of 4,6 cm² active area press cell (graphite electrode for H₂ side, TiN electrode for O₂ side), Nafion N 115 membrane, commercial reformate anode gas diffusion layer (GDL) with Pt loading of 300 μg/cm² on H₂ side (Alfa Aesar) and above mentioned Pt-Ir coated carbon GDL on O₂ side (Pt-Ir loading: 150 μg/cm²).

Morphology of carbon GDL was studied by means of scanning electron microscopy (SEM) Tescan MIRA III with inbuilt Energy-dispersive X-ray spectroscopy (EDX) Bruker Xflash 6|10. Synchrotrone radiation photoelectron spectroscopy (SRPES) was performed at MSB Elletra in Trieste with synchrotron light energy tuned to 180 eV (for SRPES purposes Pt-Ir film was sputtered onto glassy carbon instead of carbon paper).

III. RESULTS

Consecutive sputtering of 200 nm Ti sublayer and 70 nm Pt-Ir catalytic film led to roughening of carbon GDL's surface (Fig. 1a). EDX mapping proved homogeneous dispersion of Ti, Pt and Ir over the sample (Fig. 1b) and Pt:Ir ration to be (1:1).



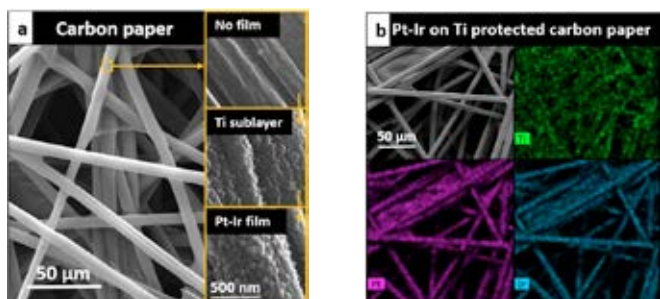


Fig. 1. SEM (a) and EDX (b) analysis

Pt binding energy upshift and Ir downshift relative to metallic Pt and Ir reference, seen on Pt-Ir SRPES spectra (Fig. 2), suggests formation of an alloy. Similar observations, correlated with intra-atomic charge transfer from Pt to Ir, were reported elsewhere [7].

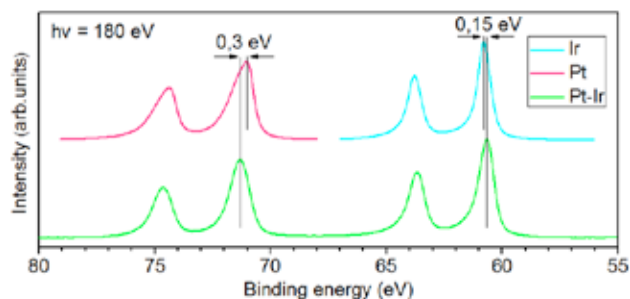


Fig. 2. SRPES analysis

Performance measurement of experimental URFC in “electrolyzer” operation mode is shown in Fig. 3. Afterwards, performance in “fuel cell” mode was tested (Fig. 4). To complete the cycle, URFC was once again operated in “electrolyzer” mode to confirm reversibility of the system. Results were identical to those seen in Fig. 3. Note that specific current (power, respectively) was calculated considering total catalyst loading of $450 \mu\text{g}/\text{cm}^2$ ($150 \mu\text{g}/\text{cm}^2$ O₂ side, $300 \mu\text{g}/\text{cm}^2$ H₂ side).

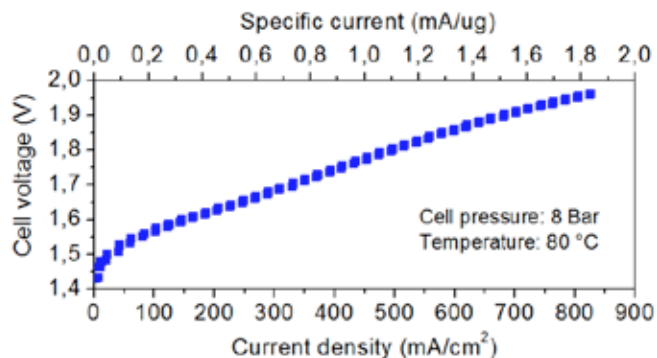


Fig. 3. “Electrolyzer” mode performance of URFC

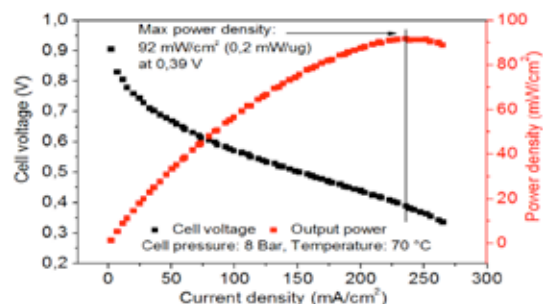


Fig. 4. “Fuel cell” mode performance of URFC

IV. CONCLUSION

Magnetron sputtering proves to be suitable method for deposition of thin catalytic films for URFC, offering precise control of noble metal loading and distribution.

Co-sputtering of Pt and Ir seems to lead to alloy formation as hinted by SRPES spectra. Also film deposition increases the roughness of carbon GDL and therefore its surface area.

Experimental URFC with thin film Pt-Ir catalyst on O₂ side of the MEA was tested in “electrolyzer” and “fuel cell” mode, giving specific performance (per Pt-Ir μg) comparable or superior to systems with much higher loading [5].

Experimental URFC system was stable during 24 hour test period with no performance drops in either of operation modes.

ACKNOWLEDGMENT

This project was supported by Charles University Grant Agency (GAUK No. 236214) and by EU FP-7-NMP-2012 project chipCAT under contract No. 310191.

REFERENCES

- [1] Armaroli, N., Balzani, V., The Hydrogen Issue, ChemSusChem, Volume 4, 2011, Pages 21-36
- [2] Carmo, M., Fritz, D. L., Merge, J., Stolten, D., A comprehensive review on PEM water electrolysis, International Journal of Hydrogen Energy, Volume 38, 2013, Pages 4901-4934
- [3] Gasteiger, H. A., Kocha, S. S., Sompalli, B., Wagner, F. T., Activity benchmarks and requirements for Pt, Pt-alloy, and non-Pt oxygen reduction catalysts for PEMFCs, Applied Catalysis B: Environmental, Volume 56, 2005, Pages 9-35
- [4] Fiala, R., Václavů, M., Vorokhta, M., Khalakhan, I., Lavková, J., Potin, V., Matolinová, I., Matolín, V., Proton exchange membrane fuel cell made of magnetron sputtered Pt–CeOx and Pt–Co thin film catalysts, Journal of Power Sources, Volume 273, 2015, Pages 105-109
- [5] Antolini, E., Iridium As Catalyst and Cocatalyst for Oxygen Evolution/Reduction in Acidic Polymer Electrolyte Membrane Electrolyzers and Fuel Cells, ACS Catalysis, Volume 4, 2014, Pages 1426-1440
- [6] Parry, S. J., Abundance and distribution of palladium, platinum, iridium and gold in some oxide minerals, Chemical Geology, Volume 43, 1984, Pages 115-125
- [7] Wang, J., Holt-Hindle, P., MacDonald, D., Thomas, D. F., Chen, A., Synthesis and electrochemical study of Pt-based nanoporous materials, Electrochimica Acta, Volume 53, 2008, Pages 6944-6952



ON-LINE IN-SITU DIAGNOSIS OF PROCESSES WITHIN HT-PEM FUEL CELL MEMBRANES BY RAMAN MICROSCOPY AND MEASUREMENTS OF FLUORESCENCE

H. Bettermann and M. Labus
Institute of Physical Chemistry
Heinrich-Heine-University of Düsseldorf
40225 Düsseldorf (Germany)

Abstract - In-situ Raman measurements and the detection of fluorescence emission were used to investigate types and distribution of molecular species inside an ABPBI membrane of a running HT-PEM fuel cell. A specific experimental setup was first engineered whereby the port which provided the observation of species inside the membrane was placed next to the cathode. Orthophosphoric acid, $H_3PO_4 \cdot H_2O$ and pyrophosphoric acid could unambiguously be identified by the analyzing the Raman spectra. Their concentrations changed individually when the current consumption of the fuel cell was changed. Raman transitions which are attributed to vibrations of the imidazole ring changed their signal heights simultaneously. In addition, the strong background fluorescence emission intensities which originates from the ABPBI membrane shows a proportionality to the current consumption.

Index Terms – fluorescence measurements, HT-PEM fuel cells, on-line measurements, Raman spectroscopy

I. INTRODUCTION

In recent years, cyclic voltammetry, impedance spectroscopy and X-ray radiography have been applied to study HT-PEFCs in operation to improve their performances. Especially phosphoric acid species, which usually promote the transport of charges through the membrane were investigated by ^{31}P -NMR spectroscopy [1]. The investigation of phosphoric acid species and the role they play for the transport of charges are again reflected in this contribution. For this, an in-situ on-line Raman spectroscopic setup was developed that enabled the observation of molecular species inside the membrane of a running HT-PEM fuel cell. A further advantage is the direct proportionality between Raman intensities of a species and its concentration. The lack that Raman signals are notoriously weak can be sur-

mounted by using laser light sources, properly chosen optic imaging conditions and very sensitive detectors.

Despite the record of phosphoric acid species within a 2,5-polybenzimidazole (ABPBI) membrane during operations of a high-temperature PEM fuel cell, the present studies are also concerned with measuring the Raman signals of the ABPBI membrane and their emission of fluorescence during changes of current consumption.

The setup was guided by minimizing the intervention into the running fuel cell. The size of the observation port was kept to a minimum and to avoid unneeded electronic excitation and resulting photochemical conversions of membrane molecules, a laser wavelength was selected which was much longer than the onset of the electronic absorption spectrum of ABPBI.

II. EXPERIMENTAL SETUP

The beam of a He-Ne laser (632.8 nm, 6 mW) passed an interference filter (Semrock, MaxLine®, 632.8 nm) and was directed to a microscope objective (Nikon, 10x, WD: 20.3 mm, NA: 0.21, focal length: 20.0 mm). The objective focused the beam through a quartz rod (diameter: 0.73 mm, length: 6 mm) into the membrane and collected the back-emitted light. The light emission was directed to a spectrograph (HoloSpec f/1.8i, Kaiser Optical Systems) via a dichroic mirror (Semrock RazorEdge® U-grade) and a plano-convex lens (focal length: 8 cm). The emission was recorded by a back-illuminated CCD-camera (Princeton Instruments PIXIS™400, 1340x400 pixels, kept at -70 °C). A block-out was milled into the endplate of the cathode to enable a proper alignment of the microscope objective. A central channel (diameter: about 5 mm) connected



the block-out with the observation hole (diameter: 0.8 mm) in which the quartz rod was inserted and fixed by a sealing agent (Scriotec 901). The hole of the GDE has a diameter of 2 mm.

The measuring time for the detection of Raman signals was set both to 10 min and to 1 min. To extract the Raman signals from the background emission, the second derivatives of the total emission spectra were analyzed.

III. RESULTS AND DISCUSSION

The emission spectra were recorded under different current settings. The total emission which consists of a dominating strong background emission and superimposed Raman transitions increased strongly when the OCV setting changed to galvanostatic operations. Going back again to the OCV condition, the emission returned to its initial OCV values after a certain delay time. The background signals are attributed to a fluorescence emission of the ABPBI-membrane although the wavelength of laser excitation was considerably longer than the wavelength of the onset of electronic absorption. Due to the arrangements of polyene chains within the membrane, the observed fluorescence may be assigned as originated from J-aggregation [2], which generally occurs from a parallel alignment of transition dipole moments of next neighbored electronically excited molecules. This is assignment could be confirmed by ex-situ fluorescence studies on the ABPBI-membranes. The series of emission spectra showed that the fluorescence intensities were proportional to the current settings.

Raman signals of the phosphoric acid species responded differently to current settings. While the Raman signal intensities of phosphoric acid and the $\text{H}_3\text{PO}_4\text{-H}_2\text{O}$ indicated by their totally symmetric P-O stretching modes changed weakly when the current was altered, a significant change of the Raman intensity could be recorded for the totally symmetric P-O stretching mode of pyrophosphoric acid (Fig.1 a). Since heated monophosphoric acid units condense into various oligophosphoric acids like pyrophosphoric acid [3] or more commonly polyphosphoric acids under the temperature conditions of HT-PEM fuel cells, these compounds are available for the charge transfer. The Raman intensities of the polyphosphoric acid were marginally affected by changes of current (Fig. 1a). This may be explained by the fact that the pyrophosphoric acid is the smallest one of the condensed species and among these species its mobility seems to be largest and it may therefore contribute best to the charge transport.

Significant signals of ABPBI are the C=C breathing vibration of the benzene ring and the totally symmetric C=N stretching mode of the imidazole unit. The imidazole ring is indirectly involved within the transport of charges by its potential protonation. The inspection of modes showed that the intensity

of the C=N stretching vibration was also affected by changes of current while the intensity of the C=C breathing mode remained constant (Fig. 1b).

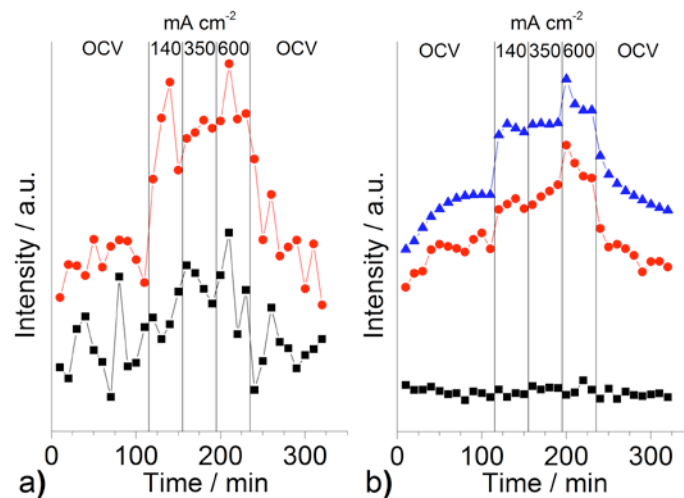


Fig. 1: Changes of Raman signal intensities and intensity changes of fluorescence emission caused by current changes (P_{HeNe} : 4.5 mW, t_{int} : 600 s)

The time intervals in which the operational conditions are set are marked by vertical lines; a) course of Raman signals: red: pyrophosphoric acid (1023 cm^{-1}), black: polyphosphoric acid (991 cm^{-1}); b) comparison of fluorescence intensities with Raman intensities: blue: fluorescence emission, red: C=N stretching mode (1573 cm^{-1}) of the imidazole unit, black: C=C breathing mode of the benzene ring (964 cm^{-1})

It is interesting to see that the course of the intensity changes of the C=N stretching mode over the current changes matches well with those intensity changes found for the fluorescence intensities. This means that the molecular state of the membrane polymer during different operating conditions of the fuel cell can be easily pursued by measuring the strong fluorescence signals while the statement which phosphoric acid species contribute to the charge transport is made by Raman spectroscopy.

REFERENCES

- [1] Suarez, S., Kodiweera, N. K. A. C., Stallworth, P., Yu, S., Greenbaum, S. G. and Benicewicz, B. C., Multinuclear NMR Study of the Effect of Acid Concentration on Ion Transport in Phosphoric Acid Doped Poly(benzimidazole) Membranes, *J. Phys. Chem. B*, 116, 2012, pp. 12545–12551
- [2] Jelley, E. E., Spectral absorption and fluorescence of dyes in the molecular state, *Nature*, 139, 1937, p. 631–632
- [3] De Jager, H.-J. and Prinsloo, L. C., The Dehydration of Phosphates Monitored by DSC/TGA and in situ Raman Spectroscopy, *Thermochim. Acta*, 376, 2001, pp. 187–196.



Effect of pH variations on the performance of anodic marine biofilm in microbial fuel cell-based biosensor.

Valeria Agostino^{1,2}, Giulia Massaglia^{1,2}, Valentina Margaria¹, Tonia Tommasi¹, Caterina Armato², Gian Paolo Salvador¹, Adriano Sacco¹, Matteo Gerosa^{1,2}, Angelica Chiodoni¹, Luisa Delmondo², Nadia Garino¹, José A. Muñoz-Tabares¹, Micaela Castellino¹, Marzia Quaglio¹.

¹Center for Space Human Robotics @PoliTo, Istituto Italiano di Tecnologia, Corso Trento 21, 10129, Torino, Italy

²Applied Science and Technology Department, Politecnico di Torino, Corso Duca degli Abruzzi 24, 10129, Torino, Italy

Abstract - Microbial fuel cells (MFCs) offer a broad range of biotechnological applications. During field application MFCs are exposed to variations in operating parameters that could affect MFC stability and performances. This work investigate the response of an anodic marine biofilm under different pH influent conditions, ranging from 3 to 13, in absence of phosphate buffer to evaluate the adaptability of the microbial community in order to better define the pH variances which can be tolerate during MFC operation. The electrochemical and biological characterization revealed a natural buffer ability of the systems, with anodic pH influent of 5 and 11. Effective changes in anodic chamber pH were only visible when MFCs were fed with influent at extreme acid and basic pH values. Our findings underline the adaptability of this microbial consortia and, therefore, the possibility for a biosensor based MFC to work effectively in a wide pH range.

Index Terms – pH, marine consortia, MFC-based biosensor

I. INTRODUCTION

Microbial Fuel Cells (MFCs) are bioelectrochemical systems that convert chemical energy into electrical energy from the respiratory metabolic profit of electrochemically active bacteria. MFCs are a versatile emerging technology, offering a broad range of biotechnological applications[1]. An important emerging field explores the use of MFCs as biosensors for pollutant analysis and in situ process monitoring due to the instant and reliable current response during the degradation of electron donors [2].

The external environment conditions affect the performances of these devices, therefore, it is necessary to discern electrochemical variations caused by operating parameters in order to detect real toxic events and prevent false positive alarms [3]. In particular, anodic pH microenvironment is one of the important factor that can influence optimal microorganism growth and substrate metabolic activity, and, in turn, affects the electron and proton generation mechanism [4]. Many studies analyzed pH variation in fed-batch mode and directly at a fixed pH, without considering how the system adapt themselves to the slowly and continuous variations caused by an unexpected polluted fluid stream that can modify the ecological equilibrium presents in natural environments. Moreover, these systems are stabilized with high concentration of phosphate buffer which represents a significative cost and energy input for real applications [5][6].

This work propose an analysis of MFC performances under different pH influent conditions, in absence of phosphate buffer, to evaluate the adaptability of an anodic marine biofilm in order to better define the pH variances which can be tolerate during MFC operation. In particular, the biofilm developed and stabilized at neutral pH, undergone a continuous and slow variation of pH mimicking field application and environmental changes. In this condition the microbial consortia has the possibility to adapt his metabolic profile in order to counteract the environmental pressure.

II. EXPERIMENTAL SECTION

A. Material and Methods

A 2 months test was conducted in triplicate in circular dual-chamber MFC (~58 mL for compartment) with the anodic chamber continuously fed with sodium acetate and with a chemical cathode (potassium ferricyanide). To sustain initial biofilm formation MFCs undergone 1 week in batch mode in neutral pH conditions. After reaching stability MFCs were running in continuous modality with influent pH modification. In particular, the test was divided into 2 phases: the first one with pH influent 7, 5, 11 and a second one with influent 7, 3 and 13 to identify pH threshold.

The system was analyzed from the electrochemical (continuous monitoring of MFCs potential and polarization curves) and biological point of view (plate count tests and FESEM analysis).

B. Results

In the 1st part of the test, under a continuously anodic feeding at pH values of 5 and 11, there are no significative differences in MFCs electrochemical performances (Fig.1), which are summarized in Table 1.

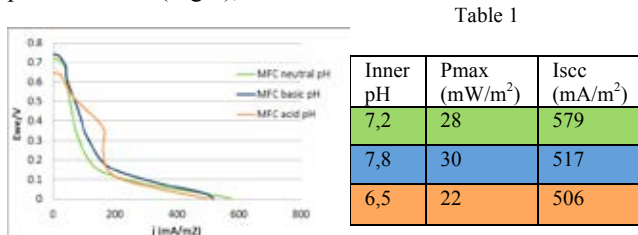


Fig. 1. Linear sweep Voltammetry at day 16 (scan rate 1 mV/s).

MFCs with acid and basic influents maintained an inner anodic pH level near the neutrality, pH 6.5 and 7.8, respectively (Fig. 2). The system showed a natural buffer ability. The marine biofilm was able to adapt its metabolic activity at pH very different from natural seawater environment .

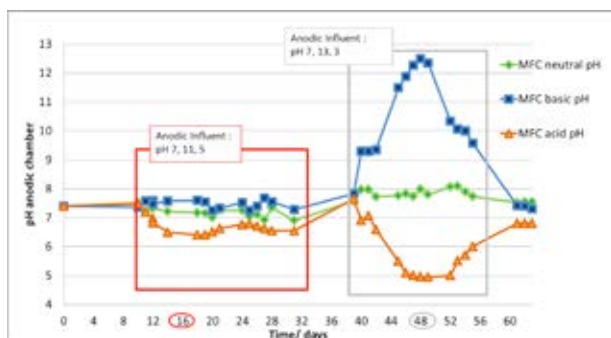


Fig. 2. Anodic values of inner pH during 2 months test. The red box on left shows the natural buffer ability of the system with influent at pH 5 and pH 11; on the right the gray box shows the anodic pH threshold reached under extreme values of pH influent (pH 3, pH 13).

To identificate the pH threshold for electrochemical performances, in the 2nd phase of the experiment, a more drastic variations of pH influent (pH 3 and 13) was

performed. In particular when the inner anodic pH was < 5 and ≥ 11 we observed a sharp drop in electrochemical MFC responses, as indicated by the polarization curves (Fig.3). These results are summarized in Table 2.

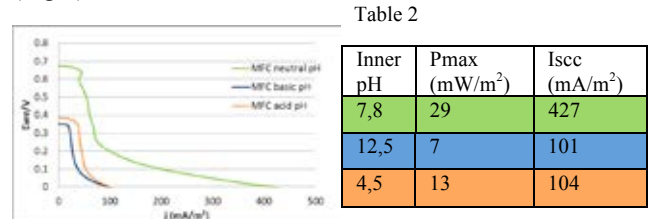


Fig. 3. Linear sweep Voltammetry at day 48 (scan rate 1 mV/s).

Plate counts test confirmed these anodic pH threshold, with a very low number of viable colonies both in acid and basic conditions.

However, the microbial consortia is able to survive to this unfavorable conditions and to re-develop an active biofilm when pH influent returns at neutral value, as confirmed by MFCs performance and inner anodic pH level.

III. CONCLUSION

The microbial adaptability and the natural buffer ability of this marine consortia reveals that pH becomes a disturbing operating parameter only when MFC influent reaches very extreme pH values. Moreover, the system is able to restart working normally in neutral conditions even after drastic pH stress. The possibility to work in a wide pH range, together with the ability to survive to extreme pH without any external maintenance, suggests the application of these type of biodetector for remote area sensing.

REFERENCES

- [1] Rabaey, K., and Verstraete, W., Microbial fuel cells: novel biotechnology for energy generation *TRENDS in Biotechnology* Vol.23, 2005, pages 291-298
- [2] Sun, J.-Z., Kingori, G.-P., Si, R.-W., Zhai, D.-D., Liao, Z.-H., Sun, D.-Z., Zheng, T. and Yong, Y.-C. Microbial fuel cell-based biosensors for environmental monitoring: a review. *Water Science & Technology* Vol.71.6, 2015, pages 801-809
- [3] Chouler, J. and Di Lorenzo, M., Water quality monitoring in developing countries; can microbial fuel cell be the answer? *Biosensgtors* Vol.5, 2015, pages 450-470
- [4] Oliveira, V.B., Simoes, M., Melo, L.F. and Pinto A. Overview on the development of microbial fuel cells. *Biochemical Engineering Journal* Vol.73, 2013, pages 53-64
- [5] Jadhav, G. S., & Ghangrekar, M. M. Performance of microbial fuel cell subjected to variation in pH, temperature, external load and substrate concentration. *Bioresource Technology*, Vol. 100(2), 2009, pages 717–23
- [6] Yong Yuan , Bo Zhao , Shungui Zhou, Shengkui Zhong , Li Zhuang Electrochemical activity of anodic biofilm responses to pH changes in microbial fuel cells. *Bioresource Technology* Vol. 102, 2011, pages 6887–6891



PFSA MEMBRANE DEGRADATION IN THE HYDROGEN INLET REGION: A MACROSCOPIC APPROACH¹

G. De Moor^{a,b}, C. Bas^{a,b}, N. Charvin^{a,b}, J. Dillet^c, G. Maranzana^c, O. Lottin^c, N. Caqué^d,
E. Rossinot^d, and L. Flandin^{a,b}

^aUniv. Savoie Mont Blanc, LEPMI, F-73000 Chambéry, (France)

^bCNRS LEPMI, F-38000 Grenoble, (France)

^cLEMETA – Univ. Lorraine – CNRS, 2 avenue de la Forêt de Haye, BP160, 54504, Vandoeuvre
les Nancy Cedex, (France)

^dAxane, 2 rue Clémencière, BP15, 38360 Sassenage, (France)

¹submitted to International Journal of Hydrogen Energy (April 2015)

Abstract - This study focuses on the characterization of a PEM Fuel Cell that has operated in stationary mode in real-life conditions for 12860 hours. We compare macroscopic analyses such as individual cell voltage, "in situ pressure drop" and "ex situ infrared imagery" leak tests with cell local performances. Results show strong heterogeneities inter and intra-stack with cells near the warmest areas as the most degraded. Infrared imageries reveal that the dry hydrogen inlet is a preferentially degraded zone with 80% of leaking cells. To develop a better understanding of the degradation process of the reinforced membrane, we build using optical microscopy images, a membrane thickness profile covering 7 channels/lands in the H₂ inlet region. We find that degradation occurs only in the channels where dry hydrogen enters. With the reinforced membrane, we dissociate the thickness variation of each layer and it reveals that degradation is initiated at the anode side.

Index Terms - PEMFC, Degradation, PTFE-reinforced membrane, Hydrogen inlet.

I. INTRODUCTION

Durability is primarily governed by membrane failure leading to high gas crossover and fast decomposition around pinholes. Thanks to a fruitful collaboration between three laboratories and Axane as fuel cell manufacturer, real life and long term operations were analyzed at different scales (MEA, catalyst layers, membrane). System lifetime was thus improved from 1500 hours until 13000 hours [1, 2]. This improvement was in major part due to the use of reinforced PFSA membrane type. These reinforced membranes have better mechanical properties and a better resistance to crack initiation and propagation [3]. In the last years, degradation mapping of the cells have proved

that the gas inlets/outlets were the main fuel cell weaknesses. If finding the defective areas inside a cell is easy, finding the degraded side in the membrane is a much more difficult task. However, being able to characterize the membrane in the cross-section and identify the degradation mechanisms as a function of the side would answer many questions. Measuring the membrane thickness is simple and routinely employed to illustrate and conclude on membrane degradation. Consequently, from thousands of optical microscopy images, we build the membrane thickness profile on a macroscopic range (>1.5cm covering 7 channels and lands). The three layers of the PTFE-reinforced membrane were studied individually and the side of degradation revealed.

II. RESULTS AND DISCUSSIONS

A. H₂ inlet/Air outlet degradation analysis protocol

Cross-section analysis of membrane and thickness measurements are commonly made using SEM images. We do believe that in a first approach, the magnification of this microscopy technique is too important. Optical microscopy with x50 magnification is sufficient to measure significant thickness variation on samples of 30-35 μm in full size. Using ImageJ, we developed a method to measure membrane thickness over more than 1.5 cm in length.

Figure 1 explains the sampling area and the methodology for thickness measurement. On the top left, there is a schematic representation of the anodic bipolar plate. Two parallel channels (red and blue) are in serpentine mode. Area of analysis is on the purple rectangle. As explained on the zoom,



the dry H₂ inlet enters in channels 1&2 meaning that the gas has traveled 1-2 cm where the sampling was made. Land2 separates channel2 from channel3. On channels3&4, H₂ has already traveled 27 cm meaning that the gas has humidified itself during this path. Channels5&6 are at more or less 1-2 centimeters identical than channels3&4. At the end, in channels 7&8, hydrogen has flowed nearly 58cm and is facing the cathode air outlet channels. The cross-section sampling area has been cut through the A-A profile, starting from a point where membrane is still under subgasket until the air outlet channels (1.5 cm). With a motorized stage on the microscope, approximately 200 pictures were taken all along the membrane. The full image was easily built using a stitching function of FIJI. Then, by thresholding the image, it was possible to separate each layer of the membrane as it is seen on the right bottom part in Figure 1. Then we measured the thickness following this procedure: (i) for each individual pixel in the y direction, we count the number of pixel for each layer in the z direction; (ii) at the end of the row, it moves forward to the next pixel in y direction and count again in the z direction. For the magnification used in this study, one pixel was equivalent to a distance of 0.08 μm. Finally, knowing the exact number of pixel for each layer and for each y value, it is possible to draw the membrane thickness profile as shown on the left bottom part.

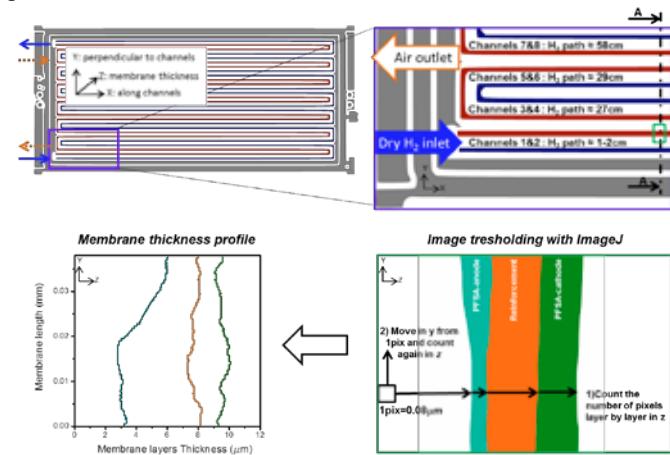


Figure 1: Protocol for membrane thickness profile measurement

Consequently, the complete profile of the membrane over the 1.5 cm has been obtained from more than 50,000 values of thickness. This is of interest for statistical analysis of the thickness variation as a function of the position in the channels or lands.

B. H₂ inlet/Air outlet cross-section degradation analysis

A major result is the radical change under the land 2 which separates the dry hydrogen in channel 2 and the humidified hydrogen in the channel 3. A very short land of 0.69 mm separates the dry hydrogen of the inlet region from humidified H₂ that traveled 26 cm in the cell. This induces a spectacular

change in the state of degradation of the membrane. The latter was measured entirely degraded on the inlet side and very closed to its initial value on the other side of the land. This phenomena is highlighted in Figure 2. We plotted the membrane thickness profile in the end of channel2, the land2 and the beginning of channel3. The red parts are related to the membrane in a channel, and the blue parts are under a land. The PFSA-anode layer is on the top, the reinforcement layer is in the middle in white and the PFSA-cathode on the bottom. It is seen that the PFSA-anode layer is very thin and fragmented at the end of channel2. This continues under the beginning of land2. However, the thickness of each layer becomes rapidly uniform and constant as in channel3.

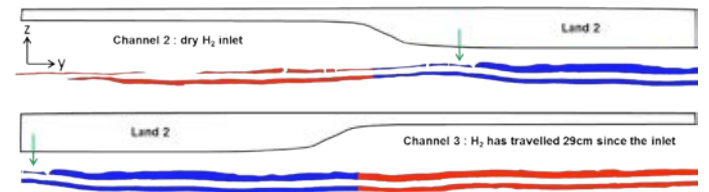


Figure 2: Transition between channel2 (dry H₂) and channel3 (wet H₂)

III. CONCLUSION

From this study, we revealed that a large majority of cells were leaking in the H₂inlet/Air outlet region. It was measured that the degraded area was only located in the two channels facing the dry hydrogen inlet. The thickness profile has been useful to determine that in this H₂ inlet area, the PFSA-anode side is degraded in first. As a conclusion, macroscopic thickness measurement appear as one of the simplest way to quickly conclude on the degradation of membrane or catalyst layers. SEM images are often used, however this study clearly show that with a too large magnification, one can pass beside information about degradation.

ACKNOWLEDGMENT

This work has been supported by the H2E (Horizon Hydrogène Energie) program supported by BPI France.

REFERENCES

- [1] L. Dubau, *et. al*, "Carbon corrosion induced by membrane failure: The weak link of PEMFC long-term performance," International Journal of Hydrogen Energy, 2014.
- [2] G. De Moor, *et. al*, "Understanding Membrane Failure in PEMFC: Comparison of Diagnostic Tools at Different Observation Scales," Fuel Cells, vol. 12, pp. 356-364, 2012.
- [3] E. Moukheiber, *et. al*, "Understanding the formation of pinholes in PFSA membranes with the essential work of fracture (EWF)," International Journal of Hydrogen Energy, 2013.



TOWARDS THE ITALIAN FUEL CELLS AND HYDROGEN PLATFORM

Angelo Moreno*, Chiara Barchiesi**, Viviana Cigolotti***,
Vanessa Rossi**, Gianni Bidini**

*ENEA, Centro Ricerche Casaccia, Via Anguillarese, 301, Roma
(Italy)

**Dipartimento Ingegneria, Università degli Studi di Perugia, Via
Goffredo Duranti, 06125 Perugia (Italy)

***ENEA, Centro Ricerche Portici, P.le Enrico Fermi, 1 - 80055
Portici, Napoli (Italy)

Abstract - In Italy the presence of an active scientific community on hydrogen and fuel cells is becoming more and more evident: an industrial sector committed to turn the innovative technological opportunities of these technologies into effective business opportunities and several public institutions supporting the integration of scientific community and industry actions. However, these initiatives often remain dispersed and efforts not sufficiently integrated. Activities are restricted to the technical experts, failing to arrive at the level of the decision makers who are in the position to establish a national framework and identify guidelines and priorities in accordance with other European countries. Indeed, despite repeated attempts to stimulate cohesive government intervention, a national platform on FC&H₂ has not yet been launched as in other countries of the world. The Italian National Agency for New Technologies, Energy and Sustainable Economic development (ENEA) and the University of Perugia (Unipg) are promoting the establishment of the Italian Fuel Cells and Hydrogen Platform in order to coordinate efforts for the development of critical technologies for the whole hydrogen cycle (production, delivery, storage, conversion and end use applications) and the overcoming of barriers, in other words, to act as a country system. The present abstract describes the activities performed so far and highlights the results achieved up to date towards the official launch of the Platform.

Index Terms – Italian Fuel Cells and Hydrogen Platform, country system, FCH₂ strategy.

I. INTRODUCTION

In the European Union, the hydrogen and fuel cell technology is one of the eight strategic priorities of the SET-Plan and some Member States have developed important programmes for its deployment. Italy is the only major EU

country having not yet developed a coordinated and long-term plan for hydrogen and fuel cells along with a national platform promoting public-private partnership in the field. This is partly due to substantial lack of interest demonstrated so far by the largest industrial groups and to the priority given to natural gas and electricity. Nevertheless, ENEA and Unipg are continuing to work towards establishing a national platform that is intended to serve as a steering committee to coordinate the many research, development and demonstration initiatives underway in the country and to plan a coherent long-term strategy. In fact, in Italy the presence of an active scientific community on FCH₂ is evident and several companies are committed to turn the innovative technological opportunities of these technologies into effective business opportunities. Last but not least, several public institutions are supporting the deployment of hydrogen as alternative fuel for stationary, mobile, and transportation applications and promoting the integration of scientific community and industry actions. It is worth to highlight that in February 2014 the Industry, Trade and Tourism Committee of the Italian Senate issued a resolution which clearly stated that a national hydrogen platform should be launched as soon as possible, also with the aim to allow Italian industry and research bodies to take full advantage of the EU funds available under Horizon 2020.

II. OBJECTIVES OF THE PLATFORM

The main objective of the Platform is to foster the development of fuel cells and hydrogen in Italy through medium- and long-term initiative policies which aim at:



- identifying the research, technical and scientific priorities as well as those of the industrial sector of the country;
- building awareness and policy consensus;
- identifying clear financial tools for supporting the development and implementation of the foreseen initiatives.

This will allow to define a shared vision and strategy for research, development, demonstration and application (RSDA) oriented towards the promotion of excellence and industrial competitiveness in the country in the field of FCH2. The ultimate goal of such an organized system will be to afford the European scenario and interact or compete with transnational initiatives.

III. METHODOLOGY

A. Identification of Italian Actors on H2FC

ENEA and Unipg have identified the Italian universities, research centers, companies, public institutions and associations working on the field. An analysis of the Italian members of the FCH2 associations has served as the primary tool for such a mapping. It followed a research about the regional, national, European and international projects and initiatives involving Italian institutions and companies. All departments of energy of the Italian Regions have been identified through their websites. A first search has been made about the Engineering, Science and Technology universities. Then, the single departments and laboratories have been approached. Category associations have been contacted for identifying the companies whose field of work is FCH2. Last but not least, personal contacts of the staff working at the Platform, have been directly approached. A mailing list has been also realized which is made up of more than 200 contacts.

B. Realization of a questionnaire

Three different questionnaires (one for universities and research centers, one for companies and one for public administrations) have been realized by experts of ENEA and Unipg. Questionnaires are made up of the following sections:

Section	Universities/ research centers	Companies	PA
General Information (name, address, contact person, email, etc...)	X	X	X
Core business		X	
Area(s) of interest (e.g. transportation, hydrogen production, etc...)	X	X	X
Specialization / expertise		X	
Field of interest		X	
Number of persons working on FCH2	X	X	X
Investments in FCH2		X	
Market potential		X	
Laboratories	X	X	
H2 Research activities (e.g. Storage, Production, Distribution, Safety,...)	X	X	
FC Research activities (e.g. materials,	X	X	

stack, system, components, ...)			
Estimated value of the main available infrastructures (in euros)	X	X	
Annual cost for the management of the research group (personnel, equipment, ...)	X	X	
Projects	X	X	X
Publications and patents	X	X	
Collaborations	X	X	X
Membership of national and international associations	X		X

The questions have been elaborated according to the variables which were needed for sizing the Italian actors playing in the field.

C. Questionnaire distribution

Questionnaires have been circulated between the identified contacts and published in the online platform <http://www.europeanfuelcell.it/survey/>

D. Questionnaire results

97 questionnaires have been received up to date (65 from universities / research centers, 8 from public administrations, 24 from industries) and a further 100 people have registered on the Platform website. It is worth to highlight that questionnaires have been answered by the single university departments or laboratories / research groups, so we have even more than one questionnaire for some universities and research centers. A detailed analysis of the survey is currently ongoing.

IV. CONCLUSION

The Italian Fuel Cells and Hydrogen Platform initiative garnered positive consensus both from the academic world and the industrial one. They have a positive attitude towards the Platform's constitution as demonstrated also by the accurate and timely information provided through the survey. Public administration institutions need to be approached once again. A map of the Italian FCH2 infrastructures and actors will be realized along with a booklet (in Italian and English) aimed at presenting the Italian FCH2 panorama. Contract talks with representatives of the Italian government are also foreseen.

The Italian Fuel Cells and Hydrogen Platform's website http://www.europeanfuelcell.it/european_fuel_cell_piattaforma_italiana_fch2.html



COUPLING OF MICROBIAL ELECTROLYSIS CELLS AND DARK FERMENTATION TO ENHANCE THE PRODUCTION OF BIOHYDROGEN FROM AGRO-INDUSTRIAL WASTEWATERS

A. Marone*, O. Ayala**, E. Trably*, A. Carmona*, R. Moscoviz*, E. Latrille*, V. Alcaraz**, and N. Bernet*

*INRA, UR0050, LBE, Avenue des Etangs, Narbonne, (France)

**Universidad de Guadalajara, CUCEI, Blvd. Gral. Marcelino García Barragán, Jalisco, (Mexico)

Abstract - The aim of this work is the development of a feasible, cascade two-step BioH₂ production process from Organic Wastewater (WW), combining dark fermentation (DF) and Microbial Electrolysis Cells (MECs). Such coupling of DF and ME constitutes a technological cornerstone within the concept of an environmental biorefinery. Five different WW coming from cheese (CW), fruit juice (FJW), paper (PW), sugar (SW) and fruit processing (FPW) factories were selected among 21 different WW collected from a wide range of industrial sectors (food, manufacturing, biofuel, wastewater treatment, among others) to evaluate the feasibility of two-step process. The results of this work show that dark fermentation linked with ME is a feasible and highly promising option in order to maximize the conversion of WW into bioenergy.

Index Terms – Dark fermentation, hydrogen, microbial electrolysis cells, wastewater treatment.

I. INTRODUCTION

Among the diverse renewable H₂-producing biotechnologies, dark fermentation (DF) of Organic Wastewater (WW) has received significant attention in recent years since it combines sustainable waste management with pollution control and generation of a highly valuable clean energy product [1]. However, fermentative H₂ production provides only a partial oxidation of the organic substrate. It is likely to be industrially viable only if fermentative bioprocesses are integrated within a stream that can utilize fermentation by-products. Microbial Electrolysis Cells (MECs) are an emerging technology that could utilize the metabolic byproducts generated by DF. Combining DF with MECs in a two-steps cascade process can result in a complete exploitation of biodegradable WW, which maximizes at the same time energy recovery and effluent depollution [2].

The aim of this research is to identify the most suitable WW for the development of a feasible, two-step BioH₂ production cascade -

process, combining DF and MC within the biorefinery concept. Five different WW coming from cheese (CW), fruit juice (FJW), paper (PW), sugar (SW) and fruit processing (FPW) factories were selected among 21 different WW collected from a wide range of industrial sectors (food, manufacturing, biofuel, wastewater treatment, among others) to evaluate the feasibility of two-step process. The selection was made on the basis of fermentative conversion efficiency (i.e., both H₂ and metabolic by-product accumulation) obtained in DF experiments. The effluents from the fermentation of CW, FJW, PW, SW and FPW were tested in two chambers MECs to further recover H₂ and WW depollution.

II. MATERIALS AND METHODS

A. Experimental set up

CW, FJW, PW, SW and FPW were selected among 21 different WW collected from a wide range of industrial sectors on the basis of fermentative conversion efficiency.

DF experiments carried out in batch reactors (pH 5.5, 37°C) using heat treated anaerobic sludge as inoculum.

MEC experiments were conducted in two chambers (400 mL wV) potentiostatically controlled systems (anode applied potential + 0.2V vs SCE, pH 7, 37°C). An electroactive biofilm enriched from anaerobic sediments using acetate as carbon source is used as biocatalyst.

B. Analytical methods

The volume of biogas production was measured using water column method. The gas compositions of the anode and cathode chambers were determined by a gas chromatograph (Clarus 580 GC). The concentration of soluble metabolic products were analyzed by high-performance liquid chromatography (HPLC).



C. Calculations

The coulombic efficiency (CE, %) was calculated as $CE = n_{ce}/n_{th}$, where n_{ce} is the moles of hydrogen that could be recovered based on the measured current, and n_{th} was the theoretical maximal production based on COD removal, calculated as described in [3].

The cathodic hydrogen recovery (r_{cat} , %) was calculated as $r_{cat} = n / n_{ce}$, where (n) was the moles of hydrogen produced at the cathode and (n_{ce}) the moles of hydrogen that could be recovered based in the measured current.

The energy yield (YE, %) is the term for energy recovery based on the energy content of the hydrogen produced compared to the electrical input. It was calculated as $YE = -W_{H_2}/W_e$, where (W_{H_2}) was the energy content of the hydrogen produced, calculated based on hydrogen combustion energy and (W_e) was the input electrical energy required to produce the hydrogen in the MEC.

III. RESULTS

The H_2 recovered in DF was linearly correlated with the initial content of soluble sugars and present in WW ($R^2 = 0.9$). The H_2 production obtained from DF of the five WW ranged from 30 to 296 mL H_2 /L and CW showed the best H_2 production yield of 120 ± 31 mL H_2 /gVS. Acetate, butyrate were the main metabolic by-products in all the experiments (Figure 1).

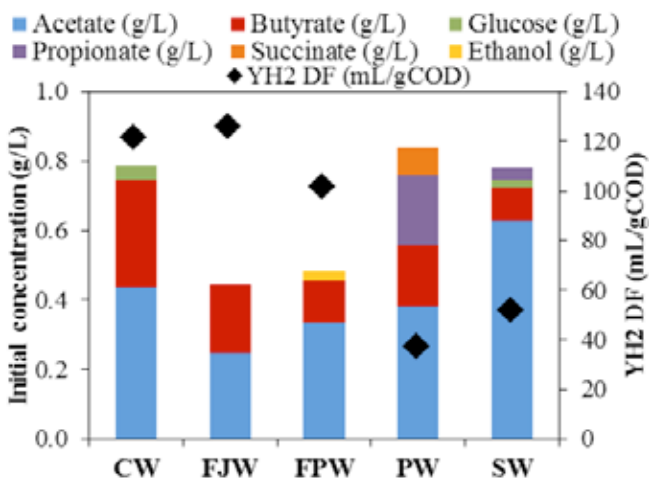


Fig. 1 - Yields of H_2 production in DF and composition of the different effluents obtained from the fermentation of CW, FJW, FPW, PW, and SW, used to feed the MECs.

MECs results show satisfactory performances in terms of Coulombic Efficiency (CE), cathodic hydrogen recovery and H_2 yield. Regarding the energy yields results showed, not only 100% of the electrical input energy could be recovered in all effluents, but at least twice energy amount (217%) could be generated by the combustion of hydrogen produced (Figure 2).

Interestingly, a complete conversion of metabolic by-products into acetate is first observed before acetate consumption started and current began to increase.

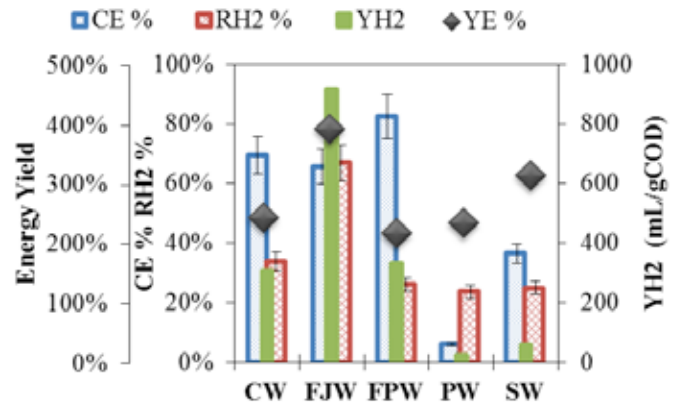


Fig. 2 - Coulombic efficiency (CE%), H_2 yield (YH₂), cathodic H_2 recovery (RH₂%) and Energy Yield (YE%) in MECs with different effluents.

IV. CONCLUSION

The results, shown in this paper, are the preliminary experimental data regarding the DF and MECs application for treatment and simultaneous energy recovery from real WWs. These results showed that coupling of DF and MEC for organic WW treatment constitutes a feasible and highly promising route in the environmental biorefinery framework.

ACKNOWLEDGMENT

This research was supported by Waste2bioHy project (FP7-MC-IEF -326974) and BITA Project (Marie Curie IRSES; PIRSES-GA-2011-295170) within the EU FP7.

REFERENCES

- [1] Hallenbeck, PC., Fermentative hydrogen production: Principles, progress, and prognosis. International Journal Hydrogen Energy, Volume 34, 2009, pp 7379-7389.
- [2] Rozendal, RA., Hamelers, HVM., Euverink, GJW., Metz, SJ., Buisman, CJN., Principle and perspectives of hydrogen production through biocatalyzed electrolysis. International Journal Hydrogen Energy, Volume 31, 2006, pp 1632-1640.
- [3] Logan, BE., Call, D., Cheng, S., Hamelers, HVM., Sleutels, THJA., Jeremiasse, AW., Rozendal, RA. Microbial electrolysis cells for high yield hydrogen gas production from organic matter. Environmental Science and Technology, Volume 42, 2008, pp 8630-8640.

MESSAGE FROM THE TRACK MANAGER

This is a study on MECs – not MFCs – which require energy to run, instead of generating energy. The Authors are therefore asked to include energy consumption figures by the MEC, and clarify whether this external energy input has been included in their coulombic efficiency calculations.



VARIABILITY AND COMPARABILITY OF TESTING PROCEDURES FOR PEMFC MODULES AND STACKS REGARDING PERFORMANCE AND SAFETY ASPECTS

Corinna Harms*, Katrin Nürnberg**, Thomas
Jungmann***, Frank Köhrmann*, Alexander Dyck*

*NEXT ENERGY · EWE Research Centre for
Energy Technology at the University of Oldenburg,
Carl-von-Ossietzky-Str. 15, 26129 Oldenburg, (Germany)

**Zentrum für BrennstoffzellenTechnik ZBT GmbH,
Carl-Benz-Straße 201, 47057 Duisburg, (Germany)

***Fraunhofer Institute for Solar Energy Systems ISE,
Heidenhofstraße 2, 79110 Freiburg, (Germany)

corresponding author: corinna.harms@next-energy.de

Performance and safety measurements are conducted in order to reach comparable and reliable testing procedures for PEMFC stacks and modules. These measurements include polarization curves and the investigation of voltage stability at different load levels. As a base the IEC 62282-2 standard is used regarding safety testing.

Index Terms - PEMFC stacks, testing procedures, performance measurement, standardization

I. INTRODUCTION

Testing procedures for fuel cells could be done on the single cell, the stack or the module level regarding different aspects like performance, endurance or safety. The values derived from these testing procedures should be comparable among different laboratories, which is an important aspect for fuel cell manufacturers and system integrators. But the prerequisites like test benches, gas qualities, sensor positions and measurement accuracies could be quite different and influence the results significantly. In order to reach comparable and reliable results a harmonization is necessary which could be reached by standardization. Fuel cell standards are available by the International Electrotechnical Commission (IEC) which

publishes International Standards, Technical Specifications and Technical Reports.

II. TESTING PROTOCOL

In this study we develop a testing protocol for PEMFC modules and stacks. A fuel cell module contains one or more fuel cell stacks and, if applicable, additional components [1]. This could be piping systems, electrical connections, means for conveying additional fluids and other [1].

The IEC 62282-2 standard is used as a base for safety testing for fuel cell modules [2]. We develop testing procedures for performance measurements which includes a reliable and reproducible polarization curve.

For the definition of the polarization curve a testing protocol generated within the European project "Development of PEM Fuel Cell Stack Reference Test Procedures for Industry (Stack-Test)" was adapted where mandatory and optional load points as well as holding times were defined [3]. These values were adapted and additionally for the PEMFC modules minimum, maximum, part and nominal load points were measured with a holding time of 30 min at each load point in order to evaluate the voltage stability over time.



The safety aspect is covered by gas leakage tests where either simultaneously the pressure on the anode and the cathode side is increased or a differential pressure is applied in order to detect external and internal leakages, respectively.

III. RESULTS

The testing protocol with the measurement of resulting terminal voltages in polarization curves and at different load points of a fuel cell module were repeated at least three times in order to evaluate the reproducibility. The resulting voltages were evaluated regarding stability at each load point.

The voltages of the fuel cell module "SuSy300" by balticFuelCells in figure 1 show a higher deviation of the voltages at low load points between the different measurements. At low voltages the voltages decrease slightly from the first to the last measurement.

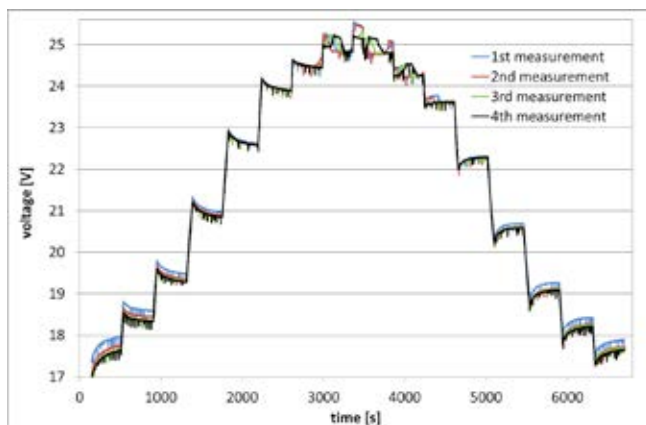


Fig. 1: Voltage characteristics of a fuel cell module during four measurements

Results from two fuel cell modules and one fuel cell stack will be presented.

IV. CONCLUSION

Testing procedures for performance and safety testing were adapted for PEMFC stacks and modules, which will help to generate a harmonization of testing and therefore to reach comparable results among various laboratories at different test bench types.

ACKNOWLEDGMENT

We acknowledge the funding for the project "VariPrüfBZ" from the Federal Ministry for Economic Affairs and Energy (BMWi) in Germany.

REFERENCES

[1] IEC 62282-1 ed3.0, Fuel cell technologies - Part 1: Terminology, publication date 2013-11-04, available to purchase on <https://webstore.iec.ch/publication/6751>

[2] IEC 62282-2 ed2.0; Fuel cell technologies - Part 2: Fuel cell modules, publication date 2012-03-26, available to purchase on <https://webstore.iec.ch/publication/6752>

[3] "Development of PEM Fuel Cell Stack Reference Test Procedures for Industry (Stack-Test)", European Union Seventh Framework Programme (FP7/2007-2013) under grant n° 303445, Polarisation Curve available at: <http://stacktest.zsw-bw.de/>



FABRICATION OF ANODE SUPPORTED MULTILAYER TAPE CASTED SOLID OXIDE FUEL CELLS: PERFORMANCE AND AGEING CHARACTERIZATION

D. Rodríguez*, B. Colldeforns**, M. Torrell**, M. Blanes*, F. Ramos*, A. Tarancón**

*FAE, Francisco Albero SAU, L'Hospitalet de Llobregat, Spain

**Catalonia Institute for Energy Research (IREC) Jardins de les Dones de Negre, 1, 08930-Sant Adrià de Besòs, Barcelona, Spain;

Performance of anode supported solid oxide fuel cells fabricated by multilayered tape casting has been characterized. Different anodic support porosity has been studied for different cells with equal thicknesses of electrodes and electrolyte. Tape casting multilayer technology allows achieving a precise control on the anode and electrolyte layers. Two different compositions of Ni-YSZ composite, 40%NiO-60%YSZ as a functional layer (AFL) and 40%NiO-60%YSZ as a support (ASL), together with a 10-15 μ m of dense YSZ layer have been fired as the base of the cell. A Ceria Gadolinium Oxide (CGO) diffusion barrier and LaSrCoFe₂O₃ (LSCF) cathode have been deposited above by screen printing generating the complete cell. A complete Solid Oxide Fuel Cell (SOFC) with excellent microstructure and performance through a fully industrial fabrication process has been obtained. Mechanical, microstructural and electrochemical characterization of the cells has been performed.

The electrochemical performance of the SOFC cell has shown a maximum power density of 850 mW/cm² at 750°C under pure H₂. Moreover a preliminary degradation test during more than 500h of galvanostatic operation has been achieved with no important degradation after a first stabilization zone.

Index Terms – Planar anode supported cells, ageing, electrochemical characterization, mechanical characterization.

I. INTRODUCTION

SOFCs are a highly efficient energy-conversion device that converts chemical energy into electric energy directly through electrochemical reaction [1], however the working temperatures and severe redox punctual conditions lead to degradation processes and a drop on the performance. [2]

The anode composition and microstructure plays a crucial role, ensuring the triple phase boundary catalytic activity and the percolation of the ionic and electronic conductivity paths [3]. Anode-supported SOFCs have been proposed as applicable

SOFCs with higher power densities, through thinner electrolytes available [4]. However, as thinner is the electrolyte, thicker anode support layers are needed in order to assure mechanical strength. Due to these thicker layers, the power densities of the cells are decreased by a larger resistance contribution of diffusion processes in the polarization resistance [5].

On the other hand, if the porosity of the anode support is increased in order to decrease the concentration polarization resistance, the activation polarization resistance is increased. To overcome these obstacles, ASL porosity has been analyzed.

Resulting from this work, anode supported cells with 20-30 μ m AFL (40%NiO-60%YSZ) and a support anodic layer (50%NiO-50%YSZ) of 160-170 μ m have been prepared, demonstrating a maximum power density of 850 mW/cm² at 750°C under pure H₂ and lifetimes over 500h with no important degradation after a first stabilization zone.

II. EXPERIMENTAL PROCEDURES

Half-cells composed of YSZ over YSZ-Ni AFL and ASL have been prepared by tape casting. YSZ (8% Y₂O₃-ZrO₂, KCeracell, South Korea), NiO (Kceracell, South Korea) and starch from rice (Sigma-Aldrich, Germany) have been used to prepare both anode layers and electrolyte. PEG 400 (Panreac, Spain), Duramax B1000 (Rohm and Hass, Germany) and Dolapix PC 75 (Zschimmer and Schwarz, Germany) have been used as plastizicer, binder and dispersant respectively, and water as solvent. The ratio of the YSZ slurry was 23:5:4:1:1 powder:solvent:binder:plastizicer:dispersant.

AFL slurry has been prepared in a similar way, mixing NiO:YSZ in a 3:2 ratio by ball milling and slurries prepared as YSZ slurries. ASL slurry has been prepared mixing NiO:YSZ:Starch in a ratio 7:4:0-1 by ball milling and slurries

prepared as YSZ and AFL ones.

The pore former has been removed at 500°C by 1h and samples sintered at 1350°C by 3h. Obtained half-cells presented an area of 11.5 cm² and a total thickness of 200-220 μm (ASL: 160-170 μm AFL: 20-30 μm Electrolyte: 8-15 μm). Single cells have been prepared by screen printing using GDC as diffusion barrier (2-3 μm) and LSCF as cathode(20-40 μm), respectively fired at 1200°C and 1050°C by 4h. Reduction was conducted heating single cells to 900°C at H₂ 5%N₂ atmosphere. Mid-long term performance has been done. Postmortem analysis comprised XRD and SEM.

III. RESULTS AND DISCUSSION

Based on the sintering program conditions as displayed in the experimental procedure, the influence of porosity in ASL on the cell performance has been determined. Different starch rates have been added obtaining porosity values reported in Table I. Porosity was found to have a significant effect on Young's modulus (E) and maximum tensile strength (σ) of half-cells before hydrogen reduction. Young's modulus and maximum tensile strength were found to decrease with porosity.

TABLE I. MECHANICAL PROPERTIES BY POROSITY

Sample	%Porosity	σ(MPa)	E (Gpa)
A	0.5	114± 34	39 ± 9
B	6.5	108 ± 25	26 ± 10
C	11.2	83 ± 32	13 ± 7
D	28	27 ± 7	8 ± 5

As it is shown in Figure 1, the power densities increase with increasing porosity, presenting a maximum in power density at C samples.

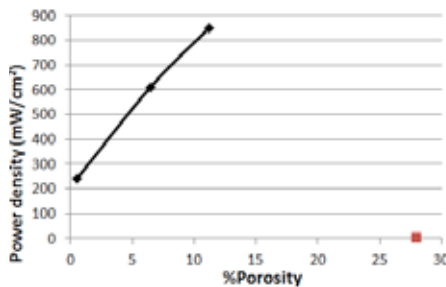


Figure 1. Relative porosity of the unreduced cells in front of power density.

Tape casted anode have shown a good microstructure with percolation of the both phases in the functional layer and an adequate value of porosity that ensures the diffusion of the H₂ and an adequate release of steam after the H₂ oxidation as it can be appreciated on the cross section micrograph of the figure 2. The power density of the tested C cell is 850mW/cm² extracting a current density of 1.3 A/cm² at 0.7V. (Figure 2)

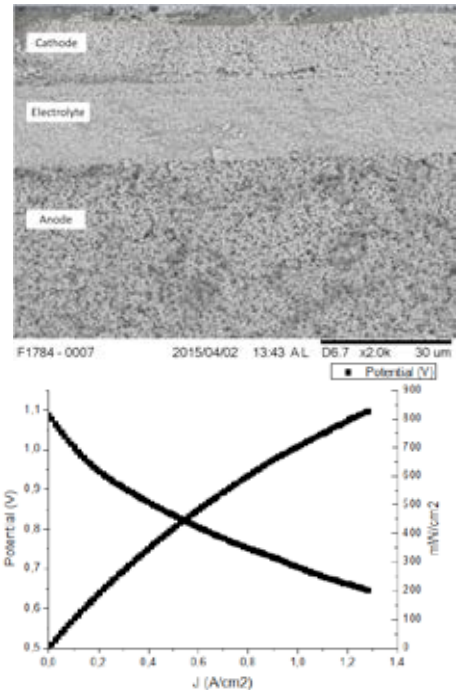


Figure 2. Cross section micrograph after reduction and polarization curve.

IV. CONCLUSIONS

Porosity represents a significant effect on the cell mechanical resistance due to young's modulus and maximum tensile strength, which was found to decrease with porosity. A value of porosity about 11% seems to bring a remarkable performance even when the cell is tested at mid-long term during 500h.

ACKNOWLEDGMENT

The authors thank to Centro para el Desarrollo Tecnológico Industrial (CDTI) for financial support (project Eureka-SCAPE-SOFC) as well as partners AMES and Kceracell.

REFERENCES

- [1] Ivers-Tiffée, E., Weber, A., Herbrist, D., Materials and technologies for SOFC-components. Journal of the European Ceramic Society, Volume 21(10), 2001, pp.1805-1811.
- [2] Ternér, M. R., Schuler, J. A., Mai, A., Penner, D., On the conductivity degradation and phase stability of solid oxide fuel cell (SOFC) zirconia electrolytes analysed via XRD. Solid State Ionics, Volume 263, 2014, pp.180-189.
- [3] Lim, T. H., Song, R. H., Shin, D. R., Yang, J. I., Jung, H., Vinke, I. C., Yang, S.S., Development of a 700W anode-supported micro-tubular SOFC stack for APU applications, Int. J. of Hydrogen Energy, Volume 33(9), 2008, pp.2330-2336.
- [4] Duncan, K. L., Lee, K. T., Wachsman, E. D., Dependence of open-circuit potential and power density on electrolyte thickness in solid oxide fuel cells with mixed conducting electrolytes. Journal of Power Sources, Volume 196(5), 2011, pp.2445-2451.
- [5] Virkar, A. V., Chen, J., Tanner, C. W., Kim, J. W., The role of electrode microstructure on activation and concentration polarizations in solid oxide fuel cells. Solid State Ionics, Volume 131(1), 2000, pp.189-198.



SOLID OXIDE CELL AND STACK TESTING, SAFETY AND QUALITY ASSURANCE (SOCTESQA)

M. Lang*, C. Auer*, K. Couturier**, E.R. Nielsen***, S.J. McPhail****,
N. Kotsionopoulos*****, Q. Fu***** and Q. Liu*****

*German Aerospace Center (DLR), 70599 Stuttgart, (Germany)

**Univ. Grenoble Alpes - CEA/LITEN, 38054, Grenoble, (France)

***Technical University of Denmark (DTU), 4000 Roskilde, (Denmark)

****Italian National Agency for New Technologies, Energy and Sustainable Economic Development (ENEA), 00123 Rome, (Italy)

*****Joint Research Centre – European Commission (JRC), 1755 LE Petten, (The Netherlands)

***** European Institute for Energy Research (EIFER), 76131 Karlsruhe, (Germany)

*****Energy Research Institute (NTU), Nanyang Technological University, Singapore 639798 (Singapore)

Abstract - For the successful market penetration of high temperature solid oxide fuel/electrolysis cell energy systems it is necessary to increase the quality assurance and the reliable assessment of the corresponding cells and stacks. Therefore in May 2014 the EU-funded project “SOCTESQA” was launched. The aim is to develop uniform and industry wide test programs for solid oxide cell/stack (SOC) assembly units. The paper presents the results which have been achieved so far, e.g. the development of a test matrix and of generic test modules for current-voltage curves, electrochemical impedance spectroscopy and long term tests. Several of these test modules were combined to a test program and applied by the different partners to an SOC stack. The test output results (TOPs) are compared to each other and possible differences are discussed in context to differences in test input conditions (sensitivity analysis). This validation process helps to improve the generic test modules and programs.

Index Terms – quality assurance, solid oxide cell/stack, standardization, test program

I. INTRODUCTION

High temperature solid oxide assembly units and the appendant test systems are very complex in structure and processing. There are many parameters which influence the test results and therefore have to be considered during testing. In order to simplify and harmonize test programs among different research facilities, laboratories and developers detailed test schemes, programs and protocols

are necessary - mainly as there is an increasing amount of application fields which are based on the operation of SOC cell/stack assembly in the fuel cell (SOFC), in the electrolysis (SOEC) and in the reversible SOFC/SOEC mode. The “SOCTESQA” project focuses on the development of robust and uniform test programs for experimental characterization of the specified SOC test object and the interpretation of measured data (Figure 1). The project builds on experiences of previous and ongoing EU-projects, e.g. “FCTESTNET” [1], “FCTESQA” [2] and “STACKTEST” [3] but also on the activities of relevant standards developing organizations, e.g. the International Electrotechnical Commission (IEC) [4].

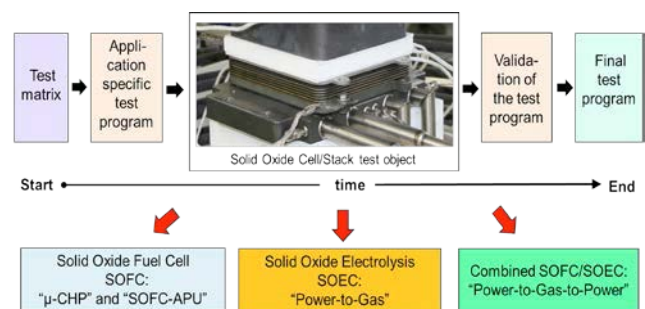


Fig. 1. Scheme of project objective

II. TEST MATRIX

A test matrix was developed which includes possible characterization methods, so called test modules (TM), covering the wide range of applications e.g. stationary SOFC μ -CHP, mobile SOFC APU and SOFC/SOEC power-to-gas systems. Altogether 18 test modules were specified. Important test modules are current-voltage curves, electrochemical impedance spectroscopy and long term tests under steady state or dynamic operating conditions.

III. INTERFACES BETWEEN TEST OBJECT AND TEST ENVIRONMENT

Special attention has to be paid on the interfaces between test object (SOC stack) and test environment (Figure 2). These interfaces can be separated in media, electric, heat and mechanical nature. Moreover the test input parameters (TIPs) and test output parameters (TOPs) at the interfaces have to be defined clearly. In the "SOCTESQA" project TIPs are defined as parameters whose values can be set in order to define the test operating conditions of the cell/stack. TIPs have to be controllable and measurable. On the other hand TOPs are parameters that indicate the performance of the cell/stack as a function of TIPs. Variation of TIPs leads to a response of the cell/stack indicated by the change of TOPs. TOPs do not have to be controllable but must be measurable.

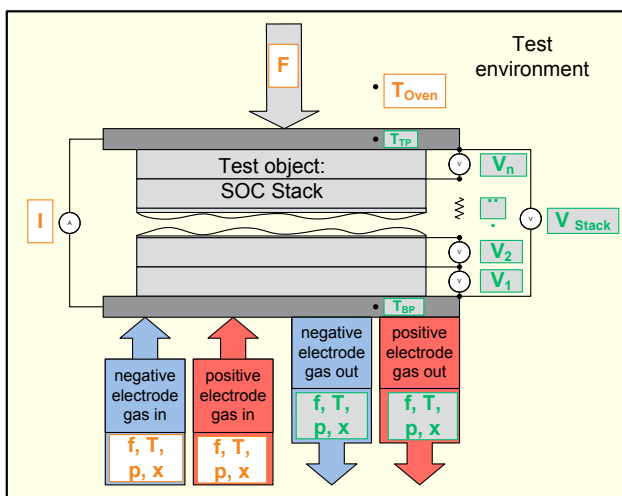


Fig. 2. Interfaces between SOC stack test object and test environment

IV. TEST PROGRAM

Fig. 3 shows a possible test program for durability testing as an example. It consists of a series of different test modules for characterization and performance evaluation, each module with its own specific objective as well as the test program objective. The initial and final current-voltage curve (TM02) qualifies the initial and final

performance. To identify the performance-limiting factor as well as the degradation mechanism the electrochemical impedance spectroscopy (TM03) is a useful tool. The applied test modules define the key parameters such as the current variation rate, gas flow rates, gas and stack temperatures, frequency range, excitation amplitude etc. as well as the way to present the data. Many applications require long term stable operation either under steady state or dynamic operation conditions. This issue is covered by the test modules "Operation under constant current" (TM12) and "Operation under varying current" (TM13), respectively.

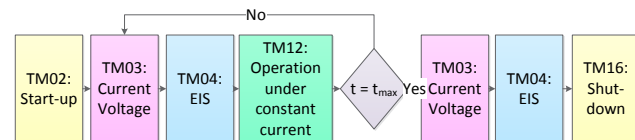


Fig. 3. Example of a test program for an SOC stack test object

This test program is currently applied by the different partners to identical SOC stacks and the results are compared to each other. With this review and validation loop the test modules and program are further optimized.

V. CONCLUSION

The proper definition and the monitoring of all interfaces between short stack and test station are very important. The first results between the partners show a high consistency. A high sensitivity of the stack behavior towards operating temperatures and the process gases was found. These high sensitivity parameters have to be addressed properly in the test modules and programs.

ACKNOWLEDGMENT

The authors gratefully acknowledge the funding of this project within the European Union's Seventh Framework Program (FP7/2007-2013) for Fuel Cells and Hydrogen Joint Undertaking (FCH-JU) under the grant agreement number 621245.

REFERENCES

- [1] FCTESTNET, WP2 Stationary Fuel Cell Systems: Test Programs and Test Modules, <http://iet.jrc.ec.europa.eu/fuel-cells/sites/fuel-cells/files/files/documents/060603%20FCTESTNET%20Stationary%20Applications.pdf>, (2006).
- [2] Website of the FCTESQA-project, <http://iet.jrc.ec.europa.eu/fuel-cells/about-fctesqa-project>.
- [3] STACKTEST, Master document, Test module drafts WP2, WP3, WP, 4, <http://stacktest.zsw-bw.de/downloads/>, (2014).
- [4] International Electrotechnical Commission: IEC TC 105, IEC 62282-1 TS: Fuel Cell technologies Part 1: Terminology, <http://webstore.iec.ch>, (2013).



COUPLING CONTINUUM AND PORE-NETWORK MODELS IN POLYMER-ELECTROLYTE FUEL CELLS

I. V. Zenyuk*, E. Medici**, J. Allen** and A.Z. Weber*

* Lawrence Berkeley National Laboratory, Berkeley, CA 94720, (USA)

** Michigan Tech. University, Houghton, MI 49931, (USA)

Abstract – Water transport in gas-diffusion layers (GDLs) with non-homogeneous morphologies was investigated with X-ray computed tomography (CT) and a combined continuum and pore-network model (PNM). The strong temperature-dependence at near-limiting current for polymer-electrolyte fuel cell (PEFC) was explained with a change in water-transport regime from liquid-phase at low temperature to vapor-phase at high temperature. Higher currents observed experimentally for stacked GDLs are possibly due to an extra low-transport resistance interfacial region that allows water redistribution between the layers.

Index Terms - Polymer-electrolyte fuel cells, coupled pore-network continuum models, x-ray computed tomography, water management

I. INTRODUCTION

Optimal water management is essential for the performance and stability of polymer-electrolyte fuel cells (PEFCs), especially those with next-generation material sets such as the nanostructured thin-film (NSTF) catalysts layers of 3M Co. [1]. Recent studies have suggested directing water transport through the anode improves low-temperature NSTF performance. Achieving high water-transport rates requires optimization of the anode GDL's morphology.

Continuum models use a volume-averaged approach to model liquid-water transport. This strategy is suitable for higher operating temperatures and homogeneous GDL morphologies. However, in this study, the optimal GDLs demonstrate a significant amount of inhomogeneity. To handle the complexity of the GDL morphology and access the expected capillary-fingering type of water transport in these porous media, pore-network models (PNMs) are utilized. While PNMs models capture water transport through the GDL, they do not contain suitable descriptions of the other layers, complex nonlinear transport, and electrochemical phenomena. Here, we combine

the advantage of both models in an iterative scheme integrating continuum and PN models to describe the multiphase and multiscale water transport properly.

This talk will discuss the work-flow between the coupled models including utilization of X-ray CT inputs. We will also provide physical understanding as to why various GDLs demonstrate different performance including optimal GDL design strategies. Of particular interest is why stacking GDLs can result in increased performance.

II. MATERIALS AND METHODS

A. X-ray Micro Computed Tomography

The tomography experiments were conducted at Beamline 8.3.2. at the Advanced Light Source (ALS). The source energy was 14 keV; the optics system consisted of sCMOS PCO.Edge camera, 0.5 mm LuAG scintillator and 5x lenses, resulting in pixel resolution of 1.33 μm . Additional details of tomography experiment are provided elsewhere [2]. The material set was single layer (1x) and two stacked layers (2x) of proprietary GDLs referenced here as X0155 GDLs.

B. Modeling

The coupling is achieved through an iterative scheme wherein the 2-D continuum PEFC model passes the calculated heat and mass fluxes to the PNM, where they act as spatially varying source terms. Subsequently, the PNM returns to the continuum model a set of effective properties, such as thermal conductivity, effective diffusivity, and permeability, which are discretized along the electrode|GDL interface. The two models are integrated within Matlab, which was also used for post-processing and data analysis. The in-depth details of the models coupling is provided in our earlier publication [3].



III. RESULTS

A. GDL Morphology

Fig. 1a shows the reconstruction of volume-rendered 2x X0155 and a cross-section grey-scale tomograph of the two layers. The fiber-density modulation is clearly seen, where regions of high and low fiber-density alternate. The in-between GDLs region features higher porosity. Fig. 1b shows the area-averaged porosity as a function of position. Significant variations (up to 0.08) in porosity are seen due to GDLs' fiber-density modulations. The interfacial porosity creates a tail in the pore-size distribution (PSD) as the inset shows. The PNM generates computational grid based on the PSD reported with X-ray CT.

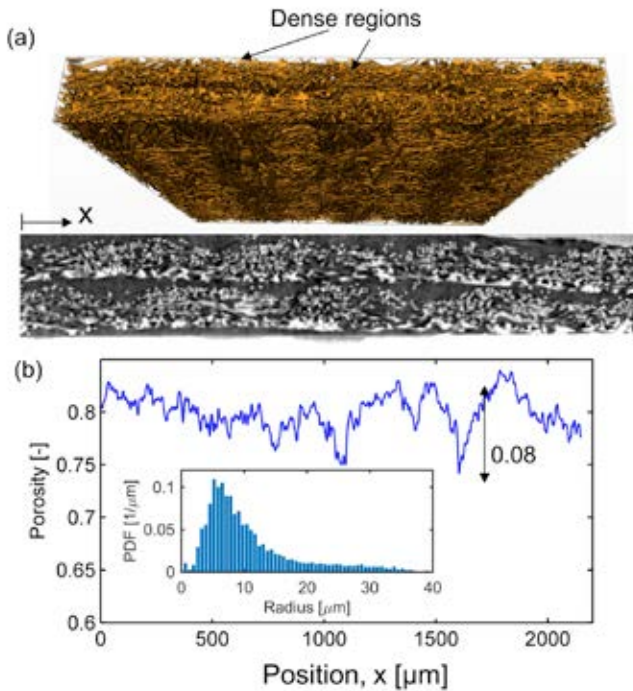


Fig. 1. a) A volume-rendered, stacked X0155 GDLs and a grey-scale tomograph. b) Associated area-averaged porosity and a pore-size distribution (inset).

B. Potentiostatic Temperature Sensitivity

Fig. 2a shows current as a function of temperature for a PEFC operating at 0.4 V, where the experimental data is complemented by modeling results for a 1x X0155 GDL. The model results are in good agreement with experimental data and a correlation is observed between the liquid pressure on the anode side and temperature.

Liquid-water pressure on the anode side at 40°C is 10 kPa and the water-front distribution by PNM is shown in Fig. 2b. In contrast, only several capillary-fingers observed at 80°C, which is in agreement with low (<1 kPa) liquid pressures in anode. At 40°C, water transport is predominantly in the liquid-phase, whereas at 80°C it is in the vapor-phase.

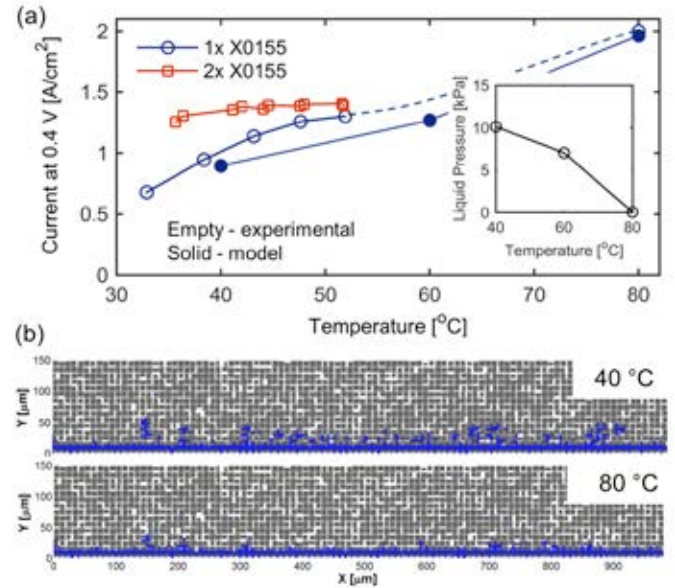


Fig. 2. a) Currents as a function of temperature and liquid pressure as inset. b) Associated water-front distributions from PNM at 40 and 80°C.

IV. CONCLUSION

Morphology of GDLs was input into a coupled Continuum-PNM to understand a correlation between porosity, PSD, anisotropy and PEFC performance. The temperature dependence of current was explained with change in transport regime from liquid- to vapor-phase going from low to high temperatures. Higher current for stacked X0155 GDL compared to single are currently under investigation.

ACKNOWLEDGMENT

This work was supported by the Assistant Secretary for EERE, FCTO, of the U.S. DOE under contract number DE-AC02-05CH11231 and DE-EE-0005667 in collaboration with 3M (who provided cost share) as well as with funds from the John F. and Joan M. Calder Endowed Associate Professor in Mech. E. – Engineering Mechanics at Michigan Tech. University. We thank beamline scientist Dr. Dula Parkinson for assistance with tomography set-up and image analysis.

REFERENCES

- [1] A.Z. Weber, R.L. Borup, R.M. Darling, P.K. Das, T.J. Dursch, W. Gu, D. Harvey, A. Kusoglu, S. Litster, M.M. Mench, R. Mukundan, J.P. Owejan, J.G. Pharoah, M. Secanell, I.V. Zenyuk, *Journal of The Electrochemical Society*, 161 (2014) F1254-F1299.
- [2] I.V. Zenyuk, D.Y. Parkinson, G. Hwang, A.Z. Weber, *Electrochemistry Communications*, 53 (2015) 24-28.
- [3] I.V. Zenyuk, Medici, E., Allen, J., Weber, A. Z., *International Journal of Hydrogen Energy* (Accepted) (2015).



THE OPENFUELCELL PROJECT: RECENT PROGRESS AND FUTURE DEVELOPMENTS

Steven Beale^{1,2}, Uwe Reimer¹, Dieter Froning¹, Werner Lehnert^{1,3,4}, Detlef Stolten^{1,5}

¹ Institute of Energy and Climate Research, IEK-3, Forschungszentrum Jülich GmbH, 52425 Jülich, Germany

² Queen's-RMC Fuel Cell Research Centre, Kingston ON K7L 3N6, Canada

³ Modelling in Electrochemical Process Engineering, RWTH Aachen University, Aachen, Germany

⁴ JARA – High-Performance Computing, Schinkelstraße 2, 52062 Aachen, Germany

⁵ Chair for Fuel Cells, RWTH Aachen University, Aachen, Germany

Abstract – This paper describes the ongoing development of a shared library of open source software, which is being used to obtain performance calculations for both high temperature polymer electrolyte, and solid oxide fuel cells. The openFuelCell code is built within the framework of the existing computational fluid dynamics suite, OpenFOAM. The present capabilities and features of the code are described together with details of applications and new developments currently in progress.

Index Terms – fuel cells, modelling and simulation, computational fluid dynamics, open source software.

I. INTRODUCTION

Computer codes have been used to model fuel cells for many years. Both polymer electrolyte membrane fuel cells and solid oxide fuel cells have benefited from the construction of mathematical models for cell and stack design, in addition to the gathering of experimental data on physical prototypes. Early researchers often compiled their own source code in FORTRAN or C. Subsequently, commercial computational fluid dynamics (CFD) packages, involving many person-years development time, and thousands (or millions) of lines of code, were adapted to include electrochemical processes; either by the code developer in conjunction with academic partners, or by the end-user using sockets provided by the vendor. See, for example, the reviews by Weber et al. [1] and Andersson et al. [2] on polymer electrolyte fuel cells (PEFCs) and solid oxide fuel cells (SOFCs), respectively.

Recently, the availability of well-written, open-source CFD codes has liberated the scientist/engineer from the dependence on commercial CFD software houses. Open source tools can themselves be used to build more open source tools. Some efforts are already underway to develop open source codes for modelling low temperature polymer electrolyte fuel cells (LT-PEFCs), for example, FAST-FC [3] and OpenFCST [4].

Novaresio et al. [5] describe a mass transfer library for SOFCs.

II. THE OPENFUELCELL CODE

A short summary of the development and structure of the code suite, openFuelCell [6], is given below. Initially a SOFC model was developed, but care was taken to design the code in a generic manner, so the subsequent adaptation to perform calculations for a high temperature polymer electrolyte fuel cell (HT-PEFC), which is the subject of a combined numerical-experimental programme of research at the Forschungszentrum Jülich, proved to be a logical extension.

The object-oriented code, OpenFOAM [7], is used as a basis for the openFuelCell library. It features a set of discretisation operators and solver classes, which allow for representation of systems of partial differential equations using equation mimicking. Virtual functions define the interface, and derived classes implement the functionality. This allows the user/programmer access to multiple choices of models, both new and pre-existing. A detailed technical description of the architecture and design of the code was given in [8].

The model is fully three-dimensional and based on a finite-volume method. Both galvanostatic and potentiostatic boundary conditions may be prescribed. At present, only steady runs have been conducted, but time-dependent operation may readily be incorporated. The model accounts for variable density, viscosity, conductivity, with several formulations for effective diffusion coefficients [9] in porous media, selectable at run-time. In the openFuelCell code, transport and electrochemistry are fully-coupled: The Nernst, Kirchhoff-Ohm, and Butler-Volmer (or Tafel) equations are solved for open-cell potential, current density, and overpotential(s) together with transport equations for pressure-coupled momentum, energy, and species.

Results have been obtained for both SOFC and HT-PEFC types. Multiple systems of equations are solved on 'child' meshes corresponding to different regions; air, fuel, membrane/electrolyte,

interconnect/bipolar plates. The energy equation is solved on a ‘parent’ mesh which encompasses all the ‘child’ meshes. Data are passed back and forth, as required. Figure 1 illustrates this schematically. The rationale facilitates code parallelization, and the code has successfully run on the Jülich Aachen Research Alliance (JARA) computing facility. Near-linear performance was observed on 960 cores.

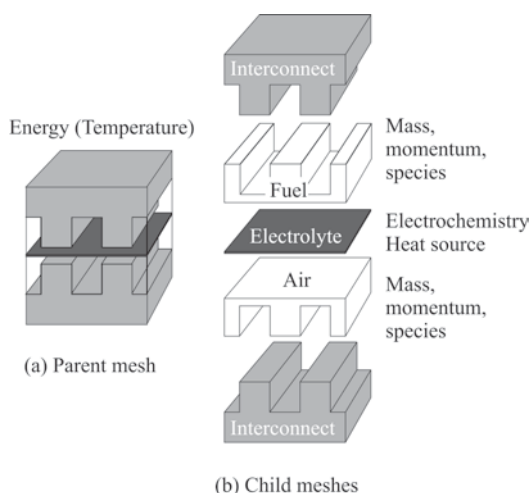


Fig. 1. Domains for ‘parent’ and ‘child’ meshes.

The openFuelCell code can also be used to model small stacks: A separate stack model based on volume-averaging, or distributed resistance analogy, has also been developed [10, 11]. Prescribing effective property values for fuel cells is a problem, since these are hard to measure. Detailed micro-scale models [12] have been used to calculate effective values of conductivities, diffusivities, and other mechanical properties. The code has also been used to conduct performance calculations for solid oxide electrolyzers [13].

The openFuelCell code is available on the open source community resource ‘SourceForge’ [6]. The source code is available to be ‘pulled’ together with documentation and instructions. The user can modify and re-compile the openFuelCell code; registered users may ‘push’ modifications onto the repository, by agreement. It is hoped to establish a special interest group of engineers and scientists advancing the state-of-the-art of fuel cell modelling, and thereby making fuel cell technology more competitive. The International Energy Agency Implementing Agreement on Advanced Fuel Cells has established an Annex [14] on open-source fuel cell modelling.

CONCLUSIONS AND FUTURE WORK

Future developments to the code include expanding the application from HT-PEFCs to include LT-PEFCs; this will involve replacing the single-phase solver with a run-time selectable two-phase scheme, and an additional module for describing water transport in the membrane and electrode passages. A more detailed cell-level model, based upon the

solution of two sets of Poisson equations for the ionic and electronic electric field potentials, in place of the Kirchhoff-Ohm approach is also currently under development.

The development of a shared library of electrochemical models will accelerate progress in research and development, by breaking down artificial barriers and avoiding unnecessary duplication of resources. The use of common platforms allows different groups to use, and add-to existing procedures, and at the same time to hide any specific details of engineering designs or scientific problems, which may be considered private intellectual property.

ACKNOWLEDGMENT

Numerous researchers contributed to the openFuelCell project. Special thanks are due to Ron Jerome, Hrvoje Jasak, Jon Pharoah, and Helmut Roth.

References

- [1] Weber, A.Z., et al., A critical review of modeling transport phenomena in polymer-electrolyte fuel cells, *Journal of the Electrochemical Society*, Volume 161 (12), 2014, pp. F1254-F1299.
- [2] Andersson, M., Yuan, J., Sundén, B., Review on modeling development for multiscale chemical reactions coupled transport phenomena in solid oxide fuel cells, *Applied Energy*, Volume 87(5), 2010, pp. 1461-1476.
- [3] <https://www.fastsimulations.com/>.
- [4] <http://www.openfest.mece.ualberta.ca/documentation.html>.
- [5] Novaresio, V., et al. An open-source library for the numerical modeling of mass-transfer in solid oxide fuel cells, *Computer Physics Communications*, Volume 183 (1), 2012, pp. 125-146.
- [6] <http://openfuelcell.sourceforge.net/>.
- [7] Weller, H.G., Tabor, G., Jasak, H., Fureby, C., A tensorial approach to computational continuum mechanics using object-oriented techniques, *Computers in Physics*, Volume 12(6), 1998, pp. 620-631.
- [8] Beale, S.B., et al. Open-source computational model of a solid oxide fuel cell, *Computer Physics Communications*, 2015, doi:10.1016/j.cpc.2015.10.007.
- [9] Cao, Q., Beale, S.B., Reimer, U., Froning, D., Lehnert, W., The Importance of Diffusion Mechanisms in High Temperature Polymer Electrolyte Fuel Cells, *ECS Transactions*, Volume 69(17), 2015, pp. 1089-1103.
- [10] Nishida, R.T., Computational Fluid Dynamics Modelling of Solid Oxide Fuel Cell Stacks, MASC thesis. Dept of Mechanical and Materials Engineering. Queen's University, 2013.
- [11] Nishida, R., Beale, S., Pharoah, J. Comparison of Solid Oxide Fuel Cell Stack Performance Using Detailed and Simplified Models. ASME 11th International Conference on Fuel Cell Science, Engineering and Technology. Minneapolis, MN, 2013.
- [12] Choi, H., Berson, A., Pharoah, J., Beale, S., Effective transport properties of the porous electrodes in solid oxide fuel cells, *Journal of Power and Energy*, Volume 225(2), 2011, pp. 183-197
- [13] Choi, H.-W., Pharoah, J.G., Ryland, D., Kettner, A., Gnanapragasam, N., Computational Fluid Dynamics Modeling of Solid Oxide Electrolysis Cell, *ECS Transactions*, Volume 57(1), 2013, pp. 3161-3170.
- [14] <http://www.ieafuelcell.com/>



SOFC IN AUXILIARY POWER UNITS (APU) FOR AERONAUTIC APPLICATIONS

L. Micoli, M. Turco, and V. Leone

University of Naples Federico II, p.le Tecchio 80 Napoli, (Italy)

Abstract - The present work is a feasibility study regarding the implementation of SOFC-APU technology in aeronautical applications. It shows the economic benefit that this solution could be introduced and a comparison in terms of emissions and reliability. Two different scenarios have been taken into account: a short-range mission with a Boeing 737-700, and a long-range mission with a Boeing 777-200LR. Also the ground emissions of Capodichino airport of Naples have been studied considering all aircrafts equipped with SOFC-APUs. The study shows that by using SOFC-APUs the fuel saved per year is more than 30%, even though the SOFC system is about four times heavier than the conventional gas turbine APU, and the corresponding weight penalty increases the amount of fuel burned by the aircraft. Also SOFC-APUs contribute to reduce CO₂, NO_x, HC and CO emissions in the airport of Naples and during the missions.

Index Terms – SOFC-APU, Aeronautic, Airport Ground Emissions.

I. INTRODUCTION

The growing attention to environmental issues and the stringent government regulations that are expected in the next future regard all the sources of pollutant emissions, including aircraft traffic. ICAO (International Civil Aviation Organization) forecasts that by 2020 the global international aviation emissions are projected to be around 70% higher than in 2005. In October 2013 ICAO agreed to develop a plan to achieve regulations for the aviation emissions by 2020.

At the present Fuel Cells (FCs) are the most promising technology in the field of power production with high efficiency and very low emissions, but they have not been employed in aeronautic yet.

Among the different types of FCs, Solid Oxide FCs (SOFCs) have recently attracted new attention due to their potential for use in stationary and distributed electric power stations as well as in transportation applications. Interest in SOFCs as an advanced Auxiliary Power Unit (APU) technology alternative for aircraft has been received increased attention [1]. Indeed, conventional APUs based on gas turbine account for 20% of

airport ground-based emissions. The reduction of airport ground emissions will continue to be a challenge due to the increased air travel. Moreover traditional APU and secondary aircraft systems are also responsible for 50% of the aircraft maintenance cost and some 15% of the delays. The APU system itself represents the third highest aircraft system cost in terms of repair and replacement [2].

The present work is a feasibility study regarding the implementation of SOFC-APU technology in aeronautical applications. It shows the economic benefit that this solution could be introduced and a comparison in terms of emissions and reliability.

Two different scenarios have been taken into account: a short-range mission, 1800 km (Naples-London) with a Boeing 737-700 equipped with the APU model GTCP 131-9B (CASE A), and a long-range mission, 9600 km (London-Tokyo), with a Boeing 777-200LR equipped with the APU model GTCP 331-500 (CASE B) [3].

Also the ground emissions of Capodichino airport of Naples have been studied considering only the mentioned aircrafts equipped with SOFC-APUs. This airport has 170 flight/day (arrivals and departures)-with an amount of about 5,8 millions of passengers per year.

II. FEASIBILITY STUDY

Generally it is complicated to assess the impact on business performance of any investment in innovation, thus it is necessary to introduce standard criteria and indicators for investments evaluation. Therefore, in addition to the assets and liabilities, for an effective economic analysis the following economic indicators have been taken into account to compare technical and strategic configurations and to identify the most appropriate scenario: the Discounted Cash Flow method (DFC), the Net Present Value (NPV) and the Internal Rate of Return (IRR) to measure and compare the profitability of investments, and the Payback Period (PBP) [4]. The period of the investment considered is 20 years.

Liabilities are costs related to the purchasing and installation of the plant, workforce, maintenance, raw materials, unexpected costs, management contracts and constitution, overheads and operating costs. These have been calculated according to the following cost modeling [5]:

$$C_j = \text{Tim} \cdot [\text{MC}_j + \text{OC}_j] \quad (1)$$

Where,

j = aircraft model,

C_j = installed APU's total operating cost for j -aircraft, for a single LTO cycle,

Tim (Time in mode) = APU operating time for each LTO cycle
 MC_j = maintenance cost for specific APU model installed on j -aircraft,

OC_j (Operating Cost) = management cost for specific APU model installed on j -aircraft, calculated considering the jet fuel consumption and costs.

Revenues consist in savings from lower fuel consumption, lower maintenance cost and lower unplanned maintenance, thanks to the SOFC technology.

Table I shows some relevant key features that have been taken into account in this feasibility study for both scenarios.

TABLE I

RELEVANT KEY FEATURES DISTINGUISHING A TRADITIONAL APU AND A SOFC-APU

Features	CASE A		CASE B	
	APU	SOFC-APU	APU	SOFC-APU
Electric Power, kWh/yr *10 ⁻³	344	299	545	471
Fuel consumption, kg/kWh	0.46	0.16	0.39	0.16
Fuel required, L/yr *10 ⁻³	194	62	251	93
Weigh, kg	160	788	245	1120
Lifetime, yr	20	5	20	5
Costs, \$ *10 ⁻³	700	280	1350	397
Maintenance costs, \$ *10 ⁻³	38	14	77	21

III. RESULTS

Table I clearly shows the economic benefit of a SOFC-APUs since it is cheaper in plant costs and maintenance costs. Furthermore this technology allows to save fuel more than 30% per year. Nevertheless the SOFC system is about four times heavier than the conventional gas turbine APU, and the corresponding weight penalty increases the amount of fuel burned by the aircraft. Moreover, the SOFC-APU must be replaced every 5 years.

Table II collects the principal economic indicators evaluated for CASE A and CASE B in order to define the strength of such investments. All indicators suggest that both investments are undoubtedly profitable, and these are more advantageous for CASE A scenario. It is worthy of note that the PBP of such investment is about 3 years.

TABLE II

ECONOMIC INDICATOR EVALUATED FOR BOTH SCENARIOS

Economic Indicators	CASE A	CASE B
NPV, \$ *10 ⁻⁶	4.9	3.0
IRR, %	49	29
PBP, yr	2.8	3.3

NPV, \$ *10 ⁻⁶	4.9	3.0
IRR, %	49	29
PBP, yr	2.8	3.3

The aircraft emissions per year have been evaluated for both scenarios. Results indicate that using a SOFC-APU the CO₂ emission are reduced by ~22% for the CASE A and by ~40% for the CASE B thanks to the fuel saved. SOx and HC emission are absent, while NOx and CO are reduced by ~40% and ~99% respectively thanks to FC technology.

Moreover the ground emissions in Capodichino airport of Naples has been taken into account considering that only the above mentioned aircrafts were equipped with a SOFC-APU. These aircrafts have 40 flights and 20 LTO cycle (Landing and Take Off) per day. Results prove that SOFC-APUs contribute to reduce by ~37% the CO₂ emission, by ~30% of CO, by ~30% of NOx, by ~70% of HC and by ~70% of SOx emission in the airport of Naples. It is worthy of note that this solution could contribute also to the reduction of noise of about 30%.

Another essential feature that should be considered in aeronautics is the failure of the applied technologies. The failure of a SOFC-APU is estimated of about 0.5 every 40000 hours of operation, this value is lower than many other devices onboard (i.e. the fuel pump is about 1.1 every 40000 h).

IV. CONCLUSION

The feasibility study conducted in this work on the implementation of SOFC-APU technology in aeronautical applications indicates that such kind of investment is profitable even though there are some points that should be improved regarding the lifetime and the weight of the SOFC.

REFERENCES

- [1] Hardman S., Chandan A., Steinberger -Wilckens R., Fuel cell added value for early market applications, Journal of Power Sources, Volume 287, 2015, pp. 297-306
- [2] Parker aerospace, Airbus to develop fuel cell tech for aviation, Fuel Cells Bulletin, Volume 2011, 2011, pp 4-10
- [3] <http://www.pmaaircraft.com/models.html>
- [4] Brealey R.A., Sandri S., Myers S.C., Principi di Finanza Aziendale - Capital budgeting, McGraw Hill
- [5] Gorinevsky, D., Dittmar, K., Mylaraswamy, D., Nwadiogbu, E., Model-based diagnostics for an aircraft auxiliary power unit, Control Applications, Volume 1, 2002, pp. 215-220



FEASIBILITY STUDY OF AN INTEGRATED PLANT ANAEROBIC DIGESTER-FUEL CELL

Angelo Ausiello, Luca Micoli, Domenico Pirozzi, Giuseppe Toscano and Maria Turco
*University of Naples "Federico II", Dipartimento di Ingegneria Chimica, dei Materiali e della
Produzione Industriale (DICMaPI), Ple Tecchio 80, 80125, Naples*

Abstract - Hydrogen can be easily converted to electricity by Fuel Cells (FCs) with high conversion efficiency and without greenhouse gas emission. At present, about 95% of H₂ is produced from fossil fuels, causing the emission of not renewable CO₂. The remaining 4% is from electrolysis and about 1% is produced from biomass. In alternative to fossil hydrogen can be produced from renewable sources, such as biomass by biological techniques. Biohydrogen can be produced by anaerobic digestion. The fermentation without light, or Dark Fermentation (DF), offers several potentialities since it is not subject to the limitations associated to the photosynthesis. The optimization of digestion process and the characterization of biogas produced are rigorously required in view of development of integrated systems digester-FCs for power production. This work is a feasibility study of a power system that integrate the FCs technology with the biohydrogen production by DF from several kinds of biomass: *Arundo donax* (not treated and treated by steam explosion), a giant reed and a Synthetic Medium were used in mesophilic conditions (38 °C). High rich hydrogen biogas were obtained with all substrates. Not treated *Arundo donax* gave the best results with H₂ concentrations up to 75% by volume.

Index Terms – *Arundo donax*, Biohydrogen, Dark fermentation, Fuel Cells

I. INTRODUCTION

Fuel Cells (FCs) are considered the solution of the future for the production of electricity for stationary and mobile power production. FCs are electrochemical devices that convert the chemical energy of a fuel, mainly H₂, directly into electricity, without an intermediate heat cycle, thus obtaining efficiencies higher than conventional thermal systems. Further advantages are related to the extremely reduced polluting emissions, the high power density and a modularity that allows a power ranges from a few kW to some MW. Hydrogen produced can be used as an energy carrier and feed a FCs to produce energy with low environmental impact [1]. Hydrogen can be produced from several kinds of biomasses by thermochemical or biological processes. In this study *Arundo donax* (giant reed), a non-food plant, has been selected as a source of lignocellulosic biomass for the production of biohydrogen by the *Dark*

Fermentation process (fermentation without light), that transforms, in presence of a pool of bacteria, sugars, starches and other carbohydrates or fermentable organic substrates into biogas containing mainly H₂ and CO₂ together with organic acids, alcohols and other by-products [2].

The objective of this work is to obtain H₂ by dark fermentation. An appropriate methodology to enhance the proliferation of hydrogen-producers bacteria to detriment of the methanogenic ones was developed. The amount of biomass needed to feed PEMFC (Proton Exchange Membrane Fuel Cell) was evaluated.

II. MATERIALS AND METHODS

A. Inoculum

In this work sewage sludge has been used as inoculum (then as pool of bacteria) obtained from a primary wastewater digester of Nola (Na). The sludge has been treated with a nutrient medium to support the growth of bacteria hydrogen producer (such as *Clostridium*) and to eliminate the methanogenic bacteria.

B. Biomass: *Arundo donax* and Synthetic Medium

Three different biomass were used: *Arundo donax* not treated (AD) and treated by steam explosion (ADexp) supplied by ENEA in Trisaia (Matera, Italy); a Synthetic Medium (SM) was used for comparison.

Arundo donax was collected from Torre Lama (Campania, Italy) agro-land. Leaves were separated from stems, washed, dried overnight at 80°C and minced with a chopper.

Tests were carried out with AD, and with ADexp treated at 210 °C for 6 min. AD and ADexp were subjected to enzymatic hydrolysis by the action of cellulase (Celluclast 1.5L, from Novozymes) and cellobiase (Novozyme 188, from Novozymes). Hydrolysis has been performed at 50°C for 72 h with 10% (w/v) of biomass in water and samples of hydrolyzed AD (ADH) and ADexp (ADHexp) have been obtained. The

hydrolyzate has been filtered (with filter paper) and the pH adjusted to 6.5.

SM was prepared with 19.6 mL of distilled water, 0.4 mL of resazurin solution 0.025% w/v; 10 mL of mineral solution (Na₂HPO₄ 7 g/L, KH₂PO₄ 3 g/L, NaCl 0.5 g/L, NH₄Cl 1 g/L and trace elements), 50 mL of solution 20 g/L of glucose; 250 µL of saline solution. For each substrates the volume was 100 mL with ratio biomass/inoculum of 80/20 (v/v). The fermentation were carried out in crimped vials with a volume of 125 mL.

C. Analytical techniques

In all tests, the microbial biomass (MB) growth, reducing sugars, volatile acids, ethanol and composition of the biogas have been monitored. The biomass concentration was monitored by measuring the optical absorbance of liquid samples at 600 nm. The concentration of glucose was measured by a modified Nelson-Somogyi method for reducing sugars. Concentration of acetic, butyric, propionic acids and ethanol was measured by GC technique, using a Shimadzu instrument GC-17A equipped with FID detector and a capillary column containing a PEG stationary phase (BP20, 30 m by 0.32 mm i.d., 0.25 µm film thickness, from SGE). Biogas (H₂ and CO₂) composition was determined by GC equipped with a TCD detector and a double packed molecular sieves-Porapack column.

III. RESULTS AND DISCUSSION

It has been developed a successful procedure to enhance the growth of hydrogen-producers bacteria to detriment the methanogenic ones. It results that for the SM, glucose concentration goes to zero after 48 h, while the biomass shows a first phase of growth, that corresponds to a peak of production of biogas, and a subsequent decrease due to death of bacteria. The trend is similar for the other two substrates, although sugars concentration goes to zero in 24 h, resulting into the higher production of biogas in the first day of testing[3]. The analysis of the liquid phase showed the presence of acetic acid, butyric acid, propionic acid and ethanol, the main product for all substrates being butyric acid (5 mg/mL for SM; 3 mg/mL for ADH and 4 mg/mL for ADHexp). The presence of VFA leads to the acidification of the solution with a consequent decrease of H₂ yield. Results indicate that the best performances are obtained by ADH with the highest MB growth and lower acids concentration. For all samples the H₂ yields are comparable or higher than literature data, so they are of interest for FCs technology and it is noticeable the absence of methane in the biogas confirming the effectiveness of the procedure used to enhance the H₂ yield. ADH gives the best results with a yield to H₂ of 1.34 with the H₂ concentration in the biogas higher than 70% (Tab. I). A feasibility study of an integrated plant digester/FCs of 1 kW with PEMFC ($\eta = 0.6$) is carried out taking into account the above results. The volume of biogas required, calculated by eq. (1), is about 560 L

$$\eta = P / (V \cdot Hi) \quad (1)$$

η = efficiency, P = power, V = volume of biogas, Hi = calorific value of hydrogen (10760 kJ/m³).

Then the amount of the raw biomass and the corresponding volume of culture are calculated and reported in table II.

TABLE I
BIOGAS COMPOSITION AND BIOHYDROGEN YIELD

Sample	V _{biogas} /V _{culture}	H ₂ (% vol)	CO ₂ (%vol)	H ₂ yield (mol H ₂ /mol glucose)
SM	2.5	36	64	0.89
AD	2.9	75	26	1.34
ADexp	2.3	69	31	1.14

TABLE II
BIOMASS REQUIRED FOR A POWER PLANT OF 1 KW

Sample	T _{digester} (°C)	Amount of substrates (kg)	Volume of culture (L)
SM	38	14.7	734.7
AD	38	17.3	193.1
ADexp	38	21.5	239.5

As expected the lowest volume and amount of culture correspond to AD. Considering that the price of AD is about 6.5 €/ton [4], a rough evaluation of the cost of the energy produced by an integrated plant digester/PEMFC is about 0.11 €/kW. This is a encouraging result because such cost should be competitive with the current price of energy (for example the ENEL price of energy is about 0.14 €/kW)–[5]. It must be remarked that the main beneficial advantage of this integrated plant is the zero environmental impact.

IV. CONCLUSIONS

This work have shown that the DF of AD is a promising process to obtain H₂ rich biogas that can be fuelled to FCs. Moreover it has been shown that this process should be competitive with the traditional fossil fuel based technology for energy production. Further studied are needed to improve the H₂ yields and to obtain a proper design of an integrated system digester/FC.

REFERENCES

- [1] Cigolotti V, McPhail S, Moreno A. Nonconventional fuels for high-temperature fuel cells: status and issues. *Journal of Fuel Cell and Science Technology*, Volume 6, 2009, pp. 021311-1-8.
- [2] Liu Y., Whitman W. B., Metabolic, phylogenetic and ecological diversity of the methanogenic archaea, *Annals of the New York Academy of Science*, Volume 1125, 2008, pp. 171-189.
- [3] Ausiello A., Micoli L., Pirozzi D., Toscano G., Turco M., Biohydrogen production by Dark Fermentation of *Arundo donax* for Feeding Fuel Cells, *Chemical Engineering Transactions*, Volume 43, 2015, pp. 385-390.
- [4] Dott. Di Benigno F., Workshop “Energia e Sostenibilità”, 20 Dec. 2013, Metaponto (Matera), Italy.
- [5] www.enel.it



THE METHOD FOR DESIGNING OXYGEN REDUCING BIOCATHODES INFLUENCES ELECTROCATALYTIC PERFORMANCES, ELECTRODES COLONIZATION AND BACTERIAL POPULATION OF THE BIOFILMS

M. Rimboud*, E. Blanchet*, A. Bergel, and B. Erable*

*Laboratoire de Génie Chimique, Université de Toulouse-CNRS, 4
allée Emile Monso, 31432 Toulouse Cedex 4 (France)

Abstract - The development of efficient microbial oxygen cathode is a determining factor for the future success of the microbial fuel cell technology. Several methods for microbial cathodes are described in the literature but nobody until now has systematically compared the interest of these different methods under identical conditions from a single source of oxygen reducing microorganisms.

Index Terms – microbial cathode, oxygen reduction, biofilm population analysis, reversible bioelectrode.

I. INTRODUCTION

Designing efficient microbial cathodes catalyzing oxygen reduction reaction (ORR) is a major issue in the development of microbial fuel cells (MFCs). The current performance of ORR microbial cathodes are limited (i) by the low solubility of oxygen in water (8 mg / L at 25 ° C) and (ii) by the low quantity of microbial catalyst that develops on the cathode [1]. A consistent part of the microbial communities selected in anodic biofilms is constituted of facultative aerobic microbes, and a first example that bioanodes could be converted into oxygen reducing biocathodes by a simple supply of air have been already demonstrated [2]. However, there are still, at present, scientific questions on these mechanisms of reversible electrochemical catalysis. Are they the same as those usually encountered in more conventional oxygen biocathodes biofilms obtained either under direct polarization or under open circuit potential of the electrodes with oxygen? Are they different microorganisms involved? And finally, is the electrocatalytic performance really better?

II. EXPERIMENTAL APPROACH

Six oxygen reducing biocathodes from compost leachate have been designed under 3 different experimental procedures: (CP: constant polarisation) two were formed under constant polarization at -0.2 V/SCE in presence of oxygen; (RE:

reversible electrode) two were polarized at the same potential in anoxic conditions and in presence of organic fuel (20 mM of acetate) before being reversed into microbial cathode by flushing the electrolyte by a constant flow of air; (OCP: open circuit potential) two were formed at open circuit (no potential applied). The performances of the six oxygen reducing microbial cathodes were compared by cyclic voltammetry, the different biofilms structures on electrodes imaged by epifluorescence and scanning electron microscopy and the microbial communities in the biofilms analyzed by 16S-DNA pyrosequencing.

III. RESULTS

A. Steady state performances for ORR at -0.2 V/SCE

After all the electrodes were colonized (15 days), the mean current densities for ORR were -0.3A/m^2 , -0.1A/m^2 and $<0.05\text{A/m}^2$ for CP, RE and OCP respectively. In steady state conditions, the forced aeration or the stirring the reaction mixture have consistently led to a reduction of the catalytic current for CP and RE biocathodes, (average values of 0.05A/m^2).

B. Colonization of electrodes by electroactive biofilms

As expected, three different types of colonization of the electrodes were observed (Fig.1). The colonization of electrodes left to the open circuit was sparse and rather diffuse. The cell density was clearly denser on conventional biocathodes formed under constant potential. Finally reversible electrodes were covered with a thick continuous biofilm encasing the entire surface of the fibers of the carbon felt.



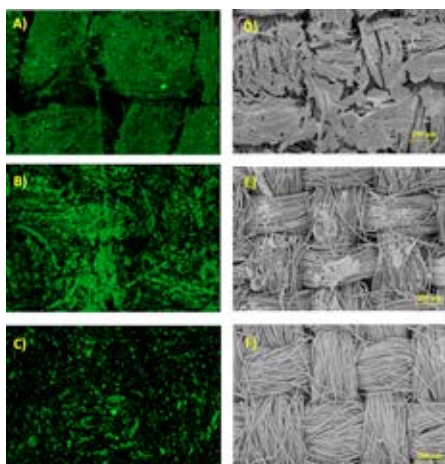


Fig. 1. Images of biofilms obtained by epifluorescence microscopy (A, B and C) and SEM (D, E, F) and respectively developed on reversible electrodes (A, D), OR biocathodes (B, E) and non-polarized electrodes (C, F).

C. Comparison of biofilms population

There are wide disparities between bacterial populations present on the electrodes depending on the different methods used for designing oxygen biocathodes (Fig.2). The populations identified on the reversible electrodes are relatively similar to those already reported in the work of Blanchet et al. [2]. The population diversity (as determined by the calculation of Simpson / Shannon indices) decreases gradually as the selection pressures are added (O_2 > potential of the electrode > acetate).

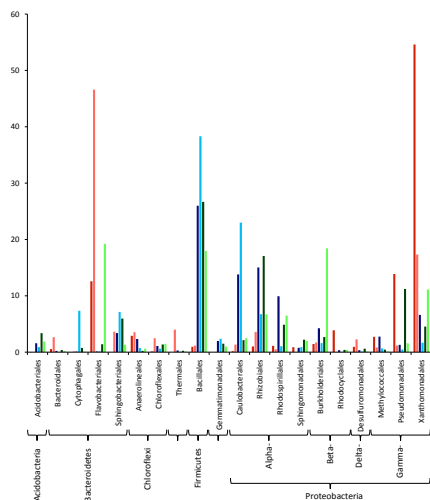


Fig. 2. Proportion of bacterial order represented in the six biofilms. Populations from reversible electrodes appeared in red, populations from OR biocathodes in blue, populations from non-polarized electrodes in green).

D. Electrocatalytic mechanisms for ORR

The two redox systems responsible for oxygen reduction identified here (Fig.3) demonstrated behaviors that made them biochemically different. They likely represented two different mechanisms for extracellular electron transfer from cathodes to

oxygen, which can be analyzed further by comparison to the existing literature.

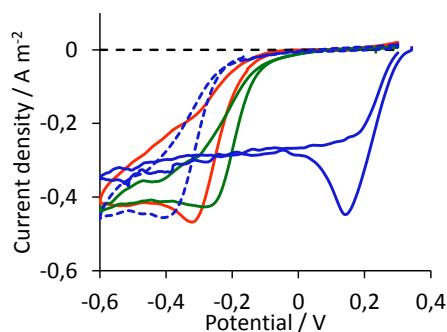


Fig. 3. Cyclic voltammeteries recorded on reversible electrode (red line), OR biocathode (plain and dotted blue lines) and non-polarized electrode (green line).

System I, centered at -0.31 V/SCE, was detected in all the biofilms grown in our experiments; it insured a basal activity for ORR in the biofilms. Comparatively, redox system II centered on $+0.19$ V/SCE developed only under sufficiently high polarization potential (potential superior to redox system I) and quiescent conditions (no hydrodynamic). The turbulences caused when gas fluxes or agitation were introduced in the reactors quickly led to disappearance, even if it was firstly briefly enhanced by the increased oxygen supply. Considering these results, it seemed logic to hypothesize that redox system II was a redox hydro soluble mediator locally concentrated inside the biofilm, which was easily washed out during supply of forced gas or under constant agitation.

IV. CONCLUSION

The method of forming oxygen biocathodes is inevitably accompanied by impacts on the electrochemical performance of the oxygen reduction mainly related to:

- (i) The structure of the catalytic interface. The mechanism and kinetics of microbial colonization are affected by the physicochemical conditions of the environment and the potential of the electrode.
- (ii) The selection of biofilm bacterial populations. Selection pressures imposed either by the potential of the electrode or by the presence of various soluble redox species in solution, lead to the predominance of different bacterial families.
- (iii) The transport phenomena in the reaction medium and in the electroactive biofilm which is set up on the electrode. Agitating the bulk is accompanied by the loss of the majority of the electrochemical signal of the oxygen reduction.

REFERENCES

- [1] Erable, B., Féron, D., Bergel, A., Microbial catalysis of the oxygen reduction reaction for microbial fuel cells: a review, *ChemSusChem*, Volume 5, 2012, pp. 975-987.
- [2] Blanchet, E., Pécastaings, S., Erable, B., Roques, C., Bergel, A., Protons accumulation during anodic phase turned to advantage for oxygen reduction during cathodic phase in reversible bioelectrodes, *Bioresource Technology*, Volume 173, 2014, pp. 224-230.



PURE HYDROGEN FEEDING A SOFC, BY THE ABATEMENT OF HYDROGEN SULFIDE AND CARBON DIOXIDE IN A CHEMICAL-LOOPING-THREE-STEPS PROCESS.

G. Mezzatesta*, S. Cavallaro*, V. Chiodo** and S. Freni**

* University of Messina – DIECII sez Chimica Ind.le, Viale Stagno
D'Alcontres, 31 - 98166 S. Agata di MESSINA, (Italy)

**ITAE-CNR, Salita S. Lucia sopra Contesse,5 - 98126 Pistunina
MESSINA, (Italy)

Abstract - This paper preliminary approaches the simultaneous separation of CO₂ and H₂S present in the composition of common flue gases. Two and three steps processes, based on traditional and innovative technologies, are comparatively examined on thermodynamic bases.

Index Terms – Carbon dioxide storage, Chemical looping combustion (CLC), Desulfurization, Multistep separation.

I. INTRODUCTION

One of the most important problems in marketing large-scale energy devices that use carbon fuels, is the management of CO₂. In particular, the SOFC with internal reforming of methane, natural gas, bio-gas from MSR or syn-gas obtained by gasification of solid fuels containing carbon, needs a reliable technology for CO₂ separation and storage. Extraction of CO₂ refers to two opposing strategic approaches: a) Post-combustion-capture: by recovering CO₂ from the anodic exhaust gas. b) Pre-combustion-capture: by the initial conversion of fuel in a gas mixture of CO₂ and H₂ followed by the separation and storage of CO₂ (at 30 to 35%). The post-combustion-capture takes advantage of the separation between anode and cathode compartments and let the SOFC behave like an "oxy-fuel" combustor, but, in any case, a pre-combustion-capture of H₂S is needed, because of the catalyst/anode easy poisoning. The chemical-looping-combustion (CLC) process is often indicated as a suitable way to separate CO₂ from fossil fuels, and further proposed as a system for increasing power station efficiency. In this paper we examine the use of a combined technology, in the aim of capture the H₂S and CO₂ before the SOFC feeding with pure hydrogen. Since the high

operating temperature of a SOFC, and the reversibility of the poison adsorption, also a reduction of H₂S can be adequate to avoid a remarkable catalytic decay.

II. THERMODYNAMICS

To quantify the adsorption behavior of mixing, as a function of temperature, a thermodynamic analysis has been made by using the *HSC-CHEM-5.1* computer program. The physical model was based on a three-steps process carried out on fluidized bed reactors filled by iron oxides. The analysis is based on the Gibbs energy minimization by assuming that:

- all stable phases have been considered
- all solids are chemically pure
- during the process T and P are constants
- equilibrium is reached.

The *HSC-CHEM-5.1* requires a pre-selection of thermodynamically stable species, but stable molecules that very slowly are formed, must be "a priori" excluded (*i.e.* diamond C). According with similar studies [1-2], we accounted as elements: the octatomic S₈, the graphitic C and the elemental Fe in a solid, crystalline form.

III. RESULTS AND DISCUSSION

As in a typical natural gas purification by an adsorber/desorber system, the H₂S-Fe₂O₃ mixture has been studied in the range 200-1000 °C. The H₂S/Fe₂O₃ molar ratio was stated to 0.001 while all other gaseous components (*i.e.* CH₄, CO_x, C_nH_(2n+2),...) have been accounted as inert (*i.e.* N₂). H₂S represents 0.7 vol% of the starting gas composition, while the solid/inert molar ratio is 8.0. Results are reported in Fig. 1a



and 1b for gaseous and solid state mix respectively. Values are normalized as 100 moles of each physical state.

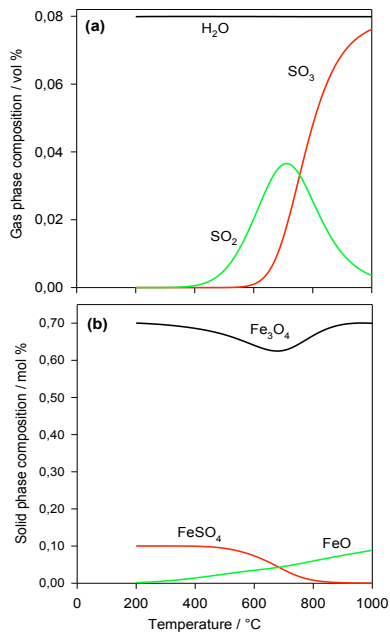


Fig. 1. Thermodynamics of H₂S on Fe₂O₃ system.

As intuitive, H₂S adsorption is stronger at lowest temperatures and the Fe₂O₃ is the most stable form of oxide (> 99 % - unreported). Some of FeSO₄ can be provided at T < 700K, while SO₂ is the main sulfured gaseous compound at mean temperatures (400-650 °C). At last, the large availability of the oxygen carrier (Fe₂O₃) moves the equilibrium to SO₃ at T > 700 °C. Alternatively, the present work propose the simultaneous CH₄ purification and transformation to H₂ by the three reactor plant used for chemical-looping hydrogen generation (CLH) system [3]. A scheme is reported in Fig. 2, while the related thermodynamic evaluations are reported in Fig. 3.

IV. CONCLUSION

With respect of other oxygen carriers, Fe₂O₃ has the advantages of being cheap and easily available, but has a relatively low active oxygen amount. Since the conversion of the fuel gas increases by increasing the solid/gas ratio, an acceptable amounts of H₂ released from the oxidizer reactor by using a molar excess of more than 5 times.

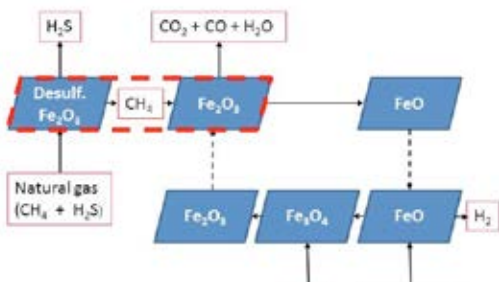


Fig. 2. CLH of poisoned methane on iron oxides.

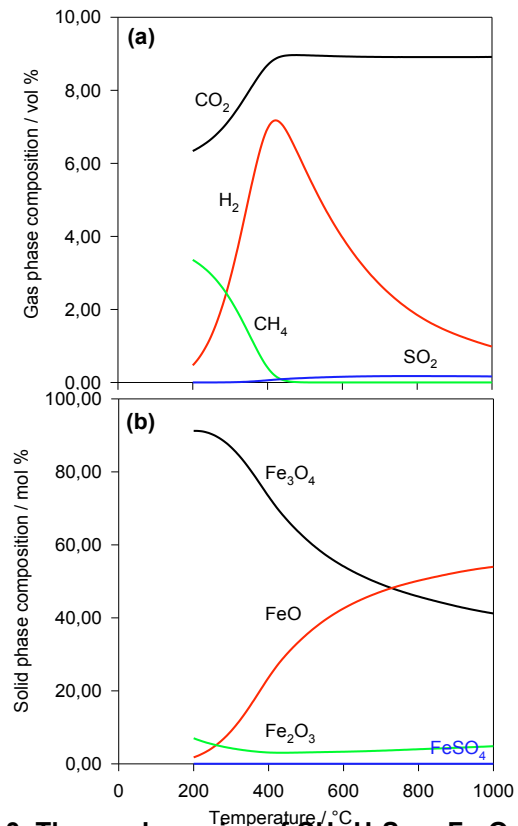


Fig. 3. Thermodynamics of CH₄-H₂S on Fe₂O₃ system.

Taking advantage of this “drawback”, the fuel doesn’t need to be desulphurised prior to combustion, because the formation of solid or liquid sulphides or sulphates, is compensated by a strong excess of iron oxide.

REFERENCES

- [1] Wang, B.; Yan, R.; Lee, D.H.; Liang, D.T.; Zheng, Y.; Zhao, H.; Zheng, C., *Energ. Fuel*, Vol. 22, 2008, pp. 1012–20.
- [2] Huang, Z.; He, F.; Zheng, A.; Zhao, K.; Chang, S.; Li, X.; Li, H.; Zhao, Z., *J. Sustain. Bioenerg. Syst.*, Vol. 3, 2013, pp. 33-9.
- [3] Kang, K.-S.; Kim, C.-H.; Bae, K.-K.; Cho, W.-C.; Kim, S.-H.; Park, C.-S., *Int. J. Hydrogen Energy* Vol. 35, 2010, pp. 12246-54.



A POWER MANAGEMENT SYSTEM FOR THE PARALLEL CONNECTION OF MICROBIAL FUEL CELLS WITH DIFFERENT ELECTRICAL CHARACTERISTICS

Diego Martínez Hernández¹, Enrico Dallago¹, Alessandro Liberale¹ and
Daniele Molognoni²

¹ Dept. of Electrical, Computer and Biomedical Engineering, University of Pavia, Pavia, Italy

² Dept. of Civil Engineering and Architecture, University of Pavia, Pavia, Italy

Abstract - In this work, we present a simple and efficient power management system for the parallel connection of an arbitrary number of Microbial Fuel Cells (MFCs), that can effectively work also with unbalanced cells (in terms of internal resistance and/or open circuit voltage). The system consists of a set of DC/DC step-up converters, namely boost converters, one for each MFC but all driven by the same signal, with a single output storage element.

Index Terms –Boost converter, Energy Harvesting, Microbial Fuel Cell, Power Management System.

I. INTRODUCTION

Microbial Fuel Cells (MFCs) are bioelectrochemical devices that convert the chemical energy contained in organic matter directly into electrical energy. So far, power achievable by a single MFC did not exceed few mW [1]. Practical MFC applications will therefore be carried out only by stacking a number of cells together (connected in series or parallel). However, both series and parallel connection of MFCs have some limitations. Series connection is only possible if the feeding lines of each MFC are kept physically separated, and with similar substrate concentration values. On the other hand, parallel connection is suitable to link MFCs immersed within the same electrolyte solution, but the cells have to be electrically similar. In this case, if one of the MFCs produces a lower voltage than the others, this cell stops working as a generator and starts acting as a load. Hence, the parallel MFCs connection, without any electronic control circuitry, is almost impracticable. In this paper, we present a simple and efficient power management system (PMS) for the parallel connection of a large number of MFCs, that can effectively work also with unbalanced cells (in terms of internal resistance and/or open circuit voltage). Each MFC is connected to its own DC/DC step-up converter (boost converter), but the output storage

element is common for all the cells. Thanks to the boost converter, it is possible to store energy at high voltage in the output capacitor. Moreover, the converter diode makes each MFC independent from all the others.

The system was designed with the aid of PSpice simulator. Values of inductances, frequency and duty cycle of the driving signal of the boost converters were chosen to make the cells work with a limited voltage ripple. An experimental set-up was afterwards developed in order to test the PMS behavior. A set of three MFCs, with different open circuit voltage (V_{OC}) and internal resistance (R_{INT}) were connected together in parallel through the proposed system, and the energy got from the MFCs was used to power a set of leds.

II. POWER MANAGEMENT SYSTEM

A detailed scheme of the system is show in Fig. 1. Each MFC is connected to an input capacitor ($10\ \mu\text{F}$), an inductor ($10\ \text{mH}$), a switch (N-channel mosfet) and a diode (BAT 85). The driving signal, the same for all the switches (a 3 kHz square wave with 50% duty cycle), is generated by a single astable multivibrator. The output capacitor C is common for all the step-up circuits, and its size can be chosen depending on the application. Every cell contributes to charging the output capacitor in a way proportional to its output electrical characteristics.

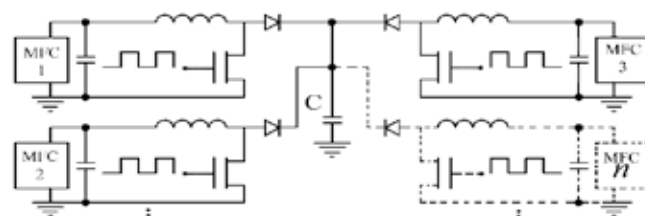


Fig. 1. Schematic design of the proposed power management system to stack MFCs in parallel configuration.

Moreover, if one or more MFCs of the stack would not work correctly, this does not affect the entire system. The number of MFCs can be extended to n units.

III. SIMULATIONS

The PMS was simulated using circuit level discrete models and a MFC basic electrical model. In particular, 3 MFCs were modelled: MFC1 had V_{OC} of 500 mV and R_{INT} of 500 Ω , MFC2 had V_{OC} of 300 mV and R_{INT} of 1000 Ω , and MFC3 had a V_{OC} of 100 mV and a R_{INT} of 1100 Ω .

Fig. 2 shows the simulated voltage across the output capacitor C (10 μ F) of the proposed system (V_{OUT_A}), together with the output voltage of other two configurations. For one of them (V_{OUT_B}), the 3 cells were linked to a single boost [2]. For the other one (V_{OUT_C}), all MFCs had their own step-up converter, as in Fig. 1, but the driving signals were feedback controlled [3]. This way, it was possible to obtain a system with maximum power point tracking (MPPT) capability [4]. It can be observed that both multiple boosts configurations (V_{OUT_A} and V_{OUT_C}) guarantee a significant efficiency improvement compared to the single boost (V_{OUT_B}). The performance difference between our proposed system (V_{OUT_A}), and a similar system implementing an additional MPPT algorithm (V_{OUT_C}), is negligible. In our opinion, the efficiency improvement due to the MPPT circuitry doesn't compensate the complexity and costs of the system.

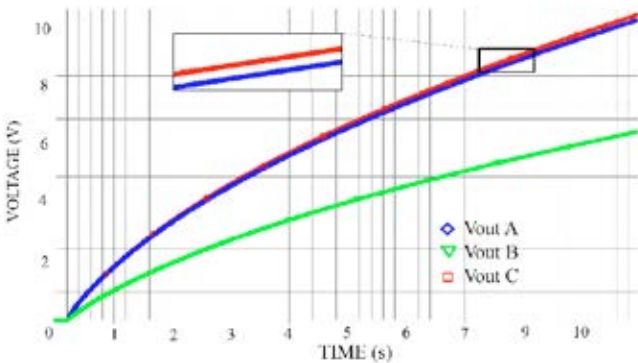


Fig. 2. Simulated voltage across the output capacitor C for three different PMS configurations.

IV. EXPERIMENTAL RESULTS

A prototype of the proposed PMS was manufactured on a board and tested with three bench-scale MFCs, as shown in Fig. 3, stacked in parallel configuration. Fig. 4 shows an experimental measurement, acquired with a Tektronix DPO4104 Oscilloscope. As load we used a set of leds, and consequently an output capacitor C of 1 mF was selected [5]. When the output capacitor is charged at 2.7 V, the load is connected to the system: the energy stored in C is used to turn the leds on, and the output capacitor is discharged. When the load operation is ended, the system restarts, recharging the capacitor.

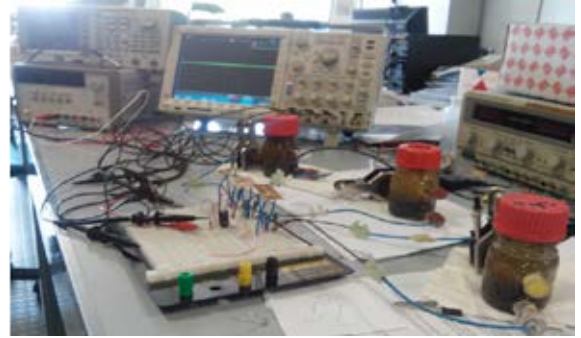


Fig. 3. Experimental set up.

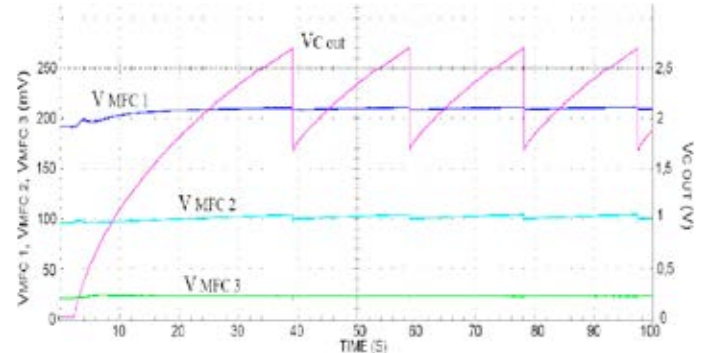


Fig. 4. Voltage across each single MFC (V_{MFC} 1, 2, 3) during the PMS operation, and voltage across the output capacitor C (V_{Cout}).

V. CONCLUSION

In this work, we present a PMS for the parallel connection of an arbitrary number of Microbial Fuel Cells, that can effectively work also in unbalanced cell conditions. The system can boost the voltage from the cells and store the energy in a single output capacitor, and every MFC contributes in a way proportional to its electrical characteristics.

ACKNOWLEDGMENT

Authors would like to thank Dr. P. Cristiani, Dr. A. Colombo and Dr. M. Grattieri for their contribution to this work.

REFERENCES

- [1] A. Meehen, H. Gao, Z. Lewandowski. "Energy harvesting with microbial fuel cell and power management system" IEEE Transactions on power electronics, Volume 26, No. 1. Pages 176-181, January 2011.
- [2] P. Wu, J. Biffinger, Fitzgerald, B. Rigeisen, "A low power DC/DC booster circuit designed for microbial fuel cells", ELSEVIER, Process Biochemistry, Volume 47, Pages 1620-1626, 2012.
- [3] N. Degrenne, B. Allard, F. Buret, P. Beliacqua. "Electrical energy generation from large number of microbial fuel cells operating at maximum power point electrical load". ELSEVIER, Journal of Power Sources. Volume 205, Pages 188-193, 2012.
- [4] D. Molognoni, S. Puig, M. D. Balaguer, A. Liberale, A. G. Capodaglio, A. Callegari, J. Colprim, "Reducing start-up time and minimizing energy losses of Microbial Fuel Cells using Maximum Power Point Tracking strategy", ELSEVIER, Journal of Power Sources, Volume 269, Pages 403-411, 2014
- [5] A. Liberale, E. Dallago, A. Lazzarini Barnabei, D. Molognoni, G. Torelli, "A self-starting power management device for Microbial Fuel Cells", 5th European Conference on Fuel Cell Technology and Applications, Rome, Italy, December 11-13, 2013.



STRONTIUM AND COPPER DOPED LANTHANUM COBALTITES: NEW CATHODE MATERIALS FOR SOLID OXIDE FUEL CELLS?

G. Eger,* A. Glisenti,* M.M. Natile,**

P. Batocchi,*** F. Mauvy***

* Dept. of Chemical Sciences - University of Padova
Via Marzolo, 1 35131 Padova, (Italy)

** CNR-IENI, INSTM; Dept. of Chemical Sciences
University of Padova Via Marzolo, 1 35131 Padova, (Italy)

*** CNRS - Université de Bordeaux, ICMCB, 87
Av. Dr. Schweitzer, F-33608 Pessac Cedex (France)

Abstract - Sr and Cu- doped Lanthanum and cobalt containing perovskites have been prepared by wet chemistry procedure and investigated. TPD experiments revealed that doping greatly increases the oxygen species desorption. The oxygen permeability was also determined in order to evaluate mixed ionic and electronic conductivity in addition to the surface activity in oxygen reduction reaction: in particular copper doping was observed to enhance permeability even at rather low temperature (500°C); the obtained results have been compared with those obtained by a Ruddlesden-Popper phase. Finally impedance spectroscopy measurements have been carried out on a symmetrical cell with $\text{Ce}_{0.9}\text{Gd}_{0.1}\text{O}_2$ as electrolyte, to better understand the effect of doping on electrochemical properties. High ionic conductivity is obtained with Sr doping.

Index Terms – MIEC, IT-SOFC, cobaltites, cathode

I. INTRODUCTION

Oxygen diffusion and mobility and ionic conductivity of LaCoO_3 have been studied as a function of oxygen partial pressure, temperature and doping [1-2]. Strontium substituted LaCoO_3 is characterized by high electronic and oxide ion conductivity and oxygen diffusivity at intermediate temperatures [3-5].

In the present work, Sr and Cu-doped LaCoO_3 have been studied and compared to undoped perovskite. Moreover a Ruddlesden-Popper perovskites was also considered.

II. EXPERIMENTAL

A. SYNTHESIS AND CHARACTERIZATION

Samples were synthesized by the well known citrate method.[6] The calcination temperatures were 600 ($\text{LaCo}_{0.5}\text{Cu}_{0.5}\text{O}_{3-\delta}$ – hereafter $\text{LaCo}_{0.5}\text{Cu}_{0.5}\text{O}_3$), 650 (LaCoO_3), 900°C ($\text{La}_{0.5}\text{Sr}_{0.5}\text{Cu}_{0.5}\text{Co}_{0.5}\text{O}_{3-\delta}$ – hereafter $\text{La}_{0.5}\text{Sr}_{0.5}\text{Co}_{0.5}\text{Cu}_{0.5}\text{O}_3$, $\text{La}_2\text{Cu}_{0.8}\text{Cu}_{0.2}\text{O}_{4+\delta}$ – hereafter $\text{La}_2\text{Cu}_{0.8}\text{Cu}_{0.2}\text{O}_{4+\delta}$).

XPS measurements were carried out with a Perkin Elmer Φ 5600ci Multi Technique System. XRD analyses with a Bruker D8 Advance diffractometer (Cu $K\alpha$ radiation). O_2 -TPD measurements (after treatment with O_2) were performed with an Autochem II 2920 Micromeritics connected with a QMS. Electrochemical measurements were performed using a Modulab Frequency Response Analyser (Modulab XM ECS).

III. RESULTS

A. CHARACTERIZATION

XRD patterns show the presence of the desired phase in all the samples. The slight shift of the peaks toward lower angles confirms the incorporation of the dopants into the perovskitic cell. XPS peak positions and shapes agree with how expected for the perovskites. The main effect of doping is in surface hydroxylation more evident in the Cu-doped perovskite. Both in the undoped and Cu-doped LaCoO_3 the surface segregation of Lanthanum is evident.



B. O₂-TPD Type Sizes and Typefaces

In the undoped LaCoO₃ β-oxygen was observed to desorb at 775°C. α- and β- oxygen species desorb from the Cu-doped LaCoO₃. In the LaCo_{0.5}Cu_{0.5}O₃ sample both α- (around 300°C) and β-oxygen desorptions (850 and 1050°C) are evident. In the Sr and Cu-doped sample the α-oxygen desorption signal shifts toward higher temperatures (370°C); the intense and broad β-oxygen desorption signal is composed by several components at 870, 910, and 1000°C corresponding to the presence of non equivalent species. The desorption of α- and β-oxygen species is significantly enhanced by Cu and Sr doping.

C. Oxygen permeability tests

Figure 1 summarizes the obtained outcomes for the oxygen permeation through LaCoO₃, La_{0.5}Sr_{0.5}Co_{0.5}Cu_{0.5}O₃ and LaCo_{0.5}Cu_{0.5}O₃, La₂Cu_{0.8}Co_{0.2}O₄ pellets.

The O₂ permeability of La_{0.5}Sr_{0.5}Co_{0.5}Cu_{0.5}O₃ at low temperatures (≤ 500°C) is very similar to that of the LaCoO₃ but significantly increases with temperature. LaCo_{0.5}Cu_{0.5}O₃ shows a better O₂ permeation than LaCoO₃ (the O₂ flow appears about 2 times higher) suggesting an interesting capability of LaCo_{0.5}Cu_{0.5}O₃ to operate as cathode. The raise in permeation performance can be due to the increase of oxygen vacancies and thus in oxygen mobility, favoured by Cu doping. Slightly higher permeation is observed with La₂Co_{0.2}Cu_{0.8}O₄ probably due to the rock salt layer [7].

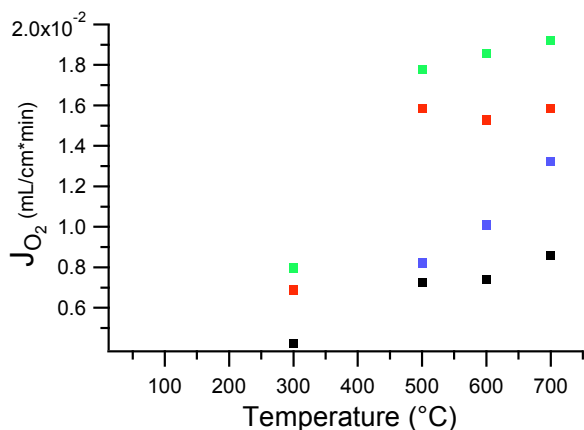


Fig. 1. Oxygen flux obtained in the permeation test for LaCoO₃ (black), LaCo_{0.5}Cu_{0.5}O₃ (red), La_{0.5}Sr_{0.5}Co_{0.5}Cu_{0.5}O₃ (blue), La₂Cu_{0.8}Co_{0.2}O₄ (green).

D. Electrochemical measures

Electrochemical measurements are carried out on two symmetric half cells: LaCo_{0.5}Cu_{0.5}O₃/CGO/LaCo_{0.5}Cu_{0.5}O₃ and La_{0.5}Sr_{0.5}Co_{0.5}Cu_{0.5}O₃/CGO/La_{0.5}Sr_{0.5}Co_{0.5}Cu_{0.5}O₃. The comparison between the obtained data and those reported in literature allows to confirm that the ASR (Area Specific

Resistance) is strongly decreased by doping; the doping with Sr and Cu, in particular, allows obtaining very interesting values (less than 0.1 Ω cm⁻¹ for T ≥ 650°C). This is presumably due to the effect of dopants in the formation of new vacancies. The global electrical conductivity can be approximated as the electronic conductivity of the material since the ionic conductivity is less than 100 mS*cm⁻¹.

IV. CONCLUSION

Cu and Sr-doped LaCoO₃ perovskites are investigated in order to verify their performances as cathode materials for IT-SOFCs and their behaviour is compared with that of the undoped LaCoO₃ and of a LaCu_{0.8}Co_{0.2}O₄ RP-perovskite. Diffraction patterns indicate the formation of the desired phase and the absence of impurity phases. The O₂-TPD results indicate that doping significantly enhances α- and β- oxygen desorption. The permeability measurements indicate good performance for the doped perovskites: Cu doping, in particular, seems to favour the permeation even at low temperature (500-600°C). Preliminary electrochemical measurements carried out on symmetric half cells seem to suggest a interesting performance of the La_{0.5}Sr_{0.5}Co_{0.5}Cu_{0.5}O₃ cathode (ASR lower than 0.1 Ω cm² at 700°C)..

REFERENCES

- [1] D.S. Tsvetkov, A.I. Vylkov, A. Yu. Zuev, A.N. Petrov The diffusion of oxygen and ion transport in lanthanum cobaltite LaCoO_{3-δ} Russ. J. of Phys. Chem. A Vol. 82, 2008, pages. 855-859.
- [2] S.Royer, D. Duprez, and S. Kaliaguine, Role of bulk and grain boundary oxygen mobility in the catalytic oxidation activity of LaCo_{1-x}Fe_xO₃ J. Catal., Vol. 234, 2005, pages 364-375.
- [3] V.V. Srdić, R.P. Omorjan, J. Seydel; Electrochemical performances of (La,Sr)CoO₃ cathode for zirconia-based solid oxide fuel cells Mater. Sci. Eng. B Vol. 116, 2005, pages 119-124 and references therein.
- [4] W. Presis, W. Bucher, W. Sitte Oxygen exchange measurements on perovskites as cathode materials for solid oxide fuel cells J. Power Sources Vol. 106, 2002, pages 116-121.
- [5] A.V. Berenov, A. Atkinson, J.A. Kilner, E. Bucher, W. Sitte; Oxygen tracer diffusion and surface exchange kinetics in La_{0.6}Sr_{0.4}CoO_{3-δ} Sol. State Ion. Vol. 181, 201, pages 819-826.
- [6] A. Glisenti, A. Galenda, M.M. Natile Steam reforming and oxidative steam reforming of methanol and ethanol: the behaviour of LaCo_{0.7}Cu_{0.3}O₃; Appl. Catal. A. Gen. Vol. 453, 2013, pages 102-112.
- [7] A. Galenda, M.M. Natile, A. Glisenti Oxygen permeation measurements: an alternative tool to select new intermediate temperature solid oxide fuel cell cathodes. Nanosci. Nanotechnol. Lett. Vol. 3, 2011, pages. 723-730.



CONVION SOFC SYSTEM DEVELOPMENT – EVALUATION OF MULTISTACK ARRANGEMENT

H. Stenberg*, K. Åström*, and E. Fontell*

*Convion Ltd., Tekniikantie 12, 02150 Espoo, Finland

Abstract - The C50 fuel cell product designed and manufactured by Convion was operated for approximately 1600 hours and produced roughly 20 kW of electric power with efficiency exceeding 50 %. The fuel cell system contained a multistack arrangement consisting of 32 MK351 stacks. The stacks performed evenly throughout the test period implying a balanced distribution of fuel. The estimated average stack degradation rate was 0.7 %/1000 h.

The behavior of individual stacks in the multistack arrangement was evaluated by changing operation conditions. The average stack voltage was decreased by 1.7 % when stack temperature was decreased by 15 °C. Stacks at higher temperatures experienced smaller voltage drops. Increasing fuel utilization by 3.5 % reduced voltages by 1.3 %, but increased electrical efficiency. Decreasing stack current by 22 % increased average stack voltage by 4.3 %, but differences in stack behavior were observed.

Index Terms – Degradation, multistack, SOFC system

I. INTRODUCTION

Convion has started validation of a new, highly innovative C50 fuel cell product able to produce 58 kW of electricity. In the validation phase, the C50 product contained a third of the nominal stack amount. The multistack arrangement consisted of 32 MK351 stacks and was designed and assembled by Convion. The MK351 stacks were produced by Fraunhofer IKTS.

The system produced roughly 20 kW of electricity with efficiency exceeding 50 % and was operated according to plans for 1600 hours before it was shut down for analysis and modifications. The purpose of this paper is to evaluate stack performance and degradation in the multistack arrangement.

II. EVALUATION OF THE MULTISTACK ARRANGEMENT

The design of the multistack arrangement was evaluated by analyzing the performance and behavior of the 32 stacks.

A. Stack Performance

The average stack performance in the multistack arrangement was in agreement with the steady state modelling results done prior to

system start. Relative stack voltages measured during the test period are presented in Fig. 1.

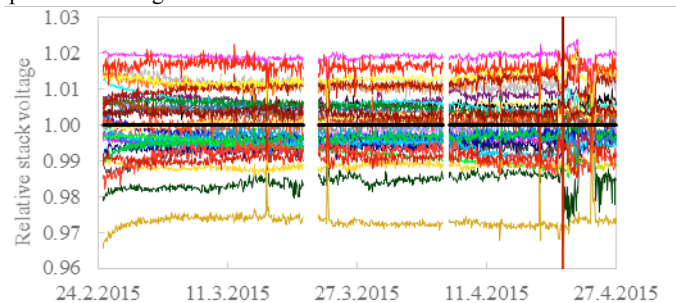


Fig. 1. Stack voltages relative to the average voltage (black line) during the test period. Different colors represent different stacks.

The stacks performed evenly throughout the test period and as seen in Fig.1, most of the stack voltages were within 1 % of the average voltage. The best stack was roughly 2 % above and the worst stack roughly 3 % below the average level.

B. Degradation

The average degradation rate during the test period was 1.4 %/1000 h. However, half of the total degradation was caused by system stops and actual stack degradation rate was estimated to be 0.7 %/1000 h. The relative evolution of stack voltages during the test period are presented in Fig. 2.

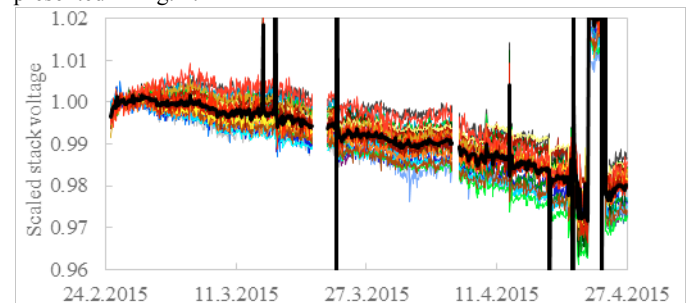


Fig. 2. Degradation of stack voltages during the test period. Different colors represent different stacks, black is the calculated average.

As seen in Fig. 2, the degradation of the stacks differed during the test period. The actual degradation rate ranged from 0.2 %/1000 h for the best stack to 1.1 %/1000 h for the worst stack. The discontinuities in Fig. 1 and Fig. 2 were caused by system stops, operation condition changes and data logging failures.

C. Stack Temperature

The effect of stack temperature on stack performance was investigated by lowering the stack temperature control set point by 15 °C. The temperature of every other stack was measured. The temperature distribution of the stacks and the effect of the temperature drop are presented in Fig. 3.

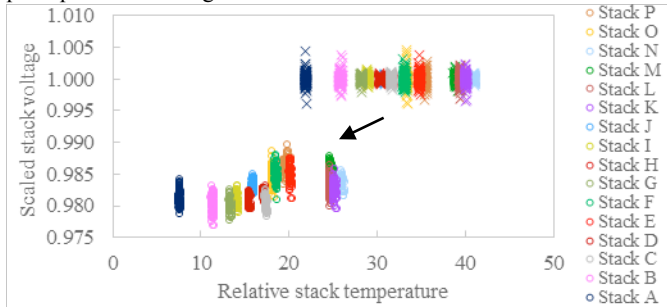


Fig. 3. Effect of changing stack temperature on stack voltages.

The stack voltages decreased by 1.4–2.0 % and the average voltage drop was 1.7 %. As seen in Fig. 3, the temperature difference between the hottest and coolest stack was more than 10 °C, and the average voltage drop of the hottest stacks was smaller than the average voltage drop of the coolest stacks.

D. Fuel Utilization

The effect of fuel utilization on stack voltages was investigated by decreasing fuel flow and thus increasing total system fuel utilization. The decrease was approximately 3.5 % of the original fuel flow. The effect of increased fuel utilization on stack voltages is presented in Fig. 4.

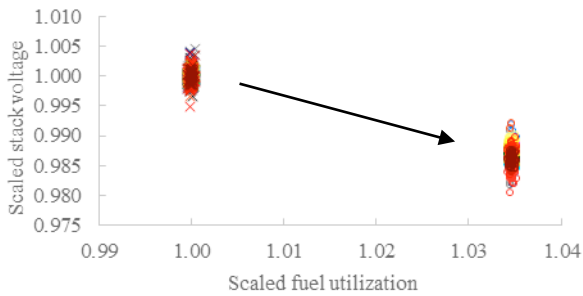


Fig. 4. Effect of changing fuel utilization on stack voltages. Different stacks shown with different colors.

Increasing fuel utilization by 3.5 % decreased the average stack voltage by 1.3 %. As a consequence, the electrical efficiency of the system was increased by 1.6 percentage points. As seen in Fig. 4, the stacks experienced nearly equal voltage drops: the voltage drops of 29 of the 32 stacks were between 1.18 % and 1.42 %. This indicated a balanced distribution of fuel to the stacks when the system is operated under the nominal load.

E. Stack Current

The effect of electric current on stack voltages was investigated by

lowering the current by approximately 22 %. Fuel utilization was not changed, hence fuel feed was also reduced by 22 %. Results are presented in Fig 5.

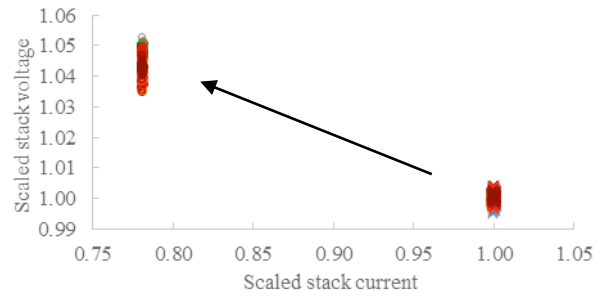


Fig. 5. Effect of changing electric current on stack voltages. Different stacks shown with different colors.

Lowering electric current by 22 % increased the average stack voltage by 4.3 %. However, as seen in Fig. 5, there were notable differences between the voltage increments of individual stacks. For example, the voltages of two worst stacks increased by 3.7 %, whereas the voltages of three best stacks increased by 4.9 %. The difference might have been caused by the smaller fuel flow and thus less well balanced distribution of fuel to the stacks.

III. CONCLUSION

The C50 product was successfully operated for 1600 hours and produced roughly 20 kW of electricity with an electrical efficiency of more than 50 %. The tested fuel cell system contained 32 stacks, far more than in typical test systems, integrated into a multistack arrangement. The MK351 stacks performed evenly in the arrangement and the actual degradation rate was anticipated. System stops affected stack degradation, but the stops were caused by signal disturbances in the instrumentation system, not by the fuel cell process.

The expected stack performance and degradation rate was an indication of good stack quality and successful multistack arrangement design. Especially the distribution of fuel flow to the stacks appeared to be very well balanced, and electrical efficiency could be further increased by finding the optimal fuel utilization. However, stack temperatures were not completely even, causing differences in stack behavior when the stack temperature set point was changed. In addition, decreasing electric current by substantially reducing fuel flow appeared to negatively affect the distribution of fuel flow to the stacks.

To summarize, the validation of the C50 product was more than successful and gave crucial information on how the multistack arrangement as well as the complete fuel cell process can be further developed.

ACKNOWLEDGMENT

The authors want to thank all partners who have helped Convion to manufacture and validate the first C50 product.



SIMULATION AND EXPERIMENTAL INVESTIGATION OF A PARALLEL SERPENTINE-BAFFLE FLOW FIELD PLATE AGAINST FUEL CROSSOVER IN A DE-PEMFC

P. Belchor^{1***}, G. S. Oliveira^{2*}, G. C. Benetti^{3*}, M. M. C. Forte^{4**}, V. Ferreira^{5*},
R. A. Milani^{6*}, and G. K. Col^{7*}

^{*}UNOESC, Rua Getúlio Vargas, 2125 – Flor da Serra, Joaçaba-SC, 89600-000, (Brazil)

^{**}UFRGS, Av. Bento Gonçalves, 9500 – Agronomia, Porto Alegre-RS, 91501-970, (Brazil)

Abstract - The negative effects of ethanol crossover through the electrolyte membrane of a direct ethanol proton exchange membrane fuel cell (DE-PEMFC), are potential reduction and cathode depolarization. In this paper, different combinations of the parallel serpentine-baffle flow field plate (PSBFFP) and parallel serpentine flow field plate (PSFFP) in the anode and cathode were investigated with the aim of minimizing ethanol crossover in the cell. Simulations and laboratory tests showed that ethanol crossover through the membrane electrolyte assembly (MEA) was minimized when the anode and cathode were fitted with PSFFP and PSBFFP, respectively. It was concluded that the greater pressure of oxygen at the cathode can decrease ethanol crossover in a DA-PEMFC. However, a decrease in the crossover is not a guarantee of improvement in the overall fuel cell performance; it must be combined with efficient removal of the water produced by the redox reaction in the cathode.

Keywords – crossover, ethanol, flow field plate, fuel cell.

I. INTRODUCTION

The performance of a direct ethanol proton exchange membrane fuel cell (DE-PEMFC) depends on numerous parameters, such as the ethanol feed concentration, the operating temperature and the rate of the ethanol crossover. The negative effects of ethanol crossover through the electrolyte membrane, from the anode to the cathode side of a DE-PEMFC, are potential reduction and cathode depolarization, which decrease the overall efficiency of DE-PEMFC. In this paper, different combinations of the parallel serpentine-baffle flow field plate (PSBFFP) and parallel serpentine flow field plate (PSFFP) in the anode and cathode were investigated with the aim of minimizing ethanol crossover in the cell.

II. MATERIALS AND METHODS

The ethanol crossover process in a DE-PEMFC prototype unit also was evaluated using the flow simulation tool of SOLIDWORKS 2014. The experimental runs in the laboratory were carried out in a DE-PEMFC prototype unit, as shown in the schematic diagram in Figure 1.

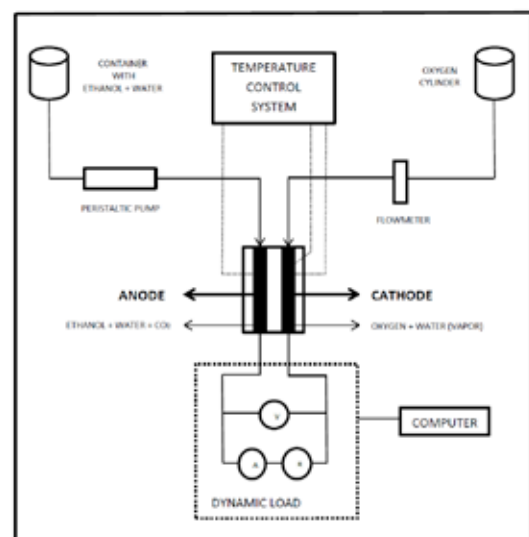


Fig. 1. Schematic DE-PEMFC unit flow diagram.

The runs in the DE-PEMFC unit with Nafion membrane were carried out using four different combinations of the plates PSFFP (A) and PSBFFP (B) in the anode and cathode sides as

shown in Figure 2. To guarantee maximum crossover during the test, the ethanol concentration was 1 M and the fuel cell operating temperature was 80°C [1].

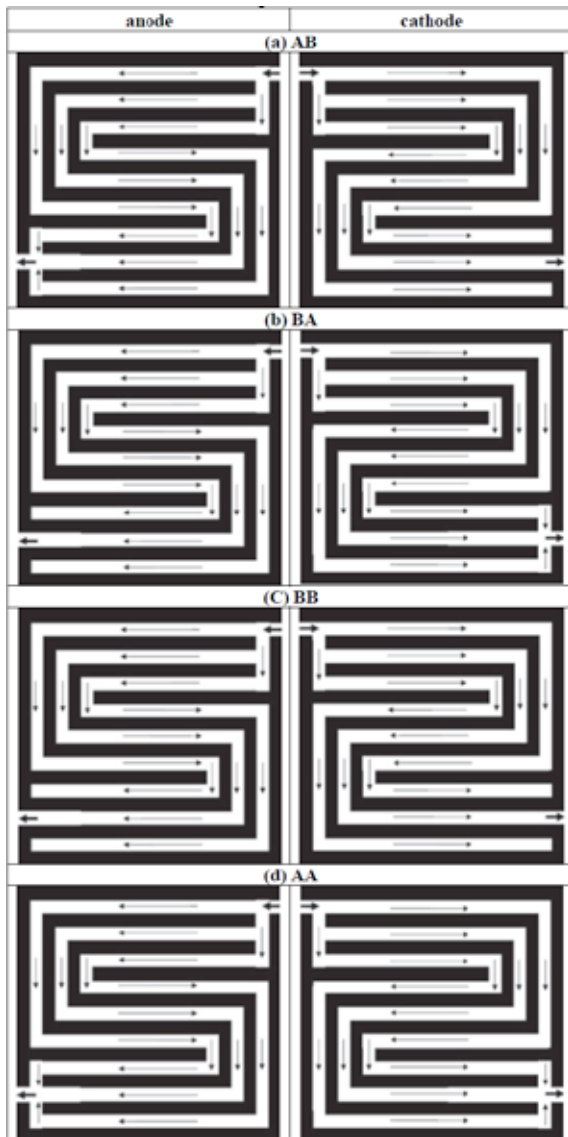


Fig. 2. Schematic diagram of the four anode/cathode flow field plates' configurations evaluated. (a) PSFFP/PSBFFP; (b) PSBFFP/PSFFP; (c) PSBFFP/PSBFFP; (d) PSFFP/PSFFP.

III. RESULTS AND DISCUSSION

The curve of experimental voltage versus current for the four combinations of PSBFFP and PSFFP are shown in Figure 7. The DE-PEMFC unit performance in the current range of 0 to 0.6 A varied according to the plate combination of the anode and cathode. Above 0.1 A, the cell with PSFFP in the anode and PSBFFP in the cathode (red curve) presented the best performance among the four combinations.

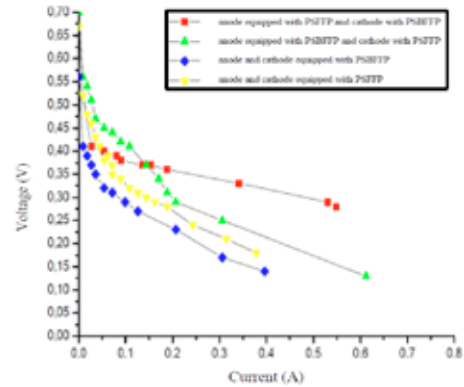


Fig. 2. Current density-voltage curves with the four anode/cathode flow field plate's configurations

This was attributed to the higher oxygen gas pressure in the discontinuous channels of PSBFFP in contact with MEA on the cathode side. On the other hand, loss of pressure and any alcohol molecule that reached the cathode by crossover occurred at the continuous channel of PSBFFP, which is also the fuel cell outlet. The water produced by the redox reaction exited the cell through the low-pressure continuous channel, which improved the overall fuel cell performance.

IV. CONCLUSION

It was concluded that the greater pressure of oxygen at the cathode, relative to the alcohol pressure at the anode, can decrease ethanol crossover in a DA-PEMFC. However, a decrease in the crossover is not a guarantee of improvement in the overall fuel cell performance; it must be combined with efficient removal of the water produced by the redox reaction in the cathode. The latter requires a large pressure loss in the cathode flow field plate that improves the cathode diffusion overpotential and decreases the overall fuel cell performance. In the present research, a perfect balance between decreasing the ethanol crossover and efficient removal of the water produced at the cathode of a DE-PEMFC was achieved without the use of peripherals by combining a PSFFP at the anode and a PSBFFP at the cathode.

ACKNOWLEDGMENT

The financial support of the Brazilian Government Agencies Coordenação de Aperfeiçoamento de Pessoal de Nível Superior (CAPES) (PROCAD 714/2008) and Conselho Nacional de Desenvolvimento Científico e Tecnológico (CNPq) (Projeto Universal 482401/2010-9) are gratefully acknowledged.

REFERENCES

- [1] Andreadis, G., Tsiakaras, P, Ethanol crossover and direct ethanol PEM fuel cell performance modeling and experimental validation, Chem Eng Sci, Volume 61, 2006, pp. 7497-7508.



SYNTHESIS AND PROPERTIES OF SULFONATED POLY(PHENYLENE)S WITH PLANAR CONFORMATION FOR PEM APPLICATIONS

H. Jang*, T. Hong*, S. Sutradhar*, J. Ha*, J. Pyo*, T. Ryu*, and W. Kim*
Department of Applied Chemistry, Konkuk University, Chungju
380-701 (Korea)

Abstract - Dichlorotetraphenylethylene was prepared by McMurry coupling reaction and 1,4-dichloro-2,5-dibenzoylbenzene was prepared from 2,5-dicarbonylchloride-1,4-dichlorobenzene and benzene with $AlCl_3$. Tetraphenylethylene is a conjugated structure which enables to form planar conformation between aromatic rings, and selective sulfonation on phenyl rings of polymer side chain. These polymers have all carbon-carbon linkages without any ether linkage on the polymer backbone, which was not easily attacked by nucleophiles and sulfonation reaction with chlorosulfuric acid. This polyphenylene structure provides a stiff and resistant backbone and also sites for chemical modifications. The structure of copolymer membranes will be studied by 1H NMR spectroscopy. The ion exchange capacity (IEC) and proton conductivity will be evaluated with increasing degree of sulfonation. The thermal and chemical stability of the prepared membrane will be characterized by thermogravimetric analysis and Fenton's reagent, respectively

Index Terms - Poly(phenylene), Nickel catalyst, Planar Structure, Proton Exchange Membrane.

I. INTRODUCTION

Polymers of using fuel cell application have received much attention because of their high thermal, oxidative, chemical stability in fuel cell environments, and also close to the Nafion's performance [1]. However, the chemical stability is unapproachable to Nafion, because of ether linkage with acid functional groups was attacked by hydrogen peroxide or peroxide radicals generated during PEMFC operation [2]. So, we focused on polyphenylene structure without ether linkage. Polyphenylene containing pendant benzoyl groups has a great of advantages, such as good durability, high performance amorphous thermoplastic, thermooxidative stability, excellent

chemical and physical properties as well as good solubility [3]. This work is an attempt to synthesize polyphenylene without ether moieties by Ni(0) catalyzed polymerization. The sulfonation reaction was controlled by varying the mole ratio of tetraphenylene monomer. The proposed polymer membranes without ether linkage structure supposed to be good chemical stability and proton conductivity. Polymer membranes will be studied by 1H NMR spectroscopy, thermogravimetric analysis, water uptake, ion exchange capacity, proton conductivity, and also by the investigation of atomic force microscopic (AFM) images.

II. EXPERIMENTAL

A. Synthesis of dichlorotetraphenylethylene

To a solution of diphenylmethane in dry tetrahydrofuran was added a 2.5 M solution of n-butyl lithium in hexane at 0 °C under nitrogen atmosphere with the 4,4-dichlorobenzophenone and stirred for 6 h at room temperature. The reaction was quenched with the addition of an aqueous solution of ammonium chloride and added methylene chloride. The separated organic layer was evaporated. The crude alcohol was dissolved in toluene in a flask fitted with a dean-stark trap. A catalytic amount of p-toluenesulfonic acid was added, and the mixture was refluxed for 4 h. The toluene layer was washed with 10% aqueous sodium bicarbonate solution and evaporated to afford the crude dichlorotetraphenyl ethylene [4].

B. Synthesis of 1,4-dichloro-2,5-dibenzoylbenzene

The mixture of 2,5-dichloro-p-xylene, potassium permanganate, pyridine, and distilled water was stirred for



12h with temperature at 100 °C. After reaction, the filtrate was acidified with hydrochloric acid to a PH of 1. White solid was filtered and dried oven at 60 °C. Dried dichloroterephthalic acid was stirred reflux condition for 24h with thionyl chloride. After reaction, thionyl chloride was evaporated and immediately, yellow solid was dissolved carbon disulfide. Benzene and aluminum chlsoride in carbon disulfide stirred at 40 °C and added yellow liquid. After 24h, the residue was poured into ice water with hydrochloric acid. Product was filtered and washed twice with water and also recrystallization used to ethyl acetate and hexane before drying in oven at 60 °C [5].

C. Synthesis of sulfonated polymer

In a typical polymerization, zinc, nickel bromide, triphenylphosphine were added to a three-necked flask under nitrogen atmosphere. Dried DMAc was transferred into the flask under a vigorous flow of nitrogen. dichlorotetraphenylethylene and 1,4-dichloro-2,5-dibenzoylbenzene were dissolved DMAc and added via a syringe into catalyst flask. The mixture was stirred at 110°C for around 24h. The mixture was poured in a 10% HCl aqueous solution. Crude polymer was filtered, dissolved in DMAc, and re-precipitated in 10% HCl aqueous solution. Finally, it was washed methanol, water, and dried at 60°C in a vaccum oven. The dried polymer was dissolved in chloroform and few DMF under nitrogen and added 0.93mL of chlorosulfonic acid under Ice bath condition. The reaction mixture was stirred at room temperature for 3h. The mixture was then poured into cold water. The polymer precipitate was filtered and washed several times to remove the acidic residue. Then filtered polymer was dried in vacuum oven at 80°C for 24h.

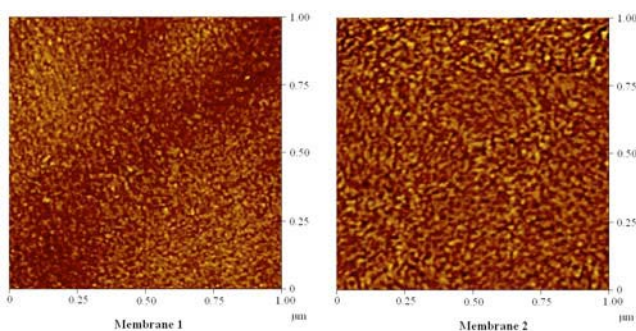


Fig. 1. AFM images of sulfonated polymers

III. RESULT AND DISCUSSION

The morphology of polymer surfaces was investigated by using an atomic force microscope (AFM) in Fig. 1. Assessment of the images revealed that the surface pattern

reflecting the hydrophilic-hydrophobic microphase separation were strongly dependent on the chemical structure. The hydrophobic domains are bright color between the hydrophilic domains which are dark brown by the cluster formation of sulfonic acids and water [6]. These morphological observations agree well with the results from the proton conductivity measurement. These conformations with four sulfonic acid groups on planar moiety provide good hydrophilic/hydrophobic phase separation and wide ionic channels as shown in the Fig. 1.

IV. CONCLUSION

These results showed that the morphology of polymer matrix greatly affected the membranes properties and stability. Membranes including conjugated segments without ether linkage also provided good dimensional stability in spite of high IEC values.

ACKNOWLEDGMENT

The Basic Science Research Program through the National Research Foundation of Korea (NRF) funded by the Ministry of Education, Science and Technology (2011-0006535).

REFERENCES

- [1] Parka, C., Lee, C., Guiver, M., Lee, Y , Sulfonated hydrocarbon membranesfor medium-temperature and low-humidity proton exchange membrane fuelcells (PEMFCs), Prog. in Polym. Sci., Volume 36, 2011, pp. 1443-1498
- [2] Hickner, M., Ghassemi, H., Kim, Y., Einsla, B., McGrath, J , Alternative Polymer Systems for Proton Exchange Membranes (PEMs), Chem. Rev., Volume 104, 2004, pp. 4587-4612.
- [3] Poppe, D., Frey, H., Kreuer, K., Heinzl, A., Mulhaupt, R , Carboxylated and Sulfonated Poly(arylene-co-arylene sulfone): Thermostable Polyelectrolytes for Fuel Cell Applications, Macromolecules, Volume 35, 2002, pp. 7936-7941.
- [4] Wang, W., Lin, T., Wang, M., Liu, T., Ren, L., Chen, D , Aggregation emission properties of oligomers based on tetraphenylethylene, J. Phys. Chem. B, Volume 114, 2010, pp. 5983-5988.
- [5] Fu, H., Yun, H., Kwei, T., Okamoto, Y., Blumstengel, S., Walser, A , Dorsinville, Blue photo- and electroluminescence Based on Poly(2-benzoyl-1,4-phenylene) and Poly(2,5-dibenzoyl-1,4-phenylene), Polym. Adv. Tech., Volume 10, 1999, pp. 259-264.
- [6] Lee, S., Shin, D., Wang, C., Lee, K., Guiver, M., Lee, Y , A capillarywater retention effect to improve medium-temperature fuel cell performance,Electrochem, Commun., Volume 31, 2013, pp. 120-124.



STRUCTURE, OXIDATION AND ELECTRICAL PERFORMANCE OF LaFeO_3 -BASED CONVERSION COATINGS ON A 13CR FERRITIC STAINLESS STEEL FOR IT-SOFC INTERCONNECT APPLICATIONS

A. Masi*[§], D. Pumiglia*[§], A. Masci*, M. Carlini[§], S. J. McPhail* and S. Frangini*

* ENEA CR Casaccia, Via Anguillarese 301 00123 Rome, (Italy)

[§] DAFNE, University of Tuscia, via San Camillo de Lellis snc 01100 Viterbo, (Italy)

Abstract – The behaviour of a commercial 13Cr ferritic SS with a LaFeO_3 conversion coating is analyzed as a potentially cost-effective strategy to produce IT-SOFC interconnects with electrically conductive and Cr-free stable surfaces. The growth of the passivation layer is evaluated by electrochemical methods, and the structure and morphology of the obtained coatings are analyzed by means of X-Ray Diffraction (XRD) and Scanning Electron Microscopy (SEM). Long-term oxidation experiments show high stability of the LaFeO_3 conversion coating at 700°C in static moist air. Electrical conductivity properties of the coated steel in SOFC environment have been investigated measuring the Area Specific Resistance (ASR) evolution at 700°C.

Index Terms – Coating, Corrosion, Interconnect, Stainless Steel.

I. NOMENCLATURE

Solid Oxide Fuel Cell (SOFC), Stainless Steel (SS), X-Ray Diffraction (XRD), Scanning Electron Microscopy (SEM), energy-dispersive X-ray (EDX), Area Specific Resistance (ASR).

II. INTRODUCTION

Following the rapid progress of Solid Oxide Fuel Cell (SOFC) technology towards the goal of average operational temperatures much below 800°C, commercial ferritic stainless steels (SSs) coated with spinel- or perovskite-type ceramic oxide layers seem to offer the most promising approach for a cost-effective fabrication of Intermediate Temperature (600-750°C) IT-SOFC interconnects with combined mechanical properties, corrosion resistance, chemical stability and negligible electrical performance loss when exposed to moist SOFC oxidizing environments and long operation times.

In an attempt to explore improved coating strategies for SSs,

a new class of chemical conversion coatings has been recently developed in our laboratory to specifically protect SSs in high temperature electrical/electrochemical applications. The method is based on forming a protective and conductive perovskite-based coating by chemical reaction of the stainless steel surface with lanthanum oxide dissolved in a molten alkali carbonate eutectic bath. At the selected processing temperatures, only the iron element is sufficiently active with lanthanum to generate a compact perovskite oxide structure, whereas chromium (and nickel, if present in the alloy) is undergoing to selective leaching in the carbonate bath, thus resulting in the formation of a Cr-free LaFeO_3 perovskite layer. The morphology of the coating is directly related to the perovskite growth mechanism and thus can be tuned by varying process parameters [1,2].

This work focuses on a thin LaFeO_3 conversion coating obtained on a commercial 13Cr ferritic SS, evaluated as a potentially cost-effective strategy to produce IT-SOFC interconnects with electrically conductive and Cr-free stable surfaces.

III. EXPERIMENTAL

A commercial grade of a 13Cr ferritic stainless steel (AISI 405) was used in this work. Perovskite conversion coatings were obtained exploiting a molten carbonate chemical process already described in previous works (5,6). After the coating passivation treatment, coupons were cleaned in boiling deionized water for not less than 6 hour to remove the excess carbonate salt still adhering to the coupon surfaces.

Steel coupons were subjected to discontinuous oxidation experiments (700°C, static ambient air, 3 vol % moisture content) and cell environment electrical experiments (700°C,



FCTS^{QA} standard conditions: Anodic flow: H₂ 35 ml/min, Humidity: 3%, Cathodic flow: Air 83 ml/min). ASR values have been obtained by means of Electrochemical Impedance Spectroscopy (EIS) measurements, (Solartron 1260 Frequency Response Analyzer (FRA) module coupled with a Solartron 1287 Electrochemical Interface, frequency scan range: 100 kHz-0.1 Hz, amplitude: 10 mV)

Morphological (JEOL JSM-5510LV with EDX) and microstructural analysis (Italstructure, INEL curved PSD detector, Cu K α source) were performed to characterize the samples before and after the test.

IV. PRELIMINARY RESULTS AND DISCUSSION

The molten carbonate process produced a thin layered coating: the surface consists in a La-Fe perovskite layer, grown through the metathesis conversion reaction of a Li-Fe spinel formed during the first hours of the synthesis process, while a mixture of Fe-rich spinel and hematite phases compose the underlying layer.

The results of the exposure test are reported in Fig. 1. In comparison with the bare stainless steel [3], the oxidation of the coated coupons occurs with an initial higher weight increase, while after the first 40h negligible weight changes are observable.

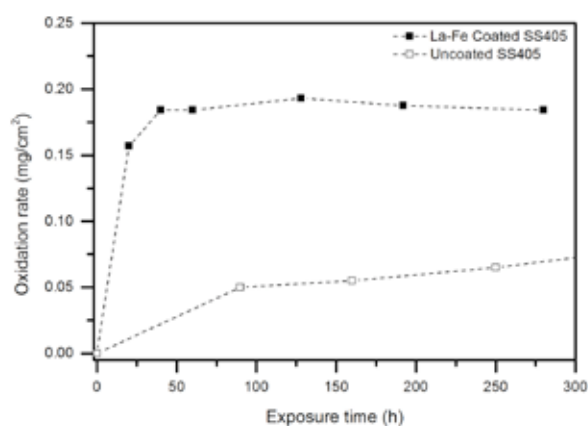


Fig. 1:oxidation curve of the coated SS405 sample compared to the uncoated sample [3].

The XRD patterns collected during the exposure test are reported in Fig. 2. The pattern sequence suggests that the initial weight gain is due to a slight growth of the Fe-rich bottom layer combined with an oxygen vacancy annihilation phenomenon. The growth of an oxygen deficient coating layer is in fact expected due to the synthesis conditions, the process being carried out under low oxygen concentration. The ASR values obtained from the coated coupon up to 500h show some fluctuation of the results in the range 0.2-0.4 Ω ·cm².

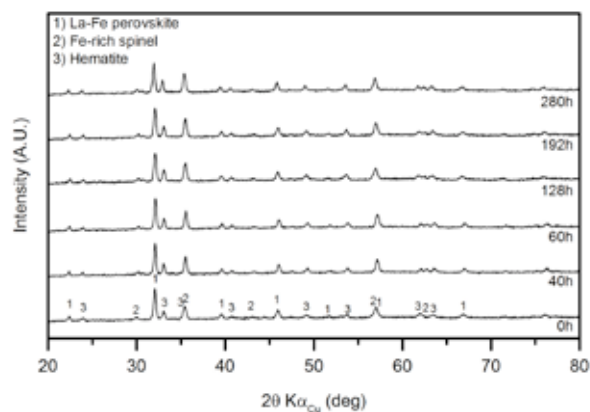


Fig. 2: XRD patterns of the SS405 coated sample collected after cooling at selected exposure time during the exposition test.

V. CONCLUSION

The initial results obtained on the coated sample suggest that the corrosion resistance of the low Cr stainless steel is largely improved in the selected condition. Apart from an initial structure evolution, the samples seem to remain unchanged during the rest of the exposure test, although the electrical properties of the coating are not optimal. Further efforts will tend towards the improvement of the surface conductivity through inclusion of dopants in the perovskite layer.

More details about the samples synthesis and characterization will be presented at the conference venue.

ACKNOWLEDGMENT

The work was partially supported by the FP7 programme SCoReD 2:0.

REFERENCES

- [1]. Frangini S, Masci A, Zaza F. Molten salt synthesis of perovskite conversion coatings: A novel approach for corrosion protection of stainless steels in molten carbonate fuel cells. *Corros Sci.* 2011;53:2539–48.
- [2]. Frangini S, Zaza F, Masci A. Molten carbonate corrosion of a 13-Cr ferritic stainless steel protected by a perovskite conversion treatment: Relationship with the coating microstructure and formation mechanism. *Corros Sci.* 2012;62:136–46.
- [3]. Frangini S, Masci a., McPhail SJ, Soccio T, Zaza F. Degradation behavior of a commercial 13Cr ferritic stainless steel (SS405) exposed to an ambient air atmosphere for IT-SOFC interconnect applications. *Mater Chem Phys.* 2014;144:491–7.



SULPHUR-TOLERANT ANODE FOR SOFCS USING BIOGAS FUEL

A. Fuerte* and M.J. Escudero*

* CIEMAT, Av. Complutense 22, 28040 Madrid, (Spain)

Abstract - The primary purpose of this work is to explore the electrode behaviour of RhCu-CaCe anode (0.4 wt.% Rh impregnated on Cu-Ca_{0.1}Ce_{0.8}O_{2+δ} mixed oxide, 40 at.% Cu) in a single cell directly operated with three different simulated biogas mixtures (equimolar to CH₄-rich biogas) that contains H₂S. The results reveal significant modifications in the structural, catalytic/redox and electrical properties of the systems as a function of the presence of Rh dopant in the formulation and the ability of this material to operate with simulated biogas mixtures without loss of single cell performance due to the formation of carbon deposits or sulphur anode poisoning.

Index Terms – Rh-Cu-ceria, SOFC, sulphur-tolerance, biogas.

I. INTRODUCTION

Biogas is a high-potential versatile raw material for reforming processes, which can be used as an alternative CH₄ source [1]. It is mainly constituted by CH₄ and CO₂ while containing a few percent of H₂, N₂ and trace contaminants such as NH₃, H₂S, halides [2] and siloxanes [3]. This composition fluctuates significantly during biogas production and it is highly dependent of the substrate used for the production process. It is well known that formation of carbon deposits on SOFC anodes can be minimize by anode morphology and operating parameters such as steam and current density. Ammonia is not practically a problem in SOFC feeds, since it is oxidised to N₂ and H₂O in a two-stage process [4]. However, sulphur impurities can cause deactivation of most methane reforming catalysts or SOFC anodes [5], so they have to be removed from biogas feedstock before its use in fuel cell.

In previous works, we have demonstrated the ability of nanocrystalline Cu-ceria based anodes to operate with different fuels: hydrogen, methane and simulated biogas containing sulphur [6-8]. The employment of bimetallic anode formulations such as Cu-Co, Cu-Ni or Cu-Ag induced changes in the properties of material in terms of enhanced catalytic activity, stability and poisoning tolerance when compared to

monometallic Cu-ceria. On the other hand, doping a basic copper-ceria formulation, Cu (40 at. %)/CeO₂, with an alkaline rare-earth (Ca²⁺) increased the oxygen vacancy concentration and concomitant oxide ion conductivity that enhanced the anode performance. Although several improvements have been achieved with the structural modifications of ceria, it is still needed to improve the activity of anode for direct electrochemical oxidation of hydrocarbon fuels.

In this context, small quantities (0.4 wt. %) of rhodium (Rh) were added to an optimised formulation based on copper-calcium doped ceria in order to enhance the catalytic activity of the conductive layer. Cu-Ca_{0.2}Ce_{0.8}O_{2+δ} was considered because of its thermal-stability, compatibility with the electrolyte, good sulphur and coke tolerance and improved oxygen-ion conductivity when compared to Cu-CeO₂ [9].

II. EXPERIMENTAL

The Rh/Cu-CeCa (0.4 wt.% Rh) was prepared by incipient wetness impregnation of the Cu-CeCa (40 at.% Cu combined with Ca_{0.1}Ce_{0.9}O_{2.δ}) previously synthesized by inverse microemulsion method [6], with an aqueous Rh(NO₃)₃ solution. After impregnation, sample was dried at 373 K and calcined under air at 1023 K for 2 h. Material was characterized by a multitechnic approach including XRD, XPS, Raman, ICP-AES and electrical conductivity measurements along with analysis of its chemical compatibility with SDC electrolyte and sulfur tolerance tests in H₂ fuel. Main results of this characterization have been previously reported [10].

For its evaluation using H₂S containing biogas a single cell with an active area of 0.3 cm², was prepared using SDC electrolyte and LSM cathode. Details of the preparation method can be found elsewhere [9]. Single cell was galvanostatically operated at 1023 K for 862 h under humidified biogas mixtures (CH₄/CO₂/H₂) containing 500 ppm (v) of H₂S (*50bioS*: 50:45:5; *60bioS*: 60:35:5; *70bioS*: 70:25:5). Impedance spectra and current-voltage curves were regularly collected.

III. RESULTS AND DISCUSSION

Rh/Cu-CeCa is mainly constitutes by a fluorite phase of $\text{Cu}_x\text{Ca}_y\text{Ce}_{1-x-y}\text{O}_{2-6}$ mixed oxide and additional phases of metal oxides that, under working conditions, are totally reduced to the corresponding metallic phases (Cu^0 and Rh^0) which coexist with the mixed oxide. It presents optimal electrical characteristics, excellent thermal compatibility, based on the TEC values that are closed to those for common SOFC electrolytes as well as good chemical compatibility with SDC electrolyte [10].

Fig. 1 shows the power densities of single cell at 1023 K as function of fuel composition. For their comparison in this figure values obtained with the same single cell running on hydrogen and simulated biogas in absence of sulphur (H_2 , 50bio-70bio) are shown. Cell voltage remained stable during all process under current demand and different fuel composition.

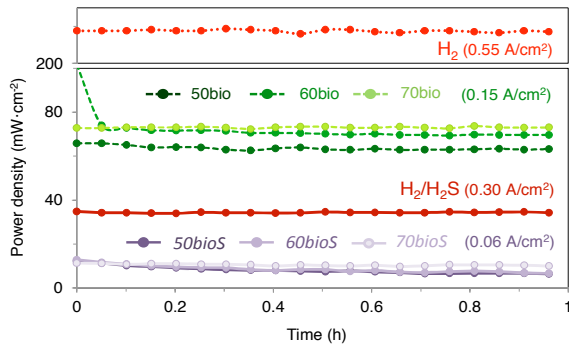


Fig. 1 Power densities of single cell at 1023 K as function of fuel composition

The main results of the single cell evaluation are collected in Table 1. The maximum current density (I_{\max}), at 0 V, under humidified H_2S (500 ppm)- H_2 was 628 mA/cm^2 , while in the presence of H_2S (500 ppm)-simulated biogas it drops to 74, 77 and 77 mA/cm^2 for 50bioS, 60bioS and 70bioS, respectively. These values are lower to those obtained with hydrogen and simulated biogas mixtures without sulphur (50bio-70bio). Impedance spectroscopy measurements were recorded after each IV curve. As seen in Table 1, the ohmic resistance (R_{Ω}) of the single is much lower in hydrogen than that running with simulated biogas mixtures due to lower $p\text{O}_2$ in the anode. On the other hand, the polarization resistances (R_p) highly increase using H_2S -containing simulated biogas as fuels. Notice R_{Ω} is not affected by the biogas composition. However, the resistance associated to electrode polarization (R_p) decrease with increasing CH_4 content.

The best single cell performance running on H_2S -containing simulated biogas was obtained with 70bioS, mixture with the highest content of methane. Although single cell performance is limited running on H_2S -containing simulated biogas, it is recovered after running in humidified hydrogen. The best single cell performance running on H_2S -containing simulated biogas was obtained with 70bioS, mixture with the highest content of methane. Although single cell performance is limited running

TABLE I
MAIN RESULTS OF Rh/Cu-CaCe /SDC / LSM SINGLE CELL EVALUATION

H_2S containing fuel*	I_{\max} (mA/cm^2)	P_{\max} (mW/cm^2)	Resistances ($\Omega\text{-cm}^2$)	
			R_{Ω}	R_p
H_2 (before S action)	1116	216	0.32	0.51
$\text{H}_2/\text{H}_2\text{S}$	628	122	0.33	0.47
50bioS	74	11	0.70	4.54
60bioS	77	11	0.70	4.40
70bioS	77	12	0.71	4.12
H_2 (after S action)	1100	236	0.28	0.19

* H_2S content= 500 ppm (v)

on H_2S -containing simulated biogas, it is recovered after running in humidified hydrogen. This fact gives evidence of the reversible carbon deposition and sulphur poisoning of the anode catalyst. Note that single cell performance is improved with the incorporation of Rh in the anode composition [10].

IV. CONCLUSION

The capability of Rh/Cu-CeCa to operate in humidified H_2S -containing simulated biogas mixtures (up to 500 ppm) at relatively low temperature (1023 K) has been demonstrated. Although maximum power density of the single cell was much lower running on H_2S -containing fuels comparing with operation using hydrogen or simulated biogas (without H_2S), mainly due to the adsorption of sulphur and carbon species, voltage remained stable and cell performance was recovered after exposition to humidified hydrogen.

ACKNOWLEDGMENT

This work has been supported by Spanish Ministry of Economic and Competitiveness (MAT2013-45043-P).

REFERENCES

- [1] Atkinson, A., Barnett, S., Gorte, R.J., Irvine, J.T.S., McEvoy, A.J., Mogensen, M.B., Shingal, S., Vohs, J.M., Nature Materials, 3, 2004, 17-27.
- [2] Haga, K., Adachi, S., Shiratori, Y., Itoh, K., Sasaki, K., Solid State Ionics, 179, 2008, 1427-1431.
- [3] Rasi, S., Lehtinen, J., Rintala, J., Renewable Energy 35, 2010, 2666-2673.
- [4] Fuerte, A., Valenzuela, R.X., Escudero, M.J., Daza, L., J. Power Sources, 192, 2009, 170-174.
- [5] Brightman, E., Ivey, D.G., Brett, D.J.L., Brandon, N.P., Journal of Power Sources, 196, 17, 7182-7187.
- [6] Fuerte, A., Valenzuela, R.X., Daza, L., J. Power Sources, 169, 2007, 47-52.
- [7] Fuerte, A., Valenzuela, R.X., Escudero, M.J., Daza, L., J. Power Sources, 196, 2011, 4324-4331.
- [8] Fuerte, A., Valenzuela, R.X., Escudero, M.J., Daza, L., Int. J. Hydrogen Energy, 39, 2014, 4060-4066.
- [9] Fuerte, A., Valenzuela R.X., Escudero M.J., Daza L., ECS Transactions, 25, 2009, 2173-2182.
- [10] Fuerte, A., Valenzuela R.X., Escudero M.J., Proceedings of 5th European Fuel Cell Piero Lunghi Conference, 2013, Rome, Italy.



THE EFFECTS OF THE COMPOSITION OF MICROPOROUS LAYERS ON THE PERMEABILITY OF GAS DIFFUSION LAYERS

Olutomisin Orogbemi, D. B. Ingham, M.S. Ismail, K. Hughes, L. Ma, M. Pourkashanian

Energy 2050, Department of Mechanical Engineering, Faculty of Engineering, The University of Sheffield, Sheffield S10 2TN, UK

ABSTRACT

The permeability significantly affects the capillary diffusivity and consequently the saturation profile within the membrane electrode assembly (MEA) in proton exchange membrane (PEM) fuel cells. Therefore, for two-phase modelling, it is important to obtain accurate values for the permeability of the porous media in the MEA. In this work, the effects of the composition of the microporous layer (MPL) on the permeability of the gas diffusion layers (GDLs) has been thoroughly investigated and presented.

1. INTRODUCTION

The microporous layer (MPL) is a key components in the membrane electrode assembly (MEA). Gas diffusion layers (GDLs) are normally coated with MPLs to mitigate water flooding in the catalyst layer and enhance the contact between the GDL and the catalyst layer [1-3]. The MPL is typically a mixture that consists of carbon black and (polytetrafluoroethylene) PTFE particles. It has been shown that the composition of this mixture has a significant effect on the influential characteristics of the GDL (e.g. the porosity, pore size, capillary diffusivity, hydrophobicity, and the gas permeability) and consequently on the overall performance of the fuel cell [1-2, 4]. To accurately model the saturation profile in the porous media in the fuel cell, one needs accurate values for the gas permeability of both the GDL and the MPL. To achieve this goal, the effects of the composition of the MPL on the through-plane gas permeability of GDLs have been experimentally investigated in this study.

2. EXPERIMENTAL DETAILS

The MPL ink (which consist of carbon black, PTFE and a dispersion agent) was prepared and applied, via manual spraying, onto one side of the GDL. The carbon loadings considered in this study are 0.5 and 2.0 mg/cm² and the

PTFE content was varied from 10 to 30 wt.% for each carbon loading. The MPL-coated GDLs were heat-treated to a temperature 120 °C for 1 hr, at 280 °C for 30 minutes and finally sintered at 350 °C for 30 minutes to uniformly distribute the PTFE throughout the MPL [4]. It should be noted that the gas permeability of the tested samples was measured before and after sintering the MPL-coated GDLs.

The thickness of the GDL was measured before and after MPL-coating by using a micrometre with an accuracy of 1 µm. The thickness of the coated GDL samples was further confirmed by employing cross-section scanning electron microscopy (SEM) images. The setup used to estimate the permeability was described in a previous work [6], see Figure 1. Briefly, in this setup, the flowing gas is forced to pass through the GDL sample at various flow rates and the pressure drop across the sample is measured for each flow rate. Further, the gas permeability was estimated by curve-fitting the experimental data to Darcy's Law. The thickness of the MPL, which is used to calculate its permeability, was estimated at as many points as possible from the cross-section images taken for the coated GDLs.

3. RESULTS AND DISCUSSION

The average thickness of 30 carbon paper substrate samples was estimated to be about 370 ± 70 µm. The averaged through-plane gas permeability for the carbon substrate samples was calculated to be 1.77×10^{-11} m².

Effect of MPL composition

Figure 2 shows the estimated through-plane permeability of the MPL-coated GDLs as a function of PTFE content for the two carbon loadings considered, namely 0.5 and 2.0 mg/cm². It can be seen that the two curves presented show different trends. For the 0.5 mg/cm² carbon loading, the permeability of the MPL-coated GDLs is a minimum at 20 % PTFE whereas, for 2.0 mg/cm², it keeps decreasing as the PTFE increases. It should be noted that the work is still proceeding in order to estimate the gas permeability of the



40 %, 50 %, etc. However, up to now, the point to emphasise is that the effects of the PTFE content present in the MPL on the gas permeability are sensitive to the carbon loading. The literature has shown that the gas permeability increases as the amount of PTFE in the MPL increases; this was attributed to the increase in the volume of the pores between the carbon agglomerates of the MPL [6, 7]. However, based on this study, this is not necessarily the case: the effects of the PTFE loading on gas permeability are dependent on the carbon loading. Therefore, care should be taken when it comes to drawing conclusions on the effects of the PTFE content of the MPL on the permeability of the GDL. As mentioned earlier, the work is still proceeding in order to cover wider ranges for the PTFE and carbon loadings to come up with more conclusive findings.

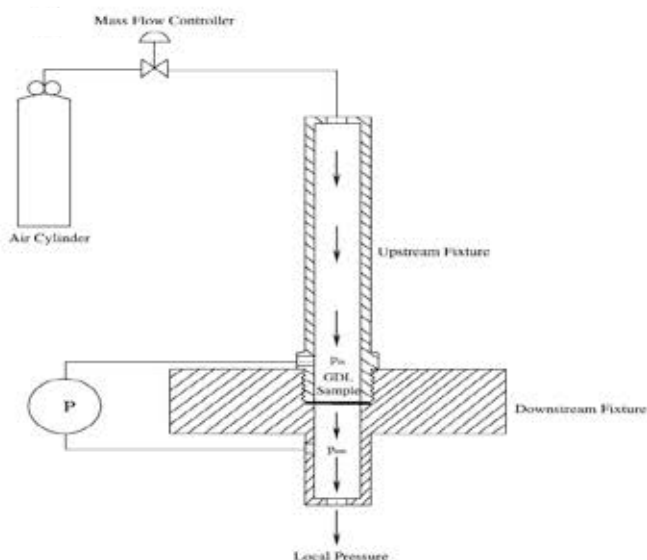


Figure 1: Schematic diagram of the experimental setup [6].

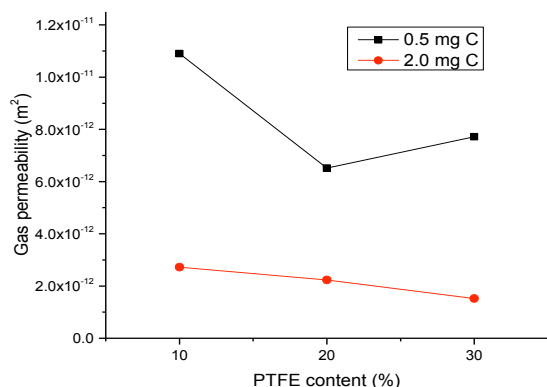


Figure 2: Effect of PTFE loading present in the MPL on the permeability of the GDL.

Through-plane Gas Permeability of MPLs

Table 1 presents the through-plane permeability of the MPLs in the MPL-coated GDLs. The procedures employed in determining the permeability of the MPL are described in [6]. The gas permeability was estimated and found to be 2 – 3 orders of magnitude lower than the corresponding GDL substrate. As expected, the trends shown in the table are in line with those shown in Figure 2.

Carbon loading (mg/cm ²)	PTFE loading (%)		
	10 wt.%	20 wt.%	30 wt.%
0.5	2.87 × 10 ⁻¹² m ²	1.42 × 10 ⁻¹² m ²	2.87 × 10 ⁻¹² m ²
2.0	9.81 × 10 ⁻¹³ m ²	5.86 × 10 ⁻¹³ m ²	4.57 × 10 ⁻¹³ m ²

Conclusions

The effects of the composition of the MPL on the through-plane permeability have been experimentally investigated. The results have shown that the effects of the PTFE content of the MPL on the gas permeability of the GDL are sensitive to the carbon loading. For the 0.5 mg/cm² carbon loading, the permeability of the MPL-coated GDLs is a minimum at 20 % PTFE whereas, for 2.0 mg/cm², it keeps decreasing as the PTFE increases. Further, the permeability of the MPLs was found to be 2-3 orders of magnitude lower than those of the corresponding carbon substrates

REFERENCES

- [1] Velayutham, G., Kaushik, J., Rajalakshmi, N. Dhathathreyan, K. S., *Effect of PTFE content in gas diffusion media and microlayer on the performance of PEMFC tested under ambient pressure*. Fuel Cells, 2007. **4**: p. 314-318.
- [2] Jordan, L. R., Shukla, A. K., Behrsing, T., Avery, N. R., Forsyth, M., *Effect of diffusion-layer morphology on the performance of polymer electrolyte fuel cells operating at atmospheric pressure*. Journal of Applied Electrochemistry, 2000. **30**: p. 641-646.
- [3] Giorgi, L., Antolini, E., Pozio, A., Passalacqua, E., *Influence of the PTFE content in the diffusion layer of low-Pt loading electrodes for polymer electrolyte fuel cells*. Electrochimica Acta, 1998. **43** (24): p. 3675 – 3680.
- [4] Ong, A. L., Bottino, A., Capannelli, G., Comite, A., *Effect of preparative parameters on the characteristic of poly (vinylidene fluoride)-based microporous layer for proton exchange membrane fuel cells*. Journal of Power Sources, 2008. **183**: p. 62-68.
- [5] Ismail, M. S., Hughes, K. J., Ingham, D. B., Ma, L., Pourkashanian, M., *Effect of PTFE loading of gas diffusion layers on the performance of proton exchange membrane fuel cells running at high-efficiency operating conditions*. Int. J. Energy Research, 2012. **10**: p. 2968
- [6] Ismail, M. S., Borman, D., Damjanovic, T. DIngham, D. B., Pourkashanian, M., *On the through-plane permeability of microporous layer-coated gas diffusion layers used in proton exchange membrane fuel cells*. Int. J. Hydrogen Energy, 2011. **36**: p. 10392.
- [7] Uchida, M., Aoyama, Y., Eda, N., Ohta, A., *Investigation of the microstructure in the Catalyst layer and effects of both Perfluorosulfonate Ionomer and PTFE-loaded carbon on the catalyst layer of polymer electrolyte fuel cells*. J. Electrochemical. Soc., 1995. **142**: p. 4143.



DETECTION OF COOLANT LEAKAGE FOR THERMAL MANAGEMENT SYSTEM OF FUEL CELL VEHICLE

Jisoo Park*, Jaeyoung Han*, Seokyeon Im** and Sangseok Yu*

*Mechanical Engineering of Chungnam National Univ., Gung-dong Yuseong-gu, Daejeon, Korea

**Automobile Engineering of Tongmyong Univ., Yongdang-dong, Nam-gu, Busan, Korea

Abstract – Proton exchange membrane fuel cell (PEMFC) which is used for fuel cell vehicle is sensitive to operating temperature because PEMFC stack is critically damaged at high temperature which is 85°C. When the coolant is leaked, temperature of PEMFC stack will rise over set value due to deficit of cooling capacity. In this study, fault detection algorithm for the coolant leakage is developed so that the controller can recognize the temperature rising. An analytic approach is applied to develop the PEMFC stack model and the cooling system is made up by model integration of radiator, fan, water pump, reservoir and 3 way valve. The idea of fault detection of coolant leakage is the correlation between the prediction value of heat balance which is sum of heat generation and cooling capacity and measured value of PEMFC stack temperature. When coolant leakage is from 0% to 75%, the algorithm predicts fault under change of various loads.

Index Terms – PEMFC, Thermal management system, Coolant leakage, Fault detection

I. NOMENCLATURE

T_{FC} : Stack temperature, °C

Q : Heat capacity, kW

track : Tracking value

II. INTRODUCTION

A proton exchange membrane fuel cell (PEMFC) has shown the most promising technology for automotive application based on their low operating temperature, faster start-up, relatively simple design and competitive power density. The performance of PEMFC is dependent on water and thermal management. And the operating temperature of PEMFC should be ranged from 60 to 70 °C under typical operating conditions.

Even though the fuel cell system has coolant leakage, thermal management system operated by regular operating algorithm. Since lower cooling capacity increases stack operating temperature, stack seems to be exposed to fatal damages. To prevent fatal damage of PEMFC stack, development of leakage detection algorithm is needed. This study presents fault detection algorithm of the coolant leakage is developed to recognize the fault of the rising stack temperature. The algorithm is confirmed with simulation of PEMFC system under various load conditions.

III. COOLANT LEAKAGE FAULT DETECTION

A. Thermal management system of PEMFC

PEMFC system model is composed of a dynamic heat generation of fuel cell stack model and dynamic cooling system

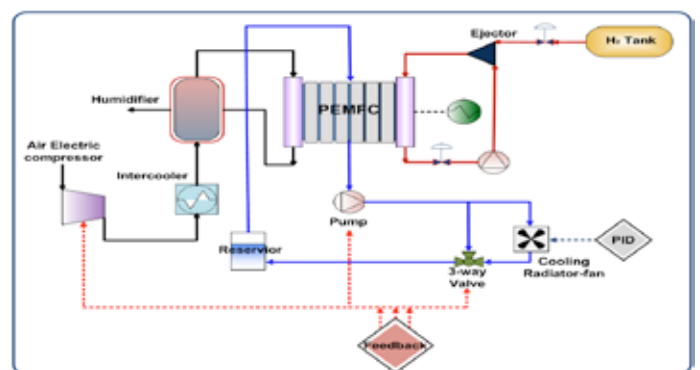


Fig. 1. Schematic of automotive PEMFC system

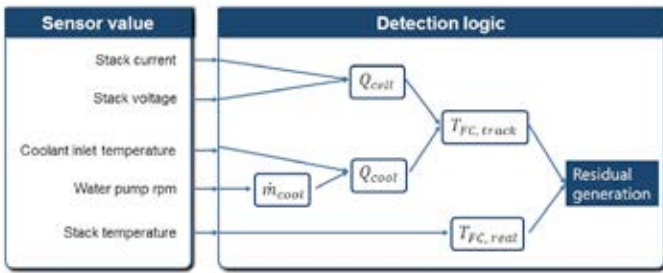


Fig. 2. Flow chart of residual generation

to maintain operating temperature. An analytic PEMFC stack model is developed and the cooling systems in Fig.1 is made up of radiator, fan, water pump, reservoir and 3 way valve. The blue line in the figure shows the flow of coolant inside the fuel cell system.

B. Fault detection method for coolant leakage

Fig.2 shows the flow chart of fault detection. The measurable data such as current and temperature is used for tracking stack temperature. Tracking temperature can be determined by using the following equation.

$$T_{FC} = \frac{T_{c,o} - T_{c,i} \exp(f(h, A, \dot{m}_c, c_p))}{1 - \exp(f(h, A, \dot{m}_c, c_p))}$$

This equation is soft sensor which is calculated to track the normal value. Although coolant is leaked, flow rate can make normal value because it is calculated by soft sensor. Therefore, rising stack temperature is able to be detected by comparing measured temperature with tracking temperature.

C. Results and discussion

We assume that coolant leakage is 10%, 30%, 50% and 70% respectively in Table 1 and input current density is set to 1A/cm². Residual is generated by comparison of sensor value with tracking value. These results show that residual is increased as leakage is increased. Especially, stack temperature is close to the damage regime when leakage rate is greater than 50% of normal amount. In this case, although water pump operates full rpm, stack temperature is increased due to lack of coolant. Otherwise, tracking value has normal stack temperature because pump speed directly changes to mass flow

TABLE I
COOLANT LEAKAGE FAULT SCENARIO

Number	Leakage amount of coolant	Residual
SC01	10% leakage of coolant	2.34
SC02	30% leakage of coolant	5.75
SC03	50% leakage of coolant	12.75
SC04	70% leakage of coolant	22.21

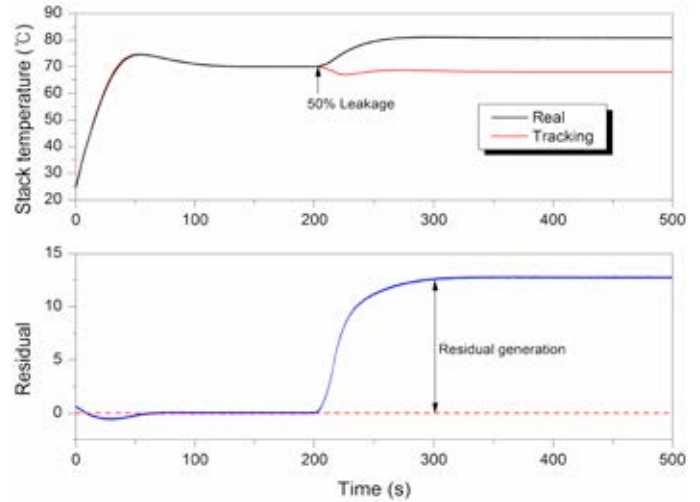


Fig. 3. Residual generation for 50% coolant leakage

lookup table. Based on residual data, signal can be used to notice the degree of danger.

IV. CONCLUSION

In this study, fault detection algorithm is developed for leakage of coolant. In five cases of leakage, we can get each residual data which extracted by analyzing the sensor and tracking value. Particularly, as leakage rate is over 50%, stack temperature rises to the risk area. Developed algorithm can give information to decide amount of coolant and how serious it is. As an alternative for heavy leakage of coolant in fuel cells, the algorithm limits input current when the fault is detected.

ACKNOWLEDGMENT

This research was supported under a Basic Science Research Program through the National Research Foundation of Korea(NRF), funded by the Ministry of Education, Science and Technology (grant number: NRF-2014R1A1A2053692)

REFERENCES

- [1] James Larminie, Fuel cell systems explained, John Willy and Sons, 2003
- [2] Jaeyoung Han, Sungsoo Kim, Sangseok Yu, Systems response of automotive PEMFC with dynamic modeling under load change, Korean Society of Automotive Engineers, 2013, Volume 21, Pages 43-50
- [3] Alex Bates, Sunwook Hwang, Santanu Mukherjee, Sang C. Lee, Osung Kwon, Gyeung Ho Choi, Sam Park, Simulation of an innovative polymer electrolyte membrane fuel cell design for self-control thermal management, International Journal of Hydrogen Energy, Volume 38, 2013, Pages 8422-8436
- [4] D. Benouioua, D. Candusso, F. Harel, L. Oukhellou, PEMFC stack voltage singularity measurement and fault classification, International Journal of Hydrogen Energy, Volume 39, 2014, Pages 21631-21637



MEASURING THE PERFORMANCE OF A DE-PEMFC SUPPLIED WITH AIR AT THE CATHODE

G. S. Oliveira^{1*}, P. Belchor^{2***}, G. C. Benetti^{3*}, M. M. C. Forte^{4**}, F. Breyer^{5*},
J. P. Bottin^{6*}, R. A. Milani^{7*}, and G. K. Col^{8*}

*UNOESC, Rua Getúlio Vargas, 2125 – Flor da Serra, Joaçaba-SC, 89600-000, (Brazil)

**UFRGS, Av. Bento Gonçalves, 9500 – Agronomia, Porto Alegre-RS, 91501-970, (Brazil)

Abstract - Oxygen is the primary oxidizer used in the cathode of a Direct Ethanol Proton Exchange Membrane Fuel Cell (DE-PEMFC) and the performance in the chemical reaction will be better if this is pure oxygen. In this paper, it was investigate the influence caused in the performance of a DE-PEMFC due to the replacement of pure oxygen at the cathode with air in a parallel serpentine-baffle flow field plate (PSBFFP). By the simulations it was possible to observe that the cell performance was better when used pure oxygen at the cathode. It was concluded that, even leading to a small deterioration in the cell operating performance of the functioning of the cell, the use of air at the cathode can be beneficial if analyzed the number of peripherals and consequent increase in costs that the use of pure oxygen could lead to the functioning of a cell in everyday practical situations.

Keywords – air, flow field plate, fuel cell, oxygen.

I. INTRODUCTION

The performance of a direct ethanol proton exchange membrane fuel cell (DE-PEMFC) depends on numerous parameters, such as the oxygen feed concentration in the cathode. [1]

In this paper, a DE-PEMFC performance was tested by using oxygen or air in the cathode.

II. MATERIALS AND METHODS

The experimental runs in the laboratory were carried out in a DE-PEMFC prototype unit, as shown in the schematic

diagram in Figure 1. In a second moment the oxygen was replaced by air.

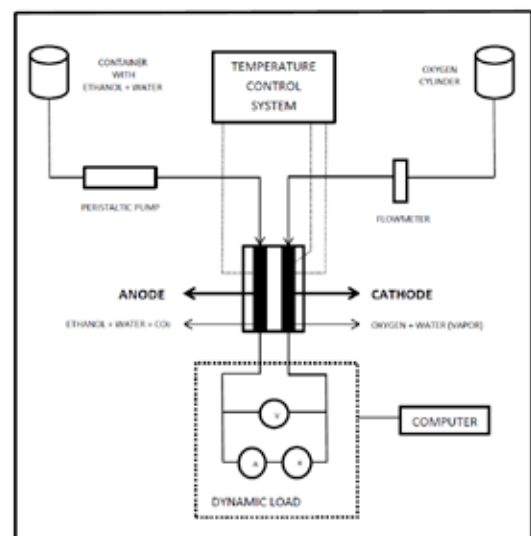


Fig. 1. Schematic DE-PEMFC unit flow diagram.

During the tests the flow variable of ethanol alcohol inserted into the anode was controlled at 12 mL/min, wherein the concentration of the alcohol used was 1 M, the cell temperature was controlled at 80°C and the torque in the threads used to compress the cell was 3 N.m. At the cathode, where there were variations in the type of reagent (oxygen and air), the flow rate was controlled at 1 L/min. Both electrodes were equipped with parallel serpentine-baffle flow field plates (PSBFFP).

III. RESULTS AND DISCUSSION

When analyzing the behaviors of voltage – current curve and power – current curve, shown in Figure 3, it was possible to observe that the cell performance was better when used pure oxygen at the cathode.

This difference in the performance of the cells becomes slightly more pronounced in the final part of the curves, due to the potential drop by diffusion occurs mainly at high current densities, caused by limitations in the mass diffusion primarily at the cathode.

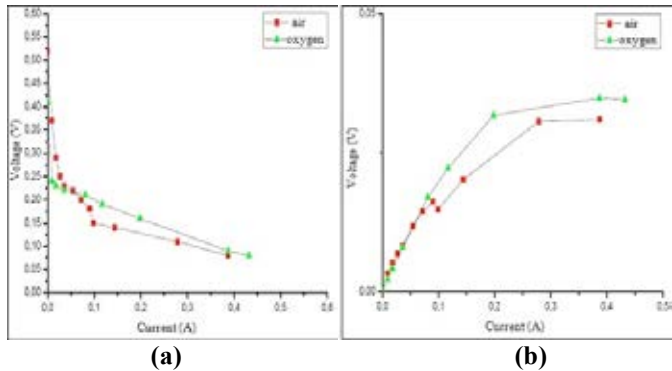


Fig. 3. (a) Current density-voltage curve and (b) Power-current curve with the cathode flow configurations

IV. CONCLUSION

As a result it was concluded that, even leading to a small deterioration in the cell operating performance of the functioning of the cell, the use of air at the cathode can be beneficial if analyzed the number of peripherals and consequent increase in costs that the use of pure oxygen could lead to the functioning of a cell in everyday practical situations.

ACKNOWLEDGMENT

The financial support of the Brazilian Government Agencies Coordenação de Aperfeiçoamento de Pessoal de Nível Superior (CAPES) (PROCAD 714/2008) and Conselho Nacional de Desenvolvimento Científico e Tecnológico (CNPq) (Projeto Universal 482401/2010-9) are gratefully acknowledged.

REFERENCES

- [1] Andreadis, G., Tsiakaras, P, Ethanol crossover and direct ethanol PEM fuel cell performance modeling and experimental validation, Chem Eng Sci, Volume 61, 2006, pp. 7497-7508.



DIFFERENTIAL PRESSURE APPARATUS: AN ENHANCEMENT OF CLASSIC SIEVERT INSTRUMENT

Matteo T., Luigi Crema (1)

(1) Foundation Bruno Kessler, Trento (I)

Abstract An Isochoric Differential Apparatus (IDA) is a differential unit that allows improving accuracy in gas sorption measurements, especially for light gases. Differential pressure measures have several advantages compared to absolute one, about accuracy, sensibility and tolerance on temperature variations, which strongly affect classic Sievert measurements. IDA has been realized and tested with standard materials for hydrogen storage (as Platinum).

Index Terms - Hydrogen Storage, Metal Hydride, Gas sorption measurement.

I. INTRODUCTION

Hydrogen storage is a limit barrier on the future coming of hydrogen's economy, expected since many years. Nowadays, main methods to store hydrogen are: liquid storage, compress gas storage and solid state storage, and only last one seems to achieve DoE 2015 target (5.5%w, 0.04 kg/L, refilling time below 3 min and more important, a cost below 2 \$ for kWh stored). [1]

In last years, incorrect and few accurate measurements about hydrogen uptake on carbon material, caused great sensations and claims for their initial anomalous results, but they renewed the attention of scientific community on these materials and hydrogen solid-state storage in general. [1] [2] [3]

Principally, measurement's errors were correlated to the kind of applied characterization method: volumetric, gravimetric and thermogravimetric one, coupled to their procedure of calibration and accuracy determinations. This problem raises because the hydrogen management is very difficult for many reasons: high gas diffusion, very low density as well as its high intervall of infammability, low activation energy of ignition and particular safety managements. Moreover, many other problems derived from the small amount of analized sample (also few tens of mg), typical for innovative nanostructure materials.

A considerable part of scientific publication about hydrogen storage topic, was focused on to enhance and to increase measurement accuracy in hydrogen sorption characterization (both kinetics and thermodynamics one). Among such techniques, there are several work about: rigorous Round Robin tests [4], new procedure and mathematical approaches [5] (i.e

more accurate gas equations [6]) and innovative instrument designs.

Volumetric techniques are widely applied for characterization of gas' sorption, and seem to be quite interesting on hydrogen storage studies, respect to gravimetric one for many reason: they have a high intrinsically accuracy in sorption characterization with light gas, as hydrogen respect to other methods, and the apparatus is cheap, versatile and simple, as well as does not require complicated management. In volumetric approach, sorption measurement are based on the variation of pressure in a fixed volume, while sample is kept at constant temperature (isothermal reaction). Accuracy of measures principally depends on calibrated volumes of instrument, accuracy of pressure sensors and the management of isothermal conditions in the apparatus.

In this context, FBK (Bruno Kessler Foundation) is developing and realizing an innovative volumetric instrument, natural evolution of standard Sievert instrument: (classic layout of volumetric apparatus for the hydrogen sorption characterization). In this brief abstract, such instrument will be exposed.

II. DIFFERENTIAL PRESSURE APPARATUS

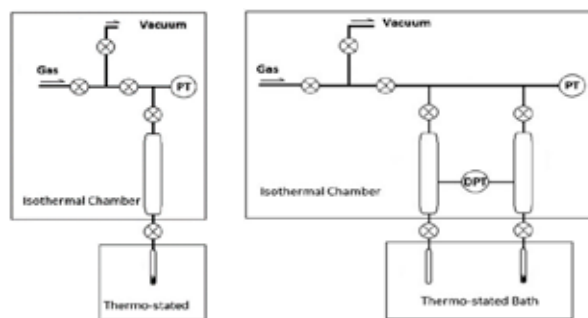


FIG. 1. COMPARISON BETWEEN CLASSICAL DESIGN OF SIEVERT (LEFT) AND DPA LAYOUT (RIGHT).

Differential Pressure Apparatus (DPA) is composed by a double Sievert design, coupled through a differential pressure transducer and gas-supplied with same inlet. Despite to original design, DPA utilizes a limb as the reference system, whereas other limb contains sample and performs the real measure. In this design, sorption measurement is correlated to differential

pressure between the two line (reference and sample). Temperature management is divided in two zones: reference volume of sample and reference line are in an isothermal zone, normally at room temperature, whereas sample and reference chambers are in a second isothermal zone at working temperature. Main advantages of this configuration are :

1. Differential pressure apparatus is more accurate than absolute one.
2. Thermal fluctuation, during measurements, in the expansion's volumes can be neglected or at least reduced.
3. Furthermore, a differential measure between two identical instrument reduce artefacts correlated to nonlinear behaviour of gas during expansion step

DPA can characterize material with low hydrogen storage potential (or to detect small amount of hydrogen uptake, high mass resolution) or, to study very small quantity of sample (typical for nanostructured materials, for synthesis reasons).

DPA is been developed to study material for hydrogen storage application in a wide range of pressure (from 0 to 100-150 Bar), so, every component is tested for high pressure). On the contrary DPA can study only material for hydrogen storage at high temperature (300-600 K, typical for metal hydrides).

Mathematical approach, adopted in our volumetric instrument, estimates hydrogen's uptake from the difference of moles between reference volumes (between initial condition, 0, and final one with closed valves, etc) and overall instrument (between previous equilibrium condition and actual one). Such formulation can be applied for all type of characterization (i.e. kinetics one) and it need not to calibrate every single volume (connections, valves, etc), focusing the calibrations on the main volumes. A critical point of volumetric techniques is to evaluate non-isothermal volume, where a temperature gradient is. Generally, calibrated values are obtained before the measurement, but in order to consider dead space of apparatus with sample, it is used to perform a pre- or post-calibration with helium (Post-calibration is preferable to avoid possible errors caused by helium adsorption). Compressibility factor, Z can be approximated to unity for high temperature and low pressure, but, it needed to be introduced with a good grade of accuracy (generally Soave-Redlich-Kwong, Benedict-Webb-Rubin or its modified expression are used to calculate Z factor) in order to develop a highly accurate instrument [1].

TABLE I

SUMMARY OF MINIMUM ACCURACY AND MAXIMUM AMOUNT OF HYDROGEN DETECTED IN DPA INSTRUMENT WITH THE DIFFERENT REFERENCE VOLUMES (SINGLE STEP).

Ref. Volume	Min. Accuracy	Max. Detection
SUPER: 30cm ³	1E-5 moles	6.1E-3 moles
SMALL: 70cm ³	2E-5 moles	13.4E-3 moles
MIDDLE:180 cm ³	5E-5 moles	40E-3 moles
BIG: 1030 cm ³	1E-4 moles	0.25 moles

A. Errors and Performance

High accuracy of differential pressure, excellent construction of instrument (with identical volumes for sample and reference

line) and small reference volume, allow very low hydrogen sorption detections.

Values reported in tab. 1, are indicative and they are been estimated on errors of calibrated volumes and accuracy of sensor at constant temperature (neglecting errors from compressibility factor). It is necessary to keep in mind errors from no-isothermal volume, which can affect final errors.

III. CONCLUSION AND FUTURE WORKS

DPA has a great potential for the characterization of materials for hydrogen storage application (from reversible metal hydrides to carbon nanostructure like graphene). Instrument is also under calibration step and it will be able to perform complete PCT study (Pressure, composition and temperature characterization) as well as kinetics one. Furthermore, it was also planned to upgrade DPA with BET measurement (specific area characterization, at nitrogen liquid temperature) and so, to develop a final apparatus, able to characterize every aspect of surface sorption, from kinetics and thermodynamics point of view. For this reason, a new system for sample's temperature management will be developed.

Contact

Dott. Matteo Testi, PhD student of University of Trento (I), tel.0461314886, via Sommarive 17, Povo (TN), Italy

REFERENCES

- [1] P.Broom, Darren, *Hydrogen Storage Materials: The Characterisation of Their Storage properties*, Warrington: Springer, 2011.
- [2] Chambers A, Park C, Baker RTK, Rodriguez NM, "Hydrogen storage in graphite nanofibers," *J Phys Chem B*, p. 4253-4256, 1998.
- [3] Dillon AC, Jones KM, Bekkedahl TA, Kiang CH, Bethune DS, Heben MJ, "Storage of hydrogen in single-walled carbon nanotubes," *Nature*, p. 377-379, 1997.
- [4] Claudia Zlotea, Pietro Moretto, Theodore Steriotis, "A Round Robin characterisation of the hydrogen sorption properties of a carbon based material," *international journal of hydrogen energy*, vol. 34, p. (2009) 3044-3057, 2009.
- [5] R. Checchetto, G. Trettel and A. Miotello, "Sievert-type apparatus for the study of hydrogen storage in solids," *Meas.Sci.Technol.*, vol. 15, p. 127-130, 2004.
- [6] H.H. Cheng, X.X. Deng, S.L. Li, W. Chen, D.M. Chen, K. Yang, "Design of PC based high pressure hydrogen absorption/desorption apparatus," *International Journal of Hydrogen Energy*, vol. 32, p. 3046 - 3053, 2007.



DURABILITY AND STABILITY OF TUNGSTEN AND NICKEL COMBINED WITH CERIA ANODE FOR SOFC WITH H₂S CONTAINING FUEL

M.J. Escudero* and A. Fuerte*
*CIEMAT, Av. Complutense 40, 28040 Madrid, (Spain)

Abstract – In the current study, a W and Ni formulation combined with CeO₂ (W-Ni-Ce) has been evaluated in single cell (W-Ni-Ce/LCD/LSGM/LSFC) as sulphur-tolerant anode for SOFC. The cell was exposed to dry 500 ppm H₂S/H₂ during 142 h and humidified 3000 ppm H₂S/H₂ during 135 h at 1023, 1073 and 1123 K. The electrochemical behaviour was investigated by IV curves, impedance spectroscopy and load demands. The results revealed no decay in the cell performance during the load tests studied under both H₂S concentrations indicating that this material is a potential sulphur-tolerant anode.

Index Terms – Anode, electrochemical performance, SOFC, sulphur, W and Ni combined with Ce.

I. INTRODUCTION

Effective utilization of sulphur-containing fuels in solid oxide fuel cells (SOFCs) has generated great interest in the development of sulphur-resistant anode material, due to the conventional Ni/YSZ cermet anode shows a low tolerance to fuel containing H₂S. Doped or undoped ceria oxides are commonly applied as sulphur tolerant components in metal cermet anodes owing to the good performance and lower cost relative to available alternatives, as well as CeO₂ is widely used in sulphur removal process [1]. In addition, WS₂ has been studied as anode material in H₂S oxidation fuel cells to improve performance [2]. Based on these studies, doping with hexavalent W to Ni-CeO₂ could increase the sulphur tolerance.

In a previous study, W-Ni formulation combined with CeO₂, (W-Ni-Ce) was used as anode material for SOFC running on H₂ with H₂S (0-500 ppm) at 1023 K. The results revealed that the cell performance was stable under load demand during 1 h in 500 ppm H₂S/H₂ [3]. Then, the purpose of this work is to investigate its performance and stability in long-terms tests at 1023, 1073 and 1123 K using dry 500 ppm H₂S/H₂ and humidified 3000 ppm H₂S/H₂ as fuel in order to verify its capacity as sulphur-tolerant anode for SOFC. The electrochemical behavior was evaluated in a single cell based on LSGM electrolyte at three mentioned temperatures.

II. EXPERIMENTAL

W-Ni combined with CeO₂ (W-Ni-Ce) with a total loading of 30 wt.% (2/1 atomic ratio for Ni/W system) was prepared by coprecipitation within reverse microemulsion and calcined in air at 1123 K for 2 h [3].

A single cell with an active area of 0.28 cm² was fabricated with LSCF as cathode, LSGM as electrolyte and W-Ni-Ce as anode material. A thin buffer layer of La_{0.4}Ce_{0.6}O_{4-δ} (LDC) was placed between the electrolyte and anode, in order to prevent formation of unwanted phases at the anode electrolyte interface. The cell was tested under dry 500 ppm H₂S/H₂ and humidified 3000 ppm H₂S/H₂ as fuel and stationary air as oxidant at 1023, 1073 and 1123 K. The electrochemical behavior was evaluated by IV curves, impedance spectroscopy and load demands.

III. RESULTS AND DISCUSSION

The voltage and power density of the cell as function of current density at three studied temperatures are displayed in Fig. 1. The values of open circuit voltage (OCV), maximum power density (MPD), ohmic resistance (R_Ω) and polarization resistance (R_p) for all tests are recollected in Table I.

TABLE I
SUMMARY OF THE CELL PERFORMANCE DATA OPERATING ON DRY 500 PPM H₂S/H₂ AND HUMIDIFIED 3000 H₂S/H₂ AT THE THREE STUDIED TEMPERATURES

Gas composition H ₂ S/H ₂	Temp (K)	OCV (mV)	MPD (mW/cm ²)	R _Ω (Ω.cm ²)	R _p (Ω.cm ²)
500	1023	1074	122	0.55	1.72
	1073	1069	226	0.35	1.06
	1123	1061	351	0.29	0.59
3000	1023	1045	94	0.65	2.14
	1073	1036	163	0.50	1.16
	1123	1026	248	0.39	0.73

As can be expected, the OCV values decreased with the increase of both temperature and sulphur content. Both trends with temperature and sulphur electrochemical oxidation agreed with the calculated OCV based on the thermodynamic equilibrium. The MPD decreased with the increasing H₂S concentration and the reduction of temperature. The MPDs decreased by 19, 28 and 29% from 500 ppm to 3000 ppm at



1023, 1073 and 1123 K, respectively. As the same time, both, R_{Ω} and R_p , resistances increase with higher sulphur content. This could be due to a rapid adsorption of S on the Ni, W and Ce surface, blocking the active sites for H_2 adsorption and oxidation, as follows [1]:

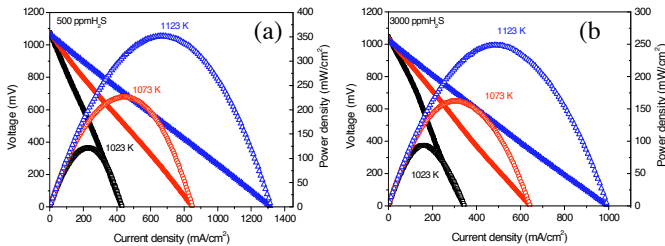
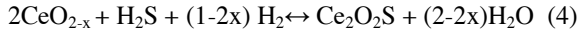
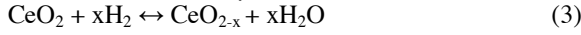
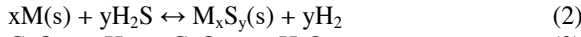
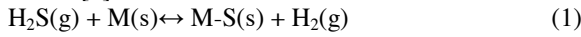


Fig. 1. IV curves of the cell in dry 500 ppm H_2S/H_2 (a) and humidified 3000 ppm H_2S/H_2 (b) at 1023, 1073 and 1123 K

Lohsoontorn et al. [4] reported the stability of nickel and ceria when are exposed to H_2S in H_2 based on thermodynamic calculations. They suggested that the reaction of Ni with sulphur becomes more favourable as temperature and pH_2 decrease, while the reaction ceria with sulphur become more favourable when pO_2 decreases and temperature increases.

In order to evaluate the tolerance of the cell towards higher H_2S concentrations, durability tests were performed under dry 500 ppm H_2S/H_2 during 70, 16.5 and 87 hours at 1023, 1073 and 1123 K, respectively; and under humidified 3000 ppm H_2S/H_2 during 48, 68 and 67 hours at the mentioned temperatures (Fig. 2). The current density demand varied in each test and corresponded to the intensity required to achieve 90% of the maximum power. Each value was obtained of IV curves measurements in identical experimental conditions before the stability test (Fig. 1).

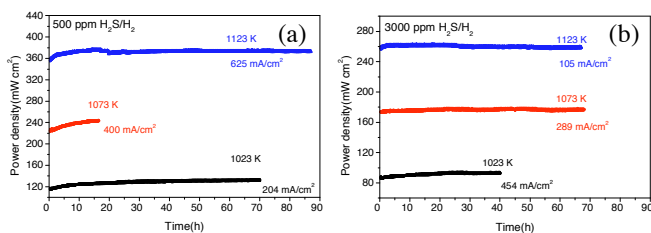
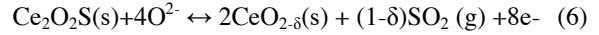


Fig. 2. Power densities of the cell under load demand in dry 500 ppm H_2S/H_2 (a) and humidified 3000 ppm H_2S/H_2 (b) at 1023, 1073 and 1123 K.

As it was supposed, the power density increases with an increase of temperature and a decrease of H_2S content in the feeding. The cell reached power densities of about 133, 243, 373 mW/cm^2 in 500 ppm of H_2S/H_2 and 93, 177 and 259 mW/cm^2 in 3000 ppm of H_2S/H_2 at 1023, 1073 and 1123 K, respectively. However, it is important to note that the cell

performance remained stable and showed a slight improvement in all compositions. This result suggested that the adsorbed sulphur on surface of nickel and Ce_2O_2S could be removed under load current conditions by reacting with oxygen ions to form SO_2 as follow [1]:



Regards to tungstate, WS_2 is very stable in H_2S atmosphere and a suitable electrocatalysts towards hydrogen sulphide oxidation. Then, the formation of WS_2 could be beneficial to the cell performance. Except for 3000 ppm H_2S at 1023 K, the IV curves measured after each stability test showed that MPD values are slightly better compared to initial measurements in identical experimental conditions. Based on these results, CeO_2 and W_2S could inhibit the sulphur poisoning of the Ni surface. Previous studies of the cell performance in humidified 500 ppm H_2S/H_2 at 750 °C revealed similar behaviour under load demand than in dry fuel. This is probably due to the formation of water in the anode that produces an analogous effect to humidify the fuel stream.

IV. CONCLUSION

W and Ni combined with CeO_2 was synthesized and examined as a candidate for sulphur anode material in single cell at 1023, 1073 and 1123 K using dry 500 ppm H_2S/H_2 and humidified 3000 ppm H_2S/H_2 as fuel. The best performance was obtained at lower sulphur content and higher temperature. The cell maximum power densities obtained at 1123 K were 351 and 246 mW/cm^2 in 500 and 3000 ppm H_2S/H_2 , respectively. Analysis of power density under load demand revealed that the cell performance remained stable after 142 h in dry 500 ppm H_2S/H_2 and during 135 h in humidified 3000 ppm H_2S/H_2 indicating that this material is a potential sulphur-tolerant anode, probably caused by the good catalytic activity for H_2 oxidation of the surface sulphides formed with tungsten and the capacity of desulfurization of CeO_2 .

ACKNOWLEDGMENT

This work was supported Spanish Ministry of Economic and Competitiveness (MAT2013-45043-P)

REFERENCES

- [1] Gong, M., Liu X., Tremblay J., Sulfur-tolerant anode materials for solid oxide fuel cell application, *J. Power Sources* 168, 2007, 289-298.
- [2] Yates, C., Winnick, J., Anode materials for a hydrogen sulfide solid oxide fuel cell, *J. Electrochem. Soc.*, 46, 1999, 2841-2844.
- [3] Escudero, M.J., Gómez de Parada, I., Fuente, A., Performance evaluation of $WNi-CeO_2$ as anode in a solid oxide fuel cell fed by simulated biogas mixtures, *Int. J. Hydrogen Energy* 40, 2015, 11303-11314.
- [4] Lohsoontorn, P., Brett, D.J.L., Brandon, N.P., Thermodynamic predictions of the impact of fuel composition on the propensity of sulphur to interact with Ni and ceria-based anodes for solid oxide fuel cells, *J. Power Sources* 175, 2008, 60-67.



EFFECT OF THE CURRENT COLLECTOR STRUCTURE ON THE PERFORMANCE OF THE MOLTEN CARBONATE FUEL CELLS: THE COMBINED COMPUTATIONAL AND EXPERIMENTAL STUDY

Chang-Wan LEE*, Mihui LEE*, Sun Hee Choi*, Sung-Pil YOON*,
Hyung Chul HAM*, Jonghee HAN* and Suk Woo Nam*
*KIST, Fuel cell researcher center

Abstract – In this work, the effect of the current collector structure on the performance of MCFCs was investigated through the computational fluid dynamics (CFD) and experiments. The three dimensional gas flow channel model for simulating current collector was considered instead of using porous media [1]. From the simulation and experiments, it was found that the current collector having large gas open area and ensuring the stable contact between components enhance the performance of the cell.

Index Terms – MCFC, Current collector, CFD

I. INTRODUCTION

The current collector of molten carbonate fuel cells (MCFCS) lies in between electrodes and the bipolar plate. The anode gas and the cathode gas flow through the current collector. In order to investigate the effect of the current collector, three types of the current collectors were compared. From the calculation of the MCFC single cell with three-dimensional fluid dynamics model, distribution of temperature, current density, gas fractions, pressure drop can be obtained. For the verification of the simulation model, the experiments of MCFCs single cell (100 mm x 100 mm) were conducted and compared with the simulation results. The geometry of the current collector for enhancing the electrochemical performance was discussed based on the simulation results and experimental results.

II. SIMULATION MODEL

In the simulation, the open circuit voltage (E_{ocv}) of MCFC is calculated from the gas partial pressure and standard potential (E_0).

$$E_{OCV} = E^0 + \frac{RT}{2F} \ln\left(\frac{P_{H_2,anode} \sqrt{P_{O_2,cathode}}}{P_{H_2O,anode}} \frac{P_{CO_2,cathode}}{P_{CO_2,anode}}\right)$$

$$E^0 = -\frac{\Delta G}{2F} = -\frac{-243730 + 48.996 \times T + 2.474 \times 10^{-3} \times T^2}{2F} \quad (1)$$

The local current density was calculated from

$$i^{x,y} = \frac{E_{OCV}^{x,y} - V_{cell}}{R_{irr}^{x,y}} = \frac{E_{OCV}^{x,y} - V_{cell}}{R_a^{x,y} + R_c^{x,y} + R_{ohm}^{x,y}} \quad (2)$$

In this work, the anode activation resistance (R_a) and cathode activation resistance (R_c) by Yuh and Selman [2] was adopted. The ohmic losses (R_{ohm}) are modelled with Arrhenius type equation and fitted with experimental results.

$$R_a = 2.27 \times 10^{-9} \exp\left(\frac{6435}{T}\right) P_{H_2}^{-0.42} P_{CO_2}^{-0.17} P_{H_2O}^{-1.0}$$

$$R_c = 7.505 \times 10^{-10} \exp\left(\frac{9289}{T}\right) P_{O_2}^{-0.43} P_{CO_2}^{-0.09}$$

$$R_{ohm} = 0.42 \times 10^{-4} \exp\left[4064\left(\frac{1}{T} - \frac{1}{923}\right)\right] \quad (3)$$

In this work, three types of the current collectors were used. The simulation model of the MCFC single cell with the current collector is shown in Fig. 1(a), (b) and (c). In case 1 and case 2, the sheets with sheared protrusions were used for the current collector [3]. In case 1, the base plate of the sheet with sheared protrusions contacts with the anode and the cathode. In case 2, the sheared protrusions contacts with the anode and the cathode. The anode and the cathode have large gas open surface. In case 3, the perforated sheet and the cell frame with flow channels were used for the comparison.

In the simulation model, nearly 400,000 tetrahedral elements and periodic boundary conditions were used. Turbulent model is not used in the simulation model for simplification because the flows in the cathode gas and the anode gas are laminar flow.

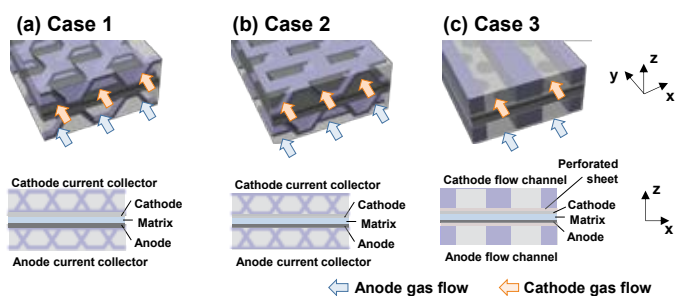


Fig. 1. Simulation model of the single cell with the current collector

III. EXPERIMENTAL SET-UP

For the single cell of MCFCs with the size of 100cm^2 , Ni-5wt%Al anode, lithiated NiO cathode, $\gamma\text{-LiAlO}_2$ matrix were used. A tape-casted Li_2CO_3 and K_2CO_3 electrolyte was used. AISI 316L was used for the cell frame and the cathode current collector. The operating temperature of the single cell is 620°C . The operating pressure is 1 atm. For the tight contact between components, the sealing pressure of 0.2 MPa was applied to the cell frame. The gas utilization at 150 mA/cm^2 is 0.4. The gas compositions are $\text{H}_2/\text{CO}_2/\text{H}_2\text{O}=72:18:10$ for the anode gas and $\text{Air}/\text{CO}_2=70:30$ for the cathode gas.

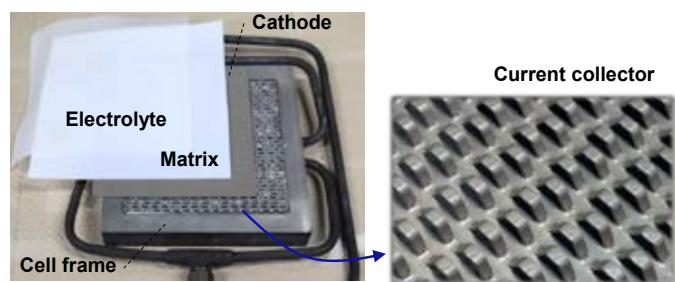


Fig. 2. Experimental set-up for the case 1 (cathode side cell frame) and the shielded slot plate for the current collector

IV. RESULTS AND DISCUSSIONS

The voltage of the single cell at 150 mA/cm^2 , N_2 crossover at the anode exit, and internal resistance (IR) of three cases were compared in Table 1. In three cases, there were no significant differences in the N_2 cross-over at anode gas exit and internal resistance (IR) of the cell. The difference of the cell voltage at 150 mA/cm^2 between the calculated results and the experimental results was less than 3mV. The simulation results show excellent agreements with the experimental results.

Both in the simulation and in the experiments, the single cell of case 2, which has the largest gas open area to the electrodes, shows better performance than other two cases.

Table I. voltage of the cell at 150 mA/cm^2

	Experimental results	Calculated results
--	----------------------	--------------------

	IR (m Ω)	N_2 cross-over (%)	Cell voltage (V)	Cell voltage (V)
Case 1	3.9 m Ω	0.35 %	0.821 V	0.823 V
Case 2	4.1 m Ω	0.32 %	0.834 V	0.832 V
Case 3	3.8 m Ω	0.34 %	0.813 V	0.816 V

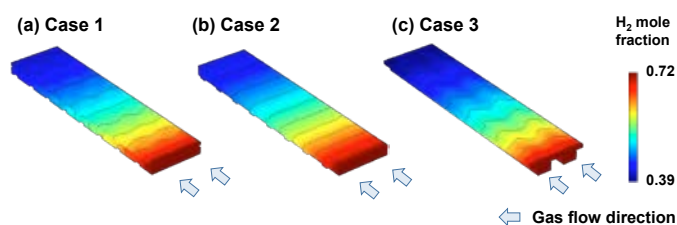


Fig. 3. H_2 mole fraction in the anode flow channel and the anode

To investigate the effect of the current collector structure, H_2 mole fractions in the anode side at 150 mA/cm^2 were compared. Fig. 3 presents H_2 mole fractions in the anode side of three cases. In case 2, the contour of the H_2 mole fraction was nearly perpendicular with the gas flow direction, because the fuel gases are supplied to electrodes more efficiently than other cases. These results indicate that the current collector with large gas open area reduces polarizations and enhances the cell performance.

V. CONCLUSION

In this work, the effect of the current collector structure on the performance of MCFCs was investigated numerically and experimentally using three types of current collectors. The simulation model precisely predicts the performance of the cell. The current collector structure, which makes large gas open area to electrodes, results in effective gas supply to electrodes, and as a result, the performance of the fuel cells increases.

REFERENCES

- [1] H. Kim, J. Bae and D. Choi, An analysis for a molten carbonate fuel cell of complex geometry using three-dimensional transport equations with electrochemical reactions, International Journal of Hydrogen Energy, Volume 38, 2013, pp. 4782-4791
- [2] C. Y. Yuh and J. R. Selman, The polarization of molten carbonate fuel cell electrodes: I Analysis of steady-state polarization data, Journal of The Electrochemical Society, Volume 138, 1991, pp. 3642-3648
- [3] C. W. Lee, D. Y. Yang, D. W. Kang and T. W. Lee, Study on the levelling process of the current collector for the molten carbonate fuel cell based on curvature integration method, International Journal of Hydrogen Energy, Volume 39, 2013, pp. 6714-6728



MODELING AND ANALYSIS OF A 5KWE HT-PEMFC SYSTEM FOR RESIDENTIAL HEAT AND POWER GENERATION

D. Han, D. Kim, and H. Ju

Department of Mechanical Engineering, Inha University, 100 Inha-ro, Nam-Gu Incheon 402-751, (Republic of Korea)

Abstract - In this study, we present a HT-PEMFC system model in which major system modules comprising a fuel reformer, PA doped PBI membrane based HT-PEMFC stack, and a heat recovery are taken account along with several BOP components and heat exchangers. In particular, the consideration of BOP components is necessary for more accurate predictions of system performance and efficiencies because the streams of fuel, air, and water are likely heated up due to the waste heat released from BOP components such as blower and pump. The proposed system model is applied to a 5 kWe HT-PEMFC system and experimentally validated using in-house test results. Thereafter, effects of key operating parameters such as an air-fuel ratio (AFR) for a burner and steam-carbon ratio (SCR) for a SR reactor in a fuel processor are numerically investigated to address their influence on product compositions and efficiencies of the HT-PEMFC system.

Index Terms - high temperature fuel cell system, phosphoric acid doped PBI membrane, steam reforming, system modeling

I. INTRODUCTION

Proton exchange membrane fuel cells (PEMFCs) combined heat and power generation (CHP) system is suitable for residential power generation system compared to CHP system based on stirling engines and internal combustion engines owing to its low greenhouse gas emissions, simple maintenance, and high electrical efficiencies [1].

In this study, we present a high temperature (HT) PEMFC CHP system model in which major system modules comprising a fuel reformer, PA doped PBI membrane based HT-PEMFC stack, and a heat recovery are taken account along with several BOP components and heat exchangers. In particular, the consideration of BOP components is necessary for more accurate predictions of system performance and efficiencies because the streams of fuel, air, and water are likely heated up due to the waste heat released from BOP components such as blower and pump. The proposed system model is applied to a 5 kWe HT-PEMFC system and experimentally validated using

in-house test results. Thereafter, effects of key operating parameters such as an air-fuel ratio (AFR) for a burner and steam-carbon ratio (SCR) for a SR reactor in a fuel processor are numerically investigated to address their influence on product compositions and efficiencies of the HT-PEMFC system.

II. NUMERICAL MODEL

Fig. 1 schematically shows displays 5kW fuel cell system that consists of three major modules, i.e., a fuel-reforming module, a HT-PEMFC stack module with PA-doped PBI membrane, and a heat recovery module, are intricately connected with the BOP components (pumps, blowers, and compressors) and heat exchangers.

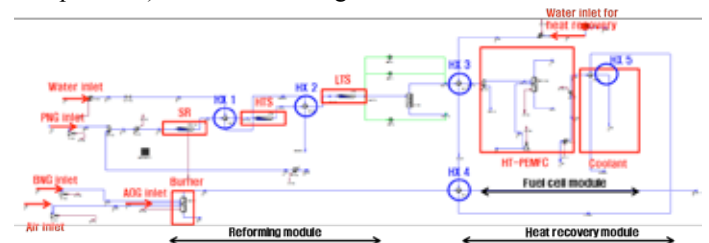


Fig. 1. Flowsheet of the 5kW_e HT-PEMFC system model

Peng-Robinson's equation of state was used to calculate the thermodynamic properties of gas mixture in individual reactors. Reaction phenomena occurring in the reactors were predicted by the plug flow kinetic model proposed by Xu and Froment [2].

The HT-PEMFC stack model is simplified from the previous three-dimensional HT-PEMFC CFD models [3-5]

III. EXPERIMENTS

An experimental fuel processor was designed and installed in the facility of Korea Gas Corporation (KOGAS). The burner is installed to maintain the operating temperature of the

reformer. The fuel processor system is composed of evaluation device, several reactors, heat-exchangers, mass flow controller (MFC), chiller, gas analyzer, manometer, thermometer, and a burner.

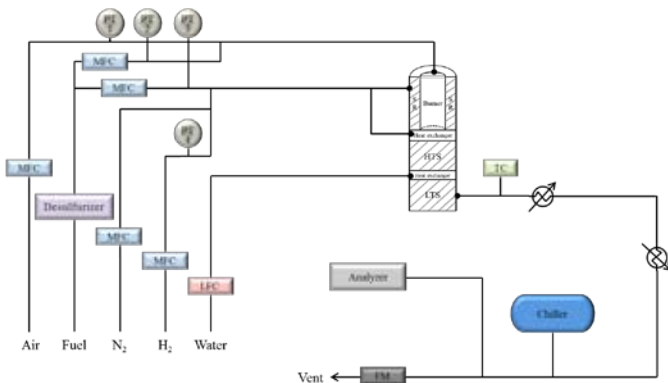


Fig. 2. Schematic of experimental setup to measure exhaust gas compositions

IV. RESULTS AND DISCUSSION

The HT-PEMFC system model accurately reproduces exhaust gas compositions and bed temperatures measured at various locations, which demonstrates the validity and accuracy of the present HT-PEMFC model. The parametric study was carried out in terms of two major operating variables, i.e., the air fuel ratio (AFR) for the burner and steam to carbon ratio (SCR) for the steam reforming (SR) reactor. As expected, the highest rate of heat supply from the burner to SR reactor was achieved with equivalent ratio (ER)=1 that corresponds to the AFR of 4.587 at the burner natural gas (BNG) flow rate of 0.3177 kg/h. If the ER is higher or lower than ER=1, the amount of heat supply decreases. The highest electrical, thermal and CHP efficiencies were obtained when ER is equal to 1.062, because the high temperature shift reactor (HTS) and low temperature shift reactor (LTS) temperatures were lowered by higher ER. However, as the ER increase more than 1.062, the hydrogen yield and stack power considerably drop due to insufficient heat supply from the burner to SR reactor. On the other hand, the effect of SCR for efficiencies of HT-PEMFC system was lower than AFR, but it had significant impact on HTS and LTS temperature. As the water stream flow rate rises, the larger portion of burner heat was consumed to heat up the larger amount of steam flow, which reduces the overall temperature of SR, HTS and LTS reactors. Therefore, the hydrogen yield was higher and the CO content was lower with the higher SCR.

V. CONCLUSION

In this study, we presented a 5kWe HT-PEMFC system model that consist of three system modules comprising a fuel reformer, PA doped PBI membrane based HT-PEMFC stack, and a heat recovery with seven BOP components and heat

exchangers. The kinetic models were simulated with commercial flowsheet simulator, ASPEN HYSYS, to implement the chemical reactions in the SR, HTS and LTS reactors, the electrochemical process of HT-PEMFC stack and the heat recovery process of HT-PEMFC system. First, the model was experimentally validated using in-house test results. Overall, the model successfully found the effects of burner AFR and SCR for HT-PEMFC system. This paper shows that the present model can maximize the system efficiencies and minimize the CO content through deriving the optimum operating conditions.

ACKNOWLEDGMENT

This work was supported by the New & Renewable Energy R&D program (grant no.20133010031751) of the Ministry of Knowledge Economy of the Government of the Republic of Korea.

REFERENCES

- [1] Alexandros Arsalis, Mads P. Nielsen, Mads P. Nielsen, Application of an improved operational strategy on a PBI fuel cell-based residential system for Danish single-family households, *Applied Thermal Engineering*, Volume 50, 2013, Pages.704-713.
- [2] Xu, J and G. F. Froment, Methane steam reforming methanation and water-gas shift. I. Intrinsic Kinetics, *AICHE J*, Volume 35. 1989, Pages 88-96.
- [3] Purushothama Chippar, Kyeongmin Oh, Whan-Gi Kim, Hyunchul Ju, Numerical analysis of effects of gas crossover through membrane pinholes in high-temperature proton exchange membrane fuel cells, *International Journal of Hydrogen Energy*, Volume 39, 2014, Pages 2863-2871.
- [4] K. Oh, G. Jeong, E. Cho, W. Kim and H. Ju, A CO poisoning model for high-temperature proton exchange membrane fuel cells comprising phosphoric acid-doped polybenzimidazole membranes, *International Journal of Hydrogen Energy*, Volume 39, 2014, Pages 21915-21926
- [5] Kyeongmin Oh, Hyunchul Ju, Temperature dependence of CO poisoning in high-temperature proton exchange membrane fuel cells with phosphoric acid-doped polybenzimidazole membranes, *International Journal of Hydrogen Energy*, Volume 40, 2015, Pages 7743-7753,



SYSTEM MODELING AND SIMULATIONS OF ACTIVE DIRECT METHANOL FUEL CELL (DMFC) SYSTEMS UNDER VARIOUS AMBIENT TEMPERATURES AND OPERATING CONDITIONS

J. Lee, D., Han, G. Gwak, and H. Ju

Department of Mechanical Engineering, Inha University, 100 Inharo, Nam-Gu Incheon 402-751, (Republic of Korea)

Abstract - Direct methanol fuel cells (DMFCs) are potential candidates for portable backup power generation and auxiliary power unit (APU) due to their advantageous features such as the ease of storage and delivery. Optimizing each components of DMFC system is critical to improve overall system performance and power density. We develop a DMFC system model in which major system components including fuel and water tanks, liquid-gas separator, heat exchangers, pumps and blowers are considered with a DMFC stack. The model is implemented within a commercial flow-sheet simulator, ASPEN HYSYS and then applied to a DMFC system to investigate the effects of DMFC operating parameters and heat management. Special emphasis is placed on establishing an active control strategies of DMFC stack temperature and methanol crossover rate via optimizing system components and operating conditions. This study contributes to identifying innovative active DMFC system designs and configuration.

Index Terms - direct methanol fuel cells (DMFCs), active DMFC system, liquid-gas separator, methanol crossover, thermal management

I. INTRODUCTION

Direct methanol fuel cell (DMFC) using liquid methanol solution as fuel has several advantages in terms of fuel storage and delivery compared to hydrogen fuel cells. That makes the DMFC technologies more suitable for small to medium scale power generation up to 1 kW. A passive fuel supply in a DMFC system is based on direct use of low concentrated methanol feed fuel (less than 4-5 M) to mitigate methanol crossover. Although the passive design enables to construct a simple system configuration, the passive DMFC system exhibits low energy density. On the other hand, the pure methanol is stored in an active DMFC system wherein the methanol feed concentration for a DMFC stack is diluted by the water produced during DMFC operations. Therefore, the active design is more efficient in terms of fuel energy density in the system. However, the active DMFC system tends to be more complicated and larger, having various additional components for fuel recirculation and phase separation. A high degree of

system optimization is required to achieve high system performance and efficiency.

Despite the considerable efforts in DMFC modeling and simulations, only few works for theoretical analysis of active DMFC system were presented in the literature [1-2]. In this paper, we develop an active DMFC system model wherein various auxiliary components such as pump, blowers, heat exchangers, and liquid-gas separator as well as a DMFC stack were rigorously taken into consideration. A one-dimensional (1-D) DMFC model developed in our previous studies [3-5] is coupled with a zero-dimensional DMFC system model in order to accurately predict the electrochemical reactions and resulting species/heat transport and methanol crossover inside a cell. Numerical simulations are conducted and DMFC performance and system efficiencies are analyzed under various system operating and external conditions. This study clearly elucidates the operating characteristics of an active DMFC system, helping to identify optimization strategies of DMFC system integration and operations.

II. NUMERICAL MODEL

To analyze an active DMFC system, the 1-D DMFC model and DMFC system model are coupled. Readers can be referred to Ko et al. [4] and Chippar et al. [5] for detailed description of model assumptions and governing equations. The main assumptions invoked in the DMFC system model are,

1. The gas phase obeys ideal gas law.
2. The exhaust temperatures of anode and cathode are same.
3. A very small fraction of carbon dioxide in the liquid-gas separator and thus, partial pressure of CO₂ is negligible.

Under a given current density, the cell voltage is calculated by the 1-D DMFC model that considers the theoretical thermodynamic potential, anode and cathode over potentials, membrane ohmic resistance, and contact resistance as follows.

$$V_{cell} = U_0 - \eta_c - \eta_a - i \frac{\delta_{mem}}{\kappa_{mem}} - iR_{cont} \quad (1)$$



The overall cell efficiency and heat balance of DMFC system can be expressed as,

$$\varepsilon_{cell} = \varepsilon_{thermal} \varepsilon_{voltaic} \varepsilon_{fuel} = \left(\frac{\Delta \bar{g}^o}{\Delta \bar{h}^o} \right) \left(\frac{V_{cell}}{U_o} \right) \left(\frac{i}{i + i_{xover}} \right) \quad (2)$$

$$\frac{(1-\eta_{cell})}{4} (i \times A_{mem}) V_{cell} N_{cell} = \left[\frac{r_{H_2O} C_{H_2O} (T_{anode} - T_{cathode})}{4} + \frac{r_{CH_3OH} C_{CH_3OH} (T_{anode} - T_{cathode})}{4} \right] + h_{H_2O} A_{mem} (T_{anode} - T_{cathode}) \quad (3)$$

In the Eq. (4), the heat generation rate of DMFC stack is estimated based on the cell voltage calculated from the 1-D DMFC model as follows,

$$Q_{gen} = \left(\frac{1 - \varepsilon_{cell}}{\varepsilon_{cell}} \right) (i \times A_{mem}) V_{cell} N_{cell} \quad (4)$$

The anode and cathode exhausts from the DMFC stack need to be mixed in the liquid-gas separator module and then additional methanol and/or water are injected into the anode fuel recirculation loop. The gas phase flow rate in the liquid-gas separator is calculated by the following equation

$$Q_{sp}^g = \frac{\left[\dot{N}_{O_2,c,in} - \left(\frac{i + i_{xover}}{4F} \right) A_{mem} \right] + \dot{N}_{N_2,c,out}}{\left[\frac{P_{sp}^g - P_{sat}(T_{sp})}{R_u T_{sp}} \right]}$$

As shown in Fig. 1, the DMFC system model comprising a DMFC stack, a liquid-gas separator module, fuel recirculation module along with several BoP(Balance of Plants) components and heat exchangers is numerically implemented using commercial software ASPEN-HYSYS.

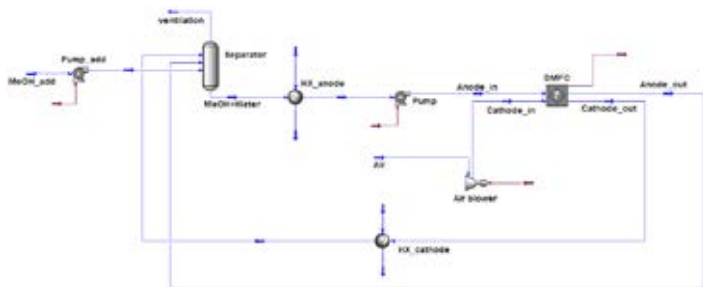


Fig. 1. Flowsheet of the active DMFC system model

III. RESULTS AND DISCUSSIONS

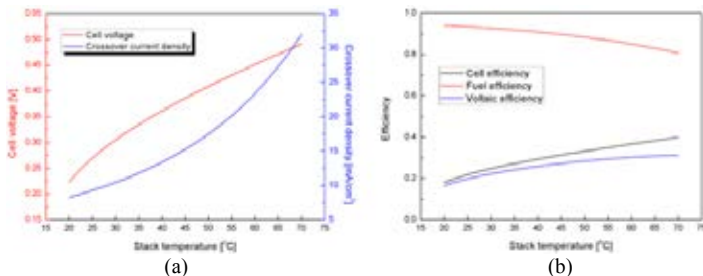


Fig.2. (a) Cell voltage and methanol crossover density and (b) efficiencies as a function of DMFC stack temperature

Fig 2a shows the effect of stack temperature on crossover

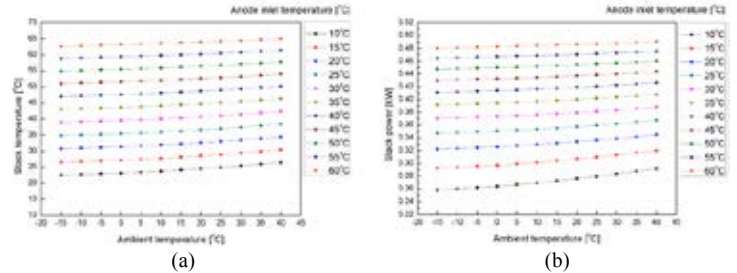


Fig.3. (a) temperature and (b) power of DMFC stack under different methanol feed and ambient temperatures

- (5) Figs 3a and 3b show the impacts of the ambient temperature and methanol feed temperature on the stack temperature and power, respectively. It is evident that both stack temperature and stack power are highly affected by the ambient temperature. The simulation results clearly indicate that as the ambient temperature varies, the methanol feed temperature should be properly adjusted to maintain optimum DMFC performance and efficiency.

ACKNOWLEDGMENT

This work was supported by the Technology Innovation Program (20143030031330, Development of Fuel Cell Technology for Charging Secondary Battery in Extreme Environment) funded By the Ministry of Trade, industry & Energy(MI, Korea).

REFERENCES

- [1] Federico Z., Ulrike K., Modelling, dynamics and control of a portable DMFC system, Journal of Process Control, Volume 20, 2010, Pages 630-642.
- [2] Stefanie A., Josefin M., Process analysis of a liquid-feed direct methanol fuel cell system, Journal of Power Sources, Volume 91, 2000, Pages 193-201.
- [3] Johan K., Kyungmun K., Sunghyun P., Whan Gi K., Soon Ho L., Hyunchul J., Effect of design of multilayer electrodes in direct methanol fuel cells (DMFCs), International Journal of Hydrogen Energy, Volume 39, 2014, Pages 1571-1579.
- [4] Johan K., Purushothama C., A one-dimensional, two-phase model for direct methanol fuel cells – Part I: Model development and parametric study, Energy, Volume 35, 2010, Pages 2149-2159.
- [5] Purushothama C., Johan K., A global transient, one-dimensional, two-phase model for direct methanol fuel cells (DMFCs) - Part II: Analysis of the time-dependent thermal behavior of DMFCs, Energy, Volume 35, 2010, Pages 2301-2308.



SYNTHESIS AND ELECTRICAL PROPERTIES OF GD-DOPED CERIA ELECTROLYTE PREPARED BY SOL-GEL PROCESS FOR IT-SOFC APPLICATIONS

S.U. Costilla^{1,2}, R.F. Cienfuegos-Pelaes¹, M.J. Escudero²

¹CIIDIT, Universidad Autónoma de Nuevo León, Km 10 de la nueva carretera al Aeropuerto Internacional de Monterrey, PIIT Monterrey, CP 66600 Apodaca, Nuevo León (México)

²CIEMAT, Av. Complutense 22, 28040 Madrid, (Spain).

Abstract - In the present work, CeO₂ doped with 10 mol% gadolinium (Gd_{0.1}Ce_{0.9}O_{1.95}, GDC) has been prepared via a polymeric route based on Pechini method which is a modified sol-gel technique. A polymer resin was prepared from different chelating and polymeric agents, it was added to a transition metal solution (TM) to obtain GDC compound. The effect of the resin nature, the complexing agent/metal transition (R=CA/TM) ratio, on the structure and the electrical properties was examined for R=1, 2 and 3. Dense GDC pellets having 97 % of the relative density were obtained at sintering temperature of 1400 °C for 2 h. For R= 2, GDC gave significantly higher total ionic conductivity of $1.2 \times 10^{-2} \text{ S cm}^{-1}$ at 600 °C. It is also found a minimum activation energy value of 0.78 eV from 500 to 800 °C, and a thermal expansion coefficient of $13.8 \times 10^{-6} \text{ K}^{-1}$

Index Terms - Gadolinium doped ceria, Solid electrolyte, SOFC, Sol-gel.

I. INTRODUCTION

Solid oxide fuel cells (SOFC) have a great potential because they show cleaner energy by their direct conversion from chemical to electrical energy. Most commonly, standard electrolyte materials, based on stabilized zirconias, require to operate at 900-1000 °C to ensure sufficient ionic conductivity. However, at high temperature operating, some destructive factors such as thermal mismatch between materials cathode and electrolyte, reactions at electrode/electrolyte interfaces, may occur. Ceria-based materials are potential electrolytes for intermediate temperature solid oxide fuel cells (IT-SOFC) due to their high ionic conductivity at relative moderate temperatures (above 600 °C). Among doped ceria compounds, Gd-doped ceria (GDC) and Sm-doped ceria (SDC), have the highest conductivity since the ionic radius of Gd³⁺ (or Sm³⁺) was close to the ionic radius of Ce⁴⁺, due to this their incorporation into ceria lattice produces less distortion in host lattice and creates more oxygen ion vacancies. This excess oxygen vacancies lead to higher ionic conductivity. Gd-doped ceria (GDC) is considered to be one of the best ceria-based solid electrolytes [1,2]. This paper present, the influences of the ratio of complexing agent to metal transition

(R=CA/TM) on the structure properties electrical. The variation of R from 1 to 3 has been investigated by impedance spectroscopy (IS). Hereafter these are abbreviated as GDCR1, GDCR2 and GDCR3.

II. EXPERIMENTAL

The different chelating and polymeric agents such as hexamethylenetetramine, acetic and acetylacetone (Gel) was added to the metal transition (Sol). The solution was maintained under stirring with temperature at 80 °C. Then, the obtained precursors (GDCR1, R2 and R3) were ground and calcined at temperature range from 400 to 900 °C in air during 1 h. The compounds were characterized by TGA/DTA, MS, XRD, and SEM-EDAX. Calcined powders were uniaxially pressed at 1 Ton/cm², the resulting green pellets were calcined at heating rate 2 °C/min, under air during 2 h at 1400 °C. The thermal expansion measurements were conducted with LINSEIS L75HS1550 dilatometer in air. Pt electrodes were coated on both sides of the dense samples and fired at 900 °C during 1 h. The ionic conductivity of the sintered GDC R1, R2 and R3 samples were collected by an AUTOLAB system as a function of temperature from 250 to 900 °C by impedance spectroscopy in a frequency range of 0.01 to 10⁶ Hz at open circuit voltage with an amplitude of mV. The impedance diagrams were analyzed by means of Zview software using equivalent circuits.

III. RESULTS AND DISCUSSION

Thermal decomposition of GDC R1, R2 and R3 samples was determined in dry air atmosphere by TGA/DTA, where the total weight loss of organic compound was found above at a temperature 750 °C [3]. Thus, in order to make sure that all organic compounds are decomposed, the lowest heating temperature for samples (GDC R1, R2, and R3) used in this work was 800 °C. On the other hand, the MS data of all the samples show that CO₂, CH₄, and H₂ gases were evolved during the



combustion reaction among the most important. XRD patterns obtained for the powders GDC R1 to R3 calcined at 800 °C, exhibited to the single-phase fluorite (cubic) structure. SEM micrographs show that the structure is composed of loosely agglomerated spheroid crystal. Samples exhibit an average particle size distribution of 3.45 μm . EDX microanalysis show that the experimental values of all samples are in good agreement with the nominal ones. The thermal expansion coefficients (TEC) of the different samples calculated in the temperature range of 150 to 800 °C were 10.5, 13.8 and 10.9 $\times 10^{-6}\text{K}^{-1}$ for GDCR1, GDCR2 and GDCR3, respectively. Therefore, the TEC value of GDCR2 is a good agreement to match between cathode and electrolyte [4].

The impedance spectra for GDCR1, GDCR2 and GDCR3 were measured in air as a function of temperature (250-900 °C) and sintered at 1400 °C, which are shown in Fig. 1. As it can be seen, two well-defined semicircular arcs merged together, corresponding to the bulk and grain boundary for the observed samples at 300 °C in air.

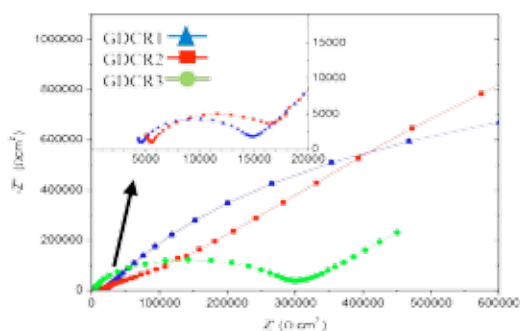


Fig. 1. Typical Nyquist plot comparing GDCR1, GDCR2 and GDCR3 at 300 °C in air sintered at 1400 °C

The semicircles corresponding to bulk and grain boundary are lost from spectrum above 500 °C, respectively. In fact, the first semicircle is attributed to high-frequency region (bulk), the second one as a medium-frequency region (grain boundary), and the third one as a low-frequency region (electrode). All experimental data were fitted to the equivalent circuit containing three resistance-constant phase element pair (R-CPE couple) connected serially.

It can be seen a similar resistive contributions for samples GDCR1 and GDCR2. In the case of GDCR3, the resistive contribution shows higher value than that of GDCR1 and GDCR2. The values of ionic conductivity (σ) and activation energy (E_a) in the temperature range from 600 to 800 °C are summarized in Table 1. The Arrhenius plot of the three samples studied in air show the activation energies of 0.66, 0.78 and 1.03 eV for GDCR1, GDCR2 and GDCR3, at the temperature range from 250 to 800 °C. It can be observed that the activation energies increase as well as R.

On the other hand, the ionic conductivity of GDCR1 and GDCR2 are similar at 600 °C, but it is higher for GDCR3.

These results are according to their activation energies.

TABLE I

SUMMARY OF MEASURED σ AND E_a OF DIFFERENT GDC (R1, R2 AND R3) IN THE TEMPERATURE RANGE 600-800 °C.

Sample	Conductivity σ (S.cm ⁻¹)			Activation energy (eV)
	600 °C	700 °C	800 °C	
GDCR1	1.37×10^{-2}	3.01×10^{-2}	5.12×10^{-2}	0.66
GDCR2	1.20×10^{-2}	2.89×10^{-2}	5.23×10^{-2}	0.78
GDCR3	2.26×10^{-3}	4.29×10^{-4}	2.23×10^{-2}	1.03

Clearly it can be seen that at 600 °C, the ionic conductivity values for the three samples tested presented good results in air atmosphere. It is important to emphasize that the GDCR2 sample presents the highest value of ionic conductivity (1.2×10^{-2} S cm⁻² at 600 °C). This indicates that there are significant changes or influences the ratio of R, in the properties.

IV. CONCLUSION

In the present work, the GDC material has been synthesized with a simple method and low-cost equipment. The results revealed that the ratio of complexing agents (R) affects their electrochemical properties. The best ionic conductivity (1.2×10^{-2} S cm⁻²) was obtained for GDCR2. However, for both GDCR1 and GDCR3 also showed good results.

ACKNOWLEDGMENT

We want to thank CONACyT (number of support-375348) and Spanish Ministry of Economic and Competitiveness (MAT2013-45043-P) for support this project.

REFERENCES

- [1] Arabaci A., Oksuzomer M.F., Preparation and characterization of 10 mol% Gd doped CeO₂ (GDC) electrolyte for SOFC applications, *Ceram. Int.* 38, 2012, 6509-6515.
- [2] Fuentes R.O., Baker R.T., Synthesis and Properties of Gadolinium-doped ceria solid solutions for IT-SOFC electrolyte, *Int. J. Hydrogen Energy*, 33, 2008, 3480-3484.
- [3] Fontaine M.L., Laberty-Robert C., Ansart F., Tailhades P., Elaboration and characterization of La₂NiO_{4- δ} powders and thin films via a modified sol-gel process, *J. Solid State Chem.* 177, 2004, 1471-1479.
- [4] Guo T., Zhang L., Song X., Dong X.L., Shirolkar, Wang M., Li M., Wang H., Influences of Gd₂Ti₂O₇ sintering M. aid on the densification, ionic conductivity and thermal expansion of Gd_{0.1}Ce_{0.9}O_{1.95} electrolyte for solid oxide fuel cells, *J. Power Sources* 262, 2014, 239-244.



CURRENT ISSUES OF HYDROGEN STORAGE TECHNOLOGY IN KOREA

Moon-Sun Chung*, Jong-Won Kim*, Jaeseung Suh**

*Hydrogen Energy R&D Center, KIER, 71-2 Jang-dong, Yuseong-gu, Daejeon, (Republic of Korea)

** Sen Tech Co., Ltd.

ABSTRACT

The main purposes of this paper are to overview the current status of research programs for hydrogen storage technologies conducted by Hydrogen Energy R&D Center based on the patent applications as well as research topics and to introduce specific achievements in each research program.

INTRODUCTION

HERC was established for fundamental technical development of clean and non-pollutant energy for the hydrogen economy in the Republic of Korea [1].

Hydrogen storage is one of the key obstacles to the commercialization as well as market acceptance of hydrogen fueled vehicle. Besides the efficiency of power system, it is an extremely challenging technology to store sufficient hydrogen on the vehicle without compromising consumer requirement such as safety, space, driving range, and fuel cost.

The hydrogen storage materials in solid state have some advantages such as high volumetric storage capacity, little energy loss, longer storage time and highest safety. Various carbonaceous and non-carbonaceous hydrogen storage materials have been studied over the past few decades. However, they still have low specific storage capacity and poor cyclic properties

HYDROGEN STORAGE TECHNOLOGIES

1. Metal hydride hydrogen storage materials and small scale storage systems for a fuel cell vehicle

The purpose of this research was to develop metal hydride hydrogen storage materials and storage system for fuel cell vehicle (FCV). In this work, we have tried to develop a process to prepare interstitial metal hydrides and metal borohydrides with more than 3% ($>120 \text{ kg H}_2/\text{m}^3$, $< 300^\circ\text{C}$) and 8 wt% ($> 100 \text{ kgH}_2/\text{m}^3$, $< 300^\circ\text{C}$, between 1 ~ 100 bar) effective hydrogen storage capacity respectively [2].

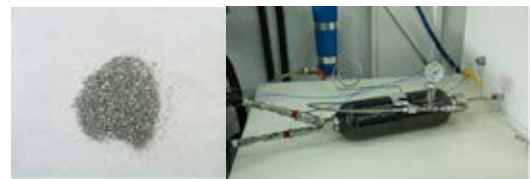


Fig. 1 Metal hydride storage system with BCC material

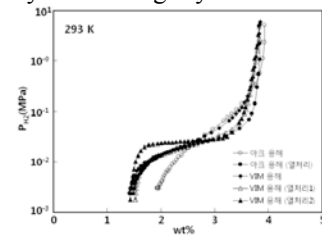


Fig. 2 Cycle performance of Ti-Cr-V-M and dehydrogenation curves of $6\text{LiBH}_4 + \text{CaH}_2$ composite with 5 wt%

2. Nano-structured materials

The porous structures of carbon also can be advantageous in hydrogen storage. And nano size metal particles, such as Ti, Cu, Cr, Ag, and Pt, will be introduced on carbon surfaces in order to gain optimal hydrogen storage capacity [3].

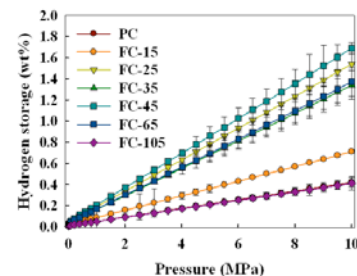
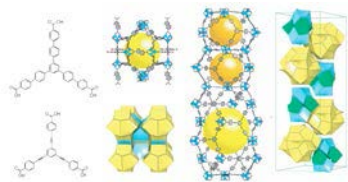
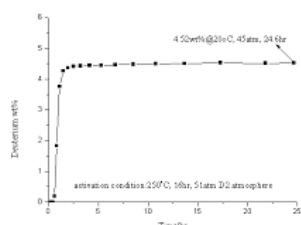


Fig. 3 nanoporous carbon with surface functionality



(a)



(b)

Fig. 4 Nanosized metal-loaded (a) MOF 210 and (b) Ni-Zr/Hf-Ti Quasicrystalline (4.52wt% at 20 °C, 45bar)

In addition, the efficient and mass storage technologies of hydrogen will be developed by using porous nanostructured material: See Reference [4, 5].

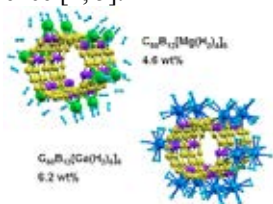


Fig. 5 Suggestion of nanostructured H₂ storage materials

Finally, the porous nanostructured materials having the hydrogen capacity of 4.0wt% at room temperature and 100 bar will be developed. Also, we have searched hydrogen storage materials based on molecular crystals and metal-dispersed materials by optimized materials design using quantum simulations and synthesis of transition metal-dispersed nanotubes.

3. Chemical hydrides

This study aims at development of compact hydrogen storage system using sodium borohydride (SBH, NaBH₄) and ammonia borane (AB, NH₃BH₃) for portable or mobile applications including unmanned aerial vehicle (UAV).



Fig. 6 UPS(100W for 6 hours) system using NaBH₄

4. Mg based storage materials

We have studied Mg based hydrogen storage materials with high capacity and application system by developing a microstructure consisting of nanocrystalline phases of Mg-Ni-X alloy with high capacity and kinetic[6].

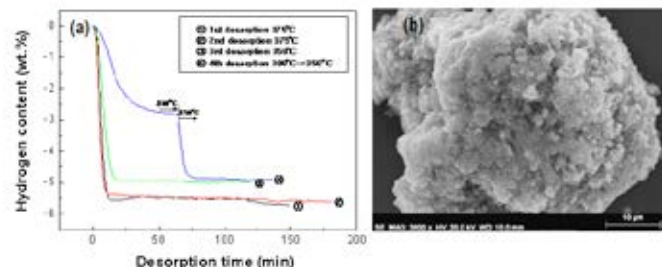


Fig. 7 96%MgH₂+5%Mg₂Ni+1%Ni alloy and hydrogen storage capacity and kinetic property

SUMMARY

The HERC has systematically supporting the wide range of research programs on hydrogen storage technologies for fuel cells. In addition, hydrogen policy and technology assessment have been investigated as well.

REFERENCES

- [1] <http://www.h2.re.kr>
- [2] Y.-W. Cho, et al., "Rehydrogenation and cycle studies of LiBH₄-CaH₂ composite", International journal of hydrogen energy, 35 (2010) 6578-6582.
- [3] Y.-S. Lee, et al., "Effect of thermal fluorination on the hydrogen storage capacity of multi-walled carbon nanotubes", International journal of hydrogen energy, 36 (2011) 1560-1567.
- [4] J. Kim, et al., "Ultrahigh Porosity in Metal-Organic Frameworks", Science, 329 (2010) 424-428.
- [5] J.-W. Choi, H.-Y. Yang, H.-J. Kim, S.-W. Son, "Organometallic Hollow Spheres Bearing Bis(N-Heterocyclic Carbene)Palladium Species: Catalytic Application in Three-Component Strecker Reactions", Angewandte Chemie Int. Ed., 49 (2010) 7718-7722.
- [6] M.-Y. Song, et al., "Effects of Transition Metal Oxide and Ni Addition on the Hydrogen Storage Properties of Mg", Journal of Materials Science, 45 (2010) 5164-5170.
- [7] 2005-N-PS04-P-02, A National Vision of the Hydrogen Economy and the Action Plan, MKE (2005).
- [8] <http://www.wips.co>



Electric conductivity of Nanostructured LaGdSmO₂-based Solid Oxide Fuel Cell

Mohamed K. Hassan^{****}, Aymen El Ameen^{**}, Mohammad S. Alsoufi^{***} and Mohammad A AbdelKareem^{****}

*Production Engineering and Design Dept., Faculty of Engineering, Minia University, 61111-el Minia, (Egypt)

**Department of Physics, Faculty of Sciences, Taibah University, Yanbu Branch, (KSA)

*** Mechanical Engineering Department College of Engineering and Islamic Arc. Umm Al-Qura University Makka (KSA)

**** Chemical Engineering Dept., Faculty of Engineering, Minia University, 61111-el Minia, (Egypt)

Abstract - Chemical stability of La_{1-x-y}Gd_xSm_yO_{2-(0.5(x+y)-δ)} with x, y = 0; 0.1 and 0.2 (LSG) as an electrolyte for solid oxide fuel cells (SOFCs) was investigated during the electrochemical measurement. At low oxygen partial pressure (0.003 atm), the LSG electrolyte partly decomposed due to the development of high over potential, and thus the induced reduction atmosphere near cathode. The morphology of LSG grain near cathode changed due to the formation of new phases. The main decomposition phases were LaO₂, and LaGdSmO₂. The polarization conductance increased due to the microstructural change in LSG and thus the increase in the specific area of the LSG electrode.

Index Terms - LaGdSmO₂, Electrical conductivity(C), Decomposition, and Chemical stability.

I. INTRODUCTION

The solid oxide fuel cells are under development for the generation of electricity with little environmental pollution. Operating of SOFC at low temperatures speeds up its commercialization due to many advantages such as broad choice of cheap interconnect materials and the long-term stability of cell components. Intensive work has been concentrated on finding an electrolyte material with higher ion conductivity than YSZ (Yttria Stabilized Zirconia) that is commercially used as an electrolyte for SOFCs [1-3]. An electrolyte for SOFCs is required not only to have high oxygen-ion conductivity but also to have a high stability under severe operating conditions, such as high temperature and large

oxygen-partial pressure (P_{O₂}) gradient for a long time. LSGM easily decomposes, especially when sintered at temperature greater than 1600 °C, due to the tendency of gallium (III) oxide reduction to gallium (I) oxide [4]. The migration of Si and Al from Pyrex sealant and Pt from electrode into the surface of LSGM electrolyte gives rise to the depletion of Ga from LSGM electrolyte [5]. Doping of lanthanum gallate with Sr and the existence of Pt enhanced the depletion of Ga from the electrolyte in the reducing atmosphere [7]. Examination of P_{O₂} dependence of over potential is one method to determine the reduction mechanism of LSGM. As P_{O₂} decreases, the cathodic over potential increases with applied current. High cathodic over potential tends to reduce the electrolyte. However, the effect of high potential on the cathode and electrolyte due to the applied current is not yet clear for LSGM electrolyte-based fuel cells. In this study, the change in cathode performance and electrolyte properties under high over potential condition was examined.

II. EXPERIMENTAL

Nanostructured samaria-and gadolinia-doped lanthania powders were synthesized at low temperature using diamine-assisted direct co-precipitation method. A series of four samples were prepared by doping LaO₂ with samaria and gadolinia separately and combined. The general formula of the prepared samples is as follow: La_{1-x-y}Gd_xSm_yO_{2-(0.5(x+y)-δ)} with x, y = 0; 0.1 and 0.2. Nano-metric powders were prepared using N,N,N',N' tetramethyl ethyldiamine (TMEDA) used as a base



in the co precipitation from nitrate water solutions of lanthania, samaria and gadolinia. Obtained samples (LaGdO_2 , LaSmO_2 , $\text{La}_{0.6}\text{Gd}_{0.2}\text{Sm}_{0.2}\text{O}_2$, and $\text{La}_{0.8}\text{Gd}_{0.1}\text{Sm}_{0.1}\text{O}_2$) were claimed at 500°C during 6h. X-ray diffraction analysis, Transmission electron microscopy (TEM) analysis and electrochemical characterization carried out for the characterization and the evaluation of the prepared materials. Fig. 1 shows the microstructure of sintered samples.

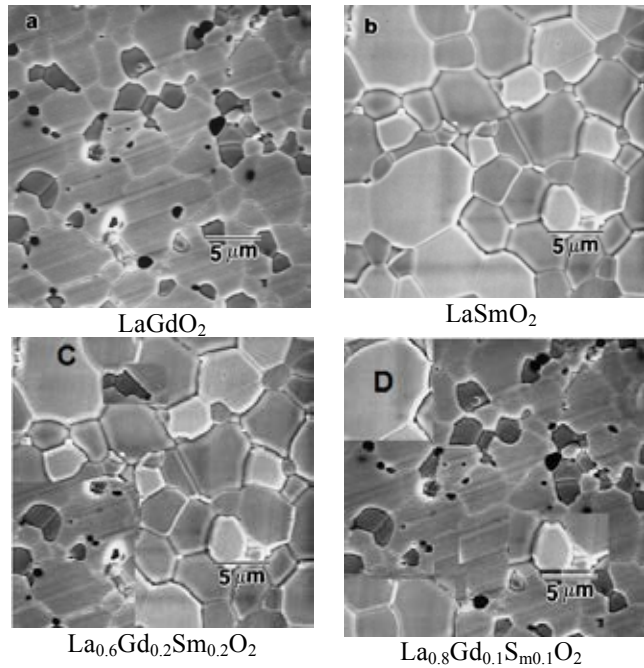


Fig. 1: Microstructure of sintered samples.

III. RESULTS AND DISCUSSION

Figures 2-4 show the effect of the chemical composition of the prepared materials on the electrical conductivity based at different operating temperatures. As being clear from the figures the sample has the composition of $\text{La}_{0.6}\text{Gd}_{0.2}\text{Sm}_{0.2}\text{O}_2$ showed the highest conductivity.

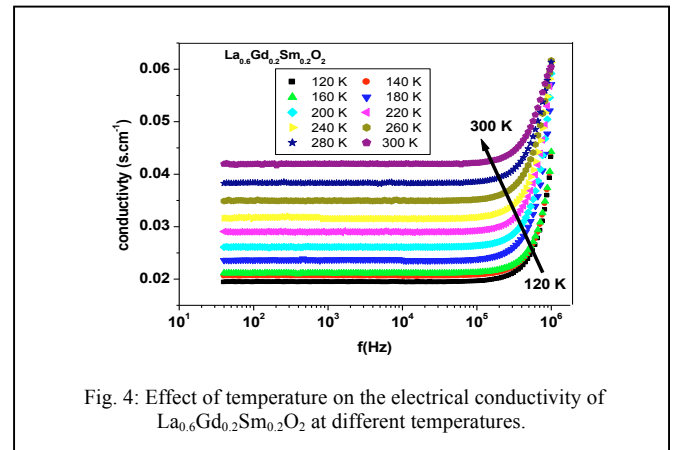


Fig. 4: Effect of temperature on the electrical conductivity of $\text{La}_{0.6}\text{Gd}_{0.2}\text{Sm}_{0.2}\text{O}_2$ at different temperatures.

IV. CONCLUSION

Chemical stability of $\text{La}_{1-x-y}\text{Gd}_x\text{Sm}_y\text{O}_{2-(0.5(x+y)-\delta)}$ with $x, y = 0; 0.1$ and 0.2 (LSG) as an electrolyte for solid oxide fuel cells (SOFCs) was prepared using diamine-assisted direct co-precipitation method. The stability of the prepared materials was investigated during the electrochemical measurement. The LSG electrolyte partly decomposed due to the development of high over potential at low oxygen partial pressure (0.003 atm). The main decomposition phases were LaO_2 , and LaGdSmO_2 . The polarization conductance increased due to the microstructural change in LSG and thus the increase in the specific area of the LSG electrode.

REFERENCES

- [1] F. Yakuphanoglu, Ph.D Thesis, Firat University, Elazig, Turkey (2002).
- [2] U. Schatzschneider, T. Weyhermüller, E. Rentschler, Eur. J. Inorg. Chem. (2001) 2569–2586.
- [3] M.S. Masoud, S.A. El-Enein, E. El-Shereafy, J. Therm. Anal. 37 (1991) 365–373.
- [4] D.F. Shriver, P.W. Atkins, C.H. Langford, Inorganic Chemistry, W.H. Freeman, New York, 1994.
- [5] K.F. Purcell, J.C. Kotz, Inorganic Chemistry, W.B. Saunders, Philadelphia, 1977.
- [6] S.R. Elliott, Adv. Phys. 36 (1987) 135–218.
- [7] M.A. Afifi, A.E. Bekheet, E. Abd Elwahabb, H.E. Atyia, Vacuum 61 (2001) 9–17.

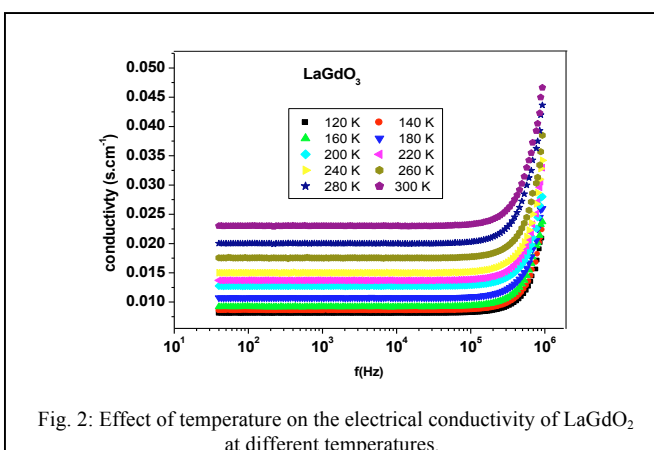
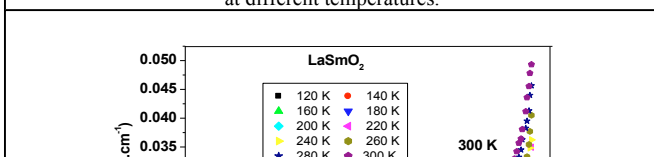


Fig. 2: Effect of temperature on the electrical conductivity of LaGdO_2 at different temperatures.



HYDROGEN RECIRCULATION AND PURGE STRATEGY IN SELF-HUMIDIFIED PEM FUEL CELL SYSTEM

F.Migliardini¹, T.M. Di Palma¹, M.F.Gaele² and P. Corbo¹

¹ Istituto Motori – National Research Council of Italy, Via G. Marconi 8
80125 Naples, (Italy)

² Università degli Studi di Napoli “Parthenope” Centro Direzionale - Isola C4
- 80143 Naples, (Italy)

Abstract –In this paper the effect of anode management in Proton Exchange Membrane (PEM) fuel cells was experimentally analyzed. In unstable operative conditions detected during system start-up in dead-end mode, the combined effect of purge, air flow rate impulse, and recycled anodic stream on individual cell performance recover was evidenced.

Anode Recirculation, Fuel Cell System, Fuel Feeding subsystem, Proton Exchange Membrane Fuel Cells

I. INTRODUCTION

Hydrogen Fuel Cell System (FCS) operation requires the utilization of balance of plant (BoP) components for reactant, thermal and water management [1]. Dead-End Anode (DEA) and Flow-Through Anode (FTA) options represent two alternative means for fuel supplying [2]. The N₂ buildup causes, for both DEA and FTA, a reversible voltage decay due to the blanketing, whereas the accumulation of water for DEA option involves fuel starvation and carbon corrosion that leads to an irreversible reduction of Electro-chemical Surface Active (ECSA) [3,4].

In the present paper an experimental analysis of a 6 kW self-humidified PEM Fuel Cell System equipped with an anode recirculation blower has been effected, evidencing the effect of the purging and of the anodic stream management on stack performance.

II. EXPERIMENTAL

The experimental tests were effected on a FCS based on a PEM stack constituted by 96 cells, able to provide a nominal power of about 6 kW. The FCS operated at low pressure and temperature without any device for external humidification. The

anode compartment was equipped with a membrane blower for hydrogen recirculation that permitted the FTA operation mode. Other experimental details are reported elsewhere [5].

III. RESULTS AND DISCUSSION

Table I summarizes the operative conditions of the dynamic tests carried out at different recirculation levels. Power consumption of recirculation blower at 100% level was about 50 W (24 V, 2,2 A) while 0% of recirculation level corresponds to a dead-end operation.

The power ranged from 1.4 to 5.8 kW, the maximum power variation rate was about 230 W/s while operative stack temperature was controlled in the range 285-330 K. The average values of stack power and purge frequency were also calculated for the entire duration of each test. The duration of each purge intervention was fixed at 1 s.

Experimental details relative to the tests N. 5 and 6 and for a time window of about 1200 s were specifically discussed. Stack power profiles were the same for the two tests passing from 1.5 to 2.8 kW in about 20 s, and this final value was maintained unchanged for the entire time window.

Temperature profiles were controlled in the range 285-316 K and resulted almost the same for the two tests in the entire time window. The steady state value of 316 K was reached after about 200 s in both tests. Cell voltage decay (dU), defined as difference between the mean cell voltage and lowest cell voltage, purge intervention, air stoichiometric ratio (λ) and recirculation level (%) were reported as function of time in Fig 1 for the test N.5 and in Fig 2 for the test N.6. Mean cell voltage profiles (not reported in Figures) resulted very similar for the two tests, reaching a steady state value of about 715 mV.

Fig 1 refers to the start-up of the system in dead-end mode from about 285 K; after about 2 minutes a progressive dU increase, due to a peripheral cell voltage decrease, was detected. This behavior was probably due to an incipient flooding phenomenon.

TABLE I
OPERATIVE CONDITIONS OF DYNAMIC TESTS EFFECTED ON THE 6 kW FCS

Test N°	Power range [kW]	Power average [kW]	Max power variation rate [W/s]	Temp. range [K]	Rec. level [%]	Mean purge frequency [min ⁻¹]	Durat. time [min]
1	1,5 - 3,7	2,7	216	301 - 320	100	0,60	7,1
2	1,5 - 5,8	3,1	225	308 - 329	100	0,80	34,5
3	1,5 - 4,8	2,8	218	292 - 318	0 - 50 - 80 - 100	0,66	18,0
4	1,5 - 4,8	2,5	216	289 - 330	0-50-100	0,65	70,4
5	1,5 - 3,7	2,6	65	284 - 317	0 - 50 - 100	0,72	42,4
6	1,5 - 4,2	2,6	167	288 - 320	100	0,60	39,4
7	2,2 - 3,8	3,0	148	291 - 332	100	0,90	29,2
8	1,5 - 3,7	2,6	127	290 - 320	0 - 50 - 100	0,60	51,4
9	1,4 - 2,5	1,6	125	307 - 320	100	0,45	9,2
10	1,4 - 3,3	1,9	156	303 - 323	100	0,48	13,8
11	1,4 - 3,3	2,1	82	312 - 328	0 - 100	0,71	25,9
12	1,5 - 3,8	2,0	85	304 - 320	0 - 100	0,69	24,7
13	1,4 - 2,7	1,9	84	291 - 317	100	0,87	18,0
14	1,4 - 2,6	1,78	103	298 - 318	100	0,83	12,9
15	1,4 - 2,6	1,9	64	302 - 317	100	0,52	27,5

An increase of purge frequency, an impulse of air flow rate at about 220 s (λ rapidly was increased from 2.2 to 3.3 for few seconds) and a λ decrease from 2.2 to 1.7 at 250 s did not result fully satisfactory to recover a stable cell performance; the partial activation of anode recirculation (50% level) at about 420 s appeared crucial to make durable and efficient all individual cell voltages in the successive entire time window.

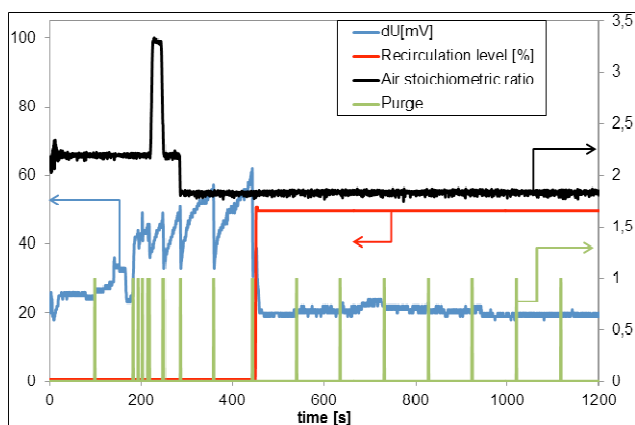


Fig. 1. Recirculation level, Purge intervention, Air stoichiometric ratio and Voltage decay (dU) as function of time for the test N. 5 during the initial time window of 1200 s.

Fig. 2 evidences that starting from 100% anode recirculation level a regular and efficient behavior of all individual cells was obtained without any exceptional management intervention (purge frequency or air flow rate increase).

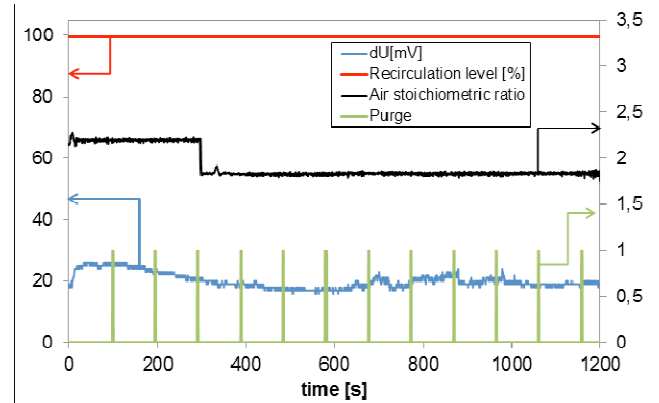


Fig. 2. Recirculation level, Purge intervention, Air stoichiometric ratio and Voltage decay (dU) as function of time for the test N. 6 during the initial time window of 1200 s.

IV. CONCLUSIONS

The effect of the purging and anodic stream management on cell performance of a self-humidified PEM Fuel Cell System equipped with a blower for fuel recirculation has been evidenced. Some unstable operative conditions encountered in dead-end mode during start-up were not completely recovered by the combined action of purge frequency and air flow rate increase, but the decisive effect of recirculation loop activation was evidenced.

ACKNOWLEDGMENT

The authors gratefully acknowledge the Italian Ministry of University and Research for financial support in "Fuel Cell Lab - Innovative systems and high efficiency technologies for polygeneration" Project.

REFERENCES

- [1] Larminie J., Dicks A., Fuel cell system explained, Chichester: John Wiley & Son, Inc., 2000.
- [2] Ahluwalia R, Wang X. Buildup of nitrogen in direct hydrogen polymer-electrolyte fuel cell stacks. Journal of Power Sources, Volume 171, 2007, pp. 63-71.
- [3] Ohs J., Sauter U., Maass S., Stolten D., Modeling hydrogen starvation conditions in proton-exchange membrane fuel cells, Journal of Power Sources, Volume 196, 2011, pp. 255-263.
- [4] Chen J., Siegel J., Matsuura T., Stefanopoulou A., Carbon corrosion in PEM fuel cell dead-ended anode operations, Journal of The Electrochemical Society, Volume 158, 2011, pp.1164-1174.
- [5] Migliardini F., Capasso C., Corbo P., Optimization of hydrogen feeding procedure in PEM fuel cell systems for transportation, International Journal of Hydrogen Energy, Volume 38, 2014, pp. 21746 – 21752.



SCHIBZ – FUEL CELLS FOR MOVABLE APPLICATIONS

A. Dipl.-Ing. Keno Leites, PMP*, B. Dipl.-Ing. Nils
Kleinohl**

*ThyssenKrupp Marine Systems GmbH, Hermann-Blohm-Str. 3,
20457 Hamburg, Germany

**OWI Oel-Waerme-Institut GmbH, Kaiserstraße 100, 52134
Herzogenrath, Germany

Abstract – This paper reports about the project *SchIBZ* which has the aim to develop and proof a diesel oil fueled fuel cell system for maritime application and transportable, temporary CHP applications. In several steps the process was developed, a small proof of concept plant build and a large demonstrator for commercial applications. The test plant was successfully operated for more than 1000h. The demonstrator will be tested for some ten months onboard a commercial vessel in international waters. The development was executed by a consortium of 6 companies and supported by the German federal ministry of transport.

Index Terms – SOFC, Diesel Fuel, maritime application, large power

I. NOMENCLATURE

DNV GL	Det Norske Veritas – Germanischer Lloyd SE
HDW	Howaldwerke-Deutsche Werft GmbH
IMO	International Maritime Organisation
LUH	Leibniz University Hannover
M&P	Motion Control & Power Electronics GmbH
NIP	National Innovation Program Hydrogen and Fuel Cell Technology
OWI	Oel-Waerme-Institut GmbH
PMP	Project Management Professional
SchIBZ	SchiffsIntegration BrennstoffZelle
SOFC	Solid Oxide Fuel Cell
TKMS	ThyssenKrupp Marine Systems GmbH

II. INTRODUCTION

In 2008 the former Blohm + Voss GmbH, today TKMS, started to investigate options for cleaner, quieter and more efficient power generation for oceangoing vessels. Different engine configurations were studied. Additionally, based on the experiences of the sister company HDW GmbH, different fuel

cell configurations were studied. The configurations included also different fuels.

After rating the features of all configurations the combination of low Sulphur diesel oil and high temperature fuel cells promised to be the best solution, although one with considerable development needs.

To execute this development TKMS sought for partners with the respective know how. Finally the consortium consists of TKMS, DNVGL, sunfire, OWI, M&P, LUH and the ship owner Braren. Additionally funding by the German government was applied for under the NIP. The project started officially June 2009 as part of a so called lighthouse initiative, named e4ships.

Actually, the large demonstrator is under construction and shall be set to work late this year.

III. DEFINING THE SYSTEM

From preliminary studies it is known, that liquid hydrocarbons can be processed to a methane and hydrogen containing fuel gas by certain catalysts. Therefore it is decided to use fuels according to EN590, since these offer well known handling and safety features and the highest volumetric energy content. Other requirements are:

- 500 kW_e
- ~50 % electrical efficiency
- Mean time between overhaul 20.000 h+
- wide operating range with high efficiency
- exhaust gas energy recovery
- comparable costs to an emission reduced diesel engine genset
- exhaust gas releasing without funnel
- capable to follow load changes as close as possible



The system has to have a high reliability and availability. To achieve this the number of moving components should be kept low.

A. Catalytic reforming

The first task of the project was to identify a catalyst which can process diesel fuel according to EN590. To perform this a small test reactor was built for testing of different materials with fuel from the next door petrol station in small scale. After several tests a catalyst was identified which proofed a high fuel processing capability at well-fitting process parameters [1].

Based on this catalyst the fuel processing section of the system was designed by using simulation methods. Special consideration was given to the recirculation. Goal was the realization of an adiabatic process.

B. Electric behavior

The second main requirement is that the power system can operate in an island mode without rotating generators. This requires power electronics to provide highly dynamic load changes and sufficient short circuit currents. The characteristic of fuel cells in turn favors smooth operation. This made it necessary to introduce an energy buffer as part of the system at the DC side.

Again utilizing simulation methods several configurations of LiIon-batteries were evaluated. They offer a good combination of energy density and power capability. Combinations with our storages are surely possible but will be investigated later. The simulations led to a configuration of multiple batteries which are not operated in parallel to prolong the lifetime.

C. Scalability

Since fuel cells are packed in stacks which have to be packed again to gain larger powers, the power output should be scalable to suite different needs in later applications.

This is realized by defining a base module, which will suite most of the spatial boundary conditions in maritime and onshore applications. By stacking these modules next to each other typical power outputs from 45 to 270kW can be realized per plant. Larger systems are possible depending on the available installation space dimensions.

IV. CONSTRUCTION AND TEST

After a proof of concept test with a 10kW_e class test rig the construction of a 50kW_e demonstration plant is actually performed. The plant will be mounted inside standard containers for easier handling. A land based test will start end of this year and the operation on board the *MS Forester* will follow up. This is a mid-size commercial vessel where the total electric energy demand is between 100 and 200kW_e. So the

demonstrator will provide a significant share to the board network and can be operated like a rotating generator. The



Fig. 1. Installation of the demonstration plant aboard the *MS Forester*[TKMS]

onboard operation will take place at least till end of 2016 with an option of 2 additionally years.

V. CONCLUSION

After working on this project for more than 7 years, we found, that liquid hydrocarbons are a valid option for certain power needs, especially in transport applications. In combination with fuel cells as energy converter liquid hydrocarbons can be utilized clean and quiet in applications with large energy demands.

Furthermore it became obvious, that HT fuel cells, especially SOFC, are at a well advanced technology state but the manufacturers need better funding. The availability of stacks on the market is not sufficient in terms of competition. Additionally the suppliers should be willing to supply stacks or stack assemblies to integrators, since single MEAs cannot be handled by many integrators.

Finally, fuel cells should always be seen as part of an aggregate, which includes the electrical side. In conjunction with energy buffers fuel cells can alter electric distribution systems a lot and offer additional efficiency gains.

ACKNOWLEDGMENT

I thank the partners in the project for the continuing support of our work.

We furthermore thank the German federal ministry of transportation for supporting the project under the NIP.

REFERENCES

- [1] Pedro Nehter, Nils Kleinohl, Ansgar Bauschulte, Keno Leites; DIESEL BASED SOFC-APU FOR MARINE APPLICATIONS; 11th European SOFC and SOE Forum (2014), Luzern



TOWARDS MINIATURE MICROBIAL FUEL CELLS FOR WATER QUALITY MONITORING

J. Chouler*, M. Di Lorenzo**

*Centre for Sustainable Chemical Technologies, University of Bath, Bath BA2 7AY, UK;
E-Mail: J.Chouler@bath.ac.uk

**Department of Chemical Engineering, University of Bath, Bath BA2 7AY, UK
E-Mail: M.Di.Lorenzo@bath.ac.uk

Abstract – To ensure adequate sanitation of water supplies a rapid, cheap and simple method to test water systems is required. The microbial fuel cell (MFC) technology has potential for the effective testing of water sources in real time. A single chamber (68 μL) miniature MFC biosensor for detection of the biological oxygen demand (BOD) of water systems and to detect toxicants is presented. The device showed a response to a change in BOD within 19 minutes. The effect of operational conditions (pH, temperature, flow rate) on current generation was shown to have a maximum sensitivity of $0.944 \mu\text{A cm}^{-2}$ per unit change of the operational parameter. The power output of the device was enhanced by a factor of 28 by doubling the length of the anodic chamber and doping the cathode with a sustainable biochar based catalyst. The promise for detection of ‘emerging’ contaminants and toxicants in developing countries is discussed.

Index Terms – Microbial Fuel Cell; microbial sensors; Toxicant; Water Quality

I. INTRODUCTION

Thousands of different chemicals contaminate water systems. Their presence and biotoxicity must be quickly and efficiently assessed to contain the associated risks on the aquatic biota and human health.

Microbial fuel cells are devices that directly convert the chemical energy in organic matter into electricity via metabolic processes of microorganisms [1]. The current generated by an MFC directly relates to the metabolic activity of the electroactive biofilm at the anode surface [2]. Any disturbances of their metabolic pathways are translated into a change in the production of electricity.

If the MFC works at saturated fuel concentration and the operational conditions (pH, salinity, temperature and anode

potential) are fixed, then variations in the current output can be associated with the presence of toxicants in the feeding stream. The MFC can therefore act as an indicator for biologically active compounds in water.

The main strength of the MFC technology relies on its simplicity. No external transducers are needed, as the presence of a pollutant in the feeding stream is immediately detected by a current change from the system. MFCs also lead to stable and cost-effective sensors that can operate infield, and continuously. Finally, the electricity generated by the MFC opens up the prospective for self-powering operations.

The work presented here looks at the use of miniature MFC-based sensors to assess the chemical and biological oxygen demand of water systems and to detect toxicants. The effect of a range of operational conditions on the MFC current (pH, temperature and flow rate), as well as methods of increasing energy generated in miniature devices by changing geometry and cathode catalyst is presented.

II. DEVICE

A miniature single MFC was constructed using a PDMS cast channel ($4 \times 4 \times 4 \text{ mm}^3$ [L, W, H] anodic chamber, anode surface area 0.16 cm^2) sandwiched between two Perspex plates, Fig.1. Carbon cloth was used for the electrode materials. All tests were performed with three identical devices and the average response taken.

III. BOD SENSING

With acetate used as a fuel source for the MFC biosensor, the effect of altering acetate concentration between 10-600 mM was studied. The sensor was capable of monitoring changes in



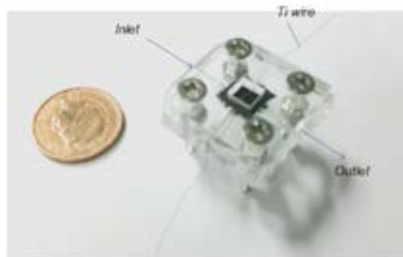


Fig. 1. Miniature single chamber MFC used in this work

the labile organic carbon content with response times on average of 19 minutes, with non-saturated conditions below 100 mM, Fig.2. For detecting toxicants in water sources the concentration of substrate must be maintained above this.

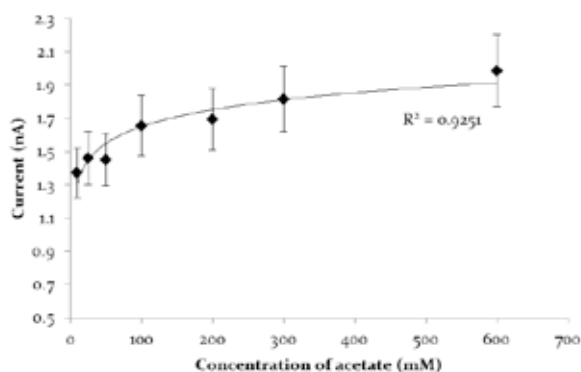


Fig. 2. Response of MFC unit to acetate concentration in feed stream, data is average of 3 MFCs with 12% error.

IV. OPERATIONAL CONDITIONS

For sensing toxicants, operational conditions such as pH, temperature, and flow rate must be controlled. The effect of these parameters on the baseline current generation was studied.

The sensitivity of these parameters within a linear range can be determined by equation 1:

$$\text{sensitivity} = \frac{\text{change in current } (\mu\text{A})}{\text{unit change in parameter} \times \text{anode surface area } (\text{cm}^2)} \quad (1)$$

The sensitivity of the MFC to temperature (15-35°C), pH (4.5-11) and flow rate (0.1-2.2 mL min⁻¹) was 0.020 $\mu\text{A } ^\circ\text{C}^{-1}$ cm⁻², 0.806 $\mu\text{A cm}^{-2}$ and 0.944 $\mu\text{A mL}^{-1}$ min cm⁻² respectively. Death of the biofilm was observed at 50 °C and at flow rates exceeding 3.5 mL min⁻¹. Response times of the MFC sensor to operational condition changes were between 14-39 minutes.

V. DEVICE GEOMETRY

To determine the effect of length on MFC performance, an additional MFC device was made with twice the length of the aforementioned device (8×4×4 mm [L, W, H], anode area 0.32 cm²). Doubling the length of the anodic chamber enhanced the maximum power density of the device from 60 to 580 mW m⁻³.

VI. CATHODE CATALYST

Usually Pt based catalysts are used at the cathode. The use of biomass based catalysts was studied for the purpose of sustainable enhanced power generation. Longer [L = 8 mm] MFC devices were prepared with 1.5 mg cm⁻² of N/S/Fe-doped biochar doped onto the cathode, and their performance compared with MFCs without a cathode catalyst. The biochar improved the maximum power density of the device from 580 to 1680 mW m⁻³.

VII. PROSPECTIVE MFC BIOSENSING

The MFC biosensor presented in this work has proven to have suitable response times and good stability for use as a rapid, simple and cost-effective device to test water quality. Looking forward, the miniature MFC device will be used to detect toxicants relevant to developing countries (NO₃⁻, heavy metals, etc.) and for 'emerging' toxicants (e.g. pharmaceuticals and their metabolites). Moreover field testing of real water systems will be pursued to ensure that the testing of multiple contaminants in water sources is feasible.

VIII. CONCLUSIONS

This work demonstrates the development of a miniature single chamber MFC biosensor for water quality monitoring. The sensitivity of the device to operational conditions such as temperature, pH and flow rate was no more than 0.944 $\mu\text{A cm}^{-2}$ per unit change, and the device was responsive to changes in BOD within 19 minutes. The maximum power density of the MFC was increased by doubling the length of the anode chamber and by adding a biochar based catalyst to the cathode, with a combined improvement by a factor of 28.

The future research goals are to test this device against toxicants relevant to developing countries and against 'emerging' contaminants in water systems. Moreover, the challenges of contaminant mixtures will be addressed by field testing the device in real water systems.

ACKNOWLEDGMENT

The authors acknowledge: EPSRC (The Engineering and Physical Sciences Research Council) and the Doctoral Training Centre for Sustainable Chemical Technologies for funding; Prof Titirici, from Queen Mary College of London, and her group for providing us the biochar used in this work.

REFERENCES

- [1] Liu, H.; Logan, B.E. Electricity generation using an air-cathode single chamber microbial fuel cell in the presence and absence of a proton exchange membrane. *Environ. Sci. Technol.* 2004, 38, 4040–4046.
- [2] Di Lorenzo, M.; Thomson, A.R.; Schneider, K.; Cameron, P.J.; Ieropoulos, I. A small-scale air-cathode microbial fuel cell for on-line monitoring of water quality. *Biosens. Bioelectron.* 2014, 62, 182–188.



DEVELOPMENT OF MINIATURE ENZYMATIC FUEL CELLS FOR HEALTHCARE APPLICATIONS

M. Di Lorenzo*, H. du Toit*, D. Ferdani** and R. B. Rashidi*

* Department of Chemical Engineering, University of Bath

** Centre for Sustainable Chemical Technologies, University of Bath
Bath, BA2 7AY, (UK)

Abstract – We report our recent results on the development of miniature glucose/oxygen enzymatic flow-through fuel cells for healthcare applications. The fuel cells implement non-toxic highly porous gold (hPG) electrodes and do not require any external mediators to facilitate the electrical communication between the enzyme redox centre and the electrode. We demonstrate power generation from transdermal fluid, obtained by reverse iontophoresis from pig skin, and prove the hPG electrodes stability towards the typical impurities of biological fluids (i.e. small proteins, amino acids). These exciting results are a step forward towards the use of EFCs for wearable healthcare devices.

Index Terms – Enzymatic fuel cell, glucose sensors, highly porous gold, wearable devices.

I. INTRODUCTION

The development of self-powered wearable biodevices is highly attractive for a number of applications, including non-invasive detection of biomarkers, transdermal drug delivery and fitness monitoring. Enzymatic fuel cells (EFCs) hold great potential as a power source for such devices. These particular types of fuel cells use redox enzymes as catalysts to convert organic substrates, such as carbohydrates, into useful electricity at body temperature. In the past few years, electricity generation from human physiological fluids *via* EFCs has been reported, which proved the possibility to harvest energy from tears [1], serum [2] and saliva [3]. Considering the short-term stability of enzymes, EFCs are suitable for non-invasive applications, such as in attachable and adhesive devices, rather than implanted devices. A recent practical example is given by the EFC tattoo that harvests energy from lactate [4].

The majority of the EFCs reported implement external electron mediators, either in solution or co-immobilised with the enzyme, to improve the electron transfer to the anode. The use of these mediators, however, limits practical applications of EFCs, due to their potential toxicity and/or risk of leaching. Moreover, these devices usually implement carbon nanotubes

or carbon nanoparticles whose toxicity is still controversial [5].

We have recently reported continuous power generation from two miniature flow-through glucose/oxygen enzymatic fuel cells [6]. The EFCs used highly-porous gold (hPG) as electrodes, as an alternative to carbon-based electrodes. hPG is characterised by a very high specific surface area, with a pore size distribution ranging from the micro to the nano scale [7]. This property, in combination with high conductivity and biocompatibility, makes hPG electrodes an ideal support for enzyme immobilisation and allows a very good electrical communication between the electrode and the enzyme [8]. We have also developed a cascade of three EFCs embedded in a compact and handy single channel device (manuscript in preparation) and we demonstrated for the first time power generation from iontophoresis extracts. Iontophoresis is a technique to extract charged and highly polar compounds across the skin *via* the application of a small electric current. Iontophoresis extracts serve as a very good approximation of sweat, since they are characterised by the same constituent compounds.

II. RESULTS

A. Fabrication of miniature EFCs

A thin film of hPG was electrochemically deposited onto platinum (Pt) wires (ID 0.5 mm) *via* a hydrogen bubbling template [7]. Glucose oxidase (GOx) and laccase (LAC), used respectively at the anode and at the cathode, were immobilized onto the hPG surface *via* electrochemical adsorption [8].

Four different devices were developed, as shown in Figure 1. A mould with the negative of the EFC device design was fabricated by 3D printing. This structure was replicated in polydimethylsiloxane *via* the *replica moulding* technique.



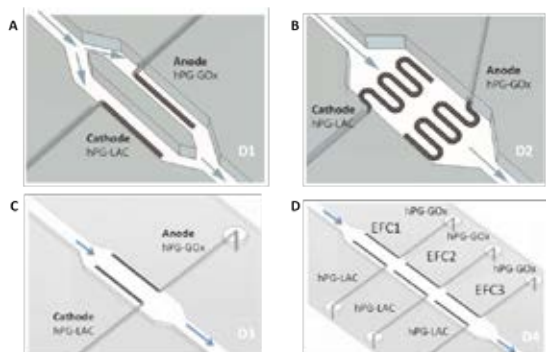


Fig. 1. The four devices studied. A) parallel channels EFC, D1; B) single channel EFC with pleated electrodes, D2; C) single channel EFC, D3; D) cascade of EFCs in a single channel device, D4.

B. Energy harvesting from glucose

Table I provides a summary of performance of the EFCs fed, continuously or in batch, with an aerated solution of glucose (27 mM) in phosphate buffer. Data is the average from two replicates.

TABLE I
SUMMARY OF PERFORMANCE OF THE EFCs.

Device	Maximum power in continuous mode (μW)	Voltage in continuous mode (mV)	Maximum power in batch mode (μW)	Voltage in batch mode (mV)
D1	1.55 ± 0.3	128	n/a	n/a
D2	0.62 ± 0.1	80	n/a	n/a
D3	0.75 ± 0.04	140	0.17 ± 0.3	76
D4 individual EFCs	EFC1: 0.168 ± 0.02 EFC2: 0.44 ± 0.05 EFC3: 0.156 ± 0.09	82 133 68	EFC1: 0.16 ± 0.02 EFC2: 0.17 ± 0.05 EFC3: 0.14 ± 0.07	68 64 66
D4 EFCs electrically connected in parallel	0.71 ± 0.12	189	0.4 ± 0.07	93

D4 was subsequently tested with iontophoresis extracts from pig-skin containing $30 \mu\text{M}$ of glucose (Fig. 2).

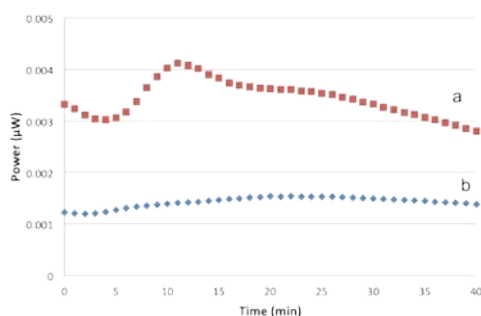


Fig 2. D4 fed with iontophoresis extracts from pig skin in batch mode. a) EFC1, EFC2 and EFC3 electrically connected in parallel; b) average of EFC1, EFC2 and EFC3 (individually connected), with 3% variation.

C. Glucose monitoring

D3 was tested as sensor for glucose, within the typical range of concentrations in sweat: $1\text{--}100 \mu\text{M}$ (Fig. 3).

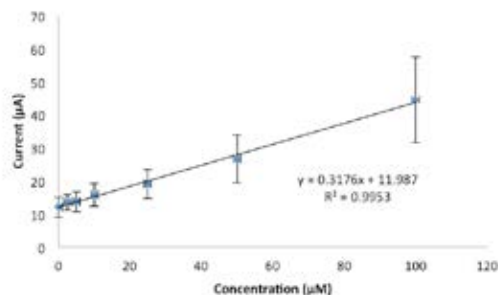


Fig. 3. Amperometric response of D3 to glucose. Data is the average of three replicates

III. CONCLUSION

- Four miniature EFCs have been developed and their performance compared. The highest power was obtained by D1. This might be due to the interference of H_2O_2 formed at the anode on the activity of LAC [6].
- In continuous mode operation, fluid dynamic effects led to different performance of the EFCs cascade in D4
- In batch, the EFCs in D4 showed similar performance.
- Energy harvesting from transdermal fluid was demonstrated, with no interferences between the impurities of this biological fluid and the hPG electrodes.
- D3 was also successfully implemented as glucose sensor.

ACKNOWLEDGMENT

Thanks to: the Bath Alumni Funds (F1314B-RS09); EPSRC and the CDT in Sustainable Chemical Technologies; M. B. Del-Charro (Univ. of Bath) for the iontophoresis extracts.

REFERENCES

- [1] Reid, R., S.D. Minter, and B.K. Gale, *Contact lens biofuel cell tested in a synthetic tear solution*. *Biosensors and Bioelectronics*, 2015. **68**: 142–148.
- [2] Wang, X., et al., *Mediatorless sugar/oxygen enzymatic fuel cells based on gold nanoparticle-modified electrodes*. *Biosensors and Bioelectronics*, 2012. **31**(1): 219–225.
- [3] Falk, M., et al., *Miniature Direct Electron Transfer Based Enzymatic Fuel Cell Operating in Human Sweat and Saliva*. *Fuel Cells*, 2014. **14**(6): 1050–1056.
- [4] Jia, W., et al., *Epidermal Biofuel Cells: Energy Harvesting from Human Perspiration*. *Angewandte Chemie international Edition*, 2013. **52**: 7233 – 7236
- [5] Bottini, M., et al., *Multi-walled carbon nanotubes induce T lymphocyte apoptosis*. *Toxicol Lett* 2006. **160**: 121–126.
- [6] du Toit, H. and M. Di Lorenzo, *Continuous power generation from glucose with two different miniature flow-through enzymatic biofuel cells*. *Biosensors and Bioelectronics*, 2015. **69**: 199–205.
- [7] du Toit, H. and M. Di Lorenzo, *Electrodeposited highly porous gold microelectrodes for the direct electrocatalytic oxidation of aqueous glucose*. *Sensors and Actuators B-Chemical*, 2014. **192**: 725–729.
- [8] du Toit, H. and M. Di Lorenzo, *Glucose oxidase directly immobilized onto highly porous gold electrodes for sensing and fuel cell applications*. *Electrochimica Acta*, 2014. **138**: 86–92.



A CASCADE OF MINIATURE MICROBIAL FUEL CELLS COUPLED WITH AN ELECTROCHEMICAL REACTOR FOR ENERGY HARVESTING

S. Monasterio*, M. Mascia*, M. Di Lorenzo**, A. Vacca*,
and S. Palmas*

*Dipartimento di Ingegneria Meccanica, Chimica e dei Materiali, Università
degli Studi di Cagliari, Piazza d'Armi, 09123 Cagliari, (Italy)

**Department of Chemical Engineering, University of Bath, Bath BA2
7AY, (United Kingdom)

Abstract – This work reports the use of the Microbial Fuel Cell (MFC) technology, in combination with an electrochemical reactor, for the generation of electricity while removing *Chlorella vulgaris* microalgae contained in wastewater.

In particular, *Chlorella vulgaris* algae was pre-treated by using an electrolytic cell. To this aim, a fixed bed reactor with 3D electrodes was employed. The pre-treated wastewater was used as feedstock for a 3D printed miniature air-cathode MFCs arranged in cascade for further algal removal and energy production.

The performance of the system was studied by measuring the chemical oxygen demand, the optical density and the recorded voltage in all the experiments. Results show that the efficiency of the system, in terms of output energy recovery and water treatment, increases when a higher number of MFCs is used in the cascade.

Index Terms - Cascade of Microbial Fuel Cells, *Chlorella vulgaris* as fuel, Electrochemical pre-oxidation step, Generation of electricity and water treatment.

I. INTRODUCTION

MFCs are particular types of fuel cell in which the energy conversion reactions are catalysed by bacteria at the anode. These devices can implement as fuel organic matter from any sort of wastewaters. Therefore, algae biomass has been investigated as fuel for the MFCs: *Synechococcus leopoliensis* was used as feedstock in a cascade of 8 MFCs without the need of energy consuming pre-treatment [1].

The use of algae biomass as fuel for MFCs is often combined with a pre-treatment. Among other methods, electrochemical pre-oxidative treatments are very efficient for the removal of pollutants and are usually based on the use of chemicals, such as hypochlorite or chlorine [2]. In this context, direct electrolysis is particularly attractive and as we have reported [3], the applied electric field and the *in situ* generation

of disinfectant agents, such as reactive oxygen species and chlorinated compounds, made possible the inactivation of *Microcystis aeruginosa* microalgae. However, oxidizing species would adversely affect the anaerobic bacteria of the MFC and therefore, it was not used in this work.

In this study, we combine a cascade of three to five 3D printed miniature air-cathode MFCs system with direct electrolysis as pre-treatment process in order to generate electricity while treating *Chlorella vulgaris* algae contained in wastewater.

II. EXPERIMENTAL SECTION

Figure 1 shows the schematic and photograph of the MFC device for two different electrode areas.

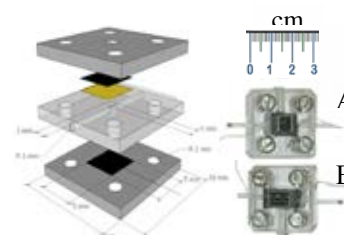


Fig. 1. Schematic and photograph of MFC sensor for this study with an electrode surface area of 0.09 cm^2 and 0.027 cm^2 of anodic volume (A) and 0.24 cm^2 and 0.072 cm^3 of anodic volume (B).

Carbon cloth was used as anode and cathode electrodes, while nafion as proton exchange membrane. Two lengths of the anode chamber (indicated as x in the figure 1) were considered: 3 and 8 mm, leading to an electrode surface area of 0.09 cm^2 and 0.24 cm^2 , respectively.

Chlorella vulgaris was adopted as a microalgae model and was removed in a previously developed fixed bed electrochemical cell [3]. The reactor was equipped with 3D electrodes in series: six discs of boron doped diamond

constituted the anode packing, while six discs of titanium grids coated with platinum constituted the cathode one. The solid surface of both electrodes was 100 cm² and the inter-electrode gap was 0.5 cm wide. Glass spheres of 0.2 mm diameter were used as filling material.

The combined experiments for algae removal and electricity generation were performed in a closed loop circuit as reported in Fig. 2.

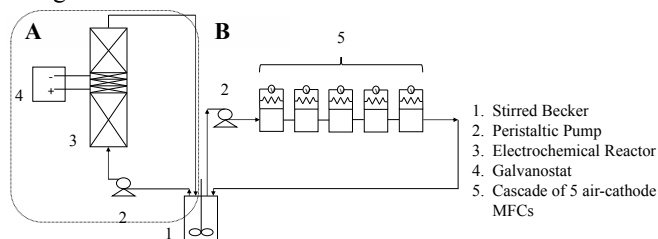


Fig. 2. Scheme of the batch-recirculating experimental apparatus used for the electrolysis of *Chlorella vulgaris* and the generation of energy by a system of a cascade of three to five air-cathode MFCs.

The wastewater contaminated by algae was pumped into the fixed bed reactor for the electrochemical pre-treatment. Electrolysis experiments were carried out in galvanostatic mode (0.2 A) at constant flow rate (0.033 L min⁻¹) for an hour with an initial algae concentration of 15x10⁶ cell mL⁻¹. The volume of the system was 200 mL. In these conditions, the 70% of algae removal was obtained. As soon as the electrolysis experiment had started, the outlet of the electrolytic cell was fed at 0.4 cm³ min⁻¹ into the MFCs cascade system. Once the pre-treatment finished, the volume of the system was directly recirculated, up to 5 days, into the cascade of three or five MFCs for energy production and further algae removal. All the MFCs were electrically independent from each other to monitor the performance of each cell in the system. The optimal external resistor (300 kΩ) of each cell was obtained by polarization curves (data not shown) for the experiments performed with the smallest electrode area in a cascade of 5 MFCs. For the rest of the experiments, a resistor of 45 kΩ for each MFC was maintained.

III. RESULTS

It results that the output power generated by the air-cathode MFCs in the cascade improves by increasing the electrode area and therefore the contacted time (HRT) in the cell being the same flow rate for both setups. As shown Fig. 3, an initial decrease in the output voltage is observed, followed by a linear increase. This trend is probably caused by the fact that initially not broken algae cells might compete with the bacteria at the anode of the MFC. However, upon completion of the electrolysis the voltage rises due to the increase of readily available organic matter in the solution. A further removal of algae was observed at the end of each experiment, for a total removal percentage higher than 85%.

Furthermore, the overall energy output (ϵ_E) of the cascade system, over a period of 28 and 120 hours, was calculated as

the sum of the ϵ_E of each MFCs:

$$\epsilon_E = \int_0^t V I dt \quad (1)$$

where, V is the cell potential (V), I is the current (A), and t is the time (s).

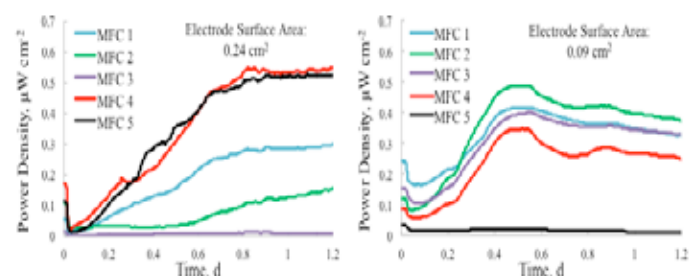


Fig. 3. Confront of power density for a cascade of five MFCs using different electrodes surface area and fixed resistor values. Left figure: 0.24 cm² and 45 kΩ; Right figure: 0.09 cm² and 300 kΩ.

Table 1 shows the ϵ_E values, of the cascade system, obtained for a period of 28 h and at two different anodic electrode area. The highest value of ϵ_E (24 mJ) was obtained with a 5 MFCs cascade system and an electrode area of 0.24 cm². Moreover, a ϵ_E of 78 mJ was obtained working with a % MFCs cascade system over a period of 120 h (with an electrode area of 0.24 cm²). This represents a 30% increase (if compared with a period of 24 h).

Electrode Area, cm ²	0.09		0.24	
No. of MFCs in the cascade	3	5	3	5
Energy Output, mJ	2.6	11	16	24

Tab. 1 Values of energy efficiencies for the experiments carried out in three and five cascade MFCs using two different sizes of electrodes for a total period of 28 h.

IV. CONCLUSION

The present study reports the combination of two advanced processes. It was demonstrated that *Chlorella vulgaris* microalgae can be successfully removed by electrochemical treatment and could feed a cascade of 3 to 5 MFCs system for energy generation and further algae removal.

ACKNOWLEDGMENT

The authors wish to thank Philippe Mozzanega (Department of Biology & Biochemistry and Department of Chemical Engineering, University of Bath, United Kingdom) for all the material borrowed.

REFERENCES

- [1] Walter, X.A., Greenman, J., Taylor, B., Ieropoulos, I.A., Microbial fuel cells continuously fuelled by untreated fresh algal biomass, *Algal Research*, Volume 11, 2015, pp. 103-107.
- [2] Gao, S., Du, M., Tian, J., Yang, J., Yang, J., Ma, F., Nan, J., Effects of chloride ions on electro-coagulation-flotation process with aluminum electrodes for algae removal, *Journal of Hazardous Materials*, Volume 182, 2010, pp. 827-834.



GELATIN AS A PROMISING PRINTABLE NUTRIENT FEEDSTOCK FOR MICROBIAL FUEL CELLS (MFC)

Pavlina Theodosiou*, Ioannis Ieropoulos***, Benjamin Taylor*, John Greenman** and Chris Melhuish*

* Bristol BioEnergy Centre, Bristol Robotics Laboratory, University of the West of England, BS16 1QY (UK)

** Biological, Biomedical and Analytical Sciences, University of the West of England, BS16 1QY (UK)

Abstract – This study describes the work carried out towards the optimization of critical MFC components with potential 3D fabricated materials. The response of the optimised fuel cells, which were fed with soft materials such as gelatin, alginate and Nafion™, is also reported. The optimised components were the membrane and the cathode electrode. Membrane was substituted with a custom made terracotta sheet and the electrode used was a single sheet of carbon veil coated with an activated carbon paste. The results showed that amongst the soft materials tested, gelatin performed better; also it revealed that even after a 10-day starvation period the gelatin had better longevity. These results show that MFCs can be potentially 3D-printed monolithically using the EvoBot platform.

Index Terms – MFC, EvoBot, Gelatin, Nutrient feedstock

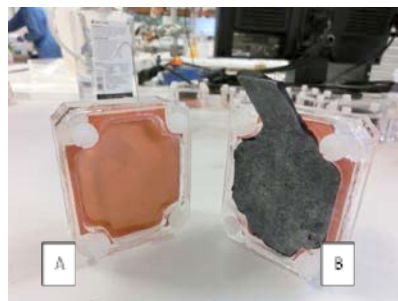
I. INTRODUCTION

Microbial Fuel Cells are energy transducers, which convert chemical energy stored in organic matter into electricity through bacterial digestion [1]. MFCs consist of two parts, the positive cathode and the negative anode. The two parts are separated by a semi-permeable membrane, which only allows ions to go through. The key to simplifying the construction of MFCs and making them more accessible is using 3D fabrication techniques and this is the aim of the EvoBot platform [2]. At first, the optimisation of the fuel as well as the membrane is needed, to make it suitable for 3D printing. This study presents the results from MFCs fed for the first time with soft materials as a nutrient feedstock. The cells had open-to-air cathodes and a single layer of terracotta clay as the membrane.

II. MATERIALS AND METHODS

Twelve analytical-type MFCs with laser-cut acrylic compartments, open-to-air cathode half-cells and 25 ml anodes, were built for this experiment (Figure 1). The cells were constructed using a flat terracotta sheet (2mm) fitted as a membrane and a single sheet of carbon veil coated with activated carbon paste as the cathode electrode. The anodes were made of carbon fibre veil with a total surface area of 270 cm² (PRF Composite Materials, UK). MFCs were inoculated with activated sludge derived from Wessex Water (Saltford, UK) and supplemented with tryptone (1%) and yeast extract (0.5%) (TYE). Triplicates of MFCs were fed under continuous flow mode with gelatin, alginate and liquid Nafion™ respectively; TYE (1:10) was also used as a background solution in all cases.

FIGURE I



OPTIMISED MEMBRANE AND CATHODE ELECTRODE MFCs

A. ANALYTICAL TYPE MFC WITH TERRACOTTA CERAMIC MEMBRANE

B. ANALYTICAL TYPE MFC WITH ACTIVATED CARBON ELECTRODE ATTACHED TO THE CERAMIC MEMBRANE AS THE AIR BREATHING CATHODE

III. RESULTS AND DISCUSSION

The initial response of the MFCs after changing the feedstock from 1.5% TYE to the target substrates is presented below (Figure 2). The MFCs fed with gelatin performed better compared to the other soft materials. The average power production of the MFCs fed with different soft materials is shown below (Figure 3). Although the gelatin output is lower than that of the control MFCs, it appeared to have better longevity, when all MFCs were starved, with its output decreasing at a slower rate than the rest. The long-chain polymer composition of gelatin renders this feedstock longer lasting as it takes longer for the microbes to break it down. The results indicated that gelatin is a suitable feedstock, which could potentially be extruded from the EvoBot platform, and incorporated as a 3D printed substrate for the MFCs. The optimised ceramic-based membrane as well as the cathode electrode paste can also be extruded from the same platform.

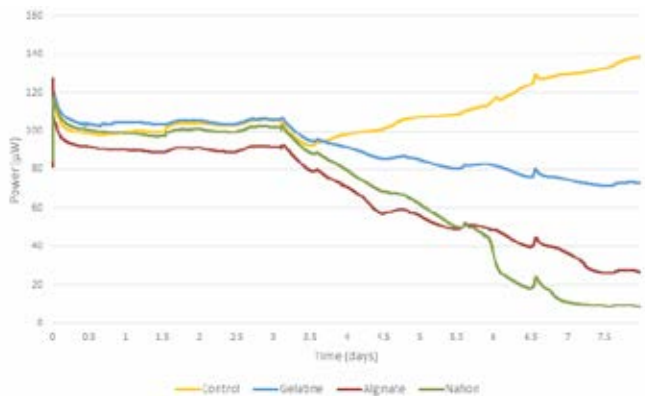


Figure 2: Time profile showing the response of MFCs after feeding with soft materials for the first time. The fuel cells were fed with 1.5% TYE for the first 3 days, and then target soft materials added as a nutrient feedstock.

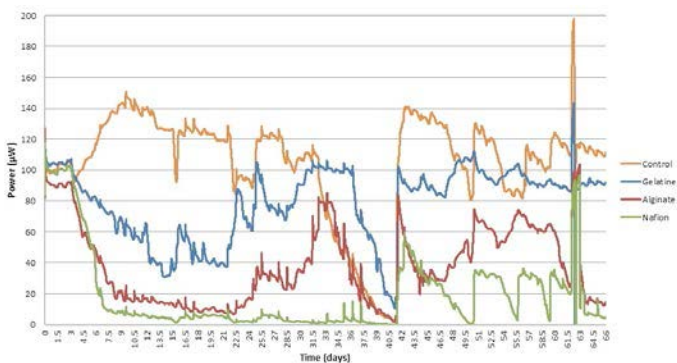


Figure 3: Average power production of MFCs after feeding with different soft materials. The spikes shown during the 62nd day are due to a polarisation experiment. The highest absolute power output for the control was 149.23 μW and for the gelatin 111.26 μW . Starvation period was between the 32nd-42nd days.

IV. CONCLUSIONS

Gelatin seems to be a promising soft material that can be 3D printed and used as a feedstock for MFC operation. Flexible materials such as ceramic clay used as a membrane, and activated carbon paste used as a cathode electrode can be used in analytical type MFC with the potential to be 3D-printed. Further work will investigate different material combinations suitable for MFC fuel and compartments, which could be used as part of an entirely 3D printable fuel cell.

ACKNOWLEDGMENT

The authors would like to thank the European Commission for the financial support of this work through the FP7-ICT, grant agreement 611640.

REFERENCES

- [1] Bennetto, H.P., Electricity generation by microorganisms. *Biotechnology Education*, Volume 1, Issue 4, 1990, Pages 163–168.
- [2] Faiña A., Nejatimoharrami F., Stoy, K, EvoBot: An Open-Source, Reactive Liquid Handling Robot, *IEEE/RSJ International Conference on Intelligent Robots and Systems (IROS)*, 2015.



OPTIMIZATION OF CO-FIRING CONDITIONS FOR LARGE-AREA SOLID OXIDE FUEL CELL FABRICATION BY CO-TAPE CASTING PROCESS

Sanghun Lee*, Joongmyeon Bae*

* Department of Mechanical Engineering, Korea Advanced Institute of Science and Technology (KAIST), Guseong-dong, Yuseong-gu, Daejeon (Republic of Korea)

Abstract - A solid oxide fuel cell (SOFCs) is one of the fuel cells, and co-tape casting process has been widely used to fabricate unit cells. In this study, each step of co-tape casting process and corresponding process conditions were studied to fabricate crack- and warp-free large-area unit cells. Thermal decomposition rate, flexural strength, and shrinkage behavior were measured by thermo-gravimetric analysis, three point flexural test, and thermo-mechanical analysis, respectively. As a result, heat treatment steps at 250 °C and 350 °C were adopted. The anode support layer composition with coarse NiO and pore former mixture of 5 wt% of carbon black and graphite was applied to obtain the highest flexural strength. The co-sintering temperature was determined at 1250 °C to have the smallest shrinkage rate difference between anode and electrolyte. Then, a warp-free large-area unit cell with a diameter of 50 mm and open circuit voltage of 1.05V was fabricated.

Index Terms - Solid oxide fuel cell, co-tape casting, shrinkage, flexural strength

I. INTRODUCTION

Recently, fuel cells has been attracting attentions due to energy depletion and environmental issues. A solid oxide fuel cell (SOFCs) is one of the fuel cells which is composed of ceramic materials. SOFCs are studied for high energy conversion efficiency, and fuel flexibility. To fabricate SOFC unit cells, tape casting process has been widely used to fabricate unit cells for low manufacturing cost and availability of mass production. Co-tape casting process is one of the tape casting process, fabricating electrolyte and anode layer by single heat treatment step. However, organic additive decomposition, shrinkage rate mismatch, and warping occur in co-tape casting process. These are factors which can cause cracks and warping. Therefore, each step of co-tape casting process and the influence of the process conditions have to be studied to fabricate crack- and warp-free large-area unit cells.

In this study, organic additive decomposition were studied by thermo-gravimetric analysis (TGA) to find optimal co-firing

conditions and temperature profiles. To minimize cracks during the organic additive decomposition, flexural strength of anode support layer after organic additive decomposition depending on compositions of NiO, Ytria-stabilized zirconia (YSZ), and pore former of carbon black and graphite was also studied. The powder composition with maximum flexural strength was determined. Finally, co-sintering temperature was determined at the temperature with minimum shrinkage rate difference of anode and electrolyte layer.

From the analyses, optimal process conditions were determined to fabricate crack- and warp-free large-area unit cells. As a result, a large-area unit cell with a diameter of 50 mm was fabricated. Also, open circuit voltage of 1.05V was obtained, indicating that a crack-free unit cell was obtained.

II. EXPERIMENTAL

To fabricate unit cell, fine NiO (AS graded, Kceracell, Republic of Korea), coarse NiO (Nickelous oxide, J.T. Baker, USA), and YSZ (TZ-8Y, TOSOH, Japan) were used. Carbon black (Raven 430, Columbian Chemicals, USA) and Graphite flake (325 mesh, Alfa Aesar) were used as pore former. For the manufacturing of green tapes, co-tape casting was conducted by slurry preparation, de-airing, casting by a doctor blade. The as-prepared green tapes were cut into button cells with 25 mm in diameter. The thermal decomposition and shrinkage rate were measured by thermal gravimetric-differential thermal analysis (TG-DTA) (TG 209 F3, NETZSCH, Germany) and Thermomechanical analyzer (TMA, TMA 402 F1, Netzsch, Germany) at a heating rate of 5 °C/min in air from room temperature to 1450 °C. The flexural strength of tapes after burn-out process at 400 °C and 600 °C was measured by three point flexure test using universal testing machine (UTM, Instron 5583, Instron Corporation, USA). A large-area unit cell was fabricated with a diameter of 50 mm, and open circuit voltage was measured (SI 1260, SI1287, Solartron, UK).



A. Influence of process conditions

The TG-DTA results are shown in Fig. 1. During the burn-out process, endothermic peak at 270 °C, and exothermic peaks at 350 °C and 400 °C were observed. It was reported that the endothermic peak can be attributed to evaporation of binder and plasticizer. The exothermic peaks were because of oxidation of chains of organic materials. Therefore, heat treatment steps at 250 °C and 350 °C were adopted to slow the reaction.

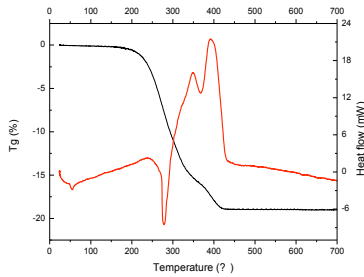


Fig. 1. TG-DTA result of the anode tape

Table I shows flexural strength of tapes after burn-out. As the burn-out temperature increased, the strength decreased due to decomposition of carbon black higher than 400 °C. Depending on the compositions of NiO, YSZ and pore former, the flexural strength changes in a wide range. Coarse NiO had lower strength than fine NiO. As the amount of YSZ increased, the strength also increased. As the pore former was changed from carbon black to graphite, the strength increased. As a result, sample 5 had the highest flexural strength.

TABLE I
FLEXURE STRENGTH RESULTS OF EACH TAPE SAMPLES WITH DIFFERENT COMPOSITIONS

Flexural strength [N]							
Sample number	NiO	Sample composition [g]			Burn-out temperature [°C]		burn-out results
		NiO:YSZ	Organic additives	Pore former	400	600	
1	Fine	62.7:37.3	26.4	Carbon black - 10	0.37	0.29	Serious fracture
2	Coarse	62.7:37.3	26.4	Carbon black - 10	0.32	0.19	Fracture
3	Coarse	62.7:37.3	21.1	Carbon black - 10	0.39	0.29	Fracture
4	Coarse	40.0:60.0	26.4	Carbon black - 10	0.5	0.33	No fracture
5	Coarse	62.7:37.3	26.4	Carbon black - 5 Graphite - 5	0.53	0.5	No fracture

Fig. 2 shows the shrinkage behavior of anode and electrolyte tapes. Anode tapes shrank more than electrolyte, which help sintering of electrolyte. The shrinkage mismatch was minimized at 1250 °C. Therefore, co-sintering was performed at

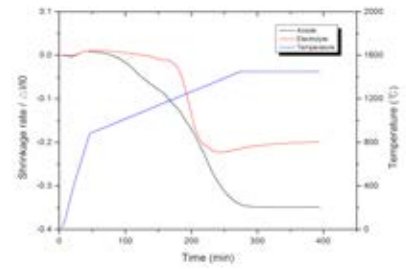


Fig. 2. Shrinkage rate of anode and electrolyte tape during the co-sintering

B. Fabrication of large-area unit cells

Based on the optimal process conditions, a large-area anode-supported electrolyte was fabricated as shown in Fig. 3. Buffer layer and cathode were coated by spin coating and screen printing, respectively. As a result, open circuit voltage of 1.05 was obtained.

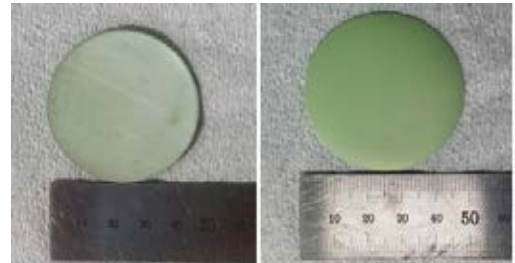


Fig. 3. Large-area anode-supported electrolyte with a diameter of 50 mm fabricated by co-tape casting process.

IV. CONCLUSION

In this study, thermal decomposition, flexural strength, and shrinkage behavior was studied, and optimal process conditions were determined. Based on the conditions, a large-area unit cell with 50 mm in diameter was successfully fabricated.

ACKNOWLEDGMENT

This research was supported by a grant from the Fundamental R&D Program for Core Technology of Materials funded by the Ministry of Knowledge Economy, Republic of Korea and the Global Frontier R&D Program on Center for Multiscale Energy System funded by the National Research Foundation under the Ministry of Education, Science and Technology, Korea. Also, this work was supported by the Korea CCS R&D Center (KCRC) grant (No 2014M1A8A1049299) funded by the Korea government (Ministry of Science, ICT & Future Planning) and KEPCO & Korea Western Power Co and the BK21 plus program through the National Research Foundation (NRF) funded by the Ministry of Education of Korea



ELECTRICITY AND CATHOLYTE PRODUCTION FROM CERAMIC MFCs TREATING URINE

I. Merino-Jimenez*, J. Greenman**, and I. Ieropoulos*

* Bristol BioEnergy Centre, Bristol Robotics Laboratory, University
of the West of England, BS16 1QY, (United Kingdom)

** Biological, Biomedical and Analytical Sciences, University of the
West of England, BS16 1QY, (United Kingdom)

Abstract –Microbial fuel cells (MFCs) offer a promising technology for electricity production. In the anodic chamber, an anaerobic biofilm breaks down the organic compounds present in the urine to generate electricity. In the cathodic chamber, the oxygen reduction reaction (ORR) contributes to the catholyte generation, together with the electroosmotic drag and the diffusion through the ceramic membrane. This work evaluates the effect of the thickness of a ceramic membrane, in the power generation, as well as for the first time study the catholyte produced from the MFCs using urine as a feedstock. Cylindrical MFCs were assembled with fine fire clay of different thicknesses (2.5, 5 and 10 mm). The power and the amount of catholyte decreased with the wall thickness, whereas the pH of the catholyte increased. The possibility to produce different quality of catholyte from urine opens a new field of study in water reuse for practical implementations.

Microbial Fuel Cell (MFC), Ceramic membrane, Catholyte production, Electroosmotic drag.

I. INTRODUCTION

Microbial Fuel Cells (MFCs) present an interesting approach to the electrical power generation technology. Urine is a free and abundant waste product, which can be treated in MFCs whilst generating electricity. An MFC consists of an anaerobic anodic chamber, a cathodic chamber and an ion exchange membrane, which separates the two. The ion exchange membrane has been shown that it can be replaced by ceramic materials [1]. The interest in using ceramic as low cost membrane materials for MFCs, is receiving increasing attention due to the positive performance in terms of power and catholyte production. The catholyte production in ceramic MFCs can be attributed to a combination of oxygen reduction reaction (ORR); water diffusion and electroosmotic drag [2]. In this

study, the catholyte produced from MFCs with different ceramic membranes was analysed and the effect of the membrane thickness was evaluated together with the power performance.

II. MATERIALS AND METHODS

A total of 12 ceramic MFCs were assembled, using fine fire clay (FFC) cylinders with three different wall thicknesses 2.5, 5 and 10 mm. The ceramics were tested in triplicates and one MFC of each thickness was left open circuit during the whole of the experiment, serving as a control. The anode electrode was constructed from 90 x 27 cm² untreated carbon veil (30 g/m², PRF Composites, Dorset, UK), which was folded and wrapped around the external surface of the ceramic cylinder. The cathode electrode consisted of a gas diffusion electrode with carbon veil as the support material and a microporous layer (MPL), which was prepared with a mixture of activated carbon (Vulcan XC-72, 80 gr/140 ml solution), polytetrafluoroethylene (PTFE) 60% wt. (Sigma-Aldrich) and deionized water [3]. The MFCs were inoculated for three days with a mixture of 50 % activated sewage sludge and 50 % fresh urine and after the third day fresh urine was continuously fed. Polarisation were performed by applying external resistances between 30 K Ω and 3.74 Ω for 5 minutes, whilst the anode and cathode electrode potentials were measured versus a Ag/AgCl reference electrode. After the first polarisation, the MFCs were loaded with the external resistance providing maximum power generation, which remained constant throughout the experiment. The catholyte was collected every 7 days, and the conductivity and pH were measured.

III. RESULTS AND DISCUSSION

The comparison of the polarisation experiments performed from each type of MFC is shown in Fig. 1. A clear difference was observed in the power output level, which was dependent on the wall thickness of the ceramic. The thinnest ceramic MFC produced the highest power of 2.1 ± 0.19 mW, followed by the medium and the thickest MFCs, which generated 1.8 ± 0.12 mW and 1.4 ± 0.21 mW, respectively.

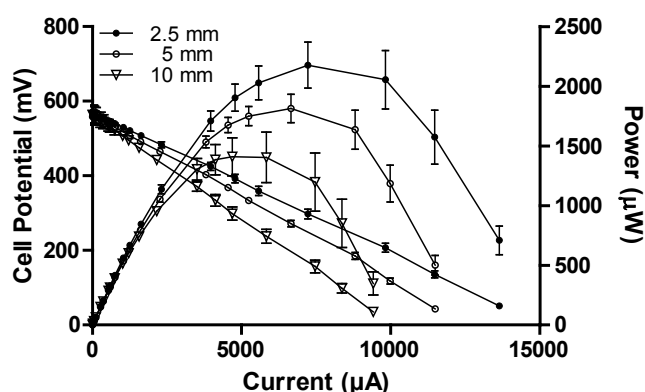


Fig. 1. Comparison of polarisation curves of the MFCs with ceramic of different wall thickness (2 mm, 5 mm, 10 mm).

A difference in the cell potential was also observed, due to a mixed dependence of the anode and cathode potentials with the ceramic thickness. The anode polarisation showed that the difference in power was due to an increase of the ohmic losses, produced by an increased internal resistance, with the ceramic thickness. There are two factors that might cause the difference in the potential losses in the cathode polarisation curves. Firstly, the wall thickness might affect the proton rate of transfer, having higher limitations to the proton flux through the ceramic membrane when it is thicker, increasing the ORR overpotential, and decreasing the cathode OCP [4]. Secondly, the difference in the catholyte accumulated in the cathodic chamber most likely has an effect in the MFC power production, by affecting the ORR in the cathode.

The amount of catholyte collected from each MFC (under load) also showed dependence on the wall thickness, collecting an average of 52.5 cm^3 from the MFCs with the thinnest membrane, which is more than 2-fold the catholyte produced in the MFCs with the 5 mm membrane (24.5 cm^3) and more than 3-fold the catholyte produced in MFCs with the thickest membrane (15 cm^3). However, the pH of the catholyte increased from 9.3 to 10, with increasing the wall thickness of the FFC membrane from 2.5 to 10 mm, respectively. The ceramic wall thickness is not the only parameter affecting the catholyte production and its quality, since the results also showed current-

dependence. For the MFCs with the same ceramic thickness, less quantity of catholyte at a lower pH was collected in the open-circuit control than in the loaded MFCs. This suggests that the difference between the collected catholyte samples was a consequence of the electroosmotic drag. Therefore, those two parameters, ceramic wall thickness and current production play an important role in the catholyte accumulation and its quality.

IV. CONCLUSION

This study compares the use of FFC ceramics with different thicknesses (2.5 mm, 5 mm and 10 mm) as low cost membrane materials for MFCs. The results show that the power produced decreased with the wall thickness, being the optimum thickness 2.5 mm for a maximum power generation of 2.1 ± 0.19 mW. The catholyte production and its composition were also found to be dependent on the membrane thickness. The amount of catholyte collected decreased with the thickness of the ceramic, but the pH increased. After seven days of operation, 15 cm^3 of catholyte at pH 10 were collected from the MFC with the thickest ceramic membrane, compared to 25 cm^3 at pH 9.3 obtained from the thinnest MFCs. This suggests the possibility of obtaining different compositions of catholyte from urine. Further work needs to be carried out in order to evaluate the possible practical applications of the catholyte collected and the potential of water reuse from urine.

ACKNOWLEDGMENT

The authors would like to acknowledge the Bill and Melinda Gates Foundation for the financial support to this project under the grant no. OPP1094890, and ROCA for providing the ceramic cylinders.

REFERENCES

- [1] Hernández-Fernández, F.J., Pérez de los Ríos, A., Salar-García, M.J., Ortiz-Martínez, V.M., Lozano-Blanco, L.J., Godínez C., Tomás-Alonso F., Quesada-Medina, J., Recent progress and perspectives in microbial fuel cells for bioenergy generation and wastewater treatment, *Fuel Processing Technology*, Volume 138, 2015, Pages 284-297.
- [2] Gajda, I., Greenman, J., Melhuish, C., Santoro, C., Li, B., Cristianie, P., Ieropoulos, I., Water formation at the cathode and sodium recovery using Microbial Fuel Cells (MFCs), *Sustainable Energy Technologies and Assessments*, Volume 7, 2014, Pages 187-194.
- [3] Papaharalabos, G., Greenman, J., Melhuish, C., Santoro, C., Cristiani, P., Li, B., Ieropoulos, I., Increased power output from micro porous layer (MPL) cathode microbial fuel cells (MFC), *International Journal of Hydrogen Energy*, Volume 38, 2013, Pages 11552-11558.
- [4] Behera, M., Ghangrekar, M.M., Electricity generation in low cost microbial fuel cell made up of earthenware of different thickness, *Water Science and Technology*, Volume 64, 2011, Pages 2468-2473.



ETHANOL ELECTROCHEMICAL CONVERSION AND PEM ELECTROLYZER OPERATION AT LOW TEMPERATURES

S.A. Grigoriev^{1*}, I.I. Nikolaev², S.E. Salnikov², V.V. Pimenov², E.K. Lutikova², S.V. Akelkina², and V.N. Fateev²

¹ National Research University "Moscow Power Engineering Institute", 14, Krasnokazarmennaya str., Moscow, 111250, Russia

² National Research Centre "Kurchatov Institute", 1, Kurchatov sq., Moscow, 123182, Russia

*E-mail: sergey.grigoriev@outlook.com

Abstract – Ethanol like some other compounds could be used for anode depolarization and reduction of energy consumption for hydrogen production by electrolysis. At the same time ethanol and ethanol solutions in water has low freezing temperature and could provide PEM electrolysis at low temperatures. In this research electrolysis of ethanol solutions in water (up to 40 vol.%) were tested for anode depolarization. Platinum, iridium and a solid solution of Pt-Ru (1:1 at. %) were used as the anode catalyst, and Pt on Vulcan XC-72 and Pt-Ru obtained by magnetron sputtering were used as the cathode one. It was demonstrated that the energy consumption for the hydrogen production by electrolysis of such solutions is lower than that for water electrolysis only at low current density and the economic feasibility of this process is doubtful. But such ethanol solutions provided possibility of “could” start of PEM electrolyzer at temperatures up to -25°C.

Index Terms – Anode depolarization, Ethanol electrochemical conversion, hydrogen production, PEM electrolysis, electrocatalyst.

I. INTRODUCTION

Recently the possibility of hydrogen production by electrochemical conversion of alcohols attracted attention of different research groups [1-3]. But such reactants and their solutions also give possibility to carry out PEM electrolysis at low temperatures [4]. Investigations of PEM electrolyzer start and operation at low temperatures practically were not done (in comparison with the investigations of PEM fuel cell cold start problem). Though application of such electrolyzers in power plants based on renewable energy systems may need such a possibility in northern regions.

This paper deals with the research that covers the possibility of using ethanol in concentrations up to 60 vol. % as an anode depolarizer for the electrolysis cell with proton-exchange membrane (PEM) for efficient hydrogen production and in order to ensure its start at low temperatures for PEM fuel cell-based power plants. Platinum, iridium and a solid solution of Pt-Ru (1:1 at. %) were used as the anode catalyst, and Pt on Vulcan XC-72 and Pt-Ru were used as the cathode one. It is shown that in all cases by using water-ethanol solutions with concentrations of ethanol up to 60 vol. % the cell voltage generally increased due to the increase of membrane resistance and decrease of rate of the cathode process of platinum catalyst passivation/poisoning by ethanol and its oxidation products. Some negative impact had strong swelling of the membrane-electrode assembly in a solution of ethanol, which leads to its partial destruction.

The energy consumption for the production of hydrogen by electrolysis of ethanol solutions is lower than that for water electrolysis at low voltage, though the economic feasibility of this process is doubtful.

The research demonstrates the electrolysis cell can withstand the freezing at the temperatures in the range of -15 to -30°C. Moreover, the resistance of the membrane in water-ethanol solutions (about 60 vol. %) is not critical at these temperatures. The feed of water-ethanol solutions in the electrolytic cell allows to start the electrolysis of water at these temperatures at a voltage of 2.0-2.2 V and currents of 0.07-0.13 A/cm². This ensures the "cold start" and subsequent self-heating of the electrolysis cell and further using deionized water as reactant.



II. EXPERIMENTAL PART

Electrolysis of ethanol solutions was investigated in a glass three-electrode and laboratory PEM electrolysis cell with Nafion membrane. Catalysts were synthesized by polyol method and using pulsed magnetron sputtering,

III. RESULTS AND DISCUSSION

At electrolysis of ethanol solutions we observed increase of the cell voltage in time in comparison with electrolysis of deionized water at initial cell voltage > 1.4 V. Main reasons are the increase of the membrane resistivity, the disruption of the MEA structure due to the membrane and catalyst layer swelling and cathode poisoning by intermediates. At high ionomer concentrations and high ethanol concentrations (60% and more) we even observed catalyst particles removing from the catalyst layer. Energy consumption for hydrogen production with ethanol solutions was lower in comparison with water electrolysis only at low current densities (less than 0.1 A/cm^2) when water electrolysis practically is not going on. The best anode and cathode catalysts were Pt-Ru compositions but even with such compositions energy consumption was more than $3 \text{ kW}\cdot\text{h/m}^3$ at 0.1 A/cm^2 (85°C). At higher current density these compositions also provided lower cell voltage in all temperature intervals but with lower stability of cell parameters. Frosting of PEM electrolysis cell up to -30°C did not influence cell parameters after cell careful heating to normal operation temperatures. Application of ethanol solutions at $-30 - 0^\circ\text{C}$ for PEM cell operation demonstrated that electrolysis is going on with reasonable speed ($0.1\text{-}0.2 \text{ A/cm}^2$) and voltage (less than 2.5 V). Heat evolution from 1 cm^2 was reaching 0.1 W which was enough for stack heating. Hydrogen purity at initial stages of the cold start was 99.98% and suitable for PEM fuel cell operation.

IV. CONCLUSION

It was shown that ethanol solutions give possibility to decrease PEM electrolyzer voltage only at low current density and low voltage (when water electrolysis practically is not going on). Even with the best anode and cathode catalysts (Pt-Ru compositions) energy consumption for hydrogen production was more than $3 \text{ kW}\cdot\text{h/m}^3$ at 0.1 A/cm^2 (85°C) and not attractive from economical point of view. The research also demonstrates the electrolysis cell can withstand the freezing at the temperatures in the range of -15 to -30°C . Moreover, the resistance of the membrane in water-ethanol solutions (about 40-60 vol. %) is not critical at these temperatures though it strongly influence cell voltage increase. The feed of water-ethanol solutions in the electrolytic cell allows to start the electrolysis of water at these temperatures at a voltage of 2.0-2.2 V and currents of $0.07\text{-}0.13 \text{ A/cm}^2$. This ensures the "cold start" and subsequent self-heating of the electrolysis cell and further using deionized water as reactant.

ACKNOWLEDGMENT

This investigation was done at the expense of a grant of the Russian Science Foundation (project No. 14-29-00111).

REFERENCES

- [1] Sasikumar G., Muthumeenal A., Pethaiah S.S., Nachiappan N., Balaji R. Aqueous methanol electrolysis using proton-conducting membrane for hydrogen production // *International Journal of Hydrogen Energy*. 2008. Vol. 33, issue 21. P. 5905–5910.
- [2] Caravaca A., Sapountzi F.M., De Lucas-Consuegra A., Molina-Mora C., Dorado F., Valverde J.L. Electrochemical reforming of ethanol water solutions for pure H_2 production in a PEM electrolysis cell // *International Journal of Hydrogen Energy*. 2012. Vol. 37, issue 12. P. 9504–9513.
- [3] Cloutier C.R., Wilkinson D.P. Electrolytic production of hydrogen from aqueous acidic methanol solutions // *International Journal of Hydrogen Energy*. 2010. Vol. 35, issue 9. P. 3967–3984.
- [4] Fateev V., Lyutikova E., Pimenov V., Akelkina S., Salnikov S., Xing W. The possibility of electrolyzer with a solid polymer electrolyte start at low temperatures // *International Scientific Journal for Alternative Energy and Ecology*. 2015. Vol. 176, issue 12. P. 28–39.



COBALT-DOPED CARBON NANOFIBERS AS AN EFFECTIVE ORR CATALYST

M. A. Abdelkareem^{1, 2}, Mohamed S. Mahmoud², Mohammad R. O. Ali³, Faiza A. Hammad²,
N.A.M. Barakat^{2,3}, and I. A. Ashour²

¹ Dept. of Sustainable and Renewable Energy Engineering, University of Sharjah, PO Box 27272, Sharjah, (U.A.E.)

² Chemical Engineering Department, Faculty of Engineering, Minia University, El-Minia, 61111, (A.R.E.)

³ Mechanical Power & Energy Eng. Dept., Faculty of Engineering, Minia University, El-Minia, 61111, (A.R.E.)

⁴ Organic Materials and Fiber Engineering Department, Chonbuk National University, Jeonju 561-756, (South Korea)

Abstract – In this work, Polyacrylonitrile (PAN) based carbon nanofibers containing different percentages of Cobalt were prepared by electrospinning. The prepared carbon nanofibers were characterized by Transmission Electron Microscopy (TEM) and X-ray Diffraction (XRD) analysis. The oxygen reduction reaction activity (ORR A) of the prepared materials was investigated in acidic medium, i.e., 0.5 M H₂SO₄. The ORR A of the prepared materials was compared with that of the commercial Pt/C catalyst. Results show that PAN based carbon nanofibers has an ORR A and this activity significantly increased with the addition of Cobalt. The ORR A of the prepared material using Cobalt has a comparable activity to that of the commercial Pt/C catalyst and considered as a promising candidates to Pt. catalyst.

Index Terms –

Carbon nanofiber, cobalt, ORR A, electrospinning.

I. INTRODUCTION

Fuel cells (FCs) have been considered to be promising power sources of alternative energy because of their cleanliness and high efficiency, usability of exhaust heat and flexibility for mobile [1]. Attention has recently been paid to proton exchange membrane FCs (PEMFCs). Nevertheless, the large scale commercialization of these cells is limited because of the high cost of the components and primarily by the cost of the Platinum catalyst that is required for hydrogen oxidation reaction (HOR) at anode and oxygen reduction reaction (ORR) at cathode. The ORR generally faces slow kinetics; therefore it requires efficient catalyst [2]. The Pt-free cathode catalyst has attracted attention over other materials such as; palladium alloys [3], metalloporphyrins [4], nitrogen doped carbon [5]. It has been proposed as potential alternative catalysts for ORR because of its relatively good electrocatalytic activity and low cost. In this paper, transition metal doped carbon nanofibers (Co-CNFs) have been fabricated using electrospinning technique using polyacrylonitrile (PAN) as precursor of carbon and nitrogen, and cobalt acetate tetrahydrate as precursor for cobalt (Co). Full characterization of the prepared materials has been carried out using SEM, TEM and XRD analysis. The ORR A of

the prepared materials was evaluated in 0.5M H₂SO₄ using three electrode cell structure (Ex-Situ cyclic voltammetry).

II. EXPERIMENTAL

Preparation of cobalt-doped carbon nanofibers is done in the following steps: 1. Preparation of PAN solution (12 wt. %). 2. Dissolve 0.06 g of Co/Ac in 1 mL of Dimethylformamide, DMF. 3. Mix the two solutions in definite ratios that give a final solution contains 1wt. % of Co to the PAN. 4. These steps were repeated to prepare the other Co wt. %, i.e., 0%, 2%, 4.6%, 6% and 9.2%. 5. Electrospinning has been carried out at 12-15 kV with a working distance of 30 cm. 5. The dried nanofiber mats were stabilized by heating it at 250° C for 4h in air. 6. The sample was carbonized in inert atmosphere at 900°C for 1h. The catalyst ink was prepared by dissolving a 2 mg of catalyst (Pt or carbon nanofiber powder) in 20 ml of Ethanol, 20 µl of Nafion solution (5wt.%), Then a 5 µl of the prepared ink was deposited on the surface of the Glassy carbon electrode.

III. RESULTS AND DISCUSSION

A. Morphology of the nanofiber

The structure and morphology of Co-CNFs catalyst was analyzed by XRD, EDX and TEM. Fig. 1 presents the TEM images of Co-CNFs catalyst. These images indicated that the nanofiber morphology was obtained. Catalyst has been prepared successfully to be in nanofiber form having a diameter of 100 nm and little micrometer length. The dots in the TEM images were related to the Co nanoparticles. We have confirmed from the XRD and the EDX that a complete reduction of the Co acetate into Co has been obtained as being clear in insert 2 of Fig. 1 and Fig.2. From this table, the obtained weight ratio of Co to C atoms were about 5% and that value was going in according to the calculated one based on the initial concentrations of the PAN and Co acetate, 4.6%, thus the catalyst is prepared successfully.



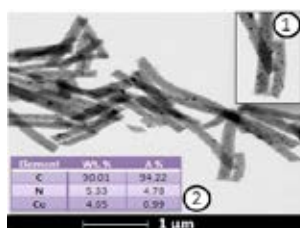


Fig.1. TEM image of Co-CNFs, insert 1: magnification of the Co-CNFs, Insert 2: Table of wt. % and atomic % of Co-CNFs catalyst from EDX analysis

Fig.2 presents the XRD pattern of Co-CNFs catalyst. It is noticed that the peaks located at 44.37, 51.52 and 75.88 are corresponding to Co (111), Co (200) and Co (220) respectively this indicates that cobalt is in metallic form not oxide form inside the carbon nanofibers.

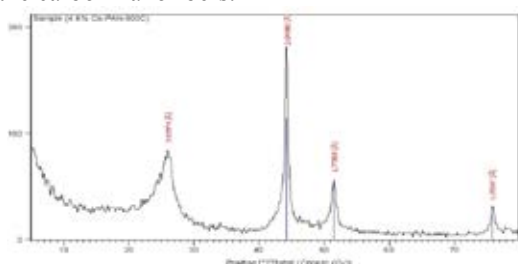


Fig.2. XRD pattern of cobalt-doped carbon nanofibers

B. Activity of catalyst prepared

The ORR activity (ORR A) of catalyst was evaluated using CV. Fig.3 (a) shows the CV of the Co-CNFs with different % of Co compared to that of commercial Pt/C catalyst. The CNF containing 0% Co showed a very plateau curve and this means a very weak ORR activity. The ORR A was significantly increased with the addition of the Co, and the highest ORR A was obtained at 4.6 wt. % Co. This activity is slightly lower than that of the Pt/C catalyst where the Onset potential of the prepared materials is lower than that of the Pt/C catalyst by 0.2V. However, the current density (limiting one) is very close to that of Pt/C catalyst. Fig. 3(b) shows the base of the calculation of the ORR A where we have subtracted N₂ current from the O₂ current to obtain the i_{ORR} current for all the samples.

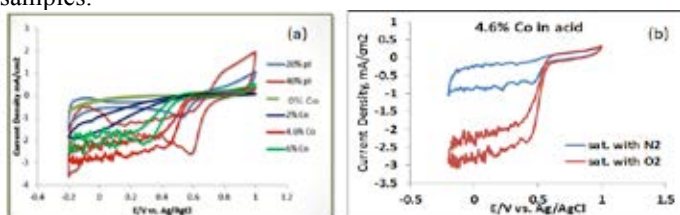


Fig.3. CVs of (Co-CNFs): (a) in O₂ saturated 0.5M aqueous H₂SO₄ at a scan rate of 5 mV/s, (b) both in O₂ and N₂ saturated acid solution

The improvement of the ORR A by the addition of the Co would be related to the enhancement of the graphitization of the carbon by the transition metal that will lead to improvement in the electrical conductivity. Also, it was reported that the ORR

A could be related to the bond between the carbon, nitrogen and the transition metal ions [6]. These results showed that carbon based carbon nanofibers containing Co is an excellent candidate to replace the Pt/C as a cathode in fuel cell applications.

IV. CONCLUSION

The conclusions can be summarized as follows:

- The catalyst in a well-defined nanofiber form, 100 nm in diameter, with uniform distribution of cobalt has been obtained.
- The cobalt in catalyst was fully reduced into the metallic form.
- Adding the Co significantly improved the ORR A; the highest activity was obtained with 4.6 wt. % Co, where the limiting current density was 3mA/cm², and onset potential 0.6V vs Ag/AgCl.
- However, the fuel cell current density when using Co-CNFs as cathode catalyst is lower than that with Pt.-catalyst, but because of Pt.-catalyst high cost, the Co-CNFs can be used as cathode catalyst for fuel cell.

ACKNOWLEDGMENT

This work was done under project funded by EU/RDI with contract no ENPI/2014/343-429.

REFERENCES

- [1] D. Yang, D. Bhattacharjya, S. Inamdar and J. Y. J. Park, "Phosphorus doped ordered mesoporous carbons with different lengths as efficient metal-free electrocatalysts for oxygen reduction reaction in alkaline media," *Journal of the American Chemical Society*, 134, 2012, 16127-16130.
- [2] F. Jaouen, J. Herranz, M. Lefèvre, J. Dodelet, U. I. Kramm, I. Herrmann, P. Bogdanoff, J. Maruyama, T. Nagaoka, A. Garsuch, J. R. Dahn, T. Olson, S. Pylypenko, P. Atanassov and E.A. Ustinov, "Cross-laboratory experimental study of non-noble-metal electrocatalysts for the oxygen reduction reaction.," *ACS Appl Mater Interfaces*, 1,2009, 1623-1639.
- [3] T. Sarakonsri, S. Suthirakun, S. Charojrochkul and T. Vilaithong, "Preparation of non-noble metal based catalysts supported on carbon for PEMFC cathodes" *J. of Ceramic Processing Research*, 10, 2009, 589-594.
- [4] M. H. Shao, T. Huang, P. Liu, J. Zhang, K. Sasaki, M. B. Vukmirovic and R. R. Adzic, "Palladium Monolayer and Palladium Alloy Electrocatalysts for Oxygen Reduction," *Langmuir*, 22, 2006, 10409-10415.
- [5] M. Lefèvre, J. Dodelet and P. Bertrand, "Molecular oxygen reduction in PEM fuelcells: evidence for the simultaneous presence of two active sites in Fe-basedcatalysts," *J. Phy. Chem. B*, 106, 2002, 8705-8713.
- [6] Paul H. Matter, Ling Zhang, Umit S. Ozkan, The role of nanostructure in nitrogen-containing carbon catalysts for the oxygen reduction reaction, *J. Catal.* 239 (2006) 83–96.



A NEW DESIGN OF MEMBRANELESS MICROBIAL FUEL CELL: ANODE AND CATHODE SHARE THE SAME SELF-STRATIFIED ELECTROLYTE OF URINE

X. A. Walter*, I. Gajda, S. Forbes*, J. Greenman** and I. A. Ieropoulos*

* Bristol BioEnergy Centre (B-BiC), Frenchay Campus, University of the West of England, Bristol, BS16 1QY, (United Kingdom)

** Microbiology Research Laboratory, Department of Biological, Biomedical and Analytical Sciences, Frenchay Campus, University of the West of England, Bristol, BS16 1QY, (United Kingdom)

Regardless of architecture, microbial fuel cell technology requires a plurality of units to achieve exploitable electrical power. This implies that each unit needs a simple design allowing the production of the needed multiplicity. Here, we present a novel design of two membraneless MFC stacks in which the anode and cathode share the same electrolyte. This design relies on the self-stratification of a liquid under the natural activity of the microbial consortia thriving in the system. Results showed that individual stacks reached a power density of $\sim 20 \text{ W.m}^3$ at 390 mV under 40 Ω . Oxygen concentration showed that the oxycline was at 0.25-0.5 cm depth (total depth of 7.5 cm). Hence, oxygen was not the dominant electron acceptor in the liquid phase. In conclusion, this simple design of microbial fuel cell demonstrated that high power density was reached even if the anode and cathode shared the same electrolyte.

Index Terms - Cathode functioning linked to nitrogen cycle membraneless stacks, self-stratifying column.

I. INTRODUCTION

The Microbial Fuel Cell (MFC) is a technology in which microorganisms employ an anode as the end-terminal electron acceptor of their electroactive anaerobic respiration. Such anaerobic electroactive respiration allows for a direct transformation of chemical energy (reduced organic matter) into electrical energy. The first working MFC was reported by Potter in 1911 [1], but it is only in the last 15 years that significant breakthroughs have been achieved. In the context of reducing energy consumption, recent studies have demonstrated the potential of using urine directly as a fuel for electricity generation [2]. Ongoing work in scaling up the microbial fuel cell technology towards out-of-the-lab applications is regularly reported,

with a number of approaches being pursued. One of these approaches is the stacking of small-scale MFC units for useful electricity generation [3]. This implies that each unit needs to have a simple design allowing easy unit replication for the collective stack. In the present study, we demonstrate the results of two membraneless MFC stacks in which the anodes and cathodes share the same electrolyte (i.e. urine). This design relied on the self-stratification of a liquid under the natural activity of the microbial consortia thriving in the system.

II. MATERIALS & METHODS

Each of the two MFC stacks comprised six ceramic vertical supports, each of which were surrounded by a cathode on the upper part and an anode on the lower part. These six units were then inserted in a container having one inlet and one outlet. The six MFCs were electrically connected in parallel forming one stack per box. The exchange volume of each stack was 200 mL. The anodes were only separated from the cathode by a horizontal 2 mm thick acrylic perforated support. Polarisation experiments were performed using a computer-controlled resistorstat. The range of resistance values was between 38k Ω - 4.36 Ω with 10-minute time intervals for each resistance.

III. RESULTS & DISCUSSION

Results showed that individual stacks reached an absolute power of $\sim 3.8 \text{ mW}$ at 390 mV under a load of 40 Ω (Figure 1a). The polarisation curves illustrate a capacitance effect (Figure 2b) that results in a 25 % increase of power output, despite the overshoot, indicating

the benefits of intermittent loading for higher power production [4].

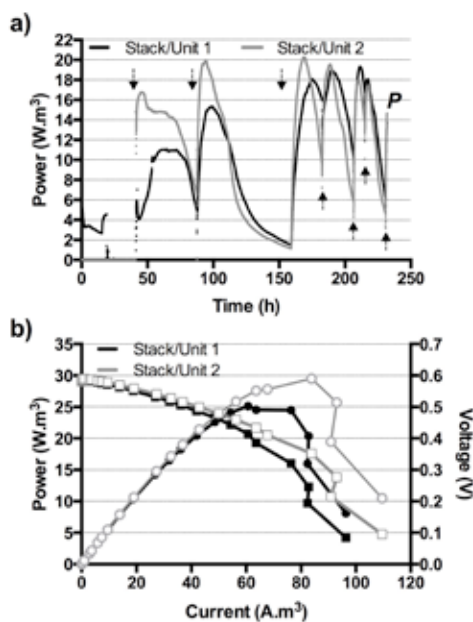


Fig. 1. Power output of individual stacks normalised by the exchange volume. **a)** Temporal data, arrows show electrolyte replenishment, and *P* indicates polarisation run. **b)** Power and polarisation data.

When the two stacks were connected in parallel, an absolute power of ~ 7 mW (418 mV, 20Ω) was achieved. When electrically connected in series, the system reached an absolute power of ~ 10.5 mW and a voltage of 900 mV (80Ω) (Figure 2). After the second replenishment, the series connection only reached an absolute power of ~ 3.4 mW at 519 mV, indicating an inhibiting effect, hence the disconnection of the series. Further investigations indicated that series connection was possible to maintain, but at a higher replenishment rate (data not shown).

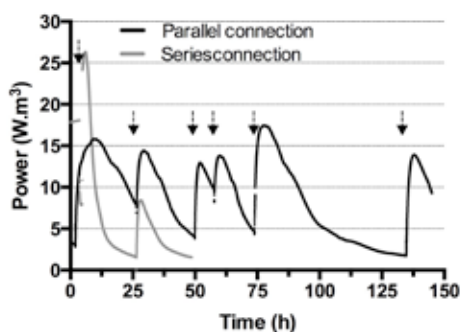


Fig. 2. Power output of the stacks when electrically connected either in parallel or series. The power was normalised by the exchange volume (200 ml). Arrows indicate the points of urine replenishment

Oxygen concentration showed that the oxycline was at 0.25 - 0.5 cm depth (total depth of 7.5 cm). Hence, the oxygen was not the dominant electron acceptor in the liquid phase (i.e. urine). Moreover, NH_4 concentration showed depletion at the limit between the anode and cathode (Figure 3). Whether NH_4 is converted into NH_3 or N_2 is to be investigated, however, this phenomenon gives rise to the hypothesis that in such a setup the cathode operation is ultimately in the nitrogen redox cycle.

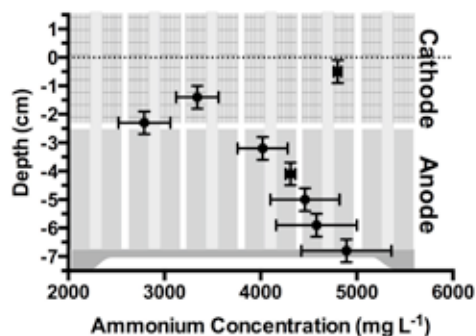


Fig. 3. Ammonium concentration profiles illustrating depletion in the lower part of the cathode. Dotted line shows the urine level in the system.

IV. CONCLUSIONS

In conclusion, this simple design of microbial fuel cell demonstrated that high power density was reached even with an anode and cathode exposed to the same electrolyte. These results are the first demonstration of a membraneless MFC whereby the insulation between cathode and anode is driven by the self-stratification of the urine. This opens up new research avenues for the identification of the electron acceptor in this new type of MFC.

ACKNOWLEDGMENT

This work has been funded by the EPSRC, grant n° EP/L002132/1.

REFERENCES

- [1] Potter, M.C, Electrical Effects Accompanying the Decomposition of Organic Compounds, Proceedings of The Royal Society B, Volume 84, 1911, pp. 260-276.
- [2] Ieropoulos I., Greenman J., Melhuish C., Urine utilisation by microbial fuel cells: energy fuel for the future, Physical Chemistry Chemical Physics, Volume 14, 2012, pp. 94-98.
- [3] Ieropoulos I., Melhuish C., Greenman J., Horsfield I., EcoBot-II: An artificial agent with a natural metabolism, International Journal of Advanced Robotic Systems, Volume 2, 2008, pp.295-300.
- [4] Walter XA, Greenman J, Ieropoulos IA. Intermittent load implementation in microbial fuel cells improves power performance. Bioresource Technology, Volume 172, 2014, pp.365-372



Use of a single-chamber, air-cathode MFC for Polycyclic Aromatic Hydrocarbons (PAHs) remediation in water environment.

Nastro R.A.*^{□#}, Toscanesi M.^{°#}, Gambino E.[^], Monteverde M.[^], Guida M.[^], Falcucci G.*[°], Minutillo M.*[°], Jannelli E.*[°], Trifuoggi M.[°]

*Department of Engineering, University "Parthenope" of Naples (Italy)

[°] Department of Chemical Sciences, University "Federico II" of Naples (Italy)

[^]Department of Biology, University "Federico II" of Naples (Italy)

[□] Corresponding author. Email: r.nastro@uniparthenope.it

[#]The authors equally contributed to this research.

Abstract - The possible utilization of MFCs technology to the remediation of waters polluted by Polycyclic Aromatic Hydrocarbons (PAHs) was explored in this work. Ten microbial strains, isolated in urban environment, were inoculated in a MFC (three replicates) fuelled by 400 ml Winogradsky saline solution containing no other carbon and energy sources than anthracene (100 ppm), naphthalene (200 ppm), phenanthrene (100 ppm), pyrene (100 ppm), benzo(a)pyrene (50 ppm) and incubated at 25°C. The performances were evaluated in terms of Power Density (PD), Current Density (CD), PAHs degradation rate and toxicity vs *Daphnia magna* and *Lepidium sativum*. A significant variability in PD ($486 \mu\text{W}/\text{m}^3$ on average) was measured along with a maximum CD of $9 \text{ mA}/\text{m}^3$. A degradation of 53% (naphthalene), 28% (anthracene and phenanthrene), 17% (pyrene) and 25% (benzo(a)pyrene) but, an increase in ecotoxicity vs *L.sativum* was measured in Winogradsky solutions+PAHs after one month.

Index Terms – Microbial Fuel Cells, bioremediation, PAHs, ecotoxicity.

I. INTRODUCTION

Polycyclic Aromatic Hydrocarbons (PAHs) are produced by the incomplete combustion of low biodegradable hydrocarbons, occurring during volcanic eruptions, forest fires, burning of fossil fuels etc. [1]. Concerns for PAHs environmental diffusion has been expressed for the mutagenic and carcinogenic activity of these compounds and sixteen of these chemicals have been regulated by the US EPA as priority pollutants [2]. Recent studies reported the possible utilization of MFCs in soil bioremediation with some encouraging results [3]. Interestingly, a certain PAHs degradation was detected in two-chamber MFCs with both

aerobic and anaerobic catholyte [3], while traditional bioremediation processes use soil aeration to stimulate the microbial metabolism. In MFCs, a higher efficiency in terms of PAHs degradation was achieved when the cathode was placed in an anaerobic environment but with less power density [3]. Nevertheless, in all the above cited researches, energy and carbon sources other than PAHs were provided by the soil itself. Our study was aimed at testing the efficiency of a microbial consortium to use five PAHs among the 16 priority pollutants as sole source of carbon and energy in Winogradsky solution used in a single chamber, air-cathode MFC.

II. MATERIALS AND METHODS

Stenotrophomonas spp., *Alcaligenes fecalis*, *Achromobacter* spp., *Xanthomonas* spp., *Staphylococcus succinus*, *Bacillus amiloliquefaciens*, *Enterobacter aerogenes*, *Arthrobacter misorens*, *Pseudomonas anguillarum* strain 1 and strain 2 were isolated from soot samples taken in urban environment. Before being used, all strains were tested for their ability to use naphthalene, phenanthrene, anthracene, pyrene and benzo[a]pyrene as sole carbon and energy sources on mineral solid media [1] and to produce surfactants [4], able to improve PAHs solubility in water. MFCs were by 500mL Duran[®] glass bottles and graphite beams, used for the electrodes assembly. Three different MFCs were set up in three replicates and fuelled respectively with 400 ml of: Winogradsky solution + PAHs + bacteria, Winogradsky solution + PAHs, Winogradsky solution. All PAHs were previously dissolved in acetone and, then, added to the Winogradsky solution with the following final concentrations: anthracene (100 ppm), naphthalene (200

ppm), phenantrene (100 ppm), pyrene (100 ppm), benzo(a)pyrene (50 ppm). Along with MFCs, 500 ml Duran[®] glass bottles (named “bioreactors”) were filled with the above solutions/suspensions (400 ml) and run for 4 weeks. PAHs were extracted by a SPE technique and analyzed by a High Pressure Chromatography (HPLC) with UV spectrometer. The environmental toxicity of each solution/suspension was evaluated vs *Daphnia magna* and *Lepidium sativum* at the beginning and at the end of the experiment. The endpoints of the ecotoxicological tests were the immobilization rate of *Daphnia magna* 24- hours newborns after 24 and 48 hrs of exposure to 50 ml of sample (four replicas) and the Germination Index (GI) of 10 *Lepidium sativum* seeds after 72 hours of exposure to 3 ml of samples (three replicas) [1]. The Germination Index (GI) was calculated according (1):

$$GI \% = \frac{G_s \times L_s}{G_t \times L_t} \times 100 \quad (1)$$

where: G_s=average number of germinated seeds in the sample, G_t=average number of seed germinated in the blank, L_s=average root length of the sample, L_t=average root length of the blank. Voltage was measured by a Keythley Instruments[®] multimeter and polarization curves were performed every 24-48 hours using a range of 5 MΩ to 1000 Ω.

III. RESULTS

P.anguilliseptica strain I was the stronger surfactant producer followed by *P.anguilliseptica* II, *Alcaligenes faecalis* and *Xanthomonas* spp. *S.succinus* and *E.aerogenes* were negative to all tests. The microbiological analyses on solid media (Oxoid[®]) at the electrodes revealed, at the anode, the abundance of all Gram negative strains with the exception of *P.anguilliseptica* and *Xantomonas* spp. present, instead, at the cathode. MFCs performances in terms of PD and CD were lower in presence of the microbial consortium, reaching a max power of 0.207 mW/m³ and 11 mA/m³ in presence of bacteria (Figure1) and 1 mW/m³ and 38 mA/m³ in MFCs with just PAHs (Figure 2).

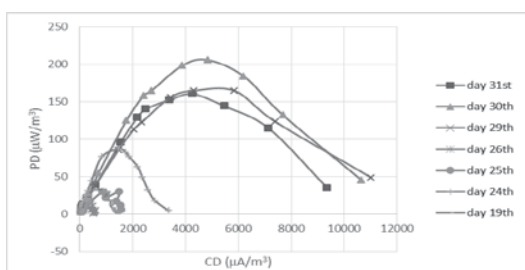


Fig.1: Polarization curves of MFCs fuelled by PAHs+bacteria.

PAHs degradation rate was higher in MFC inoculated with the microbial consortium, even in comparison with the bioreactor (Figure 3), thus proving the positive effect of the electrogenesis on PAHs degradation in water environment. The ecotoxicological essays showed a 100% immobilization of *Daphnia magna* after just 24h in all samples from both MFCs and bioreactors containing PAHs (in presence or in absence of

bacteria). As to *Lepidium sativum*, a GI<40% was measured in all MFCs and in the bioreactor in presence of bacteria and PAHs, thus demonstrating a high toxicity.

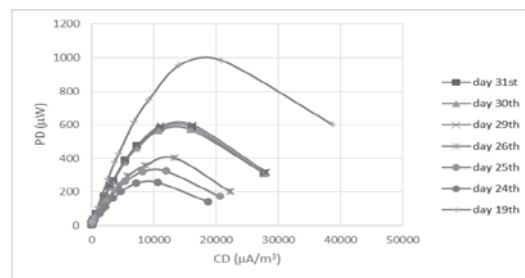


Fig.2: Polarization curves of MFCs fuelled by PAHs.

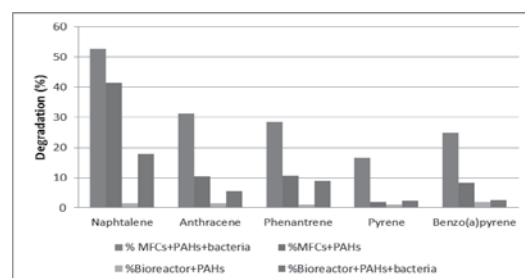


Fig.3: PAHs degradation rate in MFCs and bioreactors.

IV. CONCLUSIONS

MFCs inoculated with a PAHs solution and a specialized microbial consortium gave evidence of possible utilization in polluted waters remediation. Nevertheless, no toxicity decrease was measured after one month vs *D.magna* and *L.sativum*. This result can be explained by the generation of toxic intermediates, which are of some concern in remediation processes of both water and soil polluted by chemicals, PAHs included. Nevertheless, further investigations are needed, even to improve MFCs overall efficiency.

V. REFERENCES

- [1] Nastro R.A., Suglia A., Pasquale V., Toscanesi M., Trifuoggi M., Guida M. Bioremediation Process Efficiency for Polycyclic Aromatic Hydrocarbons Through Ecotoxicological Tests. International Journal of Performability Engineering, Volume 10, Issue 4, 2014, Pages 411-418.
- [2] Yana, J., L.Wanga, P. P. Fub and H.Yua. Photomutagenicity of 16 polycyclic aromatic hydrocarbons from the US EPA priority pollutant list. Mutation Research, Volume 557, 2004, Pages 99–108.
- [3] Sherafatmand M., Ng HY. Using sediment microbial fuel cells (SMFCs) for bioremediation of polycyclic aromatic hydrocarbons (PAHs). Bioresour. Technol., Volume 195, 2015, Pages 122-130.
- [4] Youssef N.H., Duncan K.E., Nagle D.P., Savage K.N., Knapp R.M.,McInerney M.J.Comparison of methods to detect biosurfactant production by diverse microorganisms. J. Microbiol Methods, 2004; 56(3):339-47.



PERFORMANCES AND MICROBIOLOGY OF A MICROBIAL FUEL CELL (MFC) FED WITH THE ORGANIC FRACTION OF MUNICIPAL SOLID WASTE (OFMSW).

RA Nastro**#, G. Falcucci**, Toscanesi M.*, Minutillo M.**, Pasquale V.°, Trifuoggi M.*, Dumontet S.°, Jannelli E.**

**Department of Engineering, University "Parthenope" of Naples (Italy)

°Department of Science and Technology, University "Parthenope" of Naples (Italy)

*Department of Chemical Sciences, University of Naples "Federico II" (Italy)

Corresponding author. Email: r.nastro@uniparthenope.it

Abstract - The performances and microbiology of three single-chamber, air-cathode, membraneless MFCs with the Organic Fraction of Municipal Solid Waste (OFMSW) as feedstock were investigated. Power Density (PD), Current Density (CD), organic load (COD, BOD₅, TOC) removal were evaluated. As to bacteria, lactobacilli were prevalent at the anode of all MFCs. *Lactobacillus casei* electroactivity was further studied in two-chamber MFCs, achieving a maximum PD of 77 mW/m³, with glucose as source of energy. With an electrodes distance of 2.5 cm, fuel pH was 6.8±1 and a *Pseudomonas aeruginosa* strain producing abundant pigments grew at the cathode. Even if operating in different conditions (O₂ availability, external load, initial pH, electrodes distance), all MFCs gave evidence of a possible utilization of OFMSW as source of electric power (10.8 mW/m²kg_{waste}) and current (158 mA/m²kg_{waste}), with a significant organic load removal (up to 80.4% COD, 97% BOD₅ and 83.2% TOC).

Index Terms – Lactobacilli, Microbial Fuel Cells, Organic Fraction of Municipal Solid Waste, waste valorization.

I. INTRODUCTION

The OFMSW is mainly composed by food residues, leaf and garden waste and represents about the 70% of the overall Municipal Solid Wastes (MSW) produced in Western Countries. For its composition, OFMSW could represent a suitable feedstock even in MFCs, as recently proved by Venkata Mohan & Chandrasekhar Kuppam in 2011 [1]. Nevertheless, a further studies about materials to be used in the MFC set-up as well as the operational conditions are required in order to evaluate the effectiveness of MFCs technology in OFMSW valorization and treatment. The present research was aimed to assess the influence of oxygen availability as well as the electrodes distance on OFMSW MFCs performance. The composition of electroactive microflora was investigated and,

at last, the behavior of the most abundant strain at the anodes was studied in two-chamber MFCs.

II. MATERIALS AND METHODS

A. MFC assembly

Single chambered, air-cathode and membranless MFCs were realized as describe elsewhere [1]. Graphite plates with GDL layer, were used as electrodes.in order to investigate the influence of oxygen availability in the chamber as well as the electrodes distance, three MFC were set-up: MFC₁, low oxygen internal concentration (microaerophilia), with a 5 cm electrodes distance; MFC₂, anaerobic/anoxic internal environment, with electrodes placed at 5 cm from each other. The occurrence of an overhook in MFC₂ (Figure 1) gave evidence of a possible too high electrodes distance so, in MFC₃ (anaerobic/anoxic environment), electrodes were placed at 2.5 cm from each other. MFC₂ and MFC₃ were opportunely sealed by a silionic cement. All MFCs operated in batch conditions at 25°C for 6 weeks.

B. MFC fuel preparation and analysis

An OFMSW slurry (28% of waste, 72% saline solution) was firstly homogenated by a Stomacher 400 Circulator, then incubated in anaerobic conditions at 15±2 °C for 7 days to enrich the fuel with organic substrates, thus reducing the start-CODsol, TOC, BOD₅, and pH of the waste, slurry and digestate were measured according to Standard Methods (2012).

C. MFCs monitoring

The electrodes potential vs an Ag/AgCl reference electrode was measured. Polar curves were performed using external resistors in ranging from 1 MΩ to 100Ω. Voltage was measured by a

Keythley multimeter and current produced was calculated according to Ohm's law.

D. Biofilm analysis and *L. casei* electroactivity

Biofilm at the electrodes was sampled, suspended in PBS and plated on Tryptic Soy Agar at pH 4.2 and 5.2 (in both aerobic and anaerobic conditions), MRS Agar (*Lactobacillus* spp.), McConkey Agar n°3 (*Enterobacteriaceae*) and Pseudomonas Agar Base (*Pseudomonas* spp.). All media were by Oxoid®. Microbial strains were identified via rDNA16S amplification by PCR and sequencing similarity search by BLAST algorithm against the GenBank database. A *Lactobacillus casei* suspension (0.1 DO at 600 nm) in a Minimal Salt Medium with 0.2% glucose was inoculated in two-chamber MFCs at a starting concentration of 10⁵ and 10⁶ CFU/ml. Potassium hexacyanoferrate (III) 0.01M was the electronic acceptor in the cathodic compartment.

III. RESULTS

A. MFCs performances

The organic load removal achieved 80.4% in terms of COD reduction while BOD₅ and TOC reduction were up to 97% and 83.2% respectively. MFCs achieved the maximum PD value after 3 weeks of operation with 13.1 mWm⁻²kg⁻¹ (MFC₁), 3.6 mWm⁻²kg⁻¹ (MFC₂), 1.75 mWm⁻²kg⁻¹ (MFC₃) (Figures 1 and 2). As to CD, MFCs produced 152 mA m⁻²kg⁻¹, 171 mA m⁻²kg⁻¹, 16 mA m⁻²kg⁻¹ respectively. Even if with lower PD, MFC₃ showed the highest stability in terms of both PD and CD produced in time. Moreover, the overhook observed in MFC₂ polarization curve was not present in MFC₃.

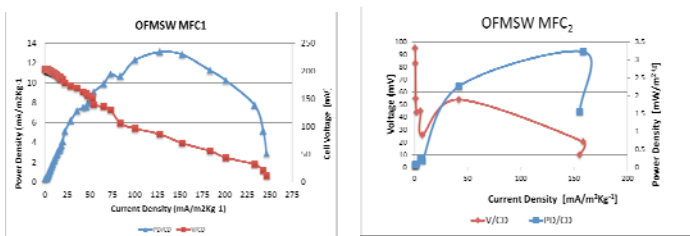


Fig. 1: Polarization curves MFC₁ and MFC₂

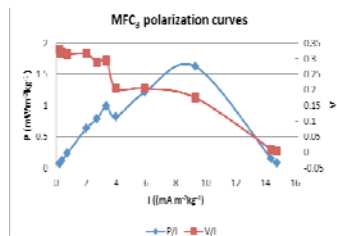


Fig. 2: Polarization curves MFC₃

A significant limitation to the MFCs performances was given by the cathode overpotential (+200±20mV vs Ag/AgCl reference electrode).

B. MFCs microbiology

Bacillus subtilis, *Rummeliibacillus pycnus*, *Bacillus amyloliquefaciens*, *Lactobacillus casei*, *Lactobacillus paracasei* and *Pseudomonas aeruginosa* were the strain isolated at the cathodes of MFCs while *Lactobacillus paracasei*, *Lactobacillus harbinensis*, *Lactobacillus casei* were prevalent at the anodes. No *Enterobacteriaceae* were isolated and yeasts were also present in the slurry as well as at the cathode, but their role in MFCs metabolism is still to be clarified.

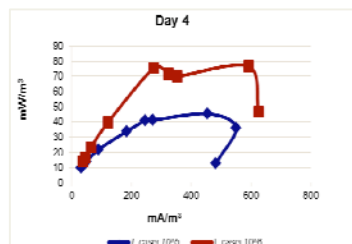


Fig. 3. *L. casei* 10⁶ and 10⁵ CFU/ml power curves.

A maximum PD of 77mW/m³ was observed in two-chamber MFCs inoculated with a 10⁶ CFU/ml *L. casei* suspension the 4th day of operation (figure 3). Nevertheless, a large overhook is present in the *L. casei* 10⁵ CFU/ml power curve probably related to the less maturity of *L. casei* biofilm.

IV. CONCLUSION

MFC provided a significant degradation rate of organic matter in terms of COD, BOD₅, and TOC in three different experimental conditions. Nevertheless, a high overpotential at the cathode limited the MFCs power production and a new graphite material is being tested at the Laboratory of Energy Systems of Parthenope University in order to overcome this issue. *Lactobacillus casei* proved to be electroactive and, according to our knowledge, this is reported for the first time. CV gave evidence of the involvement of an e⁻ donor at the anode, probably a cytochrome. Further studies are needed in order to verify this hypothesis MFCs seems to be a promising technology for the valorization of the OFMSW.

V. REFERENCES.

- [1] Nastro, R.A., S. Dumontet, S. Ulgiati, G. Falcucci, M. Vadursi, E. Jannelli, M. Minutillo, R. Cozzolino, M. Trifuoggi, G. Erme and E. De Santis. Microbial Fuel Cells Fed by Solid Organic Waste: A Preliminary Experimental Study. European Fuel Cell - Piero Lunghi Conference & Exhibition - Rome, December 11-13, 2013.
- [2] Rodrigo M.A., Cañizares P., García H., Linares J.J. and Lobato J. Study of the acclimation stage and of the effect of the biodegradability on the performance of a microbial fuel cell. *Bioresource Technology*, 2009; 100:4704-10.



POSSIBLE APPLICATIONS OF FRESHWATER SEDIMENT MICROBIAL FUEL CELLS

M. Mitov*, I. Bardarov* and Y. Hubenova**

*Innovative Center for Eco Energy Technologies,
South-West University "Neofit Rilski", 66 Ivan Mihajlov str.,
Blagoevgrad, Bulgaria

**Department of Biochemistry and Microbiology, Plovdiv
University "Paisii Hilendarski", 24 Tsar Asen str., Plovdiv, Bulgaria

Abstract – Sediment microbial fuel cells (SMFCs) gain an increasing attention as autonomous power sources for devices, operating in remote areas. This study provides data, demonstrating the ability for storing the electric energy, generated by freshwater SMFCs, and supplying low-power devices by using power management system. Modifying the explored SMFCs, possibilities for simultaneous electricity generation and denitrification were also examined.

Index Terms - sediment microbial fuel cells, electricity generation, denitrification.

I. INTRODUCTION

Sediment microbial fuel cells (SMFCs) are adaptation of the reactor-type MFCs, where the anode is embedded into aquatic sediment placed at the bottom of the reactor and the cathode is immersed in the aerobic water column above the phase boundary with the sediment. The SMFCs are considered as perspective autonomous power sources for environmental sensors located at remote areas, where frequent maintenance is infeasible [1]. However, they have some limitations, such as nonlinear scaling-up, low and variable power generation [2] and a theoretical maximum voltage of about 1.2 V, which is insufficient to power a conventional electrical device. This enforces the use of a power management system (PMS), which enables storage of the energy generated by the SMFC in ultracapacitors, boosts the voltage and supplies power to the desired electrical device in short pulses.

In this paper, the performance of freshwater SMFCs at different operation modes was examined. In addition, possibilities for coupling the biotic anode with denitrification in the cathodic chamber were also explored.

II. EXPERIMENTAL

Sediment and water samples were collected from river

Struma near the town of Blagoevgrad, Bulgaria. Twelve identical SMFCs were constructed and operated at different modes for over two years without any maintenance except a periodical addition of water to compensate the evaporation losses [3]. Different approaches were applied to determine the optimal mode for operation of the examined SMFCs as autonomous power sources. Individual or several connected in series or in parallel SMFCs were switched to 1F ultracapacitor (C 1F) and the time for charging the capacitor to 0.5 V was determined and compared. Power management systems based on LTC3105 and LTC3108 step-up DC/DC converters (Linear technology) and TPS61200 synchronous boost converter (Texas Instruments) were developed and used to extract the electrical energy from SMFCs and boost the voltage to applicable values.

The possibility for simultaneous electricity generation and denitrification was investigated by introducing a sealed cathodic chamber in the upper part of SMFC, separated by microporous membrane (Celgard) from the water column. Graphite disk or granulated activated carbon (AC) was used as a cathode in these experiments. Deaerated KNO_3 (200 mg/L NO_3^-) solution was applied as a catholyte and soluble electron acceptor. Polarization measurements at a constant load 100 Ω were performed. The nitrate removal was monitored by spectrophotometric analysis.

III. RESULTS AND DISCUSSION

The statistical evaluation of data collected during the first 18 months of SMFCs operation showed that the performance of all tested cells becomes homoscedastic after reaching a steady-state [3]. The estimated values of standard and expanded uncertainties of the electrical outputs (open circuit voltage, current and power density) indicated a high repeatability and reproducibility of the SMFCs' performance, revealing the



potentials for their practical application as autonomous power sources.

In the scope of this study, the effect of connecting multiple SMFCs in series and in parallel on the power generation was examined. When two or more SMFCs were connected in series, in most cases the voltage of one of the fuel cells became negative immediately after switching the stack to the ultracapacitor and slowly dropped over time along with the decrease of current in the circuit (Fig. 1a).

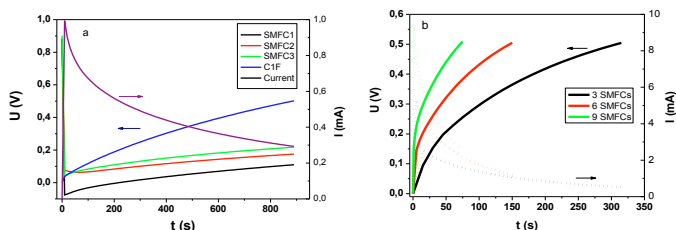


Fig. 1. Charging of 1F ultracapacitor up to 0.5 V by: a) three SMFCs, connected in series; b) 3, 6 or 9 SMFCs, connected in parallel.

The observed voltage reversal increased the time for capacitor charging, which exceeded 2.5 times that obtained when the same SMFCs were connected in parallel. Moreover, a proportional decrease of the time for charging the ultracapacitor with the increasing number of SMFCs connected in parallel has been observed (Fig. 1b), which demonstrates the ability for scaling-up the system by parallel connection of multiple cells.

The voltage reversal can be controlled by a PMS, which extracts electrical energy individually from multiple SMFCs [4]. Among the explored voltage boosters, the LTC3105 was found to be the most appropriate for our set-up. Connected to all studied SMFCs, it was able to simultaneously power a phototransistor, temperature sensor and a small LED (Fig. 2).



Fig. 2. Experimental set-up of two sensors and a LED powered by LTC3105-PMS connected to twelve SMFCs.

The replacement of the open to the air cathode with that immersed in deaerated nitrate solution resulted in a sustainable current generation (Fig. 3a). As could be expected, higher current outputs were obtained with AC cathodes, possessing much more developed surface areas.

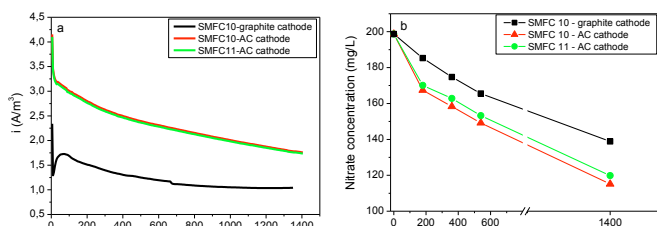


Fig. 3. a) Current generation and b) nitrate removal by SMFCs with graphite or AC cathodes immersed in deaerated KNO_3 electrolyte.

At the same time, a depletion of the nitrate content in the catholyte was registered (Fig. 3b), indicating its participation in the current generation process. Despite the nitrate removal achieved by using AC cathodes ($40.9 \pm 2.3\%$) is almost twice higher than that obtained with graphite cathodes ($23.2 \pm 1.8\%$), the estimated coulombic efficiency with both cathode types is comparable – $30.7 \pm 1.7\%$ with AC and $27.7 \pm 1.2\%$ with graphite cathodes.

IV. CONCLUSION

Freshwater SMFCs are promising autonomous power sources for low-power electronic devices and sensors, operating in remote areas. With some modification, they could be also exploited for monitoring of nitrate contamination or denitrification of polluted waters.

ACKNOWLEDGMENT

This study was supported by the National Science Fund of Bulgaria through Contracts E02/14/2014 and E02/15/2014.

REFERENCES

- [1] Ewing, T., Phuc, T.H., Babauta, J.T., Scale-up of sediment microbial fuel cells, *Journal of Power Sources*, Volume 272, 2014, pp. 311-319.
- [2] Donovan, C., Dewan, A., Heo, D., Sediment microbial fuel cell powering a submersible ultrasonic receiver: New approach to remote monitoring, *Journal of Power Sources*, Volume 233, 2013, pp. 79-85.
- [3] Mitov, M., Bardarov, I., Mandjukov, P., Hubenova, Y., Chemometrical assessment of the electrical parameters obtained by long-term operating freshwater sediment microbial fuel cells, *Bioelectrochemistry*, Volume 106A, 2015, pp. 105-114.
- [4] Tang, N., Hong, W., Ewing, T., Beyenal, H., Kim, J.-H., Heo, D., A self-sustainable power management system for reliable power scaling up of sediment microbial fuel cells, *IEEE Transactions on Power Electronics*, Volume 30, 2015, pp. 4626-4632.



CARBOHYDRATE BIOELECTROSYNTHESIS AND PHYTATE BIOREMEDIATION BY BIOFUEL CELLS

Yolina Hubenova*, Danail Georgiev*, Mario Mitov**

* Department of Biochemistry and Microbiology, University of
Plovdiv, 24 Tzar Asen Str., 4000 Plovdiv, Bulgaria

** Department of Chemistry, South-West University "Neofit
Rilski", 66 Ivan Mihajlov Str., 2700 Blagoevgrad, Bulgaria

Abstract – Recently, we found that the yeast strain *Candida melibiosica* 2491 enhances its phytase activity when cultivated under biofuel cell polarization in a nutrient-poor medium. In this study, we established that when grown in acetate buffer without any carbohydrates, this strain switches on anabolic pathways for carbohydrate synthesis from the acetate in the medium. Both findings could be useful for development of biofuel cell technology for simultaneous current generation, purification of eutrophicated with phytates waters and carbohydrate synthesis.

Index Terms - microbial fuel cells, electricity generation, redox activity, carbohydrate synthesis.

I. INTRODUCTION

Microbial fuel cells (MFCs) are bioelectrochemical devices which utilize whole living cell as biocatalysts. The technology of MFCs rapidly developed during the last decade [1]. It is supposed that it will be applicable for simultaneous electric current generation and purification of wastewaters.

Recently we reported that *Candida melibiosica* 2491 yeast strain expressed enhanced phytase activity, when grown under biofuel cell polarization in a nutrient-poor medium, containing only 3 % fructose as a carbohydrate source [2]. The phytase is an enzyme, which catalyzes the hydrolysis of myo-inositol hexakiphosphate - the main phosphorus storage form in molasses, cereal grains, oilseeds, legumes, etc. The obtained phytase activity during the cultivation of yeast under polarization reached up to 25 U per g dry biomass, exceeding with 20±3 % those of the control. At the same time, stable electrical outputs were achieved during biofuel cell operation at continuous polarization under constant load.

In the present study, we investigated biofuel cells, using as a biocatalyst *Candida melibiosica* 2491, cultivated in acidic

acetate buffer, containing fructose in different concentration as a carbohydrate source.

II. EXPERIMENTAL

Double-chamber biofuel cells (100 ml volume of each compartment) with a salt bridge (1 g agar in 10 ml 2 M KNO₃) were used. The anodic compartments were inoculated with *C. melibiosica* 2491 yeast cells, suspended in 50 ml 0.2 M sodium acetate buffer, pH 4.5, containing resp. 3 %, 0.3 %, 0.03 % fructose as well as without carbohydrate. 0.1 M K₃[Fe(CN)₆] in PBS, pH 7, served as a catholyte. Carbon felt (projected surface area 4.5 cm²; SPC-7011, 30 g/m², Weibgerber GmbH & Co. KG) was used as both cathodes and anodes. The cultivation was carried out under permanent polarization by load resistor (1 kΩ) at 23°C without aeration. The carbohydrate content was determined by means of DNS method. The current density, *j*, was calculated in respect to the geometric electrode area by using Ohm's law. The electrochemical activity was determined by CV. The yeast suspension was divided to pellet and yeast-free fraction by centrifugation of the anolyte at 5000xg for 10 minutes.

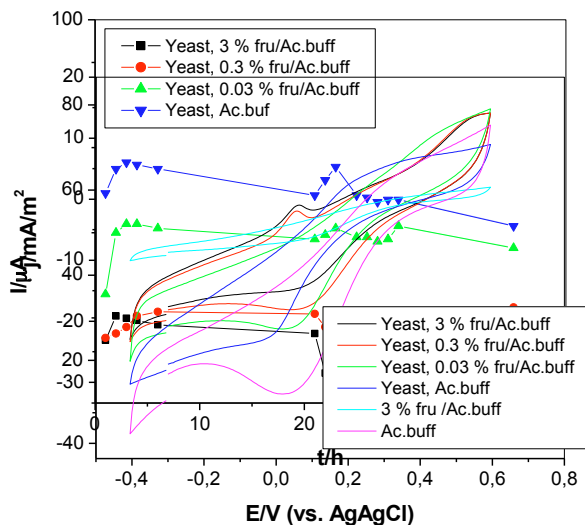
III. RESULTS AND DISCUSSION

It was observed that the current density increased with lowering the fructose content in the medium (Fig. 1). The highest value was registered for the sample without any addition of fructose. Columbic efficiency of 36 % was achieved, when 0.03 % fructose was initially used as carbohydrate source. The analyzed electrochemical activity of the anolyte (Fig. 2) showed that the cellular-free fractions of the different experimental set ups exhibited different redox activities. Oxidation peaks at a potential ca. 0.03 V in the cases



of 3 % and 0.3 % fructose-samples were observed. These peaks disappeared at a lower fructose content. We considered that the production and secretion of endogenous mediator (EM), artificially provoked by the polarization conditions of the fuel cells, depends on the carbon source and pH of the medium. The role of EM was considered as a way for enhancement of the glycolysis by insurance of NAD^+ [1, 3]. At the same time, the cathodic peak describing the redox activity of the acetate buffer showed lower currents with the increased fructose quantity, which was connected with the acetate assimilation (Fig. 2).

Fig.1. Current densities obtained over time in a batch regime of



yeast cultivation in biofuel cell. A constant load of 1 k Ω was constantly switched on in the system.

Fig. 2. Cyclic voltammograms of cellular-free fractions, obtained from the yeast suspensions by centrifugation at 5000xg for 10 min at the 24th hour.

For establishment of how the polarization influenced the metabolic processes, the fructose content was measured at the end of experimental window. We recognized, that in conditions of carbohydrate` lack, an anabolic pathway began to recover the carbohydrate content by synthesis from acetate source in the medium. Comparing the carbohydrate quantity in the medium after 24th of biofuel cell operation with the height of the reduction peaks on the voltammograms, it was calculated that about 0.3-0.4 mg/ml fructose per gram absolutely dry yeast biomass are obligatory for the yeast development and conduction of intracellular processes. The yeast are able to produce higher carbohydrate quantity (ca. 0.8 mg/ml) and even to secrete a part of it as a reserve source (0.39 mg/ml). Interpreting these data and having in mind the lack of oxidation peaks on CVs of samples with a low carbohydrate level, it was supposed that the intramolecular circulation of redox metabolites recovers the necessities the synthesis of extracellular transfer electron shuttles. Otherwise, the need of

more intensive degradation of carbohydrates within the cells requires more quantity oxidized NAD^+ . NAD^+ is delivered by switching on secondary pathways, which products transfer the captured electrons/protons from NADH through the cellular membrane to the anode [3].

IV. CONCLUSION

The present study demonstrates the principle possibility for application of the technology for purification of acidified, eutrophicated with phytates waters and suggests its future development in this direction. Furthermore, it was proved for the first time that the yeast strain applied is able to synthesize reducing sugars from acetic acid under polarization.

ACKNOWLEDGMENT

This study was supported by the National Science Fund of Bulgaria through Contracts E02/14/2014 and E02/15/2014.

REFERENCES

- [1] Hubenova, Y., Mitov, M. Extracellular electron transfer in yeast-based biofuel cells: a review. *Bioelectrochemistry*, 2015, DOI: 10.1016/j.bioelechem.2015.04.001.
- [2] Hubenova, Y., Georgiev, D., Mitov, M. Enhanced phytate dephosphorylation by using *Candida melibiosica* yeast-based biofuel cell. *Biotechnology Letters*, Volume 36 (10), 2014, pp. 1993-1997, DOI: 10.1007/s10529-014-1571-9.
- [3] Hubenova, Y., Mitov, M. Mitochondrial origin of extracellular transferred electrons in yeast-based biofuel cells. *Bioelectrochemistry*, 2014, DOI: 10.1016/j.bioelechem.2014.06.005.



ANN-SUPPORTED CONTROL STRATEGY FOR A SOLID OXIDE FUEL CELL WORKING ON DEMAND OF PUBLIC UTILITY BUILDING

L. Szablowski, J. Milewski, and K. Badyda
Institute of Heat Engineering, Warsaw University of Technology,
Poland

Abstract - The paper presents a control strategy concept of a Solid Oxide Fuel Cell working on demand of public utility building. The strategy has been achieved with the support of Artificial Neural Network. The network was used to predict the demand for electricity. The calculations were carried out on the example of building of the Institute of Heat Engineering Warsaw University of Technology. The control strategy is based on several factors and directs the operation of the unit in the context of changes occurring in the market, while taking into account the operating characteristics of the unit. The control strategy is defined by an objective function: for example, work at maximum profit, maximum service life, etc. The results of simulations of the Solid Oxide Fuel Cell at chosen loads are presented.

Index Terms - Solid Oxide Fuel Cell, SOFC, artificial neural network, distributed generation.

I. INTRODUCTION

The available data on the use of artificial neural networks to predict the demand for electricity date back to the early 90s. In [1] a model (based on artificial neural networks) is used to predict the load profile for the next 24 hours and for the very next hour was presented. The input data for the simulation were: the load profile of the two previous days and the forecasted minimum and maximum ambient temperature. The model was tested for the data of one year from the Greek interconnected power system. The resulting average absolute prediction error for this period was 2.66%. In turn, [2] presented a model which automatically adapts and is used to predict the daily and weekly demand for electricity. The error obtained in this way ranged from 2.5 to 5.1%. Similarly, the authors [3] used artificial neural networks for online load prediction. This model was tested in Italy on data from 15 February to 31 July 1993, yielding an average error of 1.93% (for maximum load) and 2.65% (for minimum load). [4] presented a fairly comprehensive assessment of the results

of the use of artificial neural networks by various centers for short-term electricity load and gas demand forecasting. However, the authors of [5] presented the benefits of a merger of Fuzzy Logic (FL) with an artificial neural network, compared to the Autoregressive Moving Average (ARMA) model for load forecasting. [6] compared the neuro-fuzzy system (a combination of artificial neural network (ANN) with a fuzzy neural network (EFuNN)) with Box-Jenkins autoregressive integrated moving average (ARIMA), a program to predict the load used by Victorian Power Exchange (VPX) and also compared with an artificial neural network only. All compared options were tested on the data describing the demand for electricity in the state of Victoria, Australia. These comparisons showed the neuro-fuzzy system was the best.

In this paper the artificial neural network was used to predict a demand to determine how load Solid Oxide Fuel Cell working on public utility building needs.

II. THEORY

A. Fuel cell

The fuel cell must run on the maximum lifetime, what we get as a result of continuous operation (without unnecessary shutdowns and start-ups). To get a decent profit (or minimize losses) in this case, the fuel cell can not be oversized. This means that for a large demand electrical energy must be purchased from the grid or produced by other sources. Technical minimum of cell operation was set at the level of 60%. However, if encountered a situation that the demand would be lower, excess of electricity produced by the SOFC fuel cell must be sold in order to avoid shutdowns and start-ups of the cell.



B. Artificial Neural Networks

An ANN is a black-box model which produces certain output data as a response to a specific combination of input data. The ANN can be trained to learn the internal relationships and predict system behavior without any physical equations. The ANN consists of neurons gathered into layers (Fig. 1).

Information is delivered to the neurons by dendrites and the activation function is realized (by the nucleus). Then, modified information is transferred forward by the axon and synapses to other neurons.

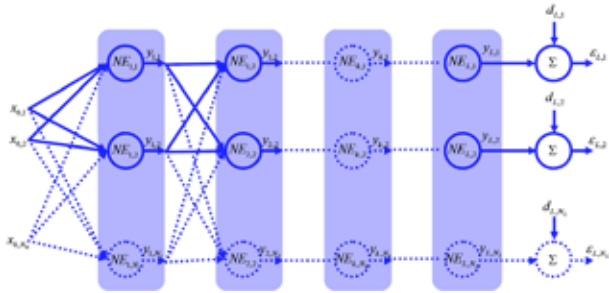


Fig. 1. Artificial Neural Network model

Each neuron in the first layer takes the input values, multiplies them by the corresponding weights and summarizes all these multiplications. Bias is added to the sum. The sum is recalculated by the neuron activation function which gives the neuron answer.

C. Costs

Fixed costs include license fees for electricity, which for the tariffs used in this analysis are about \$3.49/month gross (tariff G11 relating to power companies: “ENERGA-OBRÓT S.A.” and “Energia Operator S.A”). They also include a fixed charge of \$37.71/month gross for gas (transmission & distribution charged by the company “PGNiG”). Variable costs include primarily the purchase of electricity (\$0.11/kWh for electricity and \$0.08/kWh for transmission) and the rates of the gas group of “PGNiG” in tariff w-5 for fuel only (\$0.415/Nm³) and tariff E-1A for transmission (\$0.011/Nm³).

III. OPTIMAL CONTROL STRATEGY OF A SOLID OXIDE FUEL CELL

The neural network created as described above was trained using load data from 08.10.2011 to 15.10.2011 for part of the Institute of Heat Engineering and Central Canteens of Warsaw University of Technology.

After putting on the input of the network information about the load of 16.10.2011 together with information what day of the week it concerns was received a load of 17.10.2011, which was put on the network input together with the information about the day of the week.

This operation was repeated many times to obtain load for the entire week from 17.10.2011 to 23.10.2011.

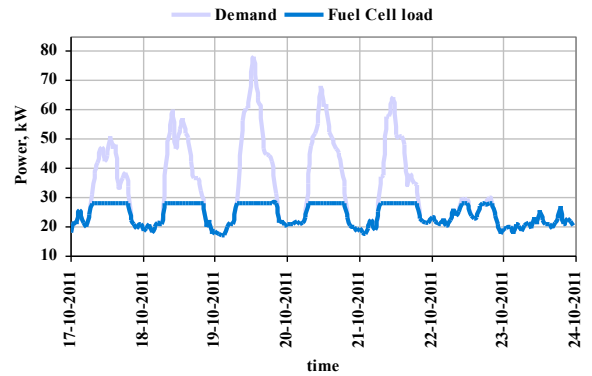


Fig. 2. Demand vs optimal load of SOFC

In the next step, a simulation of SOFC operation on the load generated by the neural network was performed (Fig. 2).

IV. CONCLUSIONS

The neural network used to predict the load was proposed and the control strategy for the SOFC working on demand of public utility building was presented. From the investigations performed, it was determined that the most appropriate objective function of the strategy is to operate the SOFC for maximum life (defined as maintaining high cell temperature).

On average, the SOFC is never turned off, even in cases of low electricity demand, or low electricity prices in the network.

Profits from operation of the SOFC depend strictly on the load profile.

ACKNOWLEDGMENT

The project was funded by the National Science Centre allocated on the basis of decision number PRO-2013/09/N/ST8/02055.

REFERENCES

- [1] Kiartzis S., Bakirtzis A., Petridis V., Short-term load forecasting using neural networks, *Electric Power Systems Research* 33, 1995, pp. 1-6.
- [2] Paarmann L. D., Najjar M. D., Adaptive online load forecasting via time series modeling, *Electric Power Systems Research* 32, 1995, pp. 219-225.
- [3] Sforna M., Proverbio F., A neural network operator oriented short-term and online load forecasting environment, *Electric Power Systems Research* 33, 1995, pp. 139-149.
- [4] Hobbs B. F., Helman U., Jitrapaikularn S., Konda S., Maratukulam D., Artificial neural networks for short-term energy forecasting: Accuracy and economic value, *Neurocomputing* 23, 1998, pp. 71-84.
- [5] Tamimi M., Egbert R., Short term electric load forecasting via fuzzy neural collaboration, *Electric Power Systems Research* 56, 2000, pp. 243-248.
- [6] Abraham A., Nath B., A neuro-fuzzy approach for modelling electricity demand in victoria, *Applied Soft Computing* 1, 2001, pp. 127-138.



DEVELOPMENT OF ULTRALIGHT AND THIN BIPOLAR PLATES USING EPOXY-CARBON FIBER PREPREGS AND GRAPHITE COMPOSITES

K. Kang, S. Park, A. Jo, K. Lee, S. Ferekh and H. Ju

Department of Mechanical Engineering, Inha University, 100 Inha-ro, Nam-Gu Incheon 402-751, (Republic of Korea)

Abstract - Using the excellent mechanical strength and in-plane electrical conductivity of epoxy-carbon fiber prepregs, we design and fabricate ultrathin composite bipolar plates (BPs) for fuel cells. For the successful fabrication of prepreg-based BPs, it is essential to increase the through-plane electrical conductivity of pristine prepregs and reduce the electrical contact resistance due to excessive surface resin extruded during compression molding. In addition, the moldability of prepreg layers should be greatly improved for the proper construction of a serpentine flow field on the prepreg surface. To resolve all these technical issues, we suggest a multilayer BP structure in which prepreg layers, pure graphite layers, and graphite-resin composite layers are combined and compression-molded. The multilayered prepreg BP is approximately 0.6 mm thick and exhibits good electrical behavior (in-plane conductivity of 172 S/cm and through-plane conductivity of 38 S/cm), with a high-quality serpentine flow channel configuration. The test results clearly demonstrate that the low through-plane electrical conductivity and poor moldability of pristine prepregs are greatly improved by our proposed BP design and fabrication.

Index Terms – fuel cell, bipolar plate, prepreg, graphite, electrical conductivity

I. INTRODUCTION

A bipolar plate (BP) is one of the major components of fuel cell systems, which performs several critical functions related to the operation of fuel cells. In a fuel cell stack, BPs provide electrical connection and mechanical support between the individual membrane electrode assemblies (MEAs). Furthermore, flow channels integrated in the BPs play a key role in the effective delivery of reactants and removal of products for stable fuel cell stack operation. Therefore, BP materials should exhibit excellent electrical conductivity and mechanical strength and allow for the construction of flow fields on their surface during the manufacturing process.

As reported in the previous papers [1, 2], despite the excellent in-plane electrical conductivity of prepreg-based

composite BPs, there are three major concerns: (1) low electrical conductivity in the through-plane direction, (2) high interfacial contact resistance, and (3) difficulty in constructing serpentine flow channels on the external BP surface. Concerns (1) and (2) are mainly due to the non-electric conducting polymer resin between preferentially oriented carbon fibers within prepregs, whereas concern (3) can be attributed to the poor moldability of prepregs because of their intrinsic structure and high flexural strength. To overcome the aforementioned three issues, we have fabricated an innovative BP in which three different layers, namely, prepreg, graphite, and graphite-composite layers, are subsequently stacked and compression-molded. The new BPs exhibit sufficient through-plane electric conductivity, a resin-free external surface, and good shape/configuration of serpentine flow channels. Sections 2 and 3 are devoted to an explanation of the BP fabrication procedures and a detailed discussion of the test results, respectively.

II. EXPERIMENTS

Fig. 1 shows a schematic of the detailed structure and fabrication procedures of the prepreg-graphite BPs with outer composite layers, herein designated composite coated graphite-prepreg hybrid BPs. The conceptual design of the new BP is a novel laminated structure in which several inner layers with graphite-coated prepregs (graphite-prepreg hybrid layers) are sandwiched between two outer layers (top and bottom) of graphite-resin composites. The main reason for using the outer layers is to facilitate the construction of serpentine flow channels by compression molding. Conversely, the major role of the graphite layers to be coated on the prepregs is to absorb the resin extruded from them during compression molding. While the excessive resin from the prepregs helps improve compaction of the graphite particles in the graphite layers,

decreased resin content in the prepregs leads to a reduction in the electrical resistance of the prepregs in the through-plane direction. The detailed fabrication procedures for the composite coated graphite-prepreg hybrid BPs are as follows:

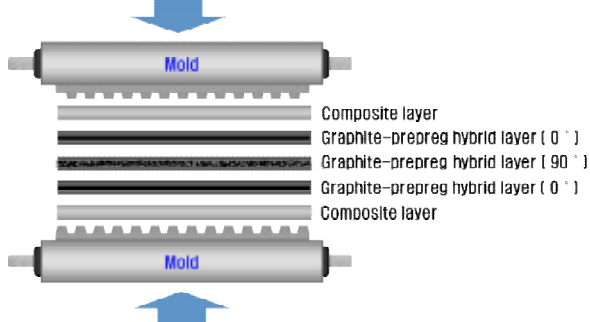


Fig. 1. Schematic of the compression molding process

To measure the electrical conductivities of the composite BPs, several sample tests were conducted in this study. The in-plane electrical conductivities of the BPs were measured using an FPP-5000 four-point probe instrument. The through-plane conductivities were measured using the contact resistance method.

III. RESULTS AND DISCUSSION

The in-plane conductivities of the graphite-prepreg hybrid layers with four different graphite particle sizes are shown in Fig. 2. Because more uniform filler distribution and better compactness were achieved with a smaller graphite particle size, the electrical conductivity decreased with the graphite particle size. While conductivity in the case of using 6-, 10-, and 20- μm particles greatly surpasses the DOE target of 100 S/cm, the lowest electrical conductivity of 63 S/cm was obtained with 40- μm graphite particles, which was because of the incomplete compaction and non-uniform distribution of the graphite particles in the layer. It should be noted that the aforementioned electrical behavior of the pure graphite layer differs from that of normal graphite-resin composite plates. In general, the electrical conductivity of graphite-resin composite plates increases with the graphite particle size when the resin content is fixed [3, 4]. This is because the smaller particles would be fully wetted by the resin more easily, decreasing the number of conductive paths and thereby reducing the bulk electrical conductivity of the composite. In contrast, in the case of the pure graphite layer with no resin, a larger number of conductive particles can be packed per unit volume as their size decreases, which increases the volumetric fraction of the graphite filler, enhancing the compactness of the layer and thus the electrical conductivity.

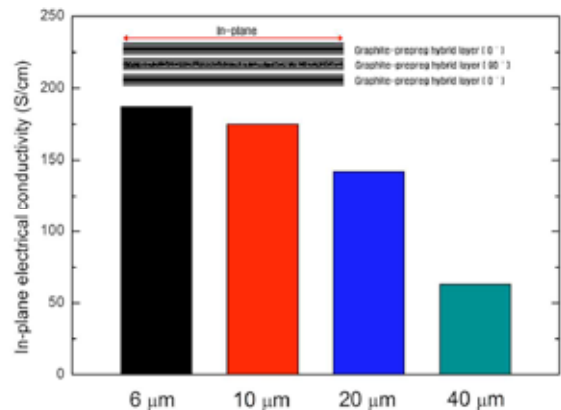


Fig. 2. In-plane electrical conductivity of the graphite-prepreg hybrid layers for graphite particle sizes of 6 μm , 10 μm , 20 μm , and 40 μm

IV. CONCLUSION

Using epoxy-carbon fiber prepregs with outstanding mechanical strength and excellent in-plane electrical conductivity, we designed and fabricated ultralight and thin composite BPs. Three technical barriers had to be overcome for the successful design of the prepreg-based BP: low through-plane electrical conductivity of pristine prepregs, high interfacial contact resistance due to excessive resin between the conductive prepreg layers, and insufficient moldability of the prepregs for the proper construction of serpentine flow channels on the BPs.

ACKNOWLEDGMENT

This work was supported by the New & Renewable Energy R&D program (grant no.20133010031751) of the Ministry of Knowledge Economy of the Government of the Republic of Korea. The authors thank Jin-soo Kim at ILDO F&C Institute of Technology for helpful discussions.

REFERENCES

- [1] I.U. Hwang, H.N. Yu, S. S. Kim, D.G. Lee, J.D. Suh, S.H. Lee, B.K. Ahn, S.H. Kim and T.W. Lim, Bipolar plate made of carbon fiber epoxy composite for polymer electrolyte membrane fuel cells, *J. Power Sources*, Volume 184, 2008, Pages 90-94.
- [2] J.W. Kim, N.H. Kim, T. Kuilla, T.J. Kim, K.Y. Rhee and J.H. Lee, Synergy effects of hybrid carbon system on properties of composite bipolar plates for fuel cells, *J. Power Sources*, Volume 195, 2010, Pages 5474-5480.
- [3] H.C. Kuan, C.C.M. Ma, K.H. Chen and S.M. Chen, Preparation, electrical, mechanical and thermal properties of composite bipolar plate for a fuel cell, *J. Power Sources*, Volume 134, 2004, Pages 7-17.
- [4] H. Chen, H. Liu, L. Yang, J. Li and L. Yang, Study on the preparation and properties of novolac epoxy/graphite composite bipolar plate for PEMFC, *Int. J. Hydrogen Energy*, Volume 35, 2010, Pages 3105-3109.



FCPOWERED RBS: A DEMONSTRATION PROJECT TO SUPPLY TELECOM STATIONS THROUGH FC TECHNOLOGY. INSTALLATION OF REMOTE SITES AND DATA ANALYSIS

S. Cordiner*, V. Mulone*, A Giordani ^, G. Tomarchio^,
T. Malkow**, G. Tsotridis**, A. Pilenga **, M.L.Karlsen*^,
J. Jensen^^

* University of Rome Tor Vergata, via del Politecnico 1, 00133 Rome (Italy)

^ ERICSSON Italy, via Anagnina 203 00118 Rome (Italy)

** EUROPEAN COMMISSION, Directorate General Joint Research Centre, Institute
for Energy and Transport, PO Box 2, 1755 ZG Petten (The Netherlands)

*^ DANTHERM POWER A/S, Majsmarken 1, DK-9500 Hobro (Denmark)

^^ GREENHYDROGEN.DK, Platinvej 29B, DK-6000 Kolding, (Denmark)

Abstract - The use of PEM FC based power generation unit has already been demonstrated with regard to the operation of off-grid RBS (Radio Base Stations) sites. In fact, in a previous paper the main design issues along with details on testing activities primarily aimed at benchmarking were illustrated. The main results showed that design has a major impact on the dependence of the RBS on external fuel supply, and thus on the overall conversion efficiency of the system.

In this paper an initial report of on field analysis is given.

Index Terms - PEM fuel cells; Alkaline electrolyzers; Radio base stations; Renewable sources; Off-grid Telecom Stations.

I. INTRODUCTION

The use of FC and H₂ electrolyzers joint to PV modules and a battery storage system is an enabling technology for the diffusion of Radio Base Stations (RBS) fueled by renewable sources [1]. The FCpoweredRBS EU project has been funded to demonstrate this potential, and consists of the experimental implementation of 13 operating sites in Italy, which have been tested so far since the beginning of 2015.

II. SYSTEM DESCRIPTION

The system layout is given in Fig. 1. It includes a PV module (5 or 10 kW_p), feeding a battery charger that is connected to a common 48V DC bus supplying power to the RBS load. In case of excess PV power, the energy can be stored in a battery pack or to power an electrolyzer (that in turn fills up 30 bar H₂ bottles). Both batteries and electrolyzer are hooked-up in parallel to the DC bus. In case, instead, of PV power lack, batteries or Fuel Cells (fueled by either 30 bar or 200 bar H₂ bottles) can supply power to the RBS load, thus ensuring its

continuous operation. A rule-based control strategy has been defined [1] to maximize the exploitation of renewable sources and FC durability.

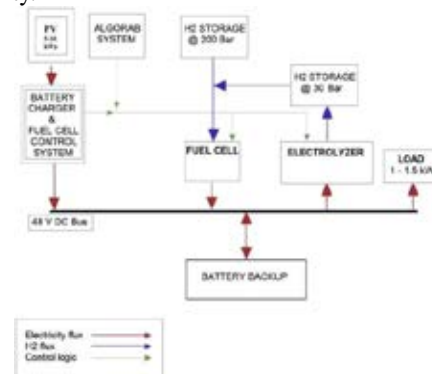


Fig. 1. FC-powered RBS system layout [1]

III. INSTALLATIONS DESCRIPTION

The systems have been installed in several locations in Italy (mainly in Lazio and Puglia), powering telecom stations owned by italian providers. The systems are characterized by a 5 kW_p power output PV system, with 640Ah@48V battery storage. The chosen FC technologies are Dantherm 1.7 kW H₂ fueled PEM Fuel Cell System, and the 1.7 kW Idatech methanol fueled PEM Fuel Cell system. Some installations have also been characterized by the installation of a H₂ GreenHydrogen.dk electrolyzer, feeding 30 bar H₂ bottles. The solutions have been deployed integrating the PV canopy, additional shelters for H₂ or Methanol storage, and external cabinets for fuel cells,

batteries and, in some cases, the electrolyzer cabinet (see Figs 2 and 3).



Fig. 2. FC-powered RBS site installation: site#1



Fig. 3. FC-powered RBS site installation: site#2

The sites have been fully equipped with sensors, and is capable of remote data gathering, with an ALGORAB acquisition data remote system (see screenshot in Fig.4). The main observed parameters during the normal FC-powered RBS operation are: current and voltage at all the different nodes of interest (PV output, battery connection, FC output, load, electrolyzer); H₂ bottle pressure and temperature.



Fig. 4. Screenshot of ALGORAB remote data acquisition system

IV. DISCUSSION OF RESULTS

Tests are currently being finalized; however since January 2015, some systems among the 13 have been analyzed.

The power output of PV modules, batteries and FC is given

as a function of time during three days in Fig.5, in one of the Dantherm sites as an example. It is evident how the FC is turned on during the first night, after the first, cloudy day, while it is switched off after the second (sunny) day during the second night.

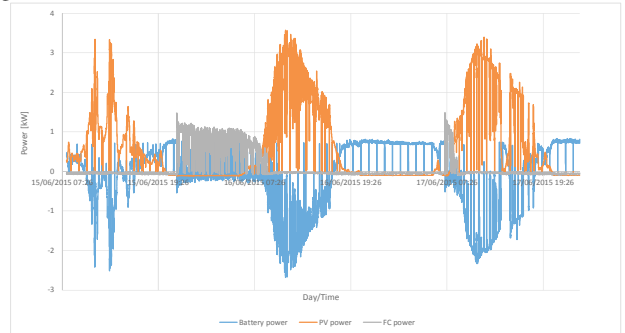


Fig. 5. Power in one of the Dantherm sites in the period 15/06/2015 to 17/06/2015

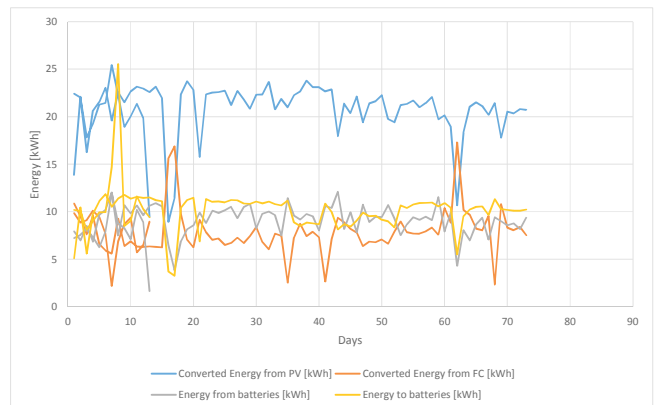


Fig. 6. Energy fluxes per day as functions of days in one of the Dantherm sites in the period May-July 2015.

Integral results, for another Dantherm site are plotted in Fig. 6, in the period between May and July 2015. It can be observed how power is consistently delivered by the system to the RBS load. This site is characterized by a fairly high required energy (in the range of 40 kWh/day), and thus the Fuel Cell is required to backup the PV power for a considerable fraction of the day (in the order of half of the energy output of the PV system). It is also evident how batteries may almost double the energy converted by the PV, as both the incoming and outgoing battery energies are continuously in the range of 10 kWh per day, similarly to the FC output.

ACKNOWLEDGMENT

This project is co-financed by funds from the european commission under FCH-JU, grant agreement number 278921.

REFERENCES

- [1] Bruni et al., Fuel Cell Based Power Systems to Supply Power to Telecom Stations, Int. J. Hydrogen Energy, 39(36):21767-21777, 2014.



ELECTROCHEMICAL AND MEMBRANE ELECTRODE ASSEMBLY (MEA) STUDIES OF PERFORMANCE STABILITY OF SUPPORTED PLATINUM CATALYST

P.Mohanta^{1*}, J.Haußmann^{2*}, L. Jörissen^{3*}

* Zentrum für Sonnenenergie- und Wasserstoff-Forschung Baden-Württemberg (ZSW), Helmholtzstraße 8, 89081 Ulm (Germany)

Abstract - One of the major causes of the Polymer Electrolyte Membrane Fuel Cells (PEMFC) performance loss is due to the degradation of the catalyst support under operation. The degradation mainly depends on the particle size of Pt, the type of catalyst support and the operating condition of the fuel cell [1]. Carbon black is widely used as Pt catalyst support for PEMFC. In this contribution, we developed a robust synthesis method of Pt on stable and non-stable carbon support by modifying the polyol method [2]. Pt particle size of ≤ 5 nm can be repeatedly synthesized by this method. The uses of other non-carbon supports are still under investigation. The electrochemical and membrane electrode assembly (MEA) performance stability of the synthesized stable carbon supported Pt catalyst has been compared with the Tanaka commercial catalyst.

Index Terms - Degradation, MEA, ORR, Pt/C

I. INTRODUCTION

The target of this work is to study of corrosion resistant cathode support materials for PEMFC. To achieve the goal, the work is divided into the development of a robust synthesis method of Pt-nanoparticles (PtNP) on different support materials, the electrochemical measurement of catalyst activity and the stability and the MEA test of the catalysts. In this contribution the modified polyol method is chosen as a promising synthesis method [2]. As a reference, the carbon black (Vulcan XC 72) has been used as support material. The synthesis method has also been used successfully to deposit PtNP on a stabilized carbon substrate. The catalysts were characterized by X-ray diffraction (XRD), TEM, potential (start-stop) cycle, load cycles, Oxygen reduction reaction (ORR) activity and MEA test.

II. EXPERIMENTAL

A. Synthesis of Pt-nanoparticles

The synthesis procedure was almost the same as described by Z. Zhou et. al, [2] except the variation of dilution and the synthesis temperature. We used 110ml solvent/g catalyst. The

starting heat up temperature was 180°C with a ramping rate of 5°C/min. The mixture was kept at 120°C for 3h. A Pt-content of 20wt% (CB20) was used with Vulcan support, while 10wt% was achieved with stabilized carbon (SC10). In order to improve the activity and the stability, the catalysts were heat treated after Pt-deposition at 250°C in Ar/H₂ atmosphere (95% Ar and 5% H₂) for 1h.

B. X-ray diffraction and TEM

The noble metal particle sizes of the synthesized catalysts were estimated by XRD using the Scherrer equation. The obtained particle sizes of Pt were ≤ 5 nm. The XRD pattern of the SC10 and CB20 are shown in fig.1.

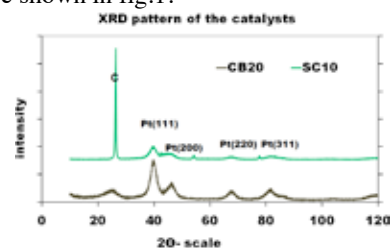


Fig. 1: XRD pattern of the catalysts

Fig. 2 is showing the comparative TEM image of the CB20 and the reference Tanaka 30wt% (TK30) catalysts.

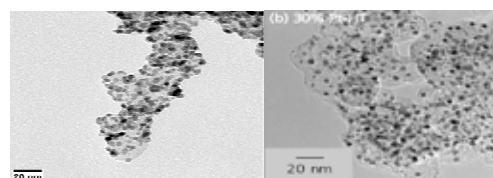


Fig.2: TEM image of CB20 (left) and TK30 (right) [3]

C. Potential cycle (Start-stop) durability test

The potential cycle tests to address support stability have been conducted in a 3 electrode cell using 0.5M H₂SO₄ solution at 25°C. The potential was cycled by a triangular wave between 1V and 1.5V at a scan rate of 500mV/s [4]. The working electrode was prepared by placing 62 μ l of catalyst ink on a

glassy carbon disk and then drying in open air. The ink composition was 5mg catalyst/ml solvent (0.05wt% of Nafion in 50% Acetone/water). The fig.3 shows that the initial electrochemical surface area (ECSA) of the TK30 is higher but it becomes lower than SC10 after 40000 cycles. The ECSA survival rate of the SC10 supported catalyst is the highest.

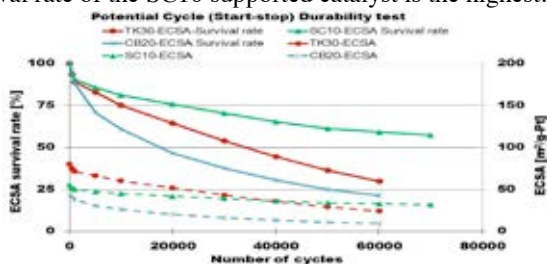


Fig.3: The degradation comparison of the supports

D. Load cycle test

The load cycle tests to address Pt-corrosion stability have been conducted in the same way as potential cycle test except the potential was cycled between 0.6V and 1.0V at a scan rate of 50mV/s [5]. The stability of the SC10 is almost the same as CB20 (as expected). Only about 20% ECSA of the catalyst SC10 is decreased after 50000 cycles. The ECSA of the TK30 catalyst is surprisingly increasing after 30000cycles.

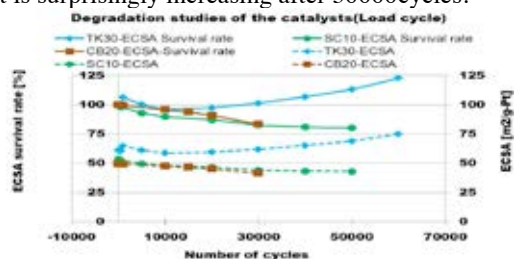


Fig.4: The degradation comparison of the catalyst

E. ORR activity

The ORR activities of the catalysts were performed by using a rotating disk electrode (RDE) in oxygen saturated 0.1M HClO₄ electrolyte. The catalyst powders were deposited on a gold RDE(4mm) from an ink prepared by suspending 2mg /ml solvent (0.02wt% Nafion in Isopropanol – Water =1:1). The Pt loading was 2μg. The activities of the catalysts were calculated from Koutecky-Levich Plot at four different rotational points. The mass activity of the SC10 is low but the specific activity is high when compared with the TK30 catalyst (see fig. 5). Almost the same activity of the SC10 has been found when compared with the Tanaka 10wt% (TK10) catalyst.

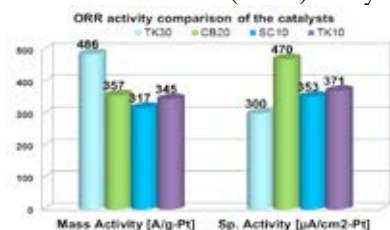


Fig. 5: ORR activity of the catalysts

F. MEA test

The MEAs of 25cm² surface areas (Pt-loading 0.3mg/cm²) have been prepared by using SC10 and TK30 catalysts. These MEAs have been tested using a Fuel Cell technologies 25cm² single cell at atmospheric pressure. The fig. 6 is showing the comparative polarization curve. The MEA using the TK30 catalyst shows the expected overall performance. The voltage of the MEA using SC10 catalyst runs slightly lower than the MEA containing TK30. The performance difference at low current density can be explained by the higher ECSA of TK30. Additional mass transport induced losses of SC10 can be explained by the thicker catalyst layer required to achieved the same noble metal loading.

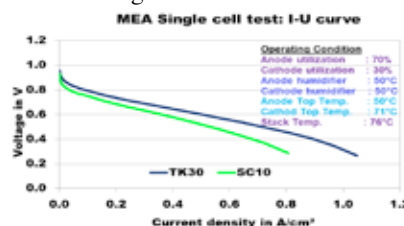


Fig.6: The performance comparison of the catalysts

III. CONCLUSION

The Pt-nanoparticles of size ≤5nm could be synthesized successfully on carbon black and stabilized carbon supports. As expected, Pt-catalysts deposited on the stabilized carbon support showed improved corrosion resistance under potential cycling compared to Pt-catalysts deposited on carbon black and as well as compared to a highly active commercial catalyst. The voltage degradation induced by Pt-corrosion of the catalysts deposited on carbon black and stabilized carbon is comparable. Surprisingly, the commercial catalyst after an initial performance decrease eventually showed increased performance under the same conditions. MEA tests showed promising results for the Pt-catalyst deposited on a stabilized carbon substrate. Further work is required to optimize the catalyst layer composition, morphology and thickness for Pt-catalysts deposited on stabilized carbon supports.

ACKNOWLEDGMENT

Funding of the project GECKO by the Federal Ministry of Education and Research (BMBF) is gratefully acknowledged.

REFERENCES

- [1] Z. Yang et. al., Systematic Study on the Impact of Pt Particle Size & Operating Conditions on PEMFC Cathode Catalyst Durability, J. Electrochem. Society, 2011 158 (11) 1439-1445
- [2] Z.Zhou et. al., Novel synthesis of highly active Pt/C cathode electrocatalyst for DMFC, chem. Commun. 2003, 394–395
- [3] K. Matsutani, et. al, Effect of Particle Size of on Stability Against Load Cycling, Platinum Metals Rev., 2010, 54, (4), 223–232
- [4] M.Brodth et. al., Fabrication, In-Situ Performance & Durability of Nanofiber FC Electrodes, J. Electrochem Soc, 2015,162 (1)84-91
- [5] T. Nagai,Y et.al, Influence of Experimental Conditions on the Catalyst Degradation in the Durability Test, J. Electrochem Society, 2014, 161 (6) , 789-794



EFFECT OF ZIRCONIA ADDITION TO NI-NI/AL ANODES ON MICROSTRUCTURE AND MECHANICAL PROPERTIES FOR MOLTEN CARBONATE FUEL CELL

G. Accardo*, D. Frattini*, A. Moreno**, S.P. Yoon***, J. Han*** and S.W. Nam***

* Department of Engineering and INSTM Research Unit, University of Naples "Parthenope", Centro Direzionale Isola C4, 80143, Naples, (Italy)

** Italian National Agency for New Technologies ENEA Casaccia Research Center, Via Anguillarese 301, 00123 Rome, (Italy)

*** Fuel Cell Research Center, Korea Institute of Science and Technology, Hwarang-ro 14-gil 5, Seongbuk-gu, Seoul (South Korea)

Abstract – Molten Carbonate fuel cell (MCFCs) are being applied in commercial power devices due to their high electrical efficiency and fuel flexibility. The anode material in MCFC should have high melting temperature, excellent oxidation resistance, good creep resistance and a good fracture toughness to be successfully used in such environments. In this work, nano zirconia particles were added to Ni-Al anode electrode and their effects on sintering and microstructure were investigated by comparing it with ZrO₂-free anode electrode. Results show that zirconia particles can effectively interact with cubic structure of Ni-Al alloys by strengthening the main slip planes thus reducing creep strain. Therefore, this study presents the possibility that nano zirconia can be added to anode for MCFC applications.

Index Terms – green sheet, molten carbonate fuel cell, Ni/Al alloys, zirconia nano powders

I. INTRODUCTION

High temperature alloys are essential to many industries that require a stable material to perform in harsh environments. They are capable of operating in oxidative environments and under high pressures in the presence of combustion gases, water vapor and high temperatures. Many of these alloys, as Ni/Al alloys, are suitable for specific applications like in Molten Carbonate Fuel Cell (MCFC) [1]. The MCFCs are directed at large-scale power generation because they can utilize a wide variety of fossil fuels at very high efficiency and minimal pollution. However, anode materials can be affected by several problems as the deformation caused by the creep and sintering. In fact, the operating conditions of MCFC, including high temperature and high pressure by cell stack, cause the creep and sintering of anodes [2]. Therefore, these effects make the thickness and porosity of the anodes decrease and the surface area and microstructure of electrode change. To improve the durability and the reliability of MCFC anode materials, additives or intermetallic phases as pure metals and oxide, including Cr, Mg, Cu, Zr, Ni₃Al, α -Al₂O₃ and LiAlO₂ can be added to Ni alloys during fabrication [3]. In this work, nano zirconia particles were added to Ni-Al anode electrode and their effects on sintering and microstructure were

investigated by comparing it with ZrO₂-free anode electrode. Anode green sheets with different zirconia content (1-10% wt.) have been fabricated by means of the conventional tape casting process. The effect of ZrO₂ addition on sintering and microstructure has been evaluated.

II. MATERIALS AND METHODS

Ni-Al-ZrO₂ green sheet was fabricated by a tape casting process. Ni powders (INCO 255, 5 μ m), Ni-Al alloy powders (Chang Sung Co, Al 5.0% wt., 5 μ m) and ZrO₂ nano powders (Alfa Caesar, 20nm) were used as raw materials. Zirconia nano powders, binder, plasticizer, dispersant, defoamer and a solvents mixture of Ethanol/Toluene (30/70% wt.) were homogeneously mixed with a ball miller in one day. After this first step, the Ni/Al anode powders were added and ball milled over two days to obtain viscous slurry. Finally, the green sheet anode was casted with a doctor blade and dried in oven after a de-airing process. Green sheet anodes (5x2x0.07 cm³) with different zirconia content (1-10% wt.) were sintered at 650°C for 3h under a nitrogen atmosphere in presence of 10% vol. of hydrogen to eliminate all organic additives. The physical and structural properties of powders and green sheet were detected by X-ray diffraction (Rigaku, Miniflex II) and SEM-EDS (InspectF50, FEI Co.). The bending strength of sintered green sheet was studied according to the ASTM E855-90 after the ex-situ sintering at 650°C.

III. RESULTS AND DISCUSSION

XRD spectra for all sintered samples have been acquired in the range 5-90°, showing high crystalline structure and two region of interest, as concern peak interpretation. The first region is around 44-45°, where a remarkable peak shift occurs in presence of ZrO₂ for all compositions. These peaks correspond to the crystallographic plane (1,1,1) of the Face-Centred Cubic (FCC) structure of Ni/Al alloy.



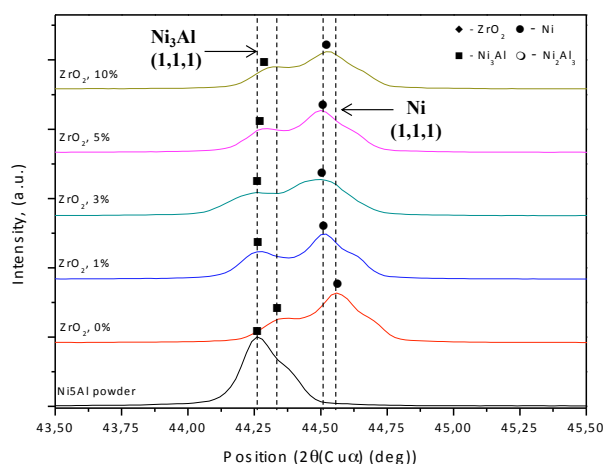


Fig. 1. Peak shift of plane (1,1,1) in presence of ZrO₂

According to the Bragg's Law, a shift to lower 2θ position indicates a modification of the interplanar distance for the plane related to the peak. The second region of interest is around $75-77^\circ$, as shown in Fig. 2.

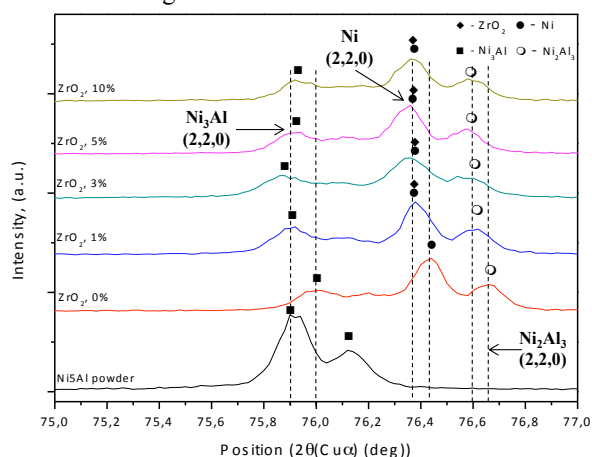


Fig. 2. Peak shift of plane (2,2,0) in presence of ZrO₂

Even in this case, a non-negligible peak shift is evident for plane (2,2,0) of Ni/Al FCC structure. Other main peaks in spectra, related to ZrO₂, concern planes (2,0,0) and (0,0,2) of the face-centred monoclinic structure. The last peak of as-received Ni5Al powder is the plane (3,0,0) and it disappears during sintering due to the diffusion at high temperature of Al atoms from this position to plane (2,2,0) of FCC structure to form the Ni₂Al₃ phase. This behavior can be explained by considering that all the mentioned planes for FCC contains octahedral and tetrahedral vacancies and intersect the plane (1,1,1), that is the main plane responsible for dislocations movement under creep. During ball milling and sintering, the addition of ZrO₂ induces a distortion in the crystal structure because Zr atoms probably tends to occupy FCC vacancies above and below the plane (1,1,1), thus reducing the space for movements and so creep deformation. The situation is better exposed in Fig. 3.

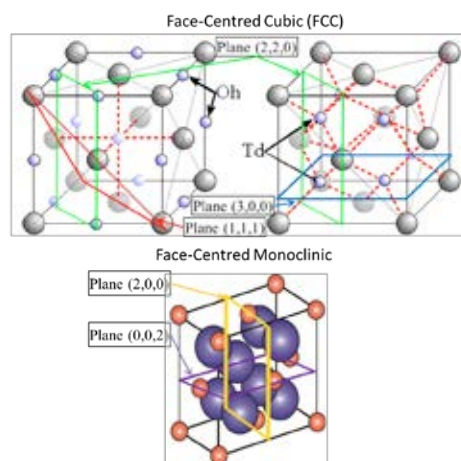


Fig. 3. Interacting planes and vacancies in Ni-Al-ZrO₂

By comparing SEM micrographs (Fig. 4) of ZrO₂-free anodes and that with 10% of nano ZrO₂, the morphological modification induced is evident, due to the deposition of the particles on the grain boundaries of the Ni/Al porous structure, obtained during elimination of organic compounds.

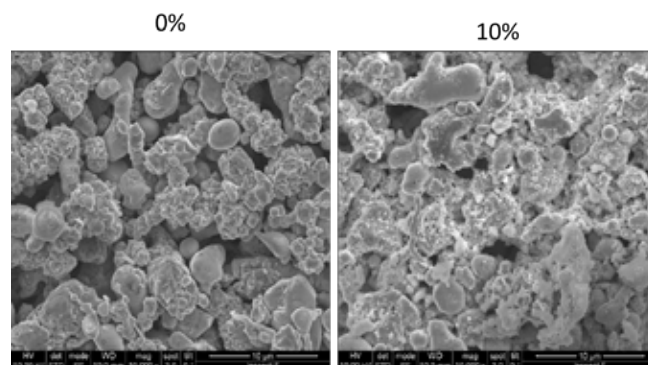


Fig. 4. SEM images of Ni-Al-ZrO₂

IV. CONCLUSION

In this work, Ni/Al anodes for MCFC application have been improved with nano ZrO₂ to modify the FCC structure. Results show that the addition of ZrO₂ can effectively modify the crystal structure, especially around the main slip plane (1,1,1) thus increasing bending strength and reducing creep strain. These evidences make the use of nano ZrO₂ of great interest to improve anode performance in MCFC.

REFERENCES

- [1] Nguyen, H.V.P., Song, S.A., Seo, D., Park, D.N., Ham, H.C., Oh, I.H., Yoon, S.P., Nam, S.W., Kim, J., Fabrication of Ni-Al-Cr alloy anode for molten carbonate fuel cells, *Materials Chemistry and Physics*, 2002, 136(2), pp. 910-916.
- [2] Nguyen, H.V.P., Othman, M.R., Seo, D., Yoon, S.P., Ham, H.C., Nam, S.W., Han, J., Kim, J., Nano Ni layered anode for enhanced MCFC performance at reduced operating temperature, *International journal of hydrogen energy*, 2014, 39(23), pp. 12285-12290.
- [3] Fang, B., Liu, X., Wang, S., Duan, J., Surface modification of a MCFC anode by electrodeposition of niobium, *Journal of Electroanalytical Chemistry*, 1998, 441(1), pp. 1-3.



HYRESPONSE: EUROPEAN HYDROGEN EMERGENCY RESPONSE: TRAINING PROGRAM FOR FIRST AID

G. Tagliabue*, F. Carletta* A. Essam Ali*

*FAST – Federazione Associazioni Scientifiche e Tecniche, Milano

Abstract: HyResponse is a 3 years European project funded by the European Commission into the Fuel Cell and Hydrogen Joint Undertaking (FC&H2). The project is the first and the most important program of its kind in the world that provides an integrated training of "first aid" in the context of applications going around hydrogen and fuel cells.

Through an online platform called European Hydrogen Safety Training Platform (EHSTP), HyResponse will provide complete training - theoretical training, operative training and virtual training, reproducing in detail one or more accident scenarios to end users (first responders, managers of companies etc.).

Index Terms – hydrogen, fuel cell technology, first responder, hydrogen safety science

I. INTRODUCTION

HyRESPONSE - under the collaboration of Ensosp, FAST, Air Liquide, University of Ulster, Areva, Global CCS, and Crise - will define innovative first responder's strategies that will describe the most appropriate actions to undergo by first responders in case of accident/incident involving a wide range of hydrogen and fuel cell technologies.

Throughout the EHSTP, first responders can use the unique hi-tech training facilities, the original training materials based on a curriculum to be developed by professionals in the field of fire and hydrogen safety science.

II. OBJECTIVES AND CONTENTS

The core-training Programme is threefold: educational training, including the state-of-the-art knowledge in hydrogen safety; operational training on mock-up real scale hydrogen and fuel cell installations; and innovative virtual reality training reproducing in detail an entire accident scenario, including influence of first responder's intervention. First responders will acquire professional

knowledge and skills to contribute to FCH permitting process as approving authority. Contemporary engineering tools to assess accident scene status and facilitate decision-making will be developed. Three pilot training sessions will be organized during the project. The Emergency Response Guide, explaining details of intervention strategy and tactics, will be developed and included into the pilot training sessions to receive attendees' feedbacks.

III. CONCLUSION

Presently the training sessions have been defined; they will be four and start from March 2016.



ALKAMMONIA: FUEL CELL FOR THE GLOBAL TELECOMMUNICATIONS INDUSTRY

Holger Schiller*, Ahmed Essam Ali**
AFC Energy - London*, FAST - Milan**

Abstract: ALKAMMONIA is a project that will revolutionise the telecommunications infrastructure due to its integration of highly efficient alkaline fuel cells - through the heating catalytic ammonia and its storage – with the installation of Base Transceiver Stations (BTSs) in remote areas of the world.

Index Terms – hydrogen, alkaline fuel cell technology, ammonia treatment, mobile telecommunication

I. INTRODUCTION

The millions of BTSs already installed have several limitations resulting mainly from the use of on-site diesel generators, but project ALKAMMONIA will overcome them and replace them with alkaline fuel cell, combined with a zero emissions ammonia treatment. The consortium started its work in 2011; it is composed of AFC Energy plc, FAST / EHA also UPS Systems plc, ZBT GmbH, Universitat Duisburg-Essen and the Paul Scherrer Institute.

II. OBJECTIVES AND CONTENTS

In order to meet the ever-increasing demand for ever improved signal coverage and greater bandwidth, millions of Base-Transceiver Stations (BTS) have been installed all over the world and their numbers continue to grow rapidly. These BTS usually require 3-5kW of electrical power. Due to the importance of the service provided, BTS are usually equipped with their own power generation equipment that serves as base-load or back-up power supply, depending on the location. In Europe, the electrical grid reaches nearly every corner of the continent and is generally very reliable, but in large areas of the world, the electrical grid is not as developed and is either unreliable or not available at all. Regions, which currently experience poor grid coverage, include large parts of Alaska, Russia, India and Africa. In these regions, a large percentage of the BTS are operated using on-site diesel generators. These diesel generators pose several problems: greenhouse gas and pollutant emissions, high operating and maintenance costs, regular fuel and generator theft and noise. In India alone, approximately 2 billion litres of diesel are used for BTS power supply yearly. The shortcomings of diesel generators for remote power

generation can be overcome if they were replaced by highly efficient and low-cost alkaline fuel cells in combination with a novel, practically emission free ammonia fuel system.

III. CONCLUSION

The idea of using ammonia (chemical formula NH_3) as a fuel is well known, combustion engines as well as fuel cells have been successfully demonstrated to run on ammonia. The most significant advantage of using ammonia as a fuel is that local CO_2 emissions are completely avoided. Ammonia is one of the most widely produced chemicals in the world, used for many processes and applications including the production of plastics, synthetic fibres, dyes, pharmaceuticals and agricultural fertilisers. Ammonia has a very high energy density even at low pressures when compared to hydrogen. This makes it economic to transport and a very attractive energy carrier in the growing hydrogen economy.



POWER UP: 500KWE ALKALINE FUEL CELL SYSTEM WITH HEAT CAPTURE

Holger Schiller*, A. Essam Ali**, Federica Carletta**

*AFC Energy – London, **FAST – Milan

Abstract: AFC Energy (AFCEN) in order to demonstrate a new efficient and sustainable production of electricity from hydrogen have created POWER-UP, a five-year EU - project that joins the efficiency of alkaline fuel cell with the stability of the AFC KORE module.

In this Project, a 500 kWe alkaline fuel cell (AFC) system will be demonstrated at Air Products industrial gas plant at Stade in Germany on a large scale.

Index Terms – hydrogen, alkaline fuel cell technology, alkaline kore module, hydrogen modular system.

I. INTRODUCTION

The use of the highest technological materials in every process level has allowed AFC Energy to develop a modular fuel cell system that can compete with conventional technologies for the production of energy.

The consortium started its work in 2013; it is composed of AFC Energy plc, FAST also Air Products PLC, GB Innomech Limited, Zentrum für Brennstoffzellentechnik ZBT GmbH and the Paul Scherrer Institute.

II. OBJECTIVES AND CONTENTS

The prototype system will be capable of assembling all the stacks in the project, and will be served as the basis for future automation industrial production to meet the increased demand for stacks, which the partners anticipate in the post-funding period.

POWER-UP will scale up manufacture of fuel cell components, reducing installation and commissioning time and reducing the cost of the system through a modular, containerised Balance of Plant.

Currently, AFCEN's fuel cells have a life expectancy of six months, but this project will achieve 12-month lifetimes.

III. CONCLUSION

POWER-UP is an opportunity to exploit the KORE module in the industrial world. This project will allow a European SME to develop to realize supply chain opportunities.

Some results have been reached:

- Site works at Stade completed;
- KORE fuel cell system manufactured and installed;
- Connection to German grid and sales contract in place joined;
- KORE single tier generation of 40kW in September 2015, on track to produce 240kWe before end of 2015
- Automation of stack assembly and significant increase in manufacturing volumes by using robot;
- Wider external partnerships established, e.g. Special Advisory Board;
- Presentation at Hannover Messe and other high-profile events, achieving a high interest from scientific community.

DON QUICHOTE: DEMONSTRATION OF HOW TO PRODUCE HYDROGEN USING WIND ENERGY

G. Tagliabue*, F. Carletta* A. Essam Ali*

*FAST – Federazione Associazioni Scientifiche e Tecniche, Milano

Abstract: The partners, with the financial support of the FCH JU, want to demonstrate the technical and economic feasibility of hydrogen storage for electricity from renewable energy.

Hydrogen storage plays an important role because it allows the achievement of European carbon reduction. This project results in much more efficiency, but the complexity and the costs of these solutions have prevented large-scale demonstrations.

Index Terms – hydrogen, fuel cell technology, hydrogen storage, renewable energy

I. INTRODUCTION

Under the co-ordination of Hydrogenics Europe, the participants in the project are Hydrogen Efficiency Technologies, WasserstoffNet vzw, Establishment Franz Colruyt NV, TÜV Rheinland Industrie Service GmbH, JRC-Joint Research Centre-European Commission, PE International AG, Icelandic New Energy Ltd and FAST.

Don Quichote is co-financed by the FCH JU (July 2012-June 2017) and want to demonstrate the technical and economic feasibility of hydrogen storage for electricity from renewable energy.

Hydrogen storage plays an important role because it allows the achievement of European carbon reduction. This project results in much more efficiency, but the complexity and the costs of these solutions have prevented large-scale demonstrations.

II. OBJECTIVES AND CONTENTS

This project brings innovations and demonstrations as:

- Extensive testing of the existing system, focused on dynamic behavior, efficiencies, and availability
- Doubling the hydrogen capacity by adding a very efficient and dynamic PEM-electrolyser (storage 130 kg/day)

- Developing, testing, demonstration and validation of direct coupling between wind turbine (1, 5 MW) and solar panels (1050 kW) and the electrolyser technology
- Adding of the conventional piston compressor by a new, high efficient compressor system based upon electrochemical compression.

The demonstrations programs consist of three phases, everyone is long twelve months (8000 hours per phase), in total 24000 hours.

- Phase 1: Adaptation of existing hydrogen fuel system (electrolyser, compressor, storage, fueling fork lifts)
- Phase 2: Research, additional storage and a fuel cell system, the latest for active balancing the grid
- Phase 3: Research, development and build of a new system for efficient, compact, modular compression and expansion of hydrogen.

III. CONCLUSION

This project combines the targets on increasing renewable electricity, grid balancing, sustainable mobility and the use of clean hydrogen in a replicable way and applications.



KNOWHY - IMPROVING THE KNOWLEDGE IN HYDROGEN AND FUEL CELL TECHNOLOGY FOR TECHNICIANS AND WORKERS

G. Tagliabue*, G. Ispano* A. Essam Ali*

*FAST – Federazione Associazioni Scientifiche e Tecniche, Milano

Abstract: The European Commission, through the Fuel Cell and Hydrogen Joint Undertaking (FCH JU), has co-founded a 3-years project titled KnowHy. KnowHy aims at providing to the widest possible audience of technicians specific training modules, practical, in an appropriate format and at affordable cost, to facilitate the deployment of the FC&H2 technologies expected to enter the market within the period 2014-2020.

Index Terms – hydrogen, fuel cell technology, training, e-learning platform

I. INTRODUCTION

Despite the fact that new job opportunities for technicians and workers regarding Hydrogen and Fuel Cells applications are expected to raise in the short term, there is an evident lack of training offers for technicians fitting market demand. KnowHy intends to overcome the gap offering a program of courses encompassing one common core module and five different specializations, among courses realized on an e-learning platform, would be held in different countries.

The project's consortium includes the following members: Delft University of Technology (Coordinator), Fundación Hidrógeno Aragón, Fundación San Valero, Technische Universität München, Environment Park, Campus Francorchamps, University of Birmingham, Técnico Lisboa, FAST – Federazione delle Associazioni SCientifiche e Tecniche, Vertigo Games, PNO Consultants, Kiwa, McPhy.

II. EXTENDED ABSTRACT PREPARATION

The objective of the KnowHy project is to create a sustainable training offer targeting professionals (technicians, workers) with the following features:

- Specific training, focused on applications, which are going to enter market rollout phase, according to the best assumptions from industry;
- An E-learning training system will allow workers and technicians more easily to participate in the courses. In order to facilitate trainee's attendance and the learning process,

training contents will be provided in mother tongue;

- KnowHy will be based in the concepts “learning by doing” and “seeing believes”. Facilities and equipment of currently existing demo projects will be used in order to provide this practical aspect to the training program;
- In order to create low cost courses, a central E-learning platform will be used and local support will be sought. As the training will be offered in widely spoken languages in Europe, it has a huge market potential; increasing the number of attendees will decrease the relative costs of the training;
- Easily adaptable to other languages or new applications, scalable and replicable. KnowHy will lead to a self-sustained training offer.

III. CONCLUSION

The project distinguishes for the importance to give to the formation, because puts interest to the training actions, mainly focused on installation, operation and maintenance of those devices.





Graphite-coated multi-walled carbon nanotubes as a cathode for bio-electrochemistry denitrification

Abbas Rezaee*, Mahdi Safari

Department of Environmental Health, Faculty of Medical Sciences, Tarbiat Modares University, Tehran, (Iran)

Abstract – The aim of this study was to evaluate the efficiency of a bio-electrochemical denitrification process include a bio-cathode of graphite-coated multi-walled carbon nanotubes. The efficiency of the bio-electrochemical denitrification was assessed as the function of various operational parameters, such as current density, pH and retention time. A plexiglass reactor consists of two chambers separated by a cation exchange membrane was utilized for the experiments. The electrodes were placed on a bioreactor and connected to DC power supply. Increasing the current densities up to 10 mA/cm², nitrate reduction efficiency was increased from 43% to 95%. Maximum nitrate reduction in bio-electrochemistry reactor used in this study was carried out at 10 mA/cm² current density and neutral pH values. According to the obtained results, at higher current density, nitrate reduction rate was decreased. At a constant condition, and initial pH values of 6.0, 7.0, 8.0 and 9.0, nitrate removal efficiency were 55, 95, 84 and 43, respectively.

Index Terms - Autohydrogenotrophic, Bio-electrochemistry, Biocathode, Denitrification

Removal of nitrate from aqueous solutions due to various health and environment problems is urgent and has been a hot topic in environmental health. The nitrate removal can be utilized by various biological or physico-chemical process [1]. Different techniques have been presented for nitrate treatment, such as ion exchange, reverse osmosis, adsorption, electrocoagulation, electromagnetic, and biological process [2, 3]. Biological denitrification is an environmental friendly technique for nitrate removal from environment [4]. In bio-electrochemical denitrification, autotrophic denitrifying bacteria utilize hydrogen gas, which is generated at the cathode by the electrolysis of water, as an electron donor to reduce nitrate into nitrogen gas [5]. Material of electrodes, electrical current, electrodes configuration, electrolyte, pH and nitrate concentration are include in the operating parameters in a bio-electrochemical process that have principal impacts on nitrate reduction. Bio-cathode could directly affect to denitrifying bacteria attachment, hydrogen production, electron transfer and other properties [6]. Hence, the development and fabrication of

novel electrode materials is an important subject in bio-electrochemical systems. Various criteria such as large active surface areas, excellent biocompatibility and conductivity, and non-toxicity towards bacteria are a priority. Therefore, the introduction of a new electrode material may be of interest and could change the course of new studies [7]. Various materials, such as carbon nanotubes, conductive polymers, metals, conductive nano-materials and activated carbon have been used for modification of cathode [8]. Between the various bio-electrode materials, carbon materials such as graphite, carbon clothes and carbon paper are used as a cathode in bio-electrochemical denitrification. Graphites are preferable as they have good mechanical and structural integrity. Also, cathode modification using carbon nanotube, improved bacterial attachment and facilitate electron transfer between bacteria and cathode surface [9]. Multi-Walled Carbon Nanotubes (MWCNTs) are selected for modification of graphite and producing the graphite/MWCNT cathode. MWCNT was added into 100 mL of mixture of concentrated sulfuric and nitric acid (3:1, vol. ratio) and sonicated for 3 h for good dispersion. The mixture was centrifuged at 5000 rpm for 10 min. The concentrated MWCNT treated with deionized water to achieved pH 6-7. Ethanol was added to MWCNT slurry and sonicated to obtain a dispersed MWCNT solution. Graphite was immersed into the MWCNT solution for 2h and then dried at 150 °C for 1 h [6]. A plexiglass reactor consists of two chambers separated by a cation exchange membrane was utilized for the experiments. It was consisted of an anode and a cathode chamber with the working volume of 2 L. Bio-electrochemical reactor were fed by the synthetic wastewater and inoculated with enriched denitrifying bacteria. The effect of different operating parameters such as current density (5 - 30 mA/cm²), pH (6 - 9), ORP (0 - -200 mV), initial nitrate concentrations (25 - 120 mg/L NO₃-N) and retention time (2 - 24 h), were studied in the bio-electrochemical reactor.

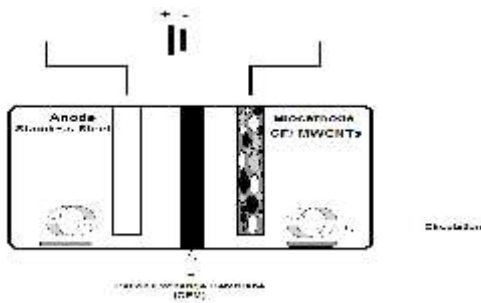


Fig. 1. Schematic diagram of the bio-electrochemical denitrification reactor

In order to evaluate the effect of graphite/MWCNT electrode on the bio-electrochemical denitrification, the efficiency of graphite/MWCNT and graphite alone were examined at the same optimum operation condition (Fig. 2). Regarding these results, it can be found that graphite/MWCNT have higher removal efficiency for nitrate than graphite. The graphite/MWCNT cathode have nitrate removal efficiency 95% after 8 h. This means that, using graphite/MWCNT composite cathode reduction rate on cathode increased and therefore running time is reduced for achieving the standard.

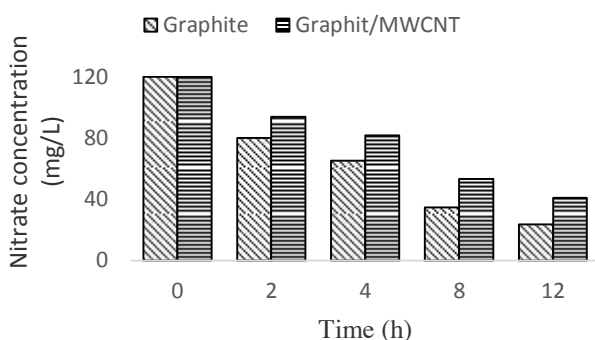


Fig. 2. Comparison of graphite and graphite/MWCNT as a bio-cathode on bio-electrochemical nitrate reduction (pH 7, ORP = -100, $\text{NO}_3^- = 120 \text{ mg/L}$, Current density = 15 mA/cm^2)

It seems that, higher efficiency of the prepared bio-cathode is due to increase the surface area of cathode, enhance the conductivity and electron transfer, increase hydrogen production, facilitate bacteria attachment on bio-cathode surface and prevention of cathode inactivation by biomass and by product. Therefore, utilization of MWCNT as cathode modifier increase the nitrate reduction efficiency about 14 percent. The use of MWCNT can increase biofilm formation and the reduction time for achieving to WHO nitrate standard was reduced. By increasing the time, nitrate reduction efficiency was increased. At retention time of 2 to 12 h nitrate reduction efficiency was increased from 43% to 92%. While at retention time of 12 to 24 h denitrification rate was limited due to

increasing accumulation of H_2 and nitrate byproducts such as nitrite and ammonia in the surface of cathode. Increasing the retention time in the reactor makes the denitrifying bacteria consume greater extent of nitrate

CONCLUSION

The obtained results show that the graphite/MWCNT, increases the nitrate removal efficiency. In this study, optimum ORP, pH, current density and retention time were -100mV, 7, 10 mA/cm^2 and 8 h, respectively. The best nitrate removal efficiency at optimum condition was 95% for graphite/MWCNT bio-cathode. Running time for achieving the nitrate standard using graphite/MWCNT was 8 h.

ACKNOWLEDGMENT

The authors thank the Tarbiat Modares University for all the support provided.

REFERENCES

- [1] Pandian, G., Kamaraj, R., Vasudevan S. Application of isotherm, kinetic and thermodynamic models for the adsorption of nitrate ions on graphene from aqueous solution. *Journal of the Taiwan Institute of Chemical Engineers*, 44, 2013, pp. 808-814.
- [2] Rezaee, A., Godini, H., Jorfi, S., Nitrate removal from aqueous solution using MgCl_2 impregnated activated carbon. *Environmental Engineering and Management Journal*, 9, 2010, pp. 449-452.
- [3] Hayrynen, K., Pongracz, E., Vaisanen, V., Pap, N., Manttari, M., Langwaldt J., Keiski R.L., Concentration of ammonium and nitrate from mine water by reverse osmosis and nanofiltration. *Desalination*, 240, 2009, pp. 280-289.
- [4] Godini, H., Rezaee, A., Khavanin, A., Nili, Ahmadabadi, A., Rastegar, S.O., Hossini H., Heterotrophic Biological Denitrification Using Microbial Cellulose as Carbon Source. *Journal of Polymer and Environment, J. Polymer Environ.* 19, 2011, 283-287
- [5] Pérez, R.G., Dosta, J., Mata-Álvarez J., Biological nitrogen removal (BNR) using sulfides for autotrophic denitrification in a sequencing batch reactor (SBR) to treat reject water. *Industrial & Engineering Chemistry Research*, 46, 2007, 6646-6649.
- [6] Tsai, H.Y., Wu, C.C., Lee, C.Y., Shih, E.P. Microbial fuel cell performance of multiwall carbon nanotubes on carbon cloth as electrodes. *Journal of Power Sources*. 194, 2009, 199-205.
- [7] Hossini, H., Rezaee, A., Ayati, B., Mahvi, A.H. Simultaneous nitrification and denitrification using a polypyrrole/microbial cellulose electrode in a membraneless bio-electrochemical system *RSC Adv.*, 2015, 5, 72699
- [8] Rozendal, R.A., Hamelers, H.V.M., Rabaey, K., Keller, J., Buisman, C.J.N. Towards practical implementation of bioelectrochemical wastewater treatment. *Trends in Biotechnology*, 26, 2008, 450-459.
- [9] Chen, W.X., Tu, J.P., Wang, L.Y., Gan, H.Y., Xu, Z.D., Zhang X.B., Tribological application of carbon nanotubes in a metal-based composite coating and composites. *Carbon*, 41, 2003, 215-222.



IODINE DOPED GRAPHENE AS CATALYST FOR LOW COST FUEL CELLS

A. Marinoiu*, I. Iordache*, M. Raceanu*, C. Teodorescu**,
A. Soare*, M. Constantinescu*

* RD Institute for Cryogenics and Isotopic Technologies- ICIT,
4Uzinei St., Rm Valcea, Romania

**Research Center OLTCHIM SA, Rm Valcea, Romania

Abstract - Iodine doped graphene were prepared in order to allow the study about the possibility of their using as catalyst support for PEMFC applications, due to their unique structural properties or to the prominent characteristics, such as high surface area, uniform pore size, ordered pore structure. The influence of the preparation method was experimentally evaluated, namely: the electrophilic substitution starting from commercial graphene; the catalyzed reduction with HI and AlI_3 ; and the reduction with HI as non-catalyzed reaction. The structure and morphology of prepared samples were characterized using BET method, during different preparation steps, Scanning Electron Microscopy (SEM), Raman investigation, X-ray photoelectron spectroscopy (XPS) analysis. Raman and XPS studies validated the presence of elemental iodine in the form of triiodide and pentaiodide. It was also stuck trapped between graphene layers, leading to interactions with C atoms. Iodine-doped graphenes have been successfully obtained through a simple, economical and relevant approach.

Index Terms - Iodine doped graphene, Catalysts, Fuel cell, Electrophilic substitution.

I. INTRODUCTION

PEM fuel cells exhibit good energy efficiency and high power density per volume. The high costs due to the noble metal catalysts, electrolyte membranes, and bipolar plates coerce the large scale marketing [1]. The membrane electrode assemblies (MEAs) fabrication costs can be reduced through several approaches. The remarkable proprieties make graphene promising candidate for these strategies. Our strategy to lower the MEA costs is to develop more efficient catalyst support systems which have the following properties: high specific surface area; an improved chemical and electrochemical stability; high catalytic activity for hydrogen oxidation. Among currently expensive noble metals, Pt is the most widely studied

noble metal as electrocatalyst [2]. Nevertheless, Pt-based catalysts still suffer from poor tolerance against carbon monoxide poisoning and fuel crossover. Thus, the development of a new class of materials with low-cost, high-efficiency for oxygen reduction reaction (ORR) and good durability is required to recognize fuel cells as one of the most promising energy sources. In the last years, graphene-nanocomposites have attracted an intense interest as functional components for fuel cells [3].

In respect to this trend, the electrochemical performance of carbon base support could be improved by introducing of extraneous elements, developing surface functional groups or suitable physico-chemical modification. Chemical doping of graphene with varied elements offers a proper solution to modify the electronic proprieties. The attempts were focused on nitrogen or boron doped graphene. Nowadays, the developing of a new graphene-iodine catalyst is more affordable, by far, than platinum-based fuel cell catalysts and more easily to be obtained.

There are only few papers which report the preparation of iodine base graphene, mostly by chemical vapor deposition CVD.

II. EXPERIMENTAL

In this paper, we prepared doped graphene materials in order to study the possibility of their using as catalyst support in PEMFC due to the unique structural and electrical properties and due to the prominent characteristics, such as high surface area, relatively uniform pore size and ordered pore structure. Several methods were approached for their synthesis: the reduction with HI catalyzed by AlI_3 , starting from graphite (Gri1), the reduction with HI as non-catalyzed reaction, starting



from graphite (Gri2) and the electrophilic substitution, starting from commercial graphene (Gri3).

Iodine-doped graphene has been successfully obtained through a simple, economical and relevant approach. The structure, morphology and properties were characterized using BET method during different preparation steps, Scanning Electron Microscopy (SEM), Raman investigation, XPS analysis. The high BET surface area of prepared graphene base materials indicated a significant extent of delamination during the proposed technology ($630 \text{ m}^2/\text{g}$).

Figure 1 show the electron microscopic image of iodine doped graphene, which tends to exhibit a very rough surface structure. As can be seen, the flakes built a very good connected network which is crucial for the electronic transport for fuel cell applications.

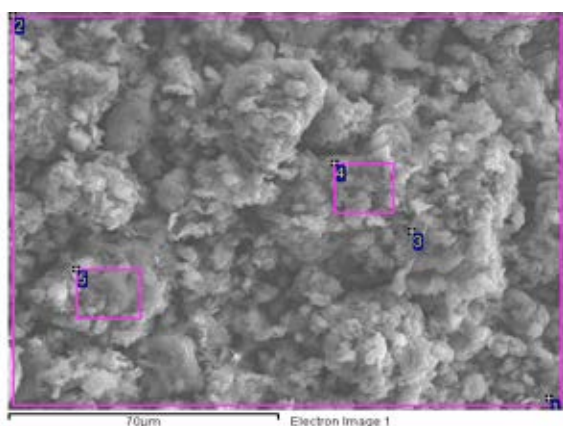


Fig. 1. SEM analysis of the prepared iodine doped graphene nanocomposite

Raman spectroscopy having laser excitation energy of 488 nm and 514 nm, provided a facile structural and quality characterization of the synthesized iodine-carbon materials (Fig. 2).

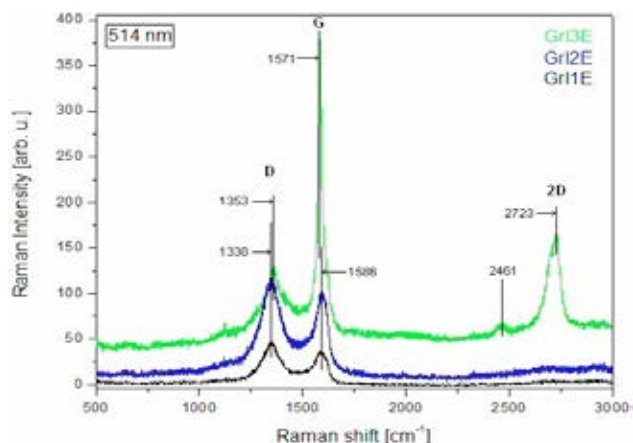
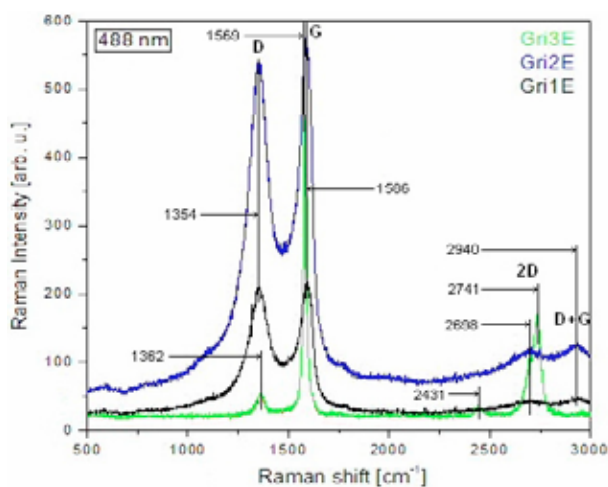


Fig. 2. Raman spectrum of iodine doped graphene

The prepared materials shows a low intense disorder-induced D band, a strong graphitic band and a second order 2 D Raman peak. The sharp G peak in comparison to D peak corresponding to Gri3 indicates highly crystalline graphene structure with minimum defects.

III. CONCLUSION

In this paper, we demonstrated an easy and verifiable process in order to obtain iodine doped-graphene materials, using three synthesis routes: the reduction with HI catalyzed by AlI_3 , the reduction with HI as non-catalyzed reaction and the electrophilic substitution. The high BET surface area indicated a significant extent of exfoliating during the proposed technology. SEM image illustrates a very rough surface structure and a very good connected network, which arguably favor the electronic transport in fuel cell applications. The sharp G peak in comparison to D peak corresponding to Gri3 indicates highly crystalline graphene structure with minimum defects.

ACKNOWLEDGMENT

This work is supported by the National Agency of Scientific Research from Romania by the National Plan of R & D, Project No. PN 09 19 01 16.

REFERENCES

- [1] Kakaei, K., Zhiani, M., A new method for manufacturing graphene and electrochemical characteristic of graphene-supported Pt nanoparticles in methanol oxidation, *Journal of Power Sources*, Volume 225, 2013, Pages 356-363.
- [2] Ban, F.Y., Majid, S.R., Huang, N.M., Lim, H.N., Graphene Oxide and Its Electrochemical Performance, *International Journal of Electrochemical Science*, Volume 7, 2012, Pages 4345 – 4351.
- [3] Kalita, G., Wakita, K., Takahashi, M., Umeno, M., Iodine doping in solid precursor-based CVD growth graphene film, *Journal of Materials Chemistry*, Volume 21, 2011, Pages 15209-15213.



Catalytic Hydrogen Production from Ammonia over Ru/La(x)-Al₂O₃ (x=0–10 mol %)

Dan Bi Chung,^{1,3} Hyo Young Kim,¹ Mina Jeon,¹ Hyun S. Park,^{1,2} Dae Hyung Lee,¹ Jin Young Kim,¹ Sun Hee Choi,¹ Suk Woo Nam,¹ Kwan-Young Lee,^{3,*} Chang Won Yoon^{1,2,*}

¹Fuel Cell Research Center, Korea Institute of Science and Technology, 39-1, Hawolgok-dong, Seongbuk-gu, Seoul 136-791, Republic of Korea

²Clean Energy and Chemical Engineering, Korea University of Science and Technology, Korea

³Department of Chemical and Biological Engineering, Korea University, Anam-Dong, Seongbuk-Gu, Seoul 136-701, Republic of Korea

ABSTRACT

Ru (1 wt%)-based catalysts supported on La(x)-Al₂O₃ (x=0, 1, 5, and 10 mol%) were synthesized and characterized by X-ray diffraction, Brunauer-Emmett-Teller measurement, scanning electron microscopy, scanning transmission electron microscopy, and temperature-programmed reduction. The as-prepared catalytic materials possessed strong metal-to-support interactions (SMSI) between Ru and La(x)-Al₂O₃. The La-doped catalysts were excellent for the dehydrogenation of ammonia; among them, the Ru (1wt%)/La(10)-Al₂O₃ catalyst exhibited superior performance and improved thermal stability with nearly 100% conversion of ammonia at 650 °C. The incorporated element La is thought to play an important role in enhancing SMSIs, ultimately facilitating ammonia dehydrogenation even at low temperatures.

INTRODUCTION

Growing concerns on issues of energy and environment make hydrogen attractive as an important alternative source of energy, particularly in the context of fuel cells, replacing the current carbon-based economy [1]. To establish hydrogen economy for the future, it is essential to develop economically viable technologies for hydrogen production, storage, and utilization. One of the main

hurdles in the implementation of hydrogen economy is the safe storage of large quantities of hydrogen. In this context, significant efforts have been made to explore highly capable hydrogen storage materials over the last decade.

As a promising candidate for chemical hydrogen storage, ammonia has recently attracted increasing attention [2]. First, ammonia possesses a significantly high hydrogen storage density of 17.8 wt% and can liberate hydrogen on demand in the presence of a proper catalyst. Additionally, this material can readily be condensed under mild conditions (20 °C and 0.8 MPa), which facilitates its high transportability and efficient delivery to the desired site employing the current infrastructure. Moreover, ammonia decomposes upon dehydrogenation to release nitrogen gas free of carbon containing impurities that deactivate platinum catalysts utilized in polymer electrolyte membrane fuel cells (PEMFCs). This allows for the compact designing of hydrogen storage/release systems.

In this research, a series of Ru catalysts supported on La-incorporated alumina, Ru/La(x)-Al₂O₃ (x= 0, 1, 5, and 10 mol%), were prepared for ammonia dehydrogenation and characterized using various analytical techniques such as X-ray diffraction (XRD), Brunauer-Emmett-Teller (BET) measurement, scanning electron microscopy (SEM), scanning transmission electron microscopy (STEM), and temperature-programmed reduction (H₂-



TPR). The dehydrogenation activities of the catalysts were also evaluated, and potential roles of the doped La element on H₂-release were elucidated.

RESULTS AND DISCUSSION

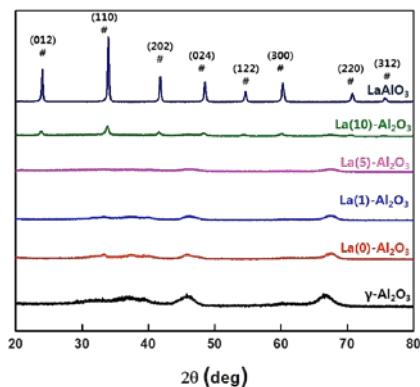


Fig. 1 XRD patterns of the La(x)-Al₂O₃ supports (x=0, 1, 5, and 10 mol%)

Fig. 1 shows the XRD patterns of the La(x)-Al₂O₃ supports (x=0, 1, 5, and 10 wt %) with different La contents. The XRD pattern of the γ -Al₂O₃ support, calcined at 900 °C for 5 h, displayed three broad peaks centered at ca. 38°, 46°, and 67° (Fig. 1, red), indicating the residual γ -Al₂O₃ phase (Fig. 1, black) following the heat treatment. The intensities of the characteristic peaks corresponding to γ -Al₂O₃ decreased as the La content increased from 0 mol % to 1 mol %, 5 mol %, and 10 mol %. Notably, upon the addition of 10 mol % La, a new peak attributed to the formation of a new phase, LaAlO₃, which has a crystalline perovskite-like structure [3]. Given the low La content (10 mol %, 26 wt %), the LaAlO₃ phase formed upon heat treatment may remain well dispersed on the surface of the Al₂O₃ support. No diffraction peaks corresponding to La₂O₃ were detected, indicating that the added La elements are well dispersed on the Al₂O₃ support.

The Ru metals were then impregnated onto the as-prepared supports using a conventional procedure, and their morphologies were analyzed using STEM (not shown). Regardless of the La quantity, the Ru nanoparticles (Ru NPs) generated during reduction were uniformly dispersed on the supports, and their crystallite sizes were in the range of 1–3 nm. Additional XRD patterns obtained using Ru (1wt%)/La(x)-Al₂O₃ (x=0, 1, 5, and 10) showed identical peaks to La(x)-Al₂O₃ with no peaks corresponding to metallic Ru species, confirming that the Ru NPs formed on La(x)-Al₂O₃ were small and well dispersed.

The Ru(1wt%)/La(0)-Al₂O₃ catalyst showed slightly increased activity while Ru(1wt%)/La(x)-Al₂O₃ (x= 5 and 10 mol%) displayed dramatically increased activities; e.g.,

Ru(1wt %)/La(10)-Al₂O₃ exhibited activity even at 400 °C and showed nearly 100% conversion at 650 °C.

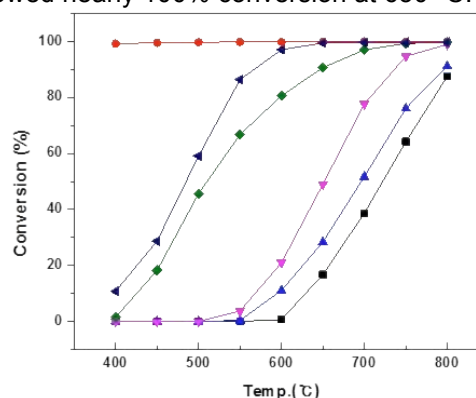


Fig. 2 Catalytic performances of the as-prepared catalysts for NH₃ dehydrogenation: (■) no catalyst, (▲) Ru(1wt%)/La(0)-Al₂O₃, (▼) Ru(1wt%)/La(1)-Al₂O₃, (◆) Ru(1wt%)/La(5)-Al₂O₃, (▲) Ru(1wt%)/La(10)-Al₂O₃, and (●) thermodynamic equilibrium values

In all cases, the ammonia conversion increased with increasing temperature, which is in agreement with the endothermic nature of the dehydrogenation. The quantities of H₂ released during NH₃ dehydrogenation at different temperatures from 400 – 800 °C increased linearly within the period of 1h. The significantly enhanced activity for Ru(1wt%)/La(x)-Al₂O₃ could be attributed to the interaction between Ru and La(x)-Al₂O₃.

CONCLUSIONS

In summary, Ru-based catalysts, Ru(1wt%)/La(x)-Al₂O₃ (x=0, 1, 5, and 10 mol%), were synthesized and characterized. Among the as-prepared catalysts, the Ru(1wt%)/La(x)-Al₂O₃ materials (x=5 and 10 mol %) were highly active for ammonia dehydrogenation. The enhanced activities of these catalysts were proposed to originate from the interaction between RuO_x and La(x)-Al₂O₃, which further resulted in reduced Ru sintering. The as-applied doping strategy would thus offer valuable insight into the development of highly efficient, transition-metal-based catalysts for ammonia dehydrogenation.

REFERENCES

- [1] Mazloomi K, Gomes C, Renew Sustainable Energy Rev **2012**, *16*, 3024.
- [2] Schuth F, Palkovits R, Schlogl R, Su DS, Energy Environ Sci **2012**, *5*, 6278.
- [3] Lima E, Villafuerte-Castrejón M-E, Saniger JM, Ibarra-Palos A, Sánchez-Sánchez JE, Álvarez LJ, Solid State Ionics **2008**, *178*, 1944.



SOFC STACK COUPLED WITH DRY REFORMING

L. Barelli, G. Bidini*, G. Cinti*, M. Pöniz**

*Università degli Studi di Perugia, via Duranti 66, 06125 Perugia, (Italy)

** EBZ GmbH

Abstract - The study proposes an innovative CHP system based on the coupling of carbon dioxide dry reforming (CDR) and solid oxide fuel cell (SOFC) technology. To supply CO₂ at the CDR unit, increasing at the same time the overall utilization factor, SOFC anode off-gases are recycled for fuel reforming. In the CDR unit, in fact, the CO₂ produced at the anodic exhausts reacts with feeding low carbon fuels (in this case natural gas) producing hydrogen and carbon monoxide for the SOFC feeding, thus allowing an internal CO₂ reuse. In particular, the SOFC, characterized by high operating temperatures and significant recoverable heat, guarantees suitable temperature of the CDR process, highly endothermic. Moreover, compared to traditional CDR applications, lower temperatures are acceptable because SOFC tolerates feeding gas containing limited amounts of CO and CH₄. According to this concept, the SOFC stack can be conveniently fed by a dry reformer reactor. The present study addresses the experimental characterization of SOFC short-stacks performance, in terms of produced power and thermal behavior, when fed by different fuel mixtures produced through dry reforming.

Index Terms – Dry reforming, SOFC, stack test, microCHP

I. INTRODUCTION

Carbon dioxide is the major greenhouse gas that contributes to the global warming. Therefore, enforcing technological strategies aiming to avoid or reuse CO₂ emissions becomes crucial, in order to mitigate GHG environmental impact. In [1], an innovative CHP system based on the coupling of carbon dioxide dry reforming (CDR) and solid oxide fuel cell (SOFC) technology is proposed. According to this concept, the SOFC stack can be conveniently fed by a dry reformer reactor [1]. Anode off-gases, containing CO₂, feed the dry reformer, where CO₂ produced at the anodic exhausts reacts with the fuel (e.g. natural gas) producing hydrogen and carbon monoxide. This syngas is then used for the SOFC feeding, resulting in an

internal CO₂ reuse. The heat required by the dry reforming process can be guaranteed by a suitable thermal integration of the SOFC stack and the reformer unit. Preliminary modelling results [1] evidenced that the innovative proposed system layout exhibits, in the case of natural gas feeding, an electric efficiency over 65%, with a related CO₂ emission factor significantly lower than the one characteristic of the best conventional fuel cell-based CHP system (reduction of about 10%). Also higher global efficiencies are expected in CHP applications. To support this analysis a deep investigation is needed at both stack and reformer level, to determine components behavior and performance under these specific operative conditions. The present work, in particular, addresses the investigation of SOFC behavior when fed by concentrated fuel mixtures as the ones obtainable through dry reforming process. First results, characterized by a limited increase in stack temperature and produced power increasing with the fuel mixture concentration, support this particular SOFC application.

II. METHODS

The aim of the test campaign is to evaluate SOFC short-stack performances when fed by dry reforming compositions. The short-stack is made of 4 ASC cells, 80 cm² active area. From our previous modeling at stack and system level [1] and experimental activity on dry reforming catalysts, 5 compositions were selected for the anode feeding as reported in Table 1. Test compositions are divided into two groups: A and B. Compositions A come from model simulations in Aspen Plus environment, while compositions B from experimental activities on a dry reforming reactor loaded with a specific Ni-Co catalyst supported on MgO-Al₂O₃. In details, relative to the dry reformer operative temperature, A1 refers to 809°C, A2 to 840°C and A3 to 960°C, while a constant CH₄/CO₂ ratio (0.6) was maintained at the reactor inlet. Regarding compositions B, B1 was obtained from experimental tests on dry reforming reactor with reactor temperature of 700°C, while B2



composition with reactor temperature of 750°C. Moreover, both compositions B refer to a 0.6 CH₄/CO₂ ratio at the dry reforming reactor inlet. Table 1 shows also the mixtures dilution (in terms of the content of H₂O and CO₂ inert species). It is expected that both produced power and equilibrium temperature increase with low dilution values of the fuel mixture. Total anodic inlet flow was designed keeping all compositions with the same amount of equivalent H₂ flow (80 NI/h). Tests were performed varying U_f (0.7, 0.6, 0.5) keeping constant inlet fuel and U_{ox} (0.2) for each compositions.

	A1	A2	A3	B1	B2
H ₂	25%	26%	31%	40,0%	43,8%
CH ₄	11%	11%	6%	5,3%	2,3%
H ₂ O	6%	6%	6%	4,2%	3,5%
CO	37%	38%	43%	43,1%	45,6%
CO ₂	21%	19%	14%	4,2%	3,5%
Inert	27%	25%	20%	8.4 %	7%

Table 1 Gas composition (mol.) used during test activity

III. RESULTS

Main focus of the study is the evaluation of the high power compositions into thermal equilibrium. The analysis focuses on two main parameters: average temperature (T_{av}) between T1 (anode inlet) and T2 (cathode inlet) and temperature difference (DT) between the two values. The first parameter gives an indication of the amount of heat that is released by the stack, while the second one indicates the distribution of the heat inside the cells. Graphs in Figure 1 show that all the temperature curves referring U_f have the same trends indicating that U_f effect does not differ with composition variation.

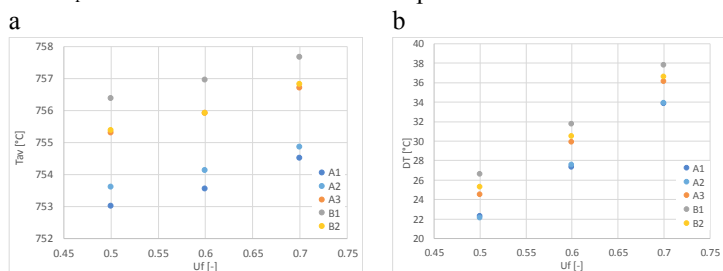


Figure 1 Temperature analysis: average temperature (a) and temperature difference (b) as function of U_f

Regarding the absolute values both graphs show similar values between A1 and A2 that are very similar compositions. For the same reason, similar values were obtained for A3 and B2, while B1 has the higher values. Globally temperature trends are correlated with fuel dilution. Specifically, both T_{av} and DT parameters increase at dilution decreasing. Anyway, T_{av} increases of 3°C maximum varying the fuel composition, while a maximum increase of about 5°C in the spatial temperature difference is measured. Consequently, the use of fuel mixtures produced through dry reforming doesn't significantly affect thermal stresses phenomena. Figure 2 reports stack power as function of U_f for all tested compositions. Higher powers were obtained for B compositions for all U_f values. Such difference comes mainly from the fuel concentration that permits an

increase of OCV values and, consequently, of all the voltages. This is confirmed by the trends of the curves that are similar.

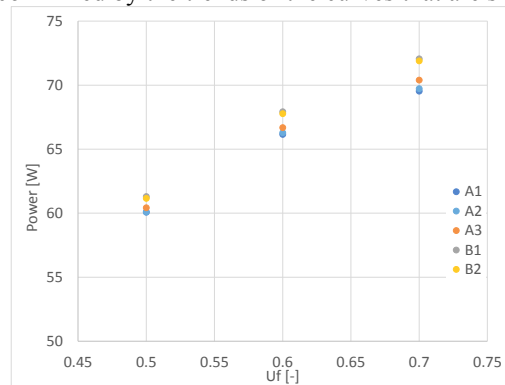


Figure 2 Power as function of U_f

IV. CONCLUSIONS

The obtained results show that high concentrated compositions like the one used for the test do not cause a significant increase of temperature into the stack. In addition, produced power increases for highly concentrated fuel mixtures. For what above, among all the tested compositions the one obtained from dry reforming experiments (B1 and B2) are the most performing. Thus the coupling of dry reforming with SOFC is feasible. Further studies will focus on long term operation to investigate the effect of carbon deposition.

ACKNOWLEDGMENTS

This work was carried out with the support of the European Community. We appreciate the support of the European Research Infrastructure H2FC European Infrastructure (funded under the FP7 specific program Capacities, Grant Agreement Number 284522).

REFERENCES

- [1] L. Barelli, A. Ottaviano. Solid oxide fuel cell technology coupled with methane dry reforming: A viable option for high efficiency plant with reduced CO₂ emissions. *Energy* 71 (2014) 118-129
- [2] S.M. Stagg, E. Romeo, C. Padro, D.E. Resasco. Effect of Promotion with Sn on Supported Pt Catalysts for CO₂ Reforming of CH₄. *Journal of Catalysis* 178/1 (1998) 137-145
- [3] H.J. Alves et al. Overview of hydrogen production technologies from biogas and the applications in fuel cells. *International Journal of Hydrogen Energy* 38/13 (2013) 5215–5225
- [4] M.E.E. Abashar. Coupling of steam and dry reforming of methane in catalytic fluidized bed membrane reactors. *International Journal of Hydrogen Energy* 29 (2004) 799 – 808.



A NEW CONTROL STRATEGY FOR FUEL CELL-BATTERY-ULTRACAPACITOR POWER SUPPLY SYSTEM WITH LIFE AND EFFICIENCY CONSIDERED

Jenn-Jong.Shieh¹, Chung-Hsing Chao^{2*}, and William Fang³.

^{1,2} Department of Electrical and Electronic Engineering, Ta Hwa University of Science and Technology
Hsinchu County, 30740, Taiwan

³Department of Aeronautical Engineering, University of Michigan,
Michigan, USA

ABSTRACT

Fuel Cells are an upcoming technology that has promise in future clean and efficient transportation. More specially, use in electric scooters as a hybrid system is an attractive option due to its ability to provide clean efficient power while keeping the speed of refueling that traditional combustion engines possess. Therefore an intelligent control system must be developed to maximize the advantage of fuel cells. Additionally, regenerative braking using super capacitors can be also used to allow farther range and longer battery life especially in city environments. Thus, different topologies that utilize battery, ultracapacitor and fuel cell technologies with regenerative braking have been examined to find an efficient design. Further, using SIMULINK/MATLAB simulation software, these systems can be simulated to monitor the characteristics of both the electrical system and the overall dynamics.

I. INTRODUCTION

With zero emissions and multiple fuel options, fuel-cell (FC) powered vehicles are an appealing alternative. Currently, due to the cost of larger high powered fuel cell systems in the price and weight, a system using a smaller fuel cell is preferred. Unfortunately, a low powered fuel cell is insufficient to power open throttle at high speeds on its own, and must rely on battery. This will reduce battery life and range of the vehicle. However, in urban use with lots of stop and go traffic, these disadvantages can be downplayed with use of regenerative braking and a higher efficiency system. A lot of energy is lost in stopping then accelerating the vehicle back up to speed. Thus, regenerative braking provides a solution to this. By removing voltage to the motor, the spinning motor becomes a generator and provides a braking force, transforming the kinetic energy of the scooter into electric energy captured to a capacitor rather than lost in heat in conventional braking. Then when power is needed to accelerate again, this energy is used first, thereby decreasing the demand on the battery and fuel cell, preserving fuel and battery life. Fuel cells and motors operate on different voltages, therefore a DC/DC converter is needed to allow this discrepancy. Many conventional design topologies include multiple converters which increase total mass, cost and complexity. A control strategy to allocate power is developed to give higher efficiency with a difference of consolidating the two converters into one. The battery and fuel cell operate in certain regimes which lower losses and the depth of discharge of the battery operates for longer life of the battery. Therefore, the goal of the present study presents a new control strategy can maximize the life and efficiency of a system.

II. SYSTEM ANALYSIS

In the design outlined herein, a topology that allows the fuel cell to operate in its high efficiency range and allow regenerative braking is proposed. One problem with this topology is that during braking, when the capacitor is fully

charged, the excess energy is lost. Therefore a design that allows charge back into the battery is sought. In order to allow this, a proposed design with a MOSFET allowing charge back into the battery is seen in Figure 1. A MOSFET with resistors to tune the gate voltage to open when the capacitor reaches the target voltage are added. The resistors are very large to prevent current leakage. This allows current to bypass the diode and into the battery when the capacitor reaches a target voltage. However, this design includes several flaws that make it suboptimal. An additional battery charger and DC/DC converter is required to prevent dangerous voltages/current that may be going to the battery. This increases operating costs as there is additional resistance. Further, system complexity is increased, resulting in higher cost and an increase in mass. Therefore it is more practical to correctly size the capacitor as capacitor costs have lowered in the past few years. The current design includes a single DC/DC converter. Although this removes the benefit of trickle charging the battery, lithium-ion batteries charge at close to 99% efficiency below 0.8C. In this model, a 20 Ah battery is used. 1C is the current to fully charge or discharge the battery in one hour which is the same as the capacity of the battery. Therefore this efficiency is obtained at 16 amps. Using a 200W fuel cell, the maximum current available to charge the battery is about 4 amps, well under 16 amps. Instead, weight and complexity is reduced, with all of the other advantages this method provides. When the vehicle braking, the motor becomes a power source, and charges the capacitor to a larger voltage. Thus when discharging, the motor pulls from the higher voltage capacitor until it reaches the battery voltage, and then are discharged concurrently. During braking, after the capacitor is full, the rest of the braking energy is dissipated as heat lost through friction in the mechanical brakes. However, if the capacitor is sized correctly, the mechanical brakes serve only as an emergency brake.

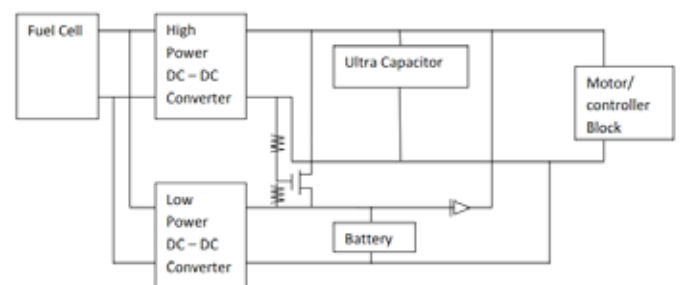


Fig. 1 Chargeback Circuit Topology

It is chosen to allow braking within 10 seconds from high speeds. Therefore with this information, it can be seen that theoretically, without friction, that the brakes can absorb approximately 30 KJ (60 km/h) and 80 KJ

(110 km/h). Thus, a capacitor size can be chosen. Scooters will be used in an urban setting; therefore regaining the energy from 60 km/h is more important. Further, because the capacitor will charge to the bus voltage of 48V, the braking energy must then be in stored in voltages higher than 48V. The upper cap of 53 Volts is chosen to allow for a smaller sized capacitor. A higher voltage would require a form of DC/DC conversion to the motor block. Although a lower voltage would reduce the risk of damage to the motor block and keep the voltage more constant, the current price of ultracapacitor offsets this advantage.

Energy in a capacitor is defined by:

$$w = \int_{Q_1}^{Q_2} v dq \quad (1)$$

Capacitance is defined by the ratio of charge over voltage, in differential form. Therefore work of Eq. (1) can be rewritten as

$$w = \int_{V_1}^{V_2} VCdv \quad (2)$$

V_1 and V_2 are known, so we can solve for C is 118.8 F.

In order to better select parts, a simulation for the hybrid system is developed to test how certain parts their control design will behave. Therefore, a MATLAB/SIMULINK model was developed. Because each part of the power system cannot supply enough power, a strategy is developed to distribute power to the motor. The power requested is passed along to the fuel cell controller. If the power demand is within the higher efficiency region, the fuel cell will provide as much power as it can the remainder is split between the capacitor and battery. If the capacitor has a voltage higher than the battery, it will discharge until the voltages are the same. Then, the battery and capacitor discharge simultaneously. If the capacitor voltage goes below the battery, the battery charges the capacitor to the battery voltage. When the power demand is less than zero, and power is coming into the system, the capacitor takes the excess power, and its voltage increases. No power goes to the battery due to a diode.

III. RESULT AND DISCUSSION

Figure 2 shows the velocity of the vehicle. This is given by the standard scooter testing specifications for Taiwan. The simulation was run with 3 different velocities of 3m/s, 5.8m/s and 8m/s. This was tested to see how the power distribution would handle, and to see where the fuel cell would power the scooter itself. Looking at the power distribution, the fuel cell is not on during the first 50 seconds. This is because no power is going to charge the battery, and if the fuel cell were to power both the motor and battery, it would be its low efficiency region. Thus, the battery is the pure provider of power. After, the scooter goes to 5.8 m/s. During the acceleration, charge is pulled from the capacitor, battery and fuel cell. This is when the fuel cell turns on. The fuel cell powers the scooter as well as charges the battery. When the scooter accelerates again, the battery and capacitor provide power, helping in acceleration. Here, the battery provides about the same amount of power as the fuel cell. Then the scooter decelerates to stop, and the energy is absorbed by the capacitor. During this period where the fuel cell power is above the required power, the fuel cell charges the battery and capacitor to the nominal voltage. Then the scooter accelerates and runs at 3 m/s. The fuel cell powers the motor, while charging the battery. When the scooter accelerates again to 5.8 m/s, the fuel cell turns off. This is because the battery is full of charge and the fuel cell is running in a low efficiency region. If the simulation were to run at 5.8 m/s, the fuel cell would power the scooter; however, this speed was purposely chosen to show that the fuel cell is shut off to ensure high efficiency. When the scooter accelerates again, the capacitor dumps its energy, and after, the battery and fuel cell both provide energy.

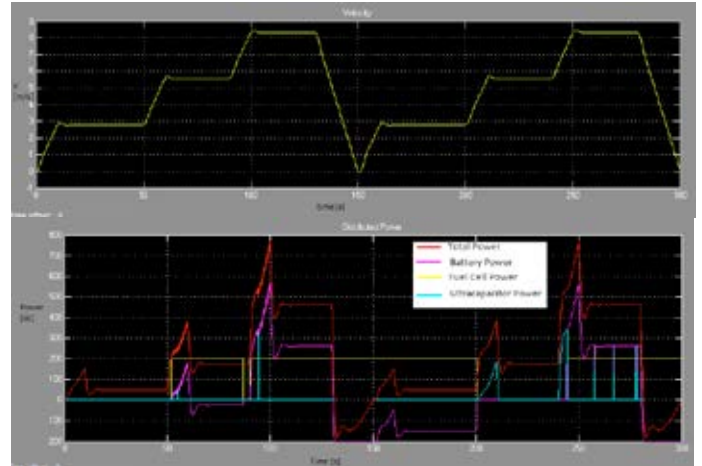


Fig. 2 Velocity of Simulation and Power distribution at 3 m/s, 5.8 m/s and 8 m/s

IV. CONCLUSION

A MATLAB/SIMULINK model simulation was written to predict the behavior of fuel cell-battery-ultracapacitor power supply system with life and efficiency considered. A large capacitor is needed to recover the energy from braking. However, following the driving pattern prescribed, a much lower capacity capacitor can be substituted. Regenerative braking, however, still makes a large impact on battery life, as much less cycles are on it, and less depth of discharge before recharging. A new control strategy was developed to ensure that the fuel cell is in its optimal power supplying state, and also increases the life and efficiency of the system with a topology which utilizes only a single DC/DC converter.

REFERENCE

1. M. Farooque, C. T. Danbury, and H. C. Maru, Fuel Cells The Clean and Efficient Power Generators, Proceedings of the IEEE (2001), Vol. 89, Issue 12, pp. 1819-1829.
2. A. Emadi, S. S. Williamson, A. Khaligh, Power Electronics Intensive Solutions for Advanced Electric, Hybrid Electric, and Fuel Cell Vehicular Power Systems," IEEE Trans. on Power Electronics (2006), Vol. 21, Issue 3, pp. 567-577.
3. D. Wu and S. S. Williamson, Status Review of Power Control Strategies for Fuel Cell Based Hybrid Electric Vehicles, IEEE Electrical Power Conference (2007), Canada, Oct. 25-26, pp. 218-223.
4. J. Bauman and M. Kazerani, A Comparative Study of Fuel-Cell-Battery, Fuel-Cell-Ultracapacitor, and Fuel-Cell-Battery-Ultracapacitor Vehicles, IEEE Transactions on Vehicular Technology (2008), Vol. 7, Issue 2, pp. 760-769.
5. J. Bauman, O. Waterloo, and M. Kazerani, An Improved Powertrain Topology for Fuel Cell-Battery-Ultracapacitor Vehicles, IEEE International Symposium on Industrial Electronics (2009), June 30 - July 2, Seoul, Korea, pp. 1483-488.
6. M. Bowkett, K. Thanapalan, T. Stockley, and M. Hathway, Design and implementation of an optimal battery management system for hybrid electric vehicles, 19th International Conference on Automation and Computing (2013), Sept. 13-14, London, pp. 1-5.
7. <https://www.tecategroup.com/ultracapacitors-Ultracapacitors/ultracapacitors.php/>
8. https://batteryuniversity.com/learn/article/charging_lithium_ion_batteries/
9. https://www.vespalabs.org/Vespa_101/Dynamics/Aerodynamics/
10. https://wiki/rolling_resistance_coefficient/



VOLTAGE PEAK ATTENUATION OBTAINED WITH THE INTEGRATED STEAMER IN THE OPEN-FLANGES™ SET-UP

R. Ihringer*, A. Bourradou*, and P. Coquoz*

* Fiaxell Sàrl, PSE-A 1015 Lausanne, Switzerland
tel.: +41 21 693 86 13 info@fiaxell.com www.fiaxell.com

Abstract – Electrolysis experiments have been carried out on a commercial cell with the Open Flanges™ test Set-Up and its integrated steamer. During operation under galvanostatic conditions, voltage peaks could be observed and were studied. It appeared that these fluctuations (amplitude and periodicity) were linked to different parameters as water utilization (WU) and type of peristaltic pump head (3 rollers or 10 rollers). Correlation between peristaltic pump head rotation and voltage peaks periodicity are presented through different graphs. This paper also presents a new kit with ceramic components for gas analysis.

Index Terms –SOFC, EIS, Integrated steamer for Electrolysis, SOEC.

I. INTRODUCTION

With the Open-Flanges™ Set-Up, Fiaxell is proposing an *integrated steamer* that allows direct injection of water in the test rig. The later replaces the typical external steamer and its complex heated lines to avoid condensation often used in SOEC research labs.

The amount of water flowing in the *integrated steamer* is controlled directly thanks to a peristaltic pump and the evaporation occurs in the hot zone of the set-up, before reaching the cell. An interchangeable ceramic cartridge inside the steamer ensures continuous water evaporation and thus a constant flux of steam. The interchangeable ceramic cartridge can also be impregnated with catalyst and the integrated steamer becomes a reactor for fuel processing (POX, SR etc.).

More and more lab research groups are using the integrated steamer for SOEC experiments as for instance EPFL [1] (Lausanne-CH), Eifer (Karlsruhe-DE), ICGM (Montpellier-FR), IMN (Nantes-FR), Sintef (Oslo-NO) and many others.

The electrolysis experiments carried out at EPFL (Swiss Institute of Technology) show that constant and smooth flux of steam allows for accurate impedance measurements as it can be seen on Fig. 1. Nevertheless, when zooming in the potential response, peaks become visible as it will be shown in the next figures and in Fig. 2.

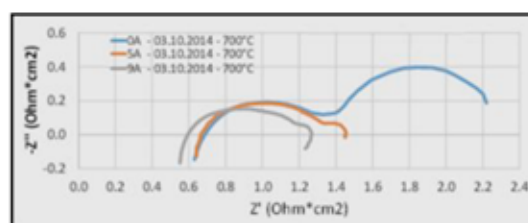


Fig. 1. Galvanostatic EIS at OCV, 5 A and 9 A, 700°C, 90% H₂O, 10% H₂, carried out at EPFL (JVH group, Swiss Institute of Technology, Lausanne-CH)

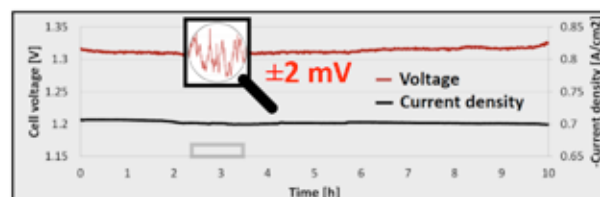


Fig. 2. Polarization at 0.7 A/cm², 750°C, 90% H₂O, 10% H₂, carried out at EPFL (JVH group, Swiss Institute of Technology, Lausanne-CH)

II. VOLTAGE PEAK ATTENUATION WITH THE INTEGRATED STEAMER

The origin of the cell voltage peaks has been investigated in the following experimental conditions: a commercial cell (ASC700 from SOLIDpower—with standard LSCF cathode electrode) is tested in the Open Flanges™ test Set-Up (see www.fiaxell.com). The steam is produced directly in the setup thanks to the integrated steamer which smoothly evaporates the water injected with a calibrated peristaltic pump. Formiergas (92% N₂, 8% H₂) was flushed along with the steam to ensure a reducing atmosphere on the nickel side of the cell. During all the experiments, a constant flux of 60% H₂O, 37% N₂ and 3 % H₂ was fed to the cell.

The influence of two parameters was studied, the type of pump head (3 or 10 rollers) and the water utilization, WU (7.5 and 45 %). The water utilization is defined by the ratio of the current going through the cell over the current necessary to electrolyze all the injected water (during the experiments, only the current density is modified).

Fig. 3 shows the evolution of the potential over time at 7.5 % WU (0.2 A/cm^2) with a 3-rollers pump head. No apparent periodicity was observed and the range of fluctuations did not go higher than 1 mV.

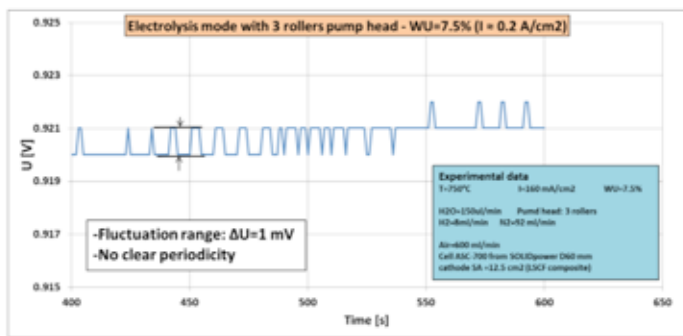


Fig. 3. Evolution of the potential over time at 0.2 A/cm^2 and 7.5 % WU, with 3 rollers pump head

However when the WU was increased (45% WU, 1 A/cm^2) peaks appeared with a higher fluctuation range (20-25 mV), Fig. 4. These peaks had a period of 8 seconds. It appeared that this corresponds to a third of the 3 rollers pump head rotation period, implying that this phenomenon is related to mechanical action of the rollers on the tube.

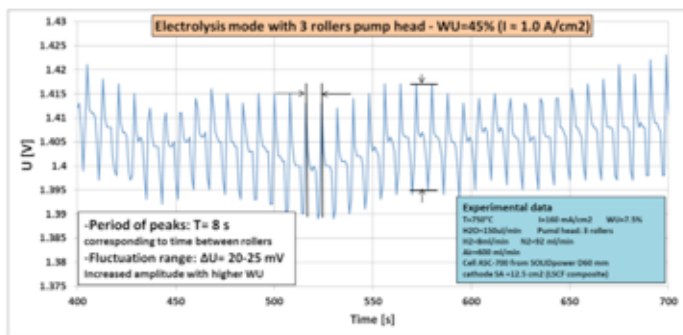


Fig. 4. Evolution of the potential over time at 1 A/cm^2 and 45 % WU, with 3 rollers pump head (fluctuations of 20-25 mV; peak period of 8 sec.)

In order to reduce the range of fluctuations a 10-rollers head was installed on the peristaltic pump. The water flow and WU (45%) were kept the same. Figure 5 shows the voltage of the cell over time. At 45 % WU, the 10-rollers head reduced the fluctuation range to 5mV. No apparent periodicity could be observed during our two days experiment.

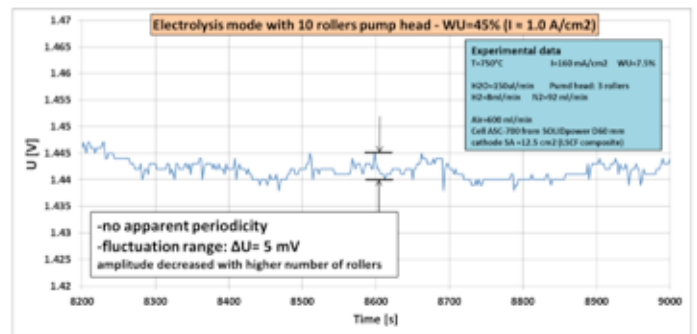


Fig. 5. Evolution of the potential over time at 1 A/cm^2 and 45 % WU, with 10 rollers pump head (fluctuations of 5 mV; no apparent peak periodicity)

Following researchers request in protonic conducting ceramics and SOEC material development, Fiaxell is designing a new testing kit for the Open-Flanges™ Set-Up answering the following targets: 1) Fully made of alumina ceramic to avoid any gas reaction with stainless steel or nickel 2) gas recovery and steam injection on both anode and cathode side 3) easy sealing with special arrangement of Vermiculite material (till 50 kg of weight on the cell edges and few hundred grams/cm² on the electrodes) or standard glass/gold sealing 4) Variable cell size and shape (from 25 mm till 50 mm in diameter) and fixed electrode surface area of 14 mm in diameter. 5) Catalyst assisted gas processing in the fuel feeding tube with temperature control. The kit will be presented in the full paper and available first quarter of 2016.

III. CONCLUSION

The stability of the cell potential with the Open Flanges Set-up and the integrated steamer is influenced by the choice of pump head and the water utilization. With the 3 roller head at 7.5% WU the fluctuation range is only 1 mV, but is increased to 20-25 mV at 45% WU. The use of a 10 roller head produced a fluctuation range five times smaller. The difference with 3 and 10 rollers head is significant, suggesting that the number of rollers is the main factor causing the instability.

IV. FURTHER WORK

The tests were performed using our Fiaxell Pro steamer. Further tests will be done with other version of our steamer, the full ceramic and the easy version.

V. REFERENCES

- [1] G. Rinaldi, S. Diethelm, J. Van herle, Steam and Co-electrolysis Sensitivity Analysis on Ni-YSZ Supported Cells, ECS Transactions, 68 (1) 3395-3406 (2015)



HYBRID SOLID OXIDE FUEL CELLS – GAS TURBINE SYSTEMS FOR COMBINED HEAT AND POWER: A REVIEW

A. Buonomano*, F. Calise*, M. Dentice d'Accadia*, A. Palombo*, M. Vicidomini*

*Department of Industrial Engineering, University of Naples Federico II
P.le Tecchio 80, 80125 – Napoli, (Italy)

Abstract - This paper presents a review of the possible layout of hybrid power plants based on the integration of Solid Oxide Fuel Cells (SOFC) and Gas Turbine (GT) technologies. SOFC/GT plants were investigated by numerical and experimental analyses, thermo-economic optimizations, etc.. Most of such systems are fed by methane converted by an internal reforming process into hydrogen and are based on the pressurized arrangement, showing lower capital costs and higher efficiencies. The steam required to drive the reforming reaction can be supplied by the anode recirculated stream or produced externally, by using the heat of exhaust gases. In this case, steam can be used also for thermal purposes and/or further system hybridization. More complex SOFC/GT configurations, including: IGCC SOFC/GT power plants, ORCs, and also hybrid SOFC/GT plants fed by alternative fuels (coal and biomass) are investigated. Finally an analysis of SOFC/GT control strategies and part-load performance is also presented.

Keywords: CHP, fuel cells, Gas Turbine, Hybrid systems, SOFC.

I. INTRODUCTION

Fuel cell are considered energy conversion systems characterized by low emissions, intrinsic modularity and highly exothermic electrochemical reactions that can be used also in cogeneration purposes (space heating, domestic hot water, steam production, etc.) [1]. High temperature SOFC (up to 1000°C) is the most attractive FC technology for possible hybrid power plants [2], including steam, Organic Rankine and Bryton cycles etc. In this case, theoretical efficiencies up to 70% can be reached [3]. Among such technologies, SOFC/GT plants are the possible candidate for energy conversion of the next future and represent a current interesting research topic. As a consequence, in order to provide a useful guide for system designer and for academia, this work resumes a literature overview of SOFC/GT taking into account layouts classification, control strategy and possible alternative fuels.

II. SOFC/GT LAYOUTS CLASSIFICATION

During last years in the plurality of SOFC/GT configurations aiming at improving the electrical efficiency and to reduce capital costs, type of fuel and steam reforming process, type of Bryton cycle, operating temperature and pressure of the SOFC stack were investigated. The operation of the FC under

atmospheric pressure should be preferred since SOFC is completely independent from the GT, being such subsystems separated by a heat exchanger. On the other hand, lower the electrical efficiencies with respect to the pressurized one (Fig. 1). Here, the SOFC stack acts as a combustor of a Bryton cycle, producing also an additional amount of electricity.

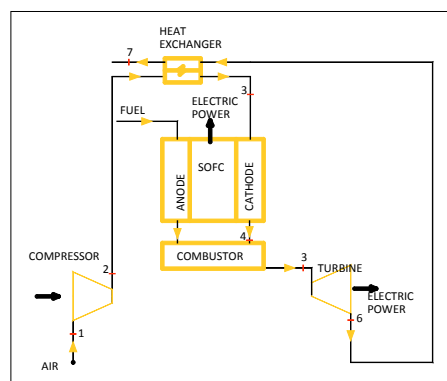


Fig. 1. Hybrid SOFC/GT Bryton cycle [3]

This configuration is cheaper than the atmospheric one, since no expensive heat exchanger is needed. Pressurized configuration is very complex to be designed since the restricted operating domain of pressures and mass flow rates of the GT, further restricts the operating domain of SOFC/GT power plants [4].

III. SOFC/GT PRESSURIZED CYCLES

The classification of pressurized SOFC/GT cycles and their main features and disadvantages are summarized:

Internally reformed SOFC/GT Cycle: this cycle is fed by natural gas, internally reformed inside the SOFC stack; a pre-reformer can be used resulting in an enhanced power production and higher efficiency. The Internal Reforming configuration can be Direct (DIR) or Indirect (IIR). In DIR natural gas is converted into a Hydrogen-rich mixture inside the anode compartment. This is a simpler and lower capital costs configuration than IIR. Anyway in DIR the anode compartment needs a proper catalyst for the Steam Methane Reforming (SMR) reaction and the risk of carbon deposition is possible. In

IIR, SMR reactions occur in a compartment separated by the anode side, which receives the heat required to support the SMR reaction from the FC. Furthermore, another important selection regards the utilization of the exhaust heat, which may be converted or not in steam by a Heat Recovery Steam Generator (HRSG). This steam can be also used to support the reforming process. When no HRSG is used, this required steam can be obtained by an anode recirculation arrangement, achieved through the use of an ejector that uses the steam produced at the anode compartment by the electrochemical reaction to support the internal SMR process. This second option is typically cheaper and more efficient; however, the control of the steam-to-carbon ratio (required to prevent carbon deposition) inside the stack may be less accurate with respect to the HRSG configuration [5].

Externally reformed SOFC/GT Cycle: this cycle is driven by the SOFC exhaust gases and can be fed by more complex types of fuels (biogas, syngas, liquids, etc.), which cannot be safely supplied directly to the SOFC stack. Then, more complex thermal management and higher capital costs are required. Lower efficiency than internally SOFC/GT plants are obtained.

Hybrid SOFC/GT-Steam Turbine: when the temperature of the exhaust stream is sufficiently high to drive an additional bottoming cycle (Rankine cycle) ultra-high efficiency combined systems are obtained. If the heat source temperature is low, water may result inadequate and organic fluids are typically utilized, Organic Rankine Cycle (ORC).

Hybrid SOFC/GT with air recirculation or Exhaust Gas Recirculation (EGR): in the first configuration a Recuperative Heat Exchanger (RHE) preheats the air entering the cathode compartment of the fuel cell, using the exhaust gases from the combustor. Anyway combustor outlet stream is cooled in RHE before entering the GT. This may seriously affect the efficiency of the turbomachinery; in the second configuration part of combustor outlet stream is recirculated to the cathode inlet, increasing the cathode inlet temperature. Anyway when the Turbine Inlet Temperature (TIT) increases, the efficiency decreases more than RHE cycle.

IV. SOFC/GT PLANTS FED BY ALTERNATIVE FUELS (COAL AND BIOMASS)

SOFC can be theoretically fed by a plurality of fuels (hydrogen, methane, ammonia, carbon monoxide, biogas, syngas, methanol, ethanol etc.) other than natural gas. The best candidates are commonly considered the syngas obtainable from biomass gasification [6], in order to include the utilization of a renewable energy source, and coal [7] due to their large availability and their low cost. The most ultra-high efficient coal technology with low environmental impact is probably the Integrated Gasification Combined Cycle (IGCC), which consists in a conventional combined cycle (Bryton +Rankine cycle) fed by the coal syngas produced by gasification.

V. SOFC/GT POWER PLANT: CONTROL STRATEGIES

During part-load operation performance of SOFC/GT plants significantly decreases both due to long start-up and shut down times of SOFC module and to significant decrease of GT efficiency. An efficient control strategy for a SOFC/GT plant is extremely complex since a number of several parameters and constraints (SOFC operating temperature and pressure, fuel utilization factor, TIT, power, temperature gradients, reforming reaction rate) must be simultaneously taken into account. Theoretical and experimental studies showed different control strategies for maximizing the part-load performance of such hybrid systems. An efficient technique, leading to higher part-load efficiencies, consists in reducing both fuel and air flow rates by a reduction of the rotational speed of turbomachinery; instead a simpler strategy may consist in the reduction of fuel and/or air mass flow rates, at constant turbomachinery speed. A schematic flow chart of this complex operating principle of the control strategies is shown in (Fig. 35) in [8].

VI. CONCLUSION

During last years research studies regarding SOFC/GT plants are carried out and the following findings can be summarized:

- Pressurized cycles have higher efficiencies, lower capital cost and more complex management despite of atmospheric cycles;
- Most of SOFC supplied by natural gas use an external steam methane reforming process;
- Control strategies must be carefully designed by avoiding the degradation of part-load performance;
- Very attractive are systems fed by renewable source as gasified biomass and the IGCC power plants fed by coal.

In conclusions, authors recommend to focus the future research on SOFC technologies much more on materials and economically viable fabrication techniques, since the economic profitability of SOFC is not competitive with alternative conventional systems.

REFERENCES

- [1] Analysis of a 1 kW residential combined heating and power system based on solid oxide FC. Applied Thermal Engineering.
- [2] Single-level optimization of a hybrid SOFC GT power plant. Journal of Power Sources.
- [3] SOFC and MCFC: Commonalities and opportunities for integrated research. International Journal of Hydrogen Energy.
- [4] Integrated model framework for the evaluation of an SOFC/GT system as a centralized power source.
- [5] A finite-volume model of a parabolic trough photovoltaic/thermal collector: Energetic and exergetic analyses. Energy.
- [6] Cost modeling approach and economic analysis of biomass gasification integrated solid oxide FC systems.
- [7] Performance evaluation of a direct-biogas SOFC-micro gas turbine (SOFC-MGT) hybrid combined heat and power (CHP) system. Journal of Power Sources.
- [8] Hybrid SOFCs- GT systems for combined heat and power: A review. Applied Energy.

Copyright © 2015



FUEL CELL POWER SYSTEM DESIGN FOR GENERAL AVIATION AIRCRAFT

D. Guida*, M. Minutillo**, and F. Curreri*

*Centro Italiano Ricerche Aerospaziali, Capua, Via Maiorisi, (Italy)

**Università di Napoli Parthenope, Napoli, (Italy)

Abstract – The application of PEM fuel cell technology to the aircraft propulsion and/or to auxiliary energy supply has a great interest for the advantages in terms of pollution emissions, noise reduction and fuel consumptions.

In this paper the sizing procedure for a PEM fuel cell system, designed for aviation applications, is presented. The main requirement of the proposed procedure regards the specific energy that has to allow to the fuel cell system to reach better performance with respect to a battery system.

In order to guarantee fixed climate conditions in which the power system has to work, a containment chamber has been designed to ensure that inside the microclimatic conditions are compliant with the specifics of the off-the-self-components. This study has been conducted in the framework of Long Endurance Demonstrator (LED) project.

Index Terms – PEM Fuel Cell, aviation, electrical motor, Specific energy

I. INTRODUCTION

Many research groups have developed fuel cell-powered aircrafts to demonstrate the possibilities of fuel cells as the new power source alternative to existing batteries in the field of the electric power supply systems [1,2,3]. The main problem that has to be overcome is the energy to mass ratio of the power system that has to be better than that of batteries.

In 2013, CIRA (Italian Research Aerospace Centre) started a research project whose goal was the design of a power system for the electrical motor, to be installed on a general aviation aircraft in the class of AERMACCHI SF 260.

According to the project, LED should guarantee at least 10% endothermic engine maximum power, assumed equal to 220 kW (300hp). The high level requirements are summarized as follows:

- REQ1** LED is a fully electric power system;
- REQ2** LED is a system maximum power of 25 kW
- REQ3** LED has to supply power for 6 hrs
- REQ4** LED operates at an altitude of 3000 m;

REQ5 LED maximum weight must be less than 400 kg

II. DESIGN OF AN ELECTRICAL POWER SYSTEM

A. Battery vs. Fuel cells

The design of an electrical power system must start from the energetic mission profile. Thus, in the choice of the power system it is possible to affirm, in first analysis, that fuel cells are recommended for high energy-consuming missions, while, batteries are more suitable when the mission is characterized by low-energy/high power. Moreover, the specific energy requirement of a fuel cell system must be of 0.35-0.4 kWh/kg, if the system aims to be more competitive than commercial LiPo batteries characterized by a specific energy of 0.2 kWh/kg. Thus, the analysis on a PEM fuel cell system for aviation applications has to be defined in terms of power requirements and mission duration, in order to evaluate if, once assigned a specific mission, the fuel cell power system is better than a battery system.

B. System off-the-self components

A proposed power supply system, designed to operate on an aircraft, must be realized with the components listed in the table 1. Starting from these components, a sizing procedure has been carried out to find the number of fuel cells stacks, model A1000 (the system component that most affects the overall performance), that maximizes the system specific energy for an assigned mission (25 kW for 6 hr); in fact, for a given electric load, the weight of the overall system depends on both the energetic mission profile and on the operating conditions of the power unit (full or partial load of the FC stack). As a consequence:

- the operating current depends on the FC stacks number;
- the H₂ mass flow rate that has to be stored to complete the mission (H₂ storage) depends on the operating current;
- the air mass flow rate and, as a consequence, the size and the number of compressors, depend on the H₂ consumption;

- the operating current influences the cooling requirements and thus the size and the weight of the heat exchangers.

Table 1. Components of a fuel cell power system

Component	Model	Weight [kg]	Power / Energy	Specific power [W/kg]
Fuel Cell (power supply unit)	Horizon A1000	2.5	1 kW	0.4
H2 Tank (storage unit)	TUFFSHELL	21.9 (1.3 H ₂)	44 kWh	-
Air Compressors (for oxidant feeding)	Airsquared, P16H36N3.25 R	6.35	0.16 kW	-
Batteries (auxiliary unit)	Thunder Power 8Ah_4s4p	0.6	2 kW	3.3
Heat exchanger (fuel cell cooling unit)	Titan AIR, H-1-20A-600	30	30 kW	1

The specific energy has been defined as a function of the power, the mission duration and the number of fuel cell stacks:

$$\rho_E = \rho_E(W_{ob}, t_{miss}, N_{STACK})$$

Moreover, the fuel cell performance has been calculated by a numerical model, properly developed by using the Aspen Plus code.

For a mission of 25 kW, with a duration of 6 hr, the specific energy vs. stack number has been plotted in Figure 1.

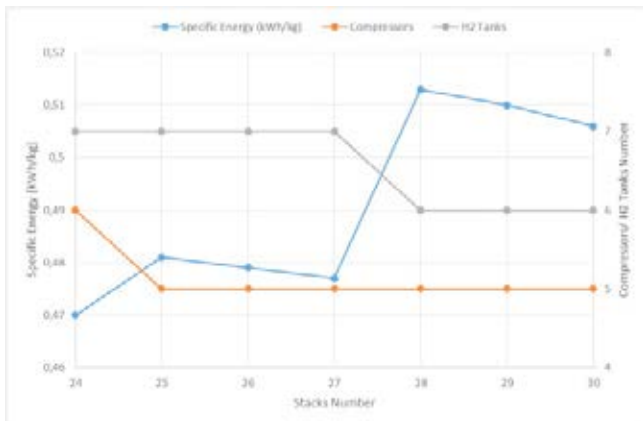


Figure 1. Specific energy, number of hydrogen tanks and number of compressors vs. stacks number

In figure 1, the number of H₂ tanks (blue line) and the number of air compressors (green line) are reported too.

It can be noted that increasing the stacks number from 24 to 25, the specific energy increases because the lowest H₂ consumption (the fuel cell works at lower load with a higher efficiency) implies a lower number of air compressors (from 6 to 5). However, even if the increasing of the stacks number from 25 to 27, causes a further reduction of the mass of H₂ (weight), it is not compensated by the increasing of overall stacks (A1000) weight. As a consequence, the specific energy decreases. Finally, by increasing again the stacks number (27 to 28), not only the H₂ consumption decreases but also the number of hydrogen tanks

(from 7 to 6). This decreasing of the H₂ tanks permits a drastic weight saving (22 kg) with a great increment of the system specific energy (0.51 kWh/kg).

It is important to highlight that the H₂ tank have the greatest influence in terms of weight percentage (table 2).

Table 2. Weight percentage with respect to the system weight

Components	Weight percentage
H ₂ Tank	47 %
Fuel Cells	24 %
Compressors	11 %
Heat exchanger	8 %
H ₂	2 %
Batteries	1 %

C. High level system design

Finally, in order to guarantee fixed climate conditions in accordance with the operation conditions of the selected components (the external conditions are $t=-5\text{ }^{\circ}\text{C}$, $P=0.74\text{ bar}$), it has been chosen to place the power system in a containment chamber as shown in Figure 3.

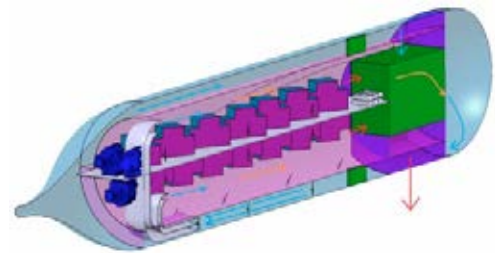


Figure 3. The containment chamber in which the power system is placed

D. Conclusions

In this paper the design of a fuel cell power system, suitable for aeronautical applications, has been reported. In order to increase the specific energy of the whole system, the number of system components has been defined by means of an optimization process. The calculated specific energy results to be equal to 0.51 kWh/kg, with a system that consists of: 28 stacks, 5 air compressors, 6 hydrogen tanks, 6 batteries and 1 heat exchanger. The total weight is 282 kg.

REFERENCES

- T. Kim, S. Kwon, Design and development of a fuel cell-powered small unmanned aircraft, *Int J of Hydrogen Energy*, 2012; 37:615-22
- O. Erdinc, M. Uzunoglu, Recent trends in PEM fuel cell-powered hybrid systems: Investigation of application areas, design architectures and energy management approaches, *Renewable and Sustainable Energy Reviews*, 2010; 14: 2874-84
- G. Romeo, F. Borello, G. Correa, E. Cestino, ENFICA-FC: Design of transport aircraft powered by fuel cell & flight test of zero emission 2-seater aircraft powered by fuel cells fueled by hydrogen, *Int J of Hydrogen Energy*, 2013;38: 469-79



EXO-ELECTROGENIC ACTIVITY OF HYDROCARBONOCLASTIC STRAINS

A. Espinoza***, A. Franzetti**, M. Daghighi**, M. Seeger*

*University Santa María, Av. España 1680, Valparaíso, (Chile)

**University Milano-Bicocca, Piazza Della Scienza 1, Milan, (Italy)

Abstract - Microbial Fuel Cells (MFCs) are a new, innovative technology for bioremediation purposes. In bioremediation, MFCs have been used to achieve the oxidation of organic matter at the anode. Bacterial metabolism can be stimulated in a MFC when an overpotential is applied. The aim of this work was to test the exoelectrogenic capacity of five hydrocarbonoclastic strains of the genera *Cupriavidus* and *Pseudomonas* and to determine if the application of overpotential stimulates the bacterial metabolism. Current density, turbidity and carbon source were monitored. Three of the five strains showed exoelectrogenic activity. Moreover, the application of different overpotentials showed an increase in current production, bacterial growth and substrate consumption.

Index Terms – Microbial Fuel Cells, Exoelectrogenic strains, Hydrocarbon bioremediation

I. INTRODUCTION

Microbial Fuel Cells (MFCs) have been applied firstly in the field of energy production and more recently for bioremediation. MFCs have been applied for bioremediation to achieve the oxidation of organic compounds (e.g. hydrocarbons) at the anode or the reduction of pollutants at the cathode.

Oil spills occur during routine activities such as extraction, refining, transportation and storage, causing damage to ecosystems and living beings. Diverse hydrocarbons are recalcitrant and toxic [1]. Bioremediation is an important technology to clean up water and soils polluted with hydrocarbons. In subsurface hydrocarbon-polluted waters, the lack of final electron acceptors may inhibit bioremediation. In this report, the use of bacteria with catabolic paths of hydrocarbon degradation [2] was analyzed in MFC.

MFC are systems with the capacity to take advantage of the electron flow of bacteria respiratory chain, converting the chemical energy of substrates in electric energy. A MFC has the configuration of an electrochemical cell and is composed by

electrodes (anode and cathode) and electrolyte [3].

MFC have been studied in bioremediation for the bacteria-mediated oxidation of organic compounds at the anode or for the reduction of polluted compounds at the cathode [4].

Bacterial metabolism can also be stimulated in a MFC when overpotential is applied between the anode and the cathode [5].

II. MATERIALS AND METHODS

A. MFCs operation

Experiments were carried out with a set of 350 mL two chambers microaerophilic MFCs. Graphite bars of 0.075 cm² were used as anodes and cathodes. The two chambers were separated by an anion-selective membrane (Membranes International). The cells were filled with 75% v/v Bushnell Haas Broth minimal medium, 22% v/v phosphate buffer, 3% v/v inoculum and supplemented with 16 mM succinate as carbon source. Anodic samples were collected periodically for 42 h for turbidity analysis. Current was measured every 60 s with a Uni-Trend UT60A Digital Multimeter.

B. Bacterial hydrocarbonoclastic strains

Pure cultures of *Cupriavidus metallidurans* CH34 (for BTEX, phenol, phenanthrene, anthracene, naphthalene degradation), *Pseudomonas* sp. DN34 and *Pseudomonas* sp. DN36 (isolated from crude oil-contaminated soil in central Chile for naphthalene, fluorene, and phenanthrene degradation), *Pseudomonas putida* G7 (for naphthalene degradation), *Pseudomonas putida* mt-2 (for toluene degradation) were tested. MFCs were inoculated with a log phase culture of the strain to a final OD₆₀₀ value of 0.6. The MFC with the bacterial cells was operated at 30 °C and agitated (150 rpm) using a magnetic stir bar. The bacterial growth was measured using a spectrophotometer at 600 nm.



C. Metabolism stimulation

Overpotentials were applied with a Tektronix PWS2323 Bench Power Supply. The anode working electrode was polarized to a constant voltage of choice: 200, 400, 600, 800 mV. A control BEC was constructed and was maintained under the same conditions but was not connected to the power supply. An abiotic BEC (without bacterial cells in the anode chamber) was operated under external voltage. Samples for bacterial OD measurements were taken periodically for 42 h and samples for succinate concentration were taken at the beginning and at the end of each experiment (0 and 42 h).

III. RESULTS

The exoelectrogenic capacity of these strains was tested by monitoring growth and current production. Three of the five strains (*Cupriavidus metallidurans* CH34, *Pseudomonas* sp. DN34 and *Pseudomonas* sp. DN36) showed exoelectrogenic activity. Current densities obtained were 0.65, 0.23 and 1.00 mA/m² respectively (Fig. 1). During the 42 h of operation *Cupriavidus metallidurans* CH34 reached an OD₆₀₀ of about 1.10, *Pseudomonas* sp. DN34 of 0.37, *Pseudomonas* sp. DN36 of 0.42 and *Pseudomonas putida* mt-2 of 0.2 (Fig. 2). *Pseudomonas putida* G7 showed no growth.

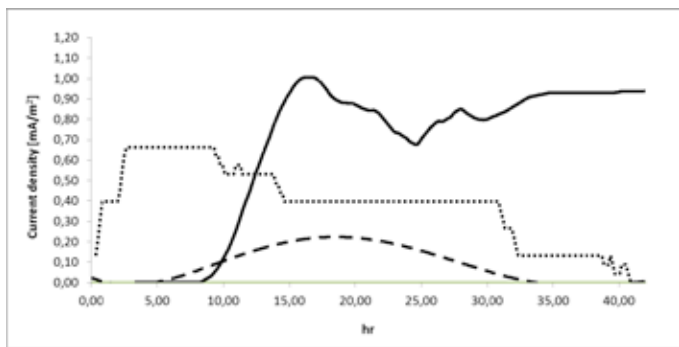


Fig. 1. Current formation in the MFC with *C. metallidurans* CH34 (—), *Pseudomonas* sp. DN34 (···), *Pseudomonas* sp. DN36 (---). No current was observed with *Pseudomonas putida* strains.

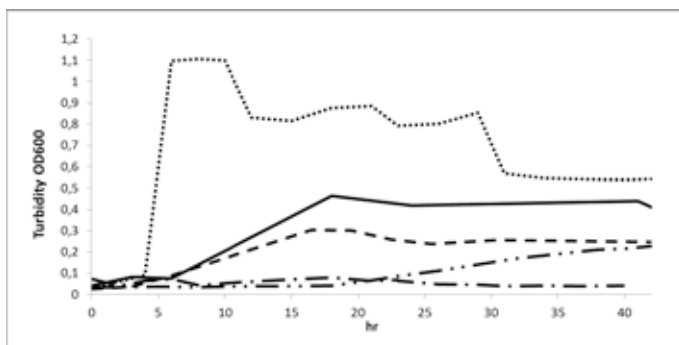


Fig. 2. Growth curve of *C. metallidurans* CH34 (···); *Pseudomonas* sp. DN34 (—), *Pseudomonas* sp. DN36 (---), *Pseudomonas putida* G7 (— · —) and *Pseudomonas putida* mt-2 (— · — · —).

When an external overpotential of 400 mV was applied over the anode in the MFC inoculated with *C. metallidurans* CH34, growth increased in about 20% and succinate removal percentage was 95.2% (while the control MFC without overpotential only reached 91.7% of succinate removal). In the case of *Pseudomonas* sp. DN34 and *Pseudomonas* sp. DN36, the overpotential that showed the most growth increase were 800 mV and 200 mV respectively. Succinate removal in these cases was 48.3% and 91.2% (in comparison with the control MFC where the removal percentages were 35.3% and 89.4% respectively).

IV. CONCLUSIONS

In this study, the exoelectrogenic capacity of hydrocarbon-degrading bacteria in MFC was analyzed. Current densities and turbidity analysis showed that *C. metallidurans* CH34, *Pseudomonas* sp. DN34 and *Pseudomonas* sp. DN36 are exoelectrogens. Moreover, the application of overpotential at the anode showed an increase in growth and succinate removal, showing that microbial metabolism was stimulated. In the future these MFCs will be studied using hydrocarbons as sole carbon and energy sources.

V. ACKNOWLEDGMENTS

The author gratefully acknowledges financial support from PIIC-2014-USM and Chilean CONICYT scholarships.

VI. REFERENCES

- [1] N. Das and P. Chandran, Microbial degradation of petroleum hydrocarbon contaminants: an overview, *Biotechnol. Res. Int.*, Vol. 2011, 2011, p. 941810.
- [2] S. Fuentes, V. Méndez, P. Aguila, and M. Seeger, Bioremediation of petroleum hydrocarbons: catabolic genes, microbial communities, and applications., *Appl. Microbiol. Biotechnol.*, Vol. 98, 2014, pp.4781-4794.
- [3] Santoro, C., Lei, Y., Li, B., & Cristiani, P.. Power generation from wastewater using single chamber microbial fuel cells (MFCs) with platinum-free cathodes and pre-colonized anodes. *Biochemical Engineering Journal*, Vol. 62, 2012, pp.8–16
- [4] Pant, D., Singh, A., Van Bogaert, G., Irving Olsen, S., Singh Nigam, P., Diels, L., & Vanbroekhoven, K., Bioelectrochemical systems (BES) for sustainable energy production and product recovery from organic wastes and industrial wastewaters. *RSC Advances*, Vol. 2 (4), 2012, pp. 1248.
- [5] Thrash, C., & Coates, J., Critical Review Review : Direct and Indirect Electrical Stimulation of Microbial Metabolism, *Environmental Science & Technology*, Vol. 42 (11), 2008, pp. 3921–3931.



ACTIVITIES FOR DEREGULATION AND STANDARDIZATION ON FUEL CELL TECHNOLOGIES

K. Shibata*, N. Hashimoto**

*Japan Electrical Manufacturers' Association, Tokyo, (*Japan*)

**Panasonic Corporation, Osaka (*Japan*)

I. INTRODUCTION

As the introduction of fuel cells is effective for electric security, reduction of environmental burden, diversification of energy supply and promotion of distributed power supplies, such effects possibly brought by their full-scale spread are expected to provide the global environmental preservation, the energy security and, furthermore, the contribution to creation of new industries. The Japan Electrical Manufacturers' Association (JEMA) has been addressing itself to the standardization of fuel cells and the proper deregulation in this regards locating them as the infrastructure establishment project for spread of fuel cells. We report the overview of activities on national standardization in Japan, International standardization on fuel cells, and national scheme of conformity testing and certification on fuel cells (review).

II. STANDARDIZATION AND CERTIFICATION IN JAPAN (JIS, JEM STANDARDS)

Since 2007, following the conducted commissioned by the Ministry of Economy, Trade and Industry of Japan (METI), and New Energy and Industrial Technology Development Organization (NEDO), preparation activities for drafting the Japanese Industrial Standards for fuel cells have been performed.

The standards (including the technical specifications) for terminology and for PAFCs have been effected by the end of 2004. Also for PEFCs, 8 national standards (JIS) have been established in July 20, 2008.

These were prepared, on one hand, based on the examination of the data and test methods acquired by the actual machine tests in the millennium project and, on the other hand, reflecting the discussions in the review process of deregulation, the autonomous safety standards of JEMA and the discussions in the international meetings for standardization. (The

millennium project was a project for establishing the infrastructure for spreading stationary PEFCs and was led mainly by Japan Gas Association commissioned by NEDO.)

The certification committee for stationary Fuel Cells for residential-use was set up in JEMA, because they have to be required certification scheme for safety in case of going on sale from 2009. It has drawn up certification standard based on JIS, and published as "Technical standard and Test method" with grid connection certification by Japan Electrical Safety & Environment Technology Laboratories, JET on Dec.2004. The certification standard has been maintained to reflect each revision of codes and the technical standard. The scope of this certification is less than 10 kW. To be called "ENE-FARM" shall meet this certification.

Furthermore, JEMA has produced JEM Standards/Technical Reports as their private standard on electrical equipment or devices, covering installation, maintenance and recycling without for certification.

III. ACTIVITIES FOR PROPER DEREGULATION

The technical committee for fuel cell power systems, which is composed of the JEMA members, has been conducting activities for promotion of the installation of fuel cells in general and for requesting the deregulations in this regards.

JEMA has been promoting proper deregulation such Electric Utility Industry Law and Fire Protect Law and so on, for diffusion from small size for residential-use to large size for independent-power-use, in cooperation with FCCJ (Fuel Cell Commercialization Conference of Japan) and JGA (Japan Gas Association) and so on.

IV. INTERNATIONAL STANDARDIZATION

JEMA promotes its activities for IEC/TC105 (Technical Committee for fuel cell technologies) in IEC (International



Electrotechnical Commission) being appointed since June 1999 as its national discussion body by the Japanese Industrial Standards Committee (JISC).

Organization and progress of work will be presented.

V. ACKNOWLEDGEMENT

JEMA has pleasure to give special thanks to Ministry of Economy, Trade and Industry, National Land and Transportation Ministry, New Energy and Industrial Technology Development Organization, and National Institute of Advanced Industrial Science and Technology for their jointly supported.



INNO-SOFC - DEVELOPMENT OF INNOVATIVE 50 KW SOFC SYSTEM AND RELATED VALUE CHAIN

O. Himanen*, V. Pulkkinen and J. Kiviaho*

*VTT Technical Research Centre of Finland Ltd.

Abstract - INNO-SOFC project combines leading European SOFC technology companies and research centres to collaborate and form required phases in the SOFC value chain. Within this project a next generation 50 kW SOFC system together with its key components will be developed, manufactured, and validated. This system includes many significant improvements compared to current State of the Art, leading to 30000 hours operating time, 4000 €/kW system costs, 60% electrical efficiency, and 85% total efficiency, which are required for large-scale commercialization of stationary fuel cells.

The project is based on the products of industrial partners (Convion, Energy Matters, Elcogen, and ElringKlinger) and motivated by their interest to further improve their products and consolidate an efficient value chain by collaboration. Research centres (VTT, Forschungszentrum Jülich, and ENEA) support these companies to develop, experimentally validate and demonstrate their products.

Index Terms – SOFC, system, value chain,

I. INTRODUCTION

Solid oxide fuel cell (SOFC) power plants are the most promising distributed stationary power plants towards the goal of decreasing CO₂, SO₂ and NO_x emissions and saving fuel and energy. However, the current SOFC power units on the market have several obstacles hindering competitiveness. The main ones are too high investment cost and insufficient life time. In order to save energy and fuel, electrical and total efficiencies also need to be increased. Minimizing the total cost of ownership also requires minimization of maintenance cost and time. Radical improvements in the SOFC technology to remedy these weaknesses will be achieved in this project. The goal is to make the SOFC units truly competitive on the distributed power market. The main objective of this project is to design, assemble and demonstrate a novel 50 kW SOFC power plant

with significant cost reduction, improved efficiency and longer life-time compared to current SOFC systems.

INNO-SOFC project is based on all-European value chain from component manufacturers to end-users. This project combines innovative and patented process integration solutions by Convion with high-performance low-temperature SOFC stacks by Elcogen. ElringKlinger is a world-leading company in the field of serial-production of high accuracy sheet metal components and in this project they are developing and manufacturing cost optimized interconnect plates for SOFC stacks manufactured by Elcogen. Energy Matters is an energy consultancy company specialized in CHP applications and will analyze different SOFC system applications and provide end-user requirements for the project. VTT, Forschungszentrum Jülich and ENEA will provide their long term experience and scientific know-how for the project to support these companies and especially validate their products.

Project started 1st of September 2015 and has a duration of 30 months.

II. PROJECT PARTNERS

VTT Technical Research Centre of Finland Ltd, coordinator
Convion Oy, Finland, system integrator
Elcogen Oy, Finland, stack manufacturer
ElringKlinger AG, Germany, interconnect manufacturer
Energy Matters, the Netherlands, end-users and applications
Forschungszentrum Jülich, Germany, research centre
ENEA, Italy, research centre

Industrial partners are operating at different phases of the value chain and are not therefore competing against each other. This enables an efficient collaboration and knowledge sharing within



the project. Research centres support these companies to develop, validate and demonstrate their products.

III. PROJECT OBJECTIVES AND APPROACH

The objectives of INNO-SOFC project are:

- Design and manufacture a 50 kW SOFC system with 60% electrical and 85% total efficiency.
- Have a system and components that enables a lifetime of 30000 hours and two years continuous operation without planned shut-downs.
- Achieve at least 30% reduction in system costs (corresponding to < 4000 €/kW).
- Reduce SOFC stack costs to < 2000 €/kW.
- Validation of stack life-time and performance in 10000 hours test.
- Validate system efficiency and life-time according to IEC standards in 3000 hours demonstration.
- Efficient all-European SOFC value chain from component manufacturers to end-users
- Identification of most promising end-users and applications for stationary SOFC systems
- Boost market penetration of stationary fuel cell products and services

Main steps to fulfil these objectives are novel and patented system design, innovative control methods, improvements in key system components and efficient European value chain. High electrical efficiency is achieved by optimizing this novel system design for Elcogen's high performance stacks. Stacks are the most important system component and Elcogen stacks have a state-of-the-art performance enabling above mentioned 60% electrical efficiency at system level. Within this project, Elcogen's stack design and manufacturing methods will be cost-optimized leading to significant cost reductions.

To boost market penetration of stationary SOFC systems, the most promising end-users and applications for SOFC technology are identified. This customer perspective is taken carefully into account by analyzing selected applications, for example greenhouses, where also CO₂ and water are valuable

products. Concept analysis is done for these selected end-user applications, where their requirements are taken into account to analyze profitability and suitability of SOFC power plants with current regulations and cost structures, but also in different future scenarios. Identified key features and requirements (such as regulations, load profile, and available fuel) will be taken into account in system design and validation, leading to a system that is optimized for these most promising applications.

IV. CONCLUSIONS

Leading European SOFC technology companies and research centres work together in INNO-SOFC project. This collaboration forms required phases in the complete SOFC value chain. INNO-SOFC focuses on the development, manufacturing, and validation of a state-of-the-art 50 kW SOFC system and its key components. The project is based on the products of industrial partners and motivated by their interest to further improve their products and consolidate an efficient value chain by collaboration. Industrial partners are operating at different phases of the value chain and are not therefore competing against each other. This enables an efficient knowledge sharing within the project. Industrial partners can optimize their products towards a common goal, which is to create a SOFC system that fulfils and exceeds end user's technical and cost targets.

ACKNOWLEDGMENT

This project has received funding from the Fuel Cells and Hydrogen 2 Joint Undertaking under grant agreement No 671403. This Joint Undertaking receives support from the European Union's Horizon 2020 research and innovation programme and Finland, Germany, Italy, and the Netherlands.



EFC15311

ARTIFICIAL NEURAL NETWORK MODEL FOR WATER GAS SHIFT REACTION IN A DENSE Pd-Ag MEMBRANE REACTOR

G. Bagnato*, S. Liguori**, A. Iulianelli*, S. Curcio***, A. Basile*

* Institute on Membrane Technology of Italian National Research Council (ITM-CNR), c/o University of Calabria Cubo 17/C, Rende (CS) – 87036, Italy.

** Dpt. of Energy Resources Engineering, Stanford University, 367 Panama Street Green Earth Sciences, Stanford, CA 94305-2220 - USA

*** Dpt. of Computer Eng., Modeling, Electronics and Systems, University. of Calabria Cubo 39/C, Rende (CS) – 87036, Italy.

Abstract – The water gas shift reaction was studied in membrane reactors for training an artificial neural network model. In particular, we have lead experiment varying many parameters as the reaction pressure, reaction temperature, gas hourly space velocity, sweep gas flow rate, H₂O/CO feed molar ratio and feed configuration have been considered from both a modelling and an experimental point of view in order to analyze their influence on the water gas shift performance in two membrane reactors. Meanwhile, the artificial neural network model has been validated by using experimental tests as training results and it was validated whit a new data set, obtained optimizing the system to achieve as much as possible high hydrogen recovery.

The model predicted the experimental performance of the water gas shift membrane reactors with an error on CO conversion lower than 0.5% and around 10% for the H₂ recovery.

Index Terms - artificial neural network, water gas shift, membrane reactor, pure hydrogen.

I. INTRODUCTION

In this pioneeristic study, we developed an Artificial Neural Networks (ANNs) model to predict the results of the WGS reaction carried out in a dense Pd-Ag MR by varying some operating conditions, with successive experimental validation. Any transport equations is used in the ANN model, helping in determining, the mutual relationships existing between the inputs and the outputs, based on fundamental principles [1-3]. ANNs are constituted of different simple interconnected computational elements, namely neurons, operating in parallel. They are inspired to biological nervous system,

reproducing some of its functions.

II. EXPERIMENTAL

The experimental results collected according to the above-described procedure are exploited to develop an ANN model aimed at identifying the non-linear relationships between the CO conversion, the H₂ recovery and composition in the permeate side and the process or operating variables, namely the transmembrane pressure from 150 to 300 kPa, the reaction temperature from 300 to 360 °C, GHSV between 2000 and 6000 h⁻¹, sweep gas flow rate (N₂) between 35.75 and 130.42 mL/min, H₂O/CO feed molar ratio from 1/1 to 4.5/1, the active membrane surface area (M1 = 15.71 cm² and M2 = 45.55 cm²) and the feed configuration (co- or counter-current with respect to the sweep gas). The available experimental data corresponded to 150 experimental tests, each of them composed of three MR performance indexes. The resulting structure of the developed neural network consisted of an input layer with 8 neurons, a first hidden layer with 20 neurons and an output layer comprising 3 neurons, Fig. 1.

III. RESULTS AND DISCUSSION

A. Influence of temperature

WGS reaction was performed in the MR at GHSV = 3340 h⁻¹, reaction pressure between 150 and 300 kPa, H₂O/CO = 3/1 and a N₂ feed composition equal to 0.257. Furthermore, the sweep gas was kept constant at 35.75 mL/min, using the membrane M2 in co-current



configuration.

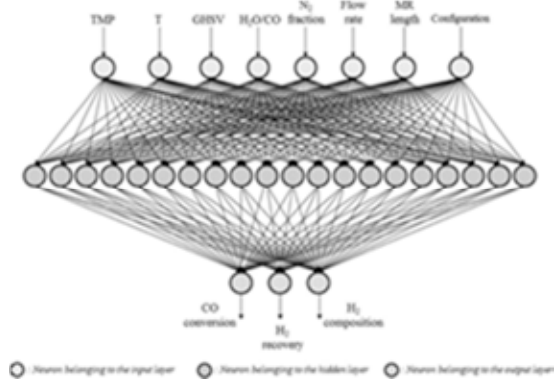


Fig. 1. Scheme of the ANNs model.

The temperature encourages the reaction kinetics and the hydrogen permeability through the membrane. Indeed, we obtained a higher H₂ recovery and CO conversion at the maximum temperature investigated (Figs. 2 and 3).

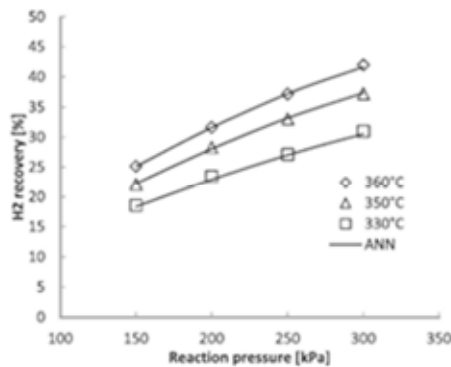


Fig. 2. H₂ recovery vs reaction pressure.

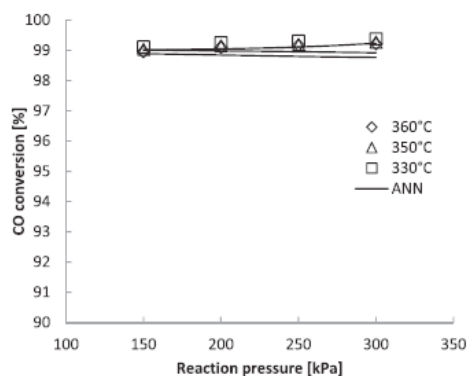


Fig. 3. CO conversion vs reaction pressure.

B. Experimental validation

We developed a neural model, capable of providing very accurate predictions of MR performance. Hence, we decided of using a set of operating conditions for achieving the maximum H₂ recovery in the range of operating conditions investigated.

The MR performance indexes obtained from the optimization were also verified experimentally under the same operating conditions. Then, the results, reported in TABLE I, show that the maximum deviation was reached in predicting the hydrogen recovery (> 10%).

TABLE I. EXPERIMENTAL VALIDATION

	ANN	Exp.	Error [%]
CO conversion [%]	99.91	99.52	0.39
H ₂ recovery [%]	85.53	76.73	10.34
H ₂ composition permeate [%]	6.65	7.18	7.91

IV. CONCLUSION

WGS reaction in MRs was simulated by a ANN model, previously trained by experimental.

In the aforementioned experimental conditions, the ANN model was validated and, then, it was used by means of an optimization algorithm to predict the best operating conditions to maximize the H₂ recovery. During the ANN model training, the error within the experimental results and the theoretical predictions ranged between 0.1 and 3. Otherwise, when the ANN model was used to optimize the H₂ recovery during WGS reaction in the MRs, the error within the experimental points and the predictions was around 10%, while it was lower than 0.5% for CO conversion.

ACKNOWLEDGMENT

The authors are grateful to the Italian Ministry of Economical Development (MISE) (Grant n. 00019EE01) for the financial support received for this research developed under MICROGEN30 project (Bando di Innovazione Industriale "Efficienza Energetica" (D.M. 05 Marzo 2008) - Codice Domanda n. EE01_00013).

REFERENCES

- [1] Reilly DL, Cooper LN. An overview of neural networks: early models to real world systems. In: Zornetzer SF, Davis JL, Lau C, editors. An introduction to neural and electronic networks. New York: Academic Press; 1990.
- [2] Curcio S, Scilingo G, Calabrò V, Iorio G. Ultrafiltration of BSA in pulsating conditions: an artificial neural networks approach. *J. Membrane Sci.*, 47 (2005) 235-246.
- [3] Moissev SN. Universal derivative-free optimization method with quadratic convergence. 2011. arXiv:1102.1347v1. *el cells, J. Power Sou.*, 273 (2015) 25-32. Li, X., Ogden, J., Yang, C, Analysis of the design and economics of molten carbonate fuel cell tri-generation systems providing heat and power for commercial buildings and H₂ for FC vehicles, *Journal of Power Sources*, Volume 241, 2015, Pages 668-679/1892, pp. 68-73.



FABRICATION & PERFORMANCE STUDY OF Pd-Au PSS SUPPORTED MEMBRANE REACTOR VIA STEAM METHANE REFORMING

B. Anzelmo*, S. Liguori*, A. Iulianelli**, A. Basile**, J. Wilcox*

*Department of Energy Resources Engineering, Stanford University, California (USA)

**ITM-CNR, Cubo 17/C, University of Calabria, Rende (CS) 87036 – (Italy)

Abstract –The mobility of hydrogen as a fuel source is paramount and if the intent in the future is to provide a clean, sustainable mobile fuel source the required production of hydrogen will need to increase. The primary industrial process for hydrogen production is natural gas reforming. It is a multi-step process in which the steam methane reforming (SMR) takes place in harsh conditions (800-1000°C and 15-20 bar) followed by two water gas shift reactors and accompanied by separation/purification steps for producing highly pure hydrogen. A Pd-based membrane reactor has the ability to replace this multi-step process providing of both the production and separation of hydrogen in only one tool.

However, the composition of natural gas for (SMR) can vary widely from source to source, but each source contains some traces of hydrogen sulfide (H₂S). This chemical compound can damage the pure Pd membrane and, consequently, can affect the overall performance of membrane reactor. Nevertheless, it has been shown that alloying the Pd membrane with another metal, namely Au, Ag, Pt or Cu provides resistance to sulfur contamination. Therefore, in this study, a Pd-Au membrane supported on porous stainless steel was fabricated to produce a pure hydrogen stream by natural gas steam reforming reaction.

Index Terms - composite membrane, hydrogen production, membrane reactor, palladium alloy

I. INTRODUCTION

One possible use for hydrogen, without direct greenhouse gas emissions, is as feed for a fuel cell (FC), with the most readily available technology being a proton exchange membrane FC (PEMFC). In order to avoid the poison of PEMFC's Pt-based catalyst due to the presence of ppm levels of CO, the hydrogen feed needs to be ultra-pure. The industrial process for hydrogen production, which is a multi-step energy intensive process followed by further separation/purification, can be a potential source [1]. However, as an alternative

method a Pd-based membrane reactor (MR) can be used owing to its ability to provide the pure hydrogen without any further purification. Moreover, the MR works at milder operating conditions compared to the traditional system.

In the last years, Pd-based composite membranes, i.e. thin metallic layer supported on such porous materials as ceramics or stainless steel, have been considered owing to their lower cost (thin Pd layer) and higher mechanical resistant (porous support) than dense Pd-based ones [2]. Moreover, the use of Pd-alloys, in particular, with Ag, Au, Pt, is grown in the last years given their ability to resist sulfur poisoning and increase the hydrogen permeability [3].

Therefore, the aim of this study is to fabricate a Pd-Au membrane supported on porous stainless steel (PSS) with the intent to produce pure hydrogen from natural gas steam reforming.

II. MEMBRANE FABRICATION

The membrane in this study was fabricated via a electroless plating technique for depositing Pd and electroplating for Au. The steps for fabricating this membrane are described in the followings: 1) oxidation of the initial support at 500 °C 2) abrasive sanding to obtain a smooth surface 3) grading of support with Pd activated Al₂O₃ particles 4) electroless plating of Pd 5) final electroplating of Au [4-8].

Each fabrication step provides a benefit relating to pore size reduction, which mitigates the defects of the support. Moreover, the grading layer of Pd activated Al₂O₃ particles not only mitigates pore size but provides an intermediate layer that limits the intermetallic discussion. This multistep process allowed for realizing a membrane characterized by a Pd-Au layer of 6.8µm with 7 wt% of Au content (Fig. 1).



Fig. 1. Fabrication Steps: [A] Initial support [B] Oxidation at 500°C [C] Grading [D] Final Pd-Au metallic layer

III. EXPERIMENTAL

The experimental plant used for carrying out the experimental measurements consists of: Brooks instruments 5850S mass-flow controllers, which regulate the gas feed flow rates; membrane module and on-line gas chromatograph (HP 6890 GC) for the gases analysis.

The steam reforming reaction will be carried out with methane and performed in a Pd-Au/PSS composite MR. In particular, the composite membrane consists of a thin Pd-Au layer deposited onto a PSS tubular support which is joined to two stainless steel tubes for the membrane housing, one of which is closed. The active area of the Pd-Au/PSS membrane is about 30.8 cm².

The Pd-Au/PSS membrane is heated up in a nitrogen atmosphere and the final temperature is kept constant at 450 °C. The pressure in the retentate side is varied from 1.5 to 3.0 bar by means of a back pressure placed at the outlet side, while the pressure in the permeate side is kept constant at 1.0 bar without using any sweep gas.

IV. RESULTS AND DISCUSSION

During the fabrication, permeation tests with pure He are carried out, at room temperature and 1 bar as pressure difference at each step. Fig. 2 shows the results of the permeation tests in which it is evident the progression and decline of He flux during the membrane fabrication process.

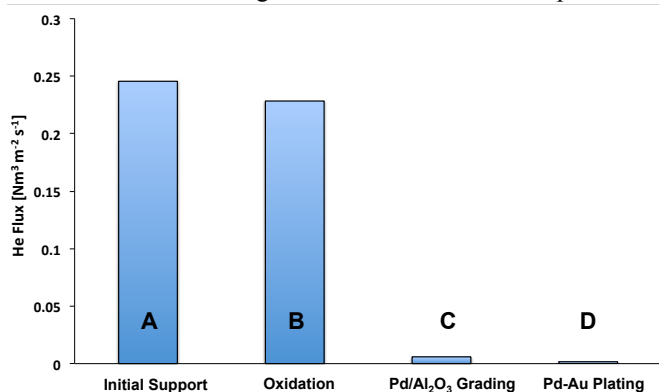


Fig. 2. He permeating flux during membrane progress ($\Delta P = 1\text{ bar}$, $T = 25^\circ\text{C}$)

The initial characterization of the membrane by way of ideal selectivity took place at 400°C with H₂, He and N₂ and ΔP in the range of 1.5 - 3.0 bar. After ideal selectivity characterization of the Pd-Au/PSS membrane, SMR reaction will be carried out and the MR performance in terms of CH₄ conversion and hydrogen production will be analyzed and discussed.

ACKNOWLEDGMENT

The authors would like to thank Prof Yi-Hua (Ed) Ma and Prof Ivan Mardilovich as well as the Worcester Polytechnic Institute's Center for Inorganic Membrane Studies.

REFERENCES

- [1] Rostrup-Nielsen, J.R., *Catalytic steam reforming*. 1984: Springer.
- [2] Liguori, S., et al., *Performance of a Pd/PSS membrane reactor to produce high purity hydrogen via WGS reaction*. *Catalysis Today*, 2012. 193(1): p. 87-94.
- [3] Chen, C.-H. and Y.H. Ma, *The effect of H₂S on the performance of Pd and Pd/Au composite membrane*. *Journal of Membrane Science*, 2010. 362(1-2): p. 535-544.
- [4] Ma, Y.H. and I.P. Mardilovich, *Composite structures with porous anodic oxide layers and methods of fabrication*, 2013, Google Patents.
- [5] Ma, Y.H., I.P. Mardilovich, and E.E. Engwall, *Thin composite palladium and palladium/alloy membranes for hydrogen separation*. *Annals of the New York Academy of Sciences*, 2003. 984(1): p. 346-360.
- [6] Ma, Y.H., I.P. Mardilovich, and E.E. Engwall, *Method for curing defects in the fabrication of a composite gas separation module*, 2007, Google Patents.
- [7] Ma, Y.H., I.P. Mardilovich, and E.E. Engwall, *Composite gas separation modules having high Tamman temperature intermediate layers*, 2007, Google Patents.
- [8] Ma, Y.H., I.P. Mardilovich, and E.E. Engwall, *Composite gas separation modules having intermediate porous metal layers*, 2007, Google Patents.



EFC15313

MICROBIAL DESALINATION CELLS: WASTEWATER TREATMENT COUPLED TO FRESHWATER PRODUCTION

Juan M. Ortiz*, Zulema Borjas*, F Rogalla**, and
A. Esteve-Nuñez*,***

* IMDEA Water C/Punto Net, 4, Parque científico tecnológico de la
Universidad de Alcalá, 28805, Alcalá de Henares, Madrid (Spain)

** FCC Aqualia, gestión integral del agua, S.A. Avenida del Camino de
Santiago, 40, , 28050 Madrid (Spain)

*** Departamento de Química, Universidad de Alcalá, , 28805, Alcalá de
Henares, Madrid (Spain)

Abstract - The aim of this communication is to demonstrate the technical feasibility of using a microbial desalination cell (MDC) for brackish water desalination using a real wastewater a fuel. By using this system, two simultaneous objectives are achieved: i) conversion of wastewater into electricity, and ii) production of drinking water from brackish water. The performance of the system is mainly affected by the concentration of organic matter in the wastewater stream as well as the initial and final conductivity of the brackish water used as inlet medium. The configuration of the MDC and the cathode reaction are parameters that should also be taken into consideration for a potential full-scale application of the system. In addition, some considerations related to the electrochemical design of the reactor are presented in order to achieve the scaling-up for real-scale applications.

Index Terms - Microbial desalination cell; electro dialysis; bio-electrochemistry, Microbial Fuel Cell

I. INTRODUCTION

A Microbial Desalination Cell (MDC) is a bio-electrochemical device where wastewater biological treatment can be effectively coupled to desalination of a saline stream. A MDC consists in an electro dialysis unit cell placed in a microbial fuel cell (MFC), in which at least one of the electrodes, usually the

anode, hosts a biofilm where the electrochemical oxidation of the dissolved organic matter takes place. By using the electric potential generated in the electrodes, the migration of the ions is produced and, therefore, the desalination occurs (Cao et al., 2009). By using wastewater as influent, we achieved simultaneous desalination of brackish water (see figure 1) and wastewater treatment without energy consumption (excluding energy needed for pumping).

II. EXTENDED ABSTRACT PREPARATION

A. Material and Methods

The MDC setup was a three chamber electrochemical reactor manufactured by ECELL (collector area 100 cm², compartment length: 12 mm). The anodic chamber was filled with carbon felt RVC 4000 (Mersen Ltd) and a graphite plate is used as electric current collector. The anodic chamber was inoculated with batch cultures of *G. sulfurreducens* (Fresh Water Medium, mineral mix, vitamin solution, 10 mM Acetate, 40 mM Fumarate, fluxed with oxygen-free N₂/CO₂ -80/20, v/v- at 30° C). Real waste water was used as inlet fuel for the anodic compartment. A graphite plate was used as cathode, and a turbulence promoter was located inside the cathodic chamber. Fe³⁺ reduction in acidic media was used as cathode reaction.



The ion exchange membranes were ion exchange conventional membranes, AMX (anionic) and CMX (cationic) from Astom Corporation (Japan). Two reference electrodes (Ag/AgCl KCl 3.5 M) were placed in the geometric center of the anodic and cathodic compartments in order to measure anode and cathode potentials. The system was operated in batch mode.

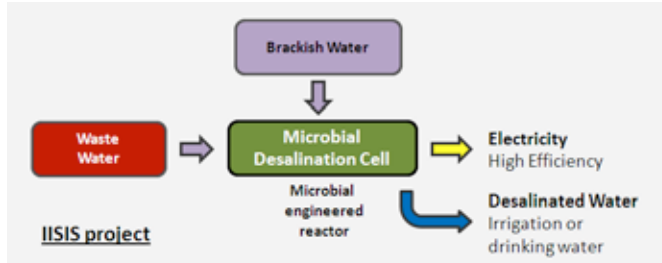


Fig 1. Scheme of the MDC system fed with wastewater as fuel

Results and Conclusions

Table 1 shows the results obtained with the MDC system under different experimental conditions. As it is noted below, the production of desalinated water depends on both i) the value of the external resistor and ii) the conductivity of the brackish water used as influent.

Table 1 MDC experimental results

Id.	Volume Anolyte/Catolyte / Saline Tanks (L)	Saline compartment length (mm)	Initial / Final Conductivity (mS/cm 25 °C)	Ext. resistor (Ohm)	Energy produced (Wh/m ²)	Desalination time (h)/ Water production (m ³ /day m ²)
1	10 / 10 / 2	12	4 - 0.5	0	0	18.2 - 0.27
2	10 / 10 / 2	6	4 - 0.5	0	0	11.0 - 0.43
3	10 / 10 / 2	6	8 - 0.5	0	0	17.6 - 0.27
4	10 / 10 / 2	6	4 - 0.5	2	52.7	15.0 - 0.32
5	10 / 10 / 2	6	8 - 0.5	2	137.8	24.5 - 0.18
6	10 / 10 / 1	6	20 - 0.5	2	213.8	28.3 - 0.08

Our results revealed that water desalination was feasible under the tested condition. However, the main limitations of MDC systems were: (a) the increase of the overall internal resistance when desalination was achieved, and (b) the low electric potential available to force ion migration. Therefore, scaling-up MDC systems requires to design parameters for minimizing internal resistance and selecting a cathode reaction able to maximize electric current in a sustainable way.

REFERENCES

- [1] Cao, X., Huang, X., Liang, P., Xiao, K., Zhou, Y., Zhan, X. and Logan, B.E. (2009), A New Method for Water Desalination Using Microbial Desalination Cells, In *Environmental Science & Technology*, 43, 7148–7152.
- [2] Luo, H., Jenkins, P. E. and Ren, Z. (2011), Concurrent Desalination and Hydrogen Generation Using Microbial Electrolysis and Desalination Cells, In *Environmental Science & Technology*, 45, 340–344.



DYNAMIC SIMULATION AND ENERGETIC-ECONOMIC ANALYSIS OF A POLYGENERATION SYSTEM BASED ON PEM FUEL CELLS AND CONCENTRATED PHOTOVOLTAIC-THERMAL COLLECTORS

Calise F. *, Figaj R. D. **, Massarotti N. **, Mauro A. **, Vanoli L. **

*Dipartimento di Ingegneria Industriale, Università di Napoli Federico II, P.le Tecchio 80, 80125, Napoli, Italy

**Dipartimento di Ingegneria, Università di Napoli "Parthenope", Centro Direzionale Isola C4, Napoli, Italy

Abstract - This paper presents a dynamic simulation model and an energetic-economic analysis of a novel polygeneration system based on PEM fuel cells, Concentrated PhotoVoltaic-Thermal collectors (CPVT) and single-stage LiBr&H₂O absorption chiller technologies. The electric energy produced by both CPVT system and PEM fuel cell is used by the user and exchanged with the grid by means of a net metering contract. Domestic hot water is produced in case of low space heating/cooling demand. The system has been designed and dynamically simulated using TRNSYS software, including a tool for the dynamic building simulation. Different time bases are used in order to present energetic, environmental and economic performance data. The energetic and economic analysis show that the system produces a significant energy saving and it can be profitable in case of a capital investment incentive.

Index Terms - PEMFC fuel cell, CPVT, solar heating and cooling, building

I. INTRODUCTION

In recent years, the interest in polygenerative systems with application of PEM fuel cell or solar technologies has grown. In particular, such technologies represent a viable option for meeting the electrical and thermal demand of buildings [1, 2]. The analysis of the available literature has shown a scarce investigation of systems employing PEM fuel cells coupled with solar technologies, in particular with the cogenerative solar ones. Moreover, no papers have been found investigating the integration of PEM fuel cell systems with CPVT in building applications. The aim of this paper is to increase the knowledge on this topic presenting a dynamic model of a polygenerative system based on PEMFC and CPVT technologies.

II. THE PROPOSED SYSTEM

The system layout is reported in Fig. 1, where the combination of SC and PEM fuel cells technologies is shown.

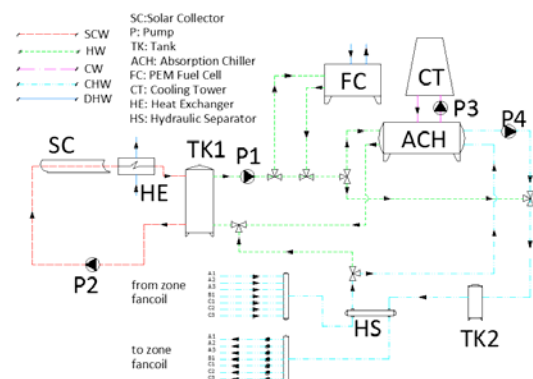


Fig. 1. Simplified layout of the proposed system

The proposed system provides space heating during winter and space cooling during summer. Moreover, electricity and domestic hot water are produced all over the year. In particular, the present system layout has been obtained modifying the one presented in a previous work [3] in order to implement the CPVT collectors (peak power of 130 kW_{th} and 50 kW_{el}). In this layout, the additional heat needed in case of scarce solar irradiation is supplied by the cogenerative fuel cell. The utilization of the fuel cell thermal energy is maximized because only a part of the maximum heating/cooling load of the building is satisfied by CPVT collectors. Furthermore, the proper operation of the absorption chiller is ensured by the



operating temperatures of the in series arrangement of CPVT and PEMFC (350 kW_{el} nominal power).

The system is made by several loops: Solar Collector Water (SCW), Hot Water (HW), Cooling Water (CW), Domestic Hot Water (DHW) and Chilled/Hot Water (CHW). The system is equipped with a complex control system able to manage all the components, whose basic operating principle is reported in [3].

III. RESULTS

The proposed system has been dynamically simulated in TRNSYS, by using both build-in and user defined components. The energetic-economic models and the building structure has been taken from [2, 3]. The electric energy purchasing/selling price has been updated referring to [4]. The main design parameters of the polygeneration system has been taken from [3], and integrated with the CPVT parameters from [2]. In particular, the solar field area considered is equal to 300 m².

The simulations have been performed for one year operation. Temperature and energy dynamic profiles have been analyzed. The weekly variation of the most important energy performance parameters during the year are reported in Fig. 2.

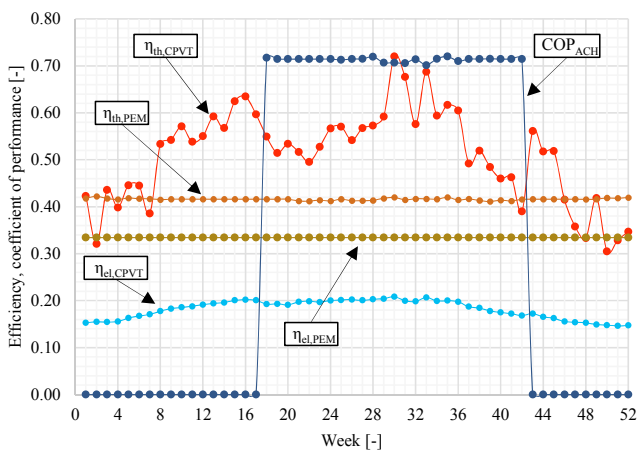


Fig. 2. Weekly efficiency and coefficient of performance

where η_{th} and η_{el} are the thermal and electrical efficiency, respectively, and COP is the Coefficient Of Performance. The results show a constant operation of the fuel cell during the year. Only a slight variation of η_{th} is observed due to the variation of the CPVT thermal energy production. The results outline also a CPVT better efficiency (calculated with respect to the beam radiation) in summer period due to the higher beam radiation with respect to winter. Moreover, the operation of the adsorption chiller is stable due to the control of hot side supply temperature.

The main yearly results obtained with an annual integration are presented in Table I, showing that the thermal and electrical energies (E_{th} , E_{el}) produced by the CPVT collectors are definitely marginal with respect to those produced by the PEM fuel cell.

Table I. Yearly simulation results

Parameter	Value	Unit	Parameter	Value	Unit
$E_{th,CPVT}$	1.41E+05	kWh	$\eta_{el,CPVT}$	0.182	-
$E_{el,CPVT}$	4.89E+04	kWh	$\eta_{th,PEM}$	0.416	-
$E_{th,PEM}$	1.18E+06	kWh	$\eta_{el,PEM}$	0.334	-
$E_{el,PEM}$	9.50E+05	kWh	COP _{ACH}	0.713	-
$E_{th,DHW}$	9.25E+05	kWh	SPB	15.4	year
$\eta_{th,CPVT}$	0.510	-	SPB 50%	7.10	year

This occurs because: i) the solar collectors field has been designed in order to satisfy only a part of the cooling demand; ii) the CPVT collectors have a scarce performance during winter season. Moreover, the DHW production is mainly due to the PEM cogenerative heat exchanger, in particular only about 5% of DHW production is due to solar thermal energy. Furthermore, the CPVT thermal efficiency, calculated with respect to the beam radiation, is over 50%. This is due to low set point temperatures of the CPVT collectors (50 and 90°C in winter and summer, respectively). For this reason, the CPVT electrical efficiency is around 20%. The fuel cell global efficiency is high (85%) and the COP of the absorption chiller is about the nominal one. The capital investment of about 1.1M€ has been obtained by the economic analysis. This value, combined with the reference system cost of 80 k€ and a saving of 68 k€/year, determines a Simple Pay Back (SPB) period of about 15 years, without funding. If a 50% capital investment subsidy for the proposed system is considered, a SPB period of 7 years can be achieved.

IV. CONCLUSIONS

A novel polygeneration system based on PEM fuel cells, CPVT collectors and absorption chiller technologies has been studied. SPB with and without incentives has been determined in 15 and 7 years, respectively. Future developments of this work include parametric analysis and optimization process.

ACKNOWLEDGMENTS

The authors gratefully acknowledge the financial support of Project PON01_2864, FC SMARTGEN R&C 2007-2013 “Fuel Cell and SMART Hybrid GENeration from fossil and renewable sources”

REFERENCES

- [1] Ham, SW., Jo, SY., Dong, HW., Jeong, JW., A simplified PEM fuel cell model for building cogeneration applications, Energy and Buildings, Volume 107, 2015, Pages 213-225.
- [2] Buonomano, A., Calise, F., Ferruzzi, G., Vanoli, L., A novel renewable polygeneration system for hospital buildings: Design, simulation and thermo-economic optimization, Applied Thermal Engineering, Volume 67, 2014, Pages 43-60.
- [3] Calise, F., Ferruzzi, G., Vanoli, L., Transient simulation of polygeneration systems based on PEM fuel cells and solar heating and cooling technologies, Energy, Volume 41, 2012, Pages 18-30
- [4] www.autorita.energia.it - July 2015





CONTENTS

AB. CODE	AUTHOR	PAGE
EFC15006	Jarosław Milewski	17
EFC15009	Valentina Zaccaria	19
EFC15013	Ioan Ioardache	21
EFC15018	Mike Musil	23
EFC15021	Dhruba Panthi	25
EFC15022	Kenichiro Ota	27
EFC15023	Tancredi Chinese	29
EFC15025	Nils Kleinohl	31
EFC15026	Giacomo Falcucci	33
EFC15029	Maren Rastedt	35
EFC15031	Daria Vladikova	37
EFC15032	Sergey Grigoriev	39
EFC15036	Rodolfo Taccani	41
EFC15037	Antonino Salvatore Aricò	43
EFC15038	Antonino Salvatore Aricò	45
EFC15040	Christian Beauger	47
EFC15041	Coz Erwan	49
EFC15043	Lorenzo Lipardi	51
EFC15045	Andreas Friedrich K.	53
EFC15048	Grazia Accardo	55
EFC15049	Domenico Frattini	57
EFC15050	Grazia Accardo	59
EFC15051	Sophie Didierjean	61
EFC15058	Alessandra Perna	63
EFC15059	Filippo Radunanza	65
EFC15060	Ramon Atochero Velasco	67
EFC15062	Vincenzo Liso	69
EFC15067	Mélanie Rolland	71
EFC15069	Fabian Grueger	73
EFC15070	Haluk Beyenal	75
EFC15071	Domenico Frattini	77
EFC15072	Yuan Tan	79
EFC15073	Ao Wang	81
EFC15074	Michel Cassir	83
EFC15075	Marta Gandiglio	85
EFC15076	Davide Papurello	87
EFC15077	Andrea Lanzini	89
EFC15078	Andrea Baricci	91
EFC15079	Gaetano Squadrito	93
EFC15080	Matteo Zago	95
EFC15082	Alessandra Palella	97
EFC15083	Alessandra Palella	99
EFC15084	Claudio Rabissi	101
EFC15085	Carmelo Lo Vecchio	103
EFC15086	Thomas Gaumont	105
EFC15087	Andreas Lindermeir	107

EFC15088	Christoph Immisch	109
EFC15089	Sami Tuomi	111
EFC15090	Eugenio Rovera	113
EFC15091	Luca Spiridigliozzi	115
EFC15092	Luca Spiridigliozzi	117
EFC15093	Luca Spiridigliozzi	119
EFC15094	Panagiotis Tsiakaras	121
EFC15095	Sven Kerzenmacher	123
EFC15100	Iwona Gadja	125
EFC15104	Vitaliano Chiodo	127
EFC15105	Matteo Grattieri	129
EFC15107	Francesca Santoni	131
EFC15108	Behzad Najafi	133
EFC15109	Francesca Pizza	135
EFC15111	Edoardo Guerrini	137
EFC15112	Gerard Mathias	139
EFC15115	Andrea Bisello	141
EFC15117	Alessandra Colombo	143
EFC15118	Roberta Cristofaro	145
EFC15119	Domenico Ferrero	147
EFC15120	Selma Aparecida Venancio	149
EFC15122	Andrea Franzetti	151
EFC15125	Domenico Frattini	153
EFC15127	Giulia Botta	155
EFC15129	Li Kang Yee	157
EFC15130	Sanggyu Kang	159
EFC15131	Vladimir Linkov	161
EFC15132	Davide Chianese	163
EFC15133	Giulio Guandalini	165
EFC15135	Daniela Barba	167
EFC15136	Giovanni Cinti	169
EFC15138	Kohei Nakashima	171
EFC15139	Linda Barelli	173
EFC15140	Concetta Ruocco	175
EFC15141	Antonio Ricca	177
EFC15142	Antonio Ricca	179
EFC15143	Bernd Cermenek	181
EFC15144	Alessandro Donazzi	183
EFC15145	Ivan Pivac	185
EFC15147	Concetta Ruocco	187
EFC15148	Francisco Elizalde	189
EFC15149	Rafal Bernat	191
EFC15151	Henrik Lund Frandsen	193
EFC15152	Marta Boaro	195
EFC15153	Sathish-kumar Kamaraj	197
EFC15154	Sathish-kumar Kamaraj	199
EFC15155	Ludwig Jörissen	201
EFC15156	Ludwig Jörissen	203

EFC15159	Panagiotis Tsiakaras	205
EFC15160	Panagiotis Tsiakaras	207
EFC15161	Panagiotis Tsiakaras	209
EFC15163	Panagiotis Tsiakaras	211
EFC15164	Marjan Bele	213
EFC15166	Stanko Hocevar	215
EFC15167	Luigi Crema	217
EFC15168	Gu Young Cho	219
EFC15170	Nathalie Monnerie	221
EFC15172	Panagiotis Tsiakaras	223
EFC15173	Andrej Lotrič	225
EFC15176	Taehyun Park	227
EFC15183	Saverio Latorrata	229
EFC15185	Giulio Cordaro	231
EFC15186	Annika Carlson	233
EFC15187	Björn Eriksson	235
EFC15188	Giulia Massaglia	237
EFC15190	Valeria Agostino	239
EFC15192	Thomas Sobi	241
EFC15193	Peter Kus	243
EFC15194	Labus Martin	245
EFC15199	Valeria Agostino	247
EFC15200	Gilles De Moor	249
EFC15202	Angelo Moreno	251
EFC15205	Antonella Marone	253
EFC15207	Corinna Harms	255
EFC15208	David Rodríguez Vidal	257
EFC15209	Michael Lang	259
EFC15211	Adam Weber	261
EFC15217	Steven Beale	263
EFC15218	Luca Micoli	265
EFC15219	Angelo Ausiello	267
EFC15222	Benjamin Erable	269
EFC15226	Stefano Cavallaro	271
EFC15227	Diego Orland Martínez Hernández	273
EFC15228	Antonella Glisenti	275
EFC15230	Henri Stenberg	277
EFC15231	Pablo M. Belchor	279
EFC15233	Hohyoun Jang	281
EFC15236	Andrea Masi	283
EFC15238	Araceli Fuerte	285
EFC15239	Olutomisin Manase Orogbemi	287
EFC15244	Jisoo Park	289
EFC15246	Oliveira Gabriela De Santini	291
EFC15248	Matteo Testi	293
EFC15249	Maria José Escudero	295
EFC15251	Whan Lee Chang	297
EFC15252	Donghee Han	299

EFC15253	Junhee Lee	301
EFC15254	Sinuhe Costilla	303
EFC15255	Moon-sun Chung	305
EFC15259	Mohamed K. Hassan	307
EFC15260	Fortunato Migliardini	309
EFC15262	Keno Leites	311
EFC15263	Jon Chouler	313
EFC15264	Mirella Di Lorenzo	315
EFC15265	Sara Monasterios Martinez	317
EFC15267	Pavlina Theodosiou	319
EFC15269	Sanghun Lee	321
EFC15270	Irene Merino-Jimenez	323
EFC15273	Sergey Grigorie	325
EFC15275	Mohamed Mahmoud	327
EFC15277	Xavier Alexis Walter	329
EFC15278	Rosanna Nastro	331
EFC15279	Rosanna Nastro	333
EFC15280	Mario Mitov	335
EFC15281	Yolina Hubenova	337
EFC15285	Lukasz Szablowski	339
EFC15286	Junhee Lee	341
EFC15287	Vincenzo Mulone	343
EFC15288	Mohanta Paritosh Kumar	345
EFC15289	Grazia Accardo	347
EFC15290	Federica Carletta	349
EFC15292	Federica Carletta	351
EFC15294	Federica Carletta	353
EFC15295	Abbas Rezaee	355
EFC15296	Adriana Marinoiu	357
EFC15297	Hyun S. Park	359
EFC15298	Giovanni Cinti	361
EFC15300	Chung-hsing Chao	363
EFC15301	Raphael Ihringer	365
EFC15302	Maria Vicidomini	367
EFC15304	Daniele Guida	369
EFC15307	Anna Speranza Espinoza Tofalos	371
EFC15308	Kazuo Shibata	373
EFC15310	Olli Himanen	375
EFC15311	Giuseppe Bagnato	377
EFC15312	Adolfo Iulianelli	379
EFC15313	Abraham Esteve-nÚñez	381
EFC15314	Francesco Calise	383



European Fuel Cell

Conference & Exhibition



TOPICS

Materials
Modeling
Lab Tests
System Design
Fuels and decarbonizing society
Fuel Cell Applications
Fuel Cells operated in reversed mode
Marketing and Policy pathways to full commercialization of Fuel Cells
Cross-cutting Issues
New ideas and bad ideas in FC

TOPICS DEDICATED TO SPECIAL SESSIONS

Safety, Regulations codes & standards in Fuel Cells
Microbial Fuel Cell
Dissemination of European project on Fuel Cell and Hydrogen

PRESENTED AT

European Fuel Cell 2015 | Piero Lunghi Conference & Exhibition
DECEMBER 16-18, 2015 | NAPLES, ITALY

ORGANIZED BY

University of Perugia
ENEA
Atena
University of Naples "Parthenope"

ORGANIZED BY

Angelo Moreno, Conference Chairman, ENEA
Viviana Cigolotti, Technical Program Manager, ENEA
Chiara Barchiesi, Michela Chianella, Vanessa Rossi, Event Coordinators, University of Perugia

THANKS AND
SEE YOU SOON | EFC17



BOOK OF PROCEEDINGS
of the 6th European Fuel Cell | Piero Lunghi Conference

creativi.biz



European Fuel Cell
Conference & Exhibition

WWW.EUROPEANFUELCELL.IT